Dissertation

submitted to the

Combined Faculty of Natural Sciences and Mathematics

of the Ruperto Carola University Heidelberg, Germany

for the degree of Doctor of Natural Sciences

Presented by	Carina Anna Lämmle M. Sc.
Born in	Ochsenhausen, Germany
Oral examination	11 March 2022

Molecular probes for DNA labeling

Referees	Prof. Dr. Dr. h.c. Hans-Georg Kräusslich
	Prof. Dr. Kai Johnsson

Acknowledgment

I would like to express my deep gratitude to Prof. Dr. Kai Johnsson for his support and helpful critiques of this research work. Assistance provided by my TAC members Prof. Dr. Dr. h.c. Hans-Georg Kräusslich and Prof. Dr. Andres Jäschke and their professional guidance was greatly appreciated.

I thank Dr. Johannes Broichhagen for his supervision and enthusiastic encouragement. I am particularly grateful for the assistance with microscopy experiments given by Dr. Birgit Koch and input for this thesis. My grateful thanks are also extended to PD Dr. Richard Wombacher for helpful discussions and Julien Hiblot for his advice. I would like to offer my special thanks to the facilities and the facility managers of the institute: In particular to Dr. Sebastian Fabritz and his team for quantification experiments and data analysis as a great contribution to this project. I want to thank Dr. Elisa D'Este for her introduction to the STED microscope.

Advice given by Thorsten Müller (AK Kräusslich) has been a great help. I would also like to thank my students Franziska Walterspiel and Luis Hauptmann for their support in the lab with the projects. Constructive recommendations provided by my subgroup D with Dr. Michelle Frei, Dr. Lin Xue and Dr. Philipp Leippe were greatly appreciated. Also a personal thanks to my office R248: Dr. Jorick Bruins and Julian Kompa.

Thanks to the technicians of the laboratory: Bettina Réssy, Cornelia Ulrich, Juliana Kling, Andrea Bergner, Dominik Schmidt, Carmen Grosskurth and Tatjana Rudi for their valuable support. My great appreciation to Gwenaëlle Matthies for arranging daily operations and schedules.

I acknowledge the Boehringer Ingelheim Fonds for giving me a PhD Fellowship. This work was also funded by the Deutsche Forschungsgemeinschaft (DFG, German Research Foundation) – Projektnummer 240245660 – SFB 1129 project. Furthermore, I am happy for the resources provided by the department, including thanks to the staff of the medium and cleaning kitchen. I want to especially mention Ioannis Karagiannis (purchasing department) and Martin Lukat (metal workshop) and Christopher Roome (IT).

I wish to thank various people for their personal support: Nicole Mertes, Dr. Marie Grünbein, Dr. Cornelia Zapp, Dr. Silvia Antona, Kevin Jahnke, Dr. Marcus Held, Veronika Burger and Tamara Naumoska. For proof-reading additional thanks to Dr. Veselin Nasufovic, Dr. Vincent Grenier, Dr. De-en Sun, Dr. Vijay Nimbarte, Nicolas Lardon, Djordje Salai and Christian Reinbold. Special thanks to our PhD coordinators Elisabeth Fuhry and Dr. Jade Cottam Jones. Finally, I wish to thank my parents and siblings for their management skills, support and encouragement throughout my PhD. Without you, I couldn't have done this.

Last but not least, I am happy to my Munich crew for taking me back. It feels like coming home.

Abstract

In my thesis, I worked on two labeling strategies for cellular DNA in fluorescence microscopy.

DNA can be studied by fluorescence microscopy with the aid of stains, that can label the total cellular DNA content in live cells. But for some applications, it is desirable that DNA labeling should only occur in specific regions. To this end, Hoechst33342 was photocaged and its in cell activation with light was investigated in a first project. The activatable DNA stain was successfully applied to label specific regions of DNA in the nucleus of living cells and in clusters of cells in zebrafish larva.

Metabolic DNA labeling is frequently applied to label newly synthesized DNA. In metabolic DNA labeling, the cell activates nucleotide precursors and incorporates them into the nascent DNA chain. In a subsequent labeling reaction, the precursors can be marked with a fluorophore. Until now, the visualization of incorporated reporter nucleosides was only amenable in fixed cells. In a second project, different approaches for metabolic DNA labeling were employed and further improved for applications in living cells.

Initially, a reported nucleoside building block, 5-vinyl-2'-deoxyuridine (VdU), which is marked in an inverse-electron demand Diels–Alder (iEDDA) reaction was explored. The building block had previously been shown to be effective for labeling of DNA in fixed cells, but not in living cells. I describe the development of a probe for a proximity-enhanced iEDDA labeling of VdU-tagged DNA in living cells.

To overcome the slow labeling observed for vinyl-modified DNA, the screening of new metabolic precursors was undertaken, in hope of finding a building block with higher reactivity. Therefore, 7-deaza-2'-deoxyadenosine derivatives were modified with more reactive dienophiles and were investigated. Their incorporation into the DNA was verified by mass spectrometry. In fluorescence imaging, they provided the first signals in the nucleus of proliferating cells. Despite faster labeling kinetics, the overall sample preparation takes long since the reporter is introduced first and visualization with a fluorophore is only possible in the second step.

Successful live cell imaging demands labeling methods with high labeling efficiency and speed. Therefore, the use of nucleosides that have the fluorophore already attached was investigated. These new metabolic precursors allowed a signal to be detected immediately after their incorporation into the nascent DNA chain. To enable better incorporation yields, the fluorescent nucleosides were further evolved into pro-nucleotides. Nuclear staining in proliferating living cells could be observed, even though it required incubation times of several hours.

In summary, all adenosine derivatives label proliferating cells. Current challenges for more demanding applications are poor spatial and temporal resolution for all metabolic approaches. In addition to low incorporation yields, the labeling is often also accompanied by undesirable cytotoxicity effects. If these drawbacks could be overcome, such could pave the way for observing processes that involve DNA synthesis in living cells. Examples of applications include the study of DNA replication, repair, or retroviral DNA synthesis.

Zusammenfassung

In meiner Doktorarbeit habe ich mich mit zwei Markierungsstrategien für zelluläre DNA in der Fluoreszenzmikroskopie beschäftigt.

DNA kann in der Fluoreszenzmikroskopie mit Farbstoffen untersucht werden, die den gesamten zellulären DNA-Gehalt in lebenden Zellen markieren. Für einige Anwendungen ist es jedoch wünschenswert, dass die Markierung der DNA nur in bestimmten Regionen erfolgt. Zu diesem Zweck wurde in einem ersten Projekt Hoechst33342 mit einer photoaktivierbaren Schutzgruppe versehen und seine Aktivierung mit Hilfe von Licht in der Zelle untersucht. Der aktivierbare DNA-Farbstoff wurde erfolgreich zur Markierung spezifischer DNA-Bereiche im Kern lebender Zellen und in Zellclustern in Zebrafischlarven eingesetzt.

Metabolische DNA-Markierung wird häufig zur Markierung neu synthetisierter DNA eingesetzt. Bei der metabolischen DNA-Markierung phosphoryliert die Zelle Nukleotidvorstufen und baut diese in die entstehende DNA-Kette ein. In einer anschließenden Markierungsreaktion kann der Baustein mit einem Fluorophor versehen werden. Die Visualisierung der eingebauten Reporternukleoside war bisher nur in fixierten Zellen möglich. In einem zweiten Projekt wurden verschiedene Ansätze zur metabolischen DNA-Markierung verwendet und für Anwendungen in lebenden Zellen weiter verbessert.

Zunächst wurde ein bekannter Nukleosidbaustein, 5-Vinyl-2'-Desoxyuridin (VdU), der mit einer Diels–Alder-Reaktion mit umgekehrtem Elektronenbedarf (iEDDA) markiert wird, untersucht. Der Baustein hatte sich bereits für Markierungen von DNA in fixierten Zellen als effektiv gezeigt, aber nicht in lebenden Zellen. Ich beschreibe die Entwicklung einer Sonde für eine durch räumliche Nähe verstärkte iEDDA-Markierung von VdU-modifizierter DNA in lebenden Zellen.

Um die langsame Markierung zu überwinden, wurde ein Screening neuer Vorstufen durchgeführt, in der Hoffnung, einen Baustein mit höherer Reaktivität zu finden. Daher wurden 7-Deaza-2'-Desoxyadenosin-Derivate mit reaktiveren Dienophilen modifiziert und untersucht. Ihr Einbau in DNA wurde durch Massenspektrometrie überprüft. In der Fluoreszenzmikroskopie lieferten sie Signale im Zellkern proliferierender Zellen. Trotz der schnelleren Markierungskinetik ist die gesamte Probenvorbereitung langwierig, da der Reporter zuerst eingeführt wird und die Visualisierung mit einem Fluorophor erst im zweiten Schritt möglich ist.

Erfolgreiche Mikroskopieaufnahmen in lebenden Zellen erfordern Markierungsmethoden mit hoher Markierungseffizienz und -geschwindigkeit. Daher wurde die Verwendung von Nukleosiden untersucht, an die das Fluorophor bereits gebunden ist. Diese neuen Vorstufen ermöglichen den Nachweis eines Signals unmittelbar nach ihrem Einbau in die entstehende DNA-Kette. Um eine bessere Ausbeute beim Einbau zu erzielen, wurden die fluoreszierenden Nukleoside zu Pro-Nukleotiden weiterentwickelt. Die Anfärbung des Zellkerns in proliferierenden lebenden Zellen konnte auch hier beobachtet werden, wenn auch erst nach einigen Stunden.

Zusammenfassend lässt sich sagen, dass alle hier entwickelten Adenosinderivate proliferierende Zellen markieren. Aktuelle Herausforderungen für anspruchsvollere Anwendungen sind die geringe räumliche und zeitliche Auflösung aller metabolischer Ansätze. Neben der geringen Einbaurate geht die Markierung häufig auch mit unerwünschten Zytotoxizitätseffekten einher. Wenn diese Nachteile überwunden werden könnten, könnten damit Beobachtungen von Prozessen in Verbindung mit DNA-Synthese in lebenden Zellen ermöglicht werden. Beispiele für Anwendungen sind DNA-Replikation, -Reparatur oder retrovirale DNA-Synthese.

Contents

Abbreviations

acac	acetyl acetone
AB	acetoxybenzyl
AIBN	azobis(*iso*butyronitrile)
AM	acetoxymethyl
AmdU	(azidomethyl)-2'-deoxyuridine
ANCHOR	DNA labeling technology ANCH DNA target sequence and OR protein
APC	aphidicolin
ATCC	American Type Culture Collection
aq.	aqueous
BCN	bicyclo[6.1.0.]nonyne
boc	*tert*-butyloxycarbonyl
BrdU	5-bromo-2'-deoxyuridine
BSA	bovine serum albumin
cDNA	copy deoxyribonucleic acid
CldU	5-chloro-2'-deoxyuridine
CLEM	correlative light and electron microscopy
CuAAC	Cu-catalyzed azide-alkyne cycloaddition
CycloSal	cyclosaligenyl
Cp	cyclopropene
Cy	cyanine
dA	(7-deaza)-2'-deoxyadenosine
DAPI	4',6-diamidin-2-phenylindol
dba	dibenzalacetone
DCM	dichloromethane
dF-EdU	2'-deoxy-2',2'-difluoro-5-ethynyluridine
DIBAL-H	di*iso*butylaluminium hydride
DIPEA	*N*,*N*-di*iso*propylethylamine
dF-EdU	2'-deoxy-2',2'- difluoro-5-ethynyluridine
DMAP	4-dimethylaminopyridine
DMF	dimethylformamide
DMSO	dimethyl sulfoxide

DNA	deoxyribonucleic acid
DTE	S-[(2- hydroxyethyl)sulfidyl]-2-thioethyl
dsDNA	double stranded DNA
EdA	5-ethynyl-2'-deoxyadenosine
EdC	5-ethynyl-2'-deoxycytidine
EDC	1-ethyl-3-(3-dimethylaminopropyl)carbodiimide
EdU	5-ethynyl-2'-deoxyuridine
eGFP	enhanced green fluorescent protein
em	emission
ESI	electrospray ionization
ex	excitation
F-ara-EdU	F-arabinose-EdU
FA	formic acid
FISH	fluorescence *in situ* hybridization
FRET	Förster resonance energy transfer
FRAP	fluorescence recovery after photobleaching
GFP	green fluorescent protein
Glide	grid-based ligand docking with energetics
h	human
H	Hoechst
H2B	histone H2B protein
Hela	immortal cell line cells from Henrietta Lacks' cervical cancer
HD	Heidelberg dye
HIV-1	human immunodeficiency virus 1
HRMS	high-resolution mass spectrometry
HMBC	heteronuclear multiple bond correlation
HOMO	highest occupied molecular orbital
HSV-1	herpes simplex virus 1
HTVS	high-throughput virtual screening
hp	hairpin
HPLC	high performance liquid chromatography
iEDDA	inverse electron demand Diels-Alder
IdU	5-iodo-2'-deoxyuridine
LC-MS	liquid chromatography coupled to mass spectrometry
LUMO	lowest unoccupied molecular orbital

MALDI	matrix assisted laser desorption ionization
MaP	Max Planck
MeTet	(4-(6-methyl-1,2,4,5-tetrazin-3-yl)phenyl)methanamine
mCLING	membrane-binding fluorophore-cysteine-lysine-palmtoyl group
mRFP	red fluorescent protein
MRM	multiple reaction monitoring
MS	mass spectrometry
MTS	(3-[4,5,dimethylthiazol-2-yl]-5-[3-carboxymethoxy-phenyl]-2-[4-sulfophenyl]-2H-tetrazolium
NBS	*N*-bromosuccinimide
NHS	*N*-hydroxysuccinimid
NMR	nuclear magnetic resonance
Nor	norbonene
ODN	oligodeoxynucleotides
OG	Oregon green
PAGE	polyacrylamide gel electrophoresis
PBS	phosphate-buffered saline
pc	photocaged
PCNA	proliferating cell nuclear antigen
PCR	polymerase chain reactions
PEG	polyethylene glycol
PET	photo-induced electron transfer
PI	Propidium iodide
PLE	porcine liver esterase
POM	pivaloyloxymethyl
PSF	point spread function
RNA	ribonucleic acid
RP-HPLC	reverse phase high performance liquid chromatography
SATE	S-acyl-2-thioethyl
SiR	silicon rhodamine
SPAAC	strain promoted azide-alkyne cycloaddition
STED	stimulated emission depletion
Su	*N*-hydroxysuccinimid
TCO	*trans*-cyclooctene
TBET	through bond energy transfer

TEAA	triethylammonium acetate buffer
TEAB	triethylammonium bicarbonate buffer
TFA	trifluoroacetic acid
TFAA	trifluoroacetic anhydride
TFE	2,2,2-trifluoroethanol
THF	tetrahydrofuran
TK	thymidine kinase
TMR	tetra-methyl rhodamine
TMS	trimethylsilyl
TLC	thin layer chromatography
TSTU	*N*,*N*,*N*',*N*'-tetramethyl-*O*-(*N*-succinimidyl)uroniumtetrafluorborate
Tz	tetrazine
U2OS	human bone osteosarcoma cell line
UV	ultra violet
VACV	vaccinia virus
VdU	5-vinyl-2'-deoxyuridine
VdUTP	VdU triphosphate
vis	visible
VTdT	vinyl thioether modified thymidine

Variables and Units

A	ampere
Å	Ångström
bar	100 kPa
bp	base pair
c	centi
°C	degree celsius, temperature relative to 273.15 K
δ	chemical shift
eq.	equivalent
g	gram
h	hour
Hz	hertz
J	coupling constant
k	kilo
K	kelvin
l	liter
m	milli, meter
M	Mega, molar
min	minute
mol	mole, 6.022×10^{23} particles
n	nano, number of moles
p	pico
Pa	pascal
ppm	parts per million
$\mathbf{T_{t,r}}$	retention time
µ	micro
V	volt
W	watt

Chemical abbreviations

Ac	acetyl
Bn	benzyl
Et	ethyl
Me	methyl
Ph	phenyl
m	meta
o	ortho
p	para
r. t.	room temperature
sat.	saturated

Part I

Introduction

1 Prologue

Deoxyribonucleic acid (DNA) is a unique molecule that is composed of monomeric units called nucleotides. Friedrich Miescher was the first to isolate and characterize DNA in the winter of 1868/9, while doing experiments on leukocytes.[1] Back then, he described DNA as a "component of all nuclei" and raised the idea that the substance could be involved in heredity.[2]

More than 80 years later, the Hershey–Chase experiments with bacteriophages confirmed that DNA carried the information for inheritance.[3] Alfred Hershey and Martha Chase received a Nobel Prize for "discoveries concerning the genetic structure of viruses".[4]

The functional mechanism behind the information transfer was completely unknown until Watson and Crick came up with the model for the double-helix structure of DNA in 1953.[5] The structure prediction was based on an X-ray diffraction image that was initially taken in the laboratory of Rosalind Franklin.[6] When James Watson and Francis Crick were awarded the Nobel Prize[7] after Franklin's death, debates were raised about who should receive credit for the discovery.

Yet, Watson and Crick were the first who postulated a copying mechanism of DNA. The hypothesis of semiconservative replication of DNA was then confirmed in the Meselson–Stahl experiment using an isotope-labeling method to distinguish between parent and newly copied DNA.[8]

Nowadays, we have detailed knowledge on DNA replication, the chromatin structure as well as the organization in the nucleus. Key technology for many discoveries was fluorescence imaging. To study DNA in cells by means of fluorescence microscopy, DNA labeling is essential.[9], [10]

Broadly applied chemical tools to visualize DNA are nucleic acid stains or metabolic DNA labeling (Chapter 2). Nucleic acid stains label the whole DNA content (Section 2.1). In contrast, metabolic DNA labeling is visualizing newly synthesized DNA only. Different metabolic precursors can be used for DNA labeling (Section 2.2) and can be combined with various bioconjugation techniques (Chapter 3).

So far, metabolic DNA labeling cannot be used in living cells, but the desire for methods that are amenable in living cells is clearly visible. One application that could benefit from these developments is the imaging of viral DNA (Chapter 4). Therefore, metabolic DNA labeling to study viruses, but also alternative methods to label viral DNA are introduced (Section 4.3).

Finally, ideas to improve metabolic labeling techniques for viruses are briefly presented in order to then elaborate on the overall scope of this work (Chapter 5).

2 Chemical tools to visualize DNA

2.1 Nucleic acid stains for DNA

Visualization of nucleic acids is a standard procedure for the detection and quantification of DNA, staining of gels in electrophoresis, in microscopy, or flow cytometry experiments.[11]

DNA stains typically show a high increase in fluorescence on DNA. Once bound to DNA, the suppression of rotational relaxation[12] and reduction of hydration[13] results in an enhancement in fluorescence.

DNA stains can be divided into cell-impermeable and cell-permeable stains. For most applications, cell-impermeable dyes are used as they are strong binders and are less toxic for the user. Cell-permeable dyes are needed as nuclear counterstains especially in live-cell microscopy.[9]

There are three main binding modes: Intercalators (mono- and bis-intercalators), groove binders (major and minor grooves), and external binders (see Figure 2.1, A).

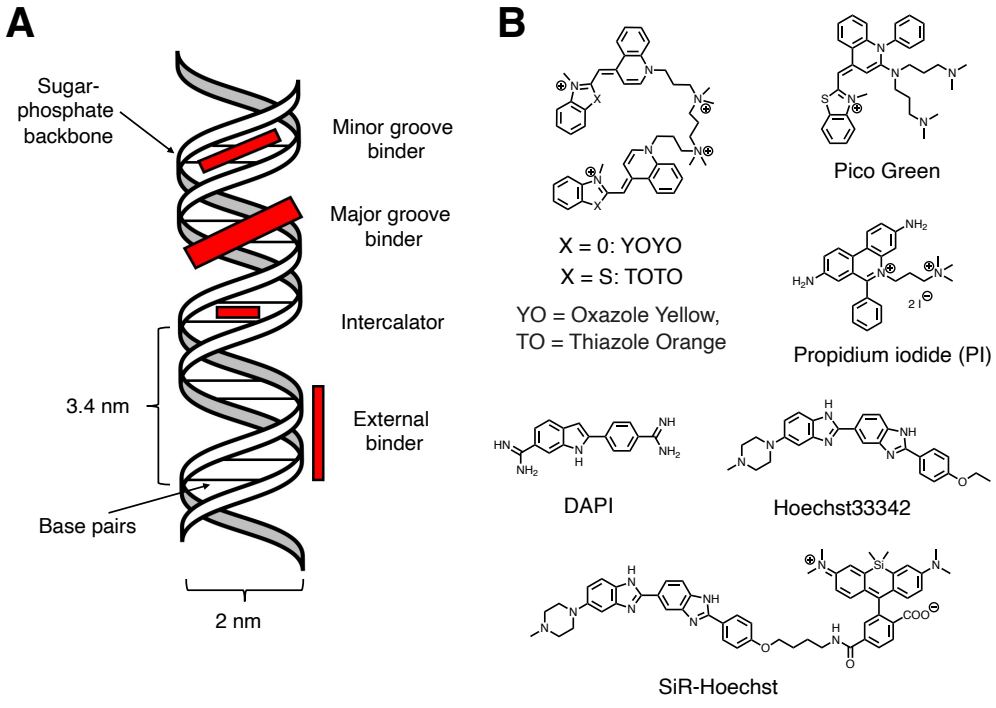

Figure 2.1: DNA binding dyes with different binding modes. (A) DNA double helix with an overview of binding modes. (B) Chemical structures of nucleic acid stains.

Classical bis-intercalators are cyanine dimers (e.g. YOYO or TOTO) and show a high affinity for nucleic acids due to interactions with the negatively charged backbone, high quantum

yield, and high fluorescence turn-on upon binding to nucleic acids. PicoGreen[14] or propidium iodine[15] are mono-intercalators and used for nucleic acid quantification or as a marker for cell cycle analysis in flow cytometry, respectively.

Indoles or imidazoles (e.g. Hoechst[16],[17],[18] and DAPI[19]) are groove-binding dyes, that preferentially bind in AT-rich regions. They are the first choices for nuclear counterstains, due to simplicity in usage, low cost, and no requirement for genetic modification.

In addition, Hoechst can be coupled with other fluorophores, which allows the detection of DNA at higher wavelengths.[20] Based on this concept, DNA probes were developed for chromatin imaging over a large spectral range and were used for STED[21], [22] and dSTORM[23] nanoscopy. In contrast to Hoechst33342, these probes show lower affinity towards DNA which results in lower toxicity and better biocompatibility. As such, 6-Hoechst-SiR enabled for the first time long-term imaging of dividing cells exhibiting low cyto- and phototoxicity compared to other DNA stains (Figure 2.1, B).[21] It is therefore widely used and is commercially available as SiR-DNA.

2.2 Metabolic DNA labeling

In metabolically DNA labeling unnatural buildling blocks are administered to replicating cells to visualize DNA.[24] Feeding nucleoside or nucleotide analogs that mimic their natural counterparts provides an opportunity for a reporter group to be inserted into the newly synthesized DNA (Figure 2.2).

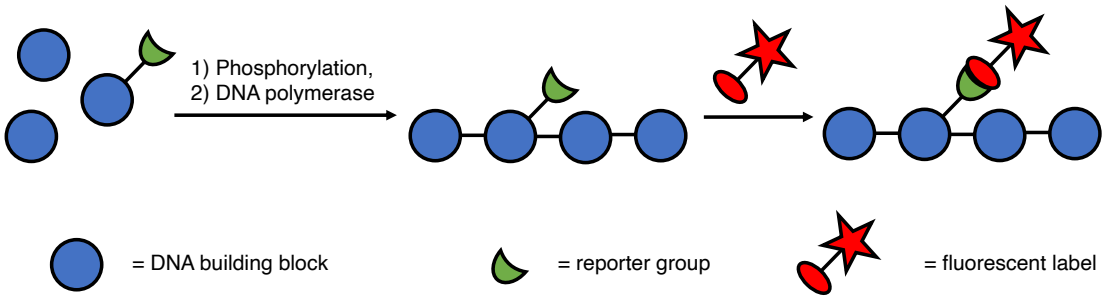

Figure 2.2: Process of metabolic DNA labeling that occurs inside a cell: DNA building blocks (= blue circles) are phosphorylated and incorporated into DNA. If reporter groups (=green half-moon) are introduced they can be targeted with a fluorescent label (=red star) that can be later detected.

Within the cell, they are phosphorylated in the nucleotide salvage pathway.[25] After their phosphorylation, the obtained nucleotide triphosphates are incorporated into DNA by polymerases, where the reporter nucleoside can be subsequently detected. Historically, autoradiography and immunofluorescence were used, more recently bioorthogonal reactions have proved to be an invaluable method for covalent labeling of reporter groups in biomolecules with fluorophores. Once marked, the nascent DNA can be localized inside a cell by means of fluorescence microscopy and the observed images give important information about its temporal and spatial synthesis, helping to get a better understanding of underlying biological processes.

2.2.1 Phosphorylation of nucleoside analogs via endogenous enzymes

To install a reporter group into nascent DNA, building blocks of DNA carrying these reporter groups are supplemented to cells. A simple building block for metabolic DNA labeling is a nucleoside. Nucleosides are uncharged molecules, that can enter a cell by passive or active transport.[26], [27] So far, mostly thymidine derivatives were employed to study DNA synthesis (Figure 2.3).[28], [29]

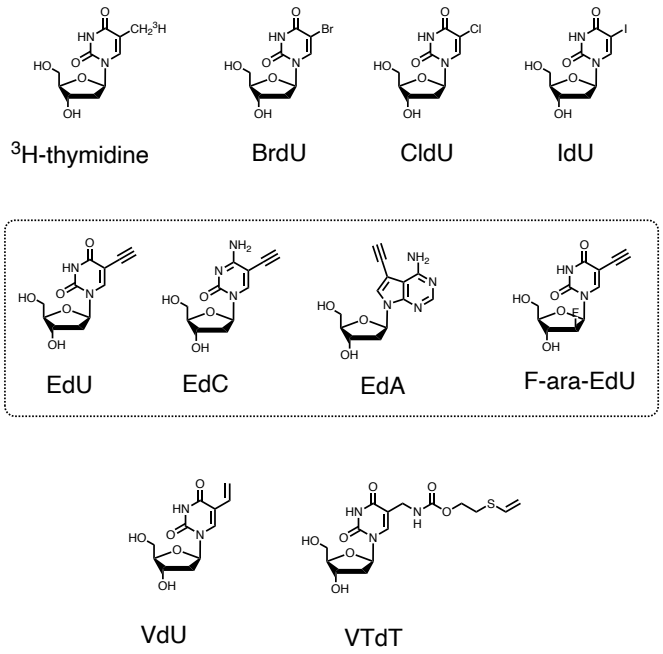

Figure 2.3: A panel of selected nucleosides for metabolic DNA labeling. Ethynyl modified nucleosides are highlighted in the box.

Radiolabeled nucleosides

Historically, ^{3}H-thymidine was used to label nascent DNA (Figure 2.3).[30] This radiolabeled nucleoside analog is structurally undistinguishable to its natural counterpart for the cell and as such efficiently incorporated into DNA. The radiolabeled DNA is subsequently detected with autoradiography or scintillation. The method was originally developed for the purpose of studying "semi-conservative replication"[30], but also used to confirm the existence of "neurogenic" zones in mice brains[31]. As the handling of a radio-labeled substrate should be avoided, and autoradiography is a time-consuming technique, there was need for new metabolic precursors.

Antibody detection

By the 1970s, advances in the production of monoclonal antibodies enabled the development of immunofluorescence.[32], [33] The emergence of an antibody against 5-bromo-2'-deoxyuridine (BrdU, Figure 2.3) laid the groundwork for the replacement of ^{3}H-thymidine with BrdU.[34], [35], [36] BrdU labeling was the key technology used to detect newly generated cells in the adult human brain and prove adult neurogenesis.[37] BrdU has been used in over 20000 published biomedical

studies in multiple fields including, stem cell research, cancer biology, parasitology and remains heavily used today.[28], [38]

To improve the accessibility of the BrdU epitope for recognition by an antibody, BrdU-labeled DNA is denatured with strong acids or partially digested with nucleases. These harsh treatments also lead to the degradation of nucleic acids or proteins and consequently negatively impact the cellular structures or disrupt tissues. Therefore, BrdU cannot be used in experiments that require analysis of protein content or molecular analysis besides BrdU staining. Its use as a quantitative tool is hence limited.[38]

Besides BrdU, other halogenated nucleosides 5-chloro-2'-deoxyuridine and 5-iodo-2'-deoxyuridine (CldU and IdU, Figure 2.3) were developed for antibody detection, but they are less frequently used.[39], [40]

Cu(I) click chemistry

A breakthrough in visualizing replicating DNA was the implementation of ethynyl groups for tagging DNA (Figure 2.3, second row). As terminal alkyne groups are rarely present in biological systems they are ideal reporters due to their small size and good metabolic stability. Alkyne groups react with azides in a Cu(I) catalyzed click reaction, without requiring additional DNA treatment and thus allow a simple and quick labeling protocol (Section 3.1).

5-Etynyl-2'-deoxyuridine (EdU) is the most prominent nucleoside that is frequently applied in proliferation assays.[41],[42] But, EdU incorporation is toxic for the cells.[43] Therefore, other alkyne modified nucleosides with lower toxicity were developed such as 5-etynyl-2'-deoxycytidine (EdC)[44],[45] and (2'*S*)-2'-deoxy-2'-fluoro-5-ethynyluridine (F-ara-EdU)[46].

Purine analogs were investigated in the context of metabolic DNA labeling. While alkyne-modified 7-deaza-2'-deoxyguanosine, did not give specific staining in cells, 7-ethynyl-7-deaza-2'-deoxyadenosine (EdA, Figure 2.3) was shown to be viable for metabolic DNA labeling, though at the cost of higher cytotoxicity compared to EdU.[47]

However, Cu(I) treatment proved detrimental to DNA and generates artifacts interfering with other fluorescent markers, such as fluorescent proteins or immunostaining by degrading epitopes for antibodies.[28] Therefore, it is not the best solution to every application and new Cu(I) free techniques for tracking DNA synthesis in proliferating cells were developed.

Cu(I) free labeling methods

The introduction of 5-vinyl-2'-deoxyurdine (VdU, Figure 2.3) was a milestone for Cu(I) free DNA labeling in cells.[48] Initially, VdU was visualized by a dipyridyl tetrazine in an iEDDA after denaturation of the DNA with hydrochloric acid and used for three-color multiplexing experiments following S-phase synthesis in a cell in combination with EdU and BrdU.

Following on from this work, Linden et al. performed VdU labeling in living cells with a methyl tetrazine attached to a BODIPY-derived singlet oxygen generator.[49] Labeling was sufficient to induce apoptosis by illuminating the bound singlet oxygen generator, but the authors could only provide poor images of fixed cells.

In addition to iEDDA reactions, a photoclick reaction of VdU with a water soluble coumarin-fused tetrazole in living cells was published.[50] The tetrazole was used at high concentrations

and showed a high background signal, indicating poor chemoselectivity.

According to observations by Tang et al., a thymidine derivative with a vinyl thioether (VTdT, Figure 2.3) was accepted as a substrate for DNA synthesis and allowed staining with an *o*-quinolinone quinone methide in cells even without DNA denaturation.[51] Incorporation of the nucleoside was confirmed by mass spectrometry analysis and fluorescence microscopy was performed. The fluorescent signal after quinone methide reaction diminished after DNA digestion, but the overall high background in the obtained images suggested low incorporation efficiency or non-specific staining of the quinone methide.

Summary

In summary, all substrates that show efficient incorporation have rather small modifications (halogen moiety, ethynyl or vinyl groups). Vinyl groups allow multiple labeling reactions and have the greatest potential of all known modifications for possible labeling in living cells. Labeling VdU in living cells would give much value.[24] However, existing methods are not yet adequate for this purpose. Therefore, the necessity persists for continuously expanding the bioorthogonal toolbox for DNA labeling.

2.2.2 Phosphorylation of nucleoside analogs via a viral kinase

In addition to attempts presented in Section 2.2.1, azide groups were integrated into DNA for Cu(I) free labeling. The resulting nucleoside 5-(azidomethyl)-2'-deoxyuridine (AmdU, Figure 2.4) was no longer incorporated into DNA due to inefficient mono-phosphorylation.[52]

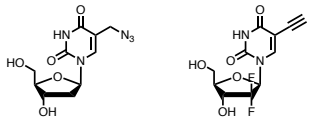

Figure 2.4: AmdU and dF-EdU are only efficiently phosphorylated by a more promiscuous viral kinase.

Phosphorylation of thymidine to its nucleotide monophsophate by human thymidine kinase 1 (hTK1) in the cytosol is commonly described as the bottleneck of the metabolic pathway.[26],[53] Therefore, researchers came up with various methods to circumvent the first phosphorylation step.

For AmdU this was done with heterologous expression of the more promiscuous herpes simplex virus thymidine kinase 1 (HSV-TK1) in Hela cells. AmdU treated Hela-HSV-TK1(+) cells exhibited (i) more intense staining after CuAAC reaction with AlexaFluor594-alkyne, and (ii) higher sensitivity to toxic effects of AmdU.[52] This clearly indicated that phosphorylation by hTK1 was the limiting step in the metabolic pathway.

After improving the incorporation of the nucleoside, the strain-promoted azide-alkyne cycloaddition (SPAAC) labeling of AmdU with BCN-AlexaFluor488 was further investigated.[52] While the SPAAC reaction gave comparable results to the Cu(I) click reaction after DNA denaturation with 1 M HCl, the staining was weaker for native DNA in fixed cells and not present in the entire nucleus. In living cells, the staining did not show any specific labeling pattern. The

experiments imply that the accessibility of the modification after incorporation into DNA poses a difficulty in its labeling. To overcome this limitation, a three-component-system was later developed that first triggers the reaction of the modifcation with an intercalator and then with the fluorophore (Section 3.4).[54],[55]

In a slightly different approach, 2'-deoxy-2',2'- difluoro-5-ethynyluridine (dF-EdU, Figure 2.4) was used for pathogen-selective labeling.[56] *In vitro* experiments showed that dF-EdU could not be phosphorylated by hTK1. Also, the crystal structure of hTK1 confirmed that the catalytic site was too small to bind the substrate. When dF-EdU was supplemented to cells, only cells that were previously infected with Herpes Simplex Virus exhibited nuclear staining upon the addition of dF-EdU and a fluorescent azide.

2.2.3 Pro-nucleotide precursors

As previously discussed in Subsection 2.2.2, nucleosides that are poor substrates for the hTK1 could be mono-phosphorylated by using a viral kinase. An alternative approach to circumvent the first intracellular phosphorylation step is the use of masked nucleotide monophosphates. These so-called pro-nucleotides are commonly found in medicinal chemistry, as (i) they exhibit enhanced bioavailability relative to the parent unphorphorylated nucleosides and (ii) the pro-drug moiety improves the pharmacological properties of nucleosides.[57]

Examples of masking groups are carbonyloxymethyl phosphotriesters (POM, POC), S-acyl-2-thioethyl (SATE) and S-[(2-hydroxyethyl)sulfidyl]-2-thioethyl (DTE) goups, cyclosaligenyl (cycloSal) phosphates and phosphonates, aryloxy phosphoramidates or phosphonamidates (ProTides), cyclic 1-aryl-1,3-propanyl ester (HepDirect) (Figure 2.5). The underlying de-masking mechanism vary for each group and rely on spontaneous or enzymatic cleavage, which is facilitated by carboxylesterases, carboxypeptidases, oxidative or reductive enzymes (e.g. cytochrome P450 or nitroreductases).

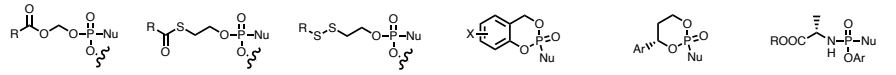

POM, POC (esterase)	**SATE** (esterase)	**DTE** (reductase)	**cycloSal** (chemical)	**HepDirect** (CYP450)	**ProTide** (peptidase)

Figure 2.5: Selected α-monophosphate groups for bioactive monophosphates in cells with their cleavage mechanisms. Nu = nucleoside.

Biolabile monophosphate groups were used for EdU and AmdU (Figure 2.6). EdU was caged with cycloSal, POM, or a simple acetyl group, and the subsequent incorporation was investigated.[58], [59] As EdU itself was already incorporated into DNA with high yield, the differences with a protecting group were marginal.

In contrast, AmdU is a great example for a poor substrate of hTK1. In an earlier publication, the first phosphorylation was bypassed with the expression of HSV-TK1 (Subsection 2.2.2).[52] To allow the incorporation of an AmdU pro-nucleotide the authors modified AmdU with three protecting groups: Pivaloyloxymethyl (POM), acetoxybenzyl (AB) and a ProTide group.[54] Modifying AmdU with a POM protecting group led to a significant improvement of the incorporation yields (Figure 2.6), while the AB-AmdU and the AmdU ProTide gave lower incorporation efficiencies in cells.

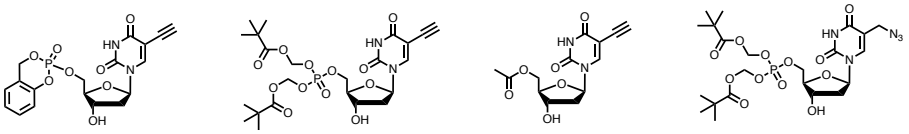

cycloSal-EdU POM-EdU ac-EdU POM-AmdU

Figure 2.6: Structures of selected pro-nucleotides for metabolic DNA labeling.

2.2.4 Delivery of nucleotide triphosphates

To completely bypass intracellular phosphorylation, nucleotide triphosphates can be used. Since they are not cell permeable, there are several delivery methods for triphosphates. However, they mostly come with drawbacks and are therefore not commonly used.

Similar to the α-protecting group presented above, γ-protecting groups were developed for triphosphates (Figure 2.7).[60],[61],[62] The main challenge is the low stability of these groups and the difficult synthesis. This could also be the reason why these protecting groups have not been used for metabolic DNA labeling so far, but have only been proposed for medicinal chemistry.

TriPPPro γ-(AB-alkyl)

Figure 2.7: Selected γ-monophosphate groups for bioactive triphosphates in cells. Nu = nucleoside.

Another possibility is the microinjection of modified triphosphates into cells. In the past, microinjections were used to deliver a fluorescent adenosine derivative into cells.[63] In microinjections, a small needle is used to manually inject a very small volume into each cell. Microinjections are tedious work and cannot be readily applied to large numbers of cells. In addition, the amount of nucleoside injected is difficult to control, and the cell can be damaged during the process. Therefore, they are often toxic to the cell.[64]

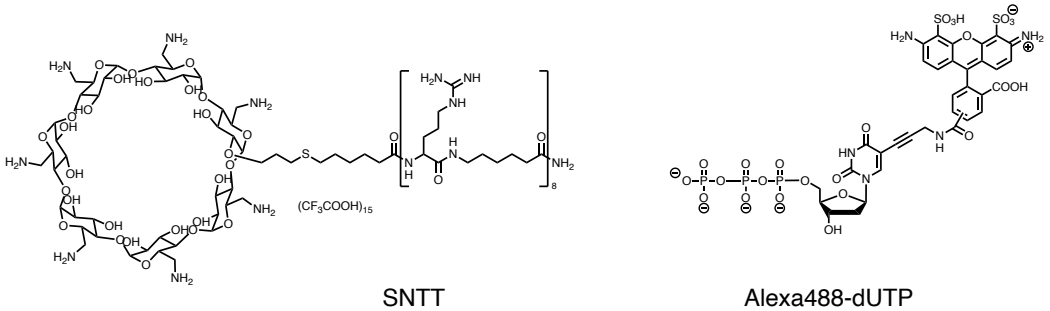

SNTT Alexa488-dUTP

Figure 2.8: Structures synthetic nucleoside triphosphate transporters (SNTT) and Alexa488-dUTP.

Recently, a synthetic nucleotide transporter (SNTT) was developed to deliver triphophates (e.g. Alexa488-dUTP) into cells (Figure 2.8).[64] The SNTT acts as a receptor for triphosphate anions and mediates cellular uptake via the polyarginine cell-penetrating peptide. Within the cell, the cargo is released from the receptor and used as a substrate for DNA synthesis. The

delivery is very rapid and can give an immediate read-out of a signal in the nucleus.[64],[65] However, strong punctae-like signals in the cytoplasm are observed. Additionally, the nucleotide triphosphates are only delivered in a short time window, which makes it difficult to observe processes that happen over a larger timeframe.

2.2.5 Polymerase-specific nucleoside precursors

For the very specific application of HIV-1 cDNA labeling, reverse transcriptase-specific nucleoside analogs were developed for subsequent staining using CuAAC chemistry.[66] Various nucleoside analogs were therefore modified with propargyl groups and screened *in vitro* for their incorporation by human polymerases and the HIV-1 reverse transcriptase.

Among the synthesized substrates, O^6-propargyl-dG and N^6-propargyl-dA were incorporated into reverse-transcribed cDNA of HIV-1, but not into genomic DNA (Figure 2.9).

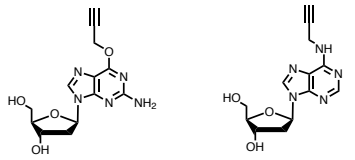

O^6-propargyl-dG N^6-propargyl-dA

Figure 2.9: Promising candidates of propargyl modified nucleoside analogs that were tested for their incorporation into HIV reverse-transcribed cDNA in cell culture experiments.

However, the staining of the viral particles was very weak, presumably due to low incorporation yields. Low incorporation yields might be due to poor phosphorylation.

2.2.6 Future developments in the field

From the previously described methods it is clear that metabolic DNA labeling is a field that is still in development. Despite new technologies BrdU and EdU are still the most broadly used methods for proliferation assays or fluorescence imaging. The reason for their use is primarily their commercial availability, but also their ease of applicability.

In addition, newly developed methods show promising potential, but the recent developments are hardly substantial enough to convince a broad community to make use of them. Only incremental technological improvements and simple applications have been achieved.

To set a further milestone it would be essential to demonstrate applications in living cells or more complex experiments. While the trend towards live-cell labeling is clearly visible, the goal has not been not achieved yet. Showing potential applications in living cells could lead to more acceptance of new methods among their users.

To enable live-cell imaging of newly synthesized DNA, bioorthogonal conjugation techniques will play a major role. Therefore, they will be briefly introduced in Chapter 3.

3 Bioconjugation techniques

3.1 Bioorthogonal reactions

Bioorthogonal reactions describe a class of reactions with diverse applications ranging from biomedical imaging, medicinal chemistry to materials and surface science.[67], [68] As the reactions proceed in biological environments, they are popular in combination with metabolic labeling of biopolymers for their visualization, cross-linking, or perturbation of their function.[69] This was demonstrated for proteins[70], [71], carbohydrates[72],[73], [74], lipids[75], [76] and nucleic acids[77], [78].

Bioorthogonal reactions have to fulfill certain criteria: (i) chemoselectivity, (ii) fast reaction kinetics, (iii) should work under physiological conditions (aqueous environment and neutral pH), (iv) ambient temperature and pressure, and (v) yield a stable covalent bond.[79], [80] Despite these requirements, numerous reactions were developed, for bioconjugation (i) *in vitro*[81],[82], (ii) on the cell surface[83], (iii) in living cells[70], [84], and (iv) *in vivo* [85], [86].

The focus here is particularly on reactions in living cells with fluorescent dyes for imaging. Reactions in living cells have the requirement that reaction partners need to be (i) cell-permeable; reaction partners and products have to be (ii) metabolically stable, and (iii) non-toxic.

3.2 Reaction kinetics

High reaction rates are required for labeling at low intracellular concentrations. As most bioorthogonal reactions follow second-order kinetics, the reaction rate depends on both concentrations of the reaction partners as well as the reaction constant.

The concentration of the tagged biomolecule and intracellular concentration of the reaction partner is typically in the low micro-molar or even nano-molar range. A plot of the conversion of a reaction for various reaction rates with both reaction partners at 1 µM concentration demonstrates that quantitative turnover within short labeling times is only achieved for reaction constants k >10 000 M^{-1} s^{-1} (Figure 3.1, A). Fortunately, bioorthogonal reactions have been developed that proceed at high reaction rates (Figure 3.1, B).

One of the first and still broadly used bioorthogonal reaction was the Cu(I)-catalyzed alkyne–azide cycloaddition (CuAAC) that was simultaneously described by Meldal and Sharpless.[81], [87] It is a robust reaction, reaching reaction rates up to 100 M^{-1} s^{-1}, whereas both reaction partners are very stable at physiological conditions. The drawback is the toxicity of Cu(I) for cells, hindering the further applications in living systems.[88] Therefore, there were many attempts to develop Cu-free alternatives.

In this process, the strain-promoted alkyne–azide cycloaddition (SPAAC) emerged.[89] It is slower compared to the CuAAC, but can be used in a living cell.[89] Similar to CuAAC, azides

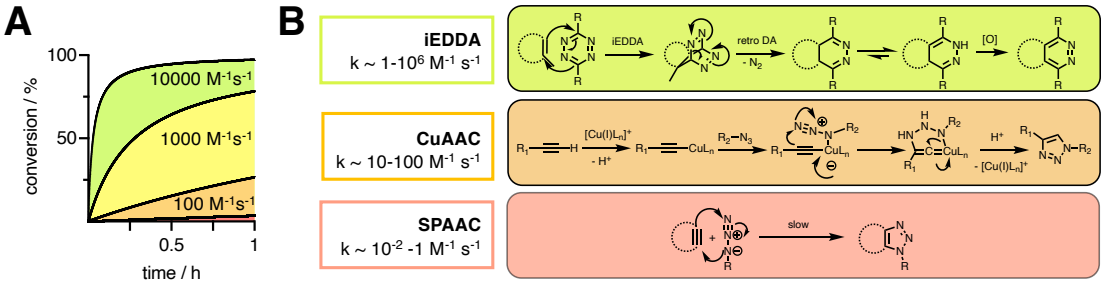

Figure 3.1: A) Conversion of a 2nd order reaction with the allocated reaction rate and 1 µM of both reactants. Therein the iEDDA reaction is the only reaction that can achieve almost quantitative conversion on a minute time scale. B) + C) Examples of bioorthogonal reactions with their reaction mechanisms and respective 2nd order rate constants.

can serve as very spatially restricted reporter groups, which makes the method interesting for metabolic labeling. However, the major drawback of the method is its slow kinetics and the susceptibility of azides to a reduction in cells.

For this reason, the inverse-electron demand Diels–Alder (iEDDA) cycloadditions between tetrazines and dienophiles became very attractive for bioorthogonal labeling in living systems. When using strained dienophiles, iEDDA are extremely fast (up to $10^6\,M^{-1}\,s^{-1}$)[90] and only generate nitrogen as a side product. The bioorthogonal handles that have to be introduced (tetrazines or strained dienophiles) are slightly larger compared to azides or alkynes and exhibit modest stability only. Nevertheless, these drawbacks are outperformed by their exceptional reaction rates and the ability of the tetrazines to show a fluorescent turn-on during the reaction when coupled to dyes, which is giving huge advantages for imaging (Section 4.1).

3.3 Inverse-electron demand Diels–Alder (iEDDA) cycloadditions

Overall, iEDDA satisfies most of the criteria for a bioorthogonal reaction in living cells and is frequently used nowadays.[91], [92]

During the reaction, a highly strained bicyclic intermediate is formed first in a 1,4-addition.[93] Then, nitrogen is released in a retro-Diels–Alder reaction to afford 4,5-dihydropyridazine, which can subsequently isomerize to the 1,4-dihydro-isomer and oxidize to form the pyridazine product (Figure 3.1, B).

On a molecular orbital scheme, electrons transfer from the highest occupied molecular orbital (HOMO) of the tetrazine to the lowest unoccupied molecular orbital (LUMO) of the dienophile (Figure 3.2). As such, the rate constant can be tuned by lifting the HOMO of the dienophile or lowering the LUMO of the tetrazine. To lift the HOMO of the dienophile (e.g. vinyl group) and increase its reactivity, typically strained alkenes and alkynes are used, such as norbonenes[94], [95], cyclopropenes [96],[97], bicycle[6.1.0.]nonyne (BCN)[98] or trans-cyclooctene (TCO)[90]. The LUMO can be lowered through electron-withdrawing substituents at the tetrazine.

In addition, sterical hindrance of the tetrazine such as methyl vs. H tetrazine plays a role in higher reactivity.[99] Among the fastest tetrazines are pyrimidyl or H tetrazines (Figure 3.2).

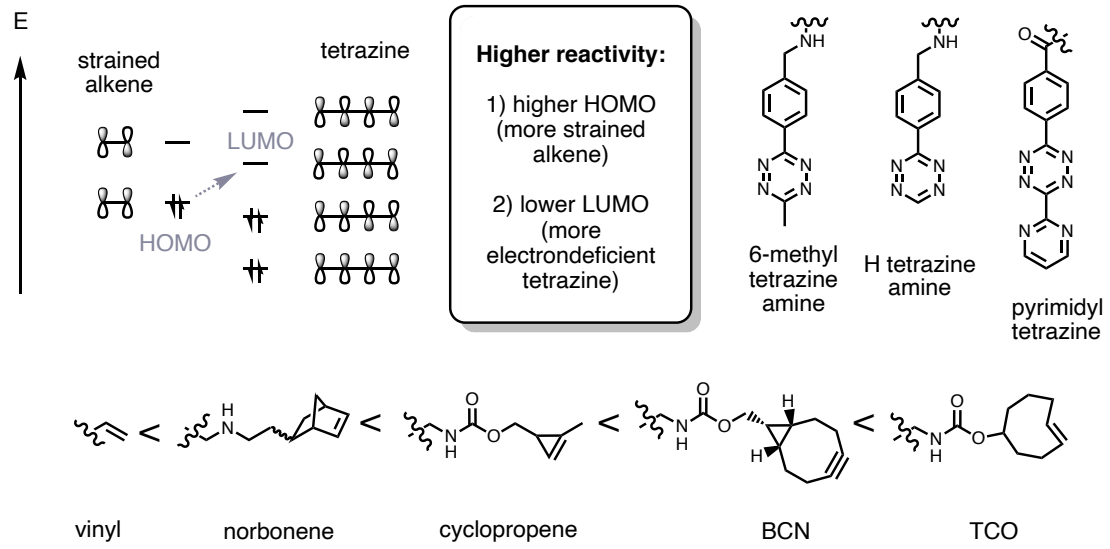

Figure 3.2: Energy diagram with molecular orbitals for an iEDDA and HOMO-LUMO gap. During a reaction, electrons of the HOMO of the dienophile move to the LUMO of the tetrazine. Higher HOMO of the dienophile and lower LUMO of the tetrazine reduce the energy gap and accelerate the reaction. The more strained the dienophiles, the higher their HOMO which results in higher reactivities in the lower panel. Electron-withdrawing substituents on tetrazines such as pyrimidyl groups lead to a lower LUMO and higher reactivity as well.

In principle, it is important to use either fast dienophiles or reactive tetrazines, but ideally both. As discussed in Section 2.2, it is sometimes difficult to use faster-reacting dienophiles, especially in metabolic labeling. One solution to this problem is to use highly reactive tetrazines. This is why the reaction of six tetrazines with vinyl-modified nucleosides was investigated in a comparative study for RNA labeling.[100] Reaction rates were determined between 10×10^{-4}–$10 \times 10^{-2}\,M^{-1}\,s^{-1}$ and guidelines derived for optimized labeling conditions. Similarly, vinyluridine was labeled in mice with a pyrimidyl tetrazine.[101]

Another possibility to boost the reaction kinetics of low reactive groups is to use proximity labeling (Section 3.4).

3.4 Proximity labeling

To improve reaction kinetics and/or selectivity of a bioorthogonal reaction, proximity labeling demonstrated great power in bioconjugation.[102]

Proximity labeling is mainly used for probing protein interactions or ligand-protein interactions.[103], [104], but there are also first applications in nucleic acid chemistry.

One example is the use of an intercalator to overcome the sterical hindrance of reactive groups that were incorporated into DNA. Therein, the Sondheimer diyne derivative DiMoc enabled the reaction between azide modified DNA and BCN, which would not occur otherwise.[54],[55] The improved labeling of the three-component system allowed the authors to efficiently label DNA without the need for an HCl denaturation step. The labeling results of native DNA are comparable to CuAAC reactions. However, no images were shown in living cells.

Also very recently, proximity-based labeling between a dienophile-modified RhoBAST ap-

tamer and its tetramethyl rhodamine methyltetrazine substrate was demonstrated.[105] The authors could specifically label an *in vitro* or *in vivo* transcribed ROI in a mixture of modified RNAs.[105]

When bioorthogonal reactions are used for imaging purposes, besides optimizing the labeling reaction, the fluorescent probes play a major role. The next Chapter 4 will therefore elaborate on the challenges associated with fluorescent probes for imaging.

4 Fluorescence microscopy as a technique to study biological processes

Fluorescence microscopy offers many possibilities to study diverse biological questions and to elucidate structural features in cells. It allows minimally invasive optical access to cellular structures and dynamics at a resolution down to the nanometer range. Combined with the right labeling technique, fluorescence microscopy allows the detection with molecular specificity. This enabled discoveries in various fields of cell biology.[106]

In particular live-cell imaging has proven a useful tool for capturing dynamic processes within living cells. To get access to information about cellular events spatial and temporal resolution are required, which are both restricted by the chosen microscopy as well as labeling technique (Sections 4.1 and 4.2).

4.1 Spatial resolution

Technical limitations

Findings of Ernst Abbe from 1879 clearly marked a physical limitation for the resolution in light microscopy, the so-called “diffraction limit”.[107] The diffraction limit is in rough approximation half of the wavelength. For UV light this means about 200 nm and for visible light 250 nm. Better resolution can be achieved using super-resolved microscopy techniques, such as stimulated emission depletion (STED) nanoscopy.[108], [106] STED uses a doughnut-shaped laser to deplete excited fluorophores to their ground state and provides a fluorophore off-switch. This then minimizes the illuminated area at the focal point and enhances the resolution.

Limitations by labeling

While technically 50 nm resolution can be achieved in STED nanoscopy, the limitation for the resolution is often the quality of the sample, in particular the labeling and not the optical setup. The perfect fluorescent probe is (i) only localized at the target, (ii) very bright and (iii) photostable.[109], [110]

However, in complex cellular environments, fluorescent probes often show off-target effects and unspecific background staining. As such, hydrophobic dyes are prone to accumulate in hydrophobic areas in the cells; positively charged dyes tend to go to mitochondria[111]; probes with weakly basic groups often show signals in lysosomes[112]. To circumvent unwanted background signals, researchers make use of fluorogenic dyes, that show environmentally-dependent fluorescence.[113], [114]

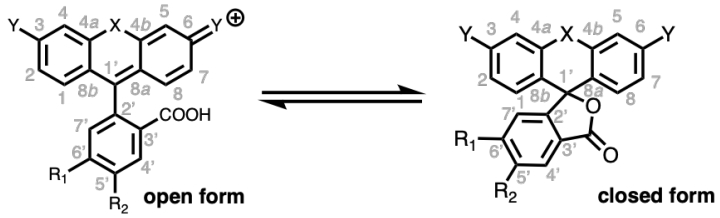

Figure 4.1: The open and closed form of xanthenes and their numbering.

Xanthenes analogs are in fact the most popular class of fluorescent probes for cellular imaging. Often, they exist in a spirolactone or -lactame equilibrium between an open, fluorescent, zwitterionic and a closed, non-fluorescent cell-permeable state (Figure 4.1). When entering the cell, they should be in a fully closed state and only open up when bound to their target. The equilibrium can be tuned by changing the nucleophilicity of the group at the C3'-position[115], [116] or by altering the electrophilicity of the central carbon on the xanthene, which can be varied by decorating the xanthene or the benzyl ring with electron-withdrawing groups[117], [118] or replacing the heteroatom (X)[119]. The sweet spot between open and closed state depends on the target.

To localize the dyes, transient or covalent interactions are used with a targeting moiety, such as a binder (e.g. inhibitor, antibody)[120], [121], [122], or by means of a covalent reaction (e.g. with a functional group or self-labeling protein, e.g. HaloTag, SNAP-tag)[123], [124].

Some probes show additional quenching mechanisms, such as dye-dye quenching through $\pi\pi$-interactions[125], photo-induced electron transfer (PET) quenching[91] or through-bond energy transfer (TBET) quenching[126].

Turn-on probes for bioorthogonal labeling

PET quenching plays a major role in bioorthogonal reactions with a turn-on effect, such as an iEDDA reaction of a tetrazine with a dienophile. Before the reaction, the fluorophore is quenched by the tetrazine. After the formation of the reaction product, fluorescence is released. The angle and point of attachment of the tetrazine to the dye are critical and was studied extensively on different scaffolds[127], positions[128] and using various linkers[129], [130]. Therein, PET quenching is observed for all dyes, TBET quenching is only discussed for dyes that are connected via a π-conjugated system.[126]

Figure 4.2 is providing an overview of several xanthene tetrazines that were synthesized with their reported turn-on values. Especially, blue-shifted dyes are well quenched via PET, as their emission spectrum shows better overlap with the absorption of the tetrazine chromophore compared to more red-shifted dyes. As such, Oregon Green probes show a turn-on up to 400-fold[96], while the highest reported turn-on for silicon rhodamine dyes is a magnitude lower around 45-fold[128].

But, also the protocols for determining the turn-on values vary in different publications (e.g. make use of organic solvents or other additives), which makes it difficult to directly compare these values. Additionally, turn-on values are measured *in vitro* only, reflecting just one important aspect of a probe that is used in cells. Selecting the turn-on as the only criterion would be too one-sided, as e.g. cell-permeability, photostability, mislocalization of dyes or water solubility

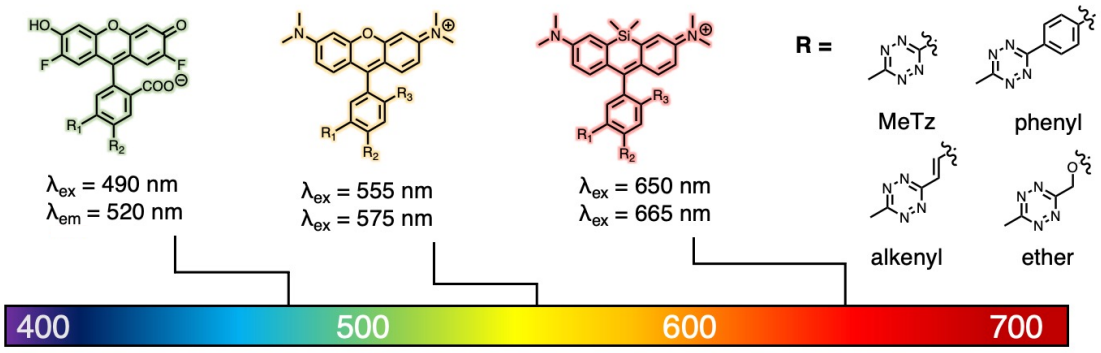

Oregon Green	Turn-on	TMR	Turn-on	SiR	Turn-on
R_1 = alkenyl R_2 = H	400 x	R_1 = alkenyl R_2 = H R_3 = COOH	76 x	R_1 = alkenyl R_2 = H R_3 = COOH	31 x
R_1 = MeTz R_2 = H	103 x	R_1 = MeTz R_2 = H R_3 = H	12 x	R_1 = phenyl R_2 = H R_3 = COOH	22 x
R_1 = H R_2 = MeTz	60 x	R_1 = H R_2 = MeTz R_3 = H	22 x	R_1 = ether R_2 = H R_3 = COOH	45 x (BCN)
		R_1 = H R_2 = ether R_3 = H	123 x (BCN)	R_1 = MeTz R_2 = H R_3 = H	3.7 x
				R_1 = H R_2 = MeTz R_3 = H	1.8 x

Figure 4.2: Chemical structure of tetrazine fluorophores based on xanthene scaffolds in a wide color range and with different linkers. The table summarizes the associated published turn-on values.[91]

are other important factors.

For bioorthogonal reactions, also the turn-over and specificity of the reaction in the cell accounts to good signal-to-noise ratios. As such, not just the choice of a good dye, but also the right bioorthogonal reaction is crucial to get a good spatial resolution. Besides, the bioorthogonal reaction is massively influencing the temporal resolution, which will be discussed in the next section (Section 4.2).

4.2 Temporal resolution

Live-cell microscopy requires a clear understanding of the time scale of the cellular process that is visualized.[10] To study a dynamic process, the chosen methods and tools must be faster than the process that should be resolved. This accounts on the one hand for the chosen microscopy technique and on the other hand for the labeling.

Technical limitations

Super-resolution microscopy is typically two to three magnitudes slower than confocal microscopy.[10] Therefore, the trade between imaging speed and resolution can be reasonable.

In the context of DNA labeling, cellular processes that are interesting to study with fluorescence microscopy are depicted in Figure 4.3. While double-strand break response or chromatin arrangements are for example very fast processes, cell division or DNA replication occur on a slower time scale. The latter processes can be readily combined with super-resolved imaging, but to resolve chromatin rearrangements image acquisition time will become more relevant.[10]

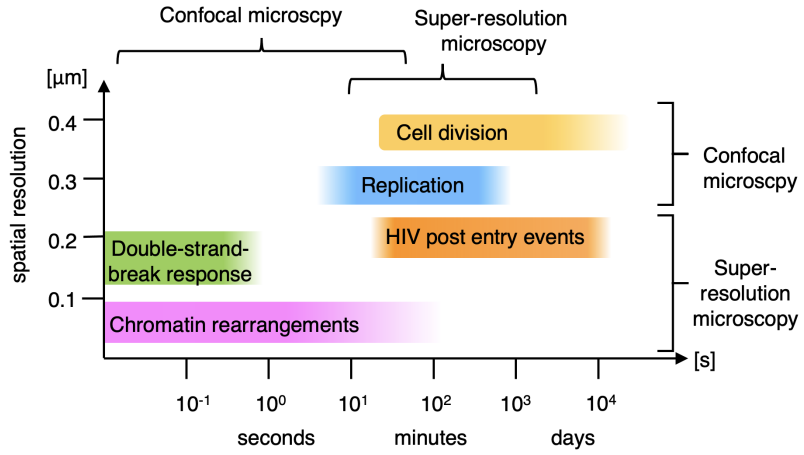

Figure 4.3: Biological processes related to DNA labeling, that can be studied with confocal or super-resolution microscopy. The requirements for spatial and temporal resolution vary with the application.

Limitations by labeling

Generally, the labeling time is a limiting factor for temporal resolution. In particular, metabolic labeling is not a fast labeling technique, as it includes various intermediate steps before visualization: (i) All compounds have to pass the cell membrane, (ii) protecting groups of monophosphates are cleaved eventually, (iii) nucleosides and nucleotide monophosphates are further phosphorylated, (iv) DNA polymerases incorporate the nucleotide triphosphates into DNA. For BrdU these steps (i)-(iv) can occur on a few-minute time scale.[28] But for nucleosides which are worse substrates for endogenous enzymes, the process might be significantly slower.

After incorporation, typically the nucleosides are marked with a fluorophore in a second step. For live-cell imaging, this will take place in the cell and delay the visual output of the process to a time point, when the reaction is completed or is stopped. Often, dyes are incubated for half an hour up to a few hours depending on the labeling kinetics of the bioorthogonal reaction.[131]

4.3 Studying viruses by means of fluorescence microscopy

Understanding the interactions between a virus and its host cell is important in order to find new targets for antiviral therapeutics and can give insights into cellular machinery observing

its defense mechanism. The dynamics of virus related processes can be studied via confocal and super-resolved fluorescence microscopy, or correlative light and electron microscopy (CLEM).[132]

Historically, fluorescence in situ hybridization (FISH) was used to label viral DNA in fluorescence microscopy.[133], [134] This method comes with some drawbacks, such as unspecific signal, incompatibility with other labeling techniques and lack of a quantitative read-out.[135] Therefore, stochastic metabolic incorporation of unnatural nucleotides into viral genomes or replication compartments is an attractive alternative and was applied for a variety of viruses.[132]

4.3.1 Metabolic labeling of viral DNA

Metabolic incorporation of unnatural nucleotides was first demonstrated with the herpes simplex virus 1 (HSV-1) using BrdU[136] and EdU[137], [138]. A few years later, EdU was also used to study post-entry events of human immunodeficiency virus 1 (HIV-1).[139] Furthermore, the vaccinia virus (VACV) was labeled with VdU.[140]

While HSV-1 and VACV are double-stranded DNA viruses and have a fairly large genome size of about 1.5×10^5 bp, the detection of the 10^4 bp reverse-transcribed cDNA of the HIV-1 is more difficult. Therefore, to study HIV in cells, the labeling method needs to be more sensitive compared to viruses with a large genome.

When working with unnatural nucleoside analogs, cytotoxic effects can occur upon prolonged incubation time. As such, metabolic pathways or genotoxic effects are discussed as modes of action for cytotoxicity.[141],[47] Therefore, the nucleoside has to be chosen carefully to retain the infectivity of the virus and to achieve the incorporation of the modified nucleoside. Another challenge when labeling viral DNA is to repress signals from genomic DNA synthesis in the nucleus. One possibility is to inhibit cellular DNA polymerases with inhibitors during infection, another is the use of reverse transcriptase-specific nucleosides (Subsection 2.2.5).

4.3.2 Protein-based labeling of viral DNA

So far, all presented approaches to label viral DNA are limited to fixed cells, as they use oligonucleotide strands, antibody staining, CuAAC or a slow iEDDA reaction. To label viral DNA in living cells, the protein-based ANCHOR labeling system was employed very recently.[142], [143]

The ANCHOR/ParB technology can detect single genes. ANCHOR is a DNA-labeling tool derived from the bacterial ParB-parS chromosomal partitioning system and uses multiple artificially introduced targeting parS seed sequences (ANCH). ANCH recruits the ParB protein (OR) that is then oligomerized at the target sequence. GFP-tagging allows the detection of the accumulated protein.[144, 145]

As such, the ANCHOR system enabled imaging of reversely transcribed HIV-1 cDNA in the nucleus and visualization of the processes of capsid uncoating during HIV-1 infection.[142] In combination with additional results[146], the authors could support the hypothesis of nuclear import of the capsid, which was previously controversially discussed.

4.3.3 State of knowledge HIV post entry events

HIV-1 post-entry events, including the latest results, are summarized in Figure 4.4. During the viral life cycle, the HIV particle releases the capsid core after fusion with the host cell membrane. Reverse transcription commences inside the capsid shortly after its fusion and the viral DNA is integrated into the host's genome after capsid uncoating in the nucleus.[147],[148]

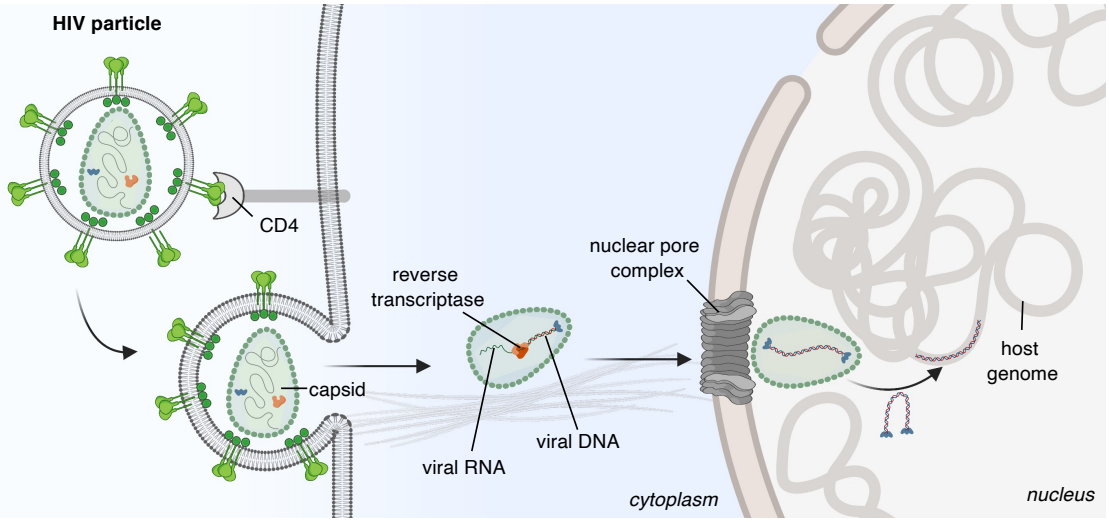

Figure 4.4: HIV particle infecting a human T-cell. In the process, the particle is fusing with the cell membrane upon CD4 receptor binding, releasing the capsid core, where viral RNA is reverse-transcribed into viral cDNA catalyzed by the reverse transcriptase. The capsid containing cDNA is then imported into the nucleus via the nuclear pore complex and the viral cDNA is then ultimately incorporated into the host genome.

Interesting questions that cannot be answered to-date are the precise onset and finalization of viral cDNA synthesis and its progression on the way into the nucleus as well as the exact post-entry dynamics. These questions are difficult to tackle with the ANCHOR system, as the system has two drawbacks: (i) proteins might not label viral cDNA shielded by the capsid or host cell proteins, (ii) non-quantitative readout for *de novo* synthesized viral DNA.

Therefore, we were interested in a tool, that would overcome these challenges to ultimately study the questions that remain unsolved during post-entry events of HIV-1. The tool should be (i) compatible with live-cell imaging, (ii) label viral DNA inside the capsid, and (iii) provide quantitative information about the amount of DNA present. We came up with different suggestions for tools to answer one of these questions (Section 5).

5 Scope of this thesis

I aimed at improving current metabolic DNA labeling strategies with the ultimate goal to label HIV-1 cDNA.

Specifically, I aimed at establishing a metabolic labeling system that is compatible with live-cell imaging and would help to track HIV-1 cDNA in a cell. Such a system would have to fulfill certain requirements (i) show fast reaction kinetics, (ii) would not require a copper catalyst or a DNA denaturation step.

Based on previously reported metabolic labeling strategies, initially, a split system was envisioned. Therein, I wanted to introduce a reactive group into DNA through the incorporation of a modified nucleoside and later click-labeling with a bioorthogonal reaction. To improve current labeling, two different strategies were attempted: (i) developing a probe for proximity labeling based on a known nucleoside analog, and (ii) using nucleosides with a more reactive group that can be used in living cells.

When the projects evolved, I additionally decided to use a one-component system of a fluorescent nucleoside with improved temporal resolution. Also, the fluorescent nucleoside was further developed as pro-nucleotide.

As a side project, an alternative approach to specifically activate a DNA stain in a cell was pursued.

Part II

Results and Discussion

1 Photocaged-Hoechst (pcHoechst)

Photo-activation allows spatio-temporal control over a synthetic molecule and is one possibility to target specific localizations in a sample. The beauty of light is being an orthogonal and rapid trigger. To harness these advantages, a DNA stain was photocaged. In the past, nucleic acid stains have been modified for activation with light for *in vitro*[149] and *in cellulo*[150] applications. None of them allows to visualize a subset of DNA in a living cell in a highly spatio-temporal manner.

As such, styrylbenzothiazole derivatives require photo-activation at 220 nm and are not compatible with cellular imaging.[149] Thiazole orange modified diarylethenes show poor cell-permeability and slow photochromism resulting in long irradiation times of the cells with UV light, limiting the approach to fixed cells.[150]

To overcome these limitations, Hoechst33342 was caged with an *ortho*-nitro benzyl group. Hoechst33342 exhibits a high affinity to DNA and good cell permeability (Theory 2.1).[16],[17],[18] The *ortho*-nitro benzyl group can be removed by activation with blue light with unmatched spatio-temporal precision and relatively low toxicity.[151], [152] Upon removal of the protecting group fluorescence signal of the dye can be observed (Figure 1.1). As such, the caged DNA stain can be activated with light in a defined region of a cell.

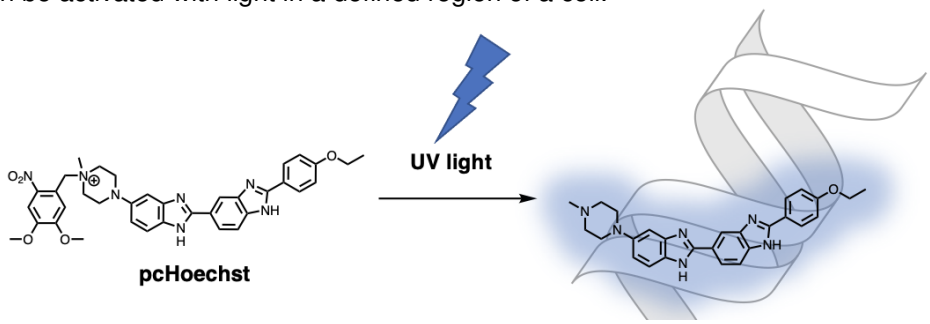

Figure 1.1: PcHoechst is non-fluorescent when caged with an *ortho*-nitro benzyl group, even in the presence of DNA. The protecting group can be then removed with UV light. After uncaging, the fluorescence signal in the presence of DNA is restored.

1.1 Synthesis and *in vitro* experiments

To cage Hoechst33342, the 4-*N*-methyl piperazino group was selectively alkylated with *O*-nitrobenzyl bromide **2** (Figure 1.1, Methods 2.2). Therefore, Hoechst33342 × HCl was free based with K_2CO_3 in an aqueous solution and yielded compound **1**. *O*-nitrobenzyl bromide **2** was synthesized from (4,5-dimethoxy-2-nitrophenyl)methanol in an Apple reaction. Free-based Hoechst33342 **1** was alkylated by adding compound **2**, base, and heating the reaction to 60 °C overnight to obtain pcHoechst **3** as a quaternary ammonium salt. Among the recovered starting

material, minor formation of bis-alkylated Hoechst33342 was observed. Structure analysis by 2D-NMR spectroscopy confirmed the regioselectivity.

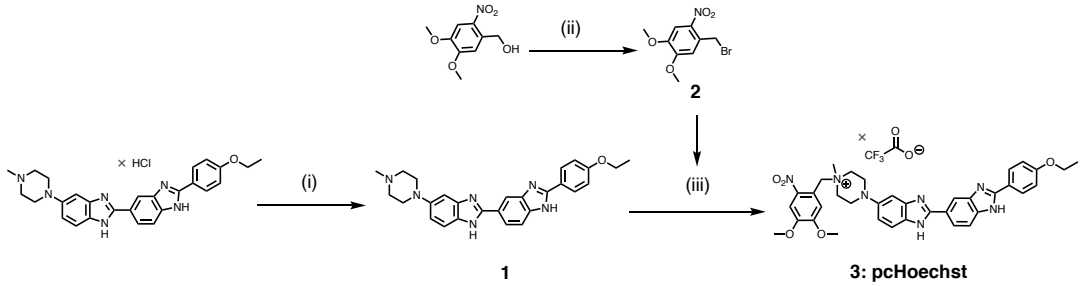

Scheme 1.1: Synthesis scheme pcHoechst: (i) K_2CO_3, H_2O, r. t., 10 min, quant., (ii) CBr_4, PPh_3, r. t., 16 h , 71%; (iii) DMF, K_2CO_3, 60 °C, o. n., 39%.

For *in vitro* characterization, UV/Vis spectra of the two starting materials Hoechst33342, compound **2**, and pcHoechst **3** were recorded (Figure 1.2, A). The absorption maximum in the UV/Vis spectrum of pcHoechst **3** differed slightly from the theoretical overlay of the spectrum from Hoechst33342 and compound **2**.

Fluorescence emission spectra were recorded in the presence of high DNA concentrations (1 mM hpDNA) and similar emission spectra were observed for both, Hoechst33342 and pcHoechst **3**. While showing the same emission spectrum, the fluorescence intensity of pcHoechst **3** was about 6-fold lower compared to Hoechst33342 at the same concentration (Figure 1.2, C). As cellular DNA concentrations are in the milli-molar range, only a weak fluorescent background signal in the cell is expected.

Titration with hairpin DNA (hpDNA, 5'-CGCGAATTCGCGTTTTCGCGAATTCGCG-3', see Figure 1.2, D, Methods 4.2.1) against pcHoechst **3** (blue) confirmed no significant turn-on in fluorescence compared to Hoechst33342, which showed an EC_{50} = 44.6 nM.

Furthermore, the increase in fluorescence quantum yield with 100 µM hpDNA, was measured as 51-fold for Hoechst33342 while only 1.6-fold for pcHoechst **3** (Table 1.1). Additionally, quantum yields were measured at low pH (pH=4) as later microscopy experiments showed a fluorescent signal in lysosomes. Therein, Hoechst33342 showed an increase in quantum yield at low pH.

Taking these results together, this showed that pcHoechst **3** is non-fluorescent or exhibits very weak fluorescence even in the presence of DNA. Possible explanations are either (i) no affinity of pcHoechst **3** for DNA, or (ii) a non-fluorescent binding mode of pcHoechst **3**.

Next, the possibility to uncage pcHoechst **3** with a strong UV lamp was tested by illuminating a solution with strong white light. Reconstruction of Hoechst33342 was subsequently verified by LC-MS analysis (Figure 1.2, E and F).[1] However, uncaging of pcHoechst **3** was not quantitative *in vitro* and further oxidation products were observed in mass spectrometry upon prolonged light exposure.

Taken together, photocaging Hoechst33342 led to an almost non-fluorescent compound pcHoechst **3**, even in the presence of hpDNA. Illumination of a solution of pcHoechst **3** then allowed to restore Hoechst33342.

[1] Presented traces were recorded by Dr. Johannes Broichhhagen, FMP Berlin.

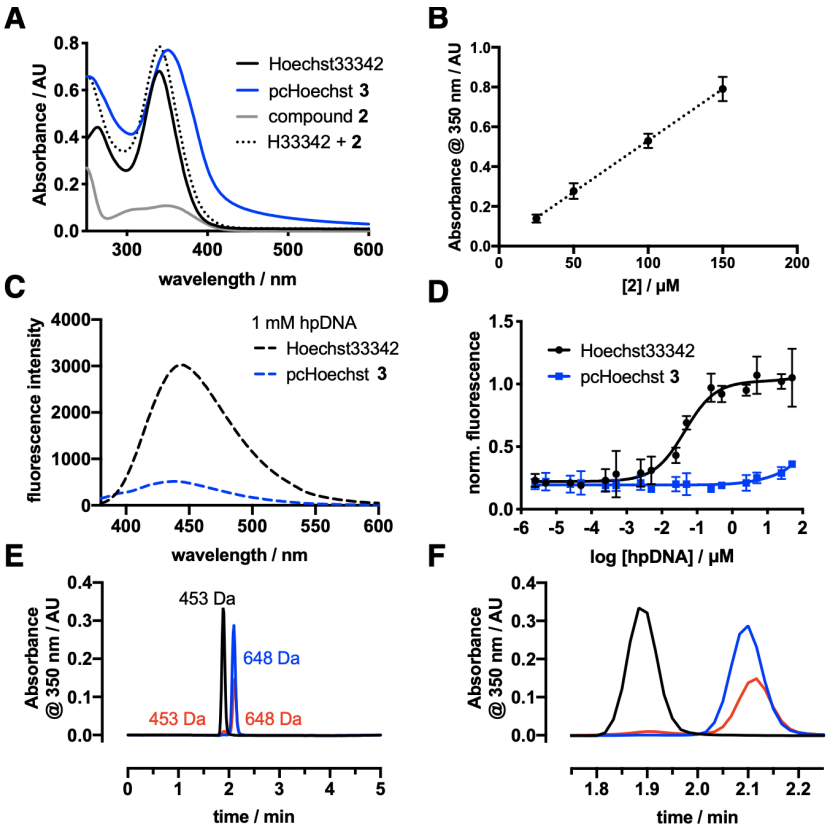

Figure 1.2: (A) UV/Vis spectra of Hoechst33342 (black), pcHoechst **3** (blue) and compound **2** (grey) recorded in PBS at 20 µM concentration. Mathematical addition of Hoechst33342 and compound **2** (dashed line). (B) Determination of the extinction coefficient of compound **2**. (C) Titration curve for 100 nM Hoechst33342 (black), and 100 nM pcHoechst **3** (blue) against hairpin DNA. (D) Fluorescence emission spectra of Hoechst33342 (black) and pcHoechst **3** (blue) in the presence of high DNA concentration (1 mM hpDNA). (E) HPLC trace of Hoechst33342 (black, 453 Da), pcHoechst **3** (blue, 648 Da) and pcHoechst **3** after uncaging for 5 min in solution with strong white light (red, both peaks). (F) Detailed view from (E).

Table 1.1: Quantum yields in % for Hoechst33342 and pcHoechst **3** in the absence and presence of 100 µM hpDNA and at low pH from N=3 measurements.

	in PBS	in 100 µM hpDNA in PBS	in citric acid buffer pH 4
Hoechst33342	1.13 ± 0.17	57.53 ± 1.68	24.53 ± 1.31
pcHoechst **3**	0.60 ± 0.14	0.97 ± 0.12	1.07 ± 00.17

1.2 Global and spatially defined uncaging in living cells

After confirming that an *o*-nitrobenzyl group efficiently silences fluorescence of Hoechst33342 in presence of DNA, uncaging of pcHoechst **3** was investigated in Hela cells (Methods 5.6.1). To study the background fluorescence of pcHoechst **3** in the nucleus, Hela cells were incubated with pcHoechst **3** in the dark and an image of the background was acquired (Figure 1.3). To my delight, the observed fluorescence signal was extremely weak as already observed in *in vitro* experiments. PcHoechst exhibits (i) poor DNA affinity or absence of fluorescence when bound to DNA in cells, and (ii) minor unspecific uncaging by ambient light.

Next, studies on the effect of pcHoechst **3** on cell division and toxicity in comparison to Hoechst33342 were performed. Therefore, dividing cells were observed and counted for 24 h in a widefield microscope with 0.1 µM and 10 µM Hoechst33342 or 10 µM pcHoechst **3** (Method 5.5).[2] While 74/97 (76%) cells divided in the control group, upon the addition of Hoechst33342 only 61/152 (40%) at 0.1 µM or 2/227 (1%) at 10 µM divided. Upon addition of pcHoechst at 10 µM, cell division was comparable to the control group with 128/152 cells (84%). As such, pcHoechst **3** exhibited significantly lower toxicity compared to Hoechst33342. For this reason, the caged compound might be a worse binder.

Before uncaging pcHoechst **3** in cells, the power of the UV laser was measured and the laser intensity per surface area on the sample was calculated (SI-Table 5.1). To liberate Hoechst33342, the cells in a field of view were irradiated with UV light under the microscope and the turn-on of the probe was observed by image acquisition in a short time series over several minutes (Figure 1.3, A, Method 5.6.1). An immediate increase in fluorescence was ob-

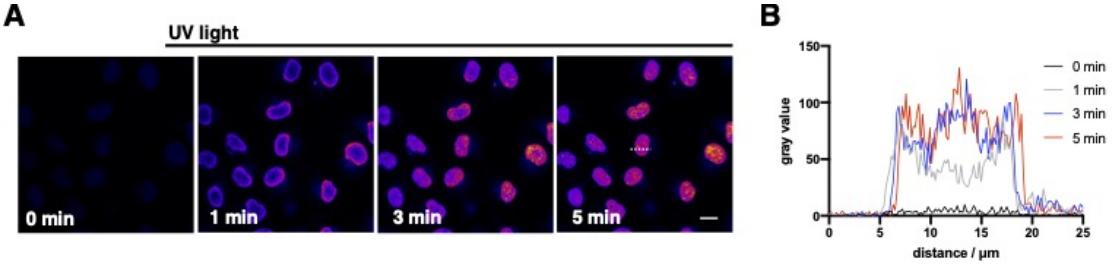

Figure 1.3: Representative confocal images of global uncaging of 10 µM pcHoechst **3** in live Hela cells from N=5 replicates at different laser intensities. Cells were incubated with 10 µM pcHoechst and incubated for 1–2 h in the dark before the first image was acquired. UV light was shone on the whole field of view between each frame and fluorescence signal intensity was subsequently recorded in the next image. Scale bar = 20 µm. B) Line profile a cell showing fluorescence increase over time.

served that reached a plateau after 5 min. The line profile for one cell was plotted and showed a 20-fold turn-on in fluorescence after 5 min (Figure 1.3, B, Method 5.6.1).

The staining in the nucleus was comparable to other Hoechst derivatives and preferentially showed condensed heterochromatic regions. In the beginning of the time series, mainly the signal at the outer regions of the nucleus was observed, while the signal was later propagated to the center of the nucleus. This could be explained by enriched heterochromatin at the nuclear lamina.[153], [154] A minor signal was observed in spots outside the nucleus which were assigned to the lysosomal system. This was later verified by co-localization experiments with mCLING and LysoTracker (SI-Figures 4.1 and 4.2).

To establish spatially controlled activation of pcHoechst **3**, the bleachpoint function of a confocal microscope was employed to target single cells and a subnuclear region in a fluorescence recovery after photobleaching (FRAP) experiment (Figure 1.4). Therefore, live HeLa cells were incubated with pcHoechst prior to imaging. First, UV illumination was applied locally to observe fluorescence signal in a single cell immediately afterward (Figure 1.4, A).

In the next step, the laser intensity was decreased in the setup, which allowed staining of

[2] Toxicity experiments were performed by Jenny Eichhorst and Dr. Martin Lehmann, FMP Berlin.

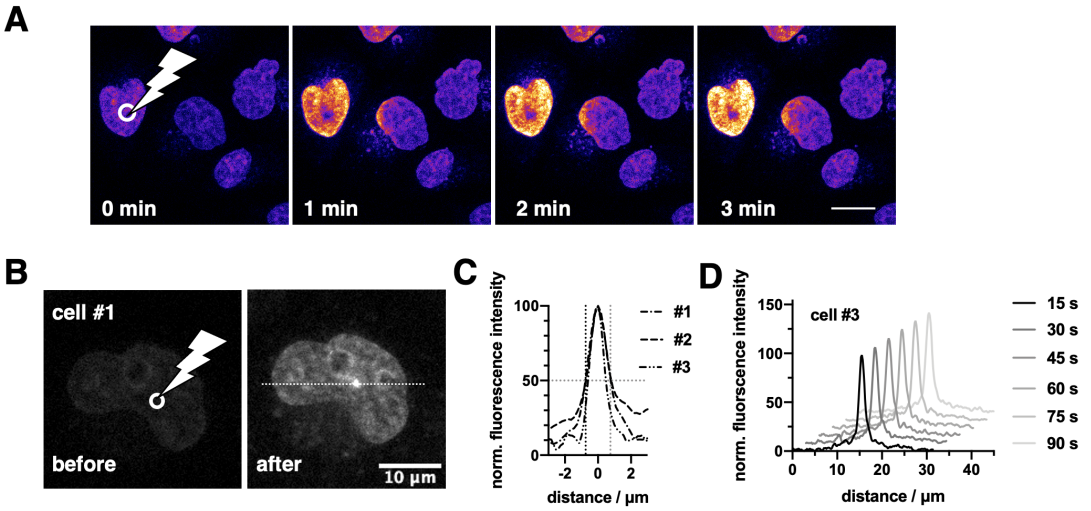

Figure 1.4: Representative confocal images of spatially controlled uncaging of 10 µM pcHoechst in live Hela cells with a UV light bleachpoint that was applied in the indicated area. Images were acquired with λ_{ex} = 355 nm, λ_{em} = 420–500 nm. UV light was shone in (A) at high laser intensity (λ_{uncage} = 355 nm, 110–1100 µW for 10–15 s) and in (B) at low laser intensity (λ_{uncage} = 355 nm, 1.42 µW for 10–15 s). In (C) and (D) the diameter of three uncaged spots, as well as a time course of the bleachpoint is shown. Experiments were performed on two independent days with different laser intensities for N >5 cells.

DNA in a more defined region with a diameter of about 1.4–1.7 µm (Figure 1.4, B and C). Subsequently, the corresponding signal was tracked over 90 s without observing significant signal broadening and allowing short-term observation of dynamics in a subnuclear fraction of DNA (Figure 1.4, D).

A dark spot appeared after excitation with high laser power (>100 kW cm^{-2}) in the illuminated region. The spot was attributed to bleaching, which was therefore investigated. Therein, Hoechst33342 was bleached in fixed cells (Figure 1.5). A reduction in the fluorescence signal was observed for medium and high laser intensities (Figure 1.5, A), while the nuclear staining with Hoechst33342 was not affected at low laser intensities. To visualize the decreased fluorescence intensity, line profiles were determined for selected cells, which showed a 3-fold and 4-fold decrease for medium and high laser intensities, respectively (Figure 1.5, B). In addition, higher laser intensities target larger areas as the signal is broadened. This was demonstrated using a cover slide that was coated with a fluorescence layer and spots on the surface of the cover slides were bleached (Figure 1.5, D).

As strong UV light can induce DNA double-strand breaks and harm the cells, the toxicity of the UV light on dividing cells was investigated (Method 5.5). Therefore, toxicity studies with dividing cells were repeated while shining UV light for 4 and 10 s this time. While in the control group 74/97 (76%) cells divided, after 4 s of UV irradiation only 104/265 (39%) and after 10 s of UV light, only 33/256 (13%) could undergo cell division. This showed the negative impact of UV light on cells due to its phototoxicity.

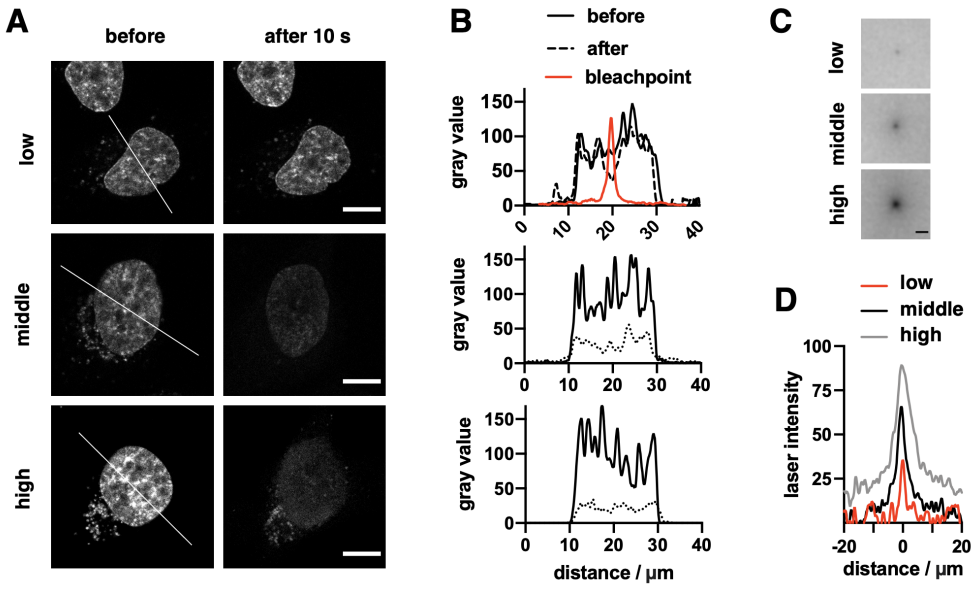

Figure 1.5: (A) Confocal images of fixed Hela cells that were incubated with Hoechst33342 and irradiated with high (1.2 MW cm^{-2}), medium (126 kW cm^{-2}), and low (1.6 W cm^{-2}) laser intensities. Scale bar = 10 µm. (B) The line profile of each cell before and after uncaging. (C) The line profile of the bleachpoint was determined on a fluorescent cover slide by bleaching the fluorescent layer and plotting the profiles in (D).

1.3 Uncaging *in vivo* in zebrafish

After successful uncaging of pcHoechst **3** in Hela cells, labeling experiments were performed in epithelial cells of living zebrafish to expand the tool to a vertebrate model organism.[3]

Before uncaging, we wanted to show that the zebrafish can tolerate pcHoechst **3**. Therefore, the dye was added to the fish tank, the viability of the zebrafish after incubation for 24 h examined and compared to Hoechst33342 (Methods 6.2). Whereas 100 µM Hoechst33342 was lethal for zebrafish, 100 µM pcHoechst **3** did not affect zebrafish development, which allowed us to move forward with uncaging pcHoechst **3** in zebrafish (Methods 6.3).

The first uncaging experiments were performed with 100 µM pcHoechst **3** and UV-LEDs at 395 nm. While zebrafish that were kept in the dark did not show nuclear staining, the uncaged compound nicely labeled the zebrafish nuclei (Figure 1.6, A).

Next, mRFP-tagged histone protein H2B (H2B-mRFP) expressing zebrafish embryos were dechorionated and incubated with 100 µM pcHoechst **3** at 32 h post-fertilization (hpf). At 52 hpf, pcHoechst **3** was activated with UV illumination at 405 nm under a confocal microscope targeting a cluster of cells. Similar to cell experiments, a bleachpoint function could be used to illuminate a small region with UV light. Only cells in that region showed a nuclear signal. The signal was then tracked for 1.5 h in time-lapse recording and was still observable 10 h post illumination (Figure 1.6, B).

[3] Images by Adam Varady, St. Anna Children's Cancer Research Institute Innovative Cancer Models, Vienna, Austria.

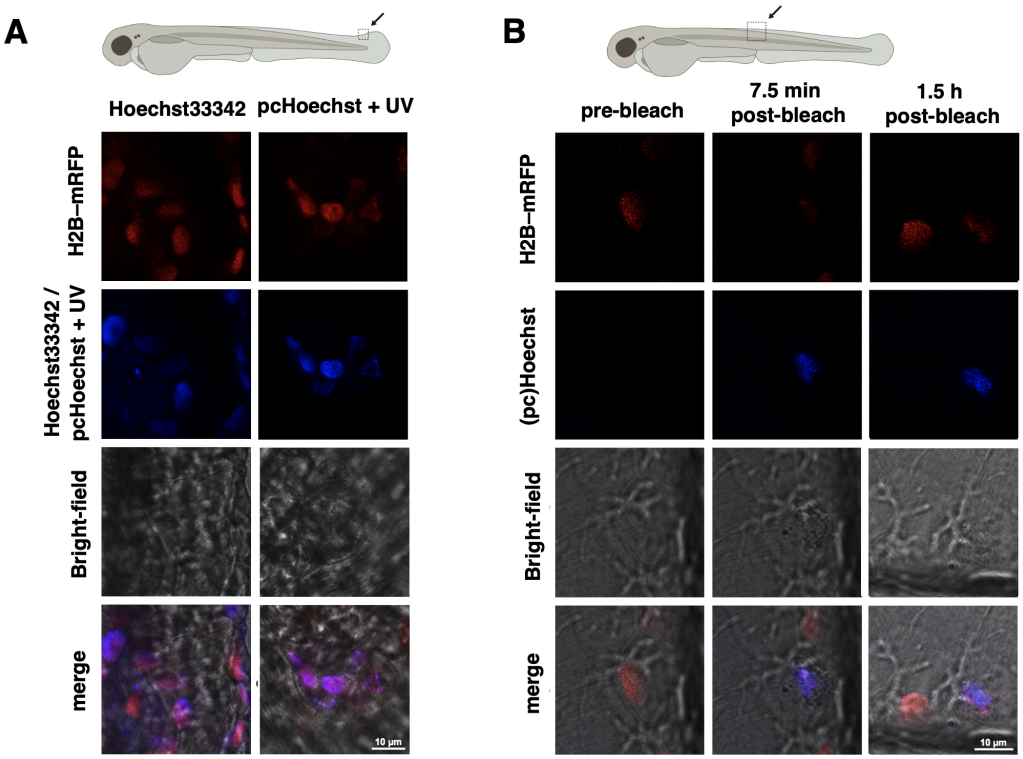

Figure 1.6: *In vivo* confocal imaging of cell nuclei in zebrafish with pcHoechst **3**. A) Agarose-embedded H2B-mRFP-expressing zebrafish embryos incubated with Hoechst33342 (10 µM, left), pcHoechst **3** (100 µM, right) overnight at 32 hpf. Uncaging with 405 nm UV laser targeted at a large cluster of cells at the zebrafish tail fin at 52–54 hpf. H2B-mRFP (=red) visualizes nuclei that co-localize with the Hoechst and pcHoechst **3** singal (=blue). Scale bar = 10 µm. B) *In vivo* uncaging of pcHoechst **3** with optimized light intensity at single-cell resolution. H2B-mRFP (red) injected zebrafish embryos were incubated with 100 µM pcHoechst **3** in the dark overnight and activated using a 405 nm UV-laser at 0.07 mW at 74 hpf. A pre-bleach confocal image, showing fluorescence background, was recorded prior to bleachpoint illumination. Post-bleach confocal images were taken 7.5 min and 1.5 h after bleaching and show signal of Hoechst (blue) that is stable for at least 1.5 h post-bleach. Scale bar = 10 µm.

1.4 Summary

In summary, pcHoechst **3** was demonstrated as a tool to activate a DNA stain under spatio-temporal control in living cells and to be a versatile method for imaging in zebrafish. In living cells, the tool allows a specific region in the nucleus to be activated and then observed over time. In zebrafish larval tissue, clusters of cells could be activated.

pcHoechst **3** promises to be able to contribute to study tumorigenesis, cell proliferation, development, and viral infections, in native tissue and wild-type animals.

To reduce phototoxicity and enable imaging in deeper tissue or for longer time periods in cells, a more red-shifted caging group such as a coumarin instead of the *ortho*-nitro benzyl group could be implemented in the future.

2 Proximity-enhanced DNA labeling

Metabolic labeling employing unnatural nucleosides was proven a powerful method for specific labeling of newly synthesized DNA (Theory 2.2.1). In recent years, new metabolic precursors were discovered for subsequent bioorthogonal reactions. Among those, VdU was the first nucleoside analog that could be labeled with an iEDDA reaction.[48] However, the reactivity of VdU is low and therefore the labeling is not compatible with live-cell imaging.

On the other hand, bioconjugation of reactive groups of low reactivity was achieved in the past through proximity labeling, which allows the enhancement of a reaction by increasing the local concentrations of the reaction partners (Theory 3.4).

Recently, Luedtke et al. published a three-component “double click” strategy, in which a DNA intercalator was used to efficiently label a previously incorporated azide-modified nucleoside.[55] While previous labeling strategies required denaturation with a strong acid or Cu(I) treatment, the authors could label native DNA for the first time. This is a milestone on the way to labeling in living cells and shows that proximity can be used to accelerate reactions on DNA. The next step now is to develop a tool to label DNA in living cells.

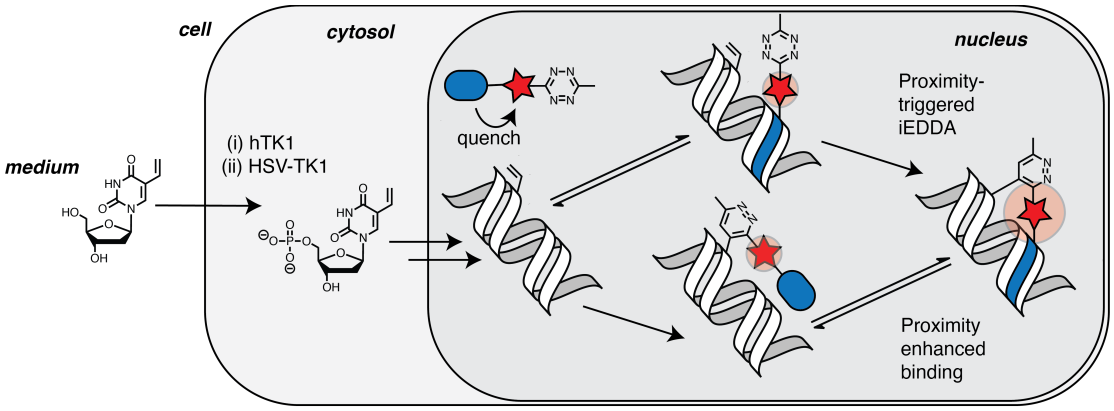

Figure 2.1: VdU is supplemented to cells and inside the cytosol phosphorylated by the hTK1 or HSV-TK1. After further phosphorylation steps, the nucleotide is then incorporated into DNA where it can be click labeled with the tetrazine probe. The SiR (red) based tetrazine probe is equipped with a DNA binding ligand (blue) and shows two modes of action: (i) transient binding to DNA and (ii) reaction with vinyl-modified DNA. When reacted and bound, the maximum fluorescence is released.

In this project, VdU was incorporated into DNA and subsequently labeled with a bifunctional probe. This fluorescent probe consists of the DNA targeting ligand Hoechst33258, silicon rhodamine (SiR), and a methyl tetrazine (MeTz) (Figure 2.1). The probe should non-covalently bind vinyl-modified DNA and react through proximity-enhancement in living cells to form a covalent bond. Before reaction, the probe is quenched from the Hoechst-ligand. Upon DNA binding, fluorescence is released and results in a bright fluorescence signal after localization to DNA.

2.1 Design of the probe and *in silico* docking

For proximity-enhanced DNA labeling, a bifunctional probe was envisioned with a probe design was based on 6-Hoechst-SiR.[21] For the reaction with vinyl-modified DNA, the probe was equipped with an additional tetrazine. In order to maintain the integrity of 6-Hoechst-SiR the best synthetically accessible point of attachment for the tetrazine was the aniline of silicon rhodamine (SiR) scaffold. The only variable part was the linker between SiR and the tetrazine.

To get a starting point for the rational design of the linker lengths, the crystal structure of the B-DNA double helix with a bound Hoechst33342 ligand (PDB: 8BNA) was used. In a double-stranded B-DNA helix, the C5-methyl group of thymidine and likewise the vinyl group of VdU were reaching in the major groove (Figure 2.2, B). Hoechst33342 is binding in the minor groove in the AATT-rich region of the oligonucleotide.

Consequently, to bring the tetrazine of the probe near the vinyl group, the distance from the minor to the major groove must be bridged by the bifunctional probe. In the consideration of finding minimal linker length, glide docking was performed, starting with a C4-linker (H-SiR-MeTz, Methods 1).

A

Binding mode	Glide score	ΔG_{bind} / kcal mol^{-1}
minor	-8.726	-119.08
minor	-6.744	-118.76
minor	-14.818	-109.76
minor	-10.202	-107.64
minor to major	-4.920	-98.66
minor	-7.474	-87.03
minor	-3.811	-81.14
minor	-0.713	-79.56
minor	-3.094	-78.22

B

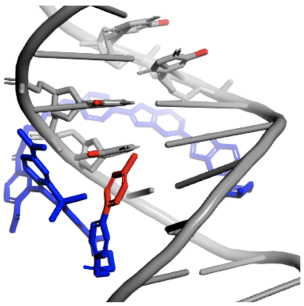

Figure 2.2: A) Glide scores and free binding enthalpies ΔG_{bind} of the conformers obtained from Glide docking. One conformer showed a binding mode from the minor to the major groove. B) Docking result of the H-SiR-MeTz (blue) bound to double-stranded DNA (grey) and reaching from the minor to major groove as a cartoon. In red highlighted is the tetrazine of the bifunctional probe and the methyl groups of thymidine. For a bioorthogonal reaction, both have to come close.

The energetic minimum was obtained for nine conformers that were all binding in the minor groove with free binding enthalpies below $\Delta G_{bind} = -75\,\text{kcal}\,\text{M}^{-1}$ (Figure 2.2, A). Additionally, the Glide score for the obtained structures was calculated, which is a measure for the likelihood of a configuration.

Among the configurations, one docking result (Glide score: -4.920, $-98.66\,\text{kcal}\,\text{M}^{-1}$) showed a scenario, in which the tetrazine could react with a modification at the C5-vinyl group of VdU (Figure 2.2, B). As the sequence of the oligonucleotide used for the calculations is the same as in the hairpin DNA for *in vitro* experiments, the reaction should occur in the *in vitro* model system. In genomic DNA reactions between two separate DNA strands could occur, due to supercoiling and dense packaging of DNA in heterochromatin regions.

To see, if longer linkers (PEG1 and PEG4) affect the labeling in cells, the probe was synthesized with three linkers (C4, PEG1 and PEG4) between the tetrazine and SiR aniline. The distance between the two reactive groups changes the local concentration of the reactants and can impact the reaction rate.

2.2 Synthesis of fluorescent bifunctional probes

For *in vitro* experiments, VdU was synthesized in two synthetic routes (Scheme 2.1, Methods 2.3). On the one hand, the product was synthesized with a Stille cross-coupling proposed by Luedkte.[48] Besides a Suzuki cross-coupling with a vinyl boronic acid was performed. Since the stannates used in Stille cross-couplings are highly toxic, the Suzuki reaction is preferred, even though the yield is slightly lower (63% versus 87%). The product was fully characterized by HRMS and NMR spectroscopy (SI-Chapter 1).

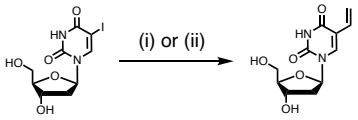

4: VdU

Scheme 2.1: Synthesis scheme VdU: (i) vinylboronic acid, $Pd(PPh_3)_2Cl_2$, *n*-Bu_3N, DMF, 80 °C, 12 h, 87% or (ii) tributyl(vinyl)tin, $Pd(PPh_3)_2Cl_2$, THF, reflux 8 h, 63%.

The bifunctional probe **7** was synthesized from commercial or custom synthesized building blocks (Scheme 2.2, Methods 2.3).

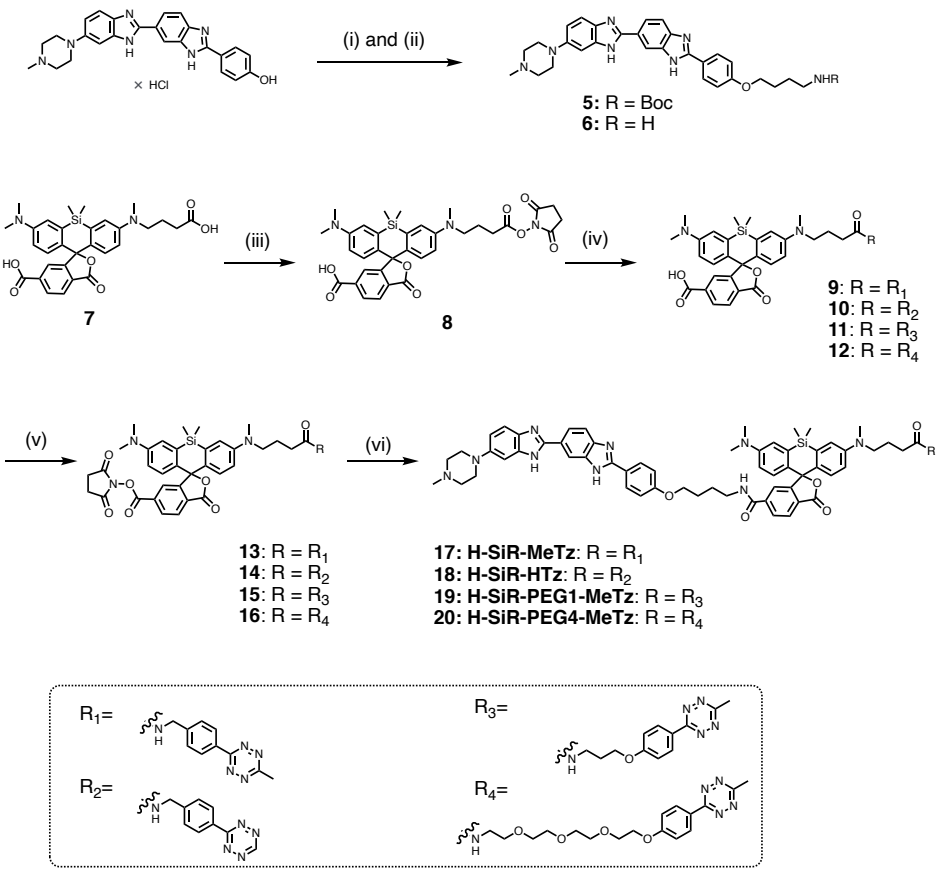

Scheme 2.2: Synthesis scheme H-SiR-Tz probes: (i) 1) K_2CO_3, H_2O, quant; 2) Br-C4-NHBoc, (ii) TFA, 0 °C, 30 min, quant. (iii) TSTU, DIPEA, DMF, r. t., 1 h, 73%, (iv) Tz-amine, DIEPA, DMF, r. t., 1 h, 50-70%, (v) TSTU, DIPEA, DMF, r. t., 1–2 h, 50-70%, (vi) compound **6**, DIEPA, DMF, r. t., 2–4 h, 30-60%.

The synthesis started with deprotonation of the phenolic alcohol of Hoechst33258 hydrochloric salt, and coupling with 4-(boc-amino)butyl bromide to obtain compound **5**. Compound **5** was then deprotected with trifluoroacetic acid (TFA) on ice to give amine **6**. Alongside, the custom synthesized asymmetric SiR precursor **7** was activated with TSTU at the aniline. TSTU was added sub-stoichiometrically to selectively target the more reactive aliphatic carboxylic acid. To avoid difficulties for purification in later steps, the activated precursor **8** was isolated from the non-reacted starting material.

By adding various commercially available tetrazine amines under basic conditions, compounds **9**-**12** were obtained. Similar to step (iii), in step (v) the other C6'-carboxylic function is activated giving rise to compounds **13**-**16**. Compounds **13**-**16** can then react with amine **6** to give the final products **17**-**20**.

The product formation was confirmed with HRMS and purity was assessed with RP-HPLC (SI-Figure 2.1). 1H and 13C-NMR were recorded for all intermediates and H-SiR-MeTz (SI-Chapter 1). The NMR assignments were supported from 2D-NMR spectra when signals were overlapping.

2.3 *In vitro* characterization

2.3.1 Photo-physical characterization and *in vitro* reaction

UV/Vis (Figure 2.3, A) and emission spectra (Figure 2.3, B) were recorded and quantum yields determined (Methods 4).

The global absorption maximum was 652 nm and the local absorption maximum was at 420 nm. For the Hoechst-conjugates, there is an additional local absorption maximum at 350 nm. Emission spectra showed an emission maximum for SiR-HTz, SiR-PEG1-MeTz, and SiR-PEG4-MeTz was at 670 nm, for SiR-MeTz at 668 nm. Hoechst-conjugates had a red-shifted emission maximum at 677 nm.

Quantum yields indicated no quenching of SiR by the tetrazine, since the SiR tetrazines **9**-**12** had similar quantum yields as SiR-COOH **7** (Table 2.1). For the Hoechst-conjugated probes (H-SiR-MeTz, H-SiR-HTz, H-SiR-PEG1-MeTz, and H-SiR-PEG4-MeTz, **17**-**20**) the quantum yield was comparable to 6-Hoechst-SiR (H-SiR) and slightly higher compared to the SiR tetrazines **9**-**12**. Quantum yields were comparable to reported values for similar probes.[125]

Table 2.1: Quantum yields of fluorescent probes measured in 0.1% SDS in PBS exciting at λ_{ex} = 650 nm from N=6 measurements on two different days.

	0.1% SDS in PBS		0.1% SDS in PBS
SiR-COOH	42.5 ± 0.163	H-SiR	52.3 ± 0.135
SiR-MeTz	35.8 ± 0.118	H-SiR-MeTz	51.5 ± 0.147
SiR-HTz	41.3 ± 0.127	H-SiR-HTz	51.9 ± 0.117
SiR-PEG1-MeTz	35.7 ± 0.791	H-SiR-PEG1-MeTz	41.5 ± 0.174
SiR-PEG4-MeTz	37.8 ± 0.079	H-SiR-PEG4-MeTz	45.3 ± 0.076

Before studying the iEDDA reaction of H-SiR-MeTz with vinyl-modified DNA in cells, the reactivity of VdU and H-SiR-MeTz was confirmed in solution (Methods 4.3). Therefore, 1 mM

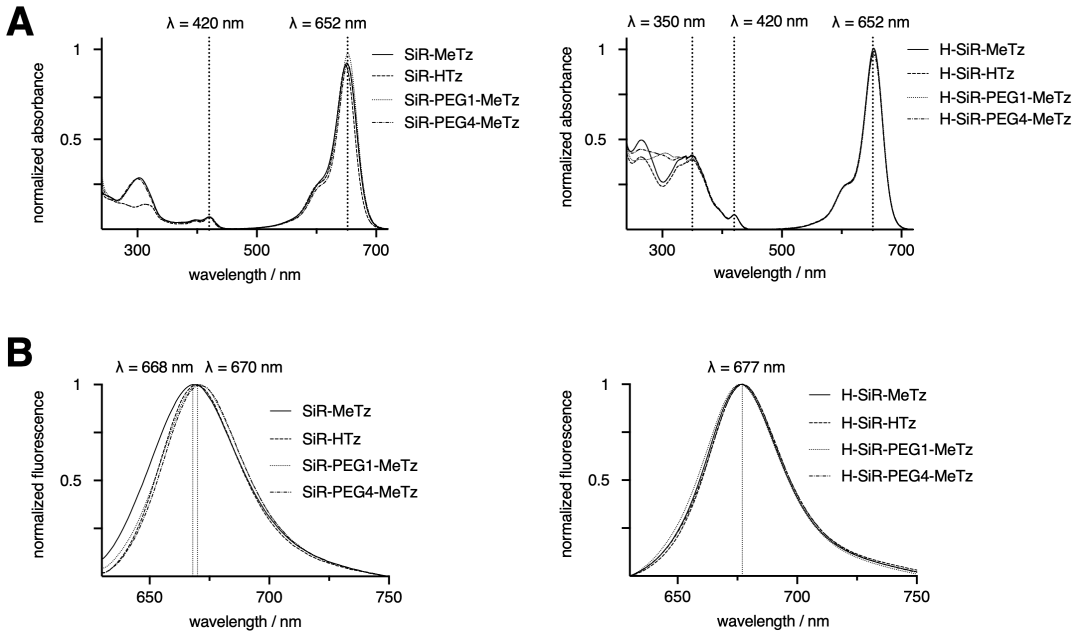

Figure 2.3: A) UV/Vis and B) fluorescence spectra (λ_{ex} = 620 nm and λ_{em} = 630–750 nm) of fluorescent probes conjugated to tetrazines with different linkers and their Hoechst-conjugates. The probes were incubated with 0.1% SDS at room temperature for 1 h before the experiment to push the spiroclactone equilibrium to an open state.

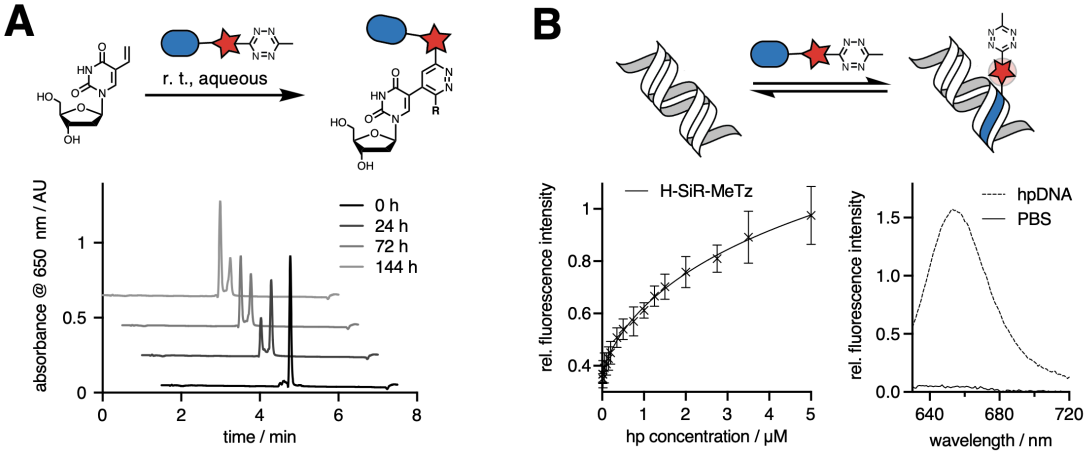

Figure 2.4: *In vitro* experiments were performed to show that: A) VdU reacts with methyl tetrazines and B) H-SiR-MeTz showed affinity towards DNA and a turn-on upon DNA binding. A) HPLC traces 10 mM VdU and 1 mM H-SiR-MeTz in methanol:water (1:1, v/v) at room temperature. B) Left: The titration curve of H-SiR-MeTz against different concentrations of hpDNA indicated an affinity for hpDNA in the micro-molar range and turn-on upon binding. λ_{ex} = 630 nm and λ_{em} 670 nm, bandwidth = 20 nm. Plotted mean values show the mean of N=6 data points measured on two independent days. Right: The emission spectra in PBS and at higher hpDNA concentrations.

H-SiR-MeTz was added to 10 mM VdU (10 eq.) in methanol:water (1:1, v/v) at room temperature under pseudo-first-order conditions. To estimate a reaction rate for VdU and H-SiR-MeTz in solution, the reaction was monitored at 650 nm over 144 h using LC-MS (Figure 2.4, A). The formation of the expected product was confirmed by HRMS. Besides, the mass of the deglyco-

sylated product was observed that formed after long reaction times.

The rate constant k_2 was roughly estimated as 4.18 $\times$ 10^{-4} M^{-1} s^{-1} and with this about 50-fold slower than the reported value for the reaction of VdU with dipyridyl tetrazine (measured at 25 °C in methanol:water, 2:1, v/v).[48] As such, a reaction between incorporated VdU and H-SiR-MeTz in a cellular environment without proximity enhancement should be negligible.

To determine the affinity of H-SiR-MeTz to a model hairpin oligonucleotide (5'-CGCGAATTC-GCGTTTTCGCGAATTCGCG-3'), a titration experiment was performed measuring the fluorescence of H-SiR-MeTz. For the titration experiment, buffer conditions for efficient hairpin folding (50 mM Tris HCl pH 7.4, 1 mM $MgCl_2$) were chosen by comparing the fluorescence emission of H-SiR-MeTz in different buffers.[1] Titration of 20 nM H-SiR-MeTz against hpDNA (10 nM to 5 µM) verified the affinity of the H-SiR-MeTz probe to DNA (Methods 4.2.2).

The turn-on values upon DNA binding are highly dependent on the concentration range (SI-Figure 3.3). H-SiR-MeTz showed a 2.7-fold turn-on in fluorescence after 1 h incubation time with 5 µM hpDNA (Figure 2.4, B). For hpDNA concentrations of 50 µM and 1 h incubation time, a 32-fold turn-on upon DNA binding was determined (Figure 2.4, B). Besides, the turn-on in fluorescence of H-SiR-MeTz with 0.1% SDS was determined 50-fold after 1 h incubation time. Hence, hpDNA is less effective in pushing the spirolactone equilibrium to the open state compared to 0.1% SDS.

2.3.2 *In vitro* kinetics oligonucleotide

To investigate the reaction kinetics of vinyl-modified DNA as well as proximity enhancement through Hoechst-tagging, *in vitro* experiments with a vinyl-modified hairpin oligonucleotide (ODN) were performed (Methods 4.4).

To obtain a vinyl-modified ODN, several options were considered: Besides solid-phase DNA synthesis and post-synthetic modifications, primer extensions are a widely used approach for incorporating unnatural nucleotide triphosphates into ODNs.[82],[77] As the vinyl modification is small and can be directly incorporated with polymerases, a primer extension was chosen.[155],[156]

A 5'-FITC-labeled 23 bp primer, which is a 3' truncated version of a full-length hpDNA from previous *in vitro* characterizations, was designed and the parameters for the primer extension were optimized (Figure 2.5). The KlenTaq and Exo Vent polymerases were able to elongate the hairpin to the desired length using all natural nucleotide triphosphates. As the primer contains a palindromic sequence, a separate template was not needed.

Next, thymidine triphosphate (TTP) was replaced by 5-vinyl-2'-deoxyuridine triphosphate (VdUTP) in the primer extension and gave a vinyl-modified hpDNA strand (Figure 2.6). As side products formed during the elongation process, a method to separate the product of the primer extension using reversed-phase HPLC (RP-HPLC) was developed. The purified product was obtained at low concentrations and MS analysis of the ODN proved difficult. Under the assumption that the right product formed, the modified ODN was incubated with tetrazines.

In the beginning, the H-SiR-MeTz probe was used up to 1 mM concentration to perform the click reaction and incubated the ODN with the tetrazine for up to 72 h. The reaction was then

[1] Experiments were carried out by Luis Hauptmann under my supervision.

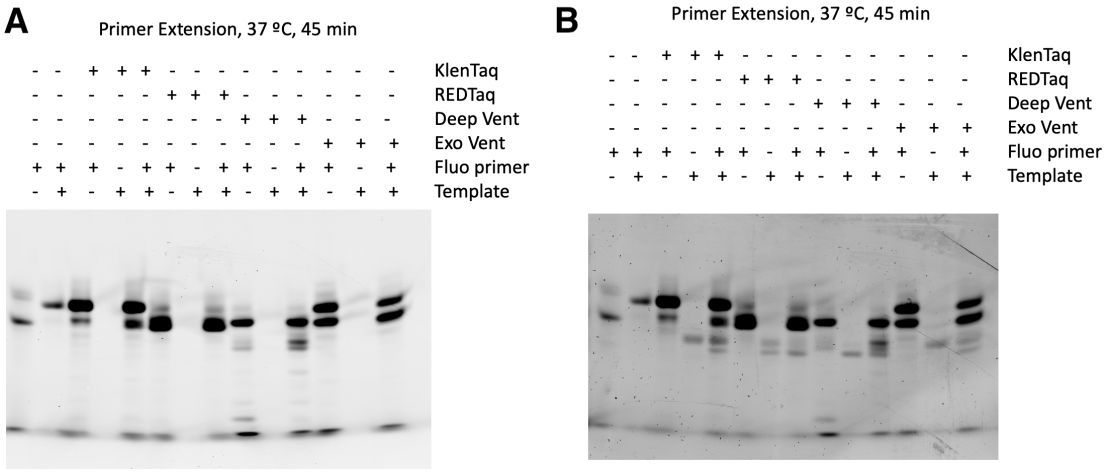

Figure 2.5: 20% Urea PAGE gel with various primer extension reactions mixtures using different polymerases and combinations of FITC-labeled primer and ODN template. All primer extensions were performed at 37 ℃ for 45 min. A) unstained gel, B) SYBR safe stained gel. Both gels were imaged in the Cy2 channel. The FITC-labeled primer and purchased 5'-FITC-labeled hairpin were loaded in the first two lines of the gel. The template was not fluorescently labeled and is therefore only visible on the stained gel. The FITC-labeled ODNs are larger, thus their mobility is higher and their bands are shifted on the gel.

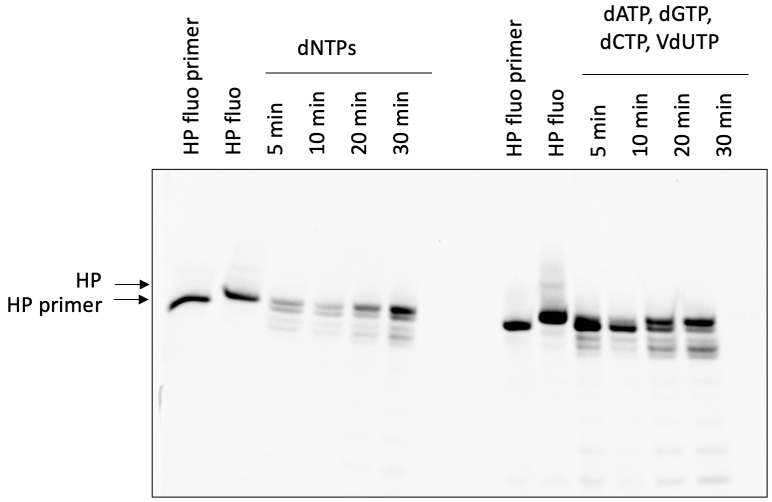

Figure 2.6: 20% Urea PAGE gel showing primer extensions using the Deep Vent polymerase and a FITC-labeled primer with natural dNTPs and VdUTP for different time points.

analyzed with a Urea PAGE gel, but no additional band on the gel was observed. Likewise, 1 mM of the soluble and highly reactive Cy5-pyrimidyl-tetrazine, which was incubated with the ODN for up to 24 h could not label the ODN.

In conclusion, the hpDNA *in vitro* system might not be ideal to study the proximity reaction of vinyl-modified DNA and a tetrazine. The folding of the hairpin might be one reason for poor accesibility of the modification, or the positioning of the modification might not be ideal. In the future, different positions for the modification could be screened to observe a reaction product (SI-Figure 3.2).

2.4 *In cellulo* characterization

2.4.1 Studying incorporation yields of unnatural nucleosides by mass spectrometry

Mammalian cells have two metabolic pathways to generate thymidine triphosphates for DNA synthesis: (i) *de novo* synthesis and via the (ii) salvage pathway. Thymidine derivatives that are delivered to the cells in metabolic labeling are metabolized via the salvage pathway and compete with the natural cellular pool of nucleosides. To get an estimate of the incorporation yield of thymidine derivatives via the salvage pathway, ^{15}N-labeled thymidine was supplemented to the growth medium of U2OS cells to a final concentration of 5–20 µM and the incorporation yield determined (Methods 5.4).

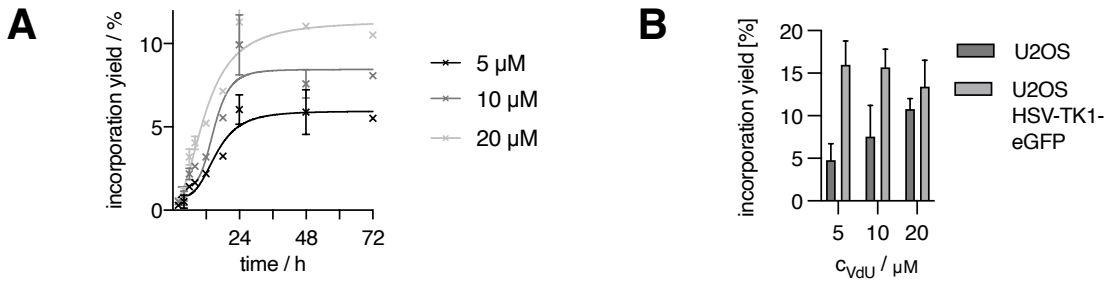

Figure 2.7: VdU incorporation yields into U2OS cells determined by MRM quantification from N=3 biological replicates in A) showing a time course between 4–72 h feeding times and in B) a comparison between a normal and U2OS HSV-TK1-eGFP(+) cell line.

After one cell division (24 h doubling time) about one-third of all thymidine in the DNA was replaced by ^{15}N thymidine that was supplemented at 10 µM (SI-Figure 4.3). This means that two out of three nucleosides are incorporated from the external pool, as only 50% of the DNA was synthesized in one cell cycle.

Next, the experiment was repeated with VdU (Figure 2.7, A) and EdU (SI-Figure 4.3). Both showed similar, but reduced incorporation compared to ^{15}N-thymidine. Up to 11.29 $\pm$ 1.21% for VdU and 21.77 $\pm$ 0.52% for EdU of the whole thymidine content in the genome were replaced with unnatural building blocks. As expected, the incorporation yield depended on the concentration of the nucleoside and is slightly increasing with higher concentrations of the nucleoside. Interestingly, the incorporation yield remained constant after 24 h. A possible explanation is the growth inhibition after one division due to the modified genome.

The limitation in the salvage pathway for the metabolic incorporation of thymidine derivatives is the human thymidine kinase (hTK1). Therefore, the incorporation yield in cells expressing the higher fidelity kinase from the herpes simplex virus (HSV-TK1) was determined as 15.97 $\pm$ 2.80%. Surprisingly, the incorporation yield was independent of the concentration that was used (Figure 2.7, B).

2.4.2 Labeling in fixed cells studied by confocal microscopy

To see if the probe keeps its promise and labels incorporated VdU in a proximity-enhanced reaction, cellular experiments were performed with H-SiR-MeTz, H-SiR-HTz, H-SiR-PEG1-MeTz

and H-SiR-PEG4-MeTz in VdU treated U2OS cells (Methods 5.6.2).

Specificity of the probe for vinyl-modified DNA

To verify the specificity of the probes for newly synthesized DNA, three criteria were applied (i) specific labeling pattern, (ii) labeling only in the presence of VdU, and (iii) the absence of labeling in the presence of a DNA synthesis inhibitor aphidicolin (APC, structure see SI-Figure 4.4, A) and VdU.

First, the labeling pattern in the nuclei was compared to the one that was obtained with EdU. In mammalian cells the S-phase takes about 8–10 h.[157] When U2OS cells are treated with VdU for 8 h, S-phase progression during the cell cycle can be visualized in an asynchronous cell population (Figure 2.8). Early S-phase cells show numerous replication foci in euchromatin, which are distributed in the whole nucleus and appear as punctual structures (I). These foci then grow bigger during S-phase progression and localize around nucleoli in mid-S-phase, giving a ring-shaped structure (II). Late S-phase cells show labeling in regions at the nuclear envelope and perinucleolar heterochromatin, making the signal more diffuse (III).[158] No labeling is observed in cells in G1/G2 phase for an 8 h VdU feeding time.

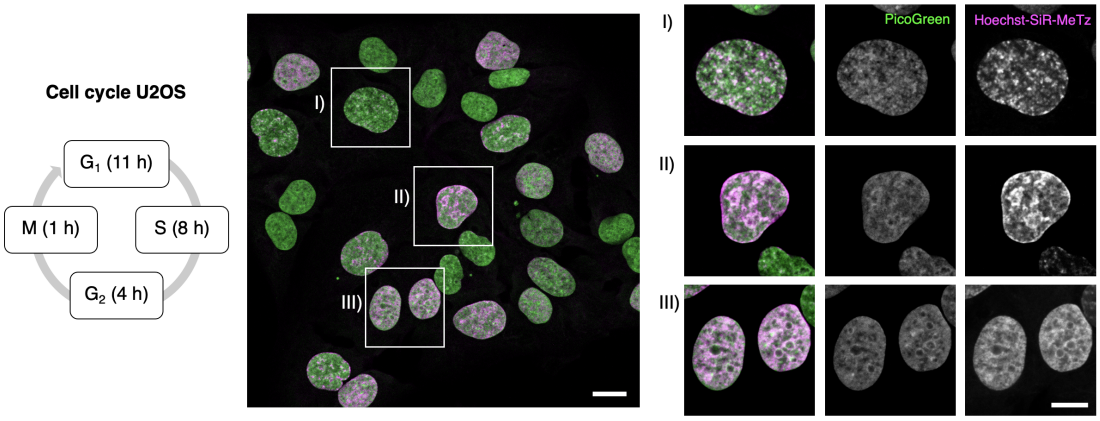

Figure 2.8: Cell cycle of U2OS cells and confocal images (63x oil objective) of U2OS TREx cells treated with 50 µM VdU for 8 h, labeled with 5 µM H-SiR-MeTz (magenta) for 16 h, and counterstained with PicoGreen (green), showing different labeling patterns that occur during the cell cycle. Scale bar left: 20 µm, right: 10 µm.

Next, the dependence of the fluorescence signal of the H-SiR-MeTz probe on the incorporation of VdU was demonstrated. Therefore, titration experiments with VdU were performed. U2OS cells were fed with various doses of VdU, fixed, and labeled with H-SiR-MeTz. Non-treated cells served as a negative control. Dose-dependent intra-nuclear staining was observed in cells treated with VdU (Figure 2.9, A). The signal co-localized with the non-covalent nuclear counterstain PicoGreen. The signal intensity of 50 µM VdU was comparable to 100 µM VdU. To reduce toxic side effects, 50 µM VdU was used for the following experiments.

To further prove the specificity of the signal for vinyl-modified DNA, DNA synthesis was inhibited with APC. Therefore, the sensitivity of U2OS cells towards APC was first studied in a titration experiment treating cells with EdU (SI-Figure 4.4, B). Therein, U2OS cells treated with EdU and 6 µM APC exhibited only little nuclear staining. When 12 µM APC were present,

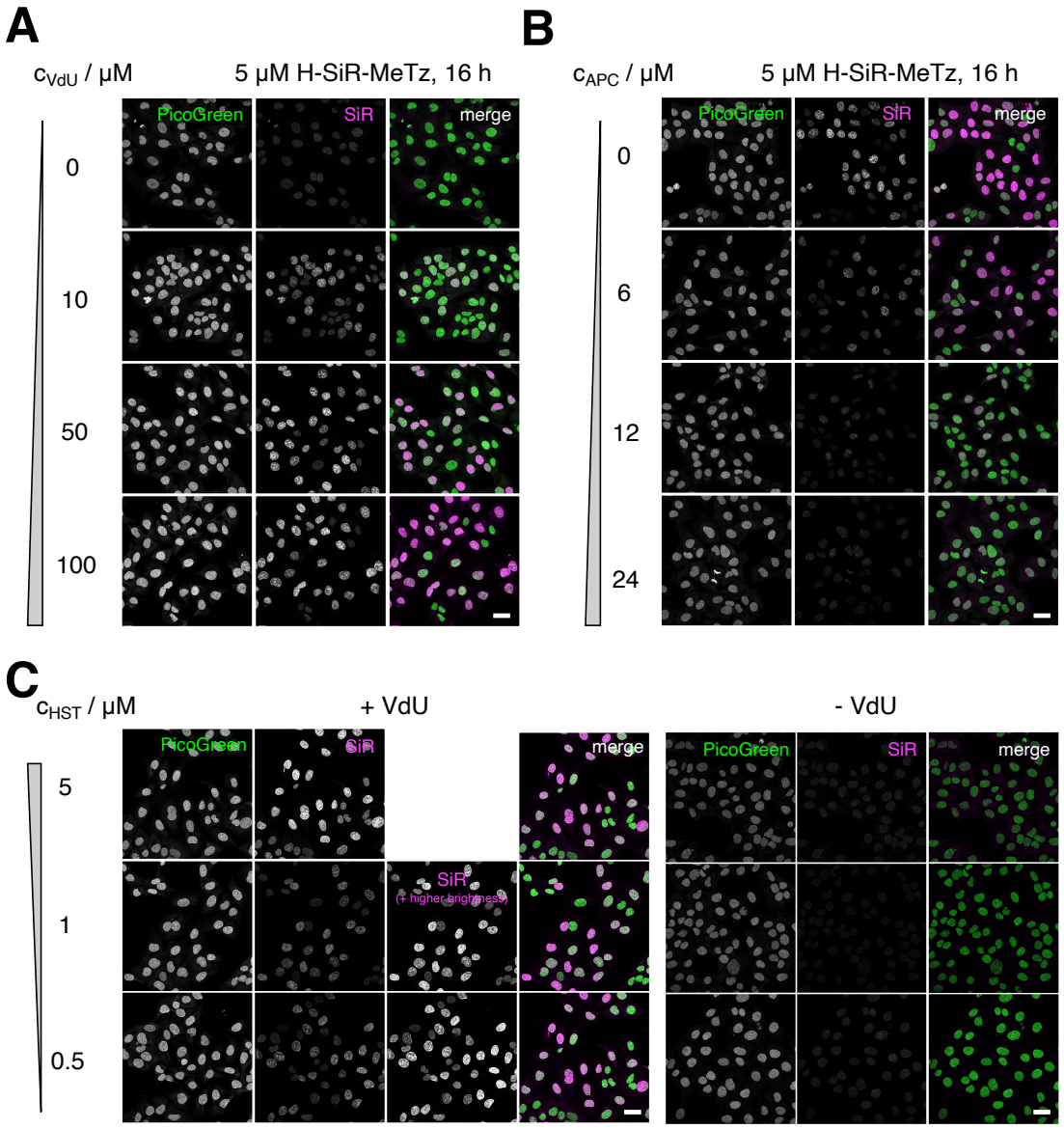

Figure 2.9: Confocal images (40x water objective) of U2OS TREx cells labeled with 5 µM H-SiR-MeTz for 16 h showing SiR (magenta) and PicoGreen (green). A) Titration feeding 0–100 µM VdU for 8 h. (B) Titration 0–24 µM APC during 8 h feeding time with 50 µM VdU. C) U2OS TREx cells optionally treated with 50 µM VdU for 8 h (left: +VdU, right: -VdU) and labeled with 0.5–5 µM H-SiR-MeTz for 16 h. Scale bar = 20 µm.

DNA synthesis, and linked EdU incorporation, was efficiently blocked. Applying 24 µM APC already showed minor toxic effects, judging from cell morphology and the occasional occurrence of dead cells. When the experiment was repeated with VdU, APC treatment led to a strong decrease in signal, showing the same trend as EdU treated cells (Figure 2.9, B). Again, the incorporation of VdU was partly blocked with 6 µM and fully with 12 µM APC. The absence of nuclear signal in cells with inhibited DNA synthesis is a strong evidence for specific labeling of the fluorescent probe for replicating cells only.

To optimize the concentration of the fluorescent probe, H-SiR-MeTz was applied at different concentrations to VdU–treated and non-treated cells (Figure 2.9, C). As expected, the signal

intensity increased with higher concentrations of H-SiR-MeTz. Even at a very low concentration of 500 nM, the signal did not completely vanish. This already indicated that the labeling could be indeed accelerated through the binding of the probe with DNA. Otherwise, labeling would not be expected at such low concentrations due to the low reactivity of VdU in the combination with methyl tetrazines.

Proximity-labeling of the probe

To investigate the hypothesis of proximity-labeling, the probe was titrated to even lower concentrations (10 nM). The fluorescence signal in the nuclei and the specific labeling pattern were still observed down to 50 nM H-SiR-MeTz (Figure 2.14, A).

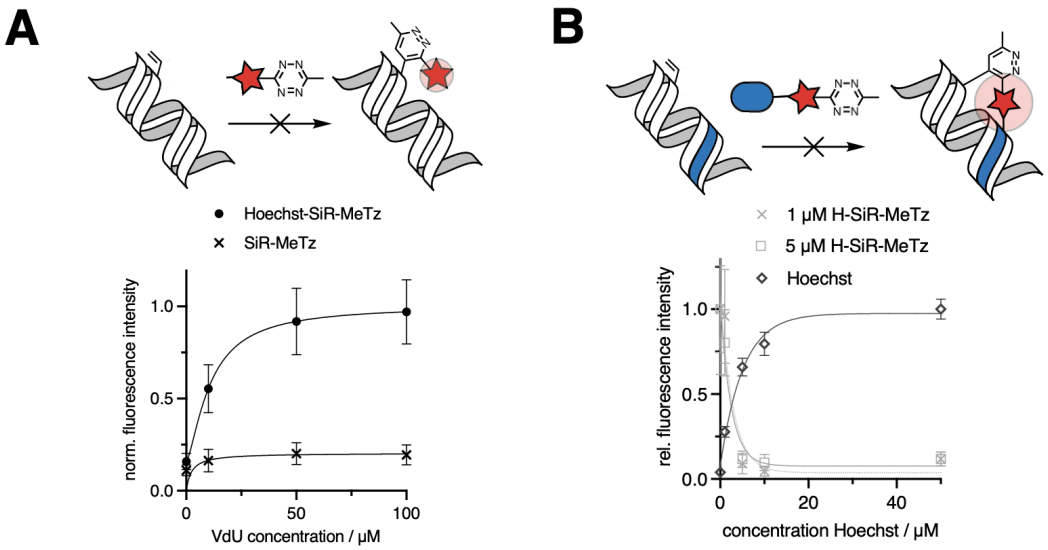

Figure 2.10: Two key experiments to study the proximity enhancement of the reaction in fixed cells. A) Showing that labeling is only efficient when the Hoechst-tagged probe is used and SiR-MeTz does not efficiently react with VdU. To visualize the effect, both dyes were used to label cells that were treated with different concentrations between 10–100 µM VdU. B) In a competition experiment of H-SiR-MeTz with Hoechst33342, increasing concentrations of Hoechst33342 led to a decrease in the labeling of the probe.

To study the influence of the targeting ligand on the reaction of H-SiR-MeTz, the labeling of H-SiR-MeTz **17** with SiR-MeTz **10** were compared. Therein, cells were treated with various doses of VdU and stained with H-SiR-MeTz and SiR-MeTz. While H-SiR-MeTz exhibited dose-dependent labeling with increasing VdU incorporation, SiR-MeTz showed hardly any signal. Higher concentrations of SiR-MeTz ($>$5 µM) led to strong signal in nucleoli. For all concentrations of SiR-MeTz that were tested, no specific pattern was observed (SI-Figure 4.7). Consequently, SiR-MeTz is not efficiently labeling vinyl-modified DNA under the used conditions. In total, this experiment showed that the presence of the ligand had a significant influence on the labeling result.

Proximity-enhancement of the labeling was then studied in a competition assay in fixed cells with Hoechst33342 (Figure 2.14, B). Hoechst33342 displays a higher affinity to DNA compared to H-SiR-MeTz. When all Hoechst binding sites of the genomic DNA are saturated with

Hoechst33342, H-SiR-MeTz cannot bind anymore. Under the assumption, that binding is essential for the click-reaction, the reaction should then not take place.

VdU–treated, fixed cells were labeled with H-SiR-MeTz in the presence of Hoechst33342. Already upon the addition of 1 µM Hoechst33342, the fluorescence intensity in nuclei dropped. At 5 µM Hoechst33342 only marginal and above 10 µM Hoechst33342 no labeling with H-SiR-MeTz was observed. The inverse trend was detected from the Hoechst33342 signal. While a weak fluorescence signal of Hoechst33342 appeared using 1 µM DNA stain, the maximum intensity was almost reached with 5 µM Hoechst33342. Judging from the Hoechst33342 labeling curve, the DNA binding sites should be highly saturated with 10 µM Hoechst33342 and above. This experiment suggests that the binding of the probe by the Hoechst ligand is critical for efficient labeling.

Displacement experiments with the probe

To verify covalent labeling and to get information about residual background binding of H-SiR-MeTz, displacement experiments were performed with 6-Hoechst-SiR (H-SiR) and H-SiR-MeTz (Figure 2.11). Upon the addition of Hoechst33342, transiently bound probes, such as 6-Hoechst-SiR (H-SiR), can be displaced. In contrast, covalently reacted probes, such as reacted H-SiR-MeTz, are displaced less efficient due to the high local concentration of the tethered probe (Figure 2.11, A and B).

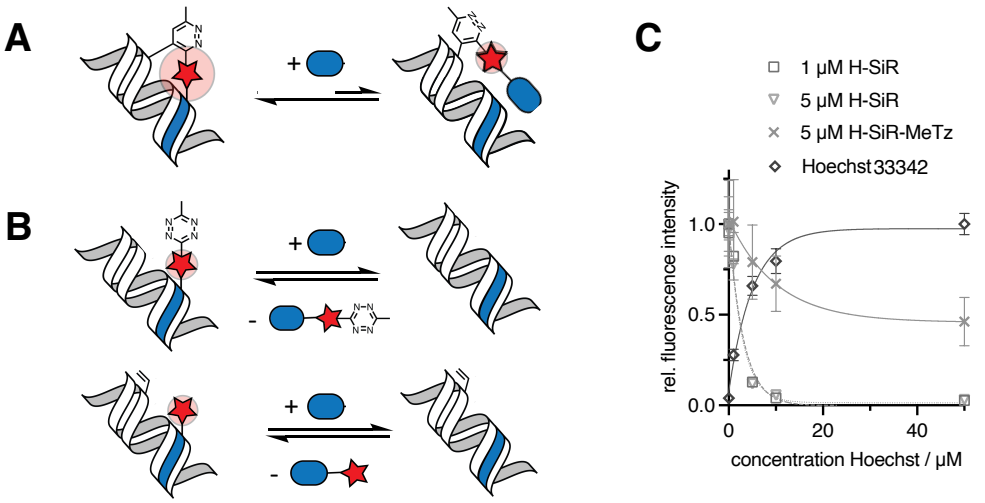

Figure 2.11: Covalently versus transiently bound dyes can be distinguished by displacement experiments in fixed cells. Situation A) shows the covalently bound H-SiR-MeTz dye that is not efficiently displaced with Hoechst33342 (=blue circle), while situation B) shows displacement of H-SiR-MeTz and H-SiR (=blue circle + red star) upon the addition of Hoechst33342. The corresponding experimental data is shown in C). While H-SiR could be fully displaced by adding Hoechst33342, the signal of H-SiR-MeTz did not fully vanish.

While the fluorescence intensity in nuclei labeled with 6-Hoechst-SiR (H-SiR) goes down to zero, the fluorescence of H-SiR-MeTz is only halved (Figure 2.11, C). This can be explained by (i) displacement of some residual, transient background binding of H-SiR-MeTz, (ii) a lower quantuum yield of displaced and tethered probe, or (iii) quenching effects from high excess of Hoechst33342.

To exclude quenching, a titration of Hoechst33342 was performed with EdU treated cells, that were labeled with SiR-azide. The fluorescence signal remained unaffected by the addition of Hoechst33342, even at high concentrations of Hoechst33342 ($>$10 µM). This led me to the assumption, that upon the addition of Hoechst33342, indeed excess, transiently bound H-SiR-MeTz is "washed out" or tethered probe is displaced.

"Washing out" dye resulted in a visible improvement of signal-to-noise ratio in the acquired image. Therefore, a short washing step (5 µM Hoechst33342, 10 min) was added to the protocol in later experiments, which helped to improve the signal-to-noise ratio.

Signal-to-noise ratios of the probe

Tetrazines are often hydrophobic and give unspecific background from the cytosol and nucleus due to miss-localization and poor quenching. Therefore the signal-to-noise ratios (S/N) were examined in more detail. To compare H-SiR-MeTz staining with other tetrazine dyes, the signal-to-noise ratio for nucleus versus cytosol (S_{nuc}/N_{cyto}) was determined staining VdU–treated cells (Figure 2.12, A and SI-Figure 4.8).

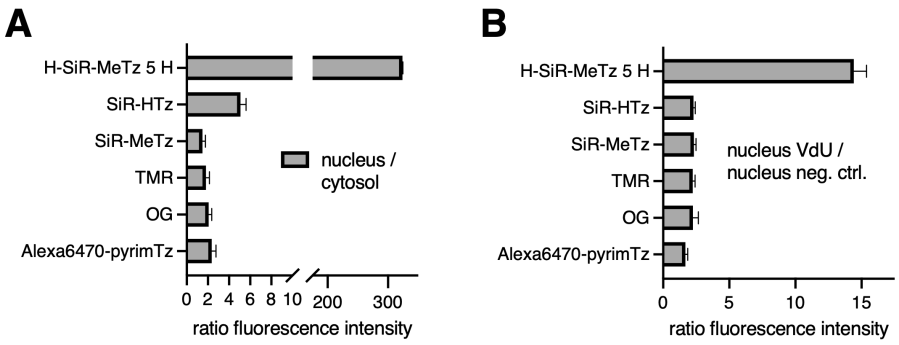

Figure 2.12: Plotted signal-to-noise ratios for different tetrazine coupled dyes that were used to label VdU–treated cells. The ratios show the fluorescence signal in the nucleus versus cytosol (S_{nuc}/N_{cyto}) and proliferating versus non-proliferating cells ($S_{pro}/N_{non\text{-}pro}$).

One example of a dye with low S_{nuc}/N_{cyto} is SiR-MeTz. It is low in reactivity, poorly quenched and hydrophobic. In contrast, OG-MeTz showed slightly improved S_{nuc}/N_{cyto} most likely due to a higher turn-on of the probe after the reaction. Also, SiR-HTz showed superior properties for S_{nuc}/N_{cyto} compared to SiR-MeTz. A possible explanation is the higher reactivity which contributes to better conversion of the bioorthogonal reaction.

The bifunctional probe H-SiR-MeTz after washing with 5 µM Hoechst33342 exceeded a S_{nuc}/N_{cyto} $>$300. Thereby, H-SiR-MeTz is clearly outperforming the other dyes, as the Hoechst ligand is effective as a targeting moiety and quencher. Thus, almost no signal was observed in the cytosol. Also, I believe that the proximity enhancement of the reaction will give higher reaction yields.

Another important criterium is the signal-to-noise in proliferating versus non-proliferating cells ($S_{pro}/N_{non\text{-}pro}$), which provides information about the specificity of the reaction for proliferating cells. Therefore, the fluorescence signal in nuclei of proliferating, VdU–treated cells was compared to non-treated cells. Again, most dyes show a 2-fold difference in fluorescence intensity of a proliferating compared to the negative control (Figure 2.12, B). Only H-SiR-MeTz after

washing with 5 µM Hoechst33342 could show two distinct populations of proliferating and non-proliferating cells with a $S_{pro}/N_{non\text{-}pro}$ of 14.42 $\pm$ 0.96 and could serve as a labeling reagent for proliferation assays with VdU.

Influence of the linker of the probe

Finally, the influence of a linker on the overall labeling result was studied. Therefore, the fluorescence signal in nuclei of cells labeled with H-SiR-PEG1-MeTz and H-SiR-PEG4-MeTz was compared to H-SiR-MeTz in VdU–treated and non-treated cells (see Figure 2.13, A).

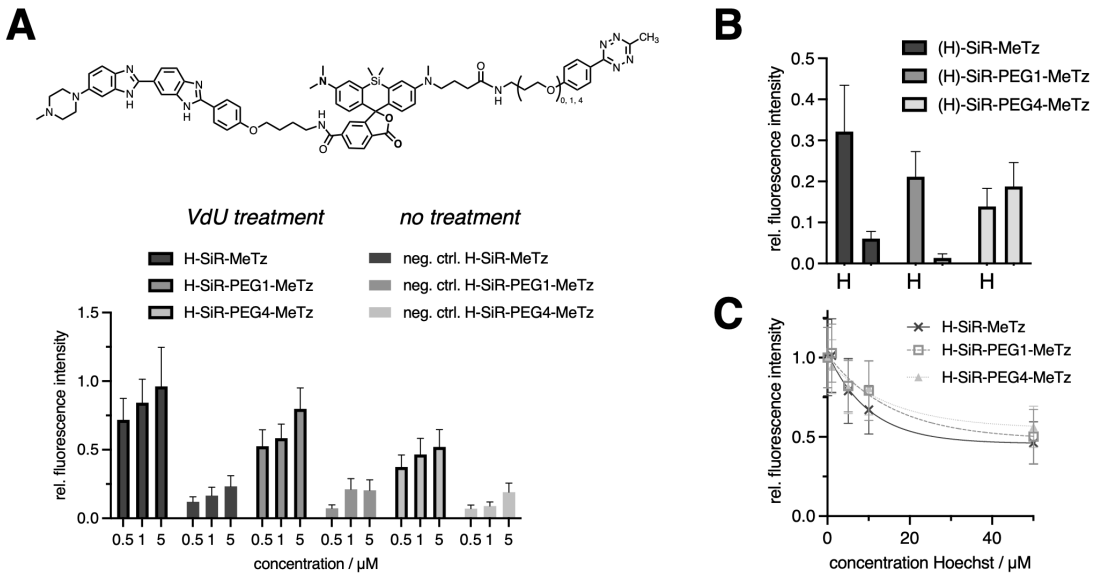

Figure 2.13: A) Comparison of H-SiR-PEG(0,1,4)-MeTz probes (see structure) of different concentrations (0.5–5 µM) in VdU–treated (50 µM), and non treated cells. B) Labeling with 5 µM (H)-SiR-PEG(0,1,4)-MeTz with and without Hoechst ligand. C) Displacement experiments for H-SiR-PEG(0,1,4)-MeTz.

The mean fluorescence intensity of the nuclei was compared and three trends were observed: (i) The signal in VdU–treated cells was brighter for all bifunctional probes compared to non-treated cells. (ii) Fluorescence signal in nuclei, but also the background of non-treated cells was increasing with higher concentrations of the fluorescent probes. (iii) Most importantly, the linker influenced the labeling: with longer linkers, the overall fluorescence signal intensity dropped. Consequently, short linkers are favored over longer linkers. Possibly, longer linkers might affect the permeability of the probes.

Besides, the influence of the Hoechst ligand on the labeling result was studied by performing similar experiments as before with SiR-MeTz, SiR-PEG1-MeTz and SiR-PEG4-MeTz (see Figure 2.13, B). Again, the signal in experiments performed with a bifunctional probe that is coupled to Hoechst is for three out of four scaffolds brighter in comparison to the SiR tetrazine probes. Here again, images of SiR tetrazine probes without Hoechst, in particular SiR-PEG4-MeTz, showed a lot of unspecific signal and accumulation in nucleoli.

Next, displacement experiments were conducted with the H-SiR-PEG1-MeTz and H-SiR-PEG4-MeTz probe with similar results as for H-SiR-MeTz (see Figure 2.13, C). The observed

trend was similar to H-SiR-MeTz, indicating covalent labeling of H-SiR-PEG1-MeTz and H-SiR-PEG4-MeTz.

Increasing the reactivity of the probe with an H tetrazine

With respect to live-cell experiments, labeling speed was improved employing a probe equipped with an H tetrazine (H-SiR-HTz). Faster labeling kinetics allow labeling at intracellular concentrations, which are typically low in living cells.

First, the labeling result of H-SiR-HTz with H-SiR-MeTz at different concentrations from 10 nM to 5 µM for 16 h in VdU–treated (50 µM, 8 h) cells was compared (Figure 2.14, A). H-SiR-HTz showed superior labeling in cells, especially at low concentrations (50 nM) (SI-Figure 4.9). At higher concentrations, a roughly 3-fold better conversion of the reaction could be reached.

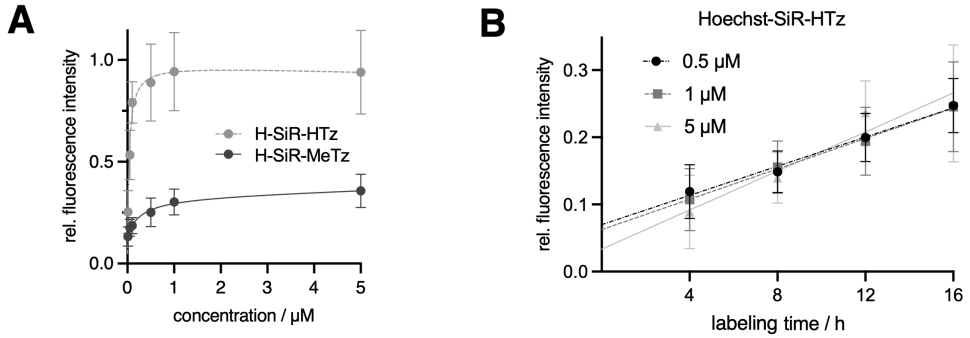

Figure 2.14: A) Comparison of H-SiR-MeTz with H-SiR-HTz showing overall labeling intensity of nuclei after 16 h staining with 5 µM probe. B) Labeling kinetics in cells with different concentrations 0.5–5 µM H-SiR-HTz.

Next, the labeling kinetics of H-SiR-HTz were investigated in more detail. Therefore, the time course of the reaction was measured. The fluorescence intensity increased linearly with labeling time (Figure 2.14, B). The labeling speed for the used concentrations was comparable. The plot indicated that labeling is still incomplete after 16 h, as the signal did not saturate.

Despite incomplete labeling, the overall good performance of the probe was encouraging to move on with live-cell experiments.

2.4.3 Labeling in living cells studied by confocal microscopy

After successful evaluation of the H-SiR-HTz probe in fixed U2OS cells, labeling in living cells was studied (Methods 5.6.3). To get staining in live U2OS cells, 0.5–5 µM H-SiR-HTz was incubated with VdU–treated cells for 8–16 h. For the experiments, U2OS-PCNA-GFP(+) or U2OS-H2B-Halo(+) cells were used, as the GFP signal or labeled HaloTag can serve as a reference for applying autofocus.

The labeling was followed live under the microscope during time-lapse imaging using 5 µM H-SiR-HTz. During the first 2 h, the fluorescence intensity was increasing in all nuclei and then remained constant, but under no-wash conditions and with short labeling times, it was hard to differentiate between proliferating and non-proliferating cells (Figure 2.15).

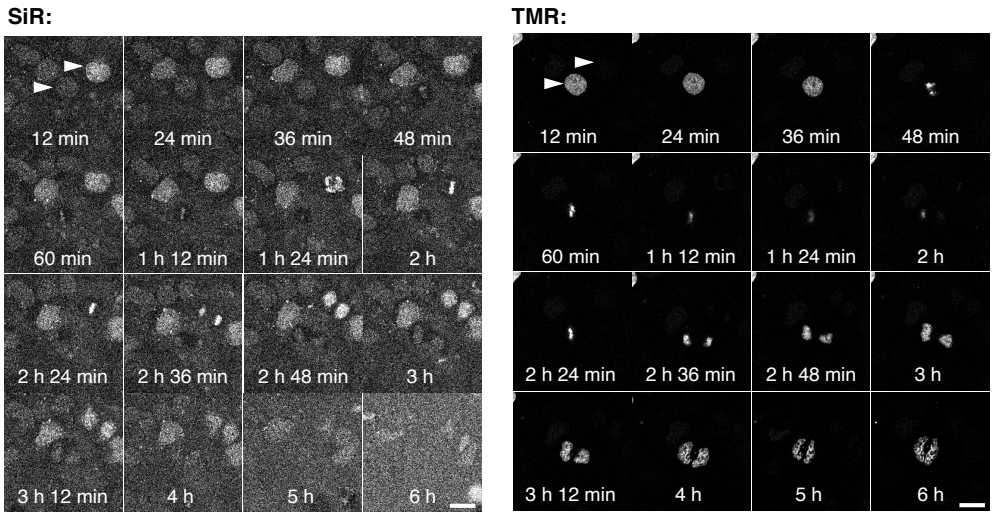

Figure 2.15: Representative confocal images of U2OS-H2B-Halo cells labeled with MAP555-chloroalkane, treated with VdU for 8 h and labeled with 5 µM H-SiR-HTz live for 2 h. Scale bar = 20 µm.

However, when the medium of the cells was changed 12–16 h after incubation with the probe, the signal cleared up in some cells within 30 min, while the signal remained in others. The labeling pattern of H-SiR-HTz indicated the labeling of incorporated VdU during the S-phase. For 5 µM of H-SiR-HTz, the signal was clearly visible, while it was weak for 0.5 µM H-SiR-HTz (Figure 2.16). The signal could be observed over several hours. If the dye would be non-covalently bound, I expect that it would be "wash out" over time. As such, the signal disappeared over time in experiments with shorter incubation times of the H-SiR-HTz probe ($<$12 h).

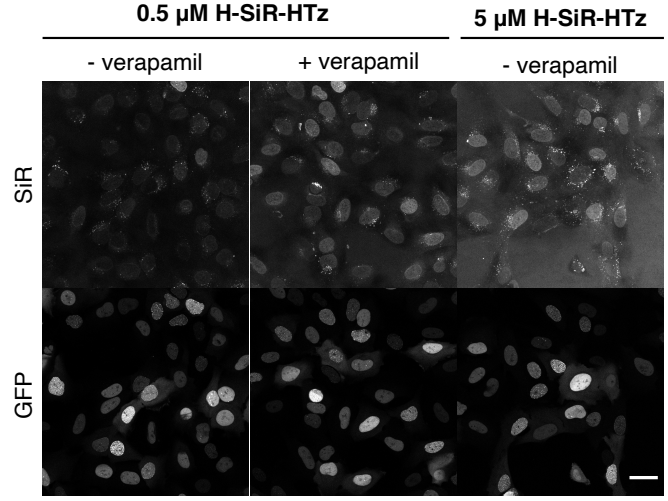

Figure 2.16: Representative confocal images of U2OS-PCNA-GFP cells treated with VdU for 8 h and labeled with H-SiR-HTz live for 16 h and optionally 10 µM verapamil. Scale bar = 20 µm.

Next, labeling with H-SiR-HTz was evaluated in the presence of the efflux pump inhibitor verapamil, which increases the intracellular concentration of the dye during labeling.[21] Therefore, VdU–treated cells were labeled with different concentrations of H-SiR-HTz in the presence and

absence of verapamil (Figure 2.16). Co-incubation with verapamil improved the signal, such that the labeling after incubation with 0.5 µM H-SiR-HTz and verapamil was comparable to incubation with 5 µM H-SiR-HTz without verapamil.

Besides labeling, toxic effects caused by the probe during imaging were observed. Judging from morphology changes and detaching cells, 5 µM H-SiR-HTz already caused toxicity issues for long incubation times of several hours. For 6-Hoechst-SiR severe toxicity was not reported up to 10 µM.[21] It is possible that a reactive probe is more toxic because it can prevent proteins from binding to DNA, whereas a transient probe can diffuse away.

Furthermore, aggregates were observed with the H-SiR-HTz probe, especially at higher concentrations (5 µM). Based on considerations of toxicity and aggregate formation, the best imaging results were achieved labeling with 1 µM H-SiR-HTz and 10 µM verapamil (Figure 2.17, A).

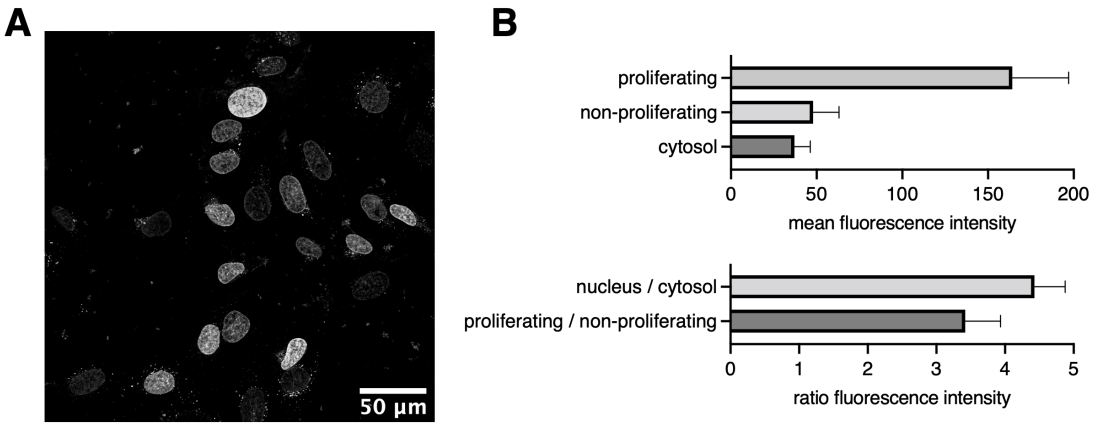

Figure 2.17: A) Confocal image (40x water) live U2OS-H2B-Halo (labeled with MAP555-CA), treated with VdU (50 µM, 8 h), stained with 1 µM H-SiR-HTz in the presence of 10 µM verapamil for 16 h. Scale bar = 50 µm. B) Quantification mean fluorescence intensity of proliferating, non-proliferating cells and in the cytosol for N=10 selected areas from a z-stack (z-projection of the maximal intensity) and the resulting ratios.

The S_{nuc}/N_{cyto} and $S_{pro}/N_{non\text{-}pro}$ were determined under these conditions in living cells (Figure 2.17, B). Both were smaller than in fixed cells, but still better compared to other tetrazine dyes in fixed cells (see above).

Finally, the signal was tracked after labeling to observe cell divisions (SI-Figure 4.10). Therefore VdU–treated and H-SiR-HTz labeled cells were imaged for 12–16 h. Unfortunately, too many cells died after several hours and only a few cells were still dividing. If the toxicity could be circumvented, the tool would be useful to study cell cycle events.

Labeling in fixed cells studied by STED super-resolution microscopy

Several cellular processes contribute to maintaining the integrity and function of the nucleus. For example, chromatin interactions with proteins are known to regulate gene activities, but the details of these mechanisms are often unknown.[159]

Super-resolution microscopy techniques were used to study these dynamics in this highly organized three-dimensional organelle. Commonly utilized strategies comprise labeling with

nucleoside analogs, but also immunochemistry.[159] But, available labeling techniques are often limited due to sterical hindrance in the densely-packed chromatin resulting in poor accessibility of labeling reagents, or artifacts as a result of harsh treatments. Additionally, when imaging within the nucleus, out-of focus light is often blurring the images.

To show that the bifunctional probe is compatible with other nucleosides as well as immunolabeling, a pulse-chase experiment with EdU and labeling with an immunostained sample was demonstrated.

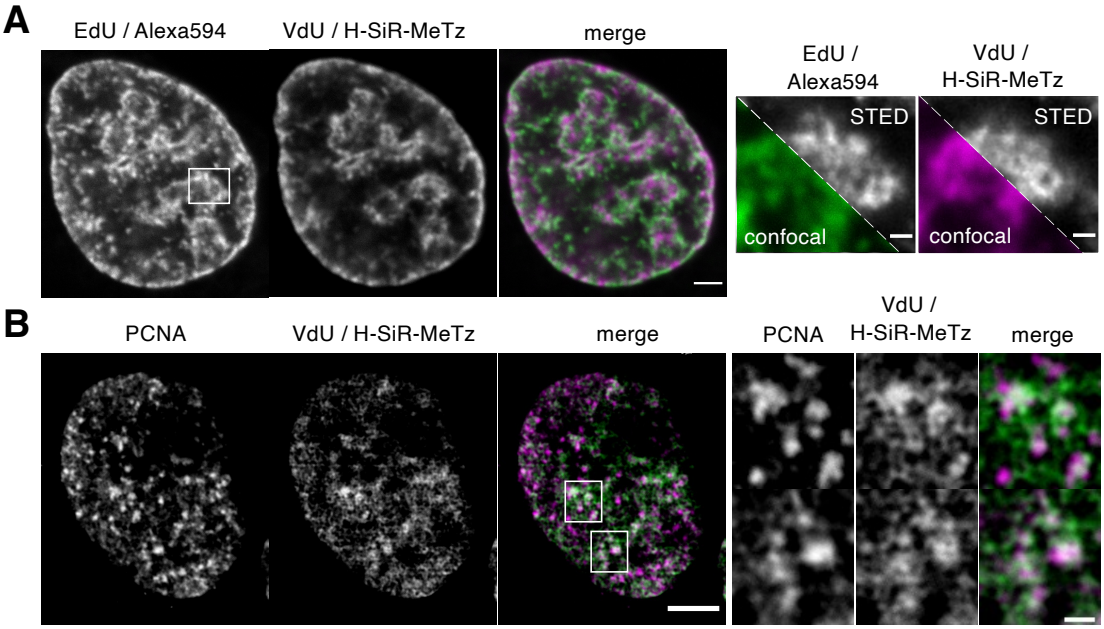

Figure 2.18: A) Confocal images (60x oil, deconvoluted, slightly smoothed), EdU pulse and VdU chase, fixed and stained with Alexa594-azide (green) and H-SiR-MeTz (magenta). The details show the higher resolved image. Scale bar = 2 µm and 500 nm. B) STED images (60x oil, mean filter (n=2)) U2OS-PCNA-GFP(+) cell line, treated with VdU for 20 min, fixed and stained with anti-GFP primary/ Alexa568-labeled secondary antibody (magenta), labeled with 5 µM H-SiR-MeTz (green) for 16 h and washed with 5 µM Hoechst. Scale bar = 5 µm and 400 nm.

For the first experiment, staining patterns of pulse-chase experiments of VdU and EdU were analyzed (Methods 5.7.1). Therein, EdU was first supplemented to the cells for 4 h before washing and adding VdU for another 4 h. Cells that show EdU and VdU signal have entered S-phase 4–8 h prior to fixation and are late S-phase cells. A commonly observed feature in the late S-phase is the formation of ring shapes in the nucleus (Figure 2.18, A). Interestingly, the signals of EdU and VdU seem to appear in different sections on these rings.

In a second experiment, replication foci and their surrounding nascent DNA were imaged. The replication marker PCNA was used to localize replication foci and study structures of replication forks that can be visualized using nucleoside analogs.[160]

By employing Cu(I) click reactions, the number of functional epitopes for antibody staining is highly reduced. HCl treatment is milder, but untreated samples can best preserve signals from fluorescent proteins or epitopes for antibodies (SI-Figure 4.5). Therefore, the performance of H-SiR-MeTz in STED nanoscopy without HCl denaturation in combination with immunostaining was demonstrated.

U2OS-PCNA-GFP(+) cells were treated with a short pulse of VdU for 20 min, fixed, and the nascent DNA was labeled (Methods 5.7.2). Afterward, the PCNA-GFP signal was detected with immunostaining using an anti-GFP primary/ Alexa568-labeled secondary antibody. In the STED microscope, early S-phase cells were then identified by the appearance of their GFP signal. To get a super-resolved image, the signal of Alexa568 was acquired to visualize replication sites.

The obtained images show a similar labeling pattern for PCNA and H-SiR-MeTz (Figure 2.18, B). This already indicated that VdU was incorporated at replication sites. Still, there is also signal from H-SiR-MeTz, which cannot be clearly allocated to a PCNA signal. One explanation might be background staining or out-of-focus light, the other that not all replication sites are fully labeled. Regardless, the result showed that it is possible to image samples at high resolution even with short VdU pulses and without HCl denaturation.

2.5 Bifunctional MAP probe

To improve the H-SiR-MeTz probe, a probe with potentially superior properties concerning (i) quenching of the dye from the tetrazine and (ii) cell permeability was proposed. Tetrazines-conjugated dyes with more efficient quenching were described in the literature (see section 4.1). Also, there is evidence that sulfonamides at the C3'-carboxylic acid of xanthenes help to improve properties of dyes, such as cell permeability and possibilities for tuning the spirolactame equilibrium.[161] Therefore, the probe design was combing both.

2.5.1 Synthesis of bifunctional MAP probe

The synthetic route for installing alkene linkers between the tetrazine and C6' of a xanthene was published by the Devaraj group.[162] Therein, the key transformation is a Heck elimination reaction between a mesylated 6-methyl-3-methoxyethyl-tetrazine and a brominated xanthene dye (Scheme 2.3).[2]

The 6-methyl-3-methoxyethyl-tetrazine **21** was synthesized in a modified Pinner synthesis from two nitriles using hydrazine in the presence of $Zn(OTf)_2$ as a catalyst. Therein the zinc(II) catalyst is likely to coordinate the nitrile and activate it which is believed to promote the formation of the amidrazone intermediate that is later further reacting in the presence of hydrazine to form a dihydrotetrazine. The dihydrotetrazine was then *in situ* oxidized with $NaNO_2$ at low pH.[163] Using two different nitriles allowed the formation of asymmetric tetrazines. In the reaction, all three combinatorial products **21**-**23** were formed and the asymmetric product was purified from the symmetric side products.

Next, the hydroxy function of **21** was mesylated (compound **24**) to generate a better leaving group which later facilitates spontaneous elimination for the Heck elimination reaction.

To obtain an isomerically pure brominated rhodamine (6-Br-TMR, compound **26**), the xanthene precursor **25** was synthesized following the instructions of Miller et al.[90] Therein, bromophthalide was converted in a two-step radical bromination followed by hydrolysis to form

[2] Franziska Walterspiel synthesized the bifunctional MAP probe for the first time in her Master's Thesis under my supervision.

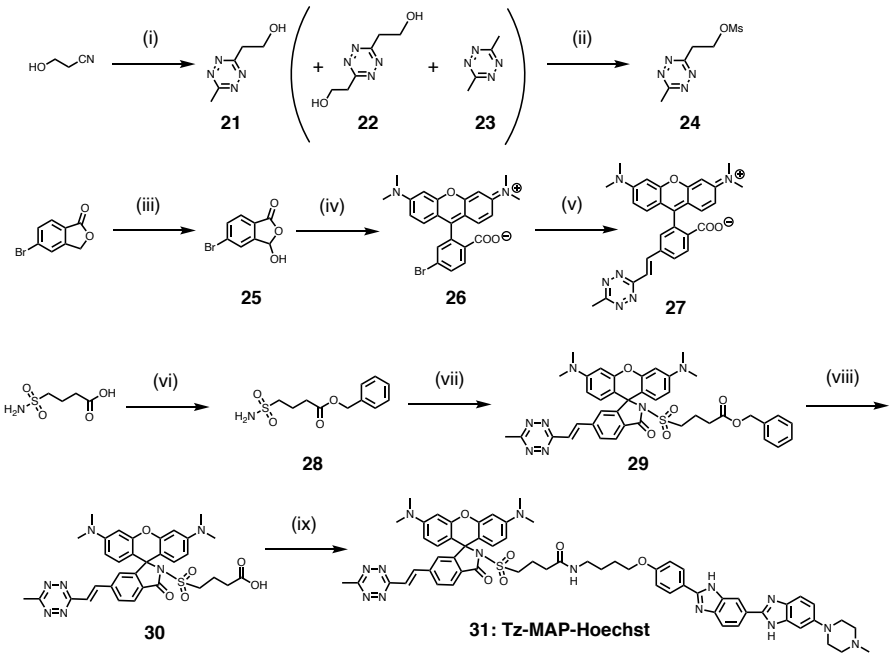

Scheme 2.3: Synthesis scheme: (i) 1) $Zn(OTf)_2$, MeCN, hydrazine hydrate, microwave, 70 °C, 15 h, 46%; 2) $NaNO_2$, 2 M HCl, pH 3 (ii) methanesulfonyl chloride, NEt_3, DCM, r. t., 10 min, 57%, (iii) 1) NBS, AIBN, DCM, reflux, 2 h; 2) water, reflux, 2 h, 94%, (iv) 3-*N,N*-dimethylaminophenol, propionic acid, *p*-TsOH, 90 °C, 18 h, 31%, (v) *N,N*-dicyclohexamethylamin, 1,2,3,4,5-pentaphenyl-1'- (di-tert-butylphosphino)ferrocene, $Pd_2(dba)_3$, DMF, microwave, 50 °C, 40 min, 57%, (vi) benzyl bromide, DIPEA, KI, DMF, r. t., 3 h, 55%, (vii) **27**, EDC $\times$ HCl, DMAP, DCM, 50 °C, o. n., 19%, (viii) H_2, Pd/C, methanol, r. t., 1 h, (ix) **6**, PyBOP, DIPEA, DMF, r. t., 2 h, 7% over 2 steps.

compound **25**. Compound **25** was then condensed with 3-dimethylaminophenol in propionic acid in the presence of catalytic amounts of *p*-TsOH to form compound **26**. In the reaction, the nucleophilic attack of 3-dimethylaminophenol occurs exclusively at the aldehyde carbonyl, ensuring the formation of the 6-regioisomer only. Compared to other procedures, there is no need for separation of the regioisomers in column chromatography, which is challenging.

The next step was the Heck elimination reaction yielding compound **27**. The *in situ* generated and highly volatile vinyl tetrazine is reacted in the microwave with compound **26** in the presence of $Pd_2(dba)_3$ and a ferrocene ligand under basic conditions. The power of the microwave was carefully chosen and turned out as a critical parameter to improve the reaction yield.

After cross-coupling, the tetrazine dye was further modified with sulfonamides. To generate a linker from the C3'-position to the Hoechst ligand, the carboxylic acid of 4-sulfamoylbutyric acid was converted into benzyl ester **28**. After activating the C3-carboylic acid of compound **27** with EDC $\times$ HCl, quenching with amine **28** in the presence of DMAP afforded compound **29**. The benzyl protecting group was then removed with H_2 and Pd/C to give compound **30**.

A final coupling step with compound **6** achieved the desired product **31**.

2.5.2 *In vitro* characterization of bifunctional MAP probe

The absorption and emission spectra of the bifunctional MAP probe were recorded (Figure 2.19). The absorption maximum is at λ= 555 nm. The emission maximum is at λ= 573 nm in PBS and shifting slightly to λ= 578 nm with hpDNA. The probe showed a weak fluorescence turn-on of 2.3-fold after 1 h incubation time.

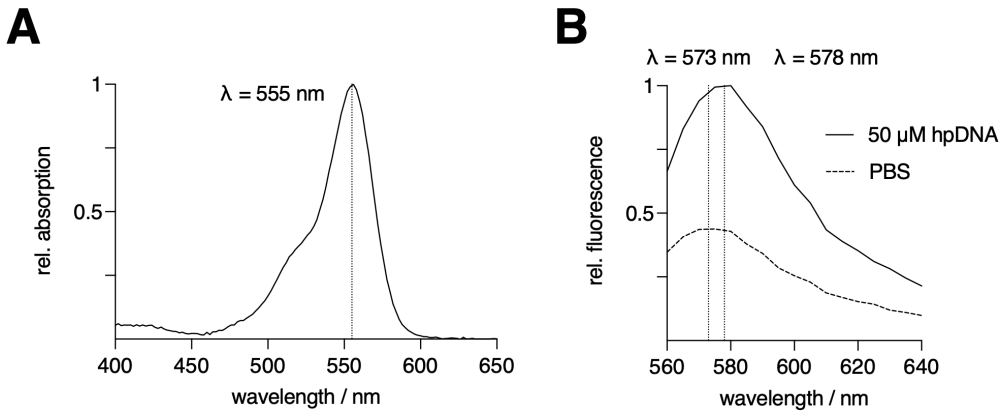

Figure 2.19: A) Absorption spectrum of 5 µM bifunctional MAP probe in 0.4% SDS. B) Emission spectrum of 5 µM bifunctional MAP probe excitation at 525 nm/10 nm and emission 560–640 nm/10 nm in PBS with and without 50 µM hpDNA after 1 h incubation time.

In comparison, H-SiR-MeTz showed 32-fold fluorescence turn-on using the same experimental conditions (see above). An explanation for the weak turn-on might be the highly closed spirolactones of MAP dyes, that might not open efficiently on DNA. Also, compared to other Hoechst-tagged xanthene dyes, the ligand is attached to a different position, which might result in worse binding or turn-on properties of the probe.

2.5.3 *In cellulo* characterization of bifunctional MAP probe

The bifunctional MAP probe **31** was tested in combination with vinyl-modified nucleosides prepared from all nucleobases (Figure 2.20, B).[3] For labeling experiments, U2OS cells were supplemented with VdU, VdA, VdC and VdG. The cells were then fixed and labeled with the bifunctional MAP probe **31** and subsequently with Hoechst33342.

The bifunctional MAP probe **31** successfully stained cells that were treated with VdU and VdC (Figure 2.20, A). The fluorescence intensity of the nuclei was then determined and visualized in a violin plot (Figure 2.20, C). VdU gave the highest fluorescence intensity, while VdC fluorescence was slightly weaker. Under the used imaging setting, no labeling was observed for VdA and VdG.

The $S_{pro}/N_{non\text{-}pro}$ of the bifunctional MAP probe **31** was lower compared to H-SiR-MeTz. For this reason, the idea was not further pursued.

[3] Franziska Walterspiel synthesized VdA, VdC and VdG in her Master's Thesis under my supervision.

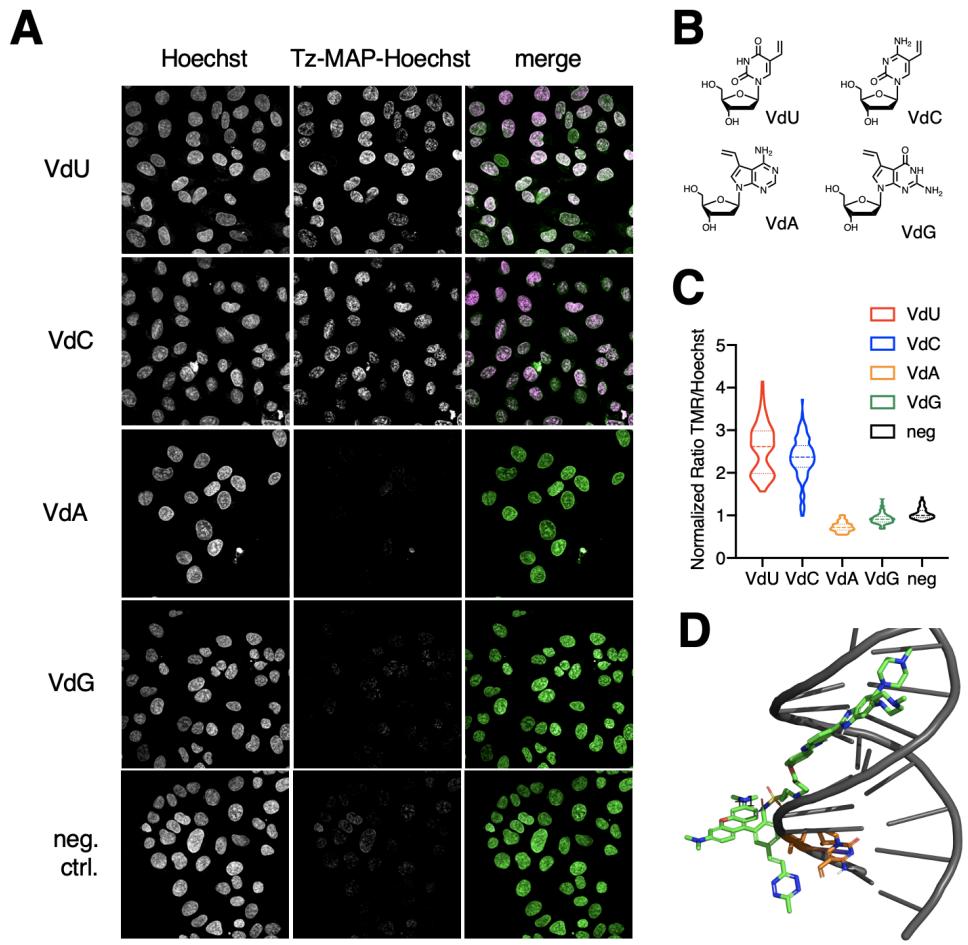

Figure 2.20: A) Confocal images (63x oil objective) of fixed U2OS TREx cells treated with VdU, VdC, VdA and VdG 100 µM each for 16 h and labeled with 0.5 µM MeTz-TMR-Hoechst **31** and subsequently Hoechst33342 (10 µg ml^{-1}). Scale bar: 20 µm. B) Chemical structures of vinyl-modified nucleosides. C) Quantification of microscopy data from experiment A (N = 62-117 cells). D) Structure created with PyMOL of MeTz-TMR-Hoechst **31** bound to DNA with tetrazine in close proximity to a modified VdC.

2.6 Summary

In summary, a probe H-SiR-MeTz **17** was developed that showed a proximity-enhanced reaction with a previously reported unnatural nucleoside, VdU, in fixed cells. Unique properties of this probe were the low background and the ability of the probe to label at very low concentrations. Besides confocal microscopy, H-SiR-MeTz **17** can be used in STED nanoscopy and the labeling in fixed cells was comparable to EdU. Replacing the methyl tetrazine with an H tetrazine in probe H-SiR-HTz **18** ultimately allowed live staining of proliferating cells.

To further improve the probe design, a probe based on the MaP strategy was synthesized. The new probe design did not show superior labeling in cells. For a future probe design, better quenching from the tetrazine and improved cell permeability would be advantageous. Similar to the probe design of the bifunctional MAP probe, a probe based on the HD dyes[128] could be envisioned.

3 Reactive adenosine derivatives

VdU was incorporated into DNA and labeled with a dipyridyl tetrazine as the first nucleoside for metabolic labeling with iEDDA.[48] While iEDDA reactions are generally suited to occur in living cells, the vinyl group reacts too slow (Theory 3.3).

To improve the labeling speed, modified nucleosides with faster reacting functional groups (e.g. norbonenes, cyclopropenes, BCN, or TCO) were investigated. Attaching those to a nucleoside would enable faster labeling after successful incorporation of the nucleoside.

Nevertheless, the incorporation of these large modifications is difficult, as the nucleoside has to be processed by various metabolic enzymes (Theory 2.2). Therefore, the nucleoside and linker have to be carefully chosen and different scaffolds, as well as linkers, should be screened.

Generally, all nucleobases can be modified without disturbing the Watson–Crick base pairing. Pyrimidine scaffolds are typically modified on position C5 of the pyrimidine ring, purines are mainly used as 7-deaza-analogs with modifications on the C7 position (Figure 3.1).

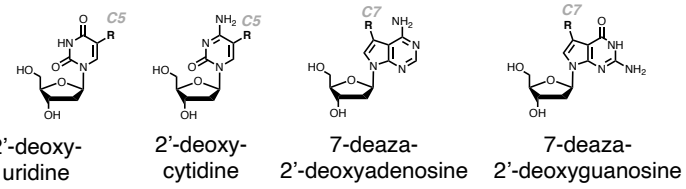

Figure 3.1: Nucleoside analog scaffolds with typical positions for modifications marked.

To date, most nucleosides for metabolic labeling are thymidine derivatives such as BrdU, EdU or VdU.[28] Additionally, thymidine derivatives are commonly used as dNTPs for *in vitro* applications.[164], [165], [166] Therefore, previous work in the Schultz lab and during my Master's project focused on modifying the thymidine scaffold. As initial attempts with thymidine derivatives did not give a signal in cells, the focus was shifted to other nucleobases.

Among purine analogs, alkyne-modified 7-deaza-2'-deoxyadenosine (EdA) was previously used for metabolic DNA labeling[47] and a variety of 7-deaza-adenosine derivatives were used for metabolic RNA labeling[100]. Similar to thymidine derivatives, modification on the C7 position of adenosine scaffolds was previously reported for *in vitro* iEDDA on oligonucleotides.[167] In particular incorporation of EdA, but also successful demonstrations of iEDDA *in vitro* were good starting points to modify a 7-deaza-adenosine derivative as a potential precursor for metabolic DNA labeling.

In addition to the nucleobase, the linker for the attachment of the modification can be of importance.[168] Therefore, reactive dienophiles were attached via different linkers (alkyne, alkane, and PEG) to 7-deaza-2'-deoxyadenosine (Figure 3.2).

To label the incorporated nucleoside, a cell-permeable tetrazine was developed based on the

MaP strategy[161] and previous findings (Chapter 2).

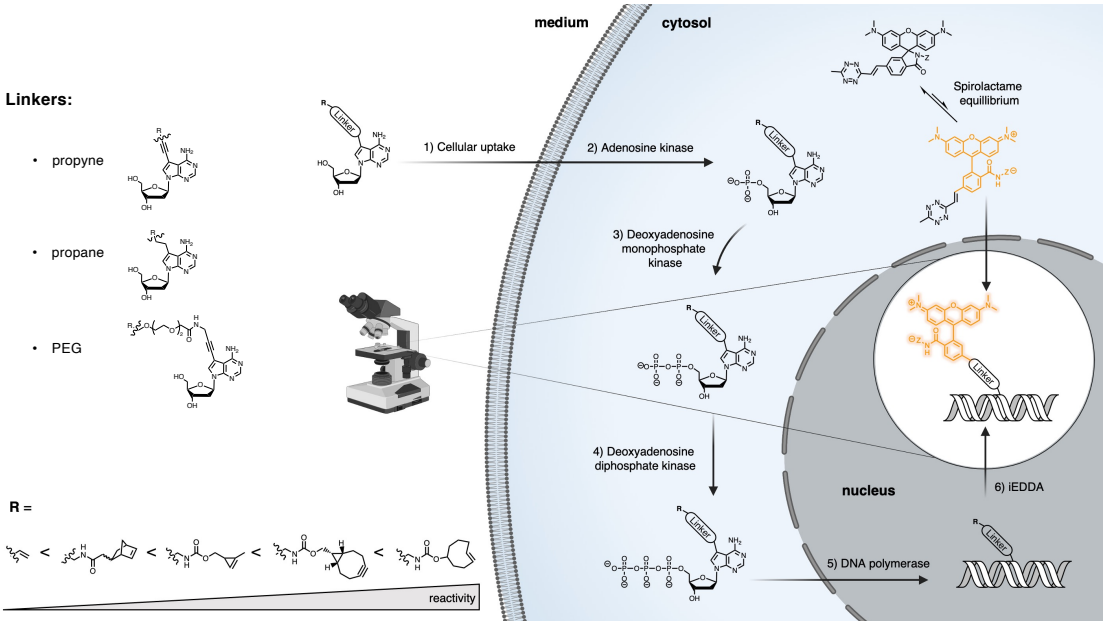

Figure 3.2: Modified 7-deaza-adenosine derivatives for metabolic DNA labeling: The nucleoside precursors are cell-permeable, then phosphorylated to their triphosphates and incorporated into DNA where they can be click labeled with a MAP tetrazine dye.

3.1 Synthesis

3.1.1 Reactive nucleosides

Adenosine derivatives were synthesized in a modular synthesis starting from commercially available nucleoside precursors (Scheme 3.1, Methods 2.4).

In a first S_N2 reaction, propargylamine was protected with trifluoroacetic anhydride (TFAA) to obtain compound **32**. Compound **32** reacted in the presence of copper(I) iodide and tetrakis-(triphenylphosphine)-palladium under basic conditions with 7-iodo-7-deaza-2'-deoxyadenosine to form compound **34** in a Sonogashira reaction. For purification purposes, an ion-exchange resin was optionally added to the reaction mixture before normal phase separation to counteract strong tendencies of nucleosides for salt formation.[169], [170] Alternatively, reversed-phase separation has proven to be an efficient purification method.

The resulting C3 propyne linker was then reduced to a saturated linker or directly deprotected in ammonia. The reduction was carried out in methanol using triethylsilane as a source of for hydrogen and Pd/C as a catalyst and resulted in the fully saturated linker of compound **39**.

The cleavage of the protecting group was realized for compounds **34** and **39** in ammonia and gave compounds **35** and **40**. Complete removal of ammonia after the deprotection was crucial as it can react with activated carboxylic acids in the subsequent coupling reactions to form amides.

The final step was the peptide bond formation with NHS esters of the respective dienophiles under standard conditions with DIPEA in DMF. This enabled the synthesis of compounds **36**-**38**,

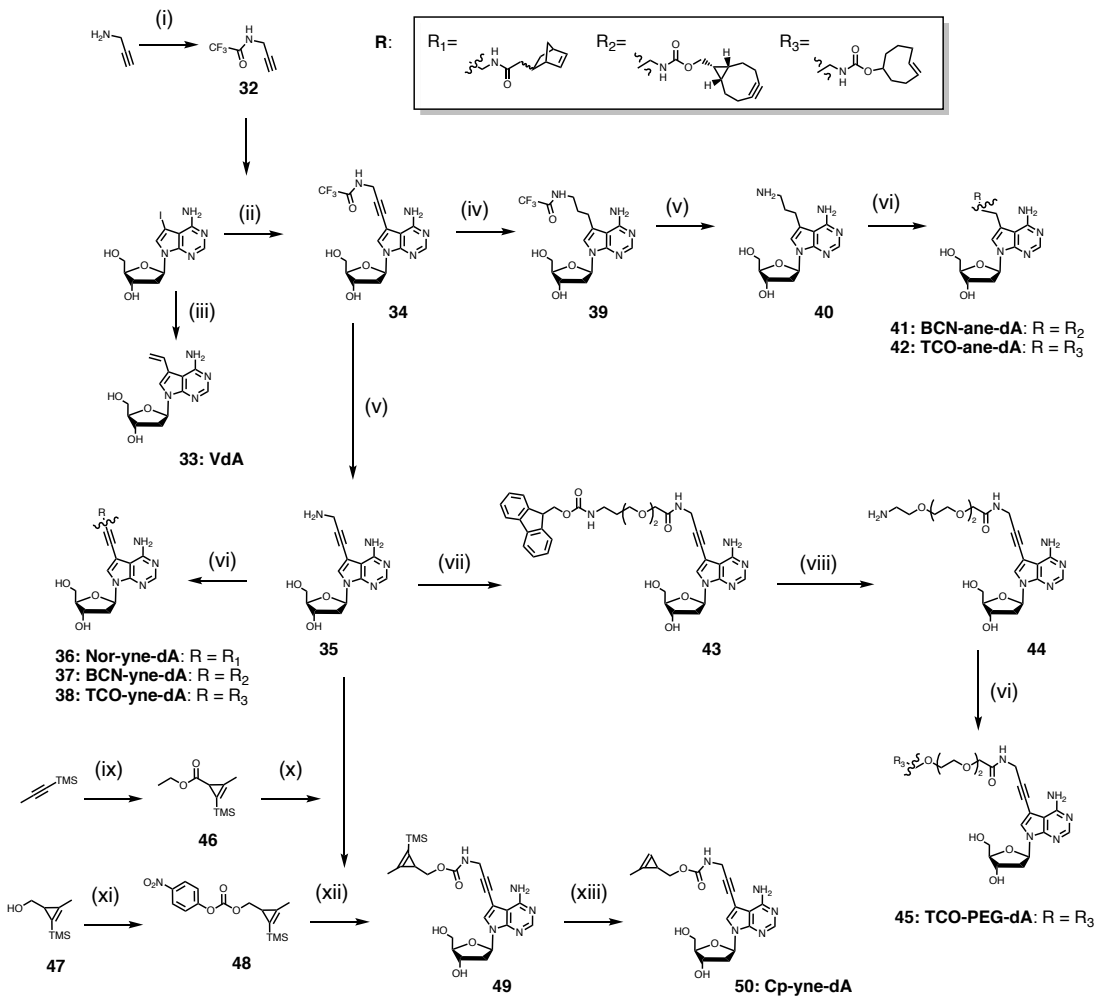

Scheme 3.1: Synthesis scheme reactive nucleosides: (i)TFAA, DCM, r. t., 16 h, 76%, (ii) CuI, $Pd(PPh_3)_4$, NEt_3, DMF, r. t., 16 h, 87%, (iii) tributyl(vinyl)tin, triphenylarsine, $Pd_2(dba)_3$, DMF, r. t., 18 h, 98%, (iv) Et_3SiH, Pd/C, MeOH, r. t., 4 h, 64%, (v) $NH_{3,aq}$, r. t., 3 h, 75%, (vi) NHS ester, DIPEA, DMF, 25–50 °C, 1–6 h, 52-83%, (vii) Fmoc-HN-PEG3-COOH, TSTU, DIPEA, DMF, r. t., 30 min, 71%, (viii) piperidine in DMF, r. t., 1 h, 82%, (ix) diazo ethyl acetate, $Rh_2(OAc)_4$, DCM, 0 °C, 4 h, (x) DIBAL-H, Et_2O, 0 °C, 30 min, 36% over two steps, (xi) *p*-nitrochloroformate, DIPEA, DMAP, DCM, r. t., 16 h, 39%, (xii) **35**, DIPEA, DMF, r. t., 16 h, (xiii) TBAF, THF, r. t., 48 h, 28% over 2 steps.

41 and **42**.

To obtain a longer linker, an amine-reactive PEG linker was installed and gave compound **43**. The bifunctional linker was initially Fmoc protected and later deprotected with piperidine to give compound **44**. The free amine **44** was then coupled as previously described yielding compound **45**.

To realize a cyclopropene modification, the TMS-protected, *p*-nitro benzyl-protected precursor was synthesized according to published procedures.[171], [172] Thereby, ethyl diazoacetate and 1-(trimethylsilyl)propyne undergo an $Rh_2(acac)_2$ catalyzed carbene insertion reaction. The volatile product, compound **46**, was then concentrated before it was reduced with DIBAL-H to the corresponding alcohol **47**.

To further couple the cyclopropene alcohol, it was activated as a *p*-nitrophenol carbamate **48**.[1] The subsequent coupling was then carried out under basic conditions in DMF to give the intermediate **49**. The cyclopropene-stabilizing TMS group was then removed and yielded the final product **50**. TBAF deprotection was a critical step, as the reaction can be slow and the yield varied with the reaction scale.

3.1.2 Tetrazine probes

Similar to the presented approach for obtaining the bifunctional MAP probe **31**, advanced tetrazine probes for labeling the modified adenosine derivatives were synthesized (see section 2.5, Scheme 3.2, Methods 2.3). Tetrazines **51** and **52** have a higher tendency to form the non-fluorescent spirolactone form compared to their TMR counterparts, which may result in better cell permeability and lower background.[115]

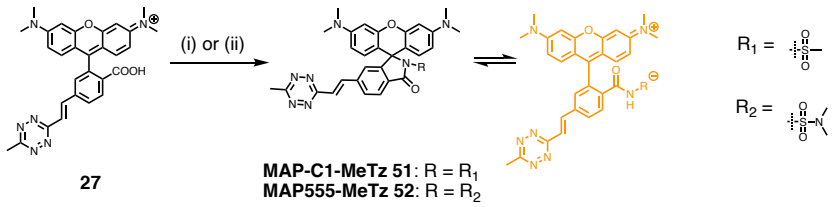

Scheme 3.2: Synthesis scheme MAP tetrazines: (i) MAP-C1-MeTz: methanesulfonamide, EDC × HCl, DMAP, MeCN, 50 °C, o. n., 26%, (ii) MAP555-MeTz: [methyl(sulfamoyl)amino]methane, EDC × HCl, DMAP, MeCN, 50 °C, o. n., 17%.

3.2 *In cellulo* characterization

After synthesizing a small library of nucleoside analogs and tetrazines, the compounds were tested in cells. In the first step, cytotoxicity of the nucleosides was addressed, before their incorporation was studied by mass spectrometry. Finally, the labeling was optimized in fixed and live cells.

3.2.1 Cytotoxicity assay

The incorporation of modified nucleosides can prove detrimental to cell viability.[173] This has been investigated using EdU, VdU and EdA, where genotoxic and cytotoxic effects have been reported.[48], [47] These likely result from interactions with enzymes of nucleoside metabolism as well as induction of double-strand breaks.[26],[53]

Importantly, a 7-deaza-adenosine derivative had been reported as cytotoxic agent with nanomolar activities in cancer cells.[174] Thus, it was investigated if the here synthesized compounds can be tolerated by cells at concentrations that allow signal generation in subsequent assays.

In the experiment, U2OS cells were treated with different doses of unnatural nucleosides and the cellular respiratory activity was measured with a MTS cytotoxicity assay (Figure 3.3,

[1] The cyclopropene alcohol was synthesized during my Master's Thesis.

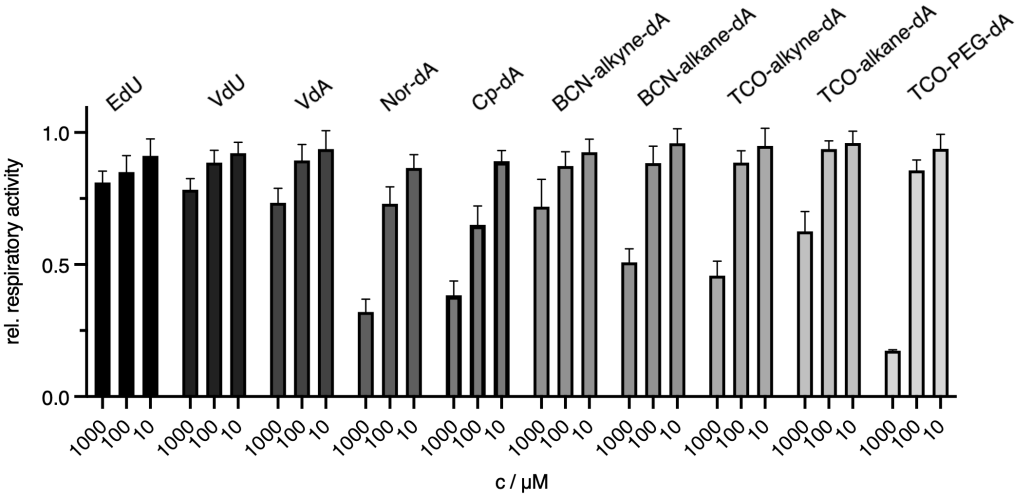

Figure 3.3: Cell viability assay of reactive 7-deaza-2'-deoxyadenosine derivatives and EdU and VdU for comparison after 24 h incubation time with U2OS TREx cells in various concentrations of nucleosides (10–1000 µM). The relative respiratory activity with respect to a DMSO negative control is plotted. Shown are N=9 replicates from three independent experiments and error bars represent the standard deviation.

Methods 5.3). The experiment confirmed slightly higher toxicity for EdU than VdU as previously reported.[48] Even higher toxicity was noticed for adenosine derivatives, similar to the reported toxicity of EdA.[47]

For microscopy experiments, the viability of $>$80% at 100 µM was considered sufficient to study the incorporation of the nucleoside by mass spectrometry and labeling by means of fluroescence microscopy in further experiments.

3.2.2 Mass spectrometry

The incorporation of unnatural nucleosides sets the basis for metabolic labeling. In addition, high incorporation yields are important for obtaining a good signal after labeling in microscopy experiments.

Mass spectrometry analysis was established to study the incorporation of new nucleoside analogs into DNA. After 1 h and 24 h incubation time of 100 µM TCO-yne-dA **38** in U2OS cells, genomic DNA was isolated, digested and subjected to multiple reaction monitoring (MRM) measurements (Methods 5.4). Stringent washing steps ensured the removal of free nucleosides and nucleotides from the analyzed samples.

For 1 h incubation time, a small signal for the MRM transition was observed, while no signal was detected in absence of nucleoside (Figure 3.6, A).[2] After 24 h incubation with TCO-yne-dA **38**, the MRM signal significantly increased, which suggests that the nucleoside was incorporated.

However, the incorporation yield was roughly 100000-fold lower than for VdU and EdU. Nevertheless, due to the expected efficient labeling reaction of the more reactive dienophiles, it was

[2]Samples were analyzed by Dr. Sebastian Fabritz, MS facility MPImR.

encouraging to evaluate the performance of the compounds in microscopy experiments.

3.2.3 Fluorescence microscopy

Fixed cells

Next, it was assessed if the incorporation yield is sufficient to generate a nuclear signal in fixed cells. The unnatural nucleosides were added to U2OS cells and labeled with MaP-C1-MeTz **51** (Methods 5.6.4).

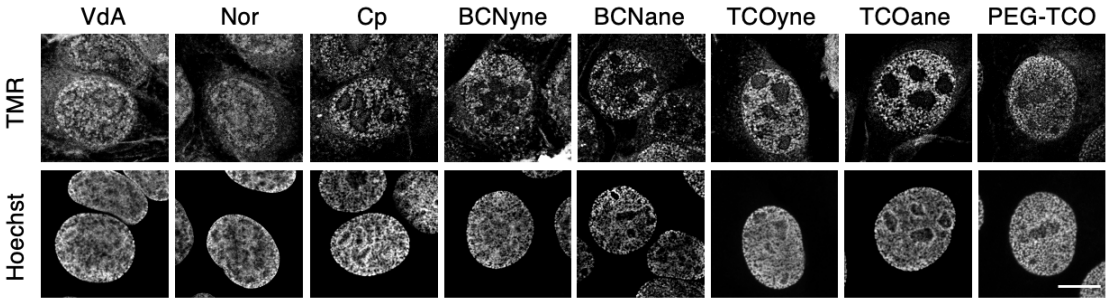

Figure 3.4: Representative confocal images of U2OS TREx cells after 8 h feeding with 100 µM nucleosides, PFA fixation, HCl denaturation, and labeling with 5 µM MAP-C1-MeTz **51** at room temperature for 16 h. Images were acquired using different laser intensities. One of two independent experiments is shown. Scale bar = 20 µm.

The samples treated with nucleoside analogs showed a brighter signal in the nuclei compared to non-treated cells. The fluorescence signal generally improved with higher reactivity of the dienophile, which indicated that only poor labeling efficiencies were achieved with low-reactive nucleosides (Figure 3.4 and SI-Figure 4.11).

Nucleosides with propane-linker showed more specific signal in the nucleus and less signal in the cytosol than with propyne-linker. The propane linker is more flexible than the propyne linker, which might be better for substrates of endogenous enzymes.

The lowest signal-to-noise was detected for VdA **33** and Nor-yne-dA **36**. The most specific signal was obtained for TCO-ane-dA **42**. Labeling was also observed for the compound containing a PEG linker, but the signal-to-noise of TCO-PEG-dA **45** was smaller compared to TCO-yne-dA **38** and TCO-ane-dA **42**. The images of TCO-PEG-dA **45** and Cp-yne-dA **50** were comparable. BCN derivatives **37** and **41** showed good nuclear signal, but also a tendency to form aggregates.

The punctuate-like labeling pattern of the cells was different from the EdU or VdU labeling pattern and most cells showed early S-phase labeling (Chapter 2). To study the adverse effects of the nucleosides on cell cycle progression, pulse-chase experiments of TCO-ane-dA **42** and EdU were performed (Methods 5.6.4). Therein, U2OS cells were first treated with TCO-ane-dA **42** for 4 h, and then EdU for 4 h before fixation and labeling with MAP-C1-MeTz **51**. In a control, only EdU was supplemented for 4 h. While signal was detected from TCO-ane-dA **42**, the EdU signal was weaker compared to the control (Figure 3.5). These data suggest that TCO-ane-dA **42** incorporation leads to stalled DNA synthesis with subsequent cell cycle arrest during S-phase.[160]

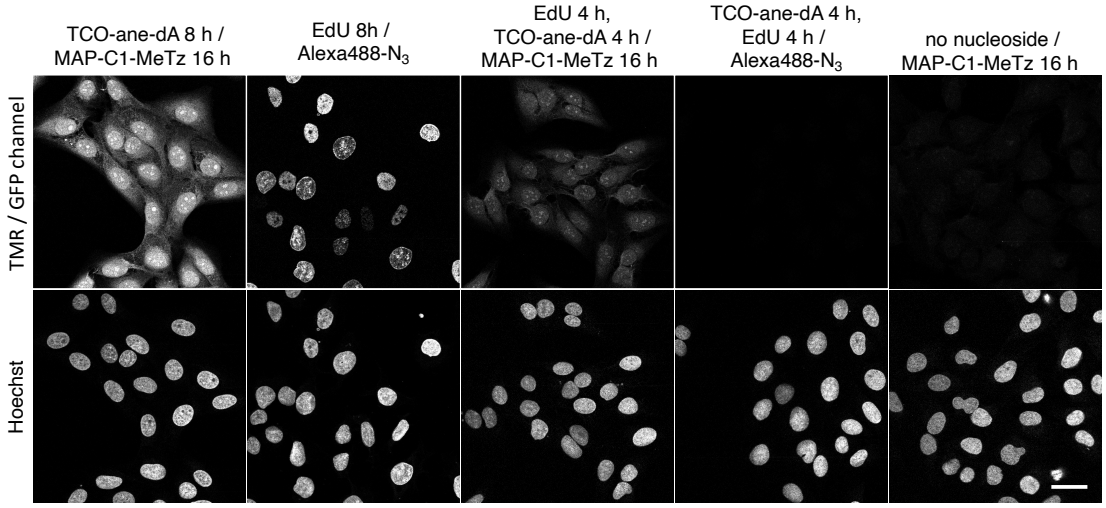

Figure 3.5: Pulse-chase experiments with TCO-ane-dA **42** and EdU. Cells were treated with 100 µM TCO-ane-dA **42** and/or 10 µM EdU, fixed and stained. Scale bar = 50 µm.

Live cells

While iEDDA reactions have been previously successfully used to label newly synthesized DNA in HCl denatured cells[48], this could not yet be achieved in living cells. Therefore, despite signs of cell cycle disruptions, the nucleosides were used to label DNA in living cells (Methods 5.6.5).

For live-cell experiments, only BCN and TCO dienophiles were suited, due to their higher reactivity. Whereas TCO nucleosides **38** and **42** gave nice labeling results in confocal imaging, the formation of aggregates was observed again for BCN nucleosides **37** and **41**.

In a comparison of different tetrazine dyes, MAP-C1-MeTz **51** was chosen for live-cell experiments, as it exhibited the brightest fluorescent signal while having low background.

For TCO-yne-dA **38** the incubation time for nucleoside treatment and labeling with MAP-C1-MeTz **51** were optimized. A minimum of 4 h for feeding and labeling time each was required to observe a signal and a washing step was included in-between. After labeling, it was sufficient to change the medium once before image acquisition.

The background in live-cell experiments cleared up within about 1 h post labeling. Before, a diffuse signal in the nuclei may be observed. Therefore, longer incubation times were generally favorable for the signal-to-noise ratios. The blurred signal is likely free nucleotide mono-, di- or triphosphate that is slowly dephosphorylated and then washed out. The presented image shows U2OS cells that were treated with TCO-yne-dA **38** for 8 h and image acquisition after another 12 h incubation time with the tetrazine (Figure 3.6, B).

Nevertheless, long incubation times come at the cost of time resolution. Also, toxic effects have to be considered, as cells can start to detach gradually after several hours. The toxicity is most likely a result of the nucleoside, but not the tetrazine (Subsection 3.2.1).

Next, the signal of TCO-yne-dA **38** and TCO-ane-dA **42** with different doses of nucleoside was compared. TCO-ane-dA **42** showed a brighter signal in the nucleus compared to TCO-yne-dA **38** (Figure 3.6, D). A brighter signal for the saturated linker confirmed the results, that were already observed in fixed cells.

To verify that the observed signal was showing incorporated nucleoside, a titration experiment

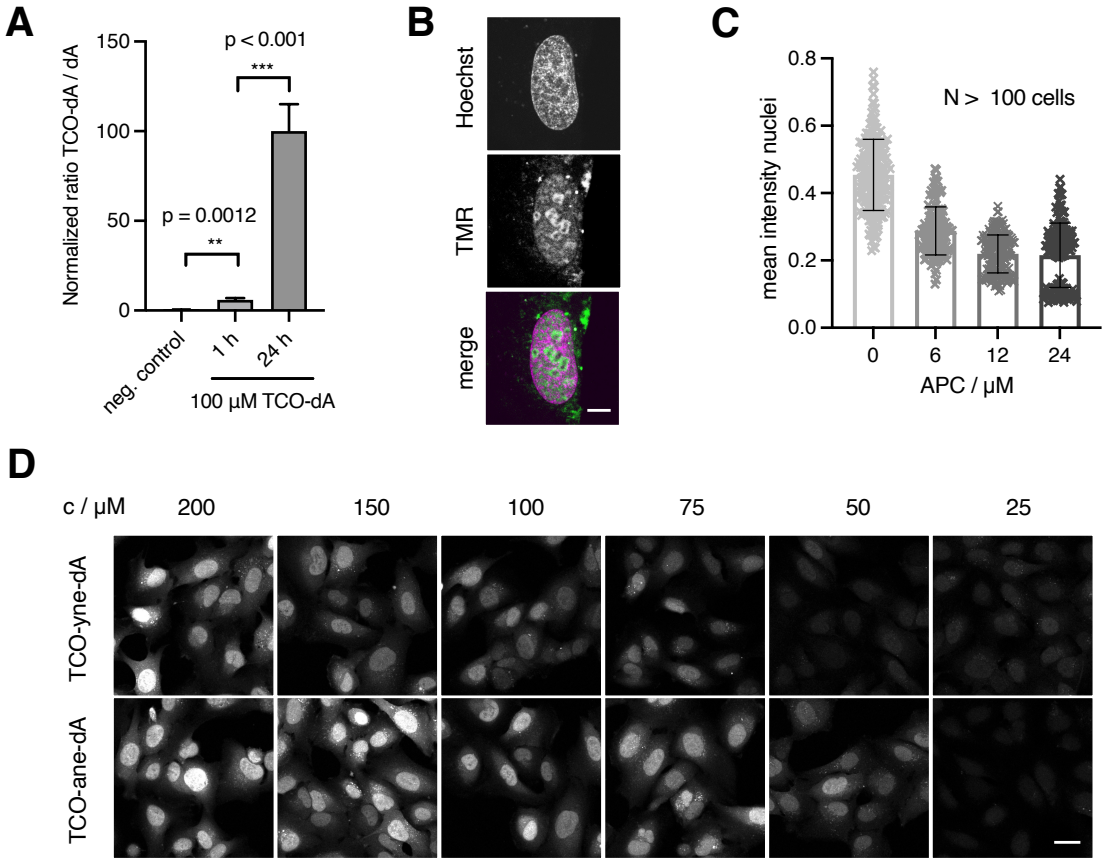

Figure 3.6: A) Incorporation yield of TCO-yne-dA **38** investigated by MS MRM analysis of digested genomic DNA isolated from 8 $\times$ 10^6 U2OS TREx cells that were fed with 100 µM TCO-yne-dA **38** for 1 h and 24 h, respectively. Data from N=3 independent experiments. Error bars represent the standard deviation. P-values were determined in GraphPad Prism 9.0 in an unpaired t-test. B) Confocal images of U2OS TREx cells after incubation with TCO-yne-dA **38** for 4 h and subsequent labeling for 11 h with MAP-C1-MeTz **51**. The cells showed a staining pattern consistent with the late S-phase.[158] Scale bar = 10 µm. C) Inhibition of DNA synthesis using APC: Cells were incubated with 100 µM TCO-ane-dA **42** for 8 h in presence of indicated concentrations of APC before fixation and click labeling. Intensities of signals within nuclei have been quantified CellProfiler 4.2.1 and normalized to the maximum gray value. D) Dose-dependent staining for 25–200 µM TCO-yne-dA **38** and TCO-ane-dA **42**. Scale bar = 20 µm.

was performed with TCO-ane-dA **42** and APC. Upon the addition of APC, the signal intensity dropped, indicating inhibition of the incorporation of the nucleoside (Figure 3.6, C).

3.3 Summary

Specific labeling of genomic DNA in living cells was achieved with 7-deaza-adenosine derivatives for the first time. This result is especially strong in consideration of low incorporation efficiencies (c.f. MS experiment) and potential disruption to DNA synthesis. If these drawbacks could be overcome in future experiments the approach could prove valuable for observing DNA synthesis in living cells. Of note, these compounds might also be employed as probes to study DNA damage following stalling of replication forks[160], but this needs to be elucidated in future

studies.

To overcome the drawback of cytotoxicity arising from 7-deaza-2'-deoxyadenosine derivatives a better understanding of their mode of action would be important.

If the toxicity was due its incorporation into DNA, DNA repair mechanisms are initiated and can be studied by immunostaining of γH2AX formation[176] or by following accumulation of 53BP1 foci[177].

In the case, that toxicity is related to interactions of metabolic enzymes, it is also possible to add another anti-metabolite to the experiments. For EdC, cytotoxicity was reduced in some cell lines after the addition of thymidine without loss of fluorescence intensity.[44] The reduction in toxicity was explained by specific interactions of EdC with the dTMP synthetase.[44] Supplementing additional nucleosides to rescue metabolic enzymes in the purine biosynthesis could be therefore imagined.

To tackle low incorporation efficiencies, metabolic enzymes (e.g. kinases, polymerases) can be engineered for more efficient phosphorylation and incorporation of 7-deaza-2'-deoxyadenosine derivatives. For proteins, a similar approach was very successfully implemented by engineering of an orthogonal tRNA synthetase.[163],[178] Originally developed in bacterial cells, the tool was in the meantime adapted for cultured mammalian cells and is widely used.[179], [180]

Viral kinases can give a starting point to engineer kinases that tolerate larger modifications (Subsection 2.2.2). As such, engineering was performed with HSV-TK1 for a gene therapy as the primary goal, but these findings could be useful to develop a molecular tool.[181],[182] Engineering was also reported for a kinase[183] and a phosphoribosyltransferase[184] involved in RNA metabolism.

All in all, the combined approach of a modified nucleoside with an engineered metabolic enzyme could pave the way for efficient labeling of DNA in living cells with good time resolution.

4 Fluorogenic nucleosides and pro-nucleotides

7-Deaza-adenosine derivatives gave signals in cells when used as metabolic precursors (Chapter 3). Due to a two-component system with a reporter nucleoside and an additional labeling reagent, the labeling was slow because the cells had to be incubated with both reagents for several hours.

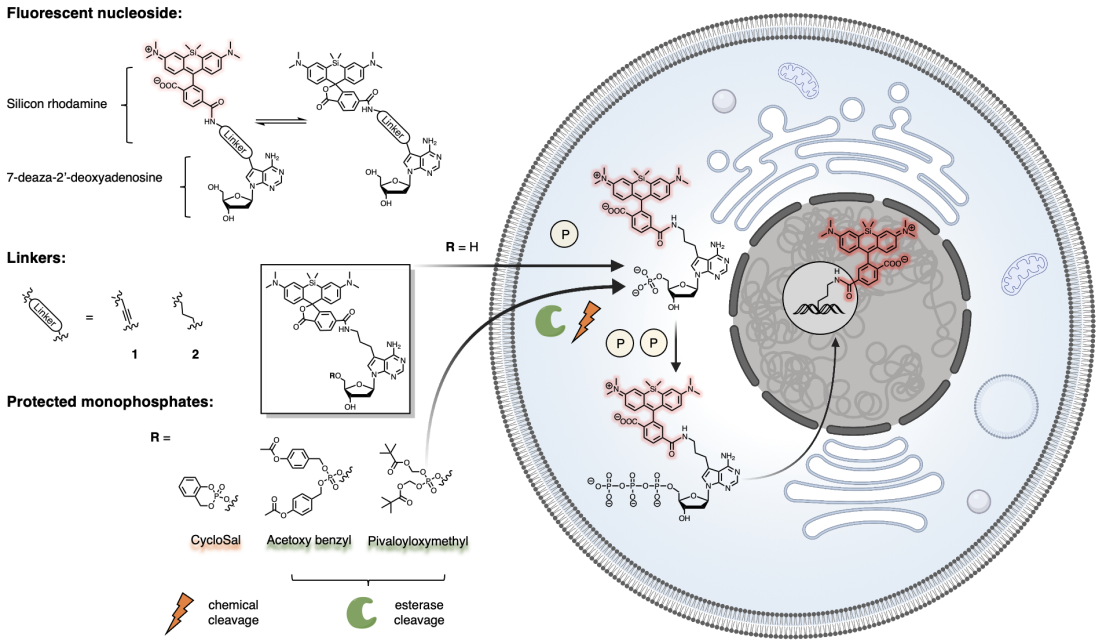

Figure 4.1: Fluorescent nucleosides based on SiR modified 7-deaza-2'-deoxyadenosine scaffolds for metabolic labeling of DNA. The unnatural nucleoside analogs were designed for delivery as nucleosides with two linkers, or protected monophosphates (pro-nucleotides) with three different protecting groups.

To improve time resolution in metabolic DNA labeling, a fluorescent nucleoside with a turn-on after incorporation into DNA was envisioned (Figure 4.1). This fluorogenic nucleoside would allow to obtain a signal directly after its incorporation and promise therefore better time resolution compared to a split system.

The chosen probe design was based on findings on reactive adenosine derivatives and the 7-deaza-2'-deoxyadenosine scaffold was this time modified with the fluorogenic SiR dye. SiR can exist in an open and closed state and can therefore be silent when only present in the cell, but is fluorescent in a polar environment (e.g. after incorporation into DNA, Theory 4.1).

To the best of my knowledge, no fluorescent nucleoside precursor was reported that was

metabolized in a cell. However, fluorescent nucleosides were previously microinjected [63] and delivered with a nucleotide transporter[64],[65] (Theory 2.2.4).

As fluorophores are significantly larger modifications compared to small reactive groups, endogenous enzymes are less likely to accept them as their substrates. Therefore, fluorogenic nucleosides were also synthesized as pro-nucleotides with different protecting groups to improve the incorporation yield as previously demonstrated for other metabolic precursors (Theory 2.2.3).

The drawbacks of pro-nucleotides are the (i) challenging synthetic preparation[185], and (ii) adjusting the right balance between extracellular stability and fast intracellular cleavage of the group.

To find a protecting group with a suited half-live, three protecting groups were used: pivaloyloxymethyl (POM) group, acetoxybenzyl (AB), and cyclosaligenyl (CycloSal) esters (Figure 4.2). The POM and AB group are cleaved by carboxylesterases, CycloSal is a chemically labile group.

I **Pivaloyloxymethyl (POM) groups** are cleaved by carboxylesterases in a two-step mechanism in two consecutive cycles. Upon cleavage of the pivaloyl ester, a chemically labile intermediate is formed. In a subsequent chemical rearrangement, formaldehyde is released to liberate a phosphate diester. In the second cycle, the same process is repeated. The second ester cleavage occurs slower as the negative charge on the monophosphate diester repels the attack of the carboxylesterase.

   POM groups were used to generate a less toxic derivative of EdU[58] or facilitate the incorporation of AmdU into genomic DNA of cells and zebrafish [54]. Apart from nucleotide prodrugs pivaloyl groups were used to cage fluorophores.[186]

II The **acetoxybenzyl (AB) esters** were developed to improve drawbacks of a POM group. Other than pivaloyl esters, methyl esters are cleaved faster due to less sterical hindrance by esterases.[187], [188],[189] Additionally, the benzoyl linker serves as a spacer between the phosphodiester after the first cleavage to shield the negative charge.[190],[191] This comes with the price that liberation of the phosphate is now limited due to a slower chemical rearrangement of the *para*-hyrodroxy benzoyl group.

   AB groups were used in a comparative study of AmdU pro-nucleotides but showed only poor performance.[54]

III **Cyclosaligenyl (CycloSal) esters** were developed by Meier et al.[192] Their advantage is their small size and fast cleavage, as they are chemically labile without the need for an enzyme. There is a major pathway of the cleavage in which nucleophilic attack of a hydroxide ion is followed by a spontaneous C-O-bond cleavage releasing a quinone methide. Besides, an S_N1 reaction can occur as a side reaction, in which a carbocation intermediate is formed, which is then attacked by a hydroxy ion. As no further cleavage for the remaining bond is observed, this is a dead-end and therefore undesired.

   CycloSal groups were used in combination with EdU for metabolic DNA labeling.[59]

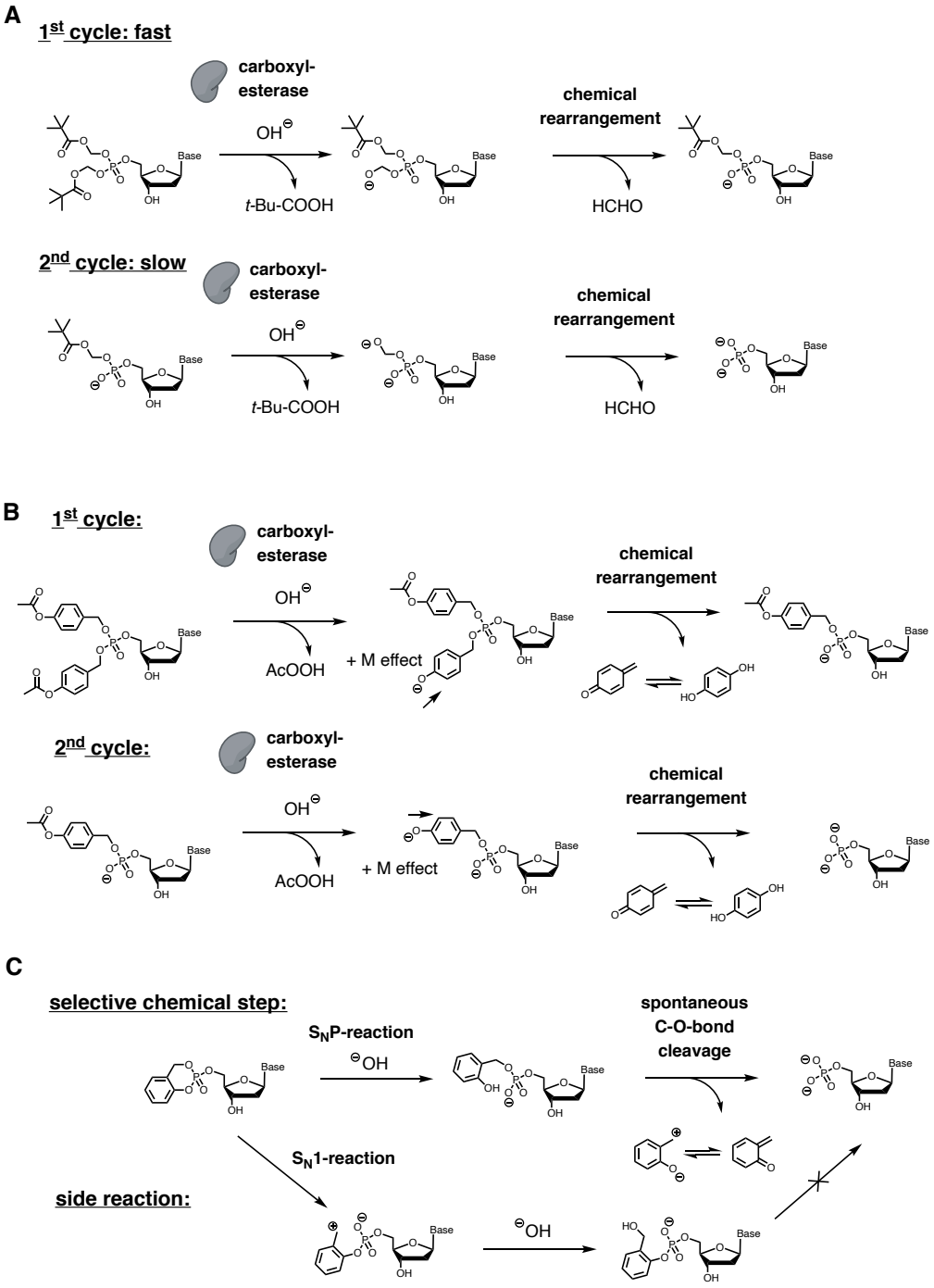

Figure 4.2: Cleavage mechanism of esterase and chemical labile protecting groups.

4.1 Synthesis

Fluorescent nucleosides SiR-yne-dA **55** and SiR-ane-dA **56** were synthesized analogical to the reactive adenosine derivatives (Scheme 4.1, Methods 2.5).

The SiR building block **53** was obtained from custom synthesis. Before coupling SiR to the nucleosides, it was activated with TSTU (compound **54**). Compound **54** then reacted with

compounds **35** and **40**, and gave compounds **55** and **56** after peptide bond formation.

To obtain the thymidine derivative SiR-yne-dU **58**, compound **54** was first coupled with propargylamine. The product **57** was then used in a Sonogashira reaction to form compound **58**. There were attempts to reduce the alkyne linker of SiR-yne-dU with H_2 and Pd/C which led to the destruction of the SiR scaffold.

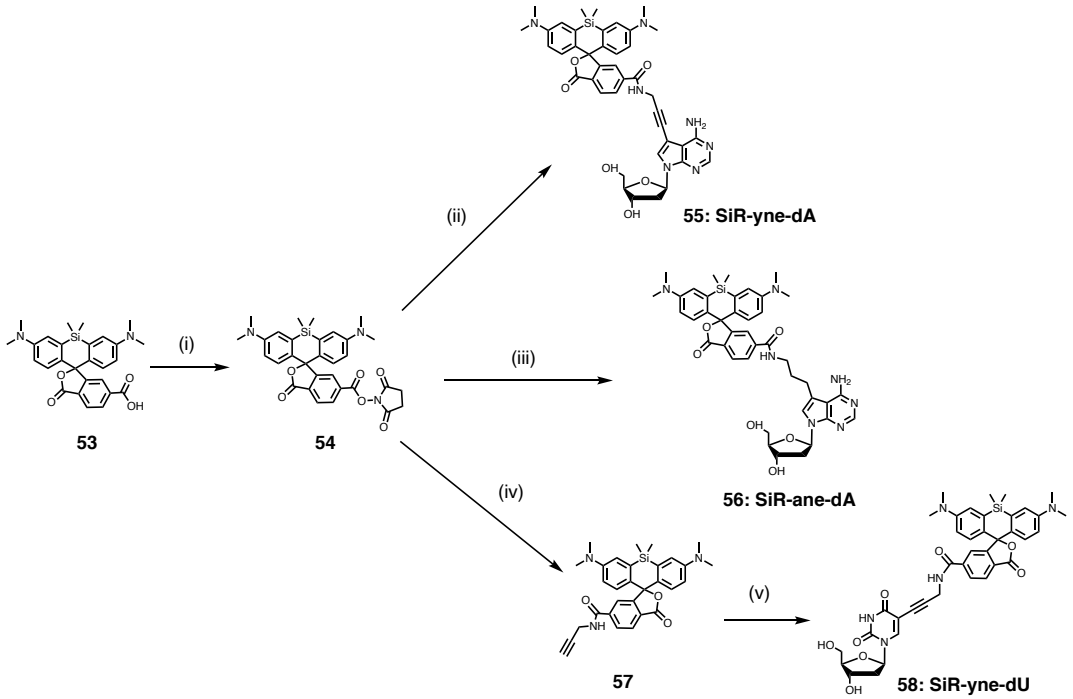

Scheme 4.1: Synthesis scheme fluorogenic nucleosides: (i) TSTU, DIPEA, DMF, r. t., 30 min, 91%, (ii) compound **35**, DIPEA, DMF, r. t., 2 h, 81%, (iii) compound **40**, DIPEA, DMF, r. t., 4 h, 74%, (iv) propargylamine, DIPEA, DMF, r. t., 30 min, 86%, (v) 5-iodo-2'-deoxyuridine, CuI, $Pd(PPh_3)_4$, DIPEA, DMF, r. t., 18 h, 40%.

Next, pro-nucleotides were synthesized from compound **56** by two synthetic routes for POM-SiR-ane-dA **63** (Scheme 4.2, Methods 2.5).

In the first route, (tris)POM phosphate **59** was synthesized from trimethyl phosphate by refluxing with chloromethyl pivalate and NaI in acetone (Scheme 4.2, A). Compound **59** was stirred in piperidine to form a bis(POM) phosphate salt **60**. After purification with an ion-exchange resin, phosphate **61** was obtained. Compound **61** was transformed into a chloride with a Vilsmeier reagent by adding thionyl chloride and catalytic amounts of DMF. The chloride **62** can then react with the SiR-ane-dA **56** to form the pro-nucleotide POM-SiR-ane-dA **63**. The route gave only small amounts of compound **63**, due to low yields in the last coupling step.

Therefore, an alternative route to synthesize POM-SiR-ane-dA **63** via alkylation of SiR-ane-dA monophosphate **68** was evaluated (Scheme 4.2, B). For this attempt, a benzyl protecting group for propargylamine was chosen, other than for the previously presented synthetic route in Scheme 3.1. The advantage was that all protecting groups could be removed at once in a later hydrogenation step.

The synthesis started by protecting propargylamine with chlorobenzyl formate. The resulting compound **64** was converted into nucleoside precursor **65** in a Sonogashira reaction. Subse-

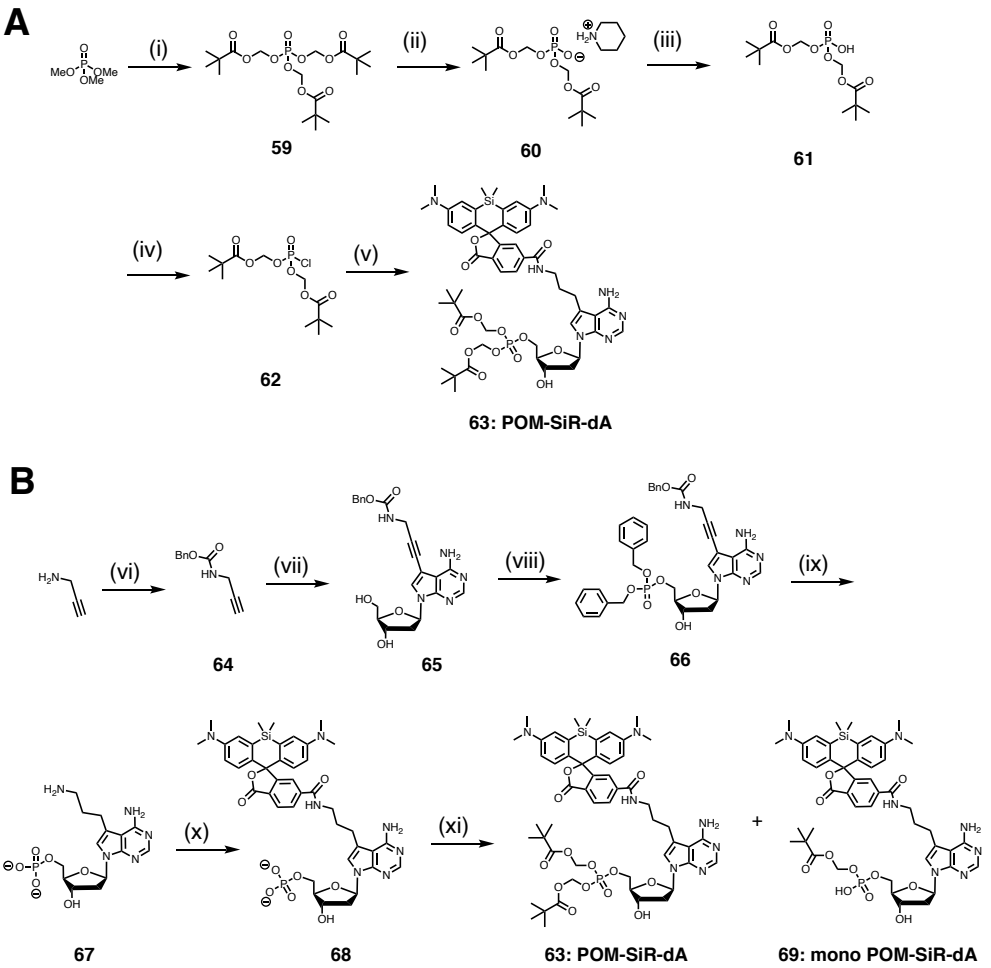

Scheme 4.2: Synthesis scheme pro-nucleotides: (A) (i) chloromethyl pivalate, NaI, acetone, reflux, 18 h, 36%, (ii) piperidine, r. t., 18 h, 63%, (iii) sephadex, 29%, (iv) $SOCl_2$, DMF_{cat}, DCM, 0 °C → r. t., 2 h, 95%, (v) pyridine, DMAP, –40 °C → r. t., 18 h, <1%; (B) (vi) chlorobenzyl formate, DIPEA, DCM, r. t., 16 h, 70%, (vii) CuI, $Pd(Ph_3)_4$, NEt_3, DMF, r. t., 16 h, 73%, (viii) 1) dibenzyl-*N,N*-di*iso*propylphosphoramidite, tetrazole, MeCN, 0 °C → r. t., 2 h, 2) AcOOH, –40 °C → r. t., 2 h, 47%, (ix) 20% Pd/C, MeOH/AcOH = 3/1, H_2, 5-10 bar, 16 h, 59%, (x) SiR-6-COOSu **54**, DIPEA, MeCN, r. t., 6 h, 54%, (xi) chloromethyl pivalate, Cs_2CO_3, DMSO, 48 h, 40 °C, 28% and 43%.

quently, a phosphate group was installed by first performing an S_N2 reaction of the 5'-OH group of compound **65** with dibenzyl-*N,N*-di*iso*propylphosphoramidite, and *in situ* oxidation with *t*-butyl hydroperoxide. All benzyl groups of compound **66** were then removed by hydrogenation giving rise to amine **67**. Amine **67** was coupled with activated SiR **54**.

In the final step, the POM protecting group was installed in an alkylation reaction by adding pivaloyloxymethyl chloride under basic conditions and stirring for 48 h. Besides the desired bisalkylated product **63**, the monoalkylated product **69** was isolated. The final alkylation step resulted in low yields presumably because the negatively charged starting material exhibited poor solubility in organic solvents.

CycloSal-SiR-dA **71** was synthesized from two routes (Scheme 4.3, Methods 2.5). Both started with phosphorus trichloride. The main difference was the reactive species that was

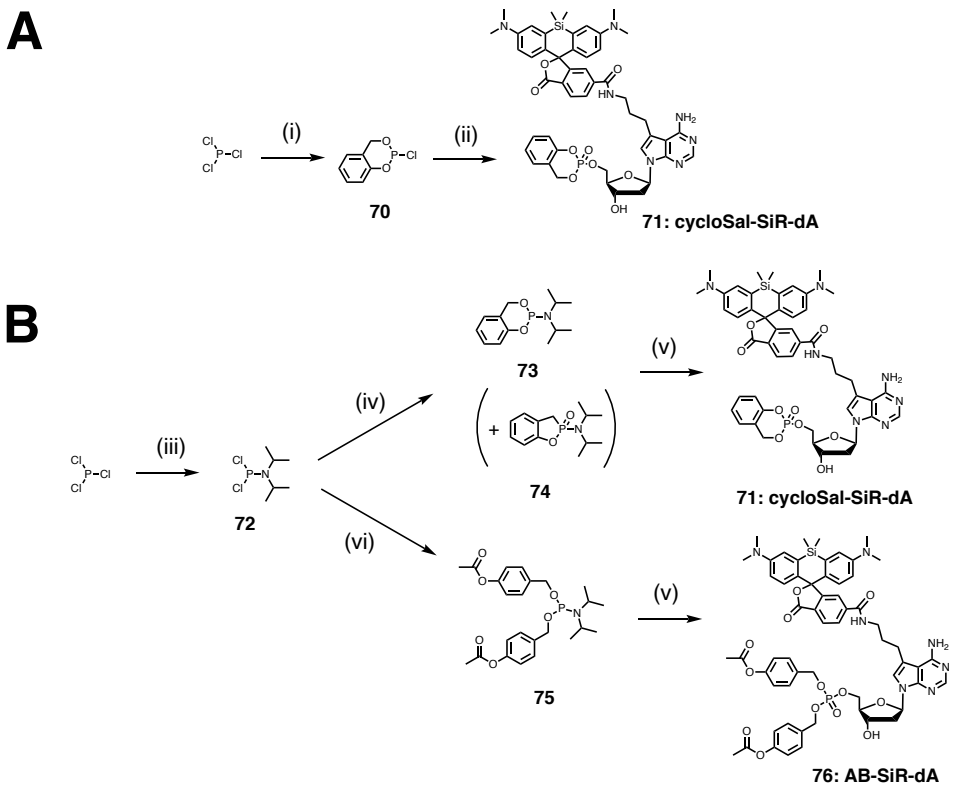

Scheme 4.3: Synthesis scheme pro-nucleotides: (i) 2-hydroxybenzyl alcohol, NEt_3, Et_2O, –10 °C, 30 min, –10 °C → r. t., 45 min, 28%, (ii) 1) SiR-ane-dA **56**, Cs_2CO_3, THF, –20 °C → 0 °C, 20 min, 2) *t*-BuOOH, THF, –20 °C → 0 °C, 10 min, 2%, (iii) di*iso*propylamine, THF, 0 °C, 30 min, 0 °C → r. t., 45 min, 68%, (iv) 2-hydroxybenzyl alcohol, NEt_3, THF, –78 °C, 1 h, –78 °C → r. t., 2 h, 55%, (v) 1) SiR-C3-ane-dA **56**, tetrazole, THF, 0 °C, 30 min, 0 °C → r. t., 30 min, 2) AcOOH, THF, –40 °C → r. t., 20 min, 2% and 33%, (vi) 4-acetoxybenzyl alcohol, NEt_3, THF, –78 °C, 1 h, –78 °C → r. t., 2 h, 73%.

used for coupling the monophosphate and the nucleoside: For route A, a chlorophosphite and for route B a less reactive di*iso*propyl phosphoramidite was used.

In the first route, the chloro phosphite **70** was synthesized in an S_N2 reaction of 2-hydroxybenzyl alcohol with phosphorus trichloride. The coupling of **70** with nucleoside **56** and *in situ* oxidation resulted in the formation of numerous side products and the desired compound **71**. This route was preferred as less side products formed.

For the alternative synthetic route, phosphorus trichloride was first reacted with di*iso*propylamine to give di*iso*propylamino dichlorophosphine **72**. In the next step, compound **72** was reacted with 2-hydroxybenzyl alcohol to give compound **73** and compound **74** as a minor side product. The final step in this route was the coupling from the phosphoramidite to the nucleoside **56** with subsequent oxidation yielding product **71**.

The third pro-nucleoside that was synthesized in this thesis was an acetoxy benzyl (AB) ester. The synthetic route was similar to the alternative cycloSal synthesis. Instead of using the salicyclic alcohol, two acetoxy benzyl groups were attached to di*iso*propylamino dichlorophosphine **72** to form the desired phosphoamidit **75**. Coupling with nucleoside **56** and oxidation worked as previously described and gave product AB-SiR-dA **76**.

4.2 *In cellulo* characterization

4.2.1 Fluorescence microscopy

Fluorogenic nucleoside

According to previous experiments (Subsection 3.2.3), in which adenosine derivatives were incorporated into DNA, SiR-conjugated nucleoside analogs were supplemented to cells to investigate the resulting labeling pattern.

To evaluate their DNA metabolic incorporation efficiencies, U2OS cells were treated with silicon rhodamine-conjugated nucleoside analogs SiR-y-dA **55**, SiR-a-dA **56**, and SiR-y-dU **58** (Methods 5.6.6).

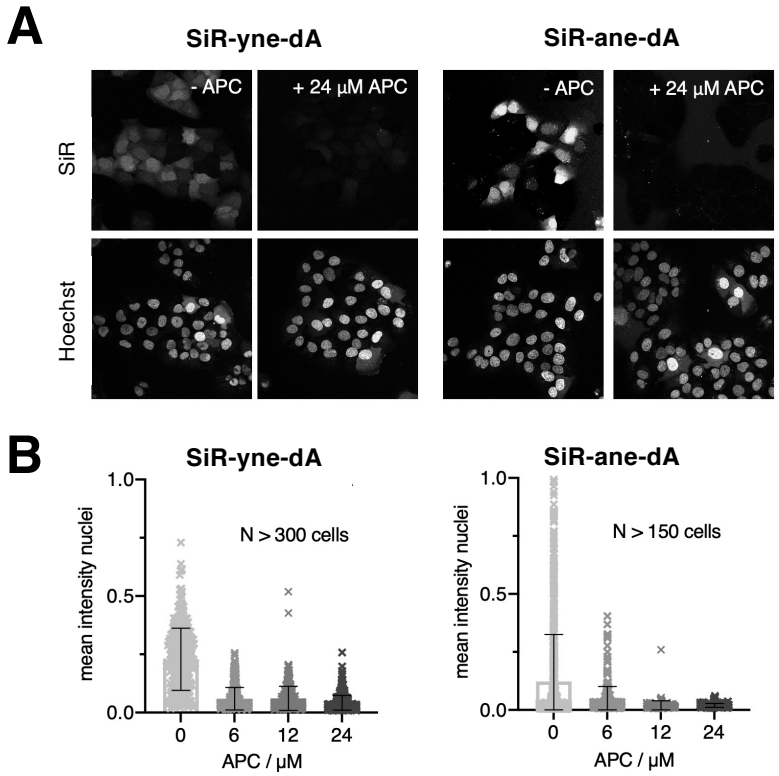

Figure 4.3: Confocal images (40x water) of live U2OS TREx cells that were supplemented with SiR-yne-dA **55** (left) and SiR-ane-dA **56** (right) (100 µM each for 4 h), optionally treated with APC (24 µM) and counterstained with Hoechst33342. Scale bar = 50 µm. The mean fluorescence intensity of the nuclei was quantified and plotted for different concentrations of APC (6–24 µM). The fluorescence signal in the nuclei disappears after treatment with APC.

Imaging revealed that uridine derivative SiR-y-dU **58** exhibited no specific staining, not even after a prolonged incubation time of 16 h (data not shown). This result was in line with published results. Therein, C5-modification of uridines (e.g. azido-methylen-groups[52] or vinyl-thioethers[51]) showed low incorporation efficiencies (Theory 2.2.1). Similarly, experiments with reactive thymidine derivatives did not give signals in cells.[1]

[1] Unpublished data from Schultz lab and my Master's thesis.

In contrast, cells treated with adenosine derivatives **55** and **56** showed nuclear signal after 4 h incubation time exhibiting the staining pattern with bright and dark cells (Figure 4.3, A). The signal co-localized with the non-covalent DNA stain Hoechst33342 and was stable over at least one hour. Besides nuclear staining, a signal was observed in endosomes. The endosomal signal may be caused by poor cell permeability or aggregation of the nucleosides.

The adenosine derivative with the flexible linker SiR-ane-dA **56** showed superior staining to SiR-yne-dA **55**. A similar effect of the linker has already been observed with the reactive adenosine derivatives (Section 3.2.3). After longer imaging times (>8 h), detaching cells were observed, which might be caused by toxic side effects.

To ensure that the signal was specific for the incorporation of the fluorogenic nucleosides, the DNA polymerase inhibitor APC was added to the experiments to inhibit DNA synthesis. When adding APC, the signal intensity dropped (Figure 4.3, B). The results were comparable with findings in a control experiment, where EdU and APC treated cells were analyzed (SI-Figure 4.4).

In summary, the results showed that it was generally possible to use modified nucleosides with fluorophores attached to the 7-deaza-2'-deoxyadenosine scaffold, and the one-component system allowed better time resolution. In these experiments, 4 h was sufficient to measure a nuclear signal in the cells. However, toxic effects occurred during the incorporation of the nucleosides and endosomes became visible in addition to the nuclear signal. To counteract this and improve incorporation yields, a pro-nucleotide strategy was investigated.

Fluorogenic pro-nucleotide

The incorporation of pro-nucleotides was studied supplementing the three pro-nucleotides POM-SiR-dA **63**, cycloSal-SiR-dA **71** and AB-SiR-dA **76** to the cells using different doses from 0.1–10 µM (Methods 5.6.6). Images were acquired after various incubation times.

The nuclear signal of pro-nucleotides was observed after a minimum incubation time of 6–8 h in U2OS cells for the cycloSal and POM group (Figure 4.4). In the case of the AB ester no signal was observed for incubation times up to 10 h. This suggests slower cleavage in the cytosol of the AB group compared to the cycloSal- and POM-protecting group or cleavage taking place in the medium before cellular uptake.

While 100 µM of the fluorescent nucleoside was used, pro-nucleotides allowed the use of lower doses (10 µM). Low doses led to a reduction of endosomal background signals. In contrast, confocal images showed no staining with SiR-yne-dA **55** and SiR-ane-dA **56** that were supplemented at 10 µM. Beyond, less toxic effects were observed, judging by the cell density and morphology. But also, the overall nuclear signal in the cells was weaker compared to their nucleoside counterparts.

When the pro-nucleotides were supplemented for longer periods (>10 h), more endosomal signal accumulated. An obvious explanation is a cleavage outside the cell and uptake of monophosphate or cleavage intermediates. To support this hypothesis, control experiments with monoalkylated POM-SiR-dA **69** and SiR-dA monophosphate **68** were performed. When supplemented to the medium of the cells, both monoalkylated POM-SiR-dA **69**, as well as SiR-dA monophosphate **68**, showed clear accumulations in endosomes (SI-Figure 4.12).

All in all, the cycloSal group gave the best results, since labeling was visible even at low

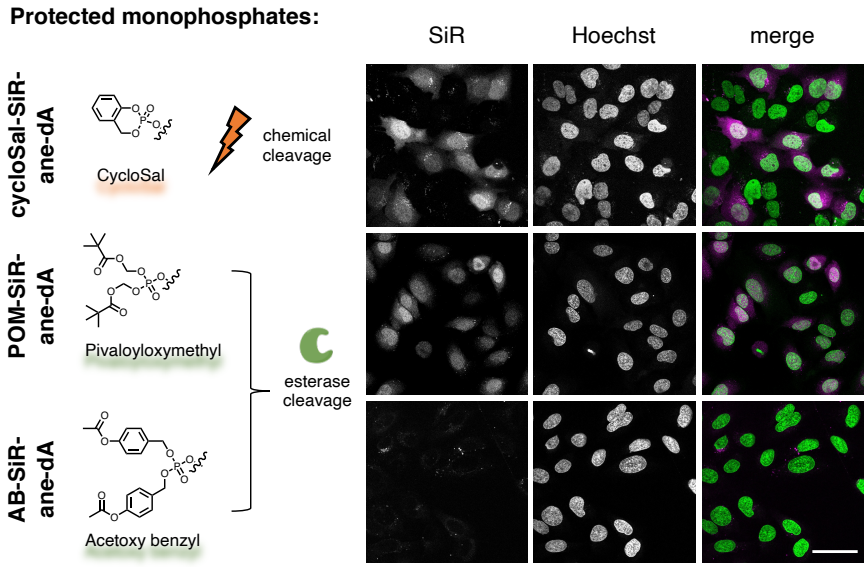

Figure 4.4: Confocal images (40x water) of live U2OS TREx cells that were supplemented with 10 µM of protected monophosphates of SiR-ane-dA **56** after 8 h incubation time. The first row is showing the signal from the nucleoside. In the second row, there is the Hoechst channel as a nuclear counterstain. In the third row, a merge of the two signals is shown (SiR = magenta; Hoechst = green). Scale bar = 50 µm.

incubation times (from 6 h onwards).

4.2.2 Flow cytometry

To get better statistical numbers flow cytometry experiments were performed with SiR-ane-dA **56**, which showed superior properties in microscopy experiments. Therein, SiR-ane-dA **56** and EdU that were supplemented to U2OS cells and incubated for 4 h. EdU treated cells were fixed and labeled, SiR-ane-dA treated cells were analyzed live (Methods 5.8). For both conditions, two populations of proliferating and non-proliferating cells can be distinguished (Figure 4.5 and SI-Figure 4.13).

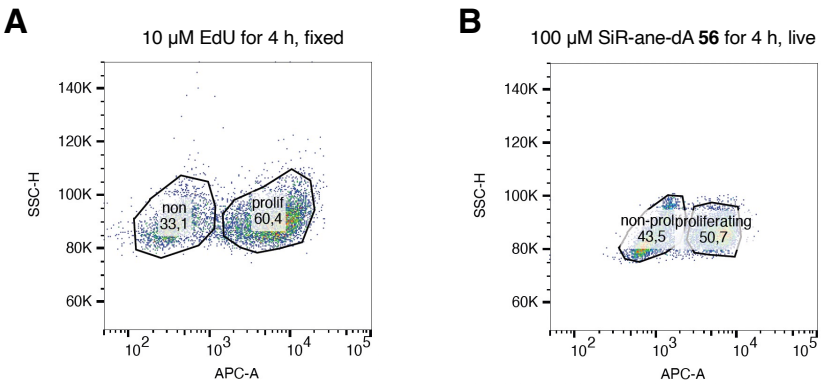

Figure 4.5: Comparison of a proliferation assay with A) EdU and B) SiR-ane-dA **56** in flow cytometry experiments. U2OS cells were treated with EdU or SiR-ane-dA **56** for 4 h. EdU treated cells were fixed before staining with Alexa-647-azide. SiR-ane-dA **56** treated cells were analyzed live. For each condition, 10000 cells were analyzed.

Statistical analysis of the two populations gave a similar number for proliferating cells in the EdU and SiR-ane-dA **56** sample (Table 4.1). Accordingly, SiR-ane-dA **56** might be useful as a proliferation marker.

Table 4.1: Flow cytometry statistics analyzing 10000 cells from N=2 experiments.

nucleoside	#	non-proliferating cells / %	proliferating cells / %
SiR-ane-dA **56**	1	31.9	58.9
SiR-ane-dA **56**	2	33.1	60.4
EdU	1	34.7	55.9
EdU	2	43.5	50.7

4.3 Summary

In summary, two fluorogenic nucleosides and three pro-nucleotide were successfully synthesized in the course of this project.

All compounds were investigated for their ability to label genomic DNA in proliferating cells.

Fluorescence imaging gave a brighter signal in the nucleus for SiR-ane-dA **56** than for SiR-yne-dA **55**. Seeing first promising data from flow cytometry experiments suggests that SiR-ane-dA **56** might be useful as a reagent for proliferation assays.

For the pro-nucleotides, labeling was observed for cycloSal-SiR-dA **71** and POM-SiR-dA **63** within a time window of a few hours. AB-SiR-dA **76** did not show nuclear signal on an hour time scale. The brightest signals were obtained with cycloSal-SiR-dA **71**, which might be due to a faster cleavage compared to POM-SiR-dA **63**. AB-SiR-dA **76** might be cleaved either already in the cytosol or very slow inside the cell.[54]

To improve the cleavage of the protecting group, a photolabile protecting group, based on the cycloSal scaffold could be envisioned.[193], [194] Therein, the chromophore of the cycloSal group would be expanded to a naphthalene- or even coumarine-like scaffold. Shining UV or blue light would then liberate the nucleoside specifically inside the cell. Besides, the cleavage of the POM group could be improved by expressing an esterase (such as the porcine liver esterase, PLE), which was already demonstrated for fluorophores.[195]

5 Conclusion and Outlook

This PhD project enabled a step towards new tools to study DNA in living cells: (i) a photoactivatable small molecule DNA binder, and (ii) metabolic DNA labeling strategies were developed. The different tools have in common that they target specific DNA in a cell. While the photocaged Hoechst (pcHoechst) allowed local staining of DNA with light, metabolic labeling approaches targeted newly synthesized DNA.

PcHoechst is not giving signals in fluorescence microscopy when caged but allows a rapid increase in signal after irradiation with UV light, which remains stable over time. The features of the tool is the high precision, simple use, and instant read-out.

There were different approaches pursued to improve metabolic DNA labeling (Scheme 5.1): (i) proximity labeling of VdU with a fluorescent probe, and (ii) novel nucleoside analogs and pro-nucleotides. Proximity labeling of VdU allowed to obtain signals in living cells with good spatial resolution, but poor time resolution. Therefore, nucleoside analogs were studied, that give faster labeling. In search for new metabolic precursors, only replacing the reactive group on the thymidine scaffold of published metabolic reporters did not result in nuclear staining in the fluorescence microscope. In contrast, adenosine derivatives, allowed to visualize proliferating cells live. For adenosine derivatives, not only modifications with a small reactive group but also the attachment of a fluorescent dye was tolerated in the cells. This eliminated the need for a second labeling step and improved the time resolution. The attempt to obtain better incorporation yields with a pro-nucleotide approach had been evaluated. While the concentration of the supplemented pro-nucleotides could be reduced significantly, the spatial and temporal resolution was comparable to their corresponding nucleosides.

Currently, an application in proliferation assays is conceivable. If the spatial and temporal resolution of the pro-nucleotides could be improved down to 100–200 nm and to a time scale of 20–60 min respectively, it might be possible to observe other dynamic processes that involve DNA synthesis. In particular, I envision that the tool could shine light on retro-viral DNA synthesis or DNA repair.

As it is not yet clear whether the challenges are more related to cellular uptake, intracellular phosphorylation by endogenous kinases, acceptance by DNA polymerases, or the accessibility of the reactive functional group in the DNA, systematic evaluation of all these points can be the first step to solve the problem. Once the limitation is clear, engineering of metabolic enzymes or *in vitro* screening of a larger library of modified nucleosides could be performed.

Since efficient phosphorylation might be the problem, the kinases could be purified and a phosphorylation assay could be used for screening a nucleoside library. Another possibility is to improve pro-nucleotide strategies to be able to skip the first phosphorylation step in the cell. Therein, the speed of the cleavage of the protecting group inside the cell should be improved. This could be tackled with a photolabile group or enzymatic cleavage by heterologously expressed enzymes. Also, if bypassing the first phosphorylation step is not enough, protected

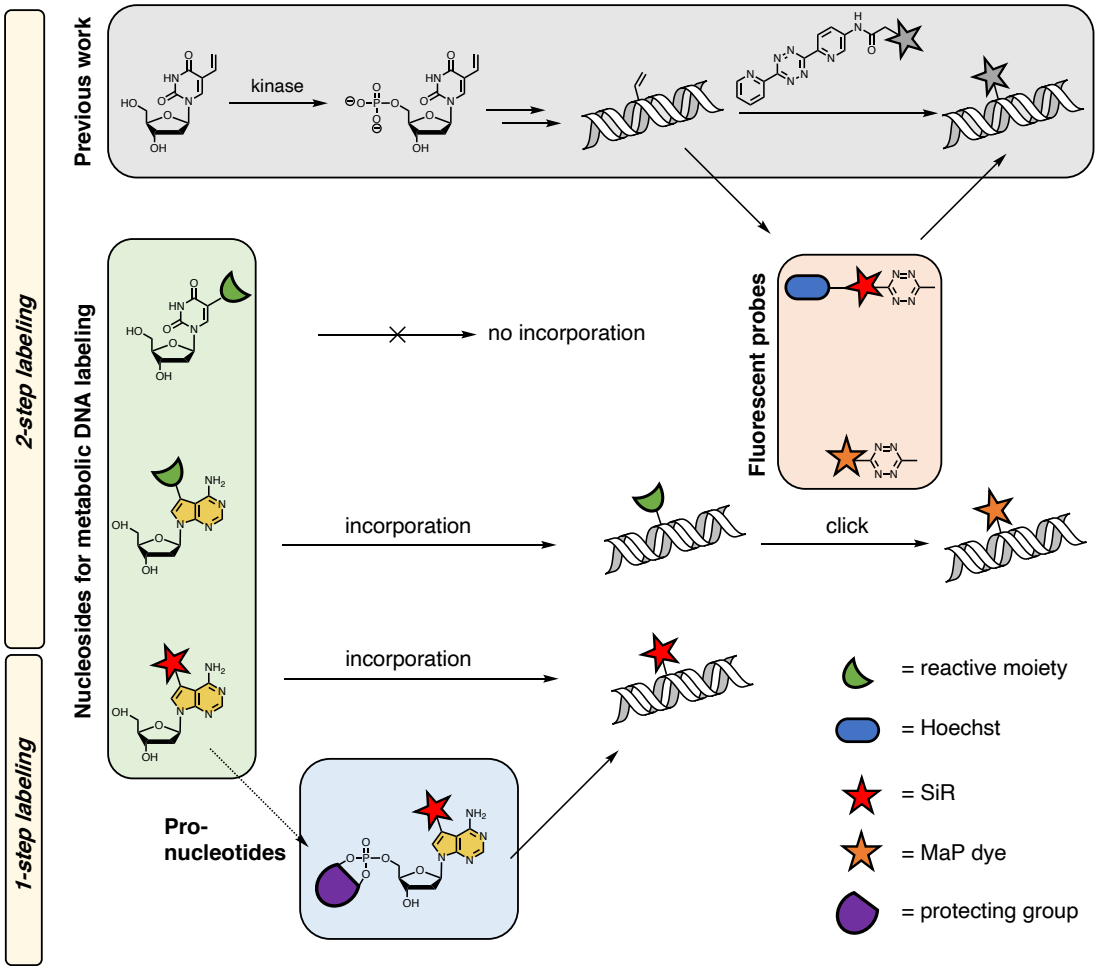

Scheme 5.1: Summary of metabolic DNA labeling approaches. Nucleosides were investigated as metabolic precursors for iEDDA and equipped with reactive moieties (= green half-moon) for a 2-step labeling or fluorophores (= red star) directly for a 1-step labeling. As thymidine derivatives were not incorporated, adenosine derivatives were used later. Fluorescent adenosine derivatives were also masked with protecting groups (= violet circle) to skip the first phosphorylation step. To label metabolic incorporated nucleosides, a bifunctional probe (Hoechst-SiR-MeTz) for proximity labeling was developed. To visualize adenosine derivatives, a MaP-tetrazine (= orange star) was used.

nucleotide triphosphates might be an attractive alternative to protected monophosphates. But, there will be tremendous efforts necessary for future research to satisfy researchers in chemical biology or imaging areas.

Part III

Material and Methods

1 *In silico* predictions

For molecular docking studies, the 8BNA crystal structure with Hoechst33342 as a co-crystal with an oligonucleotide (C-G-C-G-A-A-T-T-C-G-C-G)[196] and the Schroedinger Suite for Windows 2020-4 with Maestro 12.6 were used.

DNA prep: the 8BNA PDB structure with a bound Hoechst ligand was adjusted for docking experiments by creating formal charges and protonation states using Epik, removing water and metal ions, and then refined for minimal restrains with a OPLS_2005 force field.

Lig prep: a number of 3D structures from the ligand were generated from a 2D ChemDraw (PerkinElmer, version 19.0.0.26) file based on ionization states, tautomers, stereo chemistries, and ring conformations.

Structure ligand docking was performed with Glide (Grid-based LIgand Docking with Energetics). Grid generation was performed by selecting the bound Hoechst ligand from the 8BNA structure and extending the receptor grid to the size of the DNA structure. The docking was performed.The docking was performed without any additional constraints in a high-throughput virtual screening (HTVS) mode to obtain a set of DNA-Ligand complexes. The binding free energies of these complexes were derived from the generalized Born and surface area continuum solvation model (prime MM/GBSA) which accounts for some ligand flexibility in a frozen receptor. The structures were visualized using PyMOL^{TM} 2.4.1 (Schrodinger, LLC).

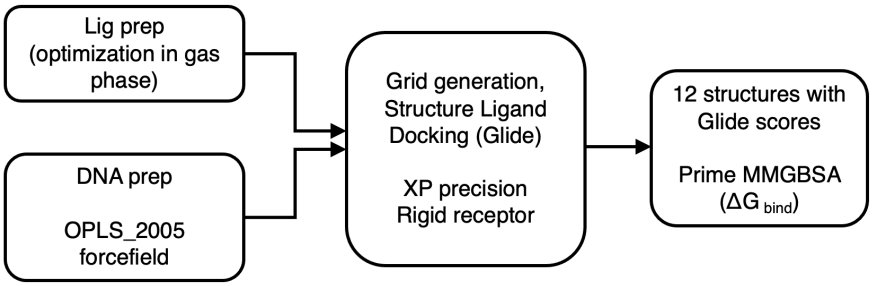

Figure 1.1: Molecular docking workflow.

2 Synthesis

2.1 General information

Chemicals: Starting materials, reactants and solvents were purchased from commercial suppliers (Sigma Aldrich, Honeywell, Alfa Aesar, Acros Organics, Fisher Scientific, Santa Cruiz, Fluka, Fluorochem, TCI etc.) in synthesis or analytical grade and were used without further purification. Nucleoside precursors were purchased from Carbosynth. The asymmetric SiR precursor was custom synthesized from AAT Bioquest, Inc. (Sunnyvale, CA, USA). Tetrazines and reactive dienophiles were purchased from Jena Bioscience (MeTet and HTet, TCO) or BroadPharm (PEG1/4-MeTet). Dry solvents were purchased from Sigma Aldrich (Acros) and if necessary were degassed by bubbling N_2 through the solvent for several minutes. Reactions that require dry conditions were performed under an argon atmosphere (argon 4.6, 99.996%) with a standard balloon technique.

Hydrogenation: Hydrogenation was performed in a hydrogenator equipped with a heater and magnetic stirrer that was operated up to 10 bar (Carl Roth GmbH, 100 mL/100 bar, model I).

Reaction controls: For reaction controls or product characterization UPLC-ESI-MS was performed on a Shimadzu LCMS-2020 instrument with a diode array detector (Nexera X2, SPD-M30A) and a Quadrupole MS analyzer. A Waters ACQUITY UPLC BEH C18 (1.7 µm, 50 $\times$ 2.1 mm) column was used. The typical gradient was from 10% B for 0.5 min $\rightarrow$ gradient to 90% B over 4.5 min $\rightarrow$ 90% B for 0.5 min $\rightarrow$ gradient to 99% B over 0.5 min with 1 ml/min flow with buffer A: 0.1% FA in H_2O and buffer B: MeCN.

Flash chromatography: Normal phase purification was performed with silica (Merck, Si 60, pore size 40–63 µm) as a stationary phase for manual column separation. Silica Gel normal phase (SiliCycle, 230-400 mesh, 40–63 µm) or SiliaSep C18 (di2chrom, SiliCycle, 230-400 mesh, 40–63 µm) reversed-phase columns were used in combination with a Biotage® flush chromatography system (Isolera™ Systems). For normal phase column separations standard solvent systems DCM/MeOH, hexanes/EtOAc (synthesis grade) were used. For reversed-phase separations, MilliQ water with 0.1% TFA (Sigma Aldrich, 99%) and HPLC grade acetonitrile (Sigma Aldrich, Honeywell) were used as mobile phase. For product detection, the instrument was equipped with a UV/vis detector.

Column chromatography: For tracking elution of column chromatography, thin layer chromatography employing silica gel on glass plates with a fluorescence indicator (Merck, silica gel Si 60, F254) was used. The spots on the plates were visualized under UV light at 254 nm or stained. For staining, the plates were dipped in the corresponding staining solution ($KMnO_4$, cerium molybdate, ninhydrin and bromocresol green) and heated for a short time with a heat gun.

RP-HPLC: RP-HPLC purification was performed on a Waters e2695 system equipped with a 2998 PDA detector. For analytical or semi-preparative separations a Supelco Ascentis® C18 HPLC Column (5 µm, 250 × 21.2 mm or 5 µm, 250 × 10 mm), MilliQ water with 0.1% TFA (Sigma Aldrich, 99%) and HPLC grade acetonitrile (Sigma Aldrich, Honeywell) were used. All products were obtained as a TFA salt. Nucleotide monophosphates were purified on a Phenomenex Gemini® 5 µm C18 110 ÅLC column (250 × 21.2 mm) using 0.1 M triethylammonium bicarbonate buffer (TEAB) and HPLC grade acetonitrile. For 500 ml 1 M TEAB buffer, 69.74 ml NEt_3 were added to 300 ml MQ water. The solution was then filled in a washing bottle, cooled with an ice bath, and vigorously stirred with a magnetic stirrer. CO_2 was passed through until the pH reaches pH 8.0 ± 0.5. The final volume was adjusted to 500 ml with MQ water. For HPLC separations, the buffer was diluted to a final concentration of 0.1 M. After HPLC purification, the products contain residual triethylammonium counterions. All aqueous fractions from reversed-phase flush chromatography and RP-HPLC purifications were lyophilized (CHRIST, alpha 2-4 LSCbasic) to obtain the final product.

Kugelrohr distillation: Phosphines were purified using a Kugelrohr distillation apparatus (BÜCHI Glasofen B-585 Kugelrohr).

HPLC traces: HPLC traces for purity assessment were recorded on a Waters H-class instrument equipped with a quaternary solvent manager, a Waters autosampler, a Waters TUV detector and a Waters Acquity QDa detector with an Acquity UPLC BEH C18 1.7 µm, 2.1 × 50 mm RP column (Waters Corp., USA).

Yields: Yields for peptide bond couplings with SiR, MAP or nucleoside derivatives at scales below 1 mg were determined using a NanoDrop™ 2000c spectrophotometer (Thermo Fisher Scientific, Waltham, MA). The sample was diluted in 0.1% SDS in PBS, 0.5% SDS in PBS or PBS and the absorbance at 650 nm, 550 nm or 290 nm was measured. The concentration was calculated using the Lambert-Beer law with their extinction coefficient (Section 4.1). The yield was calculated from the concentration.

NMR: Deuterated solvents for NMR measurements were purchased from Carl Roth GmbH. ^{1}H, ^{13}C, ^{19}F, ^{31}P NMR were recorded on a Bruker Avance III HD 400 spectrometer (400 MHz) equipped with a CryoProbe™ at ambient temperature (300 K) with the sample dissolved in $CDCl_3$, DMSO-d_6, MeOD-d_4 or D_2O. The chemical shifts are given in δ-values [ppm] and calibrated on the residual solvent signal: $CDCl_3$ (7.26 ppm / 77.16 ppm), DMSO-d_6 (2.50 ppm / 39.52 ppm), MeOD-d_4 (3.31 ppm / 49.00 ppm), D_2O 4.79 ppm. Coupling constants (J) are reported in Hertz [Hz]. For the allocation of the signals and signal multiplicities the following abbreviations were used: s (singlet), d (doublet), t (triplet), q (quartet), dd (doublet of doublets), dt (doublet of triplet), m (multiplet). For the elucidation of the obtained spectra the software MestReNova 14.1.0. was used. The multiplicities are reported based on appearance in the measured spectrum not on theoretical couplings derived from the molecular structure. The NMR signals of counterions such as trifluoroacetic acid or triethylammonium are not listed.

HRMS: High-resolution mass spectrometry (HRMS) was performed using a Bruker maXis II ETD hyphenated with a Shimadzu Nexera system. The instruments were controlled via Brukers otofControl 4.1 and Hystar 4.1 SR2 (4.1.31.1) software. Automated internal re-calibration and

data analysis of the recorded spectra were performed with Bruker's DataAnalysis 4.4 SR1 software. Measurements were performed in the MPImR MS core facility.

DMSO stock solutions DMSO solutions were prepared for cell culture experiments using DMSO-d_6 ampulla (8 $\times$ 1 ml, Sigma Aldrich). Nucleosides were stored in 1 µmol aliquots and dissolved in 10 µl DMSO before usage to give a concentration of 100 mM. Tetrazine dyes were stored in 10 nmol aliquots and dissolved in 10 µl DMSO before usage to give a concentration of 1 mM. After diluting the samples, the concentration was confirmed by NanoDrop (Thermo Fisher Scientific, Waltham, MA) measurement as described above (Section 4.1). Other dyes were kept as 1 mM DMSO stocks. All compounds and stock solutions were stored protected from light at –20 °C.

2.2 Synthesis procedures: Photocaged-Hoechst

2'-(4-Ethoxyphenyl)-5-(4-methylpiperazin-1-yl)-1*H*,1'*H*-2,5'-bibenzo[d]imidazole (free-base Hoechst33342)

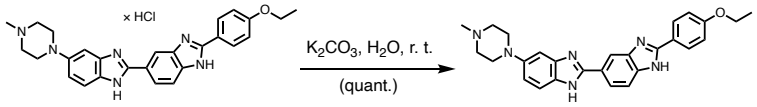

1

According to a previously described procedure [21], in a 50 ml centrifugation tube, Hoechst33342 trihydrochloride (100 mg, 178 µmol, Sigma Aldrich, #B22611-100MG) was dissolved in deionized water (20 ml). An aqueous solution of K_2CO_3 (240 µl, 2.3 M) was added. The tube was vortexed vigorously and the resulting precipitate was subsequently pelleted (4000 $\times$ g, 10 min). The supernatant was removed, the remaining residue was washed with deionized water (2 $\times$ 5 ml), centrifuged, and decanted to obtain compound **1** as a faint yellow powder after lyophilization.

1-(4,5-Dimethoxy-2-nitrobenzyl)-4-(2'-(4-ethoxyphenyl)-1*H*,1'*H*-[2,5'-bibenzo[d]imidazol]-6-yl)-1-methylpiperazin-1-ium 2,2,2-trifluoroacetate (pcHoechst)

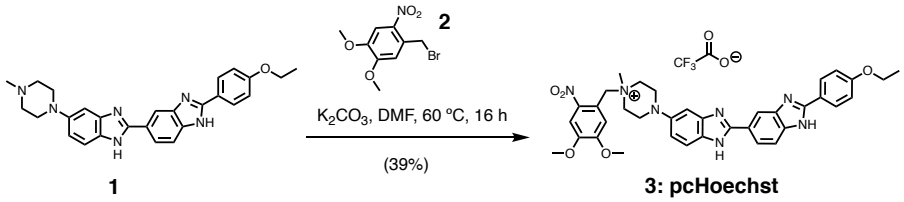

1 **3: pcHoechst**

A round bottom flask was charged with compound **1** (26 mg, 57.5 µmol, 1 eq.) and anhydrous DMF (2.5 ml) was added. K_2CO_3 (31.7 mg, 230 µmol, 4 eq.) was suspended in the reaction mixture, to which 1-(bromomethyl)-4,5-dimethoxy-2-nitrobenzene **2** (31.8 mg, 115 µmol, 2 eq.) was added in one portion. The reaction mixture was stirred for 16 h at 60 °C in the dark, before it

was quenched by the addition of 30 µl acetic acid and 100 µl water. The crude product was then subjected to RP-HPLC (Supelco Ascentis® C18 HPLC column, MeCN:H_2O:TFA = 10/90/0.1 → 90/10/0.1, v/v/v in 1 h, flow 8 ml min^{-1}, collection at λ = 360 nm) to obtain the desired product **3** (14.3 mg, 22.1 µmol) after lyophilization. **yield**: 39% (faint yellow powder). $\mathbf{R_t}$=27 min. **HRMS** (ESI): calc. for $C_{36}H_{37}N_7O_5$ $[M+H]^+$: 648.2929, found: 648.2923. **1H NMR** (400 MHz, DMSO-d_6, 300 K): δ [ppm] = 8.46 (d, J = 1.7 Hz, 1H), 8.25 – 8.17 (m, 2H), 8.07 (dd, J = 8.5, 1.7 Hz, 1H), 7.89 (d, J = 8.5 Hz, 1H), 7.81 (s, 1H), 7.73 (d, J = 9.0 Hz, 1H), 7.42 (s, 1H), 7.33 (dd, J = 9.1, 2.2 Hz, 1H), 7.26 (d, J = 2.2 Hz, 1H), 7.22 – 7.15 (m, 2H), 5.13 (s, 2H), 4.15 (q, J = 7.0 Hz, 2H), 3.98 (s, 3H), 3.94 (s, 3H), 3.90–3.79 (m, 2H), 3.78 – 3.68 (m, 2H), 3.68 – 3.61 (m, 2H), 3.51 – 3.41 (m, 2H), 3.09 (s, 3H), 1.38 (t, J = 7.0 Hz, 3H). **13C NMR** (101 MHz, DMSO-d_6, 300 K): δ [ppm] = 161.0, 158.4 (q, J = 34.2 Hz) 154.0, 152.2, 150.0, 149.5, 148.1, 143.6, 141.5 (by HMBC), 141.1 (by HMBC), 138.9 (by HMBC), 134.2 (by HMBC), 129.0, 127.3 (by HMBC), 122.1, 120.7, 120.4, 118.2, 117.8, 116.3, 116.3 (q, J = 296 Hz), 115.5, 115.1, 114.7, 114.5 (2x by HSQC), 109.3, 99.2, 64.0, 63.5, 59.0, 56.6, 56.4, 44.0, 42.8, 14.6.

2.3 Synthesis procedures: Proximity-enhanced DNA labeling

5-Vinyl-2'-deoxyurdine (VdU)

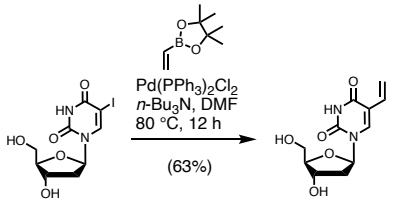

4: VdU

Anhydrous DMF (10 ml) was purged with argon for degassing for 5 min. An oven-dried Schlenck flask was charged with 5-iodo-2'-deoxyuridine (Biosynth Carbosynth®, #ND05147, 100 mg, 282 µmol, 1 eq.), $Pd(PPh_3)_2Cl_2$ (9.91 mg, 14.1 µmol, 0.05 eq.) and suspended in DMF. *n*-Bu_3N (0.5 ml) and vinylboronic acid pinacol ester (Santa Cruz, #253829, 47.8 mg, 311 µmol, 1.1 eq.) were added. The solids dissolved completely when the reaction was heated to 80 °C for 12 h. The solution turned orange after heating and brownish in the end of the reaction. The reaction was purified by reversed-phase flash chromatography (SiliaSepC18, dichrom, 40 g column, MeCN:H_2O:TFA = 0/100/0.1 → 5/95/0.1, v/v/v) after concentrating the reaction mixture under reduced pressure. Compound **4** (55 mg, 216 µmol) was obtained after lyophilization. **HRMS** (ESI): calc. for $C_{36}H_{37}N_7O_5$ $[M+H]^+$: 255.0975, found: 255.0976. **yield**: 63% (colorless powder). **1H NMR** (400 MHz, MeOD-d_4, 300 K): δ [ppm] = 8.22 (s, 1H), 6.44 (dd, J = 17.7, 11.5 Hz, 1H), 6.29 (t, J = 6.6 Hz, 1H), 5.93 (dd, J = 17.7, 1.6 Hz, 1H), 5.16 (dd, J = 11.5, 1.6 Hz, 1H), 4.42 (dt, J = 6.2, 3.7 Hz, 1H), 3.94 (q, J = 3.2 Hz, 1H), 3.90 – 3.68 (m, 2H), 2.44 – 2.13 (m, 2H). **13C NMR** (101 MHz, MeOD-d_4, 300 K): δ [ppm] = 164.5, 151.6, 139.0, 129.3, 115.2, 113.4, 89.0, 86.7, 72.0, 62.6, 41.7.

tert-butyl (4-(4-(6-(4-methylpiperazin-1-yl)-1*H*,3'*H*-[2,5'-bibenzo[d]imidazol]-2'-yl)phenoxy)butyl)carbamate (Hoechst-C4-NHBoc)

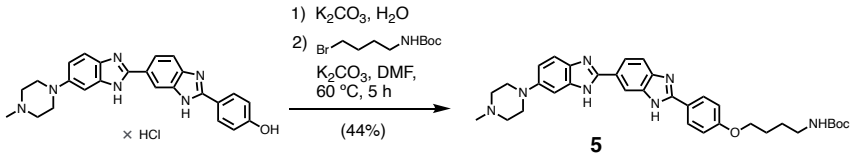

This synthesis was adapted from a published procedure.[21] Hoechst33258 (Sigma Aldrich, #B2883-500MG was free based as described for compound **1**. Hoechst33258 free base (30 mg, 48.1 µmol, 1 eq.) was dissolved in DMF (2 ml). K_2CO_3 (16.6 mg, 120 µmol, 2.5 eq.) and *N*-(4-bromobutyl)-carbamic acid (Sigma Aldrich, #90303-500MG-F, 14.5 mg, 57.7 µmol, 1.2 eq.) were added. The reaction was heated to 60 °C for 5 h. The reaction mixture was quenched with 50 µl acetic acid and diluted with 200 µl water The crude product was purified with RP-HPLC (Supelco Ascentis® C18 HPLC column, MeCN:H_2O:TFA = 20/80/0.1 $\rightarrow$ 60/40/0.1, v/v/v in 1 h, flow 8 ml min^{-1}, collection at λ = 350 nm). After lyophilization compound **5** (12.6 mg, 21.2 µmol) was obtained. **yield**: 44% (faint yellow powder). **HRMS** (ESI): calc. for $C_{34}H_{42}N_7O_3$ $[M+2H]^{2+}$: 298.6708, found: 298.6707. **1H NMR** (400 MHz, MeOD-d_4, 300 K): δ [ppm] = 8.22 (s, 1H), 8.00 (dd, J = 8.6, 1.8 Hz, 1H), 7.95 (d, J = 8.5 Hz, 2H), 7.84 (d, J = 8.6 Hz, 1H), 7.62 (d, J = 9.0 Hz, 1H), 7.29 (dd, J = 9.1, 2.2 Hz, 1H), 7.22 (d, J = 2.1 Hz, 1H), 7.02 (d, J = 8.6 Hz, 2H), 4.01 – 3.83 (m, 4H), 3.68 (d, J = 11.7 Hz, 2H), 3.32 – 3.15 (m, 4H), 3.11 (t, J = 6.9 Hz, 2H), 3.01 (s, 3H), 1.81 – 1.69 (m, 2H), 1.67 – 1.56 (m, 2H), 1.45 (s, 9H). **13C NMR** (101 MHz, MeOD-d_4, 300 K): δ [ppm] = 164.5, 159.6, 159.2, 158.8, 158.6, 154.3, 150.5, 149.1, 138.1, 135.9, 134.4, 130.7, 127.8, 124.8, 122.2, 120.1, 119.3, 119.3, 117.4, 116.5, 116.4, 115.6, 114.6, 114.4, 113.5, 100.6, 80.0, 69.3, 54.5, 43.6, 41.0, 28.8, 27.5, 27.4.

4-(4-(6-(4-methylpiperazin-1-yl)-1*H*,3'*H*-[2,5'-bibenzo[d]imidazol]-2'-yl)phenoxy)butan-1-amine (Hoechst-C4-NH_2)

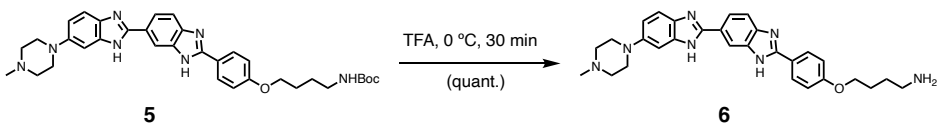

TFA (500 µl) was added to compound **5** (10 mg, 16.8 µmol, 1 eq.) on ice and the reaction mixture was stirred for 30 min at 0 °C. The reaction mixture was then allowed to warm to room temperature, while TFA was removed under a gentle stream of nitrogen and later co-evaporated with DCM (3 $\times$ 1 ml) under reduced pressure. The full conversion of the reaction was verified by LC-MS. Compound **6** was dissolved in 200 µl DMSO and used without further purification.

3-(dimethylamino)-7-((4-((2,5-dioxopyrrolidin-1-yl)oxy)-4-oxobutyl)-(methyl) amino)-5,5-dimethyl-3'-oxo-3'*H*,5*H*-spiro[dibenzo[b,e]siline-10,1'-*iso*benzo-furan]-6'-carboxylic acid (SiR-Su)

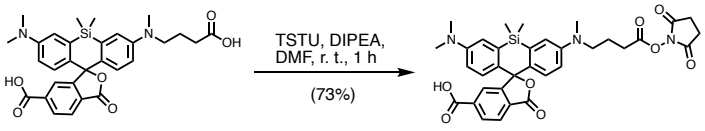

7 **8**

Compound **7** (30 mg, 55.1 µmol, 1 eq.) was dissolved in DMF (15 ml), DIPEA (18.2 µl, 110 µmol, 2 eq.) and TSTU (11.6 mg, 60.6 µmol, 1.1 eq.) were added. The reaction was stirred at ambient temperature for 1 h. Water (200 µl) and acetic acid (50 µl) were added to the reaction and the product was purified by RP-HPLC (Supelco Ascentis® C18 HPLC column, MeCN:H_2O:TFA = 20/80/0.1 $\rightarrow$ 60/40/0.1, v/v/v in 1 h, flow 8 ml min^{-1}, collection at λ = 650 nm). Lyophilization yielded compound **8** (26 mg, 40.5 µmol). **yield**: 73% (turquoise powder). **HRMS** (ESI): calc. for $C_{34}H_{36}N_3O_8Si$ $[M+H]^+$: 642.2266, found: 642.2261. **1H NMR** (400 MHz, MeOD-d_4, 300 K): δ [ppm] = 8.30 – 8.21 (m, 2H), 7.79 (dd, J = 1.5, 0.8 Hz, 1H), 7.32 (d, J = 2.9 Hz, 2H), 6.93 (dd, J = 12.2, 9.6 Hz, 2H), 6.73 (td, J = 9.4, 2.9 Hz, 2H), 3.74 – 3.66 (m, 2H), 3.27 (s, 6H), 3.22 (s, 3H), 2.81 (s, 4H), 2.72 (t, J = 6.6 Hz, 2H), 2.09 – 1.97 (m, 2H), 0.60 (s, 3H), 0.53 (s, 3H). **13C NMR** (101 MHz, MeOD-d_4, 300 K): δ [ppm] = 171.8, 170.2, 167.9, 167.8 (2C), 155.0, 154.3, 148.9, 148.2, 143.6, 140.8, 140.7, 135.5, 132.0, 131.9, 131.2, 130.2, 129.7, 122.0, 121.4, 118.7, 115.8, 115.5, 115.1, 52.9, 41.2 (2C), 39.3, 28.6, 26.5, 23.2, -0.8, -1.9.

3-((4-((4-(1,2,4,5-tetrazin-3-yl)benzyl)amino)-4-oxobutyl)(methyl)amino)-7-(di-methylamino)-5,5-dimethyl-3'-oxo-3'*H*,5*H*-spiro[dibenzo[b,e]siline-10,1'-*iso*benzo-furan]-6'-carboxylic acid (SiR-MeTz)

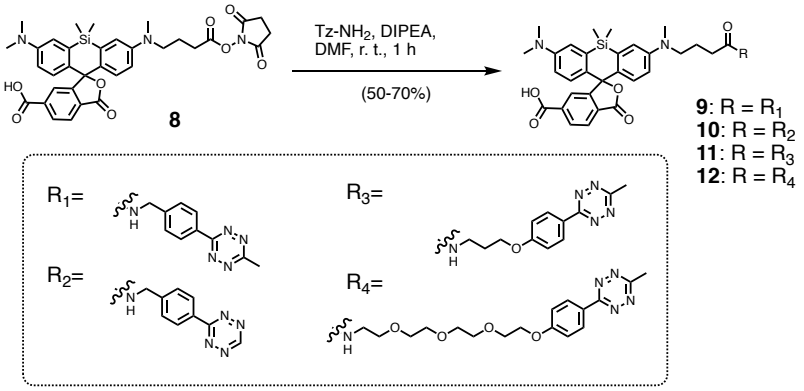

General procedure: Compound **8** (1 eq.) was diluted in DMF (1 ml). DIPEA (3 eq.) and Tz-NH_2 (1.2 eq.) were added. The reaction was stirred at ambient temperature for about 1 h. The conversion of the reaction was checked by LC-MS, before the reaction mixture was quenched with 50 µl acetic acid and diluted with 200 µl water. The reaction mixture was then subjected to RP-HPLC purification (Supelco Ascentis® C18 HPLC column, MeCN:H_2O:TFA = 30/70/0.1 $\rightarrow$

90/10/0.1, v/v/v in 1 h, flow 8 ml min^{-1}, collection at λ = 650 nm). **yield**: 50-70% (blue powder with a pinkish touch). *MeTz:* **HRMS** (ESI): calc. for $C_{40}H_{42}N_7O_5Si$ $[M+H]^+$: 728.3011, found: 728.3011. **1H NMR** (400 MHz, MeOD-d_4, 300 K): δ [ppm] = 8.46 (d, J = 8.4 Hz, 2H), 8.36 – 8.25 (m, 3H), 7.83 (dd, J = 1.5, 0.7 Hz, 1H), 7.55 – 7.45 (m, 2H), 7.44 (d, J = 2.8 Hz, 1H), 7.33 (d, J = 2.9 Hz, 1H), 6.95 (dd, J = 9.5, 5.4 Hz, 2H), 6.77 (ddd, J = 11.2, 9.5, 2.8 Hz, 2H), 4.50 – 4.41 (m, 2H), 3.70 (t, J = 7.5 Hz, 2H), 3.31 (s, 6H), 3.28 (s, 3H), 3.02 (s, 3H), 2.40 (t, J = 6.8 Hz, 2H), 2.09 – 1.91 (m, 2H), 0.65 (s, 3H), 0.57 (s, 3H). **13C NMR** (101 MHz, MeOD-d_4, 300 K): δ [ppm] = 174.8, 168.7, 167.9, 167.7, 165.1, 161.6, 161.2, 154.9, 154.5, 149.0, 148.6, 145.0 (2C), 140.9 (2C), 135.5, 135.4, 132.4, 132.1, 132.0 131.1, 129.3, 129.0, 128.8, 128.7, 121.8, 118.8, 116.3, 115.3, 115.2, 53.3, 43.9, 41.0 (2C), 39.3, 33.1, 23.9, 21.1, -0.7, -2.0. *HTz:* **HRMS** (ESI): calc. for $C_{39}H_{39}N_7O_5Si$ $[M+H]^+$: 714.2866, found: 714.2856. *PEG1:* **HRMS** (ESI): calc. for $C_{42}H_{45}N_7O_6Si$ $[M+H]^+$: 772.3273, found: 772.3276. *PEG4:* **HRMS** (ESI): calc. for $C_{47}H_{55}N_7O_9Si$ $[M+H]^+$: 890.3903, found: 890.3903.

3-((4-((4-(1,2,4,5-tetrazin-3-yl)benzyl)amino)-4-oxobutyl)(methyl)amino)-7-(di-methylamino)-5,5-dimethyl-3'-oxo-3'*H*,5*H*-spiro[dibenzo[b,e]siline-10,1'-*iso*benzo-furan]-6'-succinimidyl ester (Su-SiR-MeTz)

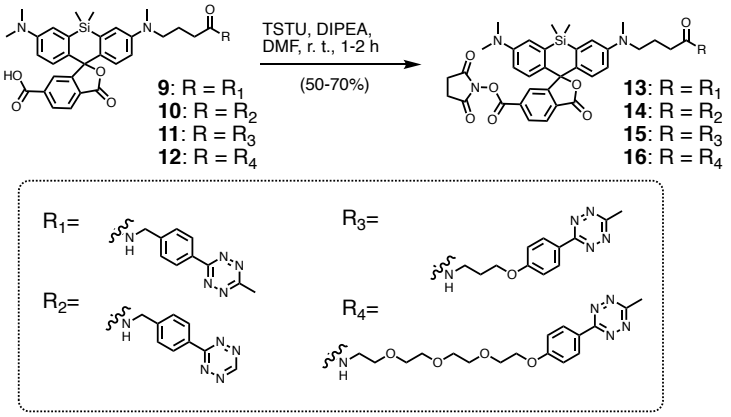

General procedure: Compounds **9**-**12** (1 eq.) were diluted in DMF (1 ml). DIPEA (3 eq.) and TSTU (1.2 eq.) were added. The reaction was stirred at ambient temperature for 1–2 h. The conversion of the reaction was checked by LC-MS, before the reaction mixture was quenched with 50 µl acetic acid and diluted with 200 µl water. The reaction mixture was then subjected to RP-HPLC purification (Supelco Ascentis® C18 HPLC column, MeCN:H_2O:TFA = 30/70/0.1 → 90/10/0.1, v/v/v in 1 h, flow 8 ml min^{-1}, collection at λ = 650 nm). The products **13**-**16** were used without further characterization. **yield**: 50-70% (based on NanoDrop measurements, blue powder with a pinkish touch).

3-(dimethylamino)-5,5-dimethyl-7-(methyl(4-((4-(6-methyl-1,2,4,5-tetrazin-3-yl)benzyl)amino)-4-oxobutyl)amino)-*N*-(4-(4-(6-(4-methylpiperazin-1-yl)-1*H*,
3'*H*-[2,5'-bibenzo[d]imidazol]-2'-yl)phenoxy)butyl)-3'-oxo-3'*H*,5*H*-spiro[dibenzo[b,e]siline-10,1'-*iso*benzofuran]-6'-carboxamide (Hoechst-SiR-MeTz)

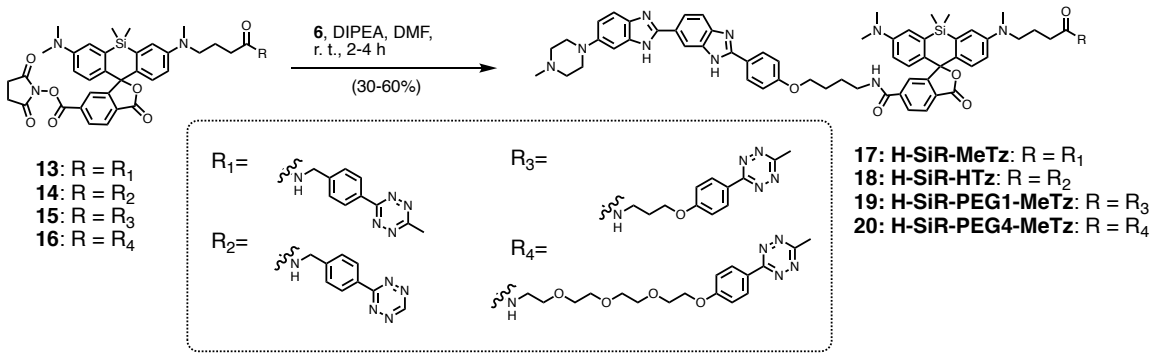

General procedure: Compounds **13**-**16** (1 eq.) were diluted in DMF (1 ml). DIPEA (3 eq.) and Hoechst-C4-NH_2 **6** (1.2 eq.) were added. The reaction was stirred at ambient temperature for 1–2 h. The conversion of the reaction was checked by LC-MS, before the reaction mixture was quenched with 50 µl acetic acid and diluted with 200 µl water. The reaction mixture was subjected to RP-HPLC purification (Supelco Ascentis® C18 HPLC column, MeCN:H_2O:TFA = 30/70/0.1 $\rightarrow$ 70/30/0.1, v/v/v in 1 h, flow 8 ml min^{-1}, collection at λ = 650 nm). **yield**: 30-60% (based on NanoDrop measurements, blue powder with a pinkish touch). *MeTz:* **HRMS** (ESI): calc. for $C_{69}H_{75}N_{14}O_5Si$ $[M+3H]^{3+}$: 402.5266, found: 402.5260. **1H NMR** (400 MHz, MeOD-d_4, 300 K): δ [ppm] = 8.83 (t, J = 5.7 Hz, 1H), 8.41 (s, 1H), 8.40 – 8.37 (m, 2H), 8.28 (d, J = 8.3 Hz, 1H), 8.12 – 8.06 (m, 3H), 8.04 (dd, J = 8.6, 1.8 Hz, 1H), 7.89 (dd, J = 8.6, 0.6 Hz, 1H), 7.75 – 7.69 (m, 2H), 7.48 – 7.43 (m, 2H), 7.42 – 7.37 (m, 2H), 7.30 (dd, J = 9.3, 2.5 Hz, 2H), 7.16 – 7.11 (m, 2H), 6.94 (d, J = 9.5 Hz, 2H), 6.78 (dd, J = 9.5, 2.8 Hz, 1H), 6.72 (dd, J = 9.6, 2.8 Hz, 1H), 4.49 – 4.38 (m, 2H), 4.13 (t, J = 6.0 Hz, 2H), 4.02 – 3.91 (m, 2H), 3.67 (t, J = 7.7 Hz, 4H), 3.52 – 3.48 (m, 2H), 3.49 – 3.44 (m, 1H), 3.28 (s, 6H), 3.25 (s, 3H), 3.24 – 3.12 (m, 2H), 3.02 (s, 3H), 2.98 (s, 3H), 2.38 (t, J = 6.8 Hz, 2H), 2.07 – 1.94 (m, 2H), 1.94 – 1.78 (m, 5H), 0.62 (s, 3H), 0.56 (s, 3H). **13C NMR** (101 MHz, MeOD-d_4, 300 K): δ [ppm] = 174.8, 168.7, 168.2, 165.1, 163.9, 162.4, 162.0, 155.9, 150.9, 150.6, 145.0, 140.9, 139.1, 135.0, 134.0, 132.3, 131.8, 130.4, 130.0, 129.6, 129.2, 128.9, 128.9, 128.6, 126.7, 125.5, 124.0, 121.5, 120.0, 119.8, 119.4, 116.5, 115.6, 115.1, 101.2, 69.1, 54.7, 53.2, 43.8, 43.6, 41.0, 40.8, 39.2, 33.0, 27.7, 27.0, 23.9, 21.1, 20.0, 17.3, -0.7, -1.9. *HTz:* **HRMS** (ESI): calc. for $C_{68}H_{70}N_{14}O_5Si$ $[M+3H]^{3+}$: 397.8547, found: 397.8547. *PEG1:* **HRMS** (ESI): calc. for $C_{71}H_{76}N_{14}O_6Si$ $[M+3H]^{3+}$: 456.5563, found: 456.5563. *PEG4:* **HRMS** (ESI): calc. for $C_{76}H_{86}N_{14}O_9Si$ $[M+3H]^{3+}$: 417.2020, found: 417.2017.

H-SiR-MeTz and VdU reaction

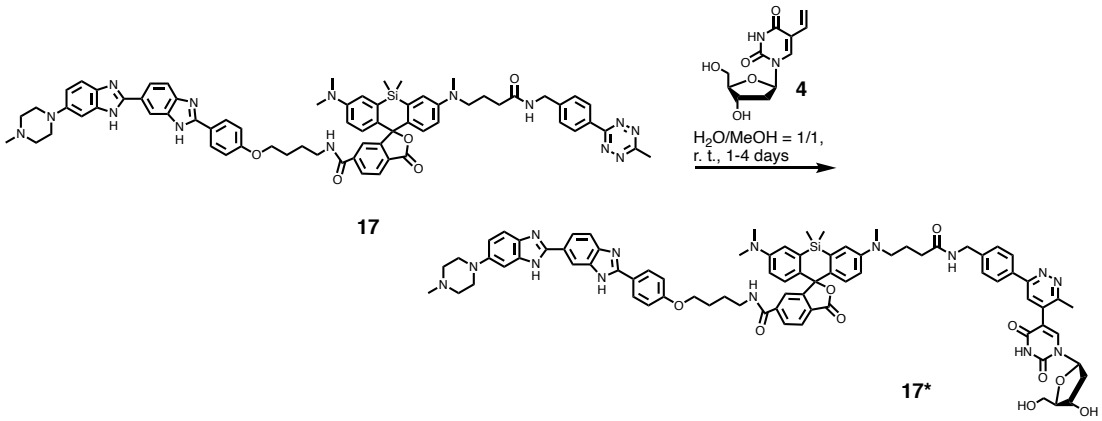

VdU (20 mM) in water was added to a solution of probe H-SiR-MeTz (2 mM) in MeOH in water/MeOH (1:1, v/v) and incubated at room temperature. **HRMS** (ESI): calc. for $C_{80}H_{84}N_{14}O_{10}Si$ $[M+3H]^{3+}$: 477.2161, found: 477.2158. Deglycosylated product: **HRMS** (ESI): calc. for $C_{75}H_{76}N_{14}O_7Si$ $[M+4H]^{4+}$: 329.1526, found: 329.1517.

2-(6-methyl-1,2,4,5-tetrazin-3-yl)ethan-1-ol

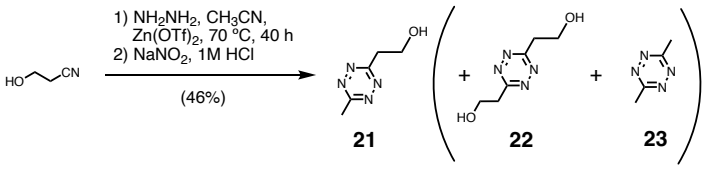

According to a published procedure[162], $Zn(OTf)_2$ (436 mg, 1.2 mmol, 1 eq.), 3-hydroxypropionitrile (273 µl, 4 mmol, 3.33 eq.), MeCN (1.05 ml, 20 mmol, 16.6 eq.), and hydrazine hydrate (1.87 ml, 60 mmol, 50 eq.) were mixed in a microwave tube. The reaction was stirred at 70 °C for 15 h in the microwave (250 W, with cooling, CEM Discover Microwave, Liberty Blue). When opening the reaction vessel, the reaction mixture started to oxidize in the presence of ambient oxygen and turned pink. Oxidation was completed by carefully adding sodium nitrite (2.76 g, 40 mmol, 33.3 eq.) and 2 M HCl to adjust to pH 3. The reaction mixture was extracted with ethyl acetate (3 × 100 ml) and dried over $MgSO_4$. The solvent was removed under reduced pressure and the residue was purified by flash column chromatography (Silica Gel, SiliCycle, 25 g, 1-10% MeOH in DCM). Compound **21** (77 mg, 0.55 mmol) was isolated besides the symmetric side products **22** and **23**. **yield**: 46% (pink oil). λ_{max} (LC-MS): 518 nm. $\mathbf{R_t}$ ($MeCN/H_2O$/TFA = 10/90/0.01 → 90/10/0.01 in 5.5 min): 1.05 min. **HRMS** (ESI): calc. for $C_5H_8N_4O$ $[M+H]^+$: 141.0771, found: 141.0772. **1H NMR** (400 MHz, $CDCl_3$, 300 K): δ [ppm] = 4.28 – 4.24 (m, 2H), 3.61 – 3.53 (m, 2H), 3.07 (s, 3H). **13C NMR** (101 MHz, $CDCl_3$, 300 K): δ [ppm] = 168.4, 168.0, 60.2, 37.5, 21.3.

2-(6-methyl-1,2,4,5-tetrazin-3-yl)ethyl methanesulfonate

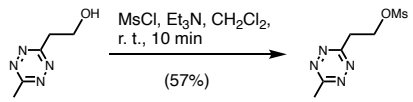

21 **24**

According to a published procedure[197], compound **21** (20 mg, 143 µmol, 1 eq.) was dissolved in DCM (2 ml). Triethylamine (23.8 µl, 171 µmol, 1.2 eq.) was added, followed by the addition of methanesulfonyl chloride (38.6 µl, 499 µmol, 3.5 eq.) in one portion. The reaction mixture was stirred at ambient temperature for 1 h. The reaction mixture was then diluted and washed with water (2 × 20 ml). The organic layer was dried over $MgSO_4$ and evaporated. The residue was purified by silica column chromatography (Silica Gel, SiliCycle, 12 g, hexanes:ethyl acetate, 1:1), yielding tetrazine **24** (17.6 mg, 81.5 µmol). **yield**: 57% (pink oil). λ_{max} (LC-MS): 521 nm. R_t(MeCN/H_2O/TFA = 10/90/0.01 → 90/10/0.01 in 5.5 min): 2.55 min. **1H NMR** (400 MHz, $CDCl_3$, 300 K): δ [ppm] = 4.87 (t, J = 6.2 Hz, 2H), 3.77 (t, J = 6.2 Hz, 2H), 3.08 (s, 3H), 3.03 (s, 3H). **13C NMR** (101 MHz, $CDCl_3$, 300 K): δ [ppm] = 168.4, 166.3, 66.1, 37.7, 34.7, 21.3.

5-bromo-3-hydroxy*iso*benzofuran-1(3*H*)-one

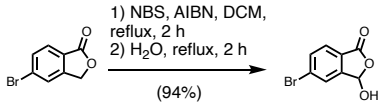

25

The synthesis followed the instructions of Kele et al.[130] In a 100 ml Schlenck flask 5-bromophthalide (TCI, #B2770, 1 g, 4.69 mmol, 1 eq.), *N*-bromosuccinimide (919 mg, 5.16 mmol, 1.1 eq.) and azobis(*iso*butyronitrile) (38.5 mg, 235 µmol, 0.05 eq.) were dissolved in DCM (20 ml). The reaction mixture was refluxed for 2 h and then kept at –20 °C for 2.5 h. Afterward, the reaction mixture was filtrated and the solvent was removed under reduced pressure. Water (20 ml) was added and the resulting mixture was refluxed for another 2 h. The reaction was cooled to 4 °C before the precipitate was filtered and washed with cold water. After drying, compound **25** (1.01 g, 4.41 mmol) was obtained. **yield**: 94% (colorless solid). **HRMS** (ESI): calc. for $C_8H_5BrO_3$ $[M+H]^+$: 228.9495, found: 228.9495. **1H NMR** (400 MHz, DMSO-d_6, 300 K): δ [ppm] = 7.93 (d, J = 1.6 Hz, 1H), 7.86 (dd, J = 8.1, 1.7 Hz, 1H), 7.76 (d, J = 8.1 Hz, 1H), 6.64 (s, 1H). **13C NMR** (101 MHz, DMSO-d_6, 300 K): δ [ppm] = 167.6, 149.4, 133.8, 128.5, 127.0, 126.5, 125.8, 97.7.

4-bromo-2-(6-(dimethylamino)-3-(dimethyliminio)-3*H*-xanthen-9-yl)benzoate

According to a published procedure[198], 3-Dimethylaminophenol (ACROS Organics™, #10486720, 273 mg, 2.00 mmol, 2 eq.), compound **25** (228 mg, 1.00 mmol, 1 eq.) and *p*-toluenesulfonic acid monohydrate (38 mg, 2.00 mmol, 0.2 eq.) were stirred in propionic acid (4 ml) at 90 °C for 18 h. The dark pink solution was cooled to ambient temperature and diluted with DCM (20 ml). The organic phase was washed with water (3 × 10 ml), brine (1 × 10 ml) and dried over $MgSO_4$.

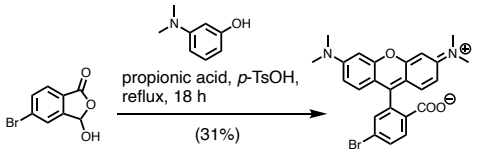

25 **26**

The solvent was removed and the crude product was purified by flash column chromatography (Silica Gel, SiliCycle, 25 g, MeOH/DCM = 5/95 → 10/90, linear gradient), affording compound **26** (145 mg,0.31 mmol). **yield**: 31% (purple solid). λ_{max} (LC-MS): 561 nm. $\mathbf{R_t}$ (MeCN/H_2O/TFA = 10/90/0.01 → 90/10/0.01 in 5.5 min): 2.75 min. **HRMS** (ESI): calc. for $C_{24}H_{21}Br_2O_3$ $[M+H]^+$: 465.0808, found: 465.0805. **1H NMR** (400 MHz, DMSO-d_6, 300 K): δ [ppm] = 7.91 (d, J = 4.7 Hz, 2H), 7.50 (s, 1H), 6.57 (d, J = 8.2 Hz, 2H), 6.52 (d, J = 8.6 Hz, 2H), 6.49 (s, 2H), 2.96 (s, 12H). **13C NMR** (101 MHz, DMSO-d_6, 300 K): δ [ppm] = 157.6, 152.0, 146.2, 133.3, 128.5, 126.5, 109.2, 97.9, 73.1.

(*E*)-2-(6-(dimethylamino)-3-(dimethyliminio)-3*H*-xanthen-9-yl)-4-(2-(6-methyl-1,2,4,5-tetrazin-3-yl)vinyl)benzoate

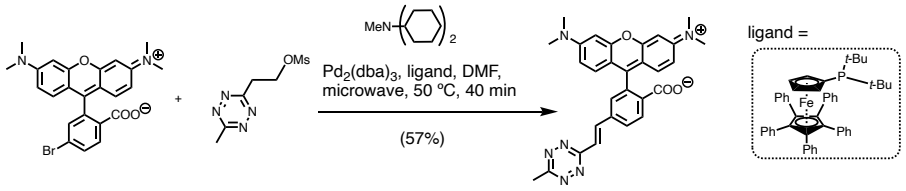

26 **24** **27**

Following the instructions of Devaraj et al.[197], compound **24** (4.12 mg, 18.9 µmol, 1.1 eq.), compound **26** (8.0 mg, 17.2 µmol, 1 eq.), *N,N*-dicyclohexalmethylamine (14.7 µl, 68.6 µmol, 4 eq.), 1,2,3,4,5-pentaphenyl-1'-(di-*tert*-butylphosphino)ferrocene (4.88 mg, 6.86 µmol, 0.4 eq.) and $Pd_2(dba)_3$ (1.57 mg, 1.72 µmol, 0.1 eq.) were dissolved in DMF (1.5 ml) and stirred in the microwave (150 W) at 50 °C for 40 min. The residue was purified by RP-HPLC (Supelco Ascentis® C18 HPLC column, MeCN:H_2O:TFA = 30/70/0.1 → 90/10/0.1, v/v/v in 1 h, flow 8 ml min^{-1}, collection at λ = 550 nm). Compound **27** (5.0 mg, 9.80 µmol) was obtained after lyophilization. **yield**: 57% (purple solid). $\mathbf{R_t}$ (MeCN/H_2O/TFA = 10/90/0.01 → 90/10/0.01 in 5.5 min): 2.80 min. **HRMS** (ESI): calc. for $C_{29}H_{27}N_6O_3$ $[M+H]^+$: 507.2139, found: 507.2137. **1H NMR** (400 MHz, MeOD-d_4, 300 K): δ [ppm] = 8.44 – 8.35 (m, 2H), 8.20 (dd, J = 8.3, 1.8 Hz, 1H), 7.82 (d, J = 1.7 Hz, 1H), 7.75 (d, J = 16.3 Hz, 1H), 7.23 (d, J = 9.5 Hz, 2H), 7.08 (dd, J = 9.5, 2.5 Hz, 2H), 7.01 (d, J = 2.4 Hz, 2H), 3.32 (s, 12H), 3.01 (s, 3H). Because of aggregation, it was not possible to measure 13C-NMR.

benzyl 4-sulfamoylbutanoate

4-Sulfamoylbutyric acid (100 mg, 598 µmol, 1 eq.), benzyl bromide (71.5 µl, 598 µmol, 1 eq.), DIPEA (98.9 µl, 598 µmol, 1 eq.) and potassium iodide (29.8 mg, 179 µmol, 0.3 eq.) were dissolved in DMF (10 ml) and stirred at ambient temperature for 3 h. The mixture was diluted

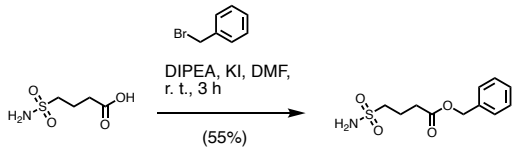

28

with ethyl acetate (100 ml), washed with water (2 × 60 ml), HCl (2 M, 1 × 100 ml), H_2O (1 × 100 ml), brine (1 × 100 ml) and dried over $MgSO_4$. The residue was purified by flash column chromatography (Silica Gel, SiliCycle, 100 g, ethyl acetate/hexane = 1/99 → 90/10). Solvent removal afforded compound **28** (85 mg, 329 µmol). **yield**: 55% (colorless solid). λ_{max} (LC-MS): 258 nm. $\mathbf{R_t}$ (MeCN/H_2O/TFA = 10/90/0.01 → 90/10/0.01 in 5.5 min): 2.07 min. **HRMS** (ESI): calc. for $C_{11}H_{15}NO_4S$ $[M+H]^+$: 258.0795, found: 258.0794. **1H NMR** (400 MHz, $CDCl_3$, 300 K): δ [ppm] = 7.51 – 7.08 (m, 5H), 5.04 (s, 2H), 4.73 (s, 2H), 3.10 (t, J = 7.0, 6.3 Hz, 2H), 2.48 (t, J = 7.0 Hz, 2H), 2.10 (p, J = 7.2 Hz, 2H). **13C NMR** (101 MHz, $CDCl_3$, 300 K): δ [ppm] = 172.5, 135.7, 128.8, 128.6, 128.5, 66.8, 54.2, 32.2, 19.5.

(*E*)-3',6'-bis(dimethylamino)-6-(2-(6-methyl-1,2,4,5-tetrazin-3-yl)vinyl)-2-(methylsulfonyl) spiro[*iso*indoline-1,9'-xanthen]-3-one

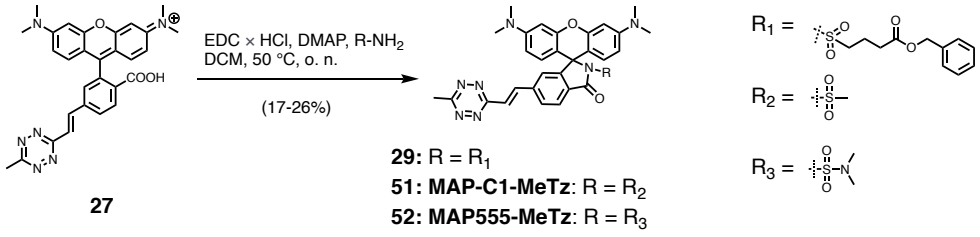

27

29: R = R_1
51: MAP-C1-MeTz: R = R_2
52: MAP555-MeTz: R = R_3

Compound 29: Compound **27** (3 mg, 5.91 µmol, 1 eq.) was dissolved in DCM (750 µl). EDC × HCl (9.06 mg, 47.3 µmol, 8 eq.), DMAP (5.78 mg, 47.3 µmol, 8 eq.) and compound **28** (2.14 mg, 11.8 µmol, 2 eq.) were added. The reaction was stirred at 50 °C overnight in a sealed vial. After solvent removel, the reaction mixture was subjected to RP-HPLC purification (Supelco Ascentis® C18 analytical HPLC column, MeCN:H_2O:TFA = 30/70/0.1 → 90/10/0.1, v/v/v in 45 min, flow 4 ml min^{-1}, collection at λ = 550 nm) and the product **29** (0.84 mg, 1.12 µmol) was obtained after lyophilization. **yield**: 19% (pink powder) λ_{max} (LC-MS): 561nm. $\mathbf{R_t}$ (MeCN/H_2O/TFA = 10/90/0.01 → 90/10/0.01 in 5.5 min): 3.18 min. **HRMS** (ESI): calc. for $C_{40}H_{40}N_7O_6S$ $[M+H]^+$: 746.2755, found: 746.2755.

Compound 51 and 52: To a solution of compound **27** (2 mg, 3.94 µmol, 1 eq.) and methanesulfonamide (750 µg, 7.88 µmol, 2 eq.) or [methyl(sulfamoyl)amino]methane (978 µg, 7.88 µmol, 2 eq.) in DCM (189 µl) was added EDC × HCl (6.04 mg, 31.5 µmol, 8 eq.) and DMAP (3.85 mg, 31.5 µmol, 8 eq.). The vial was sealed and stirred at 50 °C overnight. Compound **51** (0.60 mg, 1.03 µmol) and compound **52** (0.40 mg, 652 nmol) were obtained after RP-HPLC purification (Supelco Ascentis® C18 analytical HPLC column, MeCN:H_2O:TFA = 30/70/0.1 → 90/10/0.1, v/v/v in 45 min, flow 4 ml min^{-1}, collection at λ = 550 nm) and lyophilization. *Compound 51*: **yield**: 26% (pink powder). **HRMS** (ESI): calc. for $C_{30}H_{29}N_7O_4S$ $[M+H]^+$: 584.2075, found: 584.2076. *Compound 52*: **yield**: 17% (pink powder). **HRMS** (ESI): calc. for $C_{31}H_{32}N_8O_4S$

$[M+H]^+$: 613.2340, found: 613.2336.

(*E*)-4-((3',6'-bis(dimethylamino)-6-(2-(6-methyl-1,2,4,5-tetrazin-3-yl)vinyl)-3-oxospiro[*iso*indoline-1,9'-xanthen]-2-yl)sulfonyl)butanoic acid

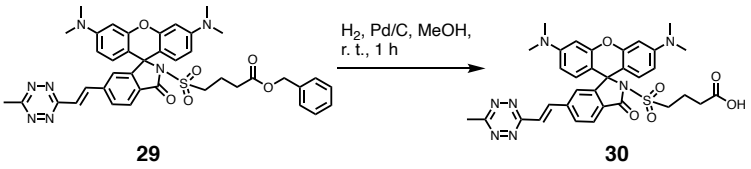

29 **30**

Anhydrous methanol was degassed by bubbling nitrogen through the solution for 5 min. Compound **29** was dissolved in methanol (1 ml) and 10 wt% of Pd/C was added. The flask was flushed with hydrogen (3 $\times$) and the reaction was stirred in a hydrogen atmosphere for 1 h. The completion of the reaction was verified by LC-MS. Product **30** was used without further purification.

(*E*)-4-((3',6'-bis(dimethylamino)-6-(2-(6-methyl-1,2,4,5-tetrazin-3-yl)vinyl)-3-oxospiro[*iso*indoline-1,9'-xanthen]-2-yl)sulfonyl)-*N*-(4-(4-(6-(4-methylpiperazin-1-yl)-1*H*,3'*H*-[2,5'-bibenzo[d]imidazol]-2'-yl)phenoxy)butyl)butanamide

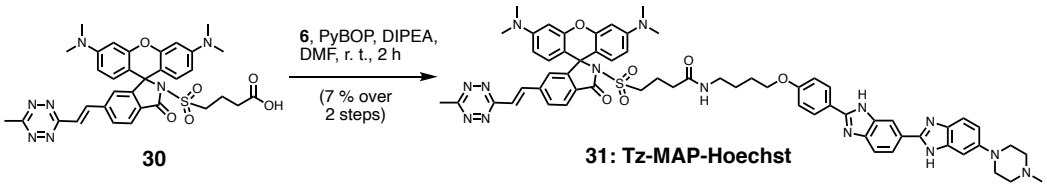

30 **31: Tz-MAP-Hoechst**

Compound **30** (1.1 mM, 0.1 ml, 0.11 µmol, 1 eq.) was dissolved in anhydrous DMF (100 µl). PyBOP (572 µg, 1.1 µmol, 10 eq.) and DIPEA (0.36 µl, 2.2 µmol, 20 eq.) were added. A solution of compound **6** (12 mM, 18.3 ml, 0.22 µmol, 2 eq.) was added dropwise over the course of 5 min. The reaction was stirred for 2 h at ambient temperature and then purified by RP-HPLC (Supelco Ascentis® C18 analytical HPLC column, MeCN:H_2O:TFA = 30/70/0.1 $\rightarrow$ 90/10/0.1, v/v/v in 45 min, flow 4 ml min^{-1}, collection at λ = 550 nm), obtaining compound **31** (12.8 µg, 11 nmol) after lyophilization. **yield**: 10% or 7% over 2 steps (pink solid). λ_{max} (LC-MS): 350 nm, 552 nm. $\mathbf{R_t}$ (MeCN/H_2O/TFA = 10/90/0.01 $\rightarrow$ 90/10/0.01 in 5.5 min): 2.75 min. **HRMS** (ESI): calc. for $C_{62}H_{65}N_{14}O_6S$ $[M+3H]^{3+}$: 379.1743, found: 379.1738.

2.4 Synthesis procedures: Reactive adenosine derivatives

Propynyl trifluoroacetamide

The synthesis followed the instructions of Novàk et al.[199] Propargylamine (1 ml, 15.6 mmol, 1 eq.) was dissolved in DCM (30 ml). A solution of the trifluoroacetic anhydride (4.34 ml, 31.2 mmol,

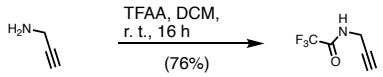

32

2 eq.) in DCM (15 ml) was added dropwise at 0 °C. The reaction mixture was stirred for 2 h, before it was poured into water. The organic phase was separated and the aqueous phase was extracted with DCM (3 × 50 ml). The combined organic phases were washed with saturated $NaHCO_3$ (3 × 50 ml), water (3 × 50 ml), brine (1 × 50 ml) and dried over $MgSO_4$. The solvent was removed under reduced pressure and the residue was purified by flash column chromatography on silica gel (Silica Gel, SiliCycle, 100 g, DCM) obtaining compound **32** (1.8 g, 11.9 mmol). **yield**: 76% (colorless liquid). $\mathbf{R_f}$(DCM)= 0.6 [Ninhydrin]. **HRMS** (ESI): calc. for $C_5H_4F_3NO$ $[M+H]^+$: 152.0318, found 152.0318. **1H NMR** (400 MHz, $CDCl_3$, 300 K): δ [ppm] = 6.71 (s, 1H), 4.15 (dd, J = 5.5, 3.0 Hz, 2H), 2.33 (t, J = 2.6 Hz, 1H). **13C NMR** (101 MHz, $CDCl_3$, 300 K): δ [ppm] = 157.11, 117.00, 114.14, 73.26, 29.70.

(2*R*,3*S*,5*R*)-5-(4-amino-5-vinyl-7*H*-pyrrolo[2,3-d]pyrimidin-7-yl)-2-(hydroxymethyl)tetra-hydrofuran-3-ol

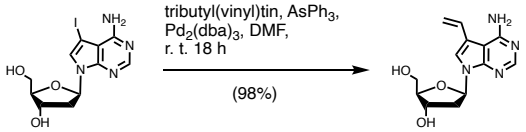

33: VdA

The reaction was adapted from Spitale et al.[184] An oven-dried Schlenk flask was charged with 7-deaza-2-deoxy-7-iodoadenosine (Biosynth Carbo-synth®, #ND06190, 50 mg, 133 µmol, 1 eq.), triphenylarsine (8.14 mg, 26.6 µmol, 0.2 eq.) and $Pd_2(dba)_3$ (6.09 mg, 6.65 µmol, 0.05 eq.). Degassed DMF (1 ml) and tributyl(vinyl)tin (46.8 ml, 160 µmol, 1.2 eq.) were added and the reaction mixture was stirred at room temperature for 10 h, before it was diluted with DCM and purified by silica flash column chromatography (Silica Gel, SiliCycle, 25 g, MeOH/DCM = 10/90) and RP-HPLC (Supelco Ascentis® C18 HPLC column, MeCN:H_2O:TFA = 1/99/0.1 → 10/90/0.1, v/v/v in 1 h, flow 8 ml min^{-1}, collection at λ = 290 nm), obtaining compound **33** (37 mg, 130 µmol). **yield**: 98% (colorless powder). λ_{max} (LC-MS): 291 nm. $\mathbf{R_t}$ (MeCN/H_2O/TFA = 10/90/0.01 → 90/10/0.01 in 5.5 min): 0.40 min, 0.68 min. **HRMS** (ESI): calc. for $C_{13}H_{16}N_4O_3$ $[M+H]^+$: 277.1295, found: 277.1294. **1H NMR** (400 MHz, DMSO-d_6, 300 K): δ [ppm] = 8.29 (d, J = 2.7 Hz, 1H), 7.92 (d, J = 2.9 Hz, 2H), 7.13 (dd, J = 17.1, 10.9 Hz, 1H), 6.54 (dd, J = 7.8, 6.0 Hz, 1H), 5.69 (dt, J = 17.2, 1.6 Hz, 1H), 5.25 (dd, J = 11.0, 1.6 Hz, 1H), 4.46 – 4.23 (m, 1H), 3.84 (dd, J = 4.6, 2.7 Hz, 1H), 3.73 – 3.47 (m, 7H).

N-(3-(4-amino-7-((2*R*,4*S*,5*R*)-4-hydroxy-5-(hydroxymethyl)tetrahydrofuran-2-yl)-7*H*-pyrrolo[2,3-d]pyrimidin-5-yl)prop-2-yn-1-yl)-2,2,2-trifluoroacetamide

The synthesis followed the instructions of Wagenknecht et al.[165] and others[200]. An oven-dried Schlenck flask was evacuated and refilled with argon (3 ×) before 7-deaza-2'-deoxy-adenosine

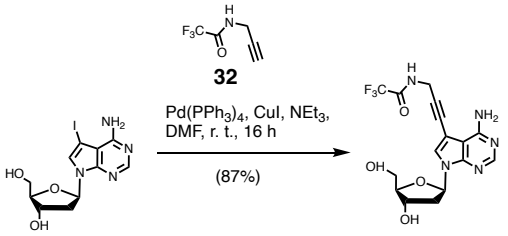

(Biosynth Carbosynth®, #ND06190, 20 mg, 53.2 µmol, 1 eq.) and copper(I) iodide (2.02 mg, 10.6 µmol, 0.2 eq.) were added and dissolved in thoroughly degassed DMF (5 ml). Compound **32** (24.1 mg, 160 µmol, 3 eq.), $Pd(PPh_3)_4$ (6.14 mg, 5.32 µmol, 0.1 eq.) and DIPEA (17.6 µl, 106 µmol, 2 eq.) were added. The reaction mixture was allowed to stirr at ambient temperature under argon atmosphere overnight. Then, it was diluted with MeOH:DCM (1:1, v/v, 5 ml) and AG-1-X8 resin (bicarbonate form, 3 g) was added. After stirring for 30 min, the crude product was filtered and the resin was rinsed once with a mixture of MeOH:DCM (1:1, v/v). The solvent was removed under reduced pressure, the crude product was redissolved in MeOH and purified by flash column chromatography (Silica Gel, SiliCycle, 5-10% MeOH in DCM). The product **34** (92 mg, 46.3 µmol) was obtained after solvent removal. **yield**: 87% (colorless solid). **1H NMR** (400 MHz, MeOD-d_4, 300 K): δ [ppm] = = 8.12 (s, 1H), 7.64 (s, 1H), 6.50 (dd, J=8.0, 6.0, 1H), 4.53 (dt, J=5.7, 2.7, 1H), 4.33 (s, 2H), 4.07 – 3.97 (m, 1H), 3.88 – 3.67 (m, 2H), 2.64 (ddd, J=13.8, 8.1, 6.0, 1H), 2.34 (ddd, J=13.4, 6.0, 2.8, 1H). **13C NMR** (101 MHz, MeOD-d_4, 300 K): δ [ppm] = = 163.1, 156.9, 152.4, 148.6, 137.7, 126.6, 87.0, 85.7, 84.0, 75.0, 70.4, 58.7, 42.01, 36.2, 31.0, 27.1.

(2*R*,3*S*,5*R*)-5-(4-amino-5-(3-aminoprop-1-yn-1-yl)-7*H*-pyrrolo[2,3-d]pyrimidin-7-yl)-2-(hydroxymethyl)tetrahydrofuran-3-ol

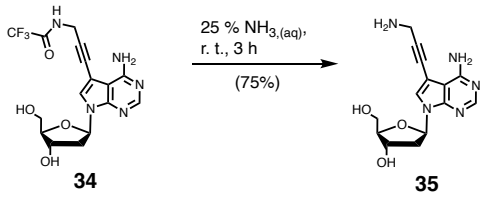

Compound **34** (9 mg, 22.5 µmol, 1 eq.) was dissolved in ammonia (25% aqueous solution, 2.5 ml) and stirred at ambient temperature for 3 h. The solvent was removed and the crude product was purified by RP-HPLC (Supelco Ascentis® C18 HPLC column, MeCN:H_2O:TFA = 1/99/0.1 → 10/90/0.1, v/v/v in 1 h, flow 8 ml min^{-1}, collection at λ = 290 nm), to obtain compound **35** (5.1 mg, 16.9 µmol) after lyophilization. **yield**: 75% (slightly brownish solid). λ_{max} (LC-MS): 284 nm. $\mathbf{R_t}$ (MeCN/H_2O/TFA = 10/90/0.01 → 90/10/0.01 in 5.5 min): 0.43 min. **HRMS** (ESI): calc. for $C_{14}H_{16}N_5O_3$ $[M+H]^+$: 304.1404, found: 304.1401. **1H NMR** (400 MHz, D_2O, 300 K): δ [ppm] = 8.34 (s, 1H), 7.92 (s, 1H), 6.65 (t, J = 6.7 Hz, 1H), 4.61 (dt, J = 6.3, 3.8 Hz, 1H), 4.14 – 4.03 (m, 3H), 3.94 – 3.59 (m, 2H), 2.70 (dt, J = 13.6, 6.6 Hz, 1H), 2.66 – 2.51 (m, 1H). **13C NMR** (101 MHz, DMSO-d_6, 300 K): δ [ppm] = 151.3, 146.7, 143.7, 130.1, 102.3, 97.0, 87.1, 84.6, 84.3, 77.4, 70.9, 61.4, 39.1, 29.9.

N-(3-(4-amino-7-((2*R*,4*S*,5*R*)-4-hydroxy-5-(hydroxymethyl)-tetra-hydrofuran-2-yl)-7*H*-pyrrolo[2,3-d]pyrimidin-5-yl)prop-2-yn-1-yl)-2-((1*R*,4*R*)-bicyclo[2.2.1]hept-5-en-2-yl)acetamide

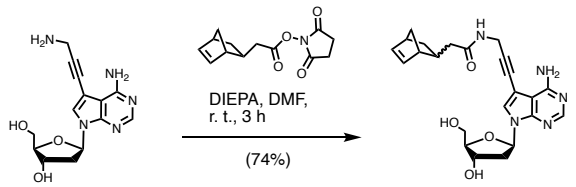

35 **36: Nor-yne-dA**

Norbornene-2-acetic acid succinimidyl ester (Sigma Aldrich, #776173-25MG, 6.2 mg, 24.7 µmol, 1 eq.) and compound **35** (9.0 mg, 29.6 µmol, 1.2 eq.) were dissolved in anhydrous DMF (0.7 ml). DIPEA (4.90 µl, 29.6 µmol, 1.2 eq.) was added. The reaction was stirred at ambient temperature for 3 h. The product was purified via RP-HPLC (Supelco Ascentis® C18 HPLC column, MeCN:H_2O:TFA = 1/99/0.1 $\rightarrow$ 10/90/0.1, v/v/v in 1 h, flow 8 ml min^{-1}, collection at λ = 286 nm). Compound **36** (8.0 mg, 18.3 µmol) was obtained after lyophilization. Endo and exo-regioisomers could not be separated. **yield**: 74% (colorless powder). **HRMS** (ESI): calc. for $C_{23}H_{28}N_5O_4$ $[M+H]^+$: 438.2136, found: 438.2132. **1H NMR** (400 MHz, MeOD-d_4, 300 K): δ [ppm] = 8.28 (s, 1H), 7.92 (s, 1H), 6.64 (dd, J = 7.4, 6.2 Hz, 1H), 6.18 (dd, J = 5.8, 3.0 Hz, 0.8H, endo), 6.08 (dd, J = 5.7, 3.0 Hz, 0.2H, exo), 6.04 (dd, J = 5.7, 2.8 Hz, 0.2H, exo), 5.99 (dd, J = 5.9, 2.9 Hz, 0.8H, endo), 4.51 (dt, J = 6.1, 3.2 Hz, 1H), 4.14 (s, 0.4H, exo), 4.12 (s, 1.6H, endo), 4.00 (q, J = 3.5 Hz, 1H), 3.82 – 3.69 (m, 2H), 2.81 (s, 0.4H, exo), 2.78 (dt, J = 3.8, 2.1 Hz, 1.6H, endo), 2.58 – 2.45 (m, 2H), 2.40 (ddd, J = 13.5, 6.2, 3.3 Hz, 1H), 2.32 (d, J = 8.0 Hz, 0.4H, exo), 2.04 (tt, J = 13.9, 6.8 Hz, 1.6H, endo), 1.97 – 1.88 (m, 1H), 1.87 – 1.78 (m, 0.2H, exo), 1.41 (ddd, J = 8.4, 4.2, 2.1 Hz, 1H), 1.28 (dt, J = 8.2, 1.6 Hz, 0.8H, endo), 1.25 – 1.16 (m, 0.2H, exo), 0.60 (ddd, J = 11.6, 4.4, 2.6 Hz, 0.8H, endo). **13C NMR** (101 MHz, MeOD-d_4, 300 K): δ [ppm] = 176.4, 176.3, 153.2, 148.0, 144.8, 138.6, 137.7, 137.4, 133.2, 129.6, 119.3, 116.4, 103.5, 99.6, 91.8, 89.4, 85.9, 73.9, 73.9, 72.6, 63.1, 50.5, 47.4, 46.9, 45.9, 43.9, 43.3, 42.1, 41.9, 36.9, 36.8, 33.2, 32.6, 30.7.

((1*R*,8*S*,9s)-bicyclo[6.1.0]non-4-yn-9-yl)methyl (3-(4-amino-7-((2*R*,4*S*,5*R*)-4-hydroxy-5-(hydroxymethyl)tetrahydrofuran-2-yl)-7*H*-pyrrolo[2,3-d]pyrimidin-5-yl)prop-2-yn-1-yl)carbamate

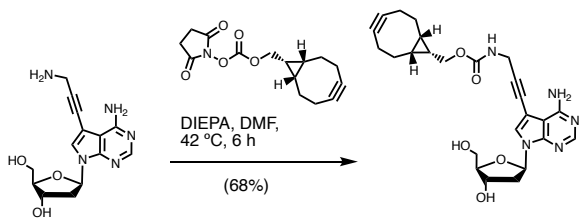

35 **37: BCN-yne-dA**

Compound **35** (5.11 mg, 16.9 µmol, 2 eq.) was dissolved in DMF (1.5 ml). DIPEA (10.4 µl,

101.1 µmol, 12 eq.) and BCN-NHS ester (Sigma Aldrich, #744867-100MG, 2.46 mg, 8.43 µmol, 1 eq.) were added. The reaction was stirred at 42 °C for 6 h. The product was purified by RP-HPLC (Supelco Ascentis® C18 HPLC column, MeCN:H_2O:TFA = 1/99/0.1 $\rightarrow$ 10/90/0.1, v/v/v in 1 h, flow 8 ml min^{-1}, collection at λ = 286 nm). Lyophilization yielded compound **37** (2.75 mg, 5.73 µmol). **yield**: 68% (colorless powder). **HRMS** (ESI): calc. for $C_{25}H_{30}N_5O_5$ $[M+H]^+$: 480.2241, found: 480.2238. **1H NMR** (400 MHz, MeOD-d_4, 300 K): δ [ppm] = 8.28 (s, 1H), 7.91 (s, 1H), 6.68 – 6.60 (m, 1H), 4.51 (dt, J = 6.1, 3.2 Hz, 1H), 4.23 (d, J = 8.2 Hz, 2H), 4.07 (s, 2H), 4.01 (q, J = 3.5 Hz, 1H), 3.83 – 3.69 (m, 2H), 2.60 – 2.47 (m, 1H), 2.46 – 2.36 (m, 1H), 2.23 (dt, J = 11.1, 3.0 Hz, 4H), 2.12 (dt, J = 14.4, 2.9 Hz, 2H), 1.69 – 1.54 (m, 2H), 1.47 – 1.34 (m, 1H), 1.01 – 0.86 (m, 2H). **13C NMR** (101 MHz, MeOD-d_4, 300 K): δ [ppm] = 158.1, 151.7, 146.6, 143.3, 128.2, 118.2, 115.0, 102.1, 98.2, 98.1, 90.9, 88.0, 84.5, 72.6, 71.2, 62.8, 61.7, 40.7, 30.6, 28.8, 20.5, 20.1, 19.6, 17.5.

(*E*)-cyclooct-4-en-1-yl (3-(4-amino-7-((2*R*,4*S*,5*R*)-4-hydroxy-5-(hydroxymethyl) tetrahydrofuran-2-yl)-7*H*-pyrrolo[2,3-d]pyrimidin-5-yl)prop-2-yn-1-yl)carbamate

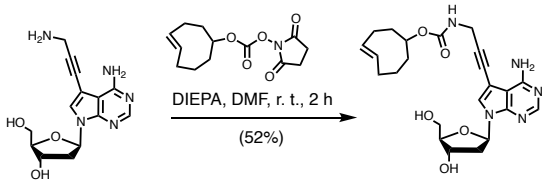

35 **38: TCO-yne-dA**

Compound **35** (5.1 mg, 16.8 µmol, 1 eq.) was dissolved in DMF (260 µl). DIPEA (4.17 µl, 25.2 µmol, 1.5 eq.) and *trans*-cyclooctene-NHS ester (Jena Bioscience, #CLK-1016-100, 5.39 mg, 20.2 µmol, 1.2 eq.) were added and the reaction mixture was stirred for 2 h at ambient temperature. The crude product was purified by HPLC (Supelco Ascentis® C18 HPLC column, MeCN:H_2O:TFA = 1/99/0.1 $\rightarrow$ 10/90/0.1, v/v/v in 1 h, flow 8 ml min^{-1}, collection at λ = 286 nm), obtaining compound **38** (4 mg, 8.74 µmol) after lyophilization. **yield**: 52% (brown oil). λ_{max} (LC-MS): 286 nm. R_t (MeCN/H_2O/TFA = 10/90/0.01 $\rightarrow$ 90/10/0.01 in 5.5 min): 2.07 min. **HRMS** (ESI): calc. for $C_{23}H_{29}N_5O_5$ $[M+H]^+$: 456.2241, found: 456.2242. **1H NMR** (400 MHz, MeOD-d_4, 300 K): δ [ppm] = 8.23 (s, 1H), 7.54 (s, 1H), 6.67 (dd, J = 7.6, 6.1 Hz, 1H), 5.66 – 5.53 (m, 1H), 5.53 – 5.41 (m, 1H), 4.52 (dt, J = 6.1, 3.1 Hz, 1H), 4.31 (dt, J = 9.3, 4.8 Hz, 1H), 3.99 (q, J = 3.7 Hz, 1H), 3.76 (qd, J = 12.0, 4.1 Hz, 2H), 3.15 (t, J = 6.9 Hz, 2H), 2.84 (t, J = 7.4 Hz, 2H), 2.60 – 2.49 (m, 1H), 2.42 – 2.24 (m, 4H), 2.03 – 1.88 (m, 4H), 1.87 – 1.79 (m, 2H), 1.77 – 1.65 (m, 2H), 1.64 – 1.52 (m, 1H). **13C NMR** (101 MHz, MeOD-d_4, 300 K): δ [ppm] = 158.9, 152.9, 149.1, 142.9, 136.1, 133.8, 123.6, 119.5, 102.4, 89.1, 85.3, 81.8, 72.7, 63.3, 42.2, 41.8, 40.7, 39.7, 35.2, 33.5, 32.1, 31.2, 24.0. **19F NMR** (376 MHz, MeOD-d_4, 300 K): δ [ppm] = -77.18.

N-(3-(4-amino-7-((2*R*,4*S*,5*R*)-4-hydroxy-5-(hydroxymethyl)tetrahydrofuran-2-yl)-7*H*-pyrrolo[2,3-d]pyrimidin-5-yl)propyl)-2,2,2-trifluoroacetamide

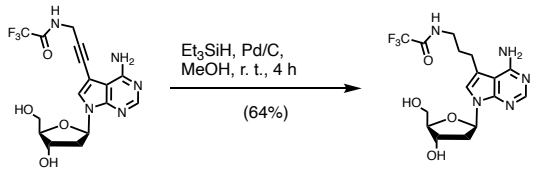

34 **39**

An oven-dried Schlenck flask was charged with palladium on activated carbon (10 wt%, 10 mg) and evacuated and purged with argon (3×). Compound **34** (50 mg, 125.2 µmol, 1 eq.) was dissolved in anhydrous methanol (4 ml) and transferred into the Schlenck flask. The solution was purged with N_2, before adding triethylsilane (303 µl, 1.88 mmol, 15 eq.) dropwise. The reaction mixture was stirred for 6 h and then filtered over Celite. The volatiles were removed under reduced pressure and the crude product was purified via reversed-phase flash chromatography (12 g C18 column, MeCN:H_2O:TFA = 99/1/0.1 → 80/20/0.1, v/v/v). After lyophilization the product **39** (32 mg, 79.3 µmol) was obtained. **yield**: 64% (colorless powder). **HRMS** (ESI): calc. for $C_{16}H_{21}F_3N_5O_4$ $[M+H]^+$: 404.1540, found: 404.1535. **1H NMR** (400 MHz, MeOD-d_4, 300 K): δ [ppm] = 8.24 (s, 1H), 7.55 (s, 1H), 6.67 (dd, J = 7.6, 6.1 Hz, 1H), 4.52 (dt, J = 6.1, 3.1 Hz, 1H), 3.99 (q, J = 3.8 Hz, 1H), 3.82 – 3.69 (m, 2H), 3.37 (t, J = 7.2 Hz, 2H), 2.93 – 2.85 (m, 2H), 2.61 – 2.50 (m, 1H), 2.42 – 2.32 (m, 1H), 1.94 (p, J = 7.4 Hz, 2H). **13C NMR** (101 MHz, MeOD-d_4, 300 K): δ [ppm] = 153.0, 149.3, 143.2, 123.7, 121.8, 119.0, 116.1, 102.4, 89.1, 85.2, 72.7, 63.3, 41.7, 39.8, 30.1, 23.9.

(2*R*,3*S*,5*R*)-5-(4-amino-5-(3-aminopropyl)-7*H*-pyrrolo[2,3-d]pyrimidin-7-yl)-2-(hydroxy-methyl)tetrahydrofuran-3-ol

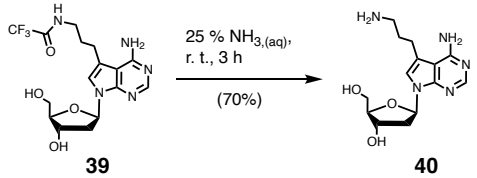

39 **40**

Compound **39** (150 mg, 376 µmol, 13.5 eq.) was dissolved in ammonia (25% aqueous solution, 3 ml) and stirred for 2 h at ambient temperature. The solvent was removed under reduced pressure and the product purified via RP-HPLC (Supelco Ascentis® C18 HPLC column, MeCN:H_2O:TFA = 1/99/0.1 → 10/90/0.1, v/v/v in 1 h, flow 8 ml min^{-1}, collection at λ = 290 nm). Product **40** (80.8 mg, 263 µmol) was obtained after lyophilization. **yield**: 70% (colorless powder). **HRMS** (ESI): calc. for $C_{14}H_{22}N_5O_3$ $[M+H]^+$: 308.1717, found: 308.1714. **1H NMR** (400 MHz, MeOD-d_4, 300 K): δ [ppm] = 8.24 (s, 1H), 7.55 (s, 1H), 6.67 (dd, J = 7.7, 6.1 Hz, 1H), 4.52 (dt, J = 6.1, 3.1 Hz, 1H), 4.03 – 3.95 (m, 1H), 3.82 – 3.69 (m, 2H), 3.37 (t, J = 7.2 Hz, 2H), 2.93 – 2.84 (m, 2H), 2.61 – 2.50 (m, 1H), 2.42 – 2.31 (m, 1H), 1.94 (p, J = 7.4 Hz, 2H).

((1*R*,8*S*,9s)-bicyclo[6.1.0]non-4-yn-9-yl)methyl (3-(4-amino-7-((2*R*,4*S*,5*R*)-4-hydroxy-5-(hydroxymethyl)tetrahydrofuran-2-yl)-7*H*-pyrrolo[2,3-d]pyrimidin-5-yl)propyl)carbamate

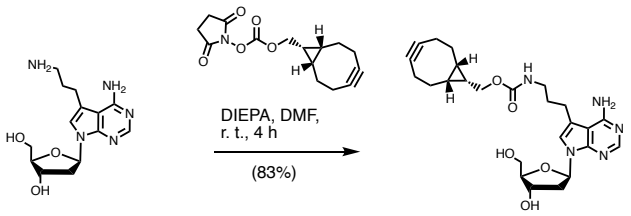

40 **41: BCN-ane-dA**

Compound **40** (8 mg, 26 µmol, 1.2 eq.) was dissolved in DMF (350 µl). DIPEA (43 µl, 260 µmol, 12 eq.) and BCN-NHS ester (Sigma Aldrich, #744867-100MG, 6.32 mg, 21.7 µmol, 1 eq.) were added. The reaction mixture was stirred for 4 h at ambient temperature. The product was purified by RP-HPLC (Supelco Ascentis® C18 HPLC column, MeCN:H_2O:TFA = 1/99/0.1 $\rightarrow$ 10/90/0.1, v/v/v in 1 h, flow 8 ml min^{-1}, collection at λ = 286 nm). The product **41** (8.8 mg, 18.0 µmol) was obtained after lyophilization. **yield**: 83% (colorless powder). **HRMS** (ESI): calc. for $C_{25}H_{34}N_5O_5$ $[M+H]^+$: 484.2554, found: 484.2547. **1H NMR** (400 MHz, MeOD-d_4, 300 K): δ [ppm] = 8.24 (s, 1H), 7.55 (s, 1H), 6.67 (dd, J = 7.7, 6.1 Hz, 1H), 4.52 (dt, J = 6.0, 3.0 Hz, 1H), 4.15 (d, J = 8.1 Hz, 2H), 3.99 (q, J = 3.7 Hz, 1H), 3.83 – 3.69 (m, 2H), 3.18 (t, J = 7.0 Hz, 2H), 2.86 (t, J = 7.4 Hz, 2H), 2.60 – 2.49 (m, 1H), 2.41 – 2.31 (m, 1H), 2.31 – 2.10 (m, 6H), 1.86 (p, J = 7.2 Hz, 2H), 1.60 (tt, J = 11.9, 5.8 Hz, 2H), 1.37 (p, J = 8.6 Hz, 1H), 1.01 – 0.87 (m, 2H). **13C NMR** (101 MHz, MeOD-d_4, 300 K): δ [ppm] = 159.5, 152.9, 149.1, 143.0, 123.6, 119.5, 119.4, 116.5, 102.4, 99.5, 89.1, 85.3, 72.7, 63.7, 63.3, 41.7, 40.7, 31.2, 30.2, 23.9, 21.9, 21.4, 18.9.

(*E*)-cyclooct-4-en-1-yl (3-(4-amino-7-((2*R*,4*S*,5*R*)-4-hydroxy-5-(hydroxymethyl)tetrahydrofuran-2-yl)-7*H*-pyrrolo[2,3-d]pyrimidin-5-yl)propyl)carbamate

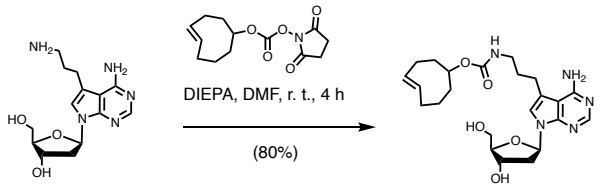

40 **42: TCO-ane-dA**

Compound **40** (4.17 mg, 13.6 µmol, 1.2 eq.) was dissolved in DMF (175 µl). DIPEA (22.4 µl, 136 µmol, 12 eq.) and *trans*-cyclooctene-NHS ester (Jena Bioscience, #CLK-1016-100, 3.02 mg, 11.3 µmol, 1 eq.) were added. The reaction mixture was stirred for 4 h at ambient temperature and then quenched with formic acid (30 µl) and water (200 µl). The product was purified by RP-HPLC (Supelco Ascentis® C18 HPLC column, MeCN:H_2O:TFA = 1/99/0.1 $\rightarrow$ 10/90/0.1, v/v/v in 1 h, flow 8 ml min^{-1}, collection at λ = 286 nm). The product **42** (6 mg, 13.0 µmol) was obtained after lyophilization. **yield**: 80% (colorless powder). **HRMS** (ESI): calc. for $C_{23}H_{34}N_5O_5$ $[M+H]^+$:

460.2554, found: 460.2552. **1H NMR** (400 MHz, MeOD-d_4, 300 K): δ [ppm] = 8.23 (s, 1H), 7.54 (s, 1H), 6.67 (dd, J = 7.6, 6.1 Hz, 1H), 5.66 – 5.53 (m, 1H), 5.53 – 5.41 (m, 1H), 4.52 (dt, J = 6.1, 3.1 Hz, 1H), 4.31 (dt, J = 9.3, 4.8 Hz, 1H), 3.99 (q, J = 3.7 Hz, 1H), 3.76 (qd, J = 12.0, 4.1 Hz, 2H), 3.15 (t, J = 6.9 Hz, 2H), 2.84 (t, J = 7.4 Hz, 2H), 2.60 – 2.49 (m, 1H), 2.42 – 2.24 (m, 4H), 2.03 – 1.88 (m, 4H), 1.87 – 1.79 (m, 2H), 1.77 – 1.65 (m, 2H), 1.64 – 1.52 (m, 1H). **13C NMR** (101 MHz, MeOD-d_4, 300 K): δ [ppm] = 158.88, 152.90, 149.12, 142.92, 136.09, 133.77, 123.63, 119.54, 102.40, 89.10, 85.30, 81.76, 72.67, 63.31, 42.21, 41.76, 40.72, 39.65, 35.16, 33.49, 32.12, 31.22, 23.95. **19F NMR** (376 MHz, MeOD-d_4, 300 K): δ [ppm] = -77.18.

(9H-fluoren-9-yl)methyl (15-(4-amino-7-((2*R*,4*S*,5*R*)-4-hydroxy-5-(hydroxymethyl)tetra-hydrofuran-2-yl)-7*H*-pyrrolo[2,3-d]pyrimidin-5-yl)-11-oxo-3,6,9-trioxa-12-azapentadec-14-yn-1-yl)carbamate

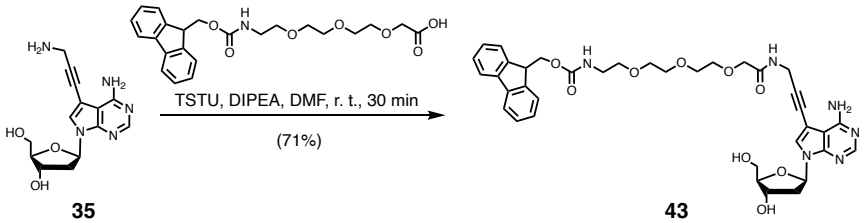

35 **43**

Fmoc-HN-PEG3-COOH (28.8 mg, 67 µmol, 1 eq.) was dissolved in DMF (600 µl), DIPEA (33.2 µl, 201 µmol, 3 eq.) and TSTU (30.3 mg, 100 µmol, 1.5 eq.) were added. The reaction was stirred at ambient temperature for 30 min. Amine **35** (20.3 mg, 67 µmol, 1 eq.) was dissolved in DMF (600 µl) and added dropwise to the solution. The product was purified via RP-HPLC (Supelco Ascentis® C18 HPLC column, MeCN:H_2O:TFA = 1/99/0.1 → 10/90/0.1, v/v/v in 1 h, flow 8 ml min^{-1}, collection at λ = 286 nm). The product **43** was obtained as a colorless solid (34 mg, 47.6 µmol) after lyophilization. **yield**: 71% (colorless solid). **HRMS** (ESI): calc. for $C_{37}H_{42}N_6O_9$ $[M+H]^+$: 715.3086, found: 715.3080. **1H NMR** (400 MHz, MeOD-d_4, 300 K): δ [ppm] = 8.20 (s, 1H), 7.82 (s, 1H), 7.72 (d, J = 7.5 Hz, 2H), 7.59 (d, J = 7.5 Hz, 2H), 7.35 (t, J = 7.4 Hz, 2H), 7.27 (td, J = 7.4, 1.2 Hz, 2H), 6.56 (dd, J = 7.3, 6.2 Hz, 1H), 4.48 (dt, J = 6.1, 3.2 Hz, 1H), 4.30 (d, J = 7.0 Hz, 2H), 4.19 (s, 2H), 4.14 (t, J = 7.0 Hz, 1H), 4.04 (s, 2H), 4.03 – 3.91 (m, 1H), 3.82 – 3.70 (m, 2H), 3.69 – 3.59 (m, 8H), 3.54 (t, J = 5.4 Hz, 2H), 3.37 – 3.22 (m, 2H), 2.58 – 2.43 (m, 1H), 2.43 – 2.30 (m, 1H). **13C NMR** (101 MHz, MeOD-d_4, 300 K): δ [ppm] = 173.5, 158.8, 152.8, 147.8, 145.3, 145.3, 144.4, 142.5, 129.7, 128.8, 128.1, 126.1, 120.9, 119.1, 116.2, 103.4, 99.5, 91.5, 89.4, 85.9, 74.1, 72.6, 72.0, 71.4, 71.4, 71.3, 71.1, 70.9, 67.7, 63.1, 42.0, 41.7, 30.4.

N-(3-(4-amino-7-((2*R*,4*S*,5*R*)-4-hydroxy-5-(hydroxymethyl)tetra-hydrofuran-2-yl)-7*H*-pyrro-lo[2,3-d]pyrimidin-5-yl)prop-2-yn-1-yl)-2-(2-(2-(2-aminoethoxy)ethoxy)ethoxy)acetamide

Compound **43** (30 mg, 42.0 µmol, 1 eq.) was dissolved in DMF (0.5 ml). Piperidine (25 µl) was added and the reaction mixture was stirred at ambient temperature for 1 h. The reaction mixture was quenched with acetic acid (20 µl), water (50 µl) and purified via RP-HPLC

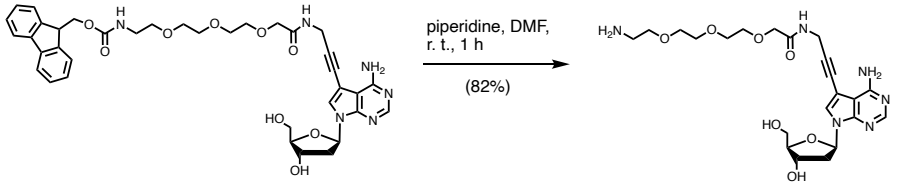

43 **44**

(Supelco Ascentis® C18 HPLC column, MeCN:H_2O:TFA = 1/99/0.1 → 10/90/0.1, v/v/v in 1 h, flow 8 ml min^{-1}, collection at λ = 286 nm). The product **44** (17 mg, 34.5 µmol) was obtained after lyophilization. **yield**: 82% (colorless solid). **HRMS** (ESI): calc. for $C_{22}H_{33}N_6O_7$ $[M+H]^+$: 515.2225, found: 515.2225. **1H NMR** (400 MHz, MeOD-d_4, 300 K): δ [ppm] = 8.29 (s, 1H), 7.91 (s, 1H), 6.63 (dd, J = 7.2, 6.2 Hz, 1H), 4.51 (dt, J = 6.2, 3.3 Hz, 1H), 4.24 (s, 2H), 4.09 (s, 2H), 4.04 – 3.97 (m, 1H), 3.83 – 3.73 (m, 1H), 3.75 – 3.60 (m, 10H), 3.13 (t, J = 5.1 Hz, 3H), 2.58 – 2.48 (m, 1H), 2.45 – 2.37 (m, 1H). **13C NMR** (101 MHz, MeOD-d_4, 300 K): δ [ppm] = 173.3, 164.9, 153.0, 148.0, 144.3, 129.8, 121.7, 118.8, 115.9, 113.1, 103.4, 99.5, 91.4, 89.4, 85.9, 74.1, 72.5, 71.8, 71.5, 71.4, 71.3, 71.2, 67.9, 63.1, 45.7, 42.1, 40.6, 37.0, 31.7, 30.4, 23.7, 23.0.

(*E*)-cyclooct-4-en-1-yl(15-(4-amino-7-((2*R*,4*S*,5*R*)-4-hydroxy-5-(hydroxymethyl)tetra-hydrofuran-2-yl)-7*H*-pyrrolo[2,3-d]pyrimidin-5-yl)-11-oxo-3,6,9-trioxa-12-azapentadec-14-yn-1-yl)carbamate

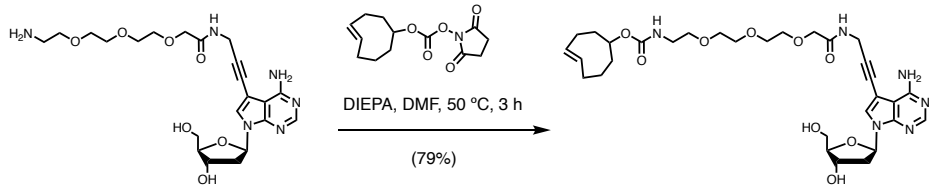

44 **45: TCO-PEG3-yne-dA**

trans-Cyclooctene-NHS ester (Jena Bioscience, #CLK-1016-100, 422 µg, 1.58 µmol, 1 eq.) was dissolved in MeCN (200 µl), DIPEA (2.09 µl, 8 eq.) was added. A solution of amine **44** (933 µg, 1.89 µmol, 1.2 eq.) in MeCN was added dropwise. The reaction was stirred for 1h at ambient temperature and then heated to 50 °C for 3 h. The reaction was quenched with acetic acid (25 µl) and diluted with water (100 µl). The product was purified with RP-HPLC (Supelco Ascentis® C18 HPLC column, MeCN:H_2O:TFA = 1/99/0.1 → 10/90/0.1, v/v/v in 1 h, flow 8 ml min^{-1}, collection at λ = 286 nm). Product **45** was obtained after lyophilization. **yield**: 79% (colorless powder). **HRMS** (ESI): calc. for $C_{31}H_{45}N_6O_9$ $[M+H]^+$: 645.3243, found: 645.3239. **1H NMR** (400 MHz, MeOD-d_4, 300 K): δ [ppm] = 8.29 (s, 1H), 7.94 (s, 1H), 6.64 (dd, J = 7.4, 6.1 Hz, 1H), 5.56 (ddd, J = 15.0, 9.5, 4.9 Hz, 1H), 5.43 (ddd, J = 16.0, 10.7, 3.5 Hz, 1H), 4.51 (dt, J = 6.0, 3.1 Hz, 1H), 4.34 – 4.24 (m, 1H), 4.23 (s, 2H), 4.06 (s, 2H), 4.01 (q, J = 3.5 Hz, 1H), 3.82 – 3.72 (m, 2H), 3.72 – 3.67 (m, 4H), 3.68 – 3.58 (m, 4H), 3.51 (t, J = 5.5 Hz, 2H), 3.25 (t, J = 5.6 Hz, 2H), 2.53 (ddd, J = 13.4, 7.4, 5.9 Hz, 1H), 2.41 (ddd, J = 13.5, 6.2, 3.3 Hz, 1H), 2.30 (qt, J = 10.6, 5.0 Hz, 3H), 1.74 – 1.63 (m, 2H), 1.62 – 1.49 (m, 1H). **13C NMR** (101 MHz, MeOD-d_4, 300 K): δ [ppm] = 173.6, 153.1, 148.0, 144.7, 136.1, 133.8, 130.8, 129.9,

119.2, 103.5, 99.5, 91.6, 89.5, 86.0, 81.8, 74.2, 72.6, 72.0, 71.4, 71.4, 71.1, 71.0, 63.1, 42.2, 42.1, 41.6, 39.6, 35.1, 33.5, 32.1, 30.4.

(2-methyl-3-(trimethylsilyl)cycloprop-2-en-1-yl)methanol

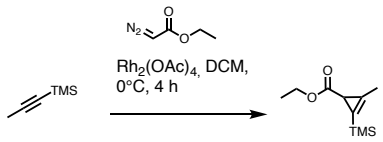

46

According to published procedures[171], [172], $Rh_2(OAc)_4$ (39.4 mg, 89.0 µmol, 0.02 eq.) was purged with nitrogen in an oven-dried Schlenk-flask, before the addition of 1-(trimethylsilyl)propyne (1.0 g, 1.33 ml, 8.91 mmol, Sigma Aldrich, #244481-25G, 2 eq.). A solution of ethyl diazoacetate (Sigma Aldrich, #E22201-5G, 13wt% in DCM, 2.94 ml, 4.45 mmol, 1 eq.) was added dropwise with a syringe pump over the course of 4 h at 0 °C. The reaction mixture was directly subjected to column chromatography (Silica 60 M, Macherey Nagel, 20% Et_2O in hexanes). The solvent was removed at 40 °C and 250 mbar to obtain the product **46** (0.31 g, 1.56 mmol). **yield**: 35% (colorless or slightly yellow liquid). $\mathbf{R_f}$ (25% DCM/hexanes): 0.1 [UV]. **1H NMR** (400 MHz, $CDCl_3$, 300 K): δ [ppm] = 4.18–3.96 (m, 2H), 2.18 (d, J = 1.5 Hz, 3H), 1.97(d, J =1.4 Hz, 1H), 1.22 (td, J = 7.1, 1.6 Hz, 3H), 0.18 (d, J =1.5 Hz, 9H). **13C NMR** (101 MHz, $CDCl_3$, 300 K): δ [ppm] = 177.2, 133.8, 122.7, 104.3, 59.9, 21.4, 14.6, 12.0, -1.4. **HRMS** (ESI): calc. for $C_{10}H_{18}O_2Si$ $[M+H]^+$: 199.1149, found: 199.1148.

ethyl 2-methyl-3-(trimethylsilyl)cycloprop-2-ene-1-carboxylate

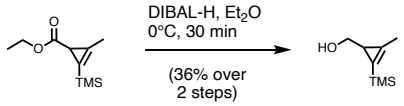

46 **47**

To a solution of compound **46** (80 mg, 0.40 µmol, 1 eq.) in Et_2O (1.2 ml), DIBAL-H (1.5 M in hexane, 800 µl, 1.20 µmol, 3 eq.) was added dropwise at 0 °C and the conversion was checked by TLC (20% Et_2O in hexanes) After the TLC showed full conversion, the reaction was quenched with a sat. aq. Rochelle's salt until a colorless gel formed. The organic layer was separated and the aqueous phase was extracted with Et_2O (3 × 20 ml). The combined organic layers were dried over $MgSO_4$ and concentrated *in vacuo* at 40 °C and 100 mbar to afford the crude product. Column chromatography (Silica 60 M, Macherey Nagel, 20% Et_2O in hexanes) yielded the product **47**. **yield**: 60% or 36% over two steps (colorless oil). $\mathbf{R_f}$ (20% Et_2O/hexanes): 0.16 [$KMnO_4$]. $\mathbf{R_t}$ (MeCN/H_2O/TFA = 10/90/0.01 → 90/10/0.01 in 5.5 min): 2.76 min. $\lambda_{\mathbf{max}}$: 222 nm. **HRMS** (ESI): calc. for $C_8H_{15}OSi$ $[M+H]^+$: 157.1043, found: 157.1043. **1H NMR** (400 MHz, $CDCl_3$, 300 K): δ [ppm] = 3.48 (d, J = 4.6 Hz, 2H), 2.22 (s, 3H), 1.56 (t, J = 4.6 Hz, 1H), 0.98 (s, 1H), 0.17 (s, 9H). **13C NMR** (101 MHz, $CDCl_3$, 300 K): δ [ppm] = 135.6, 111.4, 69.4, 22.4, 13.6, -1.0.

(2-methyl-3-(trimethylsilyl)cycloprop-2-en-1-yl)methyl (4-nitrophenyl) carbonate

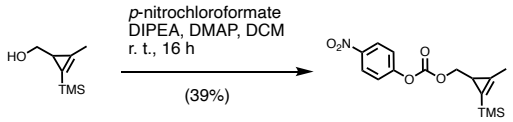

47 **48**

Cyclopropenealcohol **47** (30 mg, 0.19 mmol, 1 eq.) was dissolved in DCM (3 ml). DIPEA (49 µl, 0.29 µmol, 1.5 eq.) and DMAP (catalytic amount) were added. 4-Nitrophenyl chloroformate (46 mg, 0.23 mmol, 1.2 eq.) was added at 0 °C and the reaction mixture was allowed to warm to ambient temperature. The reaction mixture was stirred at ambient temperature for 16 h. The product was purified by flash column chromatography (SiliaSepC18, dichrom, 25 g column, 20% Et_2O/hexanes) to afford compound **48** (24 mg, 75.0 µmol). **yield**: 39% (colorless liquid). λ_{max} (LC-MS): 270 nm. $\mathbf{R_f}$ (20% Et_2O/hexanes): 0.68 [$KMnO_4$]. $\mathbf{R_t}$ (MeCN/H_2O/TFA = 10/90/0.01 $\rightarrow$ 90/10/0.01 in 5.5 min): 3.81 min.

(2-methyl-3-(trimethylsilyl)cycloprop-2-en-1-yl)methyl (3-(4-amino-7-((2*R*,4*S*,5*R*)-4-hydroxy-5-(hydroxymethyl)tetrahydrofuran-2-yl)-7*H*-pyrrolo[2,3-d]pyrimidin-5-yl)prop-2-yn-1-yl)carbamate

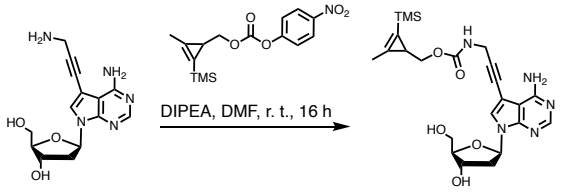

35 **49**

Compound **35** (31.7 mg, 105 µmol, 1.2 eq.) was dissolved in DMF (1.5 ml), DIPEA (17.3 µl, 105 µmol, 1.2 eq.) and compound **48** (28 mg, 87.1 µmol, 1 eq.) were added. The reaction was stirred at room temperature for 3 h. The product was purified by RP-HPLC (Supelco Ascentis® C18 HPLC column, MeCN:H_2O:TFA = 1/99/0.1 $\rightarrow$ 10/90/0.1, v/v/v in 1 h, flow 8 ml min^{-1}, collection at λ = 290 nm). Product **49** was obtained after lyophilization. The product was used without further characterization. **HRMS** (ESI): calc. for $C_{23}H_{32}N_5O_5Si$ $[M+H]^+$: 486.2167, found: 486.2163.

(2-methylcycloprop-2-en-1-yl)methyl (3-(4-amino-7-((2*R*,4*S*,5*R*)-4-hydroxy-5-(hydroxymethyl)tetrahydrofuran-2-yl)-7*H*-pyrrolo[2,3-d]pyrimidin-5-yl)prop-2-yn-1-yl)carbamate

Compound **49** (5 mg, 10.3 µmol, 1 eq.) was dissolved in THF (800 µl) and tetrabutylammonium fluoride (1 M, 93.0 µl, 103 µmol, 10 eq.) were added. The reaction was stirred for 48 h at ambient temperature before it was quenched with an aqueous $CaCl_2$ solution (1 M) and centrifuged. The supernatant was diluted with water (200 µl), acidified with acetic acid (50 µl) and purified via RP-HPLC (Supelco Ascentis® C18 HPLC column, MeCN:H_2O:TFA = 1/99/0.1 $\rightarrow$ 10/90/0.1, v/v/v

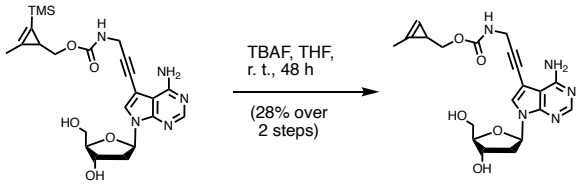

49 **50: Cp-yne-dA**

in 1 h, flow 8 ml min^{-1}, collection at λ = 286 nm). The product **50** (1.19 mg, 2.88 µmol) was obtained after lyophilization. **yield**: 28% over 2 steps (colorless powder). **HRMS** (ESI): calc. for $C_{20}H_{24}N_5O_5$ $[M+H]^+$: 414.1772, found: 414.1770. **1H NMR** (400 MHz, MeOD-d_4, 300 K): δ [ppm] = 8.25 (s, 1H), 7.88 (s, 1H), 6.66 (s, 1H), 6.62 (d, J = 6.9 Hz, 1H), 4.51 (dt, J = 6.1, 3.1 Hz, 1H), 4.07 (s, 2H), 4.06 – 3.97 (m, 2H), 3.88 (dd, J = 11.0, 5.4 Hz, 1H), 3.75 (qd, J = 12.1, 3.7 Hz, 2H), 2.60 – 2.49 (m, 1H), 2.44 – 2.34 (m, 1H), 2.13 (d, J = 1.2 Hz, 3H), 1.64 (t, J = 4.6 Hz, 1H).

2.5 Synthesis procedures: Fluorogenic nucleosides and pro-nucleotides

2,5-dioxopyrrolidin-1-yl 3,7-bis(dimethylamino)-5,5-dimethyl-3'-oxo-3'*H*,5*H*-spiro[dibenzo[b,e]siline-10,1'-*iso*benzofuran]-6'-carboxylate (SiR-6-COOSu)

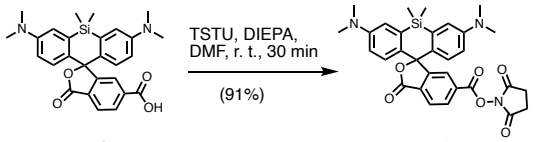

53 **54**

Compound **53** (40 mg, 84.6 µmol, 1 eq.) was dissolved in DMSO (2 ml) and DIPEA (3.56 µl, 21.5 µmol, 2 eq.). Then, TSTU (30.6 mg, 102 µmol, 1.2 eq.) was added in one portion. The reaction was stirred for 30 min at ambient temperature. The reaction was quenched with water (400 µl) and acetic acid (50 µl) and purified via RP-HPLC (Supelco Ascentis® C18 HPLC column, MeCN:H_2O:TFA = 1/99/0.1 → 10/90/0.1, v/v/v in 1 h, flow 8 ml min^{-1}, collection at λ = 650 nm). The product **54** (44 mg, 77.2 µmol) was obtained after lyophilization. **yield**: 91% (blue powder). **1H NMR** (400 MHz, DMSO-d_6, 300 K): δ [ppm] = 8.31 (dd, J = 8.0, 1.5 Hz, 1H), 8.23 (d, J = 8.1 Hz, 1H), 7.79 (s, 1H), 7.09 (s, 2H), 6.71 (d, J = 2.1 Hz, 4H), 4.33 (s, 12H), 2.88 (s, 4H), 0.63 (s, 3H), 0.53 (s, 3H). **13C NMR** (101 MHz, DMSO-d_6, 300 K): δ [ppm] = 170.0, 160.9, 130.7, 125.0 (by HMBC), 117.2, 114.1, 25.5, -0.2, -1.2.

7-Deaza-2'-deoxy-7-SiR-propynyl carbamate-adenosine (SiR-yne-dA)

Compound **54** (12 mg, 21.1 µmol, 1 eq.) was dissolved in anhydrous DMF (1 ml). DIPEA (13.9 µl, 84.3 µmol, 4 eq.) was added followed by the dropwise addition of compound **35** (7.67 mg, 25.3 µmol, 1.2 eq.) over the course of 20 min. The reaction was stirred for another 2 h at ambient

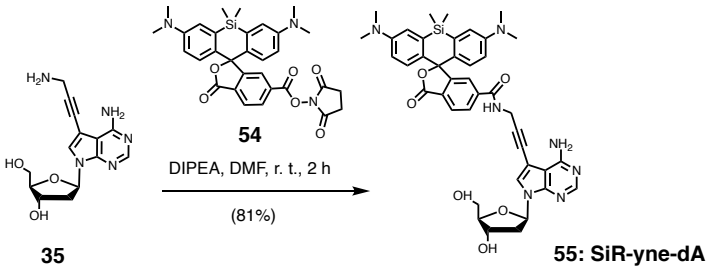

temperature. The reaction mixture was diluted with 200 µl water, acidified with 50 µl acetic acid and purified via RP-HPLC (Supelco Ascentis® C18 HPLC column, MeCN:H_2O:TFA = 1/99/0.1 $\rightarrow$ 10/90/0.1, v/v/v in 1 h, flow 8 ml min^{-1}, collection at λ = 650 nm). Compound **55** (13 mg, 177 µmol) was obtained after lyophilization. **yield**: 81% (faint blue powder). **HRMS** (ESI): calc. for $C_{41}H_{43}N_7O_6Si$ $[M+H]^+$: 758.3117, found: 758.3120. **1H NMR** (400 MHz, MeOD-d_4, 300 K): δ [ppm] = 8.33 (d, J = 8.3 Hz, 1H), 8.27 (s, 1H), 8.18 (dd, J = 8.3, 1.8 Hz, 1H), 7.92 (s, 1H), 7.78 (d, J = 1.7 Hz, 1H), 7.34 (d, J = 2.8 Hz, 2H), 6.97 (d, J = 9.5 Hz, 2H), 6.74 (dd, J = 9.6, 2.8 Hz, 2H), 6.66 – 6.58 (m, 1H), 4.49 (dt, J = 6.1, 3.2 Hz, 1H), 4.34 (s, 2H), 3.99 (q, J = 3.6 Hz, 1H), 3.81 – 3.67 (m, 2H), 3.30 (s, 12H), 2.51 (ddd, J = 13.4, 7.3, 6.0 Hz, 1H), 2.40 (ddd, J = 13.5, 6.2, 3.4 Hz, 1H), 0.64 (s, 3H), 0.58 (s, 3H). **13C NMR** (101 MHz, MeOD-d_4, 300 K): δ [ppm] = 216.1, 168.4, 167.7, 155.0, 153.0, 148.6, 148.0, 144.4, 140.9, 138.1, 134.8, 132.2, 130.0, 129.7, 129.0, 121.7, 118.7, 115.8, 115.2, 103.5, 99.6, 91.5, 89.4, 86.0, 74.3, 72.6, 63.1, 49.7, 49.6, 49.5, 49.4, 49.3, 49.2, 49.1, 49.0, 48.9, 48.8, 48.6, 48.4, 42.1, 41.0, 31.5, -0.8, -1.8.

SiR-ane-dA

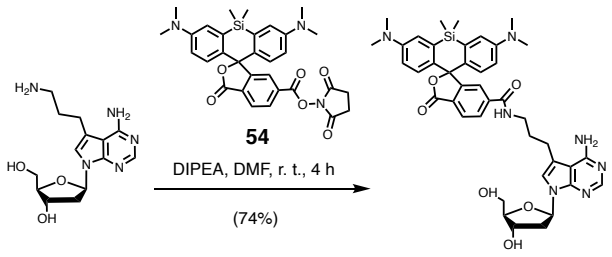

Compound **54** (135 mg, 237 µmol, 1 eq.) was dissolved in anhydrous DMF (8 ml). DIPEA (156 µl, 947 µmol, 4 eq.) was added followed by dropwise addition of compound **40** (80 mg, 260 µmol, 1.1 eq.) over the course of 20 min. The reaction was stirred for another 4 h at ambient temperature. The reaction mixture was diluted with 200 µl water, acidified with 50 µl acetic acid and purified via RP-HPLC (Supelco Ascentis® C18 HPLC column, MeCN:H_2O:TFA = 1/99/0.1 $\rightarrow$ 10/90/0.1, v/v/v in 1 h, flow 8 ml min^{-1}, collection at λ = 650 nm). Compound **56** (135 mg, 177 µmol) was obtained after lyophilization. **yield**: 74% (faint blue powder). **HRMS** (ESI): calc. for $C_{41}H_{47}N_7O_6Si$ $[M+2H]^{2+}$: 381.6751, found: 381.6750. **1H NMR** (400 MHz, MeOD-d_4, 300 K): δ [ppm] = 8.28 (d, J = 8.2 Hz, 1H), 8.20 (s, 1H), 8.07 (dd, J = 8.2, 1.8 Hz, 1H), 7.66 (d, J = 1.7 Hz, 1H), 7.55 (s, 1H), 7.33 (d, J = 2.9 Hz, 2H), 6.95 (dd, J = 9.5, 2.2 Hz, 2H), 6.75 (ddd, J = 9.6, 2.9, 0.9 Hz, 2H), 6.62 (dd, J = 7.6, 6.1 Hz, 1H), 4.49 (dt, J = 6.1, 3.1 Hz, 1H), 3.94 (q, J = 3.7 Hz, 1H), 3.79 – 3.65 (m, 2H), 3.48 (td, J = 6.9, 2.0 Hz, 2H), 3.28 (s, 12H), 2.92 (t, J =

7.3 Hz, 2H), 2.51 (ddd, J = 13.6, 7.7, 6.0 Hz, 1H), 2.32 (ddd, J = 13.4, 6.2, 3.2 Hz, 1H), 2.00 (p, J = 7.5 Hz, 2H), 0.64 (s, 3H), 0.59 (s, 3H). **13C NMR** (101 MHz, MeOD-d_4, 300 K): δ [ppm] = 168.2, 168.0, 154.7, 152.9, 149.1, 142.9, 140.1, 139.0, 134.1, 131.7, 129.9, 129.4, 128.8, 123.6, 121.4, 119.4, 119.3, 116.4, 115.2, 102.4, 89.0, 85.2, 72.6, 63.2, 41.7, 41.0, 40.4, 30.5, 24.3, -0.8, -1.7.

3,7-bis(dimethylamino)-5,5-dimethyl-3'-oxo-*N*-(prop-2-yn-1-yl)-3'*H*,5*H*-spiro[dibenzo[b,e]siline-10,1'-*iso*benzofuran]-6'-carboxamide SiR-alkyne

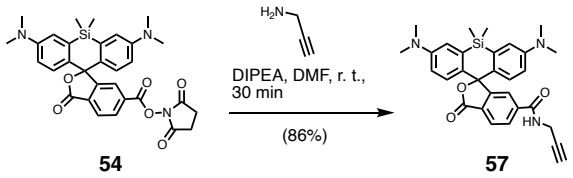

54 **57**

Compound **54** (7.15 mg, 12.55 µmol, 1 eq.) was dissolved in DMF (1 ml), DIPEA (6.22 µl, 37.6 µmol, 3 eq.) and propargylamine (2.41 µl, 37.6 µmol, 3 eq.) were added. The reaction was stirred for 30 min at ambient temperature. The reaction was stirred for 16 h at ambient temperature, quenched with water and acetic acid and purified via RP-HPLC (Supelco Ascentis® C18 HPLC column, MeCN:H_2O:TFA = 1/99/0.1 → 10/90/0.1, v/v/v in 1 h, flow 8 ml min^{-1}, collection at λ = 650 nm). Compound **57** (5.5 mg, 10.9 µmol) was obtained after lyophilization. **yield**: 86% (dark blue powder). **HRMS** (ESI): calc. for $C_{30}H_{31}N_3O_3Si$ $[M+H]^+$: 510.2207, found: 510.2201. **1H NMR** (400 MHz, MeOD-d_4, 300 K): δ [ppm] = 8.32 (d, J = 8.2 Hz, 1H), 8.12 (dd, J = 8.2, 1.8 Hz, 1H), 7.72 (d, J = 1.7 Hz, 1H), 7.34 (d, J = 2.8 Hz, 2H), 6.98 (d, J = 9.5 Hz, 2H), 6.76 (dd, J = 9.6, 2.8 Hz, 2H), 4.16 (d, J = 2.5 Hz, 2H), 3.31 (s, 12H), 2.61 (t, J = 2.5 Hz, 1H), 0.64 (s, 3H), 0.59 (s, 3H). **13C NMR** (101 MHz, MeOD-d_4, 300 K): δ [ppm] = 167.7, 155.1, 140.9, 138.4, 134.7, 132.1, 130.1, 129.8, 128.9, 121.7, 118.7, 115.2, 80.4, 72.3, 41.0, 30.1, -0.9, -1.7.

SiR-yne-dU

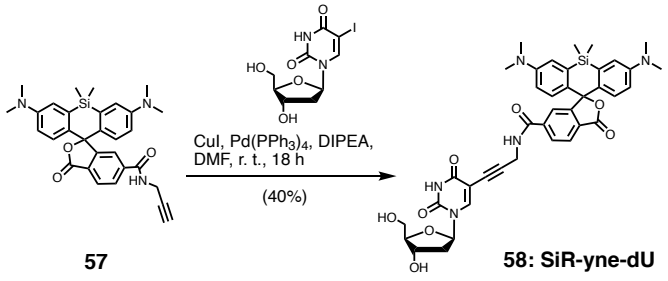

57 **58: SiR-yne-dU**

An oven-dried Schlenck flask was evacuated, refilled with argon (3 ×) before it was charged with 5-iodo-2'-deoxyuridine (Biosynth Carbosynth®, #ND05147, 2.64 mg, 7.46 µmol, 1 eq.) and copper(I) iodide (284 µg, 1.49 µmol, 0.2 eq.). The solids were dissolved in thoroughly degassed DMF (0.5 ml). Compound **57** (3.8 mg, 7.46 µmol, 1 eq.), $Pd(PPh_3)_4$ (862 µg, 0.746 µmol, 0.1 eq.) and DIPEA (2.46 µl, 14.9 µmol, 2 eq.) were added. The reaction was allowed to stir at ambient

temperature under argon atmosphere overnight. The reaction mixture was subjected to a mini-workup, diluting the solution with 0.5 ml water and extracting the product with DCM (3 × 1 ml). DCM was evaporated and the residue diluted with 200 µl water, acidified with 50 µl acetic acid and purified via RP-HPLC (Supelco Ascentis® C18 HPLC column, MeCN:H_2O:TFA = 10/90/0.1 → 40/60/0.1, v/v/v in 1 h, flow 8 ml min^{-1}, collection at λ = 650 nm). Lyophilization yielded compound **58** (1.2 mg, 3.00 µmol). **yield**: 40% (faint blue powder). **HRMS** (ESI): calc. for $C_{39}H_{41}N_5O_8Si$ $[M+H]^+$: 736.2797, found: 736.2795. **1H NMR** (400 MHz, MeOD-d_4, 300 K): δ [ppm] = 8.33 – 8.27 (m, 2H), 8.14 (dd, J = 8.2, 1.8 Hz, 1H), 7.74 (d, J = 1.7 Hz, 1H), 7.31 (d, J = 2.8 Hz, 2H), 6.95 (d, J = 9.5 Hz, 2H), 6.75 (ddd, J = 9.5, 2.9, 0.7 Hz, 2H), 6.21 (t, J = 6.6 Hz, 1H), 4.40 – 4.35 (m, 2H), 4.35 (s, 1H), 3.92 (q, J = 3.3 Hz, 1H), 3.78 (dd, J = 12.0, 3.1 Hz, 1H), 3.70 (dd, J = 12.0, 3.5 Hz, 12H), 2.30 (ddd, J = 13.6, 6.1, 3.6 Hz, 1H), 2.25 – 2.13 (m, 1H), 0.64 (s, 3H), 0.58 (s, 3H). **13C NMR** (101 MHz, MeOD-d_4, 300 K): δ [ppm] = 167.6, 164.7, 151.1, 145.5, 129.1, 121.1, 115.2, 99.7, 89.7, 89.2, 87.1, 75.4, 72.0, 62.6, 56.9, 41.7, 40.9, 31.1, 17.5, 17.3, 17.1, -0.8, -1.7.

tri((pivaloyloxy)methyl) phosphate

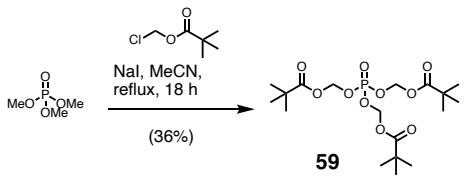

59

The synthesis was performed according to a previously published procedure.[201] Trimethyl phosphate (2.52 ml, 21.4 mmol, 1 eq.) was dissolved in MeCN (9 ml). Sodium iodide (9.63 g, 64.3 mmol, 3 eq.) and chloromethyl pivalate (Alfa Aesar™, #A11967.14, 12.1 ml, 83.5 mmol, 3.9 eq.) were added sequentially. The reaction mixture was heated to 82 °C for 24 h. The reaction mixture was diluted with Et_2O (100 ml) and washed with water, brine, and dried over $MgSO_4$. The solvent was removed under reduced pressure. The crude sample was purified by flash chromatography (SiliaSepC18, dichrom, 100 g column, DCM). The product **59** (3.4 g, 7.72 mmol) was obtained after solvent removal. **yield**: 36% (colorless oil). **HRMS** (ESI): calc. for $C_{18}H_{33}O_{10}P$ $[M+Na]^+$: 463.1704, found: 463.1702. **1H NMR** (400 MHz, $CDCl_3$, 300 K): δ [ppm] = 5.66 (d, J=13.7, 6H), 1.23 (s, 27H). **13C NMR** (101 MHz, $CDCl_3$, 300 K): δ [ppm] = 176.7, 82.9, 82.9 (d, J=5.14Hz), 38.9, 26.9. **31P NMR** (162 MHz, $CDCl_3$, 300 K): δ [ppm] = -5.24 (hept, J = 13.8 Hz).

bis((pivaloyloxy)methyl) phosphate piperidinium salt

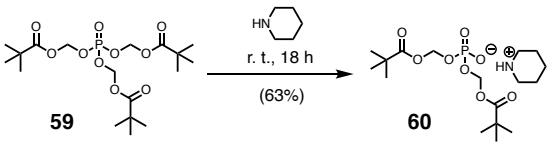

59 **60**

The synthesis was performed according to a previously published procedure.[201] Compound **59** (1.7 g, 3.86 mmol, 1 eq.) was dissolved in piperidine (10 ml) and stirred at room temperature

for 20 h. The reaction mixture was concentrated *in vaccuo* and filtered over a sephadex column g-25 to obtain the product **60** (1 g, 2.43 mmol). **yield**: 63% (colorless solid). **1H NMR** (400 MHz, $CDCl_3$, 300 K): δ [ppm] = 9.23 (s, 2H), 5.55 (dd, J = 11.81, 6.21 Hz, 4H), 2.99 (tt, J = 7.80, 3.91 Hz, 4H), 2.54 – 2.42 (m, 2H), 1.67 – 1.50 (m, 4H), 1.21 (s, 18H). **13C NMR** (101 MHz, $CDCl_3$, 300 K): δ [ppm] = 177.5, 83.5, 83.4, 44.7, 38.8, 27.1, 23.3. **31P NMR** (162 MHz, $CDCl_3$, 300 K): δ [ppm] = -4.27.

bis((pivaloyloxy)methyl) phosphate

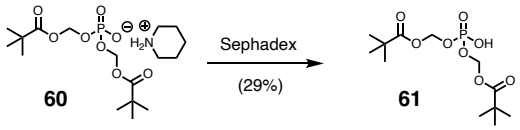

60 **61**

The synthesis was performed according to a previously published procedure.[201] Compound **60** (1 g, 2.43 mmol) was dissolved in water (20 ml) and loaded onto a cation exchange column (Dowex 50WX8, 200-400 mesh, ion-exchange resin) and then eluted with distilled water. The eluent was collected and lyophilized to give compound **61** (230 mg, 0.70 mmol). The product is hygroscopic and turns liquid if stored at 4 °C. **yield**: 29% (colorless solid). **1H NMR** (400 MHz, $CDCl_3$, 300 K): δ [ppm] = 5.65 (d, J=14.2, 4H), 1.24 (s, 18H). **13C NMR** (101 MHz, $CDCl_3$, 300 K): δ [ppm] = 82.8 (d, J=5.3), 82.8, 38.9, 26.9. **31P NMR** (162 MHz, $CDCl_3$, 300 K): δ [ppm] = -2.06.

bis((pivaloyloxy)methyl) phosphochloride

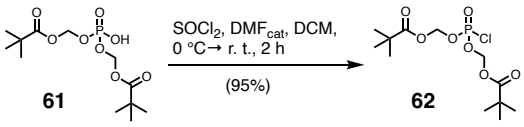

61 **62**

The synthesis was performed according to a previously published procedure.[201] To a stirred solution of oxalyl chloride (2 M in DCM, 383 ml, 766 µmol, 5 eq.) in DCM (1.5 ml), compound **61** (50 mg, 153 µmol, 1 eq.) and a catalytic amount of DMF (3 µl) was added slowly at ambient temperature. After stirring for 2 h, the solvent was removed under reduced pressure. The residue was dried *in vacuo* to give the compound **62** (50 mg, 145 µmol). The product **62** was stored up to 48 h at –20 °C and used without further purification. **yield**: 95% (slightly yellow oil). **1H NMR** (400 MHz, $CDCl_3$, 300 K): δ [ppm] = 5.81 – 5.71 (4H, m), 1.25 (s, 18H). **13C NMR** (101 MHz, $CDCl_3$, 300 K): δ [ppm] = 176.5, 83.4 (d, J=6.49), 38.9, 26.9. **31P NMR** (162 MHz, $CDCl_3$, 300 K): δ [ppm] = -2.90.

POM-SiR-ane-dA

The synthesis was performed according to a previously published procedure.[58] Compound **56** (25 mg, 32.8 µmol, 1 eq.) was dissolved in pyridine (1 ml), co-evaporated twice (2 × 1 ml) and then cooled to –40 °C. DMAP (2 mg, 16.4 µmol, 0.5 eq.) was added and the reaction mixture was allowed to stir for 20 min before a solution of compound **62** (17 mg, 49.2 µmol, 1.5 eq.) in

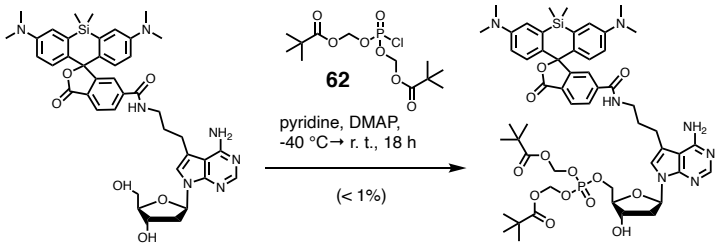

56: SiR-ane-dA **63: POM-SiR-dA**

THF (1 ml) was added dropwise. The mixture was stirred at –40 °C for 1 h and then at ambient temperature for 16 h. The reaction was diluted with ethyl acetate (20 ml) and washed with water (10 ml). The aqueous layer was re-extracted with ethyl acetate and the combined organic phases were concentrated under reduced pressure. The residue was dissolved in DMSO, water and acidified with AcOH before purification by RP-HPLC (Supelco Ascentis® C18 HPLC column, MeCN:H_2O:TFA = 30/70/0.1 → 10/90/0.1, v/v/v in 1 h, flow 8 ml min^{-1}, collection at λ = 650 nm). Lyophilization afforded product **63** (0.35 mg, 327 nmol). **yield**: 1% (blue powder). **HRMS** (ESI): calc. for $C_{53}H_{68}N_7O_{13}PSi$, $[M+2H]^{2+}$, calc.: 535.7264, found: 535.7262. **1H NMR** (400 MHz, DMSO-d_6, 300 K): δ [ppm] = 8.18 (s, 1H), 8.07 (dd, J = 8.0, 1.4 Hz, 1H), 8.01 (d, J = 8.0 Hz, 1H), 7.66 (s, 1H), 7.25 (s, 1H), 7.01 (d, J = 2.3 Hz, 2H), 6.63 (d, J = 2.5 Hz, 4H), 6.52 (t, J = 7.0 Hz, 1H), 5.53 (dd, J = 13.8, 7.0 Hz, 4H), 3.17 – 3.04 (m, 2H), 2.91 (s, 12H), 2.79 (t, J = 7.5 Hz, 2H), 2.24 – 2.16 (m, 2H), 2.01 (t, J = 7.5 Hz, 2H), 1.79 (t, J = 7.4 Hz, 2H), 1.46 (d, J = 7.8 Hz, 2H), 1.21 – 1.06 (m, 18H), 0.63 (s, 3H), 0.52 (s, 3H). **31P NMR** (162 MHz, DMSO-d_6, 300 K): δ [ppm] = -3.96.

benzyl prop-2-yn-1-ylcarbamate

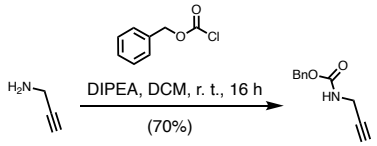

64

Propargylamine (581 µl, 9.08 mmol, 1 eq.) was dissolved in anhydrous THF (14.9 ml). K_2CO_3 (1.88 g, 13.6 mmol, 1.5 eq.) was added. The reaction mixture was cooled to 0 °C and benzyl chloroformate (1.86 g, 10.9 mmol, 1.2 eq.) was added dropwise over the course of 15 min. The reaction reaction was allowed to warm to ambient temperature and stirred for 2 h. The reaction mixture was washed with water, citric acid, brine, and dried over $MgSO_4$. The crude sample was purified by flash chromatography (SiliaSepC18, dichrom, 80 g column, DCM/MeOH 99/1 → 97/3). Solvent removal yielded compound **64** (1.20 g, 6.36 mmol). **yield**: 70% (colorless oil). $\mathbf{R_f}$(DCM) = 0.55 [UV]. **HRMS** (ESI): calc. for $C_{11}H_{11}NO_2$, $[M+H]^{1+}$, calc.: 190.0863, found: 190.0863. **1H NMR** (400 MHz, MeOD-d_4, 300 K): δ [ppm] = 7.37 – 7.25 (m, 5H), 5.09 (s, 2H), 3.88 (d, J = 2.51 Hz, 2H), 3.35 (s, 1H), 2.56 (t, J = 2.56 Hz, 1H). **13C NMR** (101 MHz, MeOD-d_4, 300 K): δ [ppm] = 158.6, 138.2, 129.5, 129.0, 128.8, 81.1, 72.0, 67.7, 31.0.

benzyl(3-(4-amino-7-((2*R*,4*S*,5*R*)-4-hydroxy-5-(hydroxymethyl)tetrahydrofuran-2-yl)-7*H*-pyrrolo[2,3-d]pyrimidin-5-yl)prop-2-yn-1-yl)carbamate

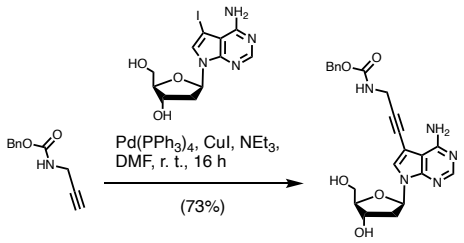

64 **65**

In an oven-dried Schlenck flask, 7-deaza-2'-deoxy-adenosine (Biosynth Carbosynth®, #ND06190, 200 mg, 532 µmol, 1 eq.) and copper(I) iodide (20.3 mg, 106 µmol, 0.2 eq.) were dissolved in thoroughly degassed DMF (4.94 ml). benzoyl propargylamine (302 mg, 1.6 mmol, 3 eq.), $Pd(PPh_3)_4$ (61.4 mg, 53.2 µmol, 0.1 eq.) and DIPEA (176 µl, 1.06 mmol, 2 eq.) were added. The reaction mixture was stirred at ambient temperature under argon atmosphere overnight. Then, the reaction mixture was diluted with a solution of MeOH:DCM (1:1) and AG-1-X8 resin (bicarbonate form, 3 g) was added. After stirring for 30 min, the crude product was filtered and the resin was once rinsed with a 1:1 solution of MeOH:DCM. The solvent was removed under reduced pressure, the crude product was redissolved in MeOH and purified by flash column chromatography (SiliaSepC18, dichrom, 40 g column) using a gradient of MeOH in DCM (5 $\rightarrow$ 10%). The product **65** (170 mg, 388 µmol) was obtained after solvent removal. **yield**: 73% (colorless powder). **HRMS** (ESI): calc. for $C_{22}H_{23}N_5O_5$ $[M+H]^+$: 438.1772, found: 438.1769. **1H NMR** (400 MHz, MeOD-d_4, 300 K): δ [ppm] = 8.32 (s, 1H), 7.92 (d, J = 2.15 Hz, 1H), 7.43 – 7.23 (m, 5H), 6.65 (t, J = 6.71 Hz, 1H), 5.16 (s, 2H), 4.52 (dt, J = 6.16, 3.22 Hz, 1H), 4.11 (s, 2H), 4.01 (dd, J = 8.56, 5.04 Hz, 1H), 3.77 (qd, J = 12.02, 3.77 Hz, 2H), 3.37 (s, 1H), 2.54 (dt, J = 13.37, 6.62 Hz, 1H), 2.43 (ddd, J = 13.50, 6.22, 3.39 Hz, 1H). **13C NMR** (101 MHz, MeOD-d_4, 300 K): δ [ppm] = 157.7, 151.6, 146.5, 142.9, 136.8, 128.3, 128.1, 127.6, 127.4, 98.3, 90.8, 88.0, 84.5, 72.7, 71.2, 66.4, 61.7, 40.7, 30.7, 15.9, 7.8.

benzyl (3-(4-amino-7-((2*R*,4*S*,5*R*)-5-(((bis(benzyloxy)phosphoryl)oxy)methyl)-4-hydroxytetrahydrofuran-2-yl)-7*H*-pyrrolo[2,3-d]pyrimidin-5-yl)prop-2-yn-1-yl)carbamate

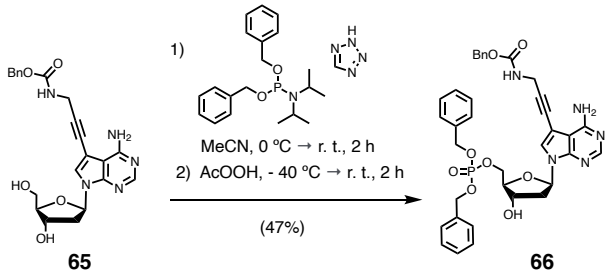

65 **66**

According to a published procedure[202], compound **65** (50 mg, 114 µmol, 1 eq.) and 2*H*-tetrazole (1 M, 137 µl, 137 µmol, 1.2 eq.) were dissolved in anhydrous MeCN (5 ml). Dibenzyl *N,N*-di*iso*propylphosphoramidite (Sigma Aldrich, #416436-5ML, 39.5 mg, 114 µmol, 1 eq.) was added at 0 °C. After stirring the reaction at 0 °C for 30 min, the reaction was allowed to warm to ambient temperature and stirred for another 30 min. The reaction mixture was cooled to –40 °C, before peroxyacetic acid (32%, 238 µl, 1.00 mmol, 8.75 eq.) was added and then allowed to warm to ambient temperature. The solvent was removed and the residue purified by flash column chromatography (SiliaSepC18, dichrom, 25 g column) using a gradient of MeOH in DCM (5 → 10%) yielding compound **66** (37.5 mg, 53.8 µmol) after solvent removal. **yield**: 47% (colorless powder). **HRMS** (ESI): calc. for $C_{36}H_{36}N_5O_8P$ $[M+H]^+$: 698.2374, found: 698.2377. **1H NMR** (400 MHz, MeOD-d_4, 300 K): δ [ppm] = 8.21 (s, 1H), 7.67 (s, 1H), 7.43 – 7.33 (m, 4H), 6.60 (t, J = 6.70 Hz, 1H), 5.17 – 5.06 (m, 3H), 5.06 – 4.95 (m, 5H), 4.46 (dt, J = 6.13, 3.74 Hz, 1H), 4.26 – 4.14 (m, 2H), 4.09 (td, J = 3.87, 2.32 Hz, 1H), 4.07 (s, 2H), 2.53 – 2.35 (m, 2H). **13C NMR** (101 MHz, MeOD-d_4, 300 K): δ [ppm] = 159.1, 148.4, 145.3, 138.2, 137.1, 137.0, 137.0, 130.0, 129.8, 129.8, 129.7, 129.7, 129.7, 129.5, 129.5, 129.1, 129.1, 128.9, 128.8, 103.7, 99.7, 92.2, 86.7, 86.6, 85.8, 74.3, 72.0, 71.0, 70.9, 68.5, 68.5, 67.8, 41.2, 32.2. **31P NMR** (162 MHz, MeOD-d_4, 300 K): δ [ppm] = -1.31.

((2*R*,3*S*,5*R*)-5-(4-amino-5-(3-aminopropyl)-7*H*-pyrrolo[2,3-d]pyrimidin-7-yl)-3-hydroxytetrahydrofuran-2-yl)methyl phosphate

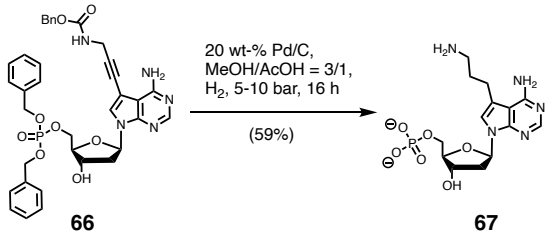

66 **67**

Compound **66** (40 mg, 57.3 µmol, 1 eq.) was dissolved in MeOH/acetic acid (3:1, v/v, 15 ml). The solution was purged with nitrogen before Pd/C (20 wt%, 8 mg) was added. The solution was then purged with hydrogen before hydrogenation was performed at 5–10 bar for 16 h. The solvent was removed under reduced pressure and the residue purified by RP-HPLC using a high pH column (Phenomenex Gemini®, MeCN:1 M TEAB = 99/1 → 95/5, v/v, 1 h, flow 8 ml min^{-1}, collection at λ = 286 nm). Lyophilization gave compound **67** (13 mg, 33.8 µmol). **yield**: 59% (colorless powder). **HRMS** (ESI): calc. for $C_{14}H_{22}N_5O_6P$ $[M+H]^+$: 388.1380, found: 388.1379. **1H NMR** (400 MHz, D_2O, 300 K): δ [ppm] = 8.10 (s, 1H), 7.50 (s, 1H), 6.67 (dd, J = 8.04, 6.26 Hz, 1H), 4.73 (dt, J = 5.51, 2.66 Hz, 1H), 4.22 – 4.16 (m, 1H), 3.92 (dtt, J = 18.65, 11.43, 3.44 Hz, 2H), 3.14 – 2.96 (m, 3H), 2.93 (t, J = 6.70 Hz, 2H), 2.76 (ddd, J = 13.94, 8.09, 5.87 Hz, 1H), 2.43 (ddd, J = 13.92, 6.30, 2.84 Hz, 1H), 2.20 – 2.01 (m, 2H), 1.92 (s, 1H). **13C NMR** (101 MHz, D_2O, 300 K): δ [ppm] = 157.6, 151.3, 150.0, 119.2, 114.9, 102.5, 86.1, 82.8, 72.1, 59.0, 38.8, 38.2, 26.1, 22.3. **31P NMR** (162 MHz, D_2O, 300 K): δ [ppm] = 3.76.

((2*R*,3*S*,5*R*)-5-(4-amino-5-(3-(3,7-bis(dimethylamino)-5,5-dimethyl-3'-oxo-3'*H*,5*H*-spiro[dibenzo[b,e]siline-10,1'-*iso*benzofuran]-6'-carboxamido)propyl)-7*H*-pyrrolo[2,3-d]pyrimidin-7-yl)-3-hydroxytetrahydrofuran-2-yl)methyl phosphate

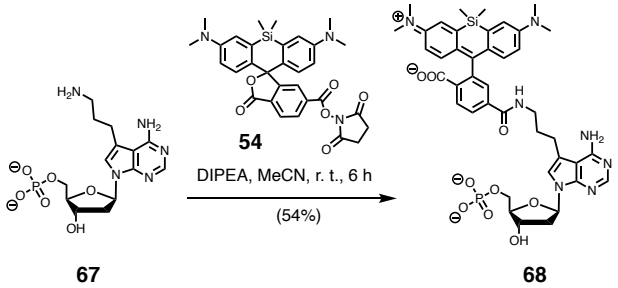

67 **68**

Compound **54** (6.13 mg, 10.8 µmol, 1 eq.) was dissolved in anhydrous DMSO (300 µl). DIPEA (3.56 µl, 21.5 µmol, 2 eq.) was added. Compound **67** (5 mg, 12.9 µmol, 1.2 eq.) was dissolved in anhydrous DMF (200 µl) and added dropwise. The reaction was stirred overnight at ambient temperature. The crude product was purified by RP-HPLC (Supelco Ascentis® C18 HPLC column, MeCN:H_2O:TFA = 1/99/0.1 $\rightarrow$ 40/60/0.1, v/v/v in 1 h, flow 8 ml min^{-1}, collection at λ = 650 nm). Lyophilization afforded product **68** (4.90 mg, 5.83 µmol). **yield**: 54% (faint blue powder). **HRMS** (ESI): calc. for $C_{41}H_{48}N_7O_9PSi$ $[M+2H]^{2+}$ = 421.6583, found: 421.6579. **1H NMR** (400 MHz, DMSO-d_6, 300 K): δ [ppm] = 8.78 (t, J = 5.56 Hz, 1H), 8.35 (s, 2H), 8.08 (dd, J = 8.02, 1.40 Hz, 1H), 8.02 (d, J = 8.03 Hz, 1H), 7.65 (s, 1H), 7.50 (s, 1H), 7.04 (s, 2H), 6.65 (d, J = 2.42 Hz, 4H), 6.55 (dd, J = 7.74, 6.16 Hz, 1H), 4.36 (dt, J = 5.73, 2.82 Hz, 1H), 3.99 (h, J = 4.18 Hz, 2H), 3.89 (dt, J = 12.43, 6.72 Hz, 2H), 3.31 (q, J = 6.59 Hz, 2H), 2.93 (s, 12H), 2.83 (t, J = 7.52 Hz, 2H), 2.49 – 2.41 (m, 1H), 2.23 (ddd, J = 13.27, 6.19, 3.08 Hz, 1H), 1.82 (p, J = 7.40 Hz, 2H), 0.63 (s, 3H), 0.52 (s, 3H). **13C NMR** (101 MHz, DMSO-d_6, 300 K): δ [ppm] = 164.8, 151.4, 149.4, 147.7, 143.2, 140.0, 130.8, 128.1, 125.5, 122.9, 121.5, 118.0, 117.8, 116.6, 114.8, 113.9, 100.7, 85.3, 82.9, 70.8, 65.7, 29.3, 22.8, -0.0, -1.2. **31P NMR** (162 MHz, DMSO-d_6, 300 K): δ [ppm] = -1.33.

(mono) POM-SiR

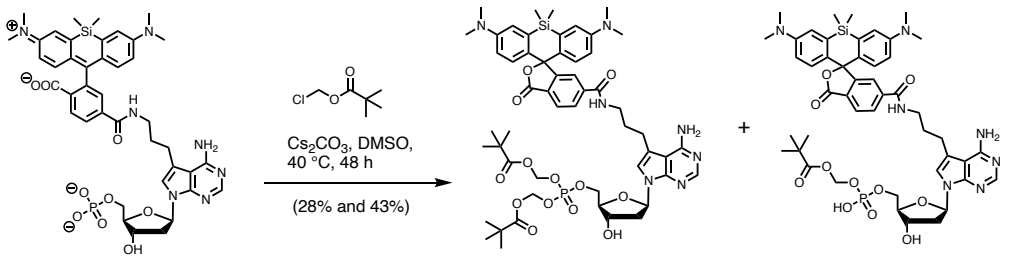

68 **63: POM-SiR-dA** **69: mono POM-SiR-dA**

Compound **68** (2 mg, 2.38 µmol, 1 eq.) was dissolved in DMSO (2.7 ml). Cesium carbonate (2.33 mg, 7.14 µmol, 3 eq.) and chloromethyl pivalate (1.38 µl, 9.52 µmol, 4 eq.) were added subsequently. The reaction was stirred for 48 h at room temperature. After 24 h chloromethyl

pivalate (1.38 µl, 9.52 µmol, 4 eq.) was added again. The reaction was quenched with 1% AcOH in MeCN and purified via RP-HPLC (Supelco Ascentis® C18 analytical HPLC column, MeCN:H_2O: TFA = 1/99/0.1 → 10/90/0.1, v/v/v in 45 min, flow 4 ml min^{-1}, collection at λ = 650 nm). Lyophilization gave compound **63** (0.71 mg, 666 nmol) and compound **69** (0.99 mg, 1.04 µmol). *POM-SiR-dA:* **yield**: 28% (blue powder). *mono POM-SiR-dA:* **yield**: 43% (blue powder). **HRMS** (ESI): calc. for $C_{47}H_{58}N_7O_{11}PSi$ $[M+H]^+$ = 956.3774, measured: 956.3774.

2-chloro-4H-benzo[d][1,3,2]dioxaphosphinine

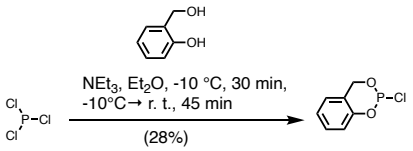

70

2-Hydroxybenzyl alcohol (Alfa Aesar™, #A14410, 3.77 g, 30.3 mmol, 1 eq.) was dissolved in anhydrous diethyl ether (40 ml) at –10 °C. Then, phosphorus trichloride (3.18 ml, 36.4 mmol, 1.2 eq.) was added slowly and carefully. To this mixture, a solution of pyridine (4.9 ml) in diethyl ether (10 ml) was added dropwise over a period of 15 min. After stirring for 1 h, the reaction mixture was allowed to warm to room temperature and stirring was continued for further 2 h. The reaction mixture was stored for about 18 h at 0 °C and the precipitated pyridinium hydrochloride was filtered off under argon using Schlenk filtration. The solvent was evaporated under reduced pressure and the residue was subjected to Kugelrohr distillation in a high vacuum. The chlorophosphane **70** (1.62 g, 8.59 mmol) was isolated and stored under argon at –20 °C. The compound spontaneously rearranges and is solidified over time. It should be prepared freshly prior to use. **yield**: 28% (colorless oil).

N-(3-(4-amino-7-((2*R*,4*S*,5*R*)-4-hydroxy-5-(((2-oxido-4H-benzo[d][1,3,2]dioxaphosphinin-2-yl)oxy)methyl)tetrahydrofuran-2-yl)-7*H*-pyrrolo[2,3-d]pyrimidin-5-yl)propyl)-3,7-bis(dimethylamino)-5,5-dimethyl-3'-oxo-3'*H*,5*H*-spiro[dibenzo[b,e]siline-10,1'-*iso*benzofuran]-6'-carboxamide

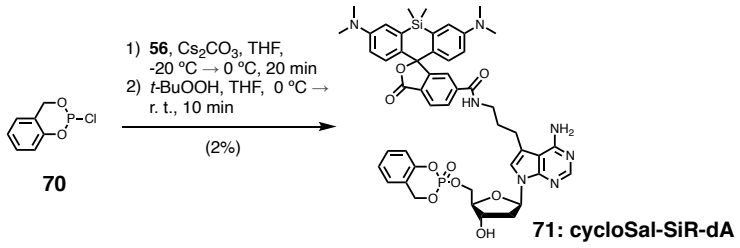

70 **71: cycloSal-SiR-dA**

Cyclosaligenyl chlorophosphit **70** (1.19 mg, 6.3 µmol, 1.2 eq.) was dissolved in THF (875 µl) and added dropwise at –20 °C to a solution of **56** (4 mg, 5.25 µmol, 1 eq.) in anhydrous THF (875 µl) and Cs_2CO_3 (4.11 mg, 12.6 µmol, 2.4 eq.) over the course of 20 min. Then, *tert*-butyl

hydroperoxide (70% , 0.676 ml, 5.25 µmol, 1 eq.) was added at 0 °C and the reaction was allowed to warm to ambient temperature before adding acetic acid and H_2O and purification via RP-HPLC (Supelco Ascentis® C18 HPLC column, MeCN:H_2O:TFA = 10/90/0.1 → 90/10/0.1, v/v/v in 45 min, flow 4 ml min^{-1}, collection at λ = 650 nm). Lyophilization afforded product **71** (0.1 mg, 0.11 µmol). **yield**: 2% (blue solid). **1H NMR** (400 MHz, DMSO-d_6, 300 K): δ [ppm] = 8.75 (q, J = 5.3 Hz, 1H), 8.24 (s, 2H), 8.14 – 7.93 (m, 2H), 7.67 (s, 1H), 7.36 – 7.22 (m, 1H), 7.20 – 7.05 (m, 5H), 6.86 – 6.74 (m, 2H), 6.63 (d, J = 1.7 Hz, 2H), 6.50 (td, J = 6.9, 2.5 Hz, 1H), 5.46 – 5.29 (m, 2H), 4.89 (d, J = 9.1 Hz, 2H), 4.33 (tt, J = 6.0, 3.8 Hz, 2H), 3.96 (q, J = 4.3 Hz, 2H), 2.91 (s, 12H), 2.78 (dd, J = 17.7, 9.1 Hz, 2H), 2.20 (ddt, J = 13.3, 6.5, 3.4 Hz, 2H), 1.78 (dd, J = 13.5, 7.1 Hz, 2H), 0.63 (s, 3H), 0.52 (s, 3H).

1,1-dichloro-*N,N*-di*iso*propylphosphanamine

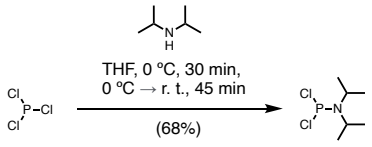

72

Di*iso*propylamine (1.45 ml, 10.3 mmol, 2.1 eq.) was added dropwise to a solution of phosphorus trichloride (427 µl, 4.88 mmol, 1 eq.) in THF (20 ml) at 0 °C over the course of 20 min. After stirring the reaction for 30 min, the reaction was allowed to warm to ambient temperature and stirred for another 45 min. The colorless precipitate was removed by filtration under nitrogen and washed with anhydrous THF. THF was removed and the crude product was distilled (1 mbar, 55 °C) to obtain the product **72** (670 mg, 3.32 mmol). **yield**: 68% (colorless liquid). $\mathbf{R_f}$ (20% EtOAc in hexanes) = 0.2 [KMnO4]. **1H NMR** (400 MHz, $CDCl_3$, 300 K): δ [ppm] = 3.93 (dhept, J = 12.9, 6.5 Hz, 1H), 1.28 (d, J = 6.8 Hz, 6H). **13C NMR** (101 MHz, $CDCl_3$, 300 K): δ [ppm] = 48.3 (d, J = 14.2 Hz), 23.6 (d, J = 8.6 Hz). **31P NMR** (162 MHz, $CDCl_3$, 300 K): δ [ppm] = 169.59.

Salicylphoshpoamidit

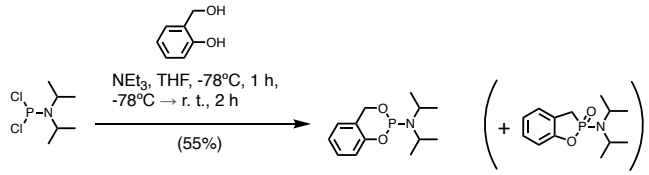

72 **73** **74**

Dichloro*iso*propylphosphoramidit **72** (400 mg, 1.98 mmol, 1 eq.) was dissolved in THF (20 ml). 2-hydroxy-benzyl alcohol (Alfa Aesar™, #A14410, 295 mg, 2.38 mmol, 1.2 eq.) and triethylamine (605 µl, 4.36 mmol, 2.2 eq.) were added dropwise at –78 °C. The solution was stirred at –78 °C for 30 min before it was allowed to warm to ambient temperature and stirred for another 1 h. The suspension was filtered under nitrogen and the filtrate concentrated, before it was subjected to column purification in a nitrogen atmosphere (ethyl acetate:hexanes:DIPEA, 30:70:0.01 →

50:50:0.01). The solvent was removed under reduced pressure to afford compound **73** (240 mg, 1.09 mmol). The product **73** was stored at –20 °C under nitrogen. The product can rearrange spontaneously to compound **74**. **yield**: 55% (colorless oil). **HRMS** (ESI): calc. for $C_{13}H_{21}NO_2P$ $[M+H]^+$: 254.1304, found: 254.1304. **1H NMR** (400 MHz, $CDCl_3$, 300 K): δ [ppm] = 7.18 (td, J = 7.7, 1.9 Hz, 1H), 7.06 – 6.87 (m, 3H), 5.14 (dd, J = 14.2, 5.1 Hz, 1H), 4.87 (dd, J = 19.5, 14.2 Hz, 1H), 3.63 (dhept, J = 10.5, 6.8 Hz, 2H), 1.24 (dd, J = 8.5, 6.8 Hz, 11H). **13C NMR** (101 MHz, $CDCl_3$, 300 K): δ [ppm] = δ 153.4 (d, J = 4.3 Hz), 128.7, 125.4, 124.5 (d, J = 13.3 Hz), 121.2, 119.2, 64.4 (d, J = 4.3 Hz), 44.4 (d, J = 12.9 Hz), 24.9 (d, J = 7.3 Hz), 24.7 (d, J = 8.3 Hz). **31P NMR** (162 MHz, $CDCl_3$, 300 K): δ [ppm] = 135.81. *Rearranged product **74**:* **1H NMR** (400 MHz, $CDCl_3$, 300 K): δ [ppm] = 7.25 – 7.16 (m, 1H), 7.00 (d, J = 7.7 Hz, 2H), 3.30 (dp, J = 19.3, 6.8 Hz, 2H), 3.16 (dd, J = 18.5, 16.3 Hz, 1H), 2.92 (dd, J = 18.5, 10.9 Hz, 1H), 1.30 (dd, J = 12.5, 6.7 Hz, 13H). **13C NMR** (101 MHz, $CDCl_3$, 300 K): δ [ppm] = 154.4 (d, J = 10.1 Hz), 129.0, 128.8, 127.2 (d, J = 17.9 Hz), 123.8 (d, J = 3.5 Hz), 122.7, 113.2 (d, J = 11.6 Hz), 46.5, 46.5, 27.9, 26.8, 23.0, 23.0, 22.5, 22.4. **31P NMR** (162 MHz, $CDCl_3$, 300 K): δ [ppm] = 47.18 (qd, J = 19.0, 11.0 Hz).

CycloSal-SiR-dA

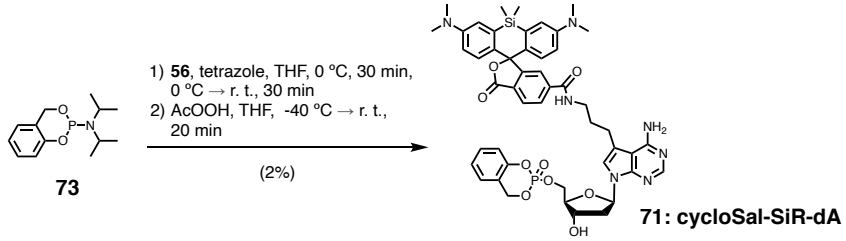

Cyclosaligenyl chlorophosphit **73** (1.19 mg, 6.3 µmol, 1.2 eq.) was dissolved in THF (100 µl) and added dropwise to a solution of compound **56** (4 mg, 5.25 µmol, 1 eq.) in THF (400 µl) with cesium carbonate (4.11 mg, 12.6 µmol, 2.4 eq.) at 0 °C. Then *tert*-butyl hydroperoxide (70%, 0.676 µl, 5.25 µmol, 1 eq.) was added at 0 °C and the reaction was allowed to warm to room temperature before adding acetic acid and water and purification via RP-HPLC (Supelco Ascentis® C18 analytical HPLC column, MeCN:H_2O:TFA = 10/90/0.1 → 90/10/0.1, v/v/v in 45 min, flow 4 ml min^{-1}, collection at λ = 650 nm). Lyophilization yielded compound **71** (0.1 mg, 108 nmol). **yield**: 2% (blue powder). **HRMS** (ESI): calc. for $C_{48}H_{52}N_7O_9PSi$ $[M+2H]^{2+}$: 465.6739, found: 465.6734.

((((di*iso*propylamino)phosphanediyl)bis(oxy))bis(methylene))bis(4,1-phenylene) diacetate (Bis-acetoxybenzyl phosphoamidit)

Dichloro*iso*propylphosphoramidit **72** (90 mg, 445 µmol, 1 eq.) was dissolved in THF (4 ml). 4-Acetoxybenzyl alcohol (Alfa Aesar™, #ACM6309462, 163 mg, 980 µmol, 2.2 eq.) and triethylamine (142 µl, 1.02 mmol, 2.3 eq.) were added dropwise at –78 °C over the course of 20 min. The solution was stirred at –78 °C for 2 h, before it was allowed to warm to ambient temperature and continued to stirr for another 1 h. After the suspension was filtered under nitrogen and the filtrate was concentrated, it was subjected to column purification in a nitrogen atmo-

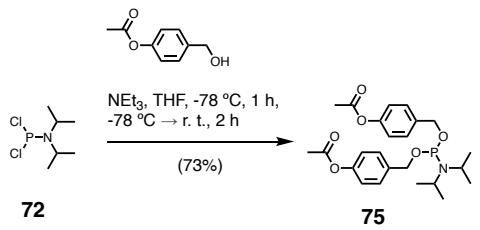

72 **75**

sphere (Silica 60 M, Macherey Nagel, ethyl acetate:hexanes:DIPEA, 30:70:0.01 → 50:50:0.01). The solvent was removed under reduced pressure and the product **75** (150 mg, 325 µmol) was stored at –20 °C under argon. **yield**: 73% (colorless solid). **HRMS** (ESI): calc. for $C_{24}H_{32}NO_6P$ $[M+H]^+$: 462.2040, found: 462.2037. **1H NMR** (400 MHz, $CDCl_3$, 300 K): δ [ppm] = 7.35 (d, J = 8.5 Hz, 1H), 7.04 (d, J = 8.6 Hz, 1H), 4.80 – 4.62 (m, 1H), 3.69 (dhept, J = 10.0, 6.8 Hz, 1H), 2.29 (s, 2H), 1.20 (d, J = 6.8 Hz, 4H). **13C NMR** (101 MHz, $CDCl_3$, 300 K): δ [ppm] = 169.7, 150.0, 137.3 (d, J = 7.7 Hz), 137.2, 128.2, 121.5, 65.0 (d, J = 18.4 Hz), 43.3 (d, J = 12.3 Hz), 24.80 (d, J = 7.4 Hz), 21.3. **31P NMR** (162 MHz, $CDCl_3$, 300 K): δ [ppm] = 147.84.

AB-SiR-dA

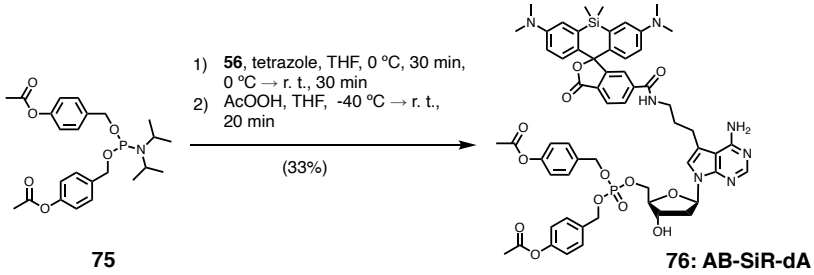

75 **76: AB-SiR-dA**

Compound **56** (2 mg, 2.62 µmol, 1 eq.) was dissolved in anhydrous MeCN (2 ml). 2*H*-tetrazole (1 M, 3.15 µl, 3.15 µmol, 1.2 eq.) and compound **75** (1.21 mg, 2.62 µmol, 1 eq.) were added at 0 °C. After stirring the reaction at 0 °C for 30 min, the reaction was allowed to warm to room temperature and stirred for another 30 min. The reaction mixture was cooled to –40 °C and peroxyacetic acid (32%, 5.46 µl, 23 µmol, 8.75 eq.) was added and then allowed to warm to room temperature. The solvent was removed and the residue purified by flash chromatography. (Silica Gel, SiliCycle, 12 g, DCM:MeOH = 98:2 → 95:5, v/v). Compound **76** (1.0 mg, 879 nmol) was obtained after solvent removal. **yield**: 33% (blue powder). **HRMS** (ESI): calc. for $C_{59}H_{64}N_7O_{13}PSi$ $[M+H]^+$: 1138.4142, found: 1138.4143. **1H NMR** (400 MHz, MeOD-d_4, 300 K): δ [ppm] = 8.78 (t, J = 5.8 Hz, 1H), 8.23 (d, J = 8.2 Hz, 1H), 8.17 (s, 1H), 8.12 (dd, J = 8.2, 1.6 Hz, 1H), 7.79 (d, J = 1.6 Hz, 1H), 7.38 (s, 1H), 7.31 – 7.17 (m, 6H), 7.05 – 6.93 (m, 4H), 6.87 (dd, J = 9.4, 5.6 Hz, 2H), 6.68 – 6.58 (m, 3H), 4.82 (t, J = 8.6 Hz, 4H), 4.40 (dt, J = 6.5, 3.7 Hz, 1H), 4.18 – 4.11 (m, 2H), 4.07 – 4.00 (m, 1H), 3.47 – 3.38 (m, 2H), 3.14 (s, 12H), 2.80 (t, J = 7.2 Hz, 2H), 2.42 (dt, J = 13.3, 6.6 Hz, 1H), 2.33 (ddd, J = 13.7, 6.5, 3.9 Hz, 1H), 2.25 (s, 3H), 2.24 (s, 3H), 2.03 – 1.89 (m, 2H), 0.63 (s, 3H), 0.56 (s, 3H). **31P NMR** (162 MHz, MeOD-d_4, 300 K): δ [ppm] = -1.68.

CycloSal TFAA-NH-C3-alkyne-dA

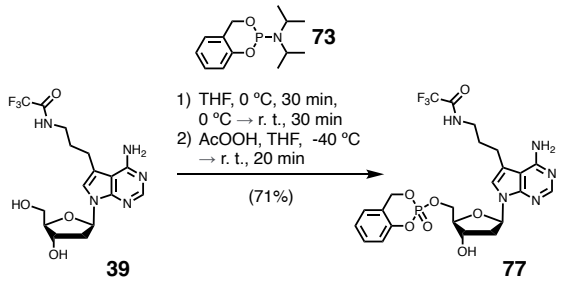

Compound **39** (20 mg, 49.6 µmol, 1 eq.) and 2*H*-tetrazole (1 M, 59.5 µl, 59.5 µmol, 1.2 eq.) were dissolved in anhydrous MeCN (2 ml). Salicylphosphoamidit (12.6 mg, 49.6 µmol, 1 eq.) was added at 0 °C. After stirring the reaction mixture at 0 °C for 30 min, the reaction mixture was allowed to warm to ambient temperature and continued to stirr for another 30 min. The reaction mixture was cooled to –40 °C and peroxyacetic acid (32%, 103 µl, 434 µmol, 8.75 eq.) was added and then allowed to warm to ambient temperature. The solvent was removed and the residue purified by RP-HPLC (Supelco Ascentis® C18 HPLC column, MeCN:H_2O:TFA = 10/90/0.1 → 90/10/0.1, v/v/v in 1 h, flow 8 ml min^{-1}, collection at λ = 290 nm). Lyophilization afforded a mixture of diastereomeres of compound **77** (20 mg, 35.2 µmol). **yield**: 71% (colorless solid). $\mathbf{R_t}$ = 32 min (RP-HPLC, 60 min 10→90%). **HRMS** (ESI): calc. for $C_{23}H_{24}N_5O_7F_3P$ $[M+H]^+$: 572.1516, found: 572.1513. **1H NMR** (400 MHz, DMSO-d_6, 300 K): δ [ppm] = 9.67 – 9.20 (m, 1H), 8.35 (s, 0.4H, diastereomere a), 8.34 (s, 0.6H, diastereomere b), 7.41 (s, 0.4H, diastereomere a), 7.35 (s, 0.6H, diastereomere b), 7.38 – 7.30 (m, 1H), 7.29 – 7.14 (m, 2H), 7.09 (ddd, J = 14.5, 8.2, 1.1 Hz, 1H), 6.53 (td, J = 6.8, 2.4 Hz, 1H), 5.52 – 5.32 (m, 2H), 4.52 – 4.28 (m, 2H), 4.23 (tdd, J = 11.3, 7.7, 6.0 Hz, 1H), 3.99 (dt, J = 6.8, 4.0 Hz, 1H), 3.26 (p, J = 6.5 Hz, 2H), 2.88 – 2.67 (m, 2H), 2.48 – 2.42 (m, 1H), 2.27 (ddt, J = 13.4, 6.4, 4.3 Hz, 1H), 1.85 – 1.68 (m, 2H). **13C NMR** (101 MHz, DMSO-d_6, 300 K): δ [ppm] = 156.4, 156.0, 151.8, 149.5 (0.5C), 149.4 (0.5C, 147.9, 147.9, 143.7, 129.8, 126.0, 124.4, 121.4 (0.5C), 121.3 (0.5C), 121.0, 120.9, 118.2, 118.2, 118.1, 118.1, 117.4, 115.1, 114.5, 100.8, 100.8, 84.4, 82.9, 82.8, 70.2, 70.1, 68.4, 68.3, 67.7, 38.6, 28.9, 28.9, 22.6. **31P 1H NMR** (162 MHz, DMSO-d_6, 300 K): δ [ppm] = -9.73 (s, diastereomere b), -9.80 (s, diastereomere a). **19F NMR** (376 MHz, DMSO-d_6, 300 K): δ [ppm] = -74.11, -74.31.

AB TFAA-NH-C3-alkyne-dA

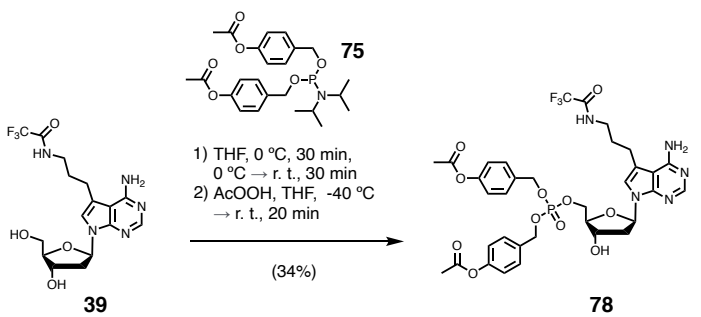

Compound **39** (20 mg, 49.6 µmol, 1 eq.) and 2*H*-tetrazole (1 M, 59.5 ml, 59.5 µmol, 1.2 eq.) were dissolved in anhydrous MeCN (2 ml). 2*H*-tetrazole (1 M, 59.5 µl, 59.5 µmol, 1.2 eq.) AB-ester phosphoamidit (22.9 mg, 49.6 µmol, 1 eq.) was added at 0 °C. After stirring the reaction at 0 °C for 30 min, the reaction was allowed to warm to ambient temperature and stirred for another 30 min. The reaction mixture was cooled to –40 °C and peroxyacetic acid (32%, 103 µl, 434 µmol, 8.75 eq.) was added and then allowed to warm to ambient temperature. The solvent was removed and the residue purified by flash chromatography (SiliaSepC18, dichrom, 12 g column, DCM:MeOH = 98:2 → 95:5). $\mathbf{R_t}$ = 36 min (RP-HPLC, 60 min 10 → 90%) **yield**: 34% (colorless powder). **HRMS** (ESI): calc. for $C_{24}H_{36}N_5O_{11}F_3P$ $[M+H]^+$: 780.2252, found: 780.2247. **1H NMR** (400 MHz, MeOD-d_4, 300 K): δ [ppm] = 9.19 (s, 1H), 8.19 (s, 1H), 7.36 (s, 1H), 7.32 (dd, J = 8.6, 6.5 Hz, 4H), 7.05 (t, J = 8.5 Hz, 4H), 6.66 (t, J = 6.7 Hz, 1H), 4.99 (dd, J = 8.7, 5.1 Hz, 4H), 4.50 (dt, J = 6.4, 3.9 Hz, 1H), 4.23 (dt, J = 6.3, 3.9 Hz, 2H), 4.09 (tt, J = 3.7, 1.9 Hz, 1H), 2.92 – 2.68 (m, 2H), 2.54 (dd, J = 13.7, 6.7 Hz, 1H), 2.52 – 2.32 (m, 1H), 2.32 – 2.28 (m, 2H), 2.27 (s, 6H), 1.93 – 1.80 (m, 2H). **13C NMR** (101 MHz, MeOD-d_4, 300 K): δ [ppm] = 171.1, 159.0, 152.7, 152.5 (d, J = 3.7 Hz), 149.4, 143.1, 134.6 (d, J = 6.5 Hz), 130.3 (d, J = 4.4 Hz), 123.0 (d, J = 3.8 Hz), 123.0, 119.2, 116.1, 102.4, 86.3 (d, J = 7.1 Hz), 85.1, 72.0, 70.3, 70.2, 70.2, 68.8 (d, J = 6.2 Hz), 40.9, 39.9, 29.9, 23.9, 20.9. **31P NMR** (162 MHz, MeOD-d_4, 300 K): δ [ppm] = -1.51. **19F NMR** (376 MHz, MeOD-d_4, 300 K): δ [ppm] = -77.2.

N-(3-azidopropyl)-3,7-bis(dimethylamino)-5,5-dimethyl-3'-oxo-3'*H*,5*H*-spiro[dibenzo[b,e]siline-10,1'-*iso*benzofuran]-6'-carboxamide

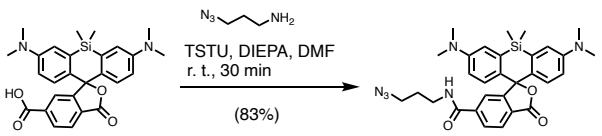

53 **79: SiR-N3**

Compound **53** (5 mg, 10.6 µmol, 1 eq.) was dissolved in DMF (1 ml). DIPEA (5.25 µl, 31.7 µmol, 3 eq.) and TSTU (4.78 mg, 15.9 µmol, 1.5 eq.) were added. The reaction was stirred for 10 min before adding 3-azido-1-propyanamine (1.27 mg, 12.7 µmol, 1.2 eq.). The reaction mixture was stirred for 30 min at ambient temperature. The reaction mixture was acidified with acetic acid and diluted with water before it was subjected to (Supelco Ascentis® C18 HPLC column, MeCN:H_2O:TFA = 10/90/0.1 → 90/10/0.1, v/v/v in 1 h, flow 8 ml min^{-1}, collection at λ = 650 nm). Lyophilization yielded product **79** (4.9 mg, 8.83 µmol). **yield**: 83% (dark blue powder). **HRMS** (ESI): calc. for $C_{30}H_{34}N_6O_3Si$ $[M+H]^+$: 555.2534, found: 555.2528. **1H NMR** (400 MHz, DMSO-d_6, 300 K): δ [ppm] = 8.80 (t, J = 5.6 Hz, 1H), 8.39 – 7.95 (m, 2H), 7.67 (s, 1H), 7.13 (s, 2H), 6.91 – 6.57 (m, 4H), 3.37 (t, J = 6.7 Hz, 2H), 3.29 (q, J = 6.5 Hz, 2H), 2.99 (s, 12H), 1.73 (p, J = 6.8 Hz, 2H), 0.65 (s, 3H), 0.53 (s, 3H). **13C NMR** (101 MHz, DMSO-d_6, 300 K): δ [ppm] = 164.9, 128.2, 119.8, 116.9, 114.2, 114.0, 111.2, 48.5, 36.9, 28.2, -0.1, -1.3.

3 Molecular cloning

Genes were obtained from Addgene (#33308[203], #26461[175], #69531[177]) and cloned in a pCDNA5/FRT/TO vector (Thermo Fisher Scientific) via Gibson assembly® (New England Biolabs, #E2611L). Primers (Eurofins, Table 3.1) were designed with Geneious® 10.2.2. The correct DNA sequence of the plasmids was verified with Sanger sequencing (Eurofins). The plasmid maps of the generated plasmids are shown in Figures 3.1 to 3.4.

Table 3.1: List of primers that were used for cloning.

name	purpose	Base sequence
cl034	pCL010 insert fwd	CTTACCACCATGATGGCTTCGTACCCCTGC
cl035	pCL010 insert rev	TAAACGGGCCCTTTACTTGTACAGCTCGTCCATGC
cl036	pCL010 vector fwd	CTGTACAAGTAAAGGGCCCGTTTAAACCCG
cl037	pCL010 vector rev	GTACGAAGCCATCATGGTGGTAAGTTTAAACGCTAGCC
cl042	pCL012 insert fwd	AAACTTACCACCATGGTGAGCAAGGGCGAG
cl043	pCL012 insert rev	TAAACGGGCCCTCTAAGATCCTTCTTCATCCTCGATCTTGG
cl044	pCL012 vector fwd	GAAGGATCTTAGAGGGCCCGTTTAAACCCG
cl045	pCL012 vector rev	CTTGCTCACCATGGTGGTAAGTTTAAACGCTAGCC
cl046	pCL013 insert fwd	CTTACCACCATGATGGTGAGCAAGGGCG
cl047	pCL013 insert rev	TAAACGGGCCCTCTACCCGGTAGAATTATC
cl048	pCL013 vector fwd	TCTACCGGGTAGAGGGCCCGTTTAAACCC
cl049	pCL013 vector rev	CTTGCTCACCATCATGGTGGTAAGTTTAAACG

Protein Sequences

For protein sequences, a one-letter-code is used.

Protein sequence HSV-TK1-eGFP:

5'-MASYPCHQHASAFDQAARSRGHSNRRTALRPRRQQEATEVRLEQKMPTLLRVYIDGPHG
MGKTTTTQLLVALGSRDDIVYVPEPMTYWQVLGASETIANIYTTQHRLDQGEISAGDAAVVM
TSAQITMGMPYAVTDAVLAPHIGGEAGSSHAPPPALTLIFDRHPIAALLCYPAARYLMGSMTP
QAVLAFVALIPPTLPGTNIVLGALPEDRHIDRLAKRQRPGERLDLAMLAAIRRVYGLLANTVRY
LQGGGSWREDWGQLSGTAVPPQGAEPQSNAGPRPHIGDTLFTLFRAPELLAPNGDLYNVF
AWALDVLAKRLRPMHVFILDYDQSPAGCRDALLQLTSGMVQTHVTTPGSIPTICDLARTFAR
DPPVATMVSKGEELFTGVVPILVELDGDVNGHKFSVSGEGEGDATYGKLTLKFICTTGKLPV
PWPTLVTTLTYGVQCFSRYPDHMKQHDFFKSAMPEGYVQERTIFFKDDGNYKTRAEVKFEG
DTLVNRIELKGIDFKEDGNILGHKLEYNYNSHNVYIMADKQKNGIKVNFKIRHNIEDGSVQLAD
HYQQNTPIGDGPVLLPDNHYLSTQSALSKDPNEKRDHMVLLEFVTAAGITLGMDELYK-3'

Protein sequence PCNA-GFP:

5'-MVSKGEELFTGVVPILVELDGDVNGHKFSVSGEGEGDATYGKLTLKFICTTGKLPVPWPTL

VTTLTYGVQCFSRYPDHMKQHDFFKSAMPEGYVQERTIFFKDDGNYKTRAEVKFEGDTLVN
RIELKGIDFKEDGNILGHKLEYNNSHNVYIMADKQKNGIKANFKIRHNIEDGSVQLADHYQQN
TPIGDGPVLLPDNHYLSTQSALSKDPNEKRDHMVLLEFVTAAGITLGMDELYKGEGQGQGQ
GPGRGYAYRSMFEARLVQGSILKKVLEALKDLINEACWDISSSGVNLQSMDSSHVSLVQLTL
RSEGFDTYRCDRNLAMGVNLTSMSKILKCAGNEDIITLRAEDNADTLALVFEAPNQEKVSDYE
MKLMDLDVEQLGIPEQEYSCVVKMPSGEFARICRDLSHIGDAVVISCAKDGVKFSASGELGN
GNIKLSQTSNVDKEEEAVTIEMNEPVQLTFALRYLNFFTKATPLSSTVTLSMSADVPLVVEYKI
ADMGHLKYYLAPKIEDEEGS-3’

Protein sequence mApple-53BP-trunc:

5’-MVSKGEENNMAIIKEFMRFKVHMEGSVNGHEFEIEGEGEGRPYEAFQTAKLKVTKGGPLP
FAWDILSPQFMYGSKVYIKHPADIPDYFKLSFPEGFRWERVMNFEDGGIIHVNQDSSLQDGV
FIYKVKLRGTNFPSDGPVMQKKTMGWEASEERMYPEDGALKSEIKKRLKLKDGGHYAAEVK
TTYKAKKPVQLPGAYIVDIKLDIVSHNEDYTIVEQYERAEGRHSTGGMDELYKGEEEFDMPQ
PPHGHVLHRHMRTIREVRTLVTRVITDVYYVDGTEVERKVTEETEEPIVECQECETEVSPSQT
GGSSGDLGDISSFSSKASSLHRTSSGTSLSAMHSSGSSGKGAGPLRGKTSGTEPADFALPS
SRGGPGKLSPRKGVSQTGTPVCEEDGDAGLGIRQGGKAPVTPRGRGRRGRPPSRTTGTRE
TAVPGPLGIEDISPNLSPDDKSFSRVVPRVPDSTRRTDVGAGALRRSDSPEIPFQAAAGPSD
GLDASSPGNSFVGLRVVAKWSSNGYFYSGKITRDVGAGKYKLLFDDGYECDVLGKDILLCDP
IPLDTEVTALSEDEYFSAGVVKGHRKESGELYYSIEKEGQRKWYKRMAVILSLEQGNRLREQ
YGLGPYEAVTPLTKAADISLDNLVEGKRKRRSNVSSPATPTASSSSSTTPTRKITESPRASMG
VLSGKRKLITSEEERSPAKRGRKSATVKPGAVGAGEFVSPCESGDNTVNDLDNSTG-3’

Protein sequence H2B-HaloTag:[1]

5’-GSEIGTGFPFDPHYVEVLGERMHYVDVGPRDGTPVLFLHGNPTSSYVWRNIIPHVAPTHR
CIAPDLIGMGKSDKPDLGYFFDDHVRFMDAFIEALGLEEVVLVIHDWGSALGFHWAKRNPER
VKGIAFMEFIRPIPTWDEWPEFARETFQAFRTTDVGRKLIIDQNVFIEGTLPMGVVRPLTEVEM
DHYREPFLNPVDREPLWRFPNELPIAGEPANIVALVEEYMDWLHQSPVPKLLFWGTPGVLIP
PAEAARLAKSLPNCKAVDIGPGLNLLQEDNPDLIGSEIARWLSTLEISG-3’

Plasmid maps

[1] H2B cell line was a gift from Dr. Michelle Frei, MPImR.

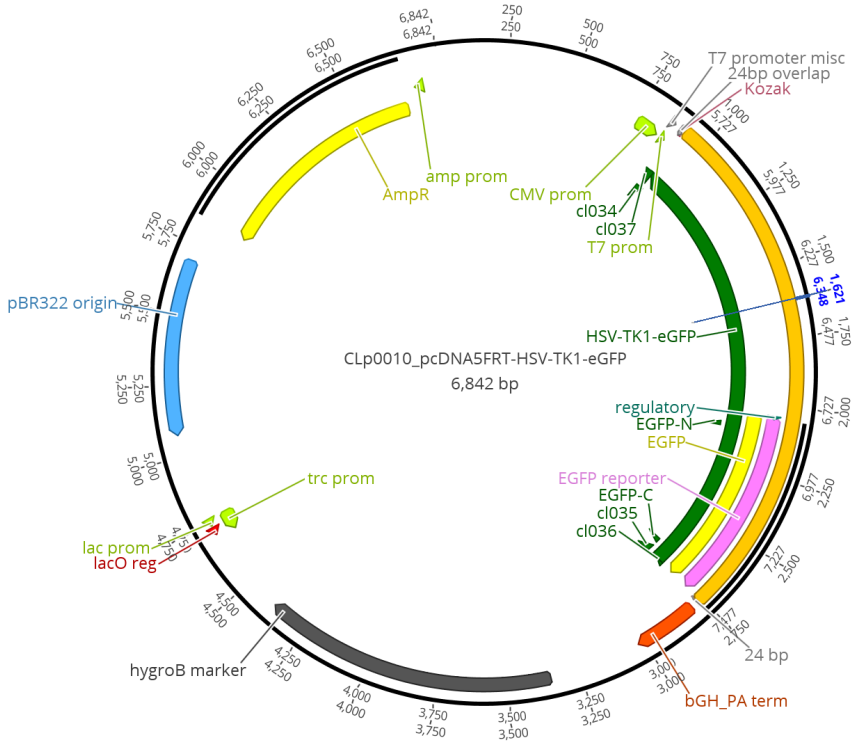

Figure 3.1: Plasmid map HSV-TK1-eGFP.

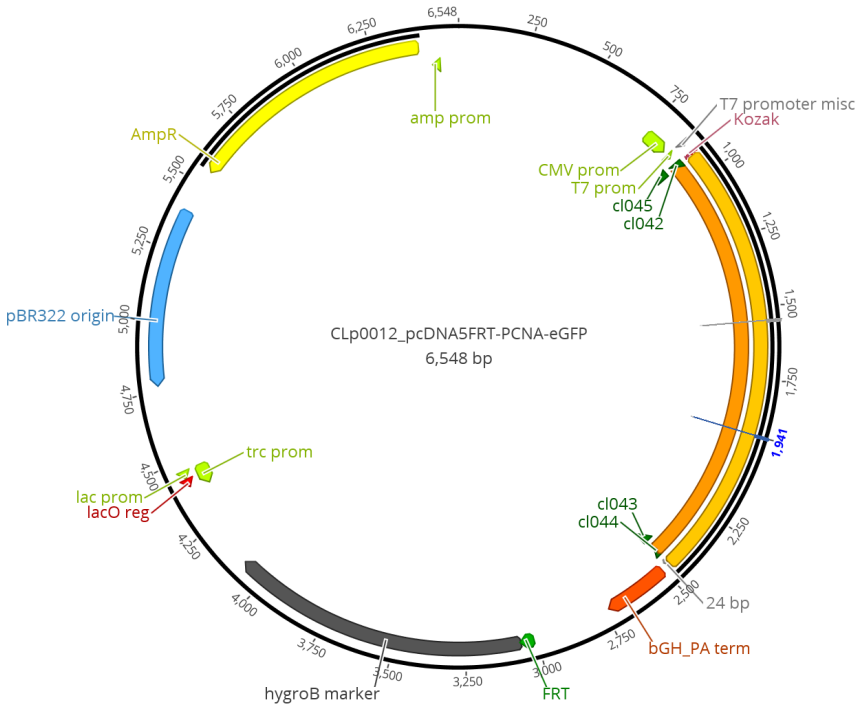

Figure 3.2: Plasmid map PCNA-GFP.

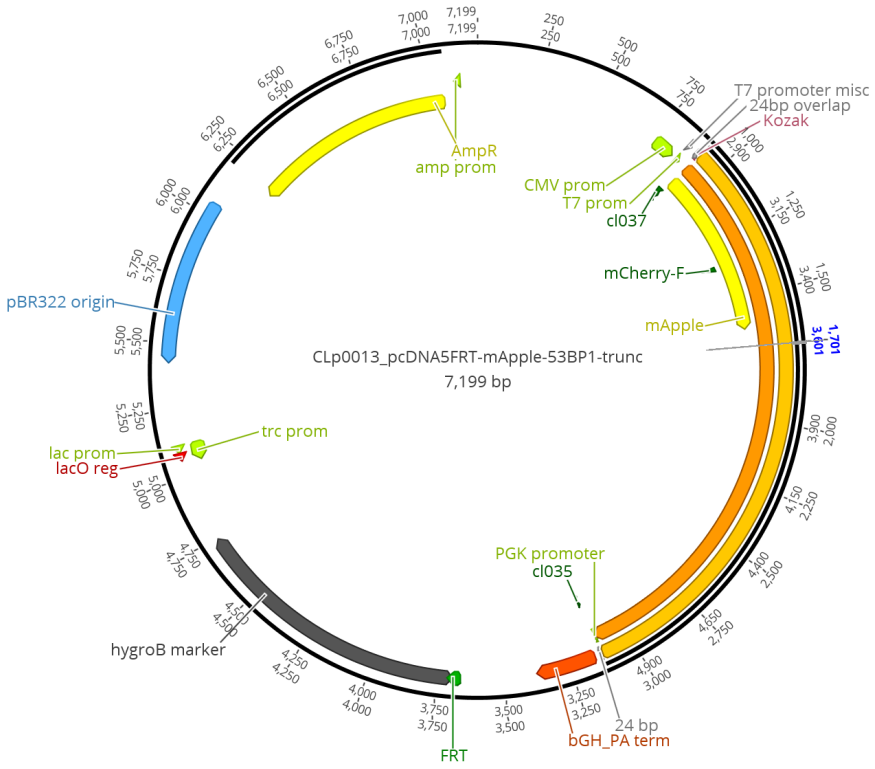

Figure 3.3: Plasmid map mApple-53BP-trunc.

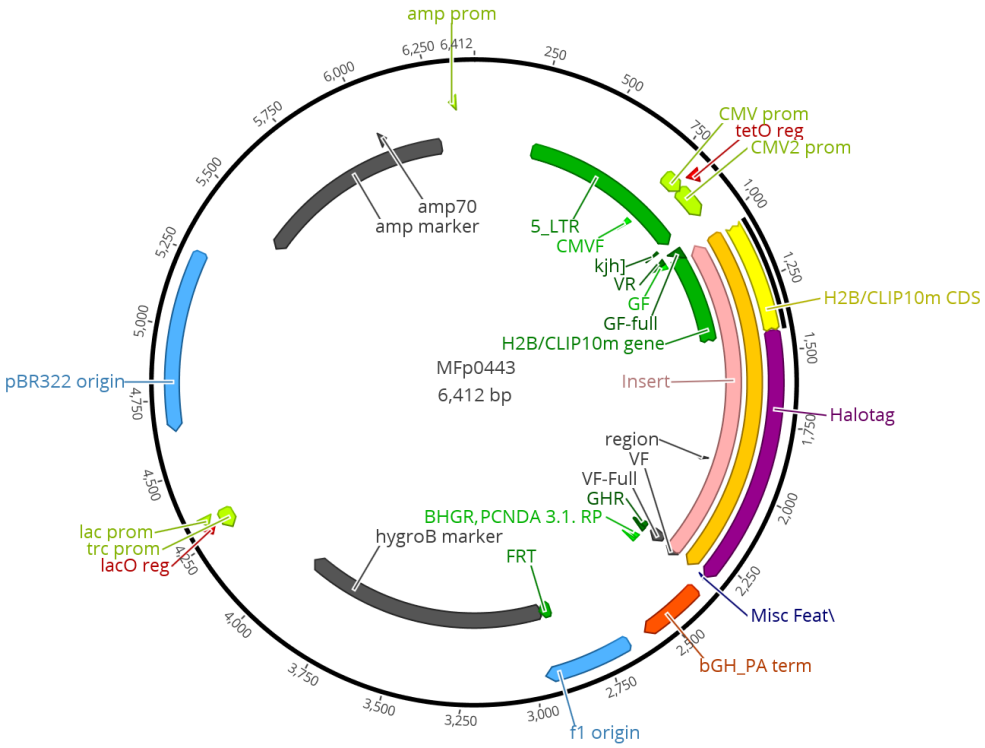

Figure 3.4: Plasmid map H2B-HaloTag.

4 *In vitro* characterization

General information: Microsoft ® Excel for Mac Version 16.53 was used to determine mean values and calculate standard deviations using STDEV.P and the n-method. Data was normalized, fitted, and plotted using GraphPad Prism 7.0 or 8.0 (GraphPad Software Inc.).

4.1 Photophysical characterization

Quantification of compounds by NMR spectroscopy: Compounds with unknown extinction coefficients, which were only available in $<$1 mg were quantified using NMR spectroscopy. 2,2,2-Trifluoroethanol (TFE) was used as an internal reference. A 1 M stock solution was prepared by adding 14.4 µl TFE to 185.6 µl DMSO-d_6 and diluting the stock solution to a final concentration of 100 mM with DMSO-d_6. The NMR sample of the unknown compound was prepared in DMSO-d_6. The concentration of the NMR sample was roughly determined with a NanoDrop (Thermo Fisher Scientific, Waltham, MA) measurement (see below). Then, an equimolar amount of TFE from the diluted stock solution was added to the sample. The peak areas of the standard with the peaks of the compound were compared. The ratio of the peak areas was used to calculate back on the exact concentration of the sample.

Determination of extinction coefficients: Approximately 1 mg was weighed on the precision scale and diluted in a defined volume of DMSO or water to obtain a stock solution in the range of 1–10 mM. For compounds that were obtained by RP-HPLC purification using acetonitrile/0.1% TFA, the mass of their TFA salts was used to determine the concentration. For compounds for which no more than 1 mg was available, the concentration was determined in NMR experiments (see above). From the stock solutions, a series of dilutions (typically in the range of 1–100 µM) was prepared and the absorbance at λ_{max} was measured. The absorbance for reactive adenosine derivatives was determined in PBS, for compound **2** in MeOH:PBS = 1:1 (v/v), for SiR-modified nucleosides 0.1% SDS in PBS. Compounds with SiR were additionally incubated for 10–15 min before the measurement. Absorbance was measured in a 1 cm quartz cuvette (Hellma Analytics) on a Jasco spectrophotometer V-770 (JASCO Deutschland GmbH, Pfungstadt, Germany). The absorbance values were plotted against the concentration and the extinction coefficient $\varepsilon_{\lambda,max}$ determined from the slope of the linear regression.

Determination of concentrations of DMSO stocks: To determine the concentration of a DMSO stock solution, the absorbance of a diluted sample was measured with a NanoDrop 2000c spectrophotometer (Thermo Fisher Scientific, Waltham, MA) in triplicates. Fluorogenic compounds are only absorbing in their open form and therefore measured in the presence of SDS, incubating the sample for 10–15 min before the measurement. For quantifications of SiR derived compounds 0.1% SDS in PBS was used, for MAP-derived compounds 0.5% SDS in

PBS was used. The stock solutions are typically diluted 1:50 or 1:100 (DMSO <2%). The concentration was calculated according to Lambert-Beer law using the extinction coefficient ε_λ as listed in Table 4.1.

$$c = \frac{E_\lambda \cdot f}{\epsilon_\lambda \cdot d} \tag{4.1}$$

whereas:

c	=	concentration / M
E_λ	=	extinction at wavelength λ
f	=	dilution factor
ϵ_λ	=	extinction coefficient at wavelength λ / M^{-1} cm^{-1}
d	=	distance light path / cm (NanoDrop = 0.1 cm)

Table 4.1: Extinction coefficients that were used for determining concentrations.

compound	solvent	$\lambda\epsilon_\lambda$/ M^{-1} cm^{-1}	
SiR / bifunctional SiR probes	650	0.1% SDS in PBS	140 000
TMR / MAP tetrazines	550	0.5% SDS in PBS	80 000
adenosine derivatives alkyne linker	290	PBS	6700
adenosine derivatives alkane linker	290	PBS	9400

UV/Vis absorption spectra: UV/Vis spectra were recorded with a Jasco spectrophotometer V-770 (JASCO Deutschland GmbH, Pfungstadt, Germany) at 21 °C using a 1 cm quartz cuvette (Hellma Analytics, Müllheim, Germany) or on a plate reader Tecan Spark® 20M (Tecan Group AG, Männedorf, Switzerland) in transparent 96-well plates (Corning Inc., NY, USA). A blank was measured before starting the measurement, or the background of the solvent was determined in a separate well and later subtracted.

Fluorescence emission spectra: Fluorescence emission spectra were recorded on a JASCO FP-8600 fluorimeter (JASCO Deutschland GmbH, Pfungstadt, Germany) in 50 µl fluorescence cuvettes (Hellma Analytics, Müllheim, Germany) or on a plate reader Tecan Spark® 20M (Tecan Group AG, Männedorf, Switzerland) equipped with a monochromator in black 96-well plates (Corning Inc., NY, USA) at room temperature.

Quantum yields: Quantum yields were determined using a Hamamatsu Quantaurus QY C11347 (Hamamatsu Photonics K.K., Hamamatsu City, Japan) with single-use quartz glass tubes (Thermo Fisher Scientific, #11732408, 0.7 ml) according to the manufacturer information in triplicates on two separate days. The excitation wavelength for SiR derivatives was 650 nm, for TMR derivatives 555 nm, fluorescein derivatives 490 nm, and for Hoechst 350 nm.

4.2 Plate reader experiments

Plate reader: Fluorescence intensity measurements were performed on a multi-well plate reader Tecan Spark® 20M (Tecan Group AG, Männedorf, Switzerland) equipped with a mono-

chromator at room temperature. The software SparkControl V3.0 was used and gain and z-position optimized in each experiment individually.

Plates: Titrations with hpDNA were performed in low-volume non-binding polystyrene 384-well plates (Corning Inc., NY, USA) in a final volume of 20 µL. Turn-on experiments were performed in 96-well plates (OptiPlate-96 Black, PerkinElmer, Inc., Massachusetts, USA) in a final volume of 100 µL.

4.2.1 Titration pcHoechst with hpDNA

hpDNA (5'-CGCGAATTCGCGTTTTCGCGAATTCGCG-3', Eurofins Scientific SE, saltfree, 2 mM in Milli-Q® water) was heated to 90 °C for 10 min and allowed to fold by slowly cooling to room temperature, before it was further diluted in Milli-Q® water in the range of 3 pM to 60 µM. Hoechst33342 and pcHoechst **3** (DMSO stock, 50 µM) were dissolved in PBS pH 7.4 (gibco, 1×, ThermoFisher) with BSA (0.1 mg ml^{-1}) to a concentration of 200 nM. 10 µL of hpDNA solution and 10 µL of dye solution were combined in each well, the plate was centrifuged and incubated for 1 h at room temperature. Fluorescence intensity was measured exciting at 350 nm (bandwidth = 20 nm) and measuring emission at 460 nm (bandwidth = 20 nm). Titrations were performed in technical triplicates on two independent days. Values were plotted on a logarithmic scale with the normalized mean fluorescence intensity $\pm$ standard deviation.

4.2.2 Titration bifunctional probe with hpDNA

hpDNA (5'-CGCGAATTCGCGTTTTCGCGAATTCGCG-3', Eurofins Scientific SE, saltfree, 2 mM in Milli-Q® water) was heated to 90 °C for 10 min and allowed to fold by slowly cooling to room temperature, before it was further diluted in Milli-Q® water in the range from 10 nM to 5 µM and from 2 nM to 200 µM, respectively. H-SiR-MeTz was diluted to 40 nM in folding buffer (100 mM Tris HCl pH 7.4, 2 mM $MgCl_2$). H-SiR-MeTz and 6-SiR-Hoechst were diluted to 40 nM in PBS pH 7.4 (gibco, 1×, ThermoFisher). 10 µL of hpDNA solution and 10 µL of dye solution were combined in each well, the plate was centrifuged and incubated for 1 h at room temperature. Fluorescence intensity was measured exciting at 640 nm (bandwidth = 10 nm) and collecting the emission at 670 nm (bandwidth = 10 nm). Titrations were performed in technical triplicates on two independent days. Values were plotted with the normalized mean fluorescence intensity $\pm$ standard deviation.

4.3 *In vitro* reaction kinetics in solution

To a solution of VdU (5 µl, 20 mM) in water was added a solution of H-SiR-MeTz (5 µl, 2 mM) in MeOH. The reaction was allowed to proceed at room temperature in water/MeOH (1:1, v/v). The conversion of H-SiR-MeTz was followed between one and six days measuring the HPLC trace at 650 nm (Shimadzu LCMS-2020 instrument with a Nexera X2, SPD-M30A diode array detector). The formation of the right product was confirmed with HRMS (see section 2.3). The reaction was performed under pseudo-1st conditions. Therefore, the mathematical correlation between the formation of the product and reaction constant $k_{1'}$ is given in equation 4.2.

$$\frac{d[P]}{dt} = k_{1'} \cdot [S] \tag{4.2}$$

whereas:

$[P]$	=	concentration of product
$[S]$	=	concentration of starting material
$k_{1'}$	=	reaction constant pseudo-1st order reaction

For the half-life $t_{1/2}$ of a pseudo-1st order reaction, the following also applies:

$$t_{1/2} = \frac{0.693}{k_{1'}} \tag{4.3}$$

$t_{1/2}$ was determined with 40 h, which gave an estimate of $k_{1'}$ of 4.18×10^{-6} s^{-1}. Herein, the order of magnitude of k_2 was roughly estimated by dividing $k_{1'}$ through the final VdU concentration of 10 mM in the reaction mixture. In this approximation, the rate constant was given as 4.18×10^{-4} M^{-1} s^{-1}.

4.4 *In vitro* kinetics with vinyl-modified hairpin

In vitro kinetics with vinyl-modified hairpin were performed (Figure 4.1). Therein, a primer extension was used to generate a vinyl-modified hairpin DNA, that was then used for experiments in which the vinyl-modified hairpin was reacted with the H-SiR-MeTz probe.

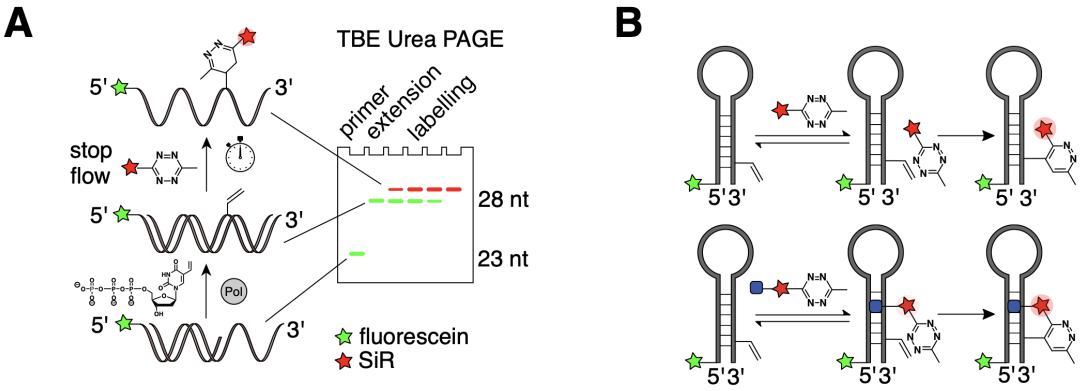

Figure 4.1: A) Kinetic measurements of a vinyl modified oligonucleotide obtained from a primer extension with a 3'-FITC-labeled primer. B) Proximity-enhancement through Hoechst ligand can be investigated using the fluorescent probe with and without Hoechst-ligand.

Primer extension with hairpin model system: A 3'-FITC-labeled primer (3'-FITC-CGCGAAT TCGCGTTTTCGCGAAT-5', Eurofins) was extended by 5 nt using a hairpin template (CGCGA ATTCGCGAAAACGCGAATTCGCG, Eurofins) and the Deep Vent® polymerase (NEB, 30 min, 37 °C). TTP was replaced with VdUTP in the same concentration as the other nucleotides (400 µM). The reaction was performed in ThermoCycler (Eppendorf AG, Hamburg, Germany) with 1 × reaction buffer containing 2% DMSO and a final reaction volume of 25 µl. Before the polymerase was added to the reaction, the master mix with primer (750 nM), template (1 µM)

and dNTPs (400 µM) was heated to 90 °C for 5 min for primer annealing. The primer extension was then performed at 37 °C for 20 min. The product was precipitated with *i*-PrOH and desalted using HiTrap desalting columns (GE Healthcare, Chicago, USA).

Table 4.2: Sequences oligos for primer extension.

name	Base sequence
hairpin fwd	3'-FITC-CGCGAATTCGCGAAAACGCGAATTCGCG-5'
hairpin fwd primer	3'-FITC-CGCGAATTCGCGTTTTCGCGAAT-5'
hairpin rev template	GCGCTTAAGCGCAAAAGCGCTTAAGCGC

Reaction kinetics with Hoechst-SiR-MeTz probe: Before performing kinetics experiments, the modified hairpin was heated to 90 °C for 5 min and directly put on ice to favor hairpin formation. Then, 2 µl Hoechst-SiR-MeTz (3 mM in PBS containing 30% DMSO, final concentration of Hoechst-SiR-MeTz 1 mM, 2000 eq.) was added to 4 µl the primer extension mixture (final concentration of primer 500 nM). The reaction was allowed to proceed at 37 °C for 4, 8, 16 h in a ThermoCycler (Veriti, 96 Well Thermal Cycler, Thermo Fisher Scientific) and then diluted with gel loading buffer (2 µl reaction mixture + 4 µl loading buffer).

Oligonucleotide synthesis and purification: Oligonucleotides were purified on a Waters e2695 system equipped with a 2998 PDA detector on a Waters XBridge Oligonucleotide C18, 2.5 µm, 2.1 × 100 mm using solvent A: TEAA buffer, solvent B: 20% MeCN in triethylammonium acetate buffer. For preparing 1 l 0.1 M TEAA buffer, 5.6 ml acetic acid was added carefully to 950 ml MQ water. 13.86 ml NEt_3 was added slowly. The pH was adjusted to pH 7.0 ± 0.5 by adding acetic acid dropwise while stirring the solution on a magnetic stirrer. The final volume was adjusted to 1 l with MQ water.

Urea PAGE gel: The purity and size of the products were analyzed on Urea PAGE gels on 20 × 20 cm glass plates with self-produced spacers and a 20-well comb (0.7 mm). Glass plates were cleaned in 2 M NaOH. After rinsing with water and ethanol, the glass was coated with Me_2SiCl_2. To prepare a stock solution for casting 20% Urea PAGE gels, 250 ml 40% solution acrylamide / bisacrylamide (19:1) were added to 50 ml 10 × TBE, 240 g Urea (8 M), was filled up with MQ water and filtered (0.22 µm membrane). To 30 ml of casting solution, 30 µl TMED and 250 µl (10% APS in water) was added, the gel (20 × 20 cm × 0.75 mm) was cast and allowed to polymerize for 45–60 min. After pre-running the gel for 15–30 min, 2 µl of sample in loading buffer were applied and the gel was run in 0.5 – 1 × TBE at 15 W in a PROTEAN II xi Cell chamber (Biorad gel system) for 2-4 hours. The gel was optionally stained with SYBR™ Gold (1:10 000 in TBE buffer) for 30 min. The gel was imaged on an Amersham™ Typhoon™ Imager (GE Healthcare, Chicago, IL, USA). FITC-labeled primers and SYBR™ were excited in the Cy2 and SiR in the Cy5 channel.

Mass spectrometry analysis of ODN: The mass of the ODN containing the unnatural nucleotide was measured using MALDI-MS and HRMS.[1] To avoid signal broadening from remaining TEAB buffer, the ODN was desalted using a desalting spin column.

[1] In collaboration with Dr. Sebastian Fabritz, MS facility, MPImR.

5 *In cellulo* characterization

5.1 Mammalian cell culture maintenance

Culture: U2OS and Hela derived immortalized cell lines (Table 5.1) were cultured in high-glucose phenol red containing Dulbecco's modified Eagle's medium supplemented with GlutaMAX (4.5 g l^{-1}) and sodium pyruvate (DMEM, Gibco™, Life Technologies #31966047) and 10% heat-inactivated fetal bovine serum (FBS, Gibco™, Life Technologies, #10270106) in a humidified 5% CO_2 incubator at 37 °C in T25 or T75 cell culture flasks. Cells were split every 2–3 d in a 1:4 ratio, every 3–4 d in a 1:10 ratio or at confluency using Gibco™ Trypsin-EDTA (0.25%, Life Technologies, #25200056) or Gibco™ Trypsin-EDTA (0.5%, no phenol red, Life Technologies, #10779413). The supernatant was regularly tested for mycoplasma contamination with a PCR mycoplasma test kit. The cells were kept in culture for up to two months or used up to a passage number of 20.

Cell counting: Cells were counted with a Countess II Automated Cell Counter (Thermo Fisher Scientific, Waltham, MA) in a bright field view after staining with Trypan Blue solution at 5×10^5 to 1×10^6 cells/ml density.

Thawing: For thawing fresh cells, the cryotubes with the frozen cells were transferred quickly to 37 °C for about 5 min until the ice inside the tube fully melted and the cryo medium was exchanged. Therein, the content of the full tube was diluted with 5 ml pre-warmed growth medium, centrifuged and the pellet resuspended in 5 ml pre-warmed growth medium. The cells were transferred into a T25 cell culture flask and recovered for two passages before they were used for experiments.

Backfreezes: Back-up cells were kept for future studies, in case of contamination and loss of cell supply. Backfreezes were made with cells from a lower passage number (<5) using 5% DMSO for cryopreservation in FBS for Hela cells and 5% DMSO in regular growth medium (10% FBS in DMEM) for U2OS cells. The cells were collected by centrifugation, resuspended in a freezing medium, and stored in cryotubes at a density of 10^6 cells/ml at –80 °C and backed up in liquid nitrogen.

5.2 Generation of stable cell lines

Transfection: The stable cell lines were generated via the FRT-Flp recombinase system co-transfecting pOG044 and the pCDNA5/FRT/TO vector with the corresponding gene in a 9:1 ratio using Lipofectamine™ 3000 reagent (Thermo Fisher Scientific, #L3000015) in Opti-MEM™ (Gibco). A selection medium containing 50 µg ml^{-1} hygromycin (Thermo Fisher Scientific, #

10687010) was added 24 h post-transfection for 24 h, and the cells were allowed to grow and recover for several days.

FACS sorting: U2OS-HSV-TK1-eGFP(+) cells were additionaly FACS sorted (BD FACS Melody™ Cell Sorter) for GFP positive cells.[1] The FACS sorted cells were grown in 50 u ml^{-1} penicillin/streptomycin for the first 24 h (Thermo Fisher Scientific, #15140122) and then again in a regular growth medium.

Table 5.1: List of cell lines generated or used in this thesis.

name	description	origin
T-REx™-HeLa	human epitheloid cervix carcinoma cells	ThermoFisher
U2OS Flip-In™ T-REx™	human bone osteosarcoma epithelial cells	ATCC
U2OS-HSV-TK1-eGFP	U2OS cells expressing HSV-TK1-eGFP	this thesis
U2OS-PCNA-GFP	U2OS cells expressing PCNA-GFP	this thesis
U2OS-p53BP-trunc	U2OS cells expressing p53BP-trunc	this thesis
U2OS-H2B-Halo	U2OS cells expressing H2B-Halo	this thesis

5.3 MTS cytotoxicity assays

Stock solution: MTS assay stock solution was prepared by dissolving MTS powder (Promega Corporation Cat.# G1111) in DPBS (Sigma) at 2 mg ml^{-1} to produce a clear golden-yellow solution. PMS (Phenazine-methosulfate pure, Serva Electrolysis) powder was added to the MTS solution to obtain a final concentration of 0.21 mg ml^{-1}. pH was adjusted to 6.5 using 1 N HCl. The resulting solution was sterile filtered through a 0.2 µm filter into a sterile, light protected container. The final stock solution was stored in aliquots protected from light at –20 °C.

Assay: 5000 cells/well were seeded in a 96-well plate (polystyrene with optical bottom, cell culture treated, Thermo Fisher Scientific) and allowed to attach overnight. On the next day, nucleoside analogs in 100 µL growth medium were added at various concentrations (10–1000 µM) for 24 h before adding 20 µL of MTS stock solution. After 4 h incubation time at 37 °C, 5% CO_2 the absorbance at 490 nm was measured and compared to a DMSO control. Each condition was measured in triplicates on three independent days. The mean $\pm$ standard deviation was plotted.

5.4 Incorporation yields via mass spectrometry

Cell culture: For studying the incorporation yield of ^{15}N-thymidine, VdU or EdU 1 $\times$ 10^5 cells were seeded in a 6-well cell culture dish. On the next day, cell culture medium was exchanged

[1] FACS sorting was performed with Dr. Birgit Koch, MPImR, Heidelberg.

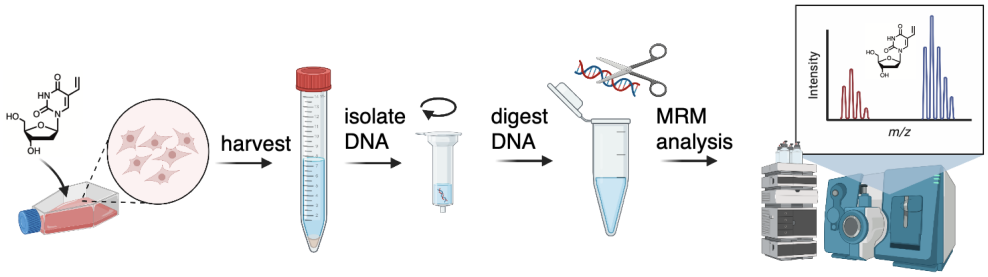

Figure 5.1: MS workflow for MRM quantification of unnatural nucleosides in DNA.

with medium containing 5, 10, 20 or 100 µM ^{15}N-thymidine (Cambridge isotope Labs), VdU or EdU and the cells were allowed to proliferate for 2–72 h. The medium was removed and the cells washed with PBS (1 × 1 ml) before 0.25% Trypsin-EDTA (0.5 ml, 2–3 min) was added until the cells were fully detached. Trypsinization was stopped by adding cell culture medium (0.5 ml). The cells were transferred in a 1.5 ml centrifugation tube and collected at 1000 × g for 1 min using a benchtop centrifuge (Eppendorf). The pellet was washed in PBS (1 ml), resuspended in PBS (50 µl) and stored up to four weeks at –80 °C.

For TCO-yne-dA **38** a T25 flask was seeded. On the next day, 100 µM TCO-yne-dA **38** was supplemented to the cells for 1 h or 24 h. The cells were trypsinized with 2 mL 0.25% Trypsin-EDTA and after 2–3 min quenched with growth medium. The cells were collected in a 5 ml centrifugation tube before they were transferred to a 1.5 ml centrifugation tube and treated as described above.

DNA isolation: The DNA was isolated using a genomic DNA extraction kit (Sigma Aldrich, GenElute™ Mammalian Genomic DNA Miniprep Kit Protocol, #G1N350). In brief, the cells were resuspended in resuspension buffer (150 µl), the samples were incubated with RNAase A solution at room temperature for 2 min before Proteinase K solution (20 µl, 10 mg ml^{-1}) was added. After adding 200 µl lysis solution C, the sample was vortexed thoroughly and the cells were lysed at 70 °C for 10 min. The DNA was finally purified using spin columns and after washing (2 ×) eluted with MQ water (50 µl).

DNA digestion: Isolated genomic DNA was diluted with Degradase reaction buffer to a final volume of 25 µl and a concentration of about 5 µg ml^{-1}. DNA Degradase Plus stock (1 µl, 5 U, Zymo Research, #E2020) was added on ice before the sample was incubated at 37 °C for 4 h to achieve full digestion. Completion of the digestion was verified with 0.6% agarose gel (SB buffer, 150 V, 15 min), loaded with 6 × loading buffer Peqlab, #PEQL98-0034), a Quick-Load® 2-Log DNA Ladder (0.1–10.0 kb, NEB, #N0469S), and stained with SYBR™ Safe DNA Gel Stain (Invitrogen, #S33102). The enzymatic reaction was quenched by diluting with 0.1% formic acid (MS grade) and the sample was subjected to MRM quantification.

MRM quantification: The MRM measurements were performed on a Shimadzu Nexera X2 connected to a Sciex QTrap 6500+ System. The following injection volumes were chosen: 5 µl ^{15}N-Thy, 6 µl VdU, 2.5 µl EdU, 10 µl TCO-yne-dA. The chromatography was performed on a Phenomenex Polar C18 column (2.1 × 100 mm, 2.6 u). For the mobile phase solvent A: H_2O + 0.1% FA (v/v, MS grade) and solvent B: MeCN, 0.1% FA (v/v, MS grade) were used at a flow of

0.45 ml min^{-1}. The gradient started from 2% B for 1 min and was ramped to 25% B in 1.5 min to 98% B in 1.5 min and remained at 98% B for 1.5 min. The system was then re-equilibrated at 2% B. The source parameters are listed in Table 5.2 Additional source parameters and transitions that were recorded for the various analytes are summarized in Table 5.3. The data was recorded with the software Analyst 1.7 with Hotfix 3 and quantified with Multiquant 3.0.2. The incorporation yield was determined as the signal intensity for thymidine derivatives with respect to the sum of the signals from thymidine and unnatural nucleoside.[2]

Table 5.2: Source parameters for MRM quantifications.

Nucleoside	CUR	CAD	temperature / °C	GS1	GS2	IS	DP	EP
Thy	45.00	medium	350	80	60	5000	20	10
^{15}N-Thy	45.00	medium	350	80	60	5000	20	10
VdU	45.00	medium	350	80	60	-4000	-40	-10
EdU	45.00	medium	350	80	60	-4000	-40	-10
TCO-yne-dA	45.00	medium	600	80	50	4500	100	10

Table 5.3: Transitions that were measured for MRM quantifications.

Nucleoside transition	ionisation mode	Q1 Mass / Da	Q3 Mass / Da	Dwell time / ms
Thy #1	pos	243.1	127.1	100
Thy #2	pos	243.1	117.1	25
^{15}N-Thy #1	pos	245.1	129.1	50
VdU #1	neg	253.0	210.0	150
VdU #2	neg	253.0	210.0	150
EdU #1	neg	251.0	208.0	150
EdU #2	neg	251.0	136.0	50
TCO-yne-dA #1	pos	456.25	340.25	200
TCO-yne-dA #2	pos	456.25	189.1	100

5.5 Widefield microscopy

Microscope Nikon TI Eclipse microscope equipped with an automated stage (Märzhäuser Tango2), a multicolor LED excitation lamp (pE4000 CoolLED), DAPI/FITC/Cy3/Cy5/Cy7 Penta LED HC Filter Set (F66-615, AHF), a 20x Plan Apo NA0.75 objective (Nikon), a sCMOS camera (Neo, Andor) and a chamber for 37 °C and CO_2 supply (Okolab) was used.

Cell culture To determine uncaging toxicity 1×10^4 Hela cells were seeded in 8-well Ibidi dishes and allowed to attach overnight. Treatment was then performed with vehicle alone, 0.1 and 10 µM Hoechst33342 or 10 µM pcHoechst **3** and cells were transferred to the microscope without washing.

[2]Mass spectrometry measurements were performed by Dr. Sebastian Fabritz, Cornelia Ulrich, Juliana Kling und Tatjana Rudi, MS core facility, MPImR, Heidelberg.

Image acquisition Cells were brought into focus in brightfield mode and a first image was acquired using Dapi Filter Set (200 ms exp. time, 365 nm Exc, Penta LED HC Filter Set, BP447/60 Em (Semrock)). Uncaging was then performed for 0, 4, or 10 s using DAPI Filter Set and a second DAPI image was acquired. Cells were then imaged for the next 24 h in phase-contrast mode every 30 minutes.

Data evaluation After the timelapse, videos were evaluated blindly for successful cell division by manual counting. Cell division was defined as one cell dividing in two living cells. Numbers were pooled from two different regions of interest and are summarized below.[3]

5.6 Laser scanning confocal microscopy (LSCM)

Microscope: Microscopy experiments were performed on a Leica DMi8 microscope (Leica Microsystems) equipped with a Leica TCS SP8 X scanhead, a SuperK white light laser, a UV CW laser (Coherent, 355 nm, 80 mW) and a heating chamber (37 °C and 5% CO_2, Life Imaging Services). The measurements were performed with a HC PL APO 63 $\times$/1.47 oil objective, a HC PL APO 40.0 $\times$/1.10 water or HC PL APO 20.0/0.75 dry objective. The fluorescence signal was collected with a HyD detector.

Image acquisition: If not stated differently, SiR was excited at λ_{ex} = 650 nm and emission sampled at λ_{ex} = 670–770 nm. Hoechst or PCNA-GFP signal were excited at λ_{ex} = 405 nm or λ_{ex} 488 nm and collected at λ_{em} = 430–530 nm or λ_{em} = 500–600 nm respectively.

Image analysis: Images were analyzed using ImageJ Fiji 2.1.0.[204] For quantitative analysis, microscopy images were analyzed with CellProfiler 4.1.3.

5.6.1 Photocaged-Hoechst: Uncaging cell experiments

Seeding and labeling: Hela T-REx™ cells were diluted to a final concentration of 2 $\times$ 10^5 cells/ml and seeded in a Greiner Bio-One CELLview™ Cell Culture Slide (10-wells, 20 000 cells/well, 100 µl culture medium) and allowed to attach overnight. The supernatant was removed and fresh medium containing 0.1–10 µM pcHoechst **3** was added 2–4 h before the experiments.

Uncaging: For global uncaging experiments the cells were irradiated with laser light at 355 nm (20-80%) for 10–15 s. The increase of the fluorescence signal was observed at 355 nm (2-5%) for 10 min by imaging one frame per minute. For long-term imaging or imaging with a higher frame rate the data was acquired at 405 nm (2%). For local uncaging of a single cell or a subnuclear fraction, the bleachpoint function or region of interest (ROI) function of the FRAP module was used. Laser intensity: 2-80%; λ= 355 nm.

Laser power and intensity calculations Laser powers were measured with a 40x water objective (NA 1.1) using a Nova II power meter (Ophir, North Logan, USA). For the 40x objective

[3] Toxicity experiments were performed by Jenny Eichhorst and Dr. Martin Lehmann, Department of Molecular Pharmacology and Cell Biology, Leibniz-Forschungsinstitut für Molekulare Pharmakologie (FMP).

the beam diameter was calculated using the following formula: 1.22 $\times$ 405 nm/ 1.1 = 449 nm and the illuminated area using the bleachpoint function was 158 478 nm^2.

5.6.2 Proximity-enhanced DNA labeling: Labeling in fixed cells

Metabolic labeling: Cells were seeded (10-well Greiner Bio-One CELLview™ Cell Culture Slide or 96-well Eppendorf plates, 2 $\times$ 10^5 cells/well, 100 µl medium) and incubated overnight. For feeding VdU (1–100 µM, Jena Bioscience, 100 mM DMSO stock, final 0.1% DMSO v/v) or EdU (10 µM, Thermo Fisher Scientific, 100 mM DMSO stock, final 0.1% DMSO v/v) the supernatant of the cells was removed and fresh medium containing the nucleosides was added. The nucleosides were incubated with the cells for 8–24 h.

APC treatment: Optionally in addition to nucleoside treatment, APC can be added to the cells to inhibit DNA synthesis. APC is added at concentrations between 6–48 µM (#A0781, Sigma-Aldrich, diluted from a 6 mM aqueous stock solution, stored in aliquots at –20 °C).

Fixation: The cells were washed with PBS (1 $\times$), fixed with 4% PFA (15 min), quenched with 50 mM glycine, 50 mM NH_4Cl (5 min), and permeabilized with 0.2% Triton X-100 in PBS (10 min).

iEDDA labeling: Cellular DNA was optionally denatured with HCl (1 M, 30 min) and neutralized applying 0.1 M aq. Borax ($Na_2B_4O_7$ $\times$ 10 H_2O, 10 min). The cells were washed with PBS (2 $\times$) before adding the methyl tetrazine dyes (5 µM in PBS, 1 mM DMSO stock, 16 h, room temperature in the dark). The cells were washed with 0.1% Triton X-100 in PBS (1 $\times$) and PBS (1 $\times$).

Cu(I) mediated labeling: Click-iT kit (Click-iT EdU Alexa Fluor 488 or 647 Imaging kit, Thermo Fisher Scientific, #C10086 or #C10340) were used. According to the manufacturer protocol, a labeling cocktail was prepared and added to the cells for 30 min. For a control experiment, 5 µM SiR-azide **79** was used in combination with the buffers from the Click-iT kit.

Hoechst or PicoGreen staining: Optionally the cells were co-stained with Hoechst33342 (1:10000 dilution, 10 mg ml^{-1} solutions, 10 min) or PicoGreen (1:2000 dilution, Quant-iT™ PicoGreen™, #P7581).

Competition labeling with Hoechst: For competition experiments, Hoechst33342 and the bifunctional probes are added simultaneously at room temperature for 16 h. A typical probe concentration is 5 µM and Hoechst33342 was varied from 0.5–50 µM.

Displacement with Hoechst: For displacement experiments, the supernatant of a well with labeled cells was removed and replaced with a solution of Hoechst33342. The conditions were equilibrated for 10 min at 37 °C before an image was acquired. The procedure was repeated with gradually increasing concentrations of Hoechst33342.

Determination of S/N in confocal microscopy images: For measuring S/N in microscopy representative spots in the images are picked manually using ImageJ Fiji 2.1.0. For each ratio, a minimum of N=10 cells were analyzed. For the cytosolic signal of the bifunctional probes, spots were picked very close to the nucleus as even with increasing brightness cytosol was

almost not visible. Proliferation was ensured with a control where EdU was incorporated into cells in a separate well when $S_{pro}/N_{non\text{-}pro}$ was determined. When the ratio was too small the differentiate proliferating and non-proliferating cells, an external control without VdU was used to determine the background in non-proliferating cells. From the positive control, only the brightest cells were picked.

Quantitative analysis confocal images: In the data processing workflow, a mask with all cell nuclei was generated using an image from a regular DNA stain (Hoechst or PicoGreen) and automated cell segmentation. For generating the mask, the diameter of the object was restricted to 50-90 pixel units and thresholding was applied with a minimum cross-entropy method and a smoothing scale factor of 1.3488. Lower and upper bounds on the threshold were set to 0.05 - 1.0. To distinguish clumped objects the distance between local maxima was calculated based on the intensity along dividing lines between them. The mask was then applied to a heterogenous labeled, asynchronous cell population ensuring that every cell was recognized. The mean fluorescence intensity was then determined for each cell and exported to a spreadsheet and further analyzed in Microsoft Excel 16.51.

When analyzing a cell pool comprised of non-proliferating and proliferating cells, only the brightest 33% of cells were considered for plots that visualize staining results. For subtracting background the average mean fluorescence intensity of the darkest 33% of cells was subtracted from the average of the 33% brightest cells. As the average duration of the cell cycle of U2OS cells is 24 h. Therefore, 8 h feeding time of nucleosides guarantees that a minimum of 33% of the cells did not enter S-phase during this time. For each condition a minimum of N=100 cells from three fields of view are analyzed. The same trends were observed by individually performed experiments on different days. Due to small changes in the output of the laser on different days, fluorescence intensities are normalized. Standard errors that are reported arise from the averaging of N cells and experiments performed on different days.

5.6.3 Proximity-enhanced DNA labeling: Labeling in live cells

Metabolic labeling: U2OS H2B-Halo cells were seeded in a 10-well Greiner Bio-One CELLview™ Cell Culture Slide at 10 000 - 15 000 cells/well density. 50 µM VdU was supplemented to the medium for 8–12 h. The cells were washed 3 $\times$ for 2 min each and incubated with fresh medium for another 30 min before the cells were labeled.

iEDDA labeling: U2OS-H2B-Halo cells were incubated with 1 µM MAP555-chloroalkane for 30 min. Then, the labeled U2OS-H2B-Halo cells or U2OS-PCNA-GFP cells were labeled with 0.5–5 µM H-SiR-HTz optionally in the presence of 10 µM verapamil for 8–16 h.

Image acquisition: While imaging z-stacks were acquired over 20 µm with a step-size of 1.5 µm using a HC PL APO CS2 20x0.75 dry objective with 2-fold zoom and 512 $\times$ 512 px.The probe was excited at 640 nm and the detector collected light from 650–750 nm. MAP555 labeled H2B was used to autofocus exciting at 540 nm and detecting 550–650 nm. PCNA-GFP was excited at 488 nm and detected at 500–600 nm. Laser power was minimized to reduce phototoxicity.

5.6.4 Reactive adenosine derivatives: Labeling in fixed cells

Metabolic labeling: Cells were seeded (10-well Greiner Bio-One CELLview™ Cell Culture Slide or 96-well Eppendorf plates, 1 × 10^5 cells/well, 100 µl medium) and allowed to settle overnight. On the next day, the medium was removed and replaced with medium containing 100 µM 7-deaza-2'-deoxyadenosine derivatives (100 mM DMSO stock, final 0.1% DMSO v/v) for 8 h.

Fixation and labeling: The cells were washed with pre-warmed PBS (1 ×), fixed with 4% PFA (15 min), quenched with 50 mM glycine / 50 mM NH_4Cl (5 min), and permeabilized with 0.2% Triton X-100 in PBS (10 min). DNA was denatured with HCl (1 M for 30 min) and neutralized applying 0.1 M aq. Borax ($Na_2B_4O_7$ × 10 H_2O, 10 min). The cells were washed with PBS (2 ×) before adding MAP-C1-MeTz **51** (5 µM) for 16 h at room temperature.

There were attempts to optimize the protocol. Some variations of the protocol are listed in Table 5.4.

Table 5.4: Parameters that were changed in the fixation protocol for imaging reactive nucleosides in fixed cells.

n^0	parameters deviating from the standard protocol
1	labeling: 0.5–5 µM tetrazine for 1–16 h
2	fixation: 20 min 1% PFA, permeabilization: 0.5% Triton X-100 in PBS
3	fixation: 10 min MeOH –20 °C
4	fixation: 5 min 4% PFA and 4 min MeOH –20 °C
5	pre-fixation: 2 min 4% PFA, pre-extraction: 0.1% TX-100 in PBS for 2 min at r. t. and wash with PBS (2 min, r. t.), fixation: 15 min 6% PFA
7	pre-fixation: 2 min 4% PFA, pre-extraction: 0.1% TX-100 in PBS for 2 min at r. t. and wash with PBS (2 min, r. t.), fixation: 10 min MeOH –20 °C
8	permeabilization: 20 min 0.2% Triton X-100 in PBS

Pulse-chase-experiments: To study the adverse effects of the nucleosides on cell cycle progression, pulse-chase experiments of TCO-ane-dA **42** and EdU were performed. In some wells, the cells were first treated with TCO-ane-dA **42** (4 h, 100 µM) and then EdU (4 h, 10 µM). In additional experiments, both were added at the same time for 4 h. The cells were fixed and labeled with 5 µM MAP-C1-MeTz **51** overnight (s. above).

5.6.5 Reactive adenosine derivatives: Labeling in live cells

Metabolic labeling: Cells were seeded (10-well Greiner Bio-One CELLview™ Cell Culture Slide or 96-well Eppendorf plates, 1 × 10^5 cells/well, 100 µl medium) and allowed to settle overnight. The nucleosides (TCO-yne-dA **38**, TCO-ane-dA **42**, BCN-yne-dA **37** and BCN-ane-dA **41**) were supplemented at 25–200 µM for 4–8 h, followed by washing with growth medium (1 × 2 min and 1 × 10 min).

Live labeling: Tetrazine dyes (MAP-C1-MeTz **51**, MAP555-MeTz **52**, HD555, HD653) were then added at 1 µM for 4–16 h. Prior to imaging the medium was exchanged once to phenol-red free medium.

Labeling in U2OS-PCNA-GFP(+) cells: U2OS-PCNA-GFP cells were seeded as described above. After the cells settled, they were treated with 100 µM TCO-ane-dA **42** for 4 h followed by washing with growth medium (1 × 2 min and 1 × 10 min) and staining with MAP-C1-MeTz **51** (1 µM, 4 h). The medium was exchanged once to phenol-red free medium before image acquisition.

5.6.6 Fluorogenic nucleosides and pro-nucleotides

Microscopy experiments were performed as described for reactive adenosine derivatives in subsection 5.6.5. The fluorogenic nucleosides SiR-yne-dA **55**, SiR-ane-dA **56** and SiR-yne-dU **58** were supplemented to the cells (100 µM, 4 h). Prior to imaging the medium was exchanged once to phenol-red free medium. Pro-nucleosides were supplemented at various concentrations from 1–50 µM in normal growth medium or phenole-red free medium for different incubation times (2–12 h). Image acquisition was performed under no-wash conditions or changing the medium once before image acquisition.

5.7 Stimulated-emission depletion (STED) super-resolution microscopy

Microscope: STED imaging was performed on an Abberior STED QUAD scanning expert line (Abberior Instruments GmbH, Göttingen, Germany) built on a motorized inverted microscope IX83 (Olympus, Tokyo, Japan). The microscope is equipped with pulsed STED lasers at 655 nm and 775 nm, with 520 nm, 561 nm, 640 nm, and multiphoton (Chameleon Vision II, Coherent, Santa Clara, USA) excitation lasers. Spectral detection was performed with two avalanche photodiodes (APD) in the spectral window 580 – 750 nm. Images were acquired with a 60x/1.42 oil immersion objective lens (Olympus). Pixel size was 20 nm. Laser powers and dwell times were optimized for each sample.

Seeding: U2OS cells (500 µl) were seeded at a density of 100 000 cells/ml on coverslips (diameter 12 mm, N_A = 1.5) that were sterilized with 70% EtOH and UV light and placed in a 24-well plate.

Fixation and labeling: Fixation and washing steps were performed in the 24-well plate. For incubating the probe, the coverslip was placed up-side-down on a sitting drop of 100 µl staining solution in a small staining chamber. For image acquisition, the coverslips were then mounted on a slide with Mowiol containing DABCO and sealed with nail polish.

5.7.1 Pulse-chase experiments EdU / VdU

Metabolic labeling: U2OS FlipIn TREx™ cells were seeded as described above and treated with 30 µM VdU for 4 h, washed with PBS (2 × 2 min) and growth medium (1 × 10 min), treated with 10 µM EdU for 4 h.

Fixation and labeling: The cells were fixed (4% PFA for 15 min). After permeabilization with 0.2% Triton X-100 in PBS for 10 min, and quenching with 100 mM NH_4Cl, 100 mM glycine the

cells were washed with PBS (2 × for 2 min). EdU-tagged DNA was labeled with 10 µg ml^{-1} Alexa594-N_3 and buffers from Click-iT EdU Imaging kit (Thermo Fisher Scientific, #C10340) according to their protocol. Before labeling of VdU-tagged DNA, the cells were denatured with 1 M HCl for 30 min, neutralized with Borax (100 mM, 5 min), washed with PBS (2 × for 2 min). Then, H-SiR-MeTz was applied for 16 h and the cells were washed with 0.1% Triton X-100 in PBS, 5 µM Hoechst33342 (each 5 min), and PBS (2 × for 5 min).

Image analysis: Deconvolution according to the Richardson-Lucy model was performed with Imspector and the PSF from equation 5.1 using an FWHM of 40 nm. Afterward, the images were slightly smoothed.

$$PSF = 2^{\frac{(-((x-\frac{X}{2})^2+(y-\frac{Y}{2})^2)}{(\frac{fwhm}{2})^2)}} \tag{5.1}$$

5.7.2 Immunofluorescence labeling of U2OS PCNA-GFP cell line

Metabolic labeling: U2OS-PCNA-GFP(+) cells were seeded on coverslips (see above) and treated with 30 µM VdU for 20 min.

Fixation and labeling: Immediately after feeding, the cells were fixed with 4% PFA for 15 min. After quenching with 100 mM NH_4Cl, 100 mM glycine the cells were washed with PBS (2 × for 2 min). Then they were labeled with 5 µM H-SiR-MeTz for 16 h, washed with 0.1% Triton X-100 in PBS, 5 µM Hoechst33342 (each 5 min) and PBS (2 × for 5 min) and immunostained. Therefore, they were incubated with primary antibody (anti-GFP IgG1 primary antibody from mouse, mixed clones 7.1 and 13.1, Roche, #11814460001, 0.4 mg ml^{-1}, 1:500) in 3% BSA in PBS for 1.5 h at ambient temperature. The secondary antibody (anti-mouse IgG H&L Alexa568 secondary goat antibody, polyclonal, invitrogen, #A11031, 1:2000) in 3% BSA in PBS was added for 1 h at ambient temperature.

Image analysis: A mean filter (N=2) was applied in ImageJ Fiji 2.1.0.

5.8 Flow cytometry analysis

Metabolic labeling: U2OS FlipIn TREx™ cells were cultured in 6-well cell culture dishes at 60-80% confluency (3 × 10^5 cells/ well) and treated with EdU (10 µM) or SiR-ane-dA **56** (100 µM) for 4 h before they were trypsinized and further analyzed. Cells were prepared by removing the growth medium from the dish and adding trypsin solution (0.5 ml) for 2–5 min until the cells fully detached and trypsinization was stopped by adding growth medium (0.5 ml). The cells were collected by centrifugation and washed (1 × PBS).

EdU treated cells: EdU treated cells were fixed with 4% PFA for 15 min, followed by washing (2 × PBS), permeabilized with 0.2% Triton X-100 in PBS, and washed (2 × PBS). Between each step, the cells were centrifuged in a benchtop centrifuge at 2000 × g. For labeling EdU, the Click-iT kit (Click-iT EdU Alexa Fluor 647 Imaging kit, Thermo Fisher Scientific, #C10340) was used. The labeling cocktail was prepared as described in the protocol using Alexa647-azide, incubated for 30 min and the cells were washed (2 × PBS). Before flow cytometry analysis, the

cells were resuspended thoroughly, filtered through the cell strainer cap (Falcon, #352235) in the Falcon® tube (12 $\times$ 75 mm).

SiR-ane-dA treated cells: SiR-ane-dA treated cells were analyzed live. Therefore, they were resuspended in FACS buffer (2% FBS in PBS) after washing and directly filtered through the Cell Strainer Cap. FACS buffer was prior prepared diluting 2% FBS in PBS and filtering through a 0.22 µm membrane.

Data acquisition and analysis: The samples were prepared in triplicates. The cells were analyzed on a BD LSRFortessa™ X-20 Flow Cytometer (Becton, Dickinson and Company, Franklin Lakes, NJ, USA) using the software BD FACSDiva™. For flow cytometry analysis, 10 000 events were recorded per condition. For gating, single cells were selected and the fluorescence in the APC signal was detected using filters 670/30 nm/nm after excitation with the 640 nm laser. The data was analyzed using FlowJo 10.7.1. The side scatter SSC was plotted vs. the signal from the APC channel.

6 *In vivo* experiments

6.1 Zebrafish strains and maintenance

Zebrafish (Danio rerio) embryos were kept in E3 medium (0.63 g L^{-1} KCl, 14.0 g L^{-1} NaCl, 1.83 g L^{-1} $CaCl_2 \times 2$ H_2O, 1.99 g L^{-1} $MgSO_4 \times 7$ H_2O, pH 7.4) containing 0.003% Phenylthiourea (PTU, Sigma-Aldrich, St. Louis, MO) after 22 hpf according to the guidelines of the local authorities under licenses GZ:565304/2014/6 and GZ:534619/2014/4. Zebrafish WT AB* (ZFIN ID: ZDB-GENO-960809-7).[1] For pcHoechst **3** uncaging experiments, zebrafish embryos were injected at the one-cell stage with an injection mix containing 25 ng μL^{-1} mRNA synthesized from pCS2+ H2B-mRFP plasmid using mMESSAGE mMACHINE™ SP6 Transcription Kit (Thermo Fisher Scientific, Waltham, MA). Injections were performed with glass capillaries pulled with a needle puller (P97, Sutter Instruments, Novato, CA), mounted onto a micromanipulator (World Precision Instruments Inc., Berlin, Germany) and connected to a microinjector (FemtoJet i4, Eppendorf, Hamburg, Germany).

6.2 (Pc)Hoechst33342 toxicity in zebrafish

For determining pcHoechst **3** toxicity and leakiness, zebrafish embryos were dechorionated after 24 hpf and embedded in 1.2% low-melting agarose (Agarose Type IX-A, Ultra-low Gelling Temperature, Sigma-Aldrich) dissolved in E3 medium on micro-slides (µ-slide 4 well, Ibidi, Gräfelfing, Germany). Subsequently, treatment with 1% DMSO (vehicle control) 100 µM pcHoechst **3** and 10 µM or 100 µM Hoechst33342 (H3570, Molecular Probes, Eugene, OR) was performed on mounted zebrafish embryos with the compounds mixed into 500 µL E3 medium containing 0.003% PTU and 0.3 mg mL^{-1} Tricaine (Ethyl 3-aminobenzoate methanesulfonate 98%, Sigma-Aldrich) layered on top of the agarose. For the incubation period, pcHoechst **3** treated embryos were kept either in the dark by wrapping the micro-slides in aluminum foil or under ambient room light. UV-LED (395 nm) illumination was carried out at 32 hpf for 5 min. Images for pcHoechst **3** toxicity were recorded at 52 hpf using a microscope camera (MC170 HD, Leica Microsystems, Wetzlar, Germany) mounted on a Leica M125 stereomicroscope and the LAS V4 software.

6.3 *In vivo* single cell uncaging in zebrafish

Zebrafish embryos were dechorionated and embedded in 1.2% low-melting agarose on microslides at 32 or 56 hpf as previously described[205] and incubated with 100 µM pcHoechst **3** or

[1] Zebrafish experiments were carried out by Adam Varady, Dr. Caterina Sturtzel, Michael Riepl under suprvision of Dr. Martin Distel from the St. Anna Children's Cancer Research Institute Innovative Cancer Models, Vienna, Austria.

10 µM Hoechst33342 for at least four hours. For the incubation period, embryos were kept in the dark by wrapping the micro-slides in aluminum foil. *In vivo* activation of pcHoechst **3** was performed using the 405 nm UV laser of a confocal microscope (Leica SP8 WLL, Leica Microsystems, Wetzlar, Germany). The respective laser power was determined using a laser power meter (LP1, Sanwa, Tokyo, Japan). The bleachpoint function of the Leica LAS software was employed to target nuclei of cells in live zebrafish for uncaging. 100 ms light-pulses of 405 nm UV light every 3 s were used for illumination of the target site, repeated for 60-100 cycles. All photoactivation experiments at the confocal microscope were conducted at 28 °C using a temperature control system (The Cube 2, Live Imaging Services, Basel, Switzerland). Confocal microscopy images were recorded using the LAS X software (Leica Microsystems, Wetzlar, Germany), videos were edited and labeled with ImageJ.

Bibliography

[1] R. Dahm, *Human genetics* **2008**, *122*, 565–581.

[2] D. P. Stern, A Short history of nearly everything, **2005**.

[3] A. Hershey, M. Chase in *Die Entdeckung der Doppelhelix*, Springer, **2017**, pp. 121–139.

[4] **2021**, https://www.nobelprize.org/prizes/medicine/1969/summary/.

[5] J. D. Watson, F. H. Crick, *Nature* **1953**, *171*, 737–738.

[6] S. Duffy, *The Yale Journal of Biology and Medicine* **2003**, *76*, 142.

[7] **2021**, https://www.nobelprize.org/prizes/medicine/1962/summary/.

[8] M. Meselson, F. W. Stahl, *Proceedings of the national academy of sciences* **1958**, *44*, 671–682.

[9] R. M. Martin, H. Leonhardt, M. C. Cardoso, *Cytometry Part A* **2005**, *67*, 45–52.

[10] L. E. Weiss, T. Naor, Y. Shechtman, *Biochemical Society Transactions* **2018**, *46*, 729–740.

[11] C. S. O'Neil, J. L. Beach, T. D. Gruber, *Journal of visualized experiments : JoVE* **2019**, DOI 10.3791/59341.

[12] A. Adhikary, V. Buschmann, C. Müller, M. Sauer, *Nucleic acids research* **2003**, *31*, 2178–2186.

[13] S. K. Pal, L. Zhao, A. H. Zewail, *Proceedings of the National Academy of Sciences* **2003**, *100*, 8113–8118.

[14] C. D. Georgiou, I. Papapostolou, *Analytical biochemistry* **2006**, *358*, 247–256.

[15] L. C. Crowley, G. Chojnowski, N. J. Waterhouse, *Cold Spring Harbor Protocols* **2016**, *2016*, 905–910.

[16] B. Chazotte, *Cold Spring Harbor Protocols* **2011**, *6*, DOI 10.1101/pdb.prot5557.

[17] M. E. Lalande, V. Ling, R. G. Miller, *Proceedings of the National Academy of Sciences of the United States of America* **1981**, *78*, 363–367.

[18] P. E. Pjura, K. Grzeskowiak, R. E. Dickerson, *Journal of Molecular Biology* **1987**, *197*, 257–271.

[19] B. Chazotte, *Cold Spring Harbor Protocols* **2011**, *6*, DOI 10.1101/pdb.prot5556.

[20] J. Bucevičius, G. Lukinavičius, R. Gerasimaite, *Chemosensors* **2018**, *6*, DOI 10.3390/chemosensors6020018.

[21] G. Lukinavičius, C. Blaukopf, E. Pershagen, A. Schena, L. Reymond, E. Derivery, M. Gonzalez-Gaitan, E. D'Este, S. W. Hell, D. W. Gerlich, K. Johnsson, *Nature Communications* **2015**, *6*, 1–7.

[22] J. Bucevičius, J. Keller-Findeisen, T. Gilat, S. W. Hell, G. Lukinavičius, *Chemical Science* **2019**, *10*, 1962–1970.

[23] X. Zhang, Z. Ye, X. Zhang, H. Man, Z. Huang, N. Li, Y. Xiao, *Chemical Communications* **2019**, *55*, 1951–1954.

[24] D. Ganz, D. Harijan, H.-A. Wagenknecht, *RSC Chemical Biology* **2020**, *1*, 86–97.

[25] E. E. Bitter, M. H. Townsend, R. Erickson, C. Allen, K. L. O'Neill, *Cell and Bioscience* **2020**, *10*, 1–16.

[26] L. P. Jordheim, D. Durantel, F. Zoulim, C. Dumontet, *Nature Reviews Drug Discovery* **2013**, *12*, 447–464.

[27] D. A. Plotnik, L. E. Emerick, K. A. Krohn, J. D. Unadkat, J. L. Schwartz, *Journal of Nuclear Medicine* **2010**, *51*, 1464–1471.

[28] B. L. Cavanagh, T. Walker, A. Norazit, A. C. Meedeniya, *Molecules* **2011**, *16*, 7980–7993.

[29] A. Ligasová, K. Koberna, *Molecules* **2018**, *23*, DOI 10.3390/molecules23113007.

[30] J. H. Taylor, P. S. Woods, W. L. Hughes, *Proceedings of the National Academy of Sciences of the United States of America* **1957**, *43*, 122.

[31] J. Altman, G. D. Das, *Journal of Comparative Neurology* **1965**, *124*, 319–335.

[32] J. Schwaber, E. P. Cohen, *Nature* **1973**, *244*, 444–447.

[33] A. Cambrosio, P. Keating, *Journal of the History of Biology* **1992**, *25*, 175–230.

[34] H. G. Gratzner, *Science* **1982**, *218*, 474–475.

[35] H. G. Gratzner, R. C. Leif, D. Ingram, A Castro, *Experimental cell research* **1975**, *95*, 88–94.

[36] W. Vogel, M. Autenrieth, G. Speit, *Human Genetics* **1986**, *72*, 129–132.

[37] P. S. Eriksson, E. Perfilieva, T. Björk-Eriksson, A.-M. Alborn, C. Nordborg, D. A. Peterson, F. H. Gage, *Nature medicine* **1998**, *4*, 1313–1317.

[38] P. Taupin, *Brain research reviews* **2007**, *53*, 198–214.

[39] T. Yokochi, D. M. Gilbert, *Current protocols in cell biology* **2007**, *35*, 22–10.

[40] A. H. Tuttle, M. M. Rankin, M. Teta, D. J. Sartori, G. M. Stein, G. J. Kim, C. Virgilio, A. Granger, D. Zhou, S. H. Long, et al., *JoVE (Journal of Visualized Experiments)* **2010**, e2166.

[41] J. Gierlich, G. A. Burley, P. M. Gramlich, D. M. Hammond, T. Carell, *Organic Letters* **2006**, *8*, 3639–3642.

[42] A. Salic, T. J. Mitchison, *Proceedings of the National Academy of Sciences of the United States of America* **2008**, *105*, 2415–2420.

[43] H. Zhao, H. D. Halicka, J. Li, E. Biela, K. Berniak, J. Dobrucki, Z. Darzynkiewicz, *Cytometry Part A* **2013**, *83*, 979–988.

[44] D. Qu, G. Wang, Z. Wang, L. Zhou, W. Chi, S. Cong, X. Ren, P. Liang, B. Zhang, *Analytical Biochemistry* **2011**, *417*, 112–121.

[45] L. Guan, G. W. van der Heijden, A. Bortvin, M. M. Greenberg, *ChemBioChem* **2011**, *12*, 2184–2190.

[46] A. B. Neef, N. W. Luedtke, *Proceedings of the National Academy of Sciences of the United States of America* **2011**, *108*, 20404–20409.

[47] A. B. Neef, F. Samain, N. W. Luedtke, *ChemBioChem* **2012**, *13*, 1750–1753.

[48] U. Rieder, N. W. Luedtke, *Angewandte Chemie - International Edition* **2014**, *53*, 9168–9172.

[49] G. Linden, L. Zhang, F. Pieck, U. Linne, D. Kosenkov, R. Tonner, O. Vázquez, *Angewandte Chemie - International Edition* **2019**, *58*, 12868–12873.

[50] Y. Wu, G. Guo, J. Zheng, D. Xing, T. Zhang, *ACS Sensors* **2019**, *4*, 44–51.

[51] A. Gubu, L. Li, Y. Ning, X. Zhang, S. Lee, M. Feng, Q. Li, X. Lei, K. Jo, X. Tang, *Chemistry - A European Journal* **2018**, *24*, 5895–5900.

[52] A. B. Neef, N. W. Luedtke, *ChemBioChem* **2014**, *15*, 789–793.

[53] K. L. Seley-radtke, M. K. Yates, *Antiviral Research* **2018**, *154*, 66–86.

[54] M. Tera, Z. Harati Taji, N. W. Luedtke, *Angewandte Chemie - International Edition* **2018**, *57*, 15405–15409.

[55] M. Tera, N. W. Luedtke, *Bioconjugate Chemistry* **2019**, *30*, 2991–2997.

[56] A. B. Neef, L. Pernot, V. N. Schreier, L. Scapozza, N. W. Luedtke, *Angewandte Chemie - International Edition* **2015**, *54*, 7911–7914.

[57] P. J. Thornton, H. Kadri, A. Miccoli, Y. Mehellou, *Journal of Medicinal Chemistry* **2016**, *59*, 10400–10410.

[58] S. Seo, K. Onizuka, C. Nishioka, E. Takahashi, S. Tsuneda, H. Abe, Y. Ito, *Organic and Biomolecular Chemistry* **2015**, *13*, 4589–4595.

[59] N. Huynh, C. Dickson, D. Zencak, D. H. Hilko, A. Mackay-Sim, S. A. Poulsen, *Chemical Biology and Drug Design* **2015**, *86*, 400–409.

[60] T. Gollnest, T. D. De Oliveira, A. Rath, I. Hauber, D. Schols, J. Balzarini, C. Meier, *Angewandte Chemie - International Edition* **2016**, *55*, 5255–5258.

[61] X. Jia, D. Schols, C. Meier, *Journal of Medicinal Chemistry* **2020**, *63*, 6991–7007.

[62] C. Zhao, S. Weber, D. Schols, J. Balzarini, C. Meier, *Angewandte Chemie* **2020**, *132*, 22247–22255.

[63] V. N. Schreier, M. O. Loehr, T. Deng, E. Lattmann, A. Hajnal, S. C. Neuhauss, N. W. Luedtke, *ACS Chemical Biology* **2020**, *15*, 2996–3003.

[64] Z. Zawada, A. Tatar, P. Mocilac, M. Buděšínský, T. Kraus, *Angewandte Chemie - International Edition* **2018**, *57*, 9891–9895.

[65] P. Güixens-Gallardo, Z. Zawada, J. Matyašovský, D. Dziuba, R. Pohl, T. Kraus, M. Hocek, *Bioconjugate Chemistry* **2018**, *29*, 3906–3912.

[66] F. De Wit, S. R. Pillalamarri, A. Sebastián-Martín, A. Venkatesham, A. Van Aerschot, X. Zeger Debyser, *Journal of Biological Chemistry* **2019**, *294*, 11863–11875.

[67] S. L. Scinto, D. A. Bilodeau, R. Hincapie, W. Lee, S. S. Nguyen, M. Xu, C. W. am Ende, M. Finn, K. Lang, Q. Lin, et al., *Nature Reviews Methods Primers* **2021**, *1*, 1–23.

[68] N. K. Devaraj, *ACS central science* **2018**, *4*, 952–959.

[69] E. M. Sletten, C. R. Bertozzi, *Angewandte Chemie - International Edition* **2009**, *48*, 6974–6998.

[70] K. Lang, L. Davis, J. Torres-Kolbus, C. Chou, A. Deiters, J. W. Chin, *Nature Chemistry* **2012**, *4*, 298–304.

[71] K. Lang, L. Davis, S. Wallace, M. Mahesh, D. J. Cox, M. L. Blackman, J. M. Fox, J. W. Chin, *Journal of the American Chemical Society* **2012**, *134*, 10317–10320.

[72] X. Ning, J. Guo, M. A. Wolfert, G. J. Boons, *Angewandte Chemie - International Edition* **2008**, *47*, 2253–2255.

[73] J. Zheng, Q. Zhan, L. Jiang, D. Xing, T. Zhang, K. L. Wong, *Inorganic Chemistry Frontiers* **2020**, *7*, 4062–4069.

[74] F. Doll, A. Buntz, A. K. Späte, V. F. Schart, A. Timper, W. Schrimpf, C. R. Hauck, A. Zumbusch, V. Wittmann, *Angewandte Chemie - International Edition* **2016**, *55*, 2262–2266.

[75] C. Y. Jao, M. Roth, R. Welti, A. Salic, *Proceedings of the National Academy of Sciences of the United States of America* **2009**, *106*, 15332–15337.

[76] A. Gaebler, A. Penno, L. Kuerschner, C. Thiele, *Journal of Lipid Research* **2016**, *57*, 1934–1947.

[77] N. Z. Fantoni, A. H. El-Sagheer, T. Brown, *Chemical Reviews* **2021**, DOI `10.1021/acs.chemrev.0c00928`.

[78] S. H. Weisbrod, A. Marx, *Chemical Communications* **2008**, 5675–5685.

[79] K. Lang, J. W. Chin, *ACS Chemical Biology* **2014**, *9*, 16–20.

[80] E. M. Sletten, C. R. Bertozzi, *Accounts of ChemicBioorthogonal turn-on probes for imaging small molecules inside living cellsal Research* **2011**, *44*, 666–676.

[81] V. V. Rostovtsev, L. G. Green, V. V. Fokin, K. B. Sharpless, *Angewandte Chemie - International Edition* **2002**, *41*, 2596–2599.

[82] N. Klöcker, F. P. Weissenboeck, A. Rentmeister, *Chemical Society Reviews* **2020**, *49*, 8749–8773.

[83] C. R. Bertozzi, E Saxon, *Science* **2000**, *287*, 2007–2010.

[84] N. K. Devaraj, S. Hilderbrand, R. Upadhyay, R. Mazitschek, R. Weissleder, *Angewandte Chemie* **2010**, *122*, 2931–2934.

[85] P. J. A., D. D. H., B. C. R., *Nature* **2004**, *430*, 873–877.

[86] P. V. Changa, J. A. Preschera, E. M. Sletten, J. M. Baskin, I. A. Miller, N. J. Agard, A. Lo, C. R. Bertozzi, *Proceedings of the National Academy of Sciences of the United States of America* **2010**, *107*, 1821–1826.

[87] C. W. Tornøe, C. Christensen, M. Meldal, *Journal of Organic Chemistry* **2002**, *67*, 3057–3064.

[88] D. C. Kennedy, C. S. McKay, M. C. Legault, D. C. Danielson, J. A. Blake, A. F. Pegoraro, A. Stolow, Z. Mester, J. P. Pezacki, *Journal of the American Chemical Society* **2011**, *133*, 17993–18001.

[89] N. J. Agard, J. A. Prescher, C. R. Bertozzi, *Journal of the American Chemical Society* **2004**, *126*, 15046–15047.

[90] M. L. Blackman, M. Royzen, J. M. Fox, *Journal of the American Chemical Society* **2008**, *130*, 13518–13519.

[91] B. L. Oliveira, Z. Guo, G. J. Bernardes, *Chemical Society Reviews* **2017**, *46*, 4895–4950.

[92] E. Kozma, O. Demeter, P. Kele, *ChemBioChem* **2017**, *18*, 486–501.

[93] R. A. Carboni, R. V. Lindsey, *Journal of the American Chemical Society* **1959**, *81*, 4342–4346.

[94] N. K. Devaraj, R. Weissleder, S. A. Hilderbrand, *Bioconjugate Chemistry* **2008**, *19*, 2297–2299.

[95] M. Vrabel, P. Kölle, K. M. Brunner, M. J. Gattner, V. Lõpez-Carrillo, R. De Vivie-Riedle, T. Carell, *Chemistry - A European Journal* **2013**, *19*, 13309–13312.

[96] J. Yang, J. Seckute, C. M. Cole, N. K. Devaraj, *Angew Chem Int Ed Engl* **2012**, *51*, 7476–9.

[97] D. M. Patterson, L. A. Nazarova, B. Xie, D. N. Kamber, J. A. Prescher, *J Am Chem Soc* **2012**, *134*, 18638–43.

[98] W. Chen, D. Wang, C. Dai, D. Hamelberg, B. Wang, *Chemical Communications* **2012**, *48*, 1736–1738.

[99] J. A. Wagner, D. Mercadante, I. Nikic, E. A. Lemke, F. Gräter, *Chemistry - A European Journal* **2015**, *21*, 12431–12435.

[100] M. Kubota, S. Nainar, S. M. Parker, W. England, F. Furche, R. C. Spitale, *ACS Chemical Biology* **2019**, *14*, 1698–1707.

[101] H. S. Liu, T. Ishizuka, M. Kawaguchi, R. Nishii, H. Kataoka, Y. Xu, *Bioconjugate Chemistry* **2019**, *30*, 2958–2966.

[102] M. Sunbul, A. Jäschke, **2019**.

[103] D. A. Erlanson, A. C. Braisted, D. R. Raphael, M. Randal, R. M. Stroud, E. M. Gordon, J. A. Wells, *Proceedings of the National Academy of Sciences* **2000**, *97*, 9367–9372.

[104] M. Cigler, T. G. Müller, D. Horn-Ghetko, M. K. von Wrisberg, M. Fottner, R. S. Goody, A. Itzen, M. P. Müller, K. Lang, *Angewandte Chemie - International Edition* **2017**, *56*, 15737–15741.

[105] D. Englert, R. Matveeva, M. Sunbul, R. Wombacher, A. Jäschke, *Chemical Communications* **2021**, *57*, 3480–3483.

[106] S. J. Sahl, S. W. Hell, S. Jakobs, *Nature Reviews Molecular Cell Biology* **2017**, *18*, 685–701.

[107] S. W. Hell, *Science* **2007**, *316*, doi: 10.1126/science.1137395., 1153–8.

[108] S. W. Hell, *Angewandte Chemie - International Edition* **2015**, *54*, 8054–8066.

[109] L. D. Lavis, R. T. Raines, *ACS Chemical Biology* **2014**, *9*, 855–866.

[110] L. D. Lavis, *Biochemistry* **2017**, *56*, 5165–5170.

[111] L. V. Johnson, M. L. Walsh, L. B. Chen, *Proceedings of the National Academy of Sciences* **1980**, *77*, 990–994.

[112] G. Y. Wiederschain, The Molecular Probes handbook. A guide to fluorescent probes and labeling technologies, **2011**.

[113] L. Wang, M. S. Frei, A. Salim, K. Johnsson, *Journal of the American Chemical Society* **2019**, *141*, 2770–2781.

[114] Y. Fu, N. S. Finney, *RSC advances* **2018**, *8*, 29051–29061.

[115] L. Wang, M. Tran, E. D'Este, J. Roberti, B. Koch, L. Xue, K. Johnsson, *bioRxiv* **2019**, *12*, 156–172.

[116] N. Lardon, L. Wang, A. Tschanz, P. Hoess, M. Tran, E. D'Este, J. Ries, K. Johnsson, *Journal of the American Chemical Society* **2021**, *143*, 14592–14600.

[117] J. B. Grimm, B. P. English, H. Choi, A. K. Muthusamy, B. P. Mehl, P. Dong, T. A. Brown, J. Lippincott-Schwartz, Z. Liu, T. Lionnet, L. D. Lavis, *Nature Methods* **2016**, *13*, 985–988.

[118] A. N. Butkevich, G. Y. Mitronova, S. C. Sidenstein, J. L. Klocke, D. Kamin, D. N. Meineke, E. D'Este, P. T. Kraemer, J. G. Danzl, V. N. Belov, S. W. Hell, *Angewandte Chemie - International Edition* **2016**, *55*, 3290–3294.

[119] L. D. Lavis, *Annual review of biochemistry* **2017**, *86*, 825–843.

[120] G. Lukinavičius, K. Umezawa, N. Olivier, A. Honigmann, G. Yang, T. Plass, V. Mueller, L. Reymond, I. R. Corrêa, Z. G. Luo, C. Schultz, E. A. Lemke, P. Heppenstall, C. Eggeling, S. Manley, K. Johnsson, *Nature Chemistry* **2013**, *5*, 132–139.

[121] G. Lukinavičius, L. Reymond, K. Umezawa, O. Sallin, E. D'Este, F. Göttfert, H. Ta, S. W. Hell, Y. Urano, K. Johnsson, *Journal of the American Chemical Society* **2016**, *138*, 9365–9368.

[122] G. Lukinavičius, G. Y. Mitronova, S. Schnorrenberg, A. N. Butkevich, H. Barthel, V. N. Belov, S. W. Hell, *Chemical Science* **2018**, *9*, 3324–3334.

[123] G. V. Los, L. P. Encell, M. G. McDougall, D. D. Hartzell, N. Karassina, C. Zimprich, M. G. Wood, R. Learish, R. F. Ohana, M. Urh, D. Simpson, J. Mendez, K. Zimmerman, P. Otto, G. Vidugiris, J. Zhu, A. Darzins, D. H. Klaubert, R. F. Bulleit, K. V. Wood, *ACS Chemical Biology* **2008**, *3*, PMID: 18533659, 373–382.

[124] A. Gautier, A. Juillerat, C. Heinis, I. R. Corrêa, M. Kindermann, F. Beaufils, K. Johnsson, *Chemistry and Biology* **2008**, *15*, 128–136.

[125] J. Bucevičius, G. Kostiuk, R. Gerasimaitė, T. Gilat, G. Lukinavičius, *Chemical Science* **2020**, *11*, 7313–7323.

[126] G. S. Jiao, L. H. Thoresen, K. Burgess, *Journal of the American Chemical Society* **2003**, *125*, 14668–14669.

[127] L. G. Meimetis, J. C. Carlson, R. J. Giedt, R. H. Kohler, R. Weissleder, *Angewandte Chemie - International Edition* **2014**, *53*, 7531–7534.

[128] P. Werther, K. Yserentant, F. Braun, K. Grußmayer, V. Navikas, M. Yu, Z. Zhang, M. J. Ziegler, C. Mayer, A. J. Gralak, M. Busch, W. Chi, F. Rominger, A. Radenovic, X. Liu, E. A. Lemke, T. Buckup, D.-P. Herten, R. Wombacher, *ACS Central Science* **2021**, DOI 10.1021/acscentsci.1c00703.

[129] A. Wieczorek, P. Werther, J. Euchner, R. Wombacher, *Chemical Science* **2017**, *8*, 1506–1510.

[130] E. Kozma, G. Estrada Girona, G. Paci, E. A. Lemke, P. Kele, *Chemical Communications* **2017**, *53*, 6696–6699.

[131] R. S. Erdmann, H. Takakura, A. D. Thompson, F. Rivera-Molina, E. S. Allgeyer, J. Bewersdorf, D. Toomre, A. Schepartz, *Angewandte Chemie International Edition* **2014**, *53*, 10242–10246.

[132] T. G. Müller, V. Sakin, B. Müller, *Molecules* **2019**, *24*, DOI 10.3390/molecules24030481.

[133] M. Lusic, B. Marini, H. Ali, B. Lucic, R. Luzzati, M. Giacca, *Cell Host Microbe* **2013**, *13*, 665–77.

[134] V. Sakin, G. Paci, E. A. Lemke, B. Muller, *FEBS Lett* **2016**, *590*, 1896–914.

[135] Y. Yamauchi, U. F. Greber, *Traffic* **2016**, *17*, 569–592.

[136] A. d. B. Kops, D. M. Knipe, *Cell* **1988**, *55*, 857–868.

[137] B. L. Strang, S. Boulant, L. Chang, D. M. Knipe, T. Kirchhausen, D. M. Coen, *J Virol* **2012**, *86*, 2089–95.

[138] I. H. Wang, M. Suomalainen, V. Andriasyan, S. Kilcher, J. Mercer, A. Neef, N. W. Luedtke, U. F. Greber, *Cell Host and Microbe* **2013**, *14*, 468–480.

[139] K. Peng, W. Muranyi, B. Glass, V. Laketa, S. R. Yant, L. Tsai, T. Cihlar, B. Müller, H. G. Kräusslich, *eLife* **2014**, *3*, e04114.

[140] L. L. Huang, K. Liu, Q. Zhang, J. Xu, D. Zhao, H. Zhu, H. Y. Xie, *Analytical Chemistry* **2017**, *89*, 11620–11627.

[141] D. Kuksin, L. C. Norkin, *J Virol* **2012**, *86*, 1555–62.

[142] T. G. Müller, V. Zila, K. Peters, S. Schifferdecker, M. Stanic, B. Lucic, V. Laketa, M. Lusic, B. Müller, H.-G. Kräusslich, *eLife* **2021**, *10*, (Eds.: W. I. Sundquist, S. L. Sawyer, E. M. Campbell), e64776.

[143] B. Mariamé, S. Kappler-Gratias, M. Kappler, S. Balor, F. Gallardo, K. Bystricky, *Journal of Virology* **2018**, *92*, DOI 10.1128/jvi.00571-18.

[144] T. Germier, S. Kocanova, N. Walther, A. Bancaud, H. A. Shaban, H. Sellou, A. Z. Politi, J. Ellenberg, F. Gallardo, K. Bystricky, *Biophysical Journal* **2017**, *113*, 1383–1394.

[145] T. Germier, A. Sylvain, K. Silvia, L. David, B. Kerstin, *Methods* **2018**, *142*, 16–23.

[146] V. Zila, E. Margiotta, B. Turoňová, T. G. Müller, C. E. Zimmerli, S. Mattei, M. Allegretti, K. Börner, J. Rada, B. Müller, et al., *Cell* **2021**, *184*, 1032–1046.

[147] M. Lusic, R. F. Siliciano, *Nature Reviews Microbiology* **2017**, *15*, 69–82.

[148] E. M. Campbell, T. J. Hope, *Nature Reviews Microbiology* **2015**, *13*, 471–483.

[149] D. Berdnikova, O. Fedorova, E. Gulakova, H. Ihmels, *Chem. Commun.* **2012**, *48*, 4603–4605.

[150] K. Liu, Y. Wen, T. Shi, Y. Li, F. Li, Y.-l. Zhao, C. Huang, T. Yi, *Chem. Commun.* **2014**, *50*, 9141–9144.

[151] P. Kla, C. G. Bochet, R. Givens, M. Rubina, V. Popik, A. Kostikov, J. Wirz, *Chemical Reviews* **2012**, *113*, 119–191.

[152] A. Patchornik, B. Amit, R. B. Woodward, *Journal of the American Chemical Society* **1970**, *92*, 6333–6335.

[153] B. Van Steensel, A. S. Belmont, *Cell* **2017**, *169*, 780–791.

[154] H. Jerabek, D. W. Heermann, *International review of cell and molecular biology* **2014**, *307*, 351–381.

[155] H. Bußkamp, E. Batroff, A. Niederwieser, O. S. Abdel-Rahman, R. F. Winter, V. Wittmann, A. Marx, *Chemical Communications* **2014**, *50*, 10827–10829.

[156] H. Cahová, A. Panattoni, P. Kielkowski, J. Fanfrlík, M. Hocek, *ACS Chemical Biology* **2016**, *11*, 3165–3171.

[157] G. M. Cooper, R. E. Hausman, R. E. Hausman, *The cell: a molecular approach*, *Vol. 4*, ASM press Washington, DC, **2007**.

[158] V. O. Chagin, J. H. Stear, M. C. Cardoso, *Cold Spring Harbor perspectives in biology* **2010**, *2*, DOI 10.1101/cshperspect.a000737.

[159] U. J. Birk, *Genes* **2019**, *10*, DOI 10.3390/genes10070493.

[160] T. Triemer, A. Messikommer, S. M. Glasauer, J. Alzeer, M. H. Paulisch, N. W. Luedtke, *Proceedings of the National Academy of Sciences of the United States of America* **2018**, *115*, E1366–E1373.

[161] L. Wang, M. Tran, E. D'Este, J. Roberti, B. Koch, L. Xue, K. Johnsson, *Nature Chemistry* **2020**, *12*, 165–172.

[162] H. Wu, J. Yang, J. Šečkute, N. K. Devaraj, *Angewandte Chemie - International Edition* **2014**, *53*, 5805–5809.

[163] S. Mayer, K. Lang, *Synthesis (Germany)* **2017**, *49*, 830–848.

[164] K. Bergen, A. L. Steck, S. Strütt, A. Baccaro, W. Welte, K. Diederichs, A. Marx, *Journal of the American Chemical Society* **2012**, *134*, 11840–11843.

[165] M. Merkel, S. Arndt, D. Ploschik, G. B. Cserép, U. Wenge, P. Kele, H. A. Wagenknecht, *Journal of Organic Chemistry* **2016**, *81*, 7527–7538.

[166] J. Schoch, A. Jäschke, *RSC Advances* **2013**, *3*, 4181–4183.

[167] D. Ploschik, F. Rönicke, H. Beike, R. Strasser, H. A. Wagenknecht, *ChemBioChem* **2018**, *19*, 1949–1953.

[168] A. Hottin, K. Betz, K. Diederichs, A. Marx, *Chemistry - A European Journal* **2017**, *23*, 2109–2118.

[169] S. Jäger, G. Rasched, H. Kornreich-Leshem, M. Engeser, O. Thum, M. Famulok, *Journal of the American Chemical Society* **2005**, *127*, 15071–15082.

[170] F. Seela, M. Zulauf, *Helvetica chimica acta* **1999**, *82*, 1878–1898.

[171] S. H. Cho, L. S. Liebeskind, *The Journal of Organic Chemistry* **1987**, *52*, 2631–2634.

[172] J. Yang, J. Šečkutė, C. M. Cole, N. K. Devaraj, *Angewandte Chemie* **2012**, *124*, 7594–7597.

[173] B. L. Cavanagh, T. Walker, A. Norazit, A. C. Meedeniya, Thymidine analogues for tracking DNA synthesis, **2011**.

[174] P. Perlíková, G. Rylová, P. Nauš, T. Elbert, E. Tloušťová, A. Bourderioux, L. P. Slavětínská, K. Motyka, D. Doležal, P. Znojek, A. Nová, M. Harvanová, P. Džubák, M. Šiller, J. Hlaváč, M. Hajdúch, M. Hocek, *Molecular Cancer Therapeutics* **2016**, *15*, 922–937.

[175] M. Held, M. H. Schmitz, B. Fischer, T. Walter, B. Neumann, M. H. Olma, M. Peter, J. Ellenberg, D. W. Gerlich, *Nature Methods* **2010**, *7*, 747–754.

[176] L. Mah, A El-Osta, T. Karagiannis, *Leukemia* **2010**, *24*, 679–686.

[177] K. S. Yang, R. H. Kohler, M. Landon, R. Giedt, R. Weissleder, *Scientific Reports* **2015**, *5*, DOI 10.1038/srep10129.

[178] T. Plass, S. Milles, C. Koehler, J. Szymański, R. Mueller, M. Wießler, C. Schultz, E. A. Lemke, *Angewandte Chemie* **2012**, *124*, 4242–4246.

[179] Z. Zhang, L. Alfonta, F. Tian, B. Bursulaya, S. Uryu, D. S. King, P. G. Schultz, *Proceedings of the National Academy of Sciences of the United States of America* **2004**, *101*, 8882–8887.

[180] K. Lang, J. W. Chin, *Chemical Reviews* **2014**, *114*, 4764–4806.

[181] M. S. Kokoris, P. Sabo, E. T. Adman, M. E. Black, *Gene Therapy* **1999**, *6*, 1415–1426.

[182] M. E. Black, T. G. Newcomb, H. M. P. Wilson, L. A. Loeb, *Proceedings of the National Academy of Sciences of the United States of America* **1996**, *93*, 3525–3529.

[183] S. Nainar, B. J. Cuthbert, N. M. Lim, W. E. England, K. Ke, K. Sophal, R. Quechol, D. L. Mobley, C. W. Goulding, R. C. Spitale, *Nature Methods* **2020**, *17*, 311–318.

[184] K. Nguyen, M. Kubota, J. D. Arco, C. Feng, M. Singha, S. Beasley, J. Sakr, S. P. Gandhi, M. Blurton-Jones, J. Fernández Lucas, R. C. Spitale, *ACS Chemical Biology* **2020**, *15*, 3099–3105.

[185] U. Pradere, E. C. Garnier-Amblard, S. J. Coats, F. Amblard, R. F. Schinazi, *Chemical Reviews* **2014**, *114*, 9154–9218.

[186] L. D. Lavis, T. Y. Chao, R. T. Raines, *Chemical Science* **2011**, *2*, 521–530.

[187] W. Li, C. Schultz, J. Llopis, R. Y. Tsien in Tetrahedron, *Vol. 53*, **1997**, pp. 12017–12040.

[188] C. Schultz, M. Vajanaphanich, A. T. Harootunian, P. J. Sammak, K. E. Barrett, R. Y. Tsien, *Journal of Biological Chemistry* **1993**, *268*, 6316–6322.

[189] S. Kantevari, G. R. Gordon, B. A. MacVicar, G. C. Ellis-Davies, *Nature Protocols* **2011**, *6*, 327–337.

[190] A. D. Briggs, M. Camplo, S. Freeman, J. Lundström, B. G. Pring, *Tetrahedron* **1996**, *52*, 14937–14950.

[191] G. J. Friis, H. Bundgaard, *European Journal of Pharmaceutical Sciences* **1996**, *4*, 49–59.

[192] C. Meier, M. Lorey, E. De Clercq, J. Balzarini, *Journal of Medicinal Chemistry* **1998**, *41*, 1417–1427.

[193] S. Arumugam, V. V. Popik, *Journal of the American Chemical Society* **2009**, *131*, 11892–11899.

[194] P. Klán, T. Solomek, C. G. Bochet, A. Blanc, R. Givens, M. Rubina, V. Popik, A. Kostikov, J. Wirz, *Chemical reviews* **2013**, *113*, 119–191.

[195] L. Tian, Y. Yang, L. M. Wysocki, A. C. Arnold, A. Hu, B. Ravichandran, S. M. Sternson, L. L. Looger, L. D. Lavis, *Proceedings of the National Academy of Sciences of the United States of America* **2012**, *109*, 4756–4761.

[196] P. E. Pjura, K. Grzeskowiak, R. E. Dickerson, *Journal of molecular biology* **1987**, *197*, 257–271.

[197] H. Wu, J. Yang, J. Šečkute, N. K. Devaraj, *Angewandte Chemie - International Edition* **2014**, *53*, 5805–5809.

[198] P. E. Deal, R. U. Kulkarni, S. H. Al-Abdullatif, E. W. Miller, *Journal of the American Chemical Society* **2016**, *138*, 9085–9088.

[199] Á. Sinai, D. Vangel, T. Gáti, P. Bombicz, Z. Novák, *Organic Letters* **2015**, *17*, 4136–4139.

[200] S. Jäger, G. Rasched, H. Kornreich-Leshem, M. Engeser, O. Thum, M. Famulok, *Journal of the American Chemical Society* **2005**, *127*, 15071–15082.

[201] Y. Hwang, P. A. Cole, *Organic Letters* **2004**, *6*, 1555–1556.

[202] M. T. Rudolf, C. Dinkel, A. E. Traynor-Kaplan, C. Schultz, *Bioorganic & medicinal chemistry* **2003**, *11*, 3315–3329.

[203] M. G. Pomper, H. Hammond, X. Yu, Z. Ye, C. A. Foss, D. D. Lin, J. J. Fox, L. Cheng, *Cell Research* **2009**, *19*, 370–379.

[204] J. Schindelin, I. Arganda-Carreras, E. Frise, V. Kaynig, M. Longair, T. Pietzsch, S. Preibisch, C. Rueden, S. Saalfeld, B. Schmid, J. Y. Tinevez, D. J. White, V. Hartenstein, K. Eliceiri, P. Tomancak, A. Cardona, *Nature Methods* **2012**, *9*, 676–682.

[205] M. Bojtár, A. Kormos, K. Kis-Petik, M. Kellermayer, P. Kele, *Organic letters* **2019**, *21*, 9410–9414.

Part IV

Supporting Information

1 NMR spectra

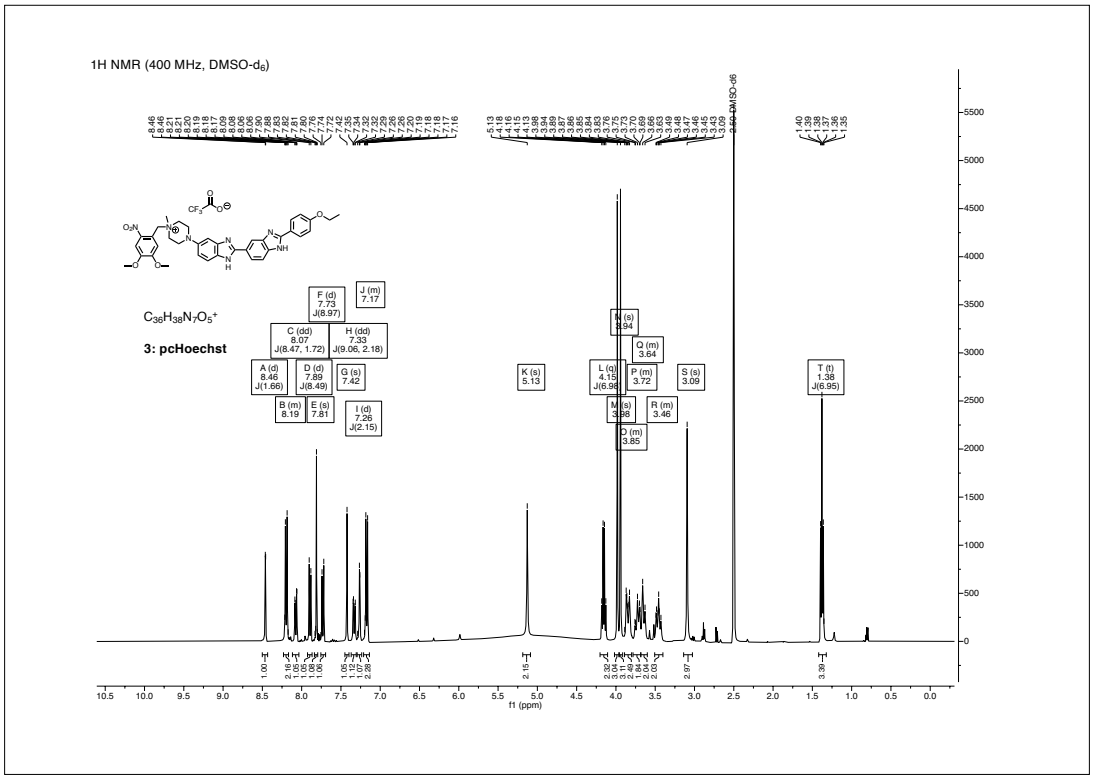
1H NMR (400 MHz, DMSO-d6)
C36H38N7O5+
3: pcHoechst
A (d) 8.46 J(1.66)
B (m) 8.19
C (dd) 8.07 J(8.47, 1.72)
D (d) 7.89 J(8.49)
E (s) 7.81
F (d) 7.72 J(8.97)
G (s) 7.42
H (dd) 7.33 J(9.06, 2.18)
I (d) 7.26 J(2.15)
J (m) 7.17
K (s) 5.13
L (q) 4.15 J(6.98)
M (s) 3.94
N (m) 3.88
O (m) 3.85
P (m) 3.72
Q (m) 3.64
R (m) 3.46
S (s) 3.09
T (t) 1.38 J(6.95)
DMSO-d6
f1 (ppm)

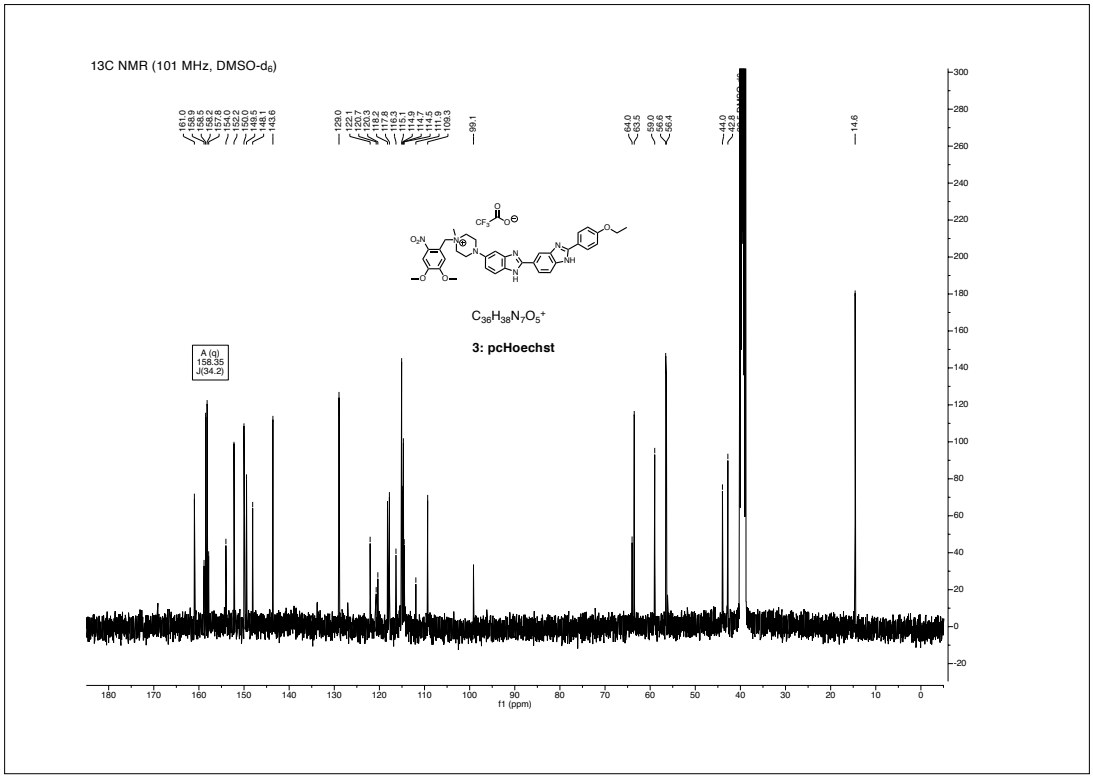
13C NMR (101 MHz, DMSO-d6)
C36H38N7O5+
3: pcHoechst
A (q) 158.35 J(34.2)
DMSO-d6
f1 (ppm)

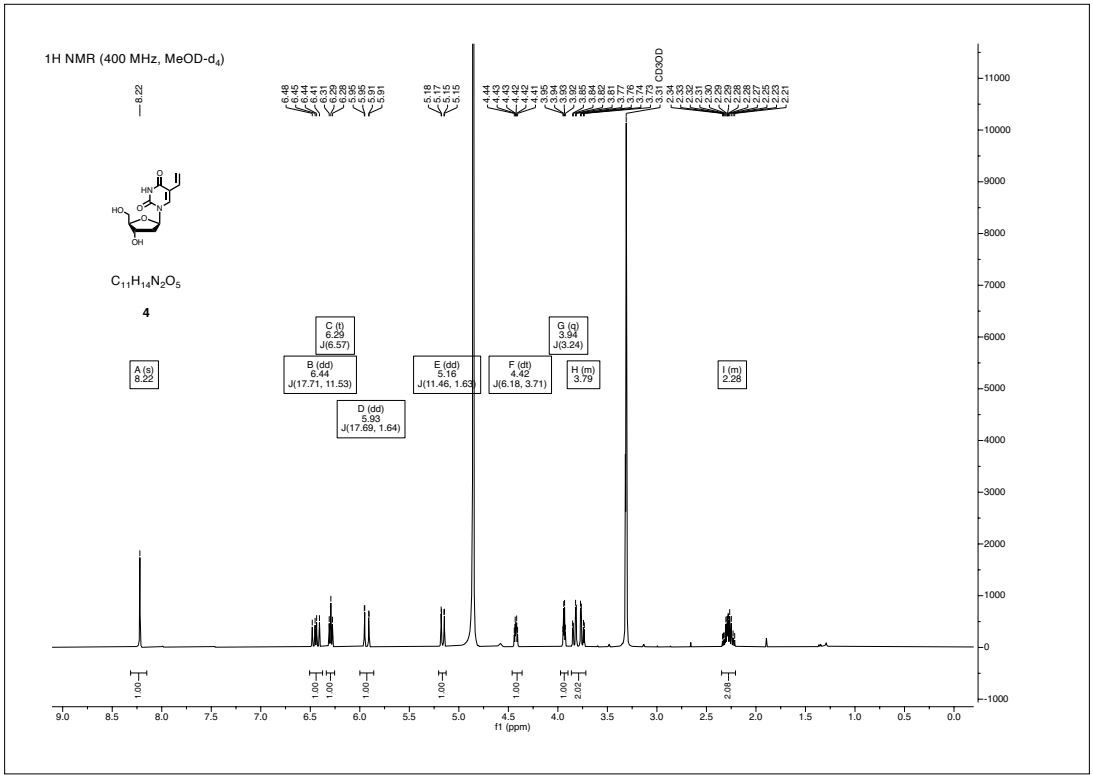
1H NMR (400 MHz, MeOD-d4)
C11H14N2O5
4
A (s) 8.22
B (dd) 5.44 J(17.71, 11.53)
C (t) 6.29 J(6.57)
D (dd) 5.93 J(17.69, 1.64)
E (dd) 5.16 J(11.46, 1.63)
F (dt) 4.42 J(6.18, 3.71)
G (q) 3.94 J(3.24)
H (m) 3.79
I (m) 2.28
f1 (ppm)

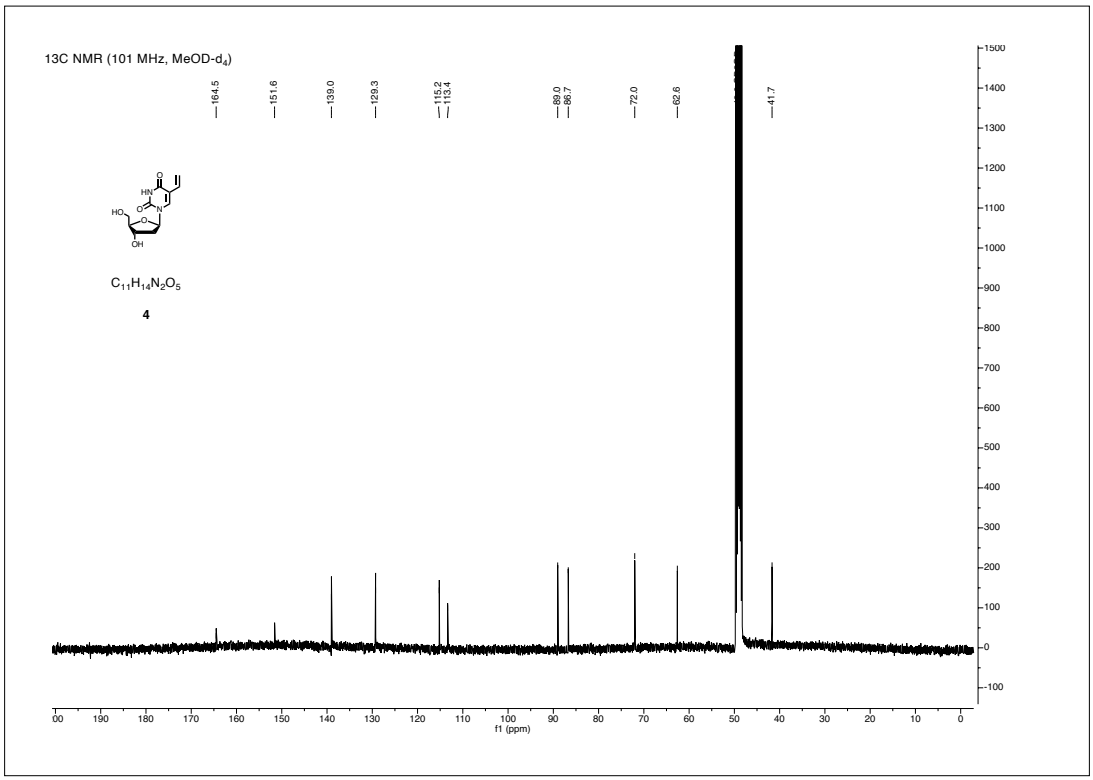
13C NMR (101 MHz, MeOD-d4)
C11H14N2O5
4
164.5
151.6
139.0
129.3
115.2
113.4
89.0
86.7
72.0
62.6
41.7
f1 (ppm)

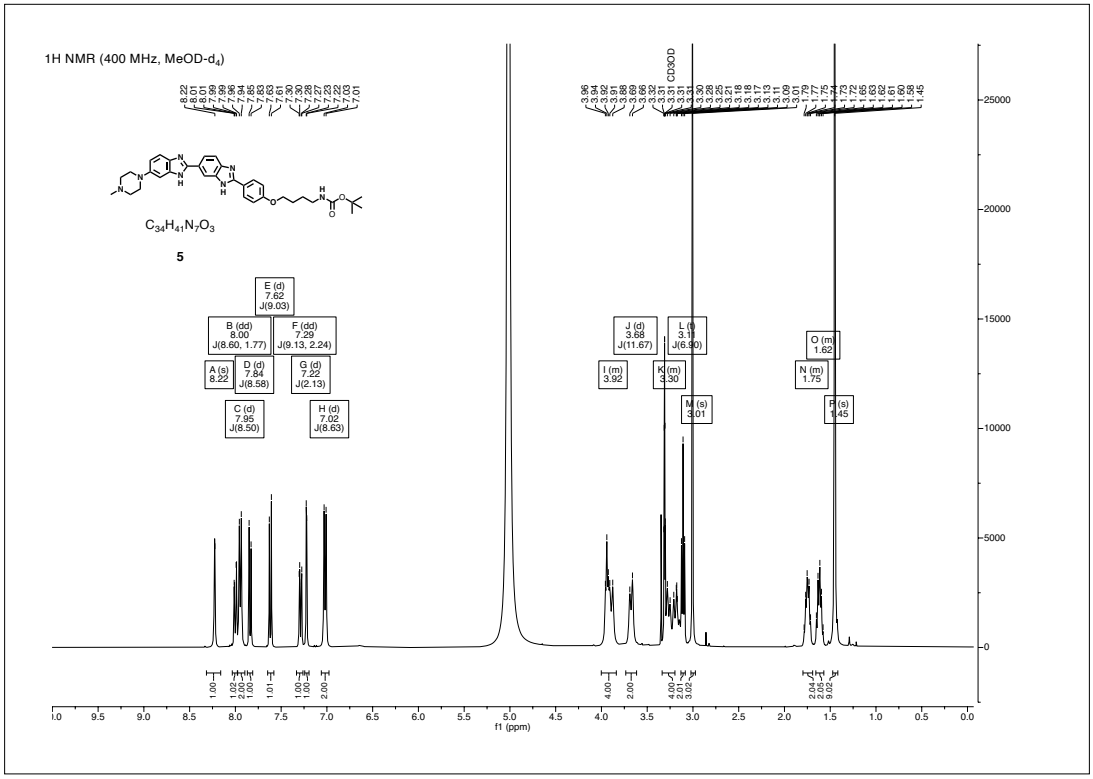
1H NMR (400 MHz, MeOD-d4)
CD3OD
C34H41N7O3
5
A (s) 8.22
B (dd) 8.00 J(8.60, 1.77)
C (d) 7.95 J(8.50)
D (d) 7.84 J(8.58)
E (d) 7.62 J(9.03)
F (dd) 7.29 J(9.13, 2.24)
G (d) 7.22 J(2.13)
H (d) 7.02 J(8.63)
I (m) 3.92
J (d) 3.68 J(11.67)
K (m) 3.30
L (t) 3.17 J(6.90)
M (s) 3.01
N (m) 1.75
O (m) 1.62
P (s) 1.45
f1 (ppm)

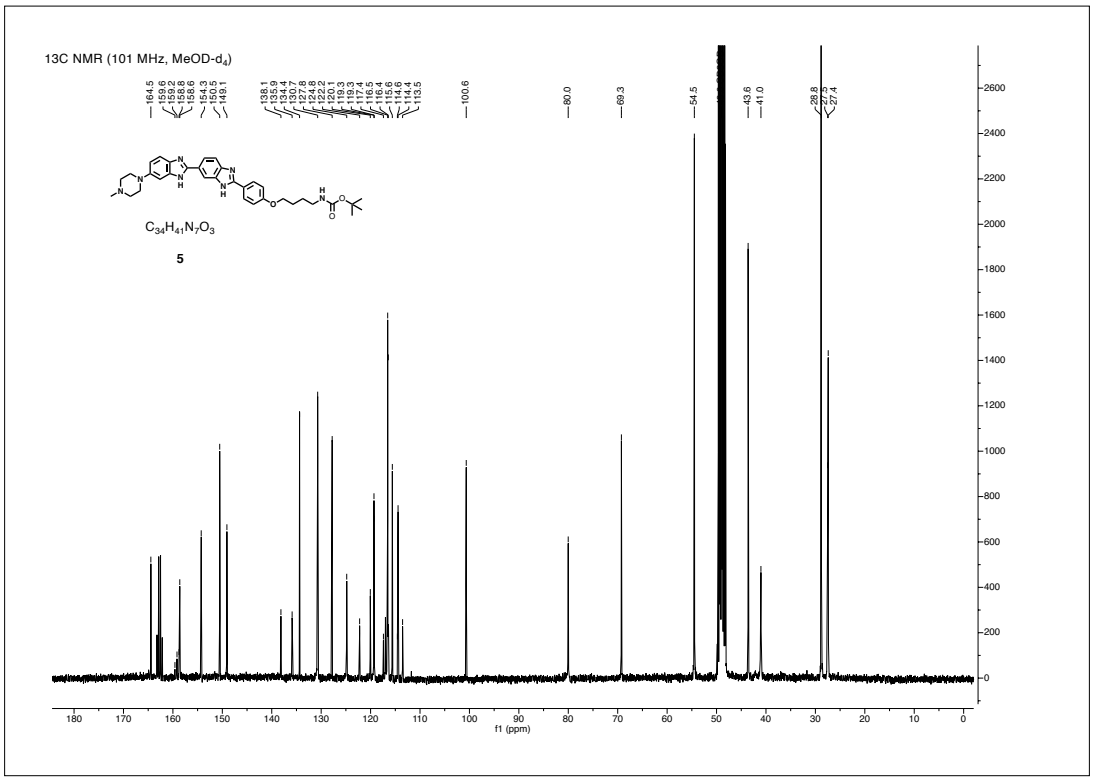
13C NMR (101 MHz, MeOD-d4)
C34H41N7O3
5
f1 (ppm)

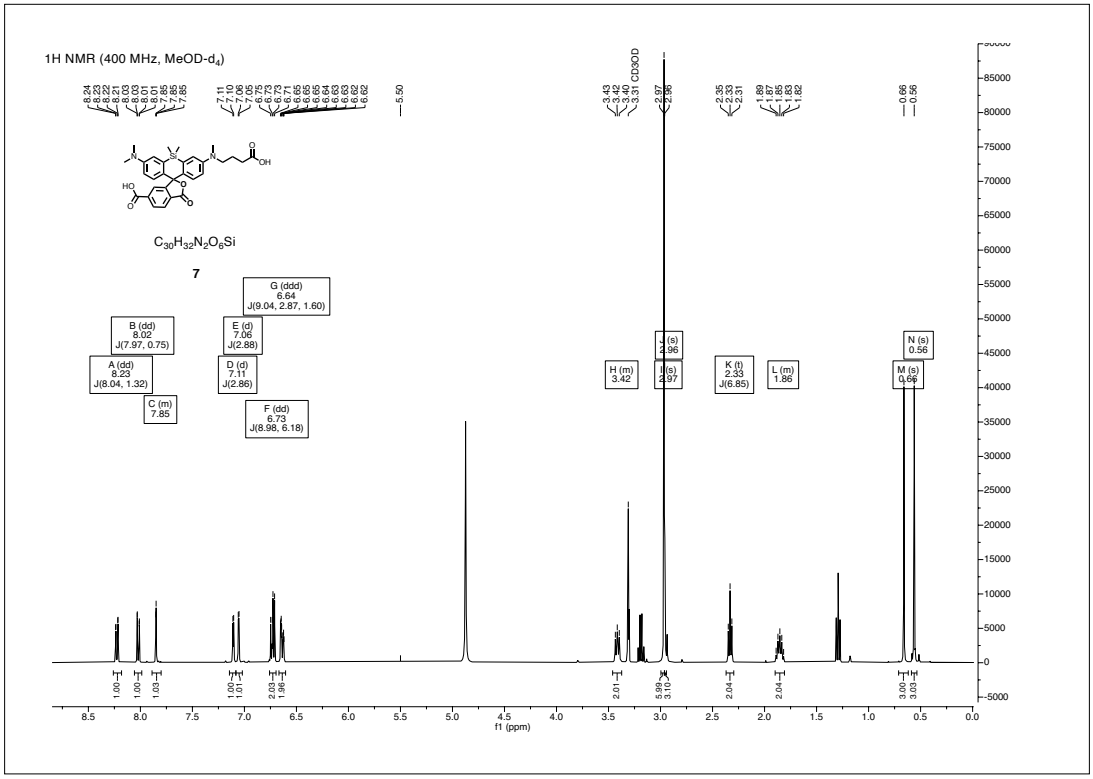
1H NMR (400 MHz, MeOD-d4)
C30H32N2O6Si
7
A (dd) 8.23 J(8.04, 1.32)
B (dd) 8.02 J(7.97, 0.75)
C (m) 7.85
D (d) 7.11 J(2.86)
E (d) 7.06 J(2.88)
F (dd) 6.73 J(8.98, 6.18)
G (ddd) 6.64 J(9.04, 2.87, 1.60)
H (m) 3.42
I (s) 2.97
J (s) 2.96
K (t) 2.33 J(6.85)
L (m) 1.86
M (s) 0.66
N (s) 0.56
f1 (ppm)

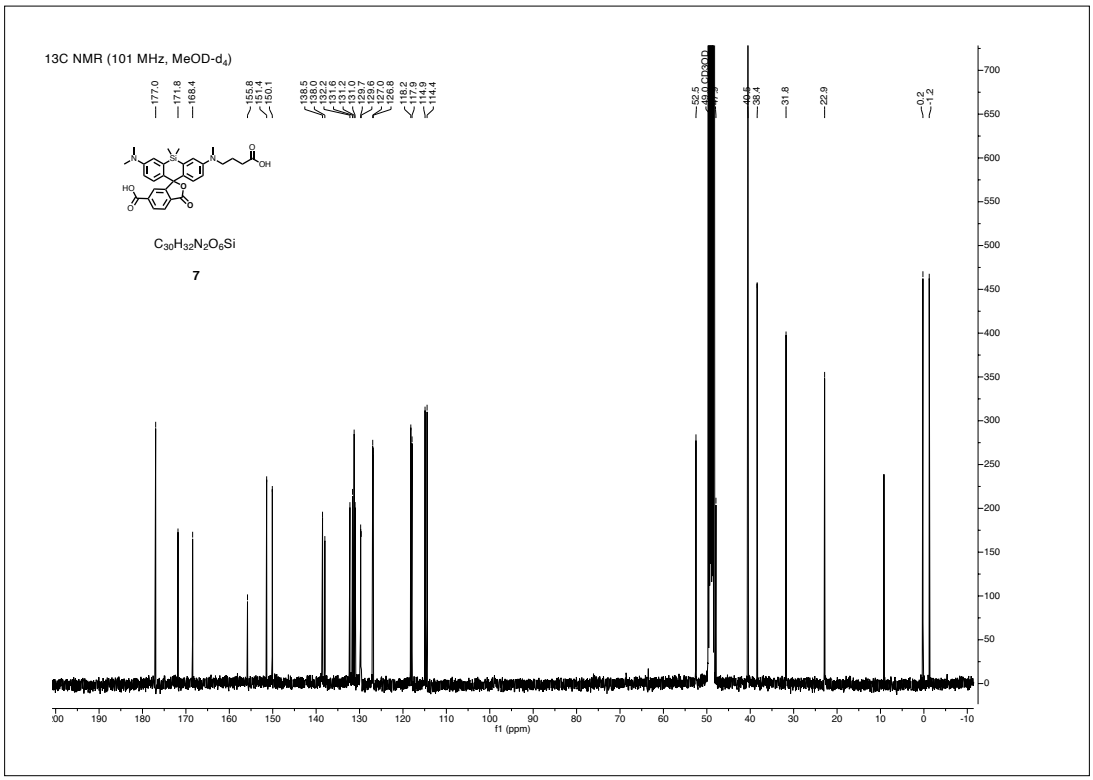
13C NMR (101 MHz, MeOD-d4)
C30H32N2O6Si
7
f1 (ppm)

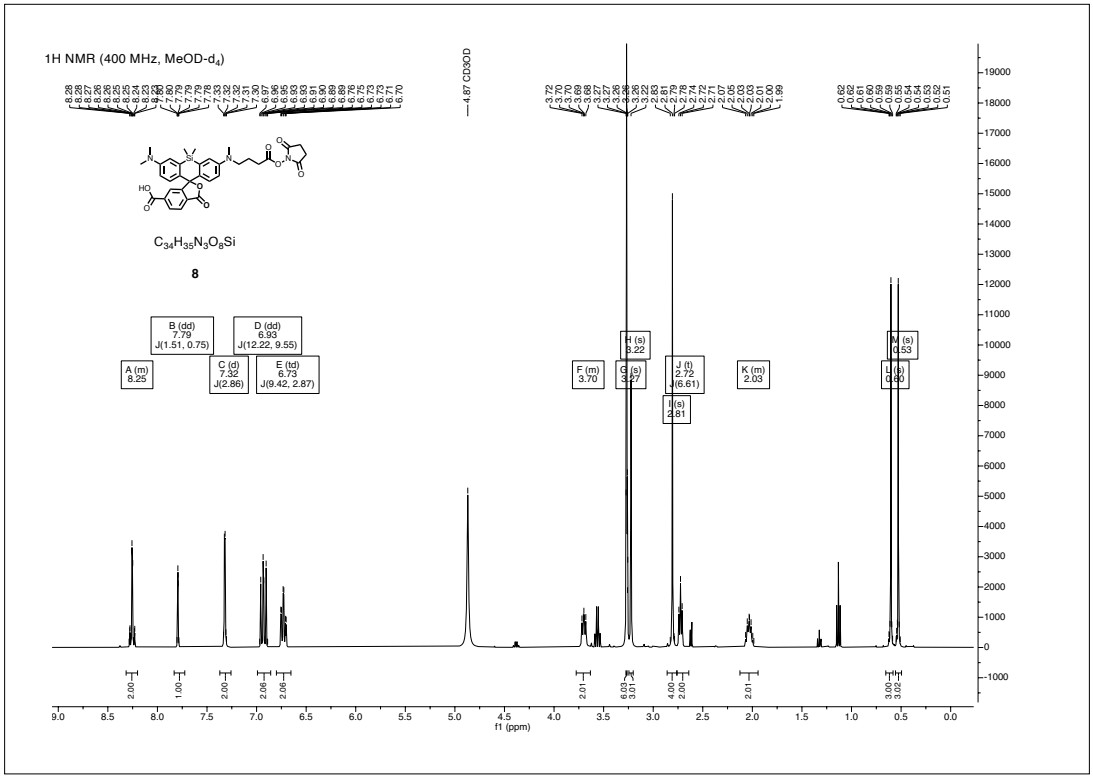
1H NMR (400 MHz, MeOD-d4)
4.87 CD3OD
C34H35N3O8Si
8
A (m) 8.25
B (dd) 7.79 J(1.51, 0.75)
C (d) 7.32 J(2.86)
D (dd) 6.93 J(12.22, 9.55)
E (td) 6.73 J(9.42, 2.87)
F (m) 3.70
G (s) 3.27
H (s) 3.22
I (s) 2.81
J (t) 2.72 J(6.61)
K (m) 2.03
L (s) 0.60
M (s) 0.53
f1 (ppm)

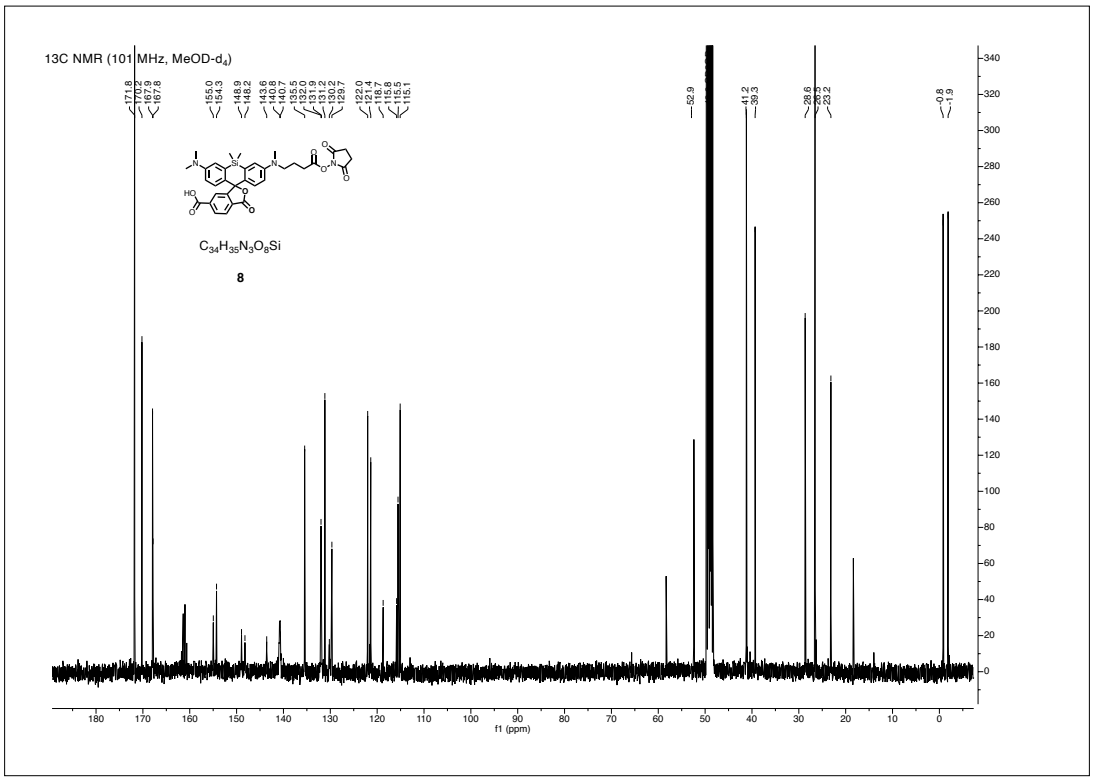
13C NMR (101 MHz, MeOD-d4)
C34H35N3O8Si
8
f1 (ppm)

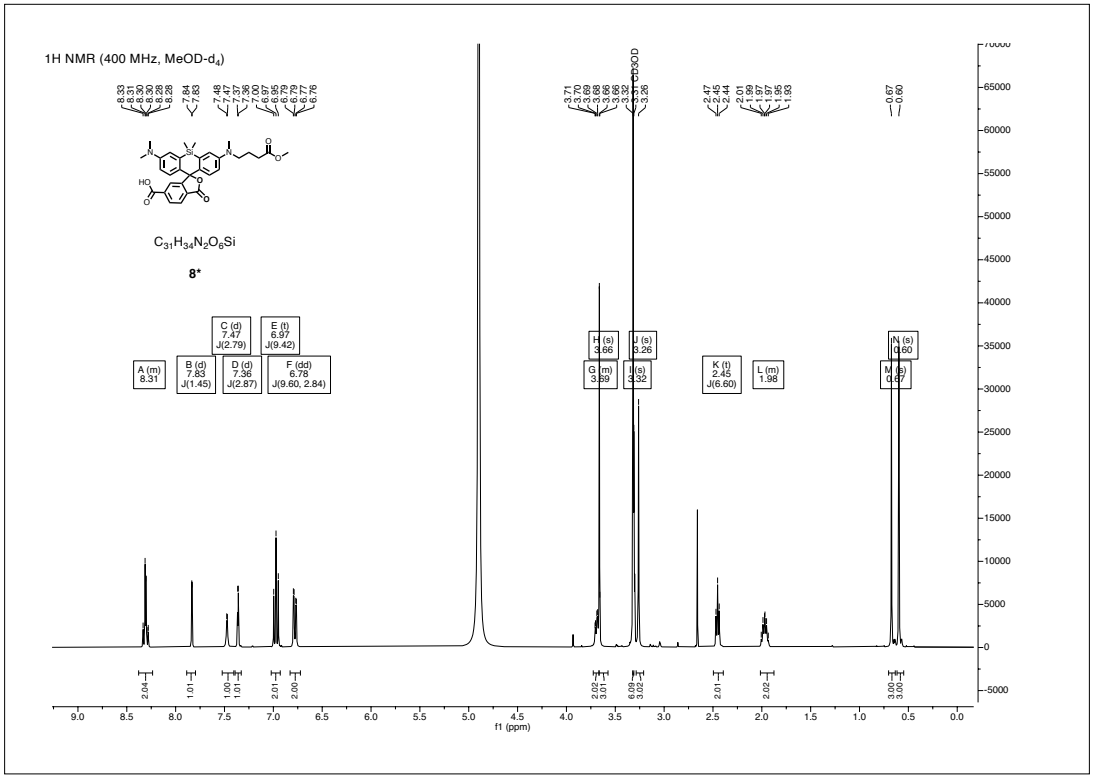
1H NMR (400 MHz, MeOD-d4)
C31H34N2O6Si
8*
A (m) 8.31
B (d) 7.83 J(1.45)
C (d) 7.47 J(2.79)
D (d) 7.36 J(2.87)
E (t) 6.97 J(9.42)
F (dd) 6.78 J(9.60, 2.84)
G (m) 3.99
H (s) 3.66
I (s) 3.32
J (s) 3.26
K (t) 2.45 J(6.60)
L (m) 1.98
M (s) 0.67
N (s) 0.60
f1 (ppm)

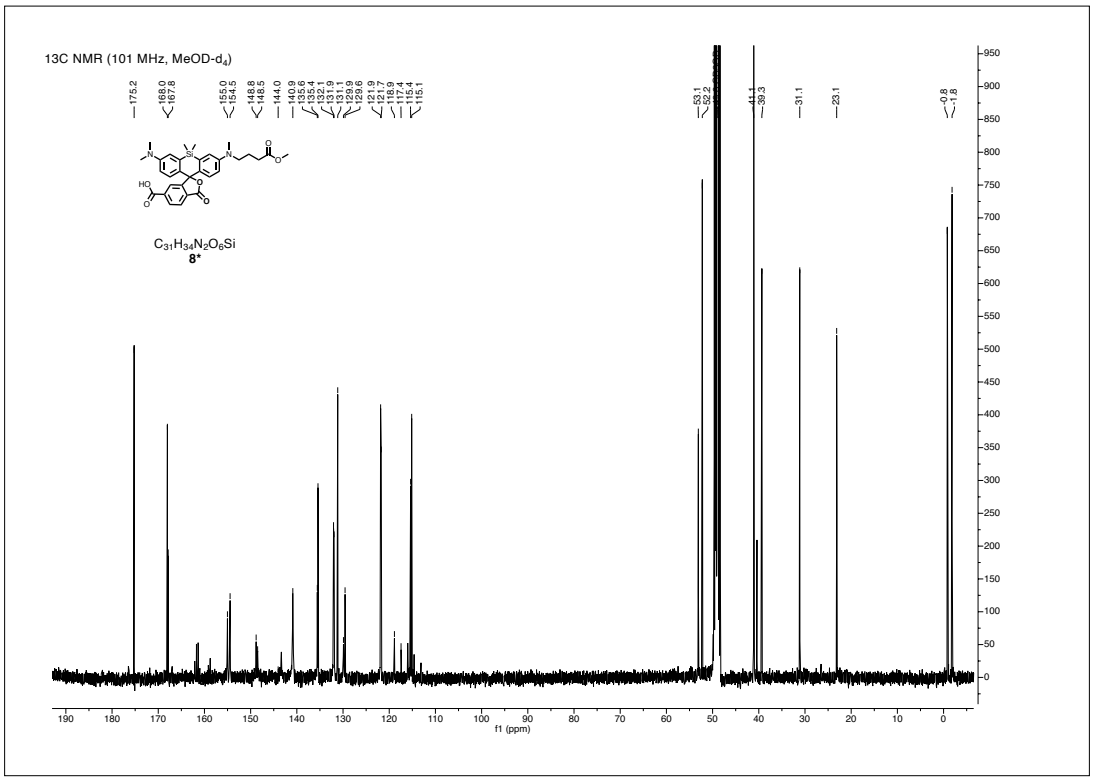
13C NMR (101 MHz, MeOD-d4)
C31H34N2O6Si
8*
f1 (ppm)

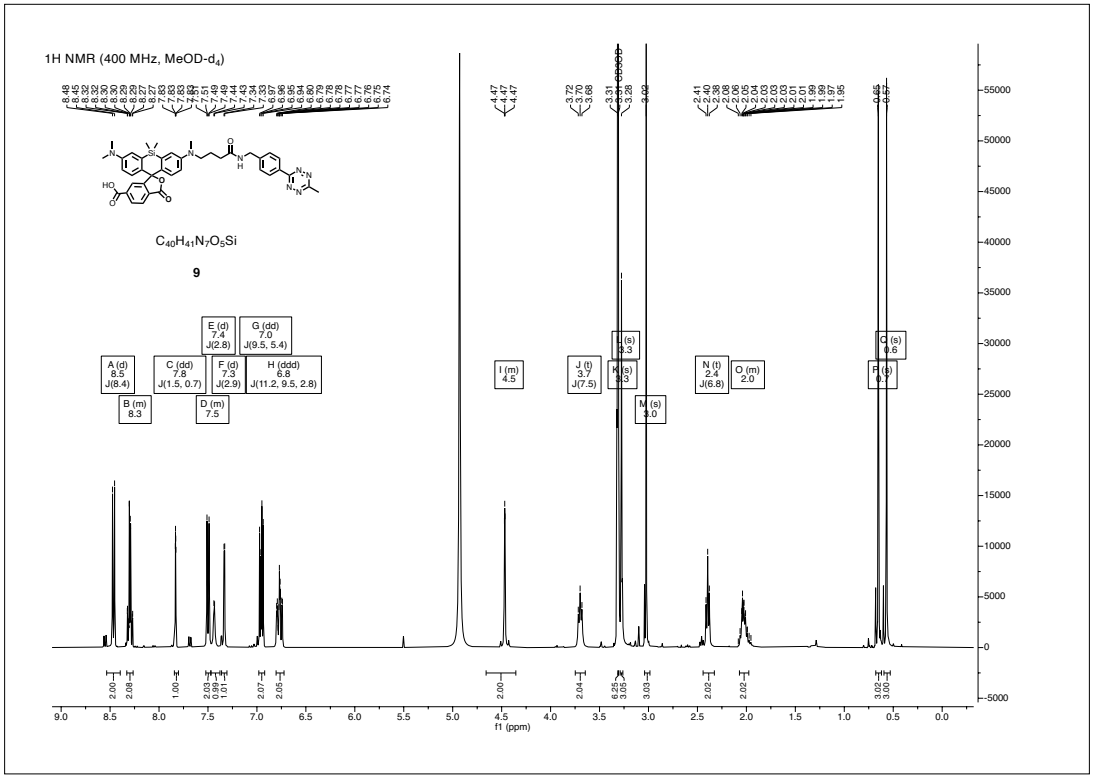
1H NMR (400 MHz, MeOD-d4)
C40H41N7O5Si
9
A (d) 8.5 J(8.4)
B (m) 8.3
C (dd) 7.8 J(1.5, 0.7)
D (m) 7.5
E (d) 7.4 J(2.8)
F (d) 7.3 J(2.9)
G (dd) 7.0 J(9.5, 5.4)
H (ddd) 6.8 J(11.2, 9.5, 2.8)
I (m) 4.5
J (t) 3.7 J(7.5)
K (s) 3.3
L (s) 3.3
M (s) 3.0
N (t) 2.4 J(6.8)
O (m) 2.0
P (s) 0.7
Q (s) 0.6
f1 (ppm)

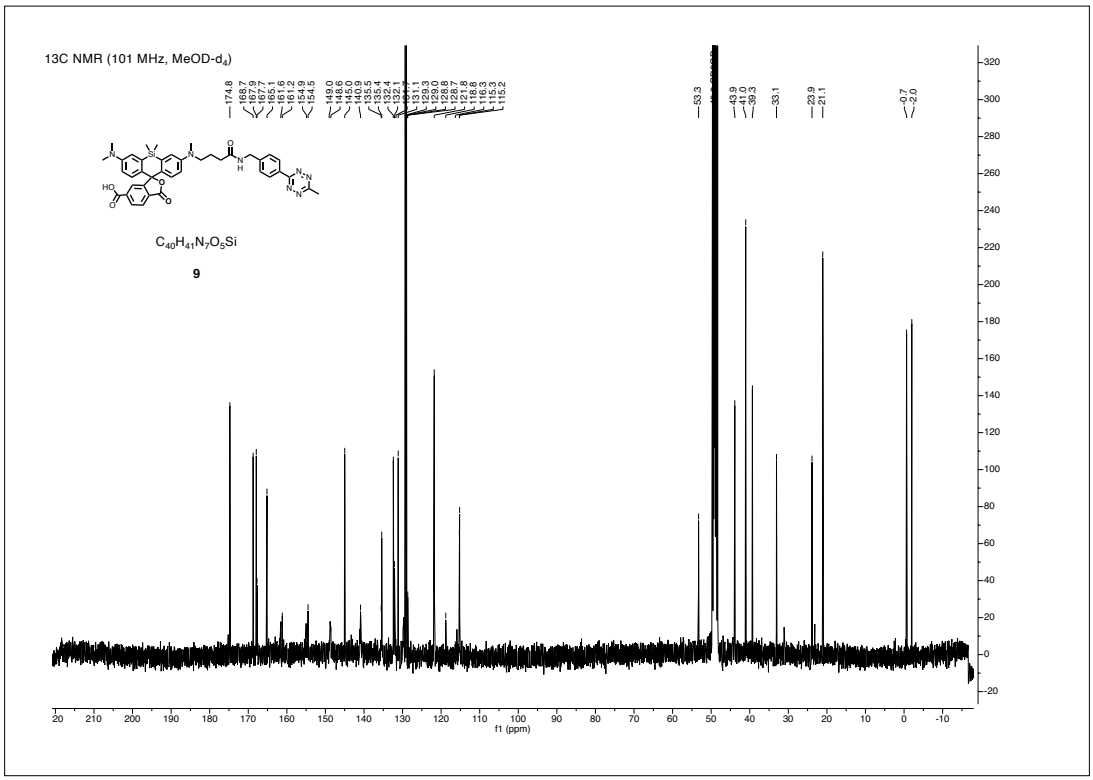
13C NMR (101 MHz, MeOD-d4)
C40H41N7O5Si
9
f1 (ppm)

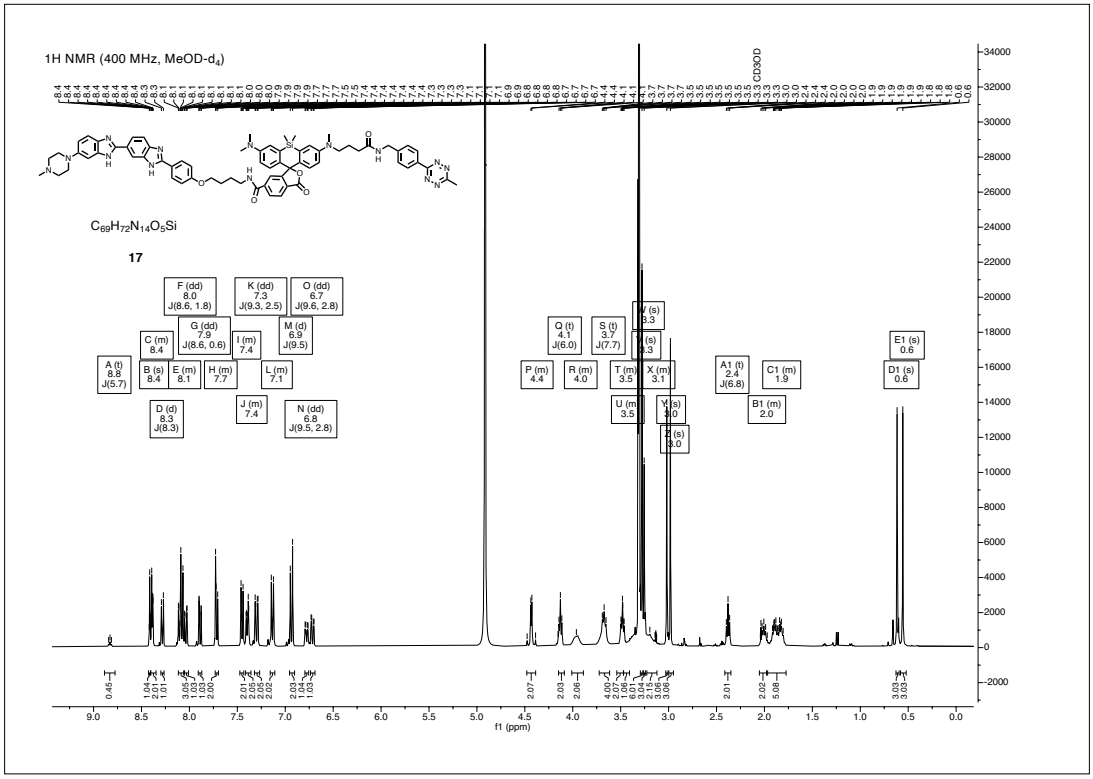
1H NMR (400 MHz, MeOD-d4)
C69H72N14O5Si
17
f1 (ppm)

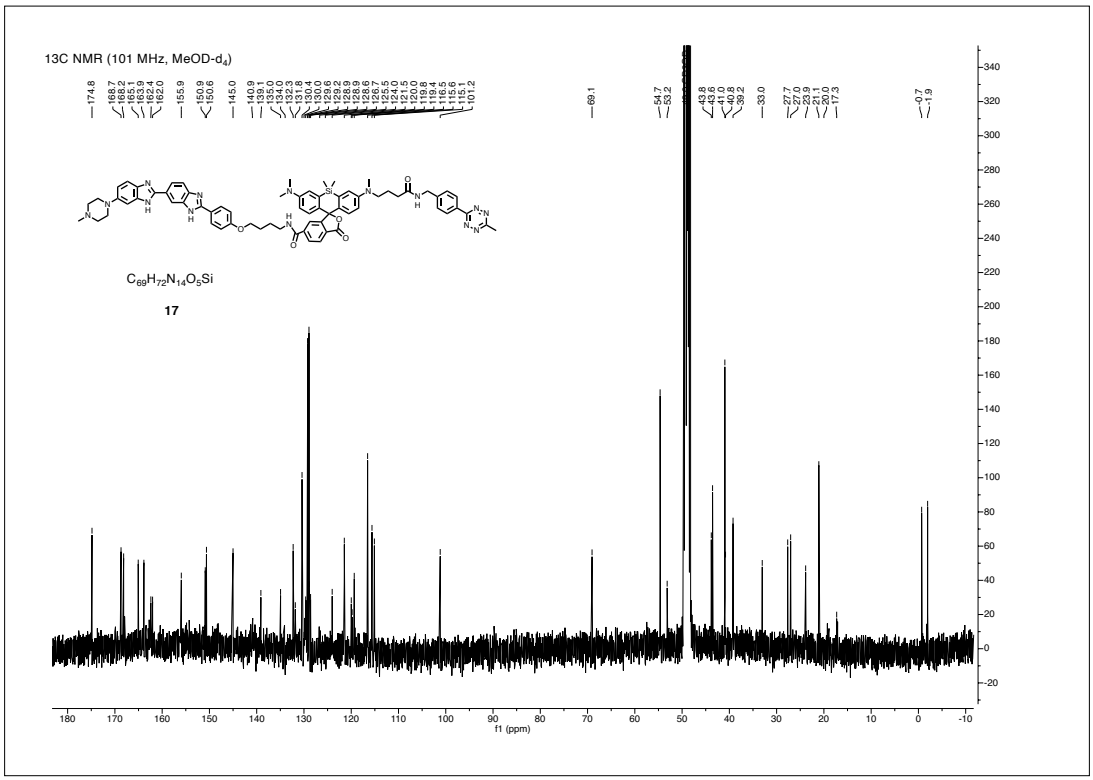
13C NMR (101 MHz, MeOD-d4)
C69H72N14O5Si
17
f1 (ppm)

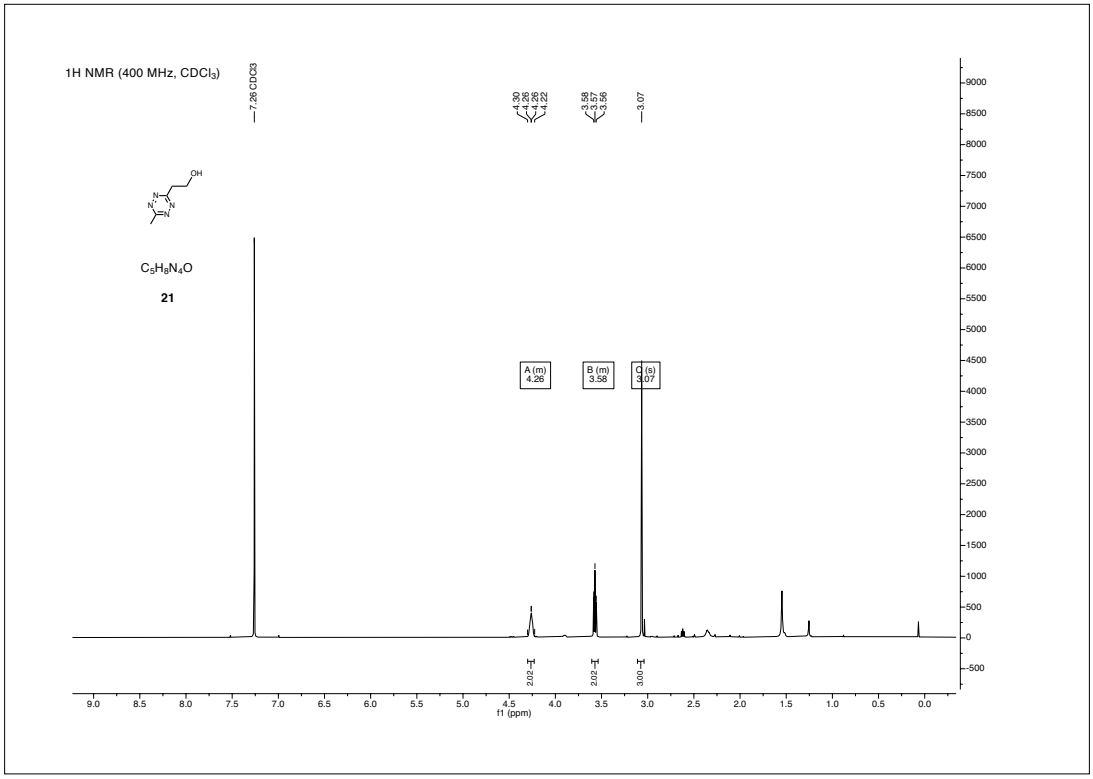
1H NMR (400 MHz, CDCl3)
7.26 CDCl3
4.30
4.26
4.26
4.22
3.58
3.57
3.56
3.07
OH
C5H8N4O
21
A (m)
4.26
B (m)
3.58
C (s)
3.07
2.02
2.02
3.00
f1 (ppm)

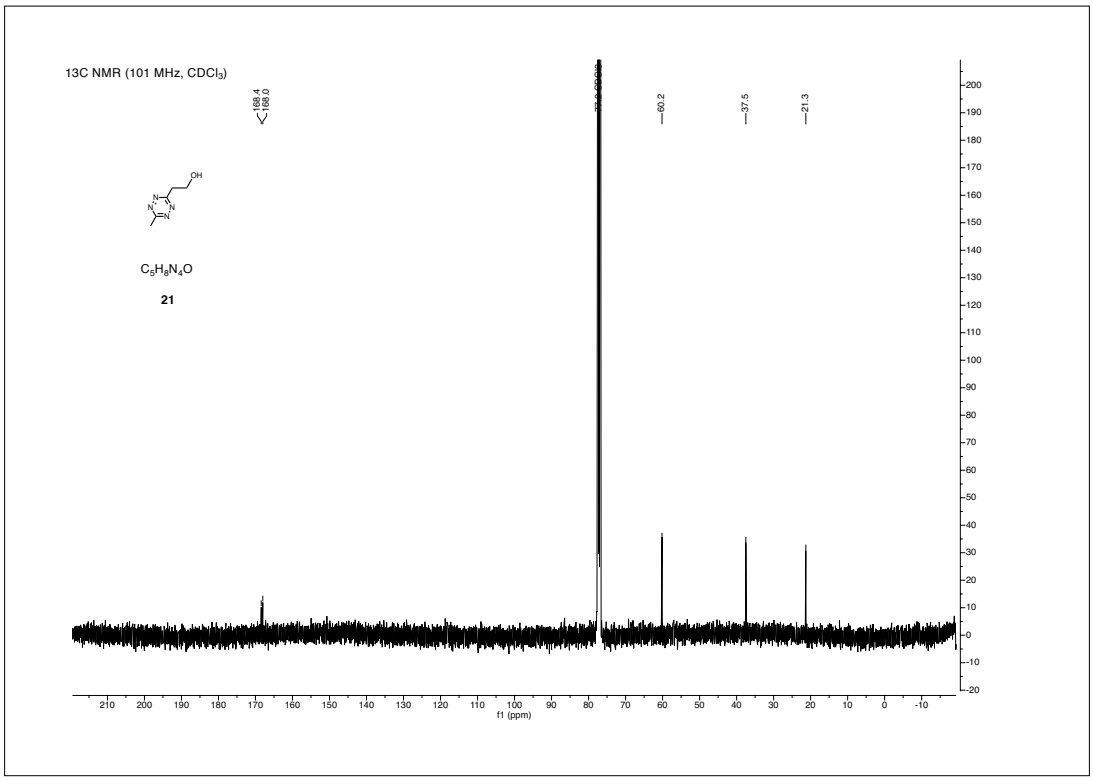
13C NMR (101 MHz, CDCl3)
169.4
168.0
77.3 CDCl3
60.2
37.5
21.3
OH
C5H8N4O
21
f1 (ppm)

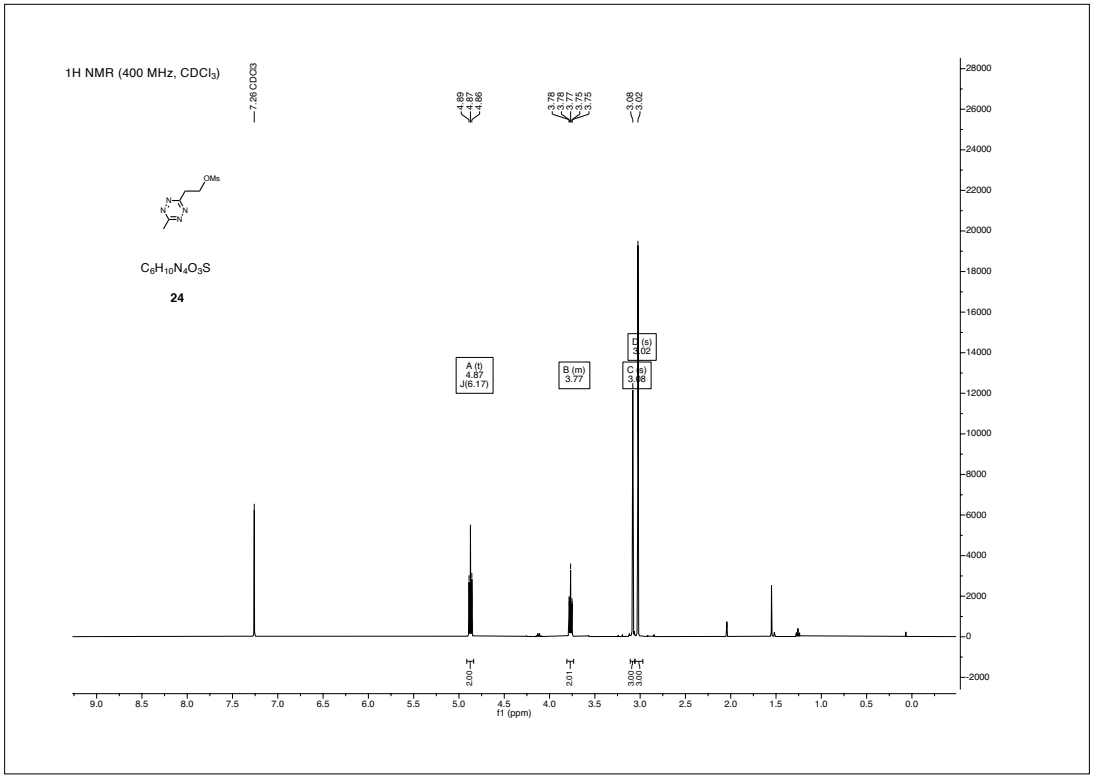
1H NMR (400 MHz, $CDCl_3$)
7.26 CDCl3
4.89
4.87
4.86
3.78
3.78
3.77
3.75
3.75
3.08
3.02
OMs
$C_6H_{10}N_4O_3S$
24
A (t)
4.87
J(6.17)
B (m)
3.77
D (s)
3.02
C (s)
3.08
2.00
2.01
3.00
3.00
f1 (ppm)

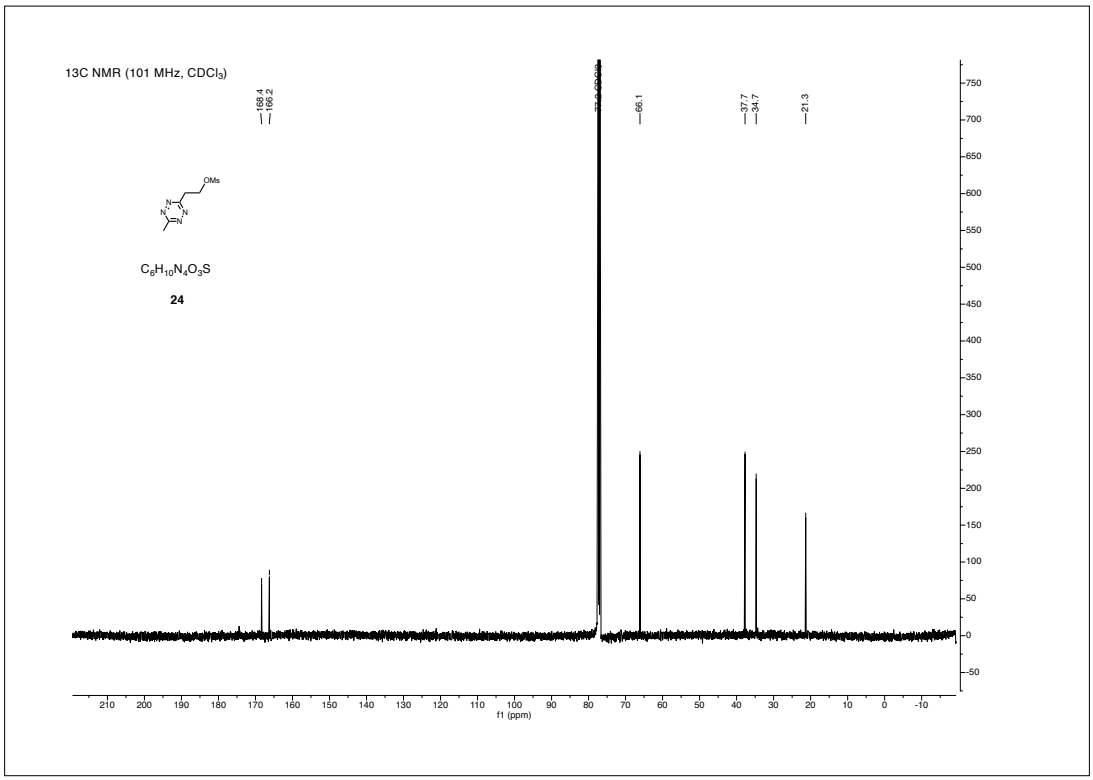
13C NMR (101 MHz, $CDCl_3$)
168.4
166.2
77.2 CDCl3
66.1
37.7
34.7
21.3
OMs
$C_6H_{10}N_4O_3S$
24
f1 (ppm)

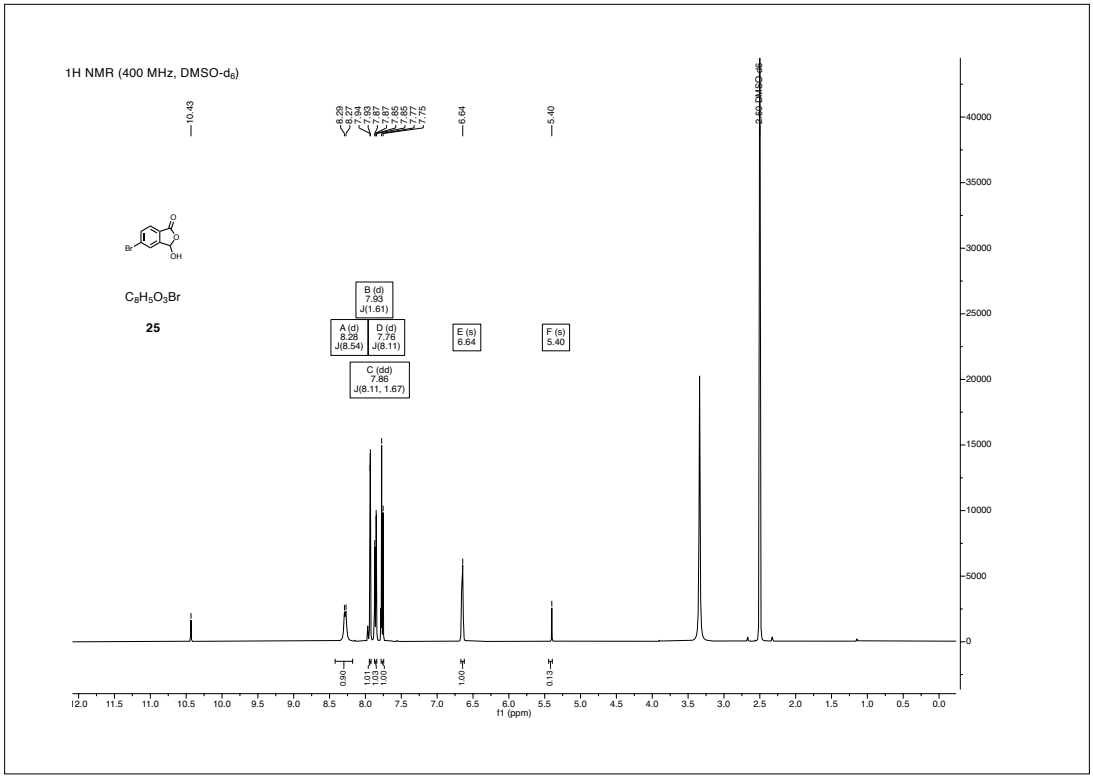
1H NMR (400 MHz, DMSO-d6)
10.43
8.29
8.27
7.94
7.93
7.87
7.86
7.85
7.77
7.75
6.64
5.40
2.50 DMSO-d6
Br
O
O
OH
C8H5O3Br
25
B (d)
7.93
J(1.61)
A (d)
8.28
J(8.54)
D (d)
7.76
J(8.11)
C (dd)
7.86
J(8.11, 1.67)
E (s)
6.64
F (s)
5.40
0.90
1.01
1.03
1.00
1.00
0.13
f1 (ppm)

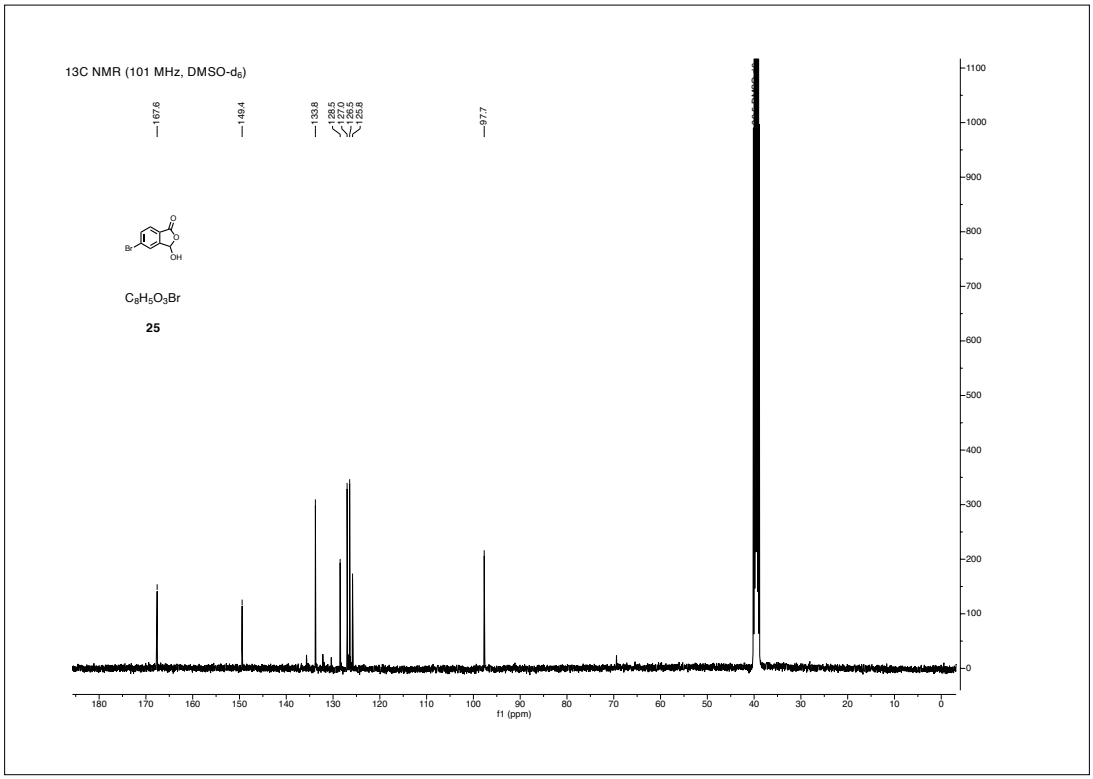
13C NMR (101 MHz, DMSO-d6)
167.6
149.4
133.8
128.5
127.0
126.5
125.8
97.7
39.5 DMSO-d6
Br
O
O
OH
C8H5O3Br
25
f1 (ppm)

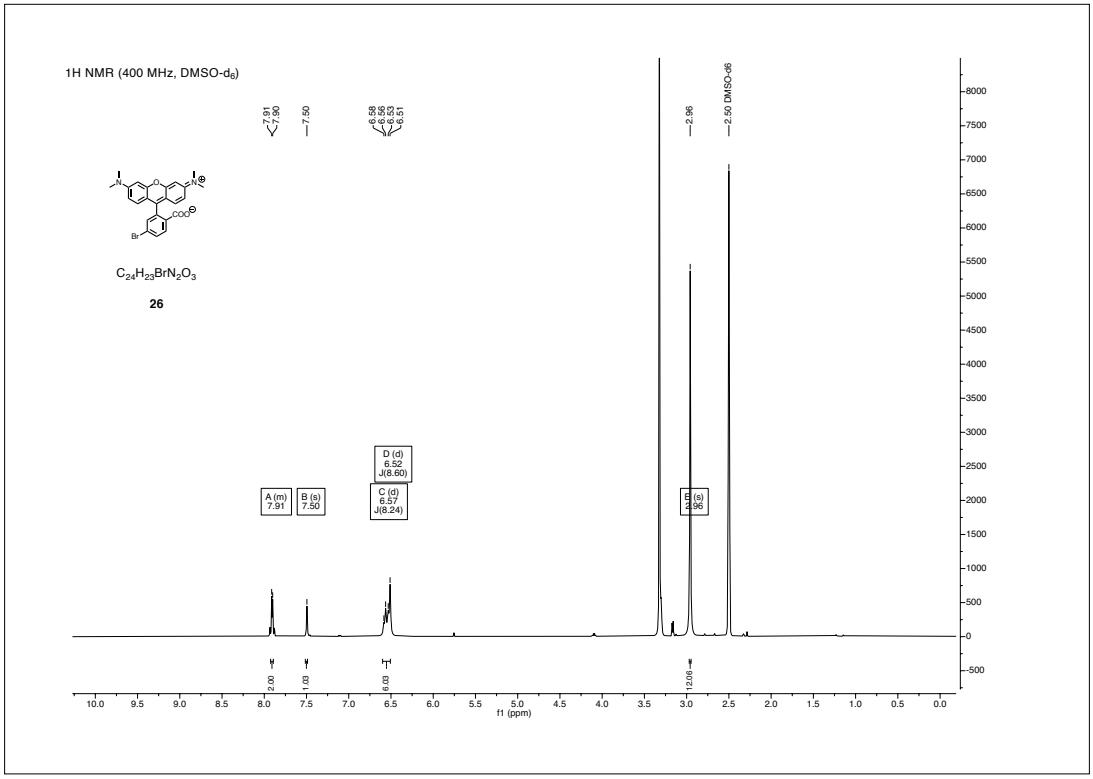

$C_{24}H_{23}BrN_2O_3$

26

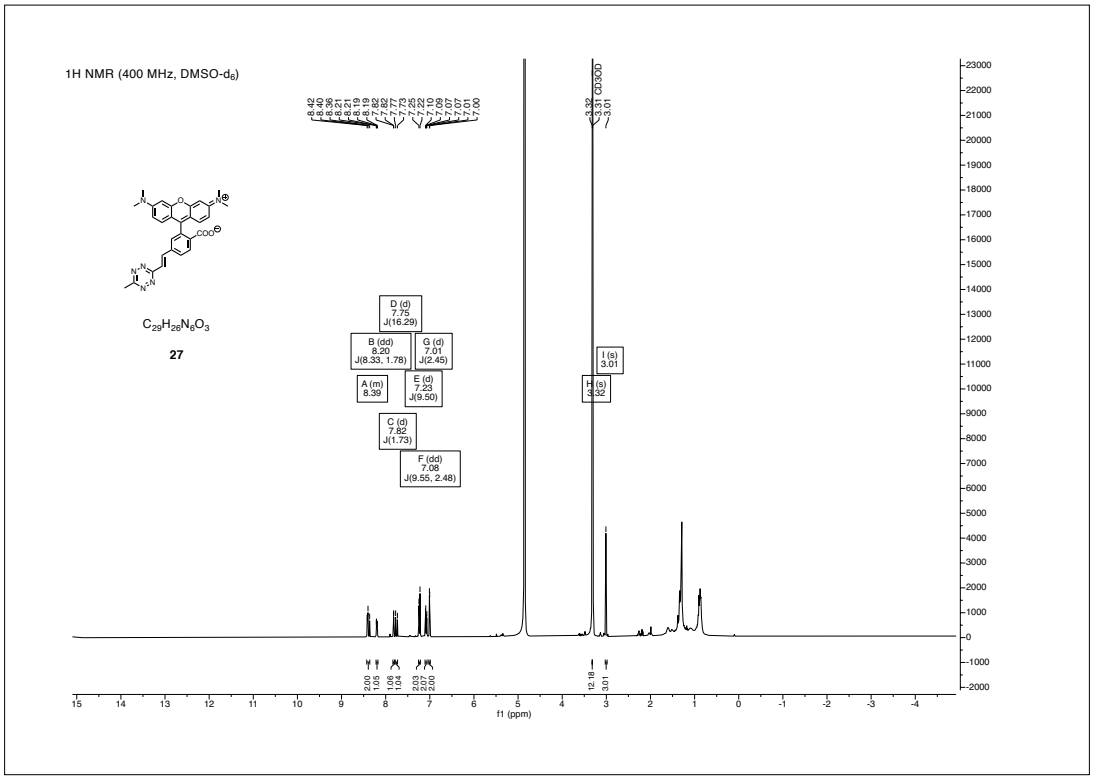

$C_{29}H_{26}N_6O_3$

27

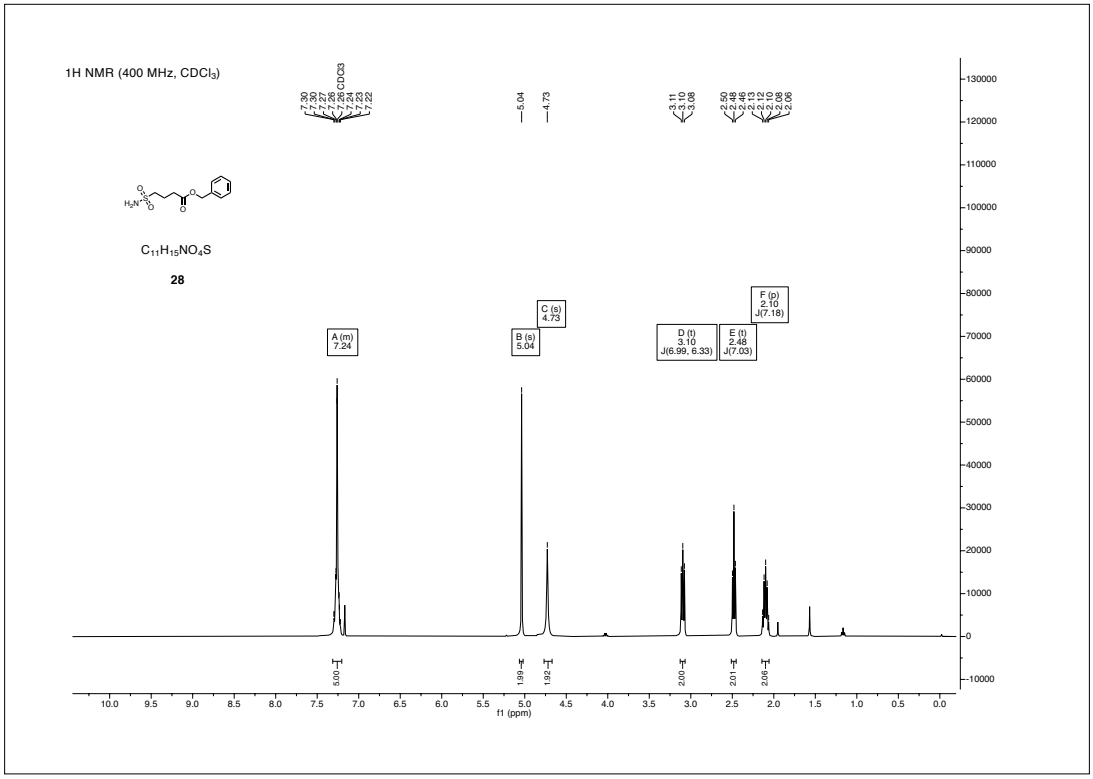
1H NMR (400 MHz, CDCl3)
7.30
7.29
7.27
7.26 CDCl3
7.24
7.23
7.22
5.04
4.73
3.11
3.10
3.08
2.50
2.48
2.13
2.12
2.10
2.08
2.06
C11H15NO4S
28
A (m)
7.24
B (s)
5.04
C (s)
4.73
D (t)
3.10
J(6.99, 6.33)
E (t)
2.48
J(7.03)
F (p)
2.10
J(7.18)
5.00
1.99
1.92
2.00
2.01
2.08
f1 (ppm)

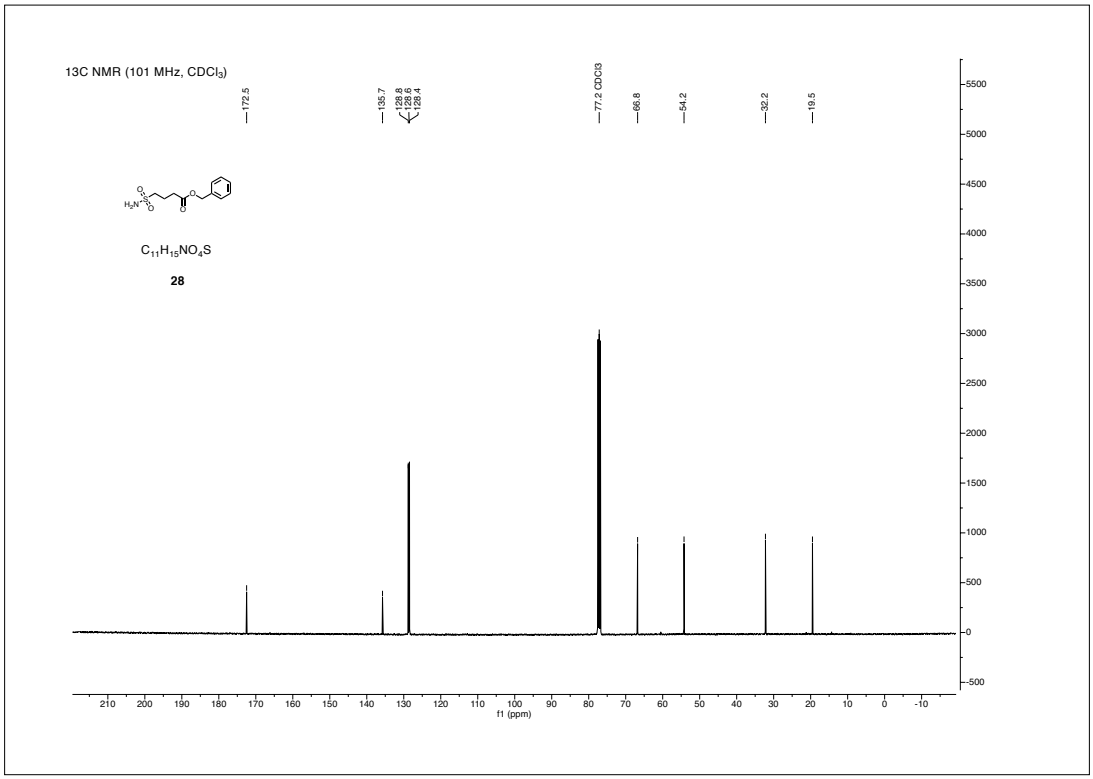
13C NMR (101 MHz, CDCl3)
172.5
135.7
128.8
128.6
128.4
77.2 CDCl3
66.8
54.2
32.2
19.5
C11H15NO4S
28
f1 (ppm)

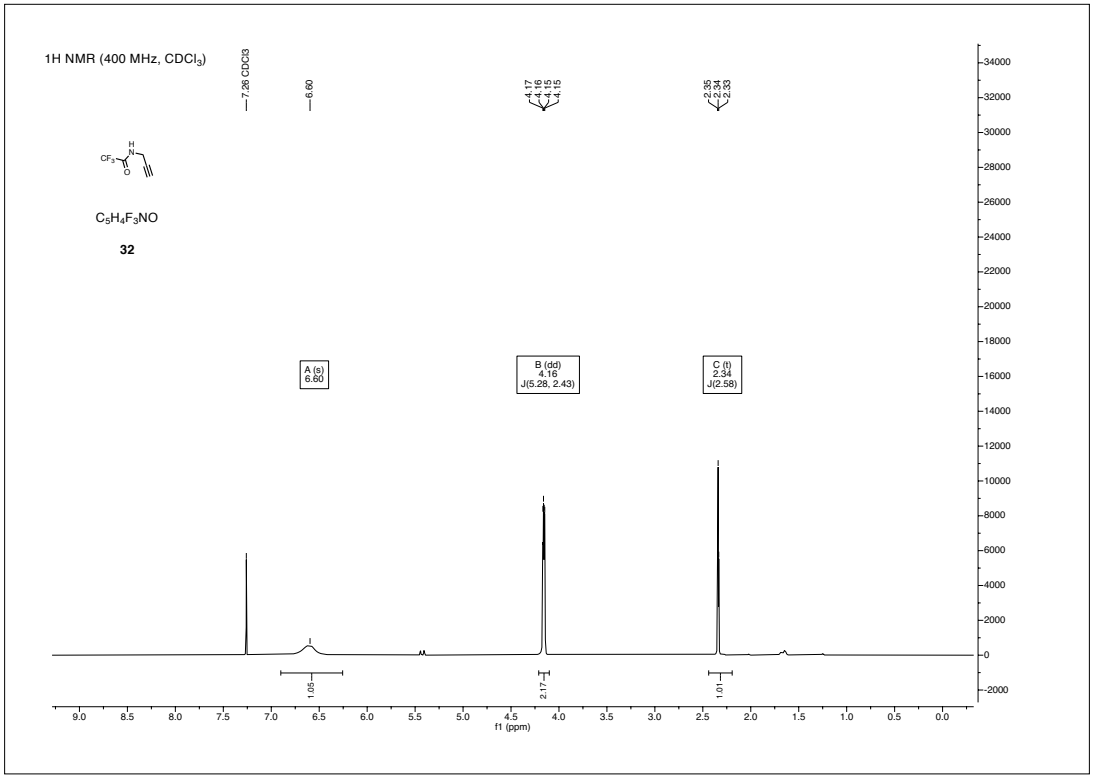
1H NMR (400 MHz, CDCl3)
7.26 CDCl3
6.60
4.17
4.16
4.15
4.15
2.35
2.34
2.33
C5H4F3NO
32
A (s)
6.60
B (dd)
4.16
J(5.28, 2.43)
C (t)
2.34
J(2.58)
1.05
2.17
1.01
f1 (ppm)

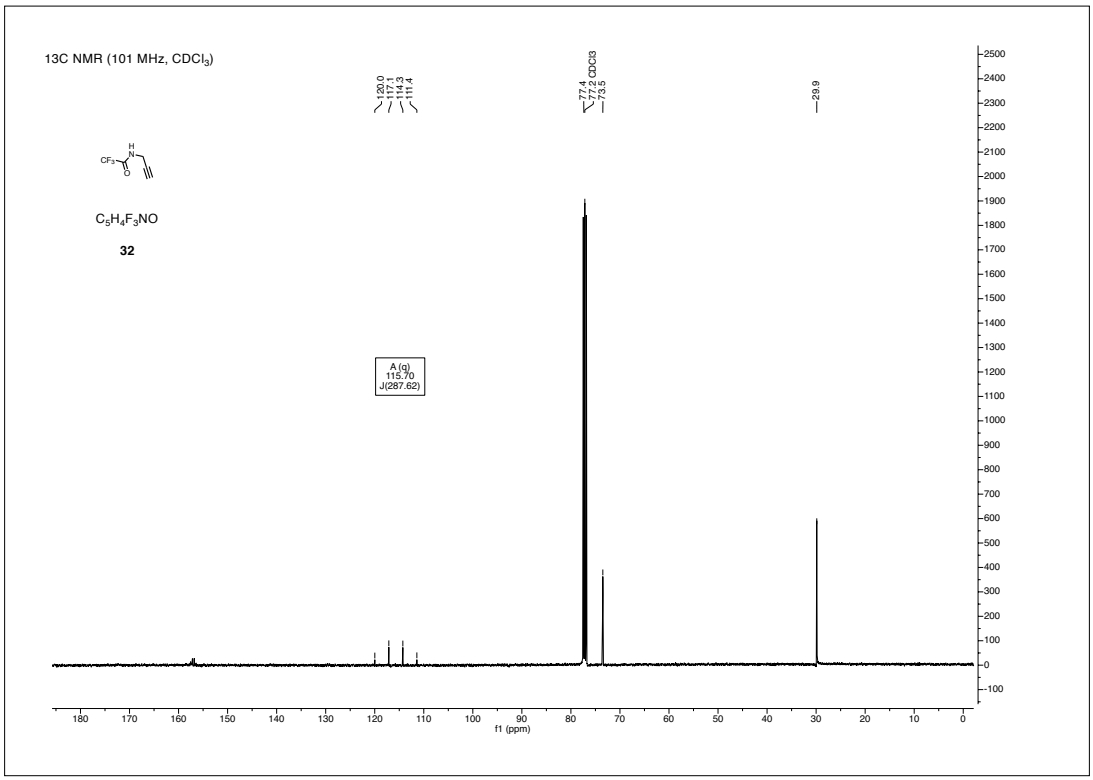
13C NMR (101 MHz, CDCl3)
120.0
117.1
114.3
111.4
77.4
77.2
CDCl3
73.5
29.9
C5H4F3NO
32
A (q)
115.70
J(287.62)
f1 (ppm)

19F NMR (376 MHz, $CDCl_3$)

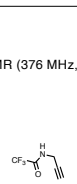

$C_5H_4F_3NO$

32

1H NMR (400 MHz, MeOD-d_4)

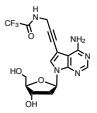

$C_{16}H_{16}F_3N_5O_4$

34

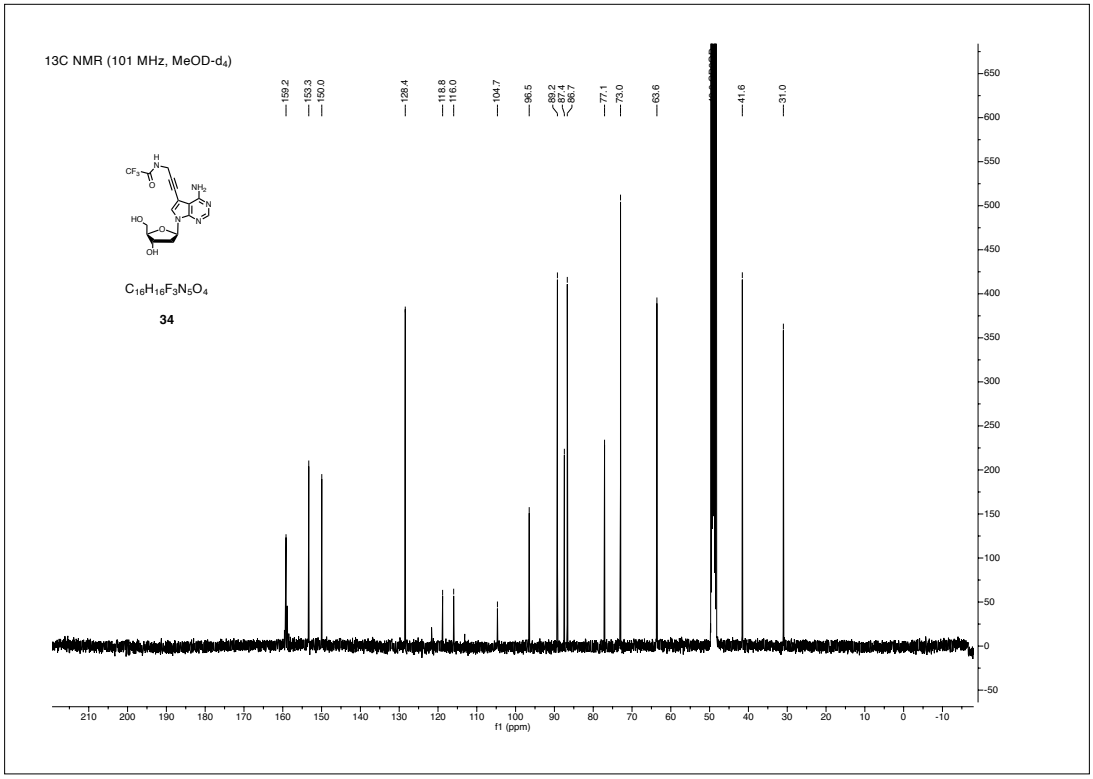
13C NMR (101 MHz, MeOD-d4)
159.2
153.3
150.0
128.4
118.8
116.0
104.7
96.5
89.2
87.4
86.7
77.1
73.0
63.6
41.6
31.0
C16H16F3N5O4
34
f1 (ppm)

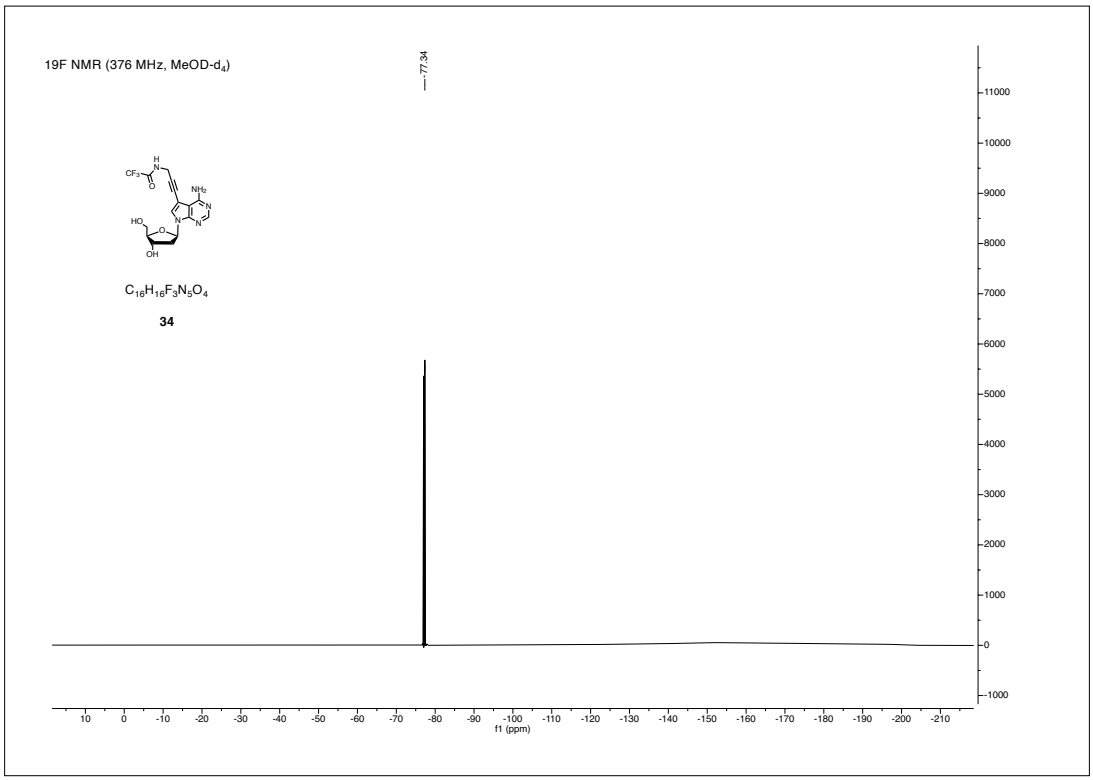
19F NMR (376 MHz, MeOD-d4)
-77.34
C16H16F3N5O4
34
f1 (ppm)

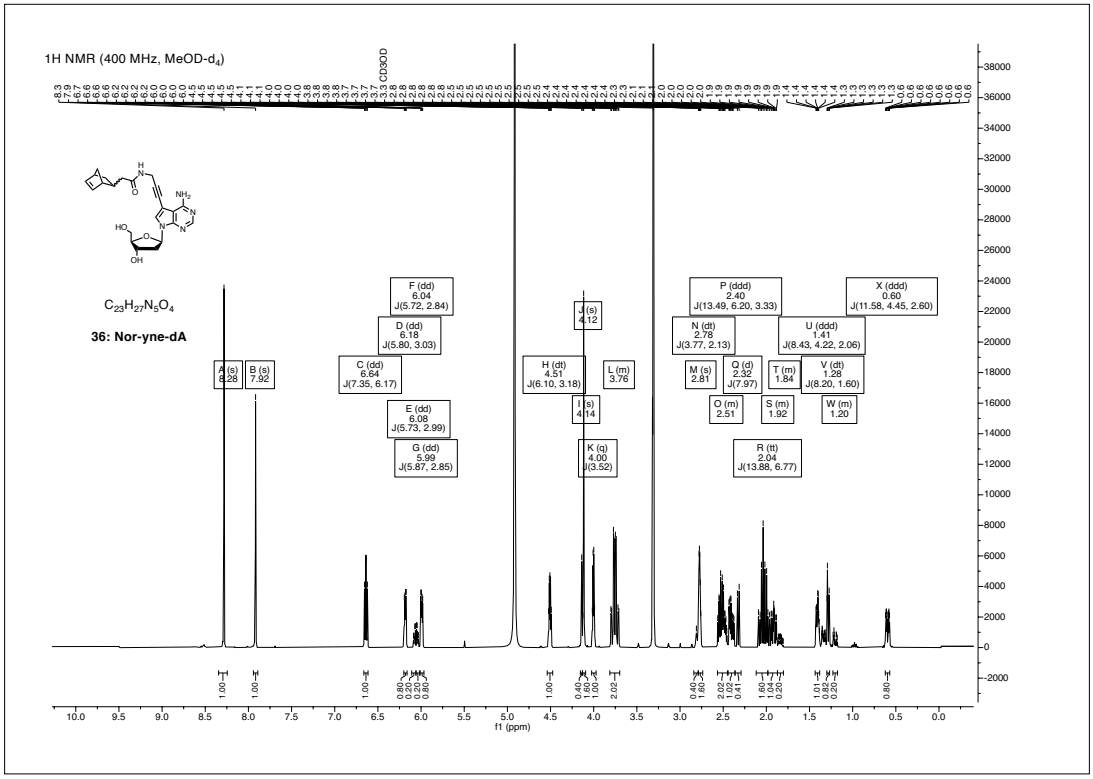
1H NMR (400 MHz, MeOD-d4)
CD3OD
A (s) 8.28
B (s) 7.92
C (dd) 6.64 J(7.35, 6.17)
D (dd) 6.18 J(5.80, 3.03)
E (dd) 6.08 J(5.73, 2.99)
F (dd) 6.04 J(5.72, 2.84)
G (dd) 5.99 J(5.87, 2.85)
H (dt) 4.51 J(6.10, 3.18)
I (s) 4.14
J (s) 4.12
K (q) 4.00 J(3.52)
L (m) 3.76
M (s) 2.81
N (dt) 2.78 J(3.77, 2.13)
O (m) 2.51
P (ddd) 2.40 J(13.49, 6.20, 3.33)
Q (d) 2.32 J(7.97)
R (tt) 2.04 J(13.88, 6.77)
S (m) 1.92
T (m) 1.84
U (ddd) 1.41 J(8.43, 4.22, 2.06)
V (dt) 1.28 J(8.20, 1.60)
W (m) 1.20
X (ddd) 0.60 J(11.58, 4.45, 2.60)
f1 (ppm)
C23H27N5O4
36: Nor-yne-dA

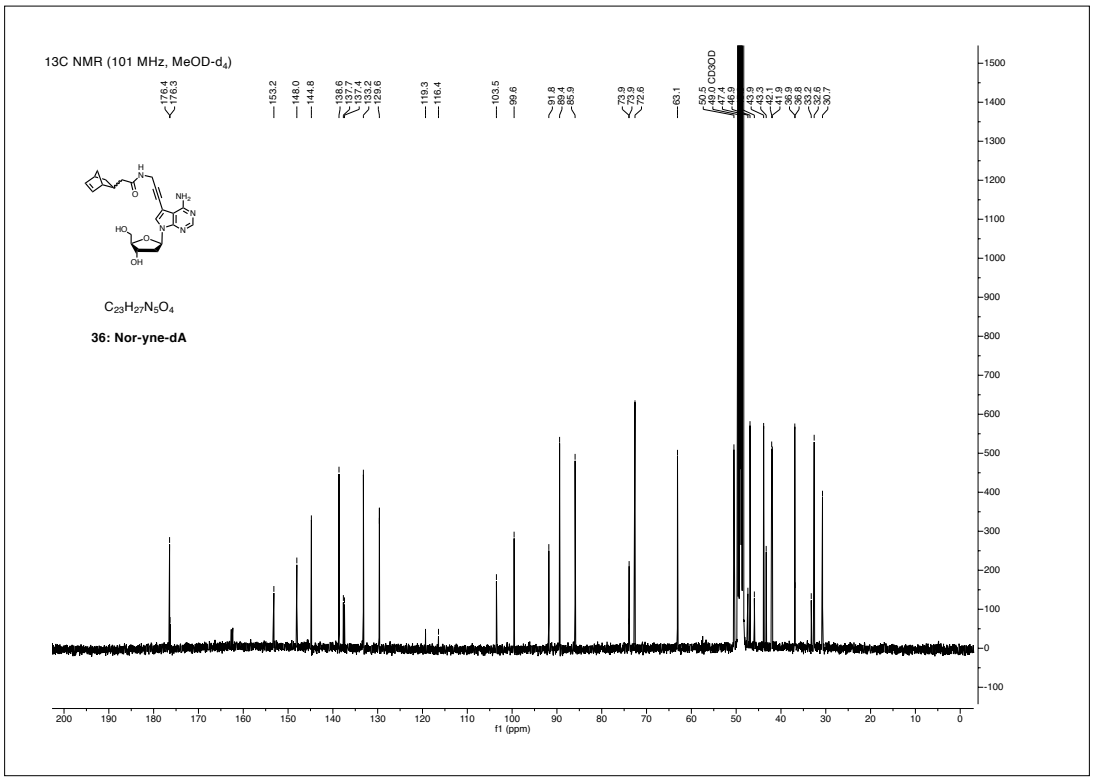
13C NMR (101 MHz, MeOD-d4)
CD3OD
f1 (ppm)
C23H27N5O4
36: Nor-yne-dA

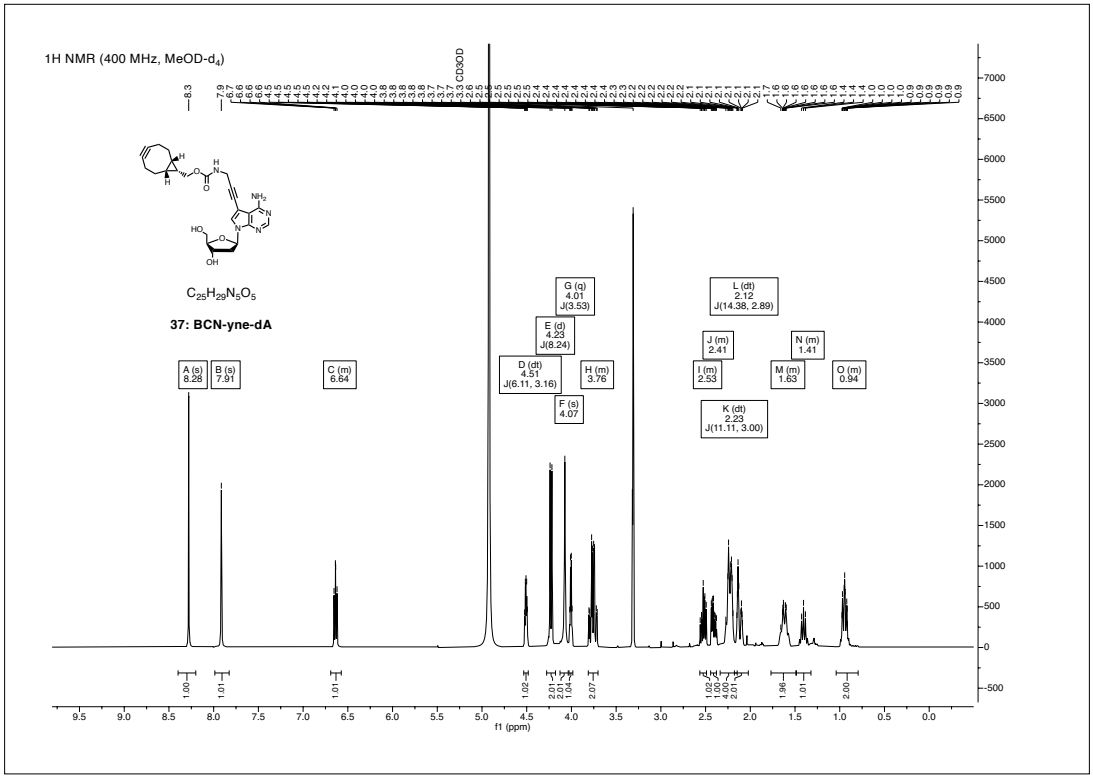
1H NMR (400 MHz, MeOD-d4)
C25H29N5O5
37: BCN-yne-dA
A (s) 8.28
B (s) 7.91
C (m) 6.64
D (dt) 4.51 J(6.11, 3.16)
E (d) 4.23 J(8.24)
F (s) 4.07
G (q) 4.01 J(3.53)
H (m) 3.76
I (m) 2.53
J (m) 2.41
K (dt) 2.23 J(11.11, 3.00)
L (dt) 2.12 J(14.38, 2.89)
M (m) 1.63
N (m) 1.41
O (m) 0.94
f1 (ppm)

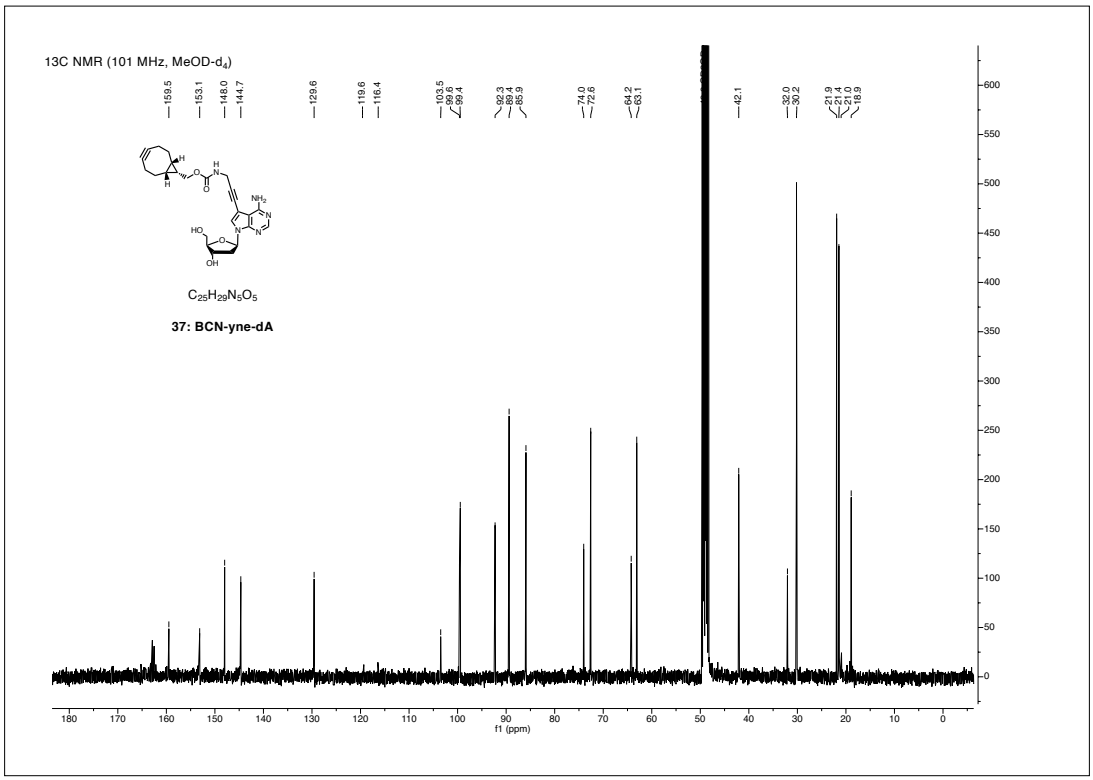
13C NMR (101 MHz, MeOD-d4)
C25H29N5O5
37: BCN-yne-dA
f1 (ppm)

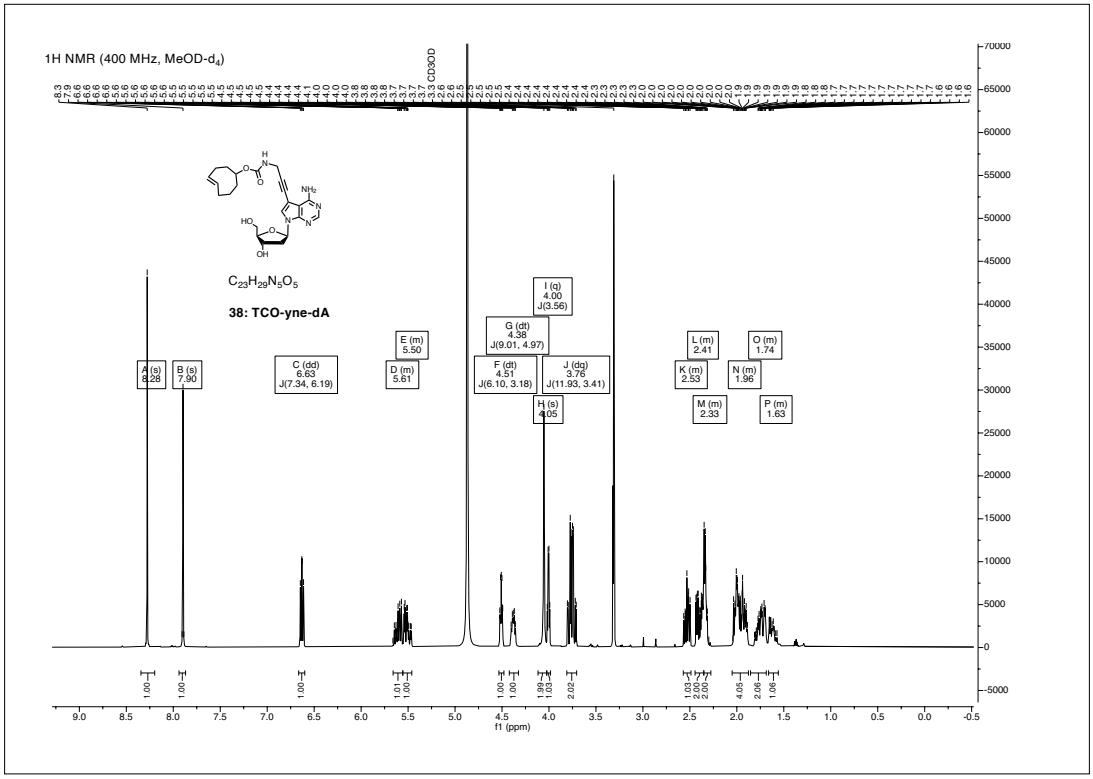

$C_{23}H_{29}N_5O_5$

38: TCO-yne-dA

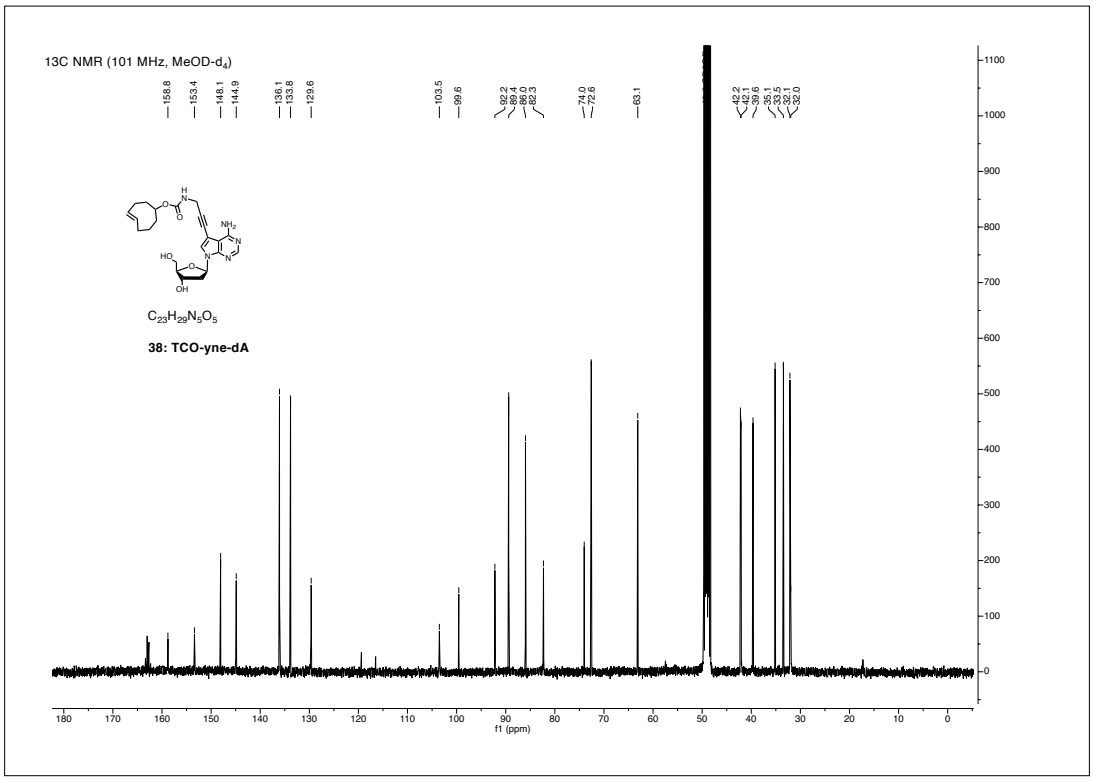

$C_{23}H_{29}N_5O_5$

38: TCO-yne-dA

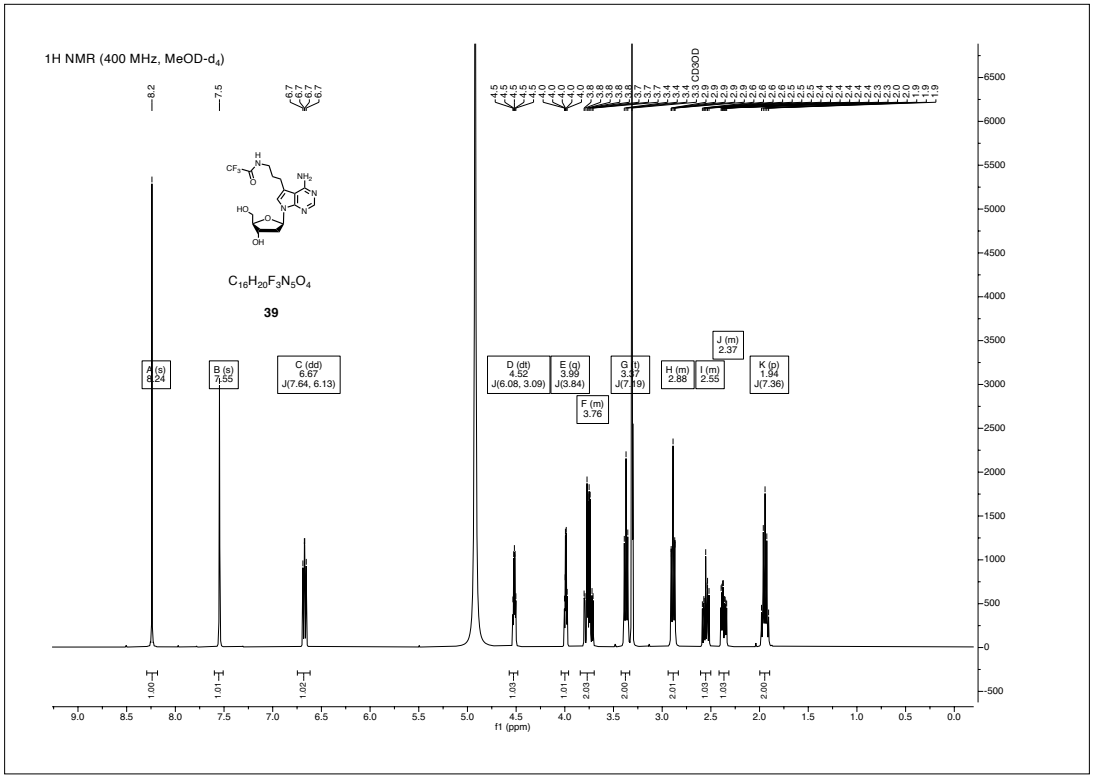
1H NMR (400 MHz, MeOD-d4)
C16H20F3N5O4
39
A (s) 8.24
B (s) 7.55
C (dd) 6.67 J(7.64, 6.13)
D (dt) 4.52 J(6.08, 3.09)
E (q) 3.99 J(3.84)
F (m) 3.76
G (t) 3.37 J(7.19)
H (m) 2.88
I (m) 2.55
J (m) 2.37
K (p) 1.94 J(7.36)
f1 (ppm)

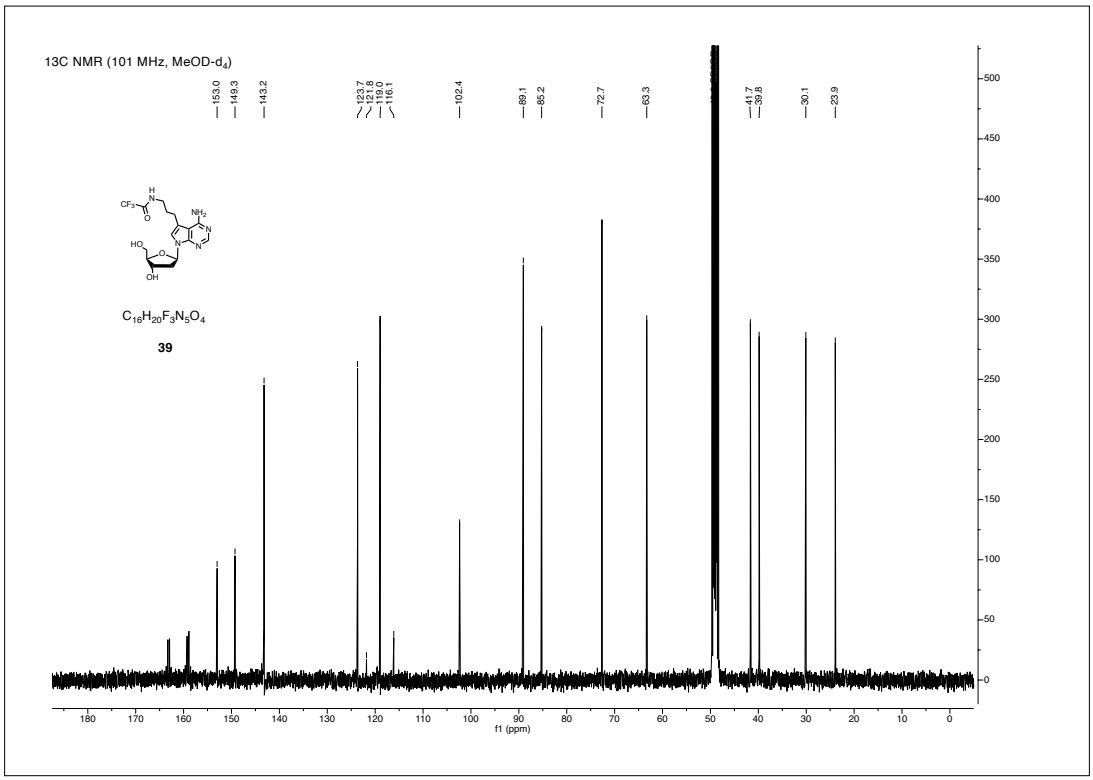
13C NMR (101 MHz, MeOD-d4)
C16H20F3N5O4
39
f1 (ppm)

19F NMR (376 MHz, MeOD-d_4)

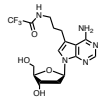

$C_{16}H_{20}F_3N_5O_4$

39

1H NMR (400 MHz, MeOD-d_4)

$C_{25}H_{33}N_5O_5$

41: BCN-ane-dA

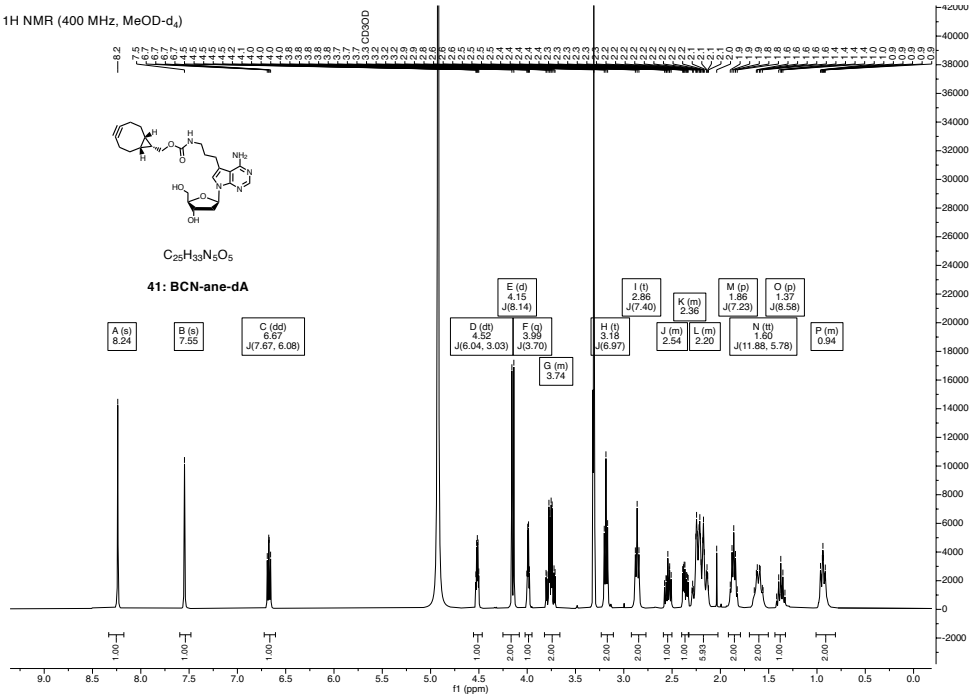

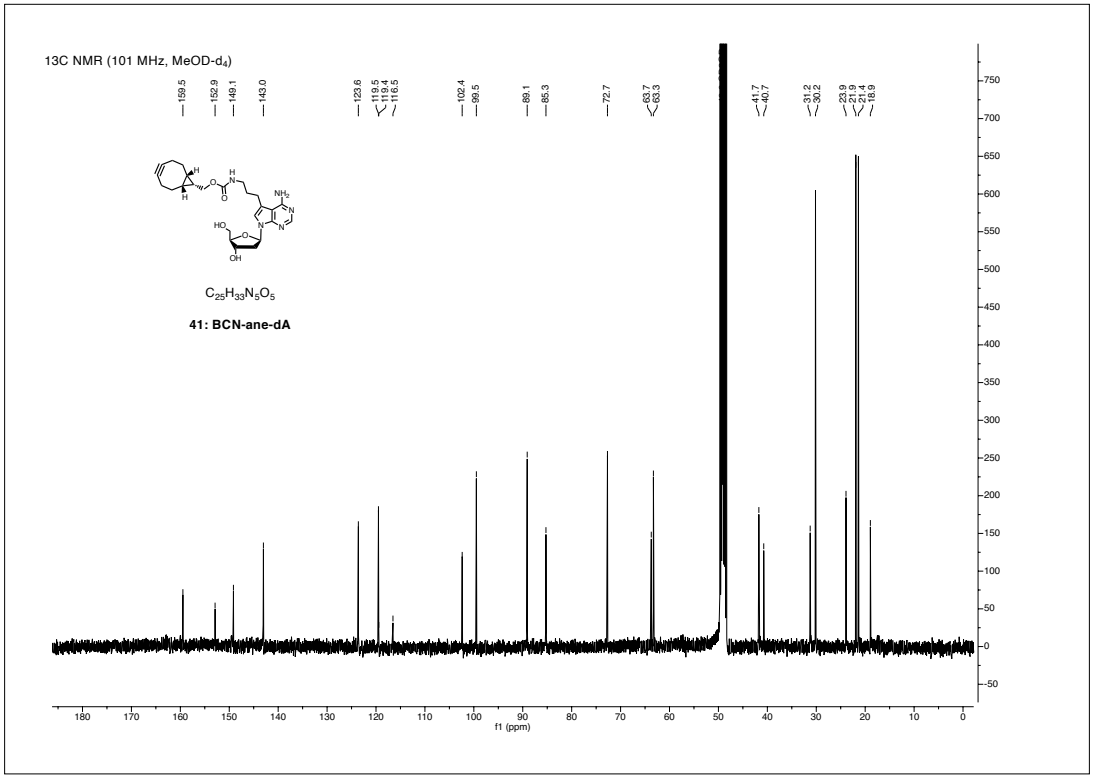
13C NMR (101 MHz, MeOD-d4)
159.5
152.9
149.1
143.0
123.6
119.5
118.4
115.6
102.4
99.5
89.1
85.3
72.7
63.7
63.3
41.7
40.7
31.2
30.2
23.9
21.9
21.4
16.9
C25H33N5O5
41: BCN-ane-dA
f1 (ppm)

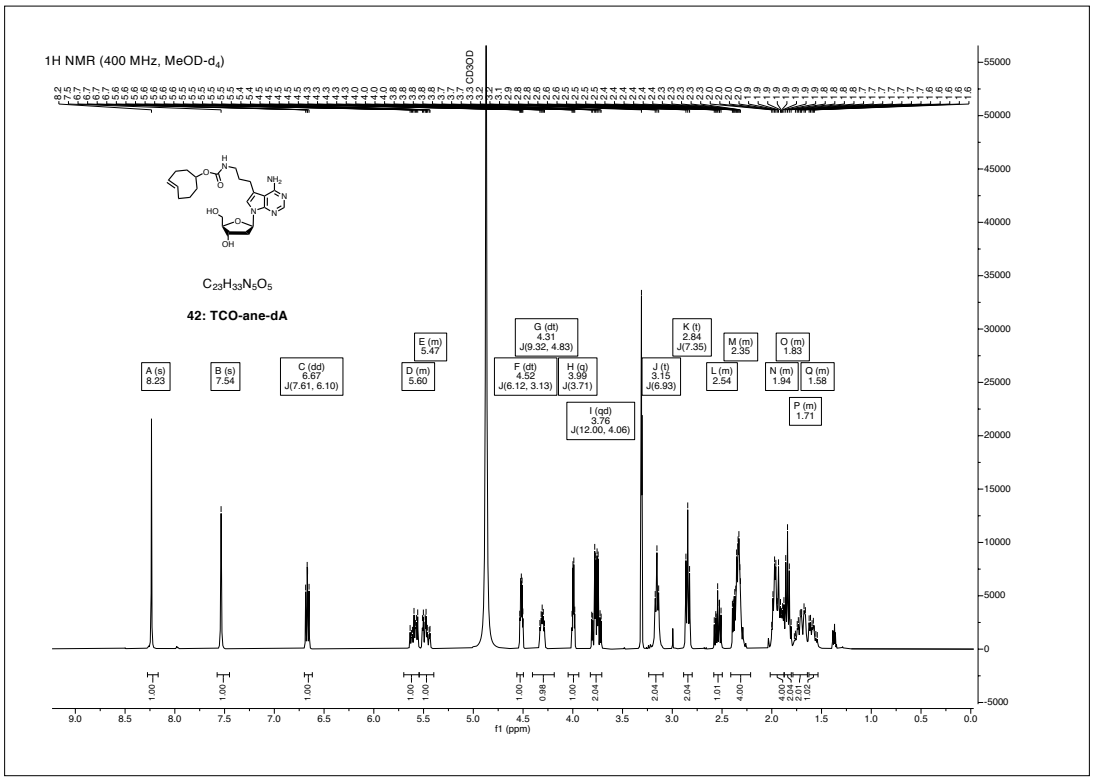
1H NMR (400 MHz, MeOD-d4)
CD3OD
C23H33N5O5
42: TCO-ane-dA
A (s) 8.23
B (s) 7.54
C (dd) 6.67 J(7.61, 6.10)
D (m) 5.60
E (m) 5.47
F (dt) 4.52 J(6.12, 3.13)
G (dt) 4.31 J(9.32, 4.83)
H (q) 3.99 J(3.71)
I (qd) 3.76 J(12.00, 4.06)
J (t) 3.15 J(6.93)
K (t) 2.84 J(7.35)
L (m) 2.54
M (m) 2.35
N (m) 1.94
O (m) 1.83
P (m) 1.71
Q (m) 1.58
f1 (ppm)

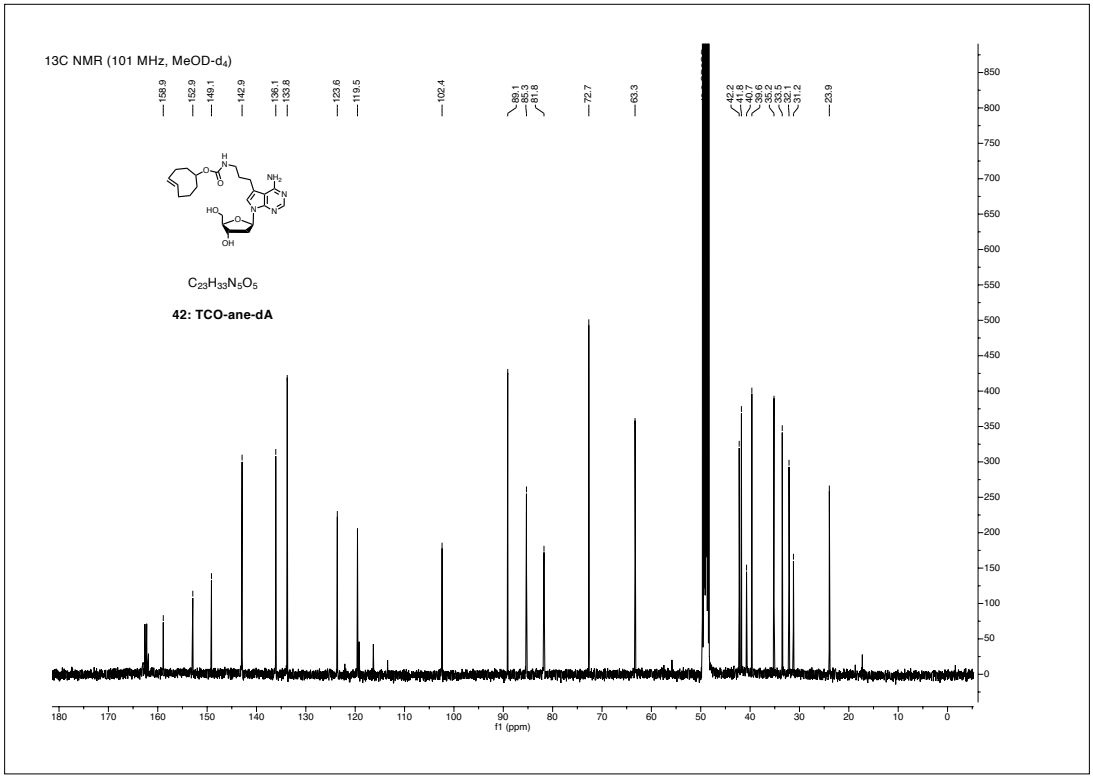
13C NMR (101 MHz, MeOD-d4)
158.9
152.9
149.1
142.9
136.1
133.8
123.6
119.5
102.4
89.1
85.3
81.6
72.7
63.3
49.0
42.2
41.8
40.7
39.5
35.2
33.5
32.1
31.2
23.9
C23H33N5O5
42: TCO-ane-dA
f1 (ppm)

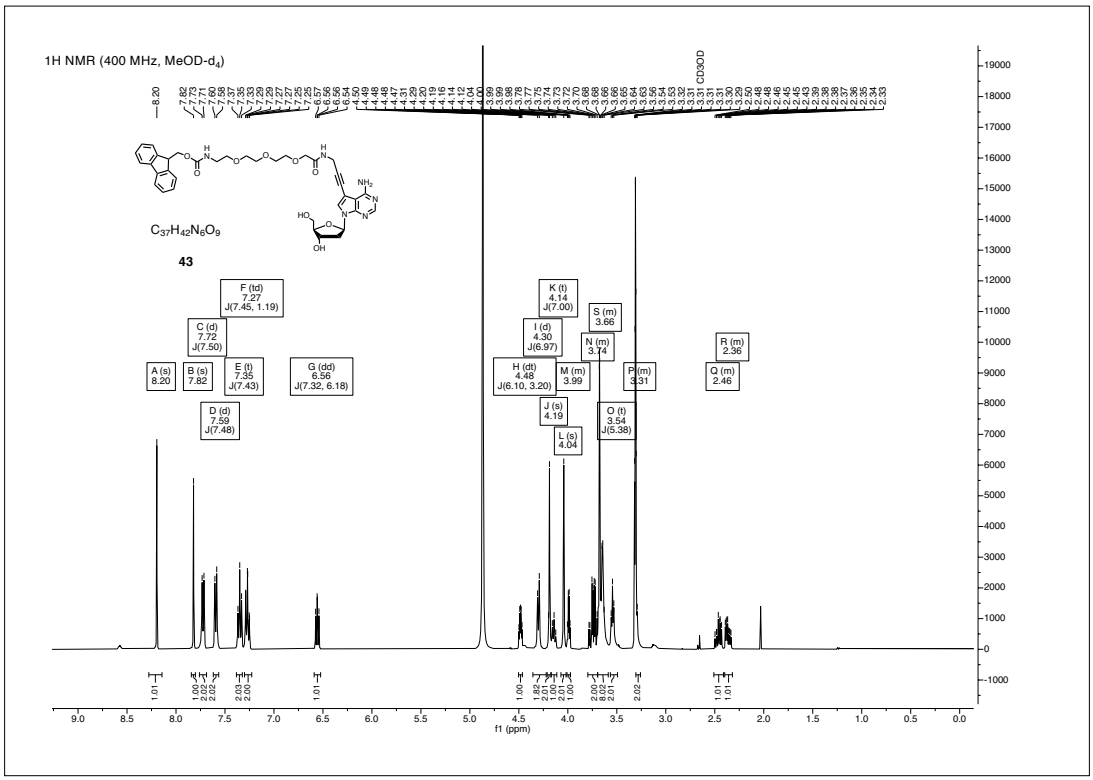
1H NMR (400 MHz, MeOD-d4)
CD3OD
C37H42N8O9
43
A (s) 8.20
B (s) 7.82
C (d) 7.72 J(7.50)
D (d) 7.59 J(7.48)
E (t) 7.35 J(7.43)
F (td) 7.27 J(7.45, 1.19)
G (dd) 6.56 J(7.32, 6.18)
H (dt) 4.48 J(6.10, 3.20)
I (d) 4.30 J(6.97)
J (s) 4.19
K (t) 4.14 J(7.00)
L (s) 4.04
M (m) 3.99
N (m) 3.74
O (t) 3.54 J(5.38)
P (m) 3.31
Q (m) 2.46
R (m) 2.36
f1 (ppm)

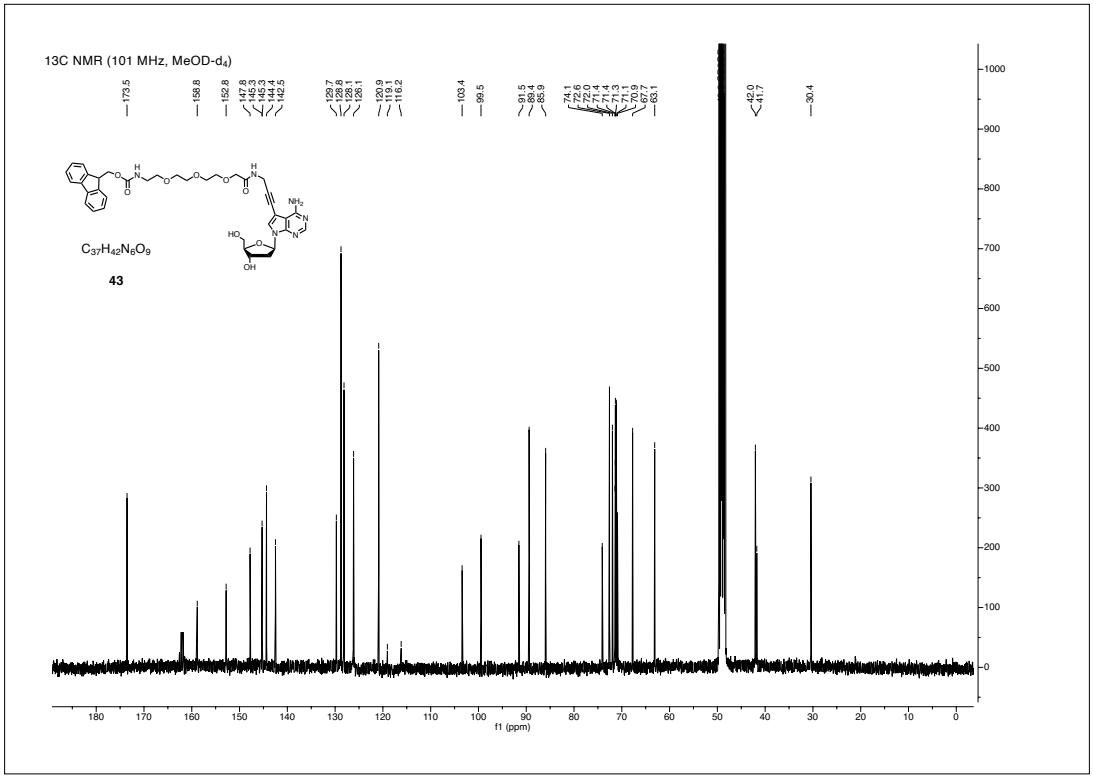
13C NMR (101 MHz, MeOD-d4)
C37H42N6O9
43
f1 (ppm)

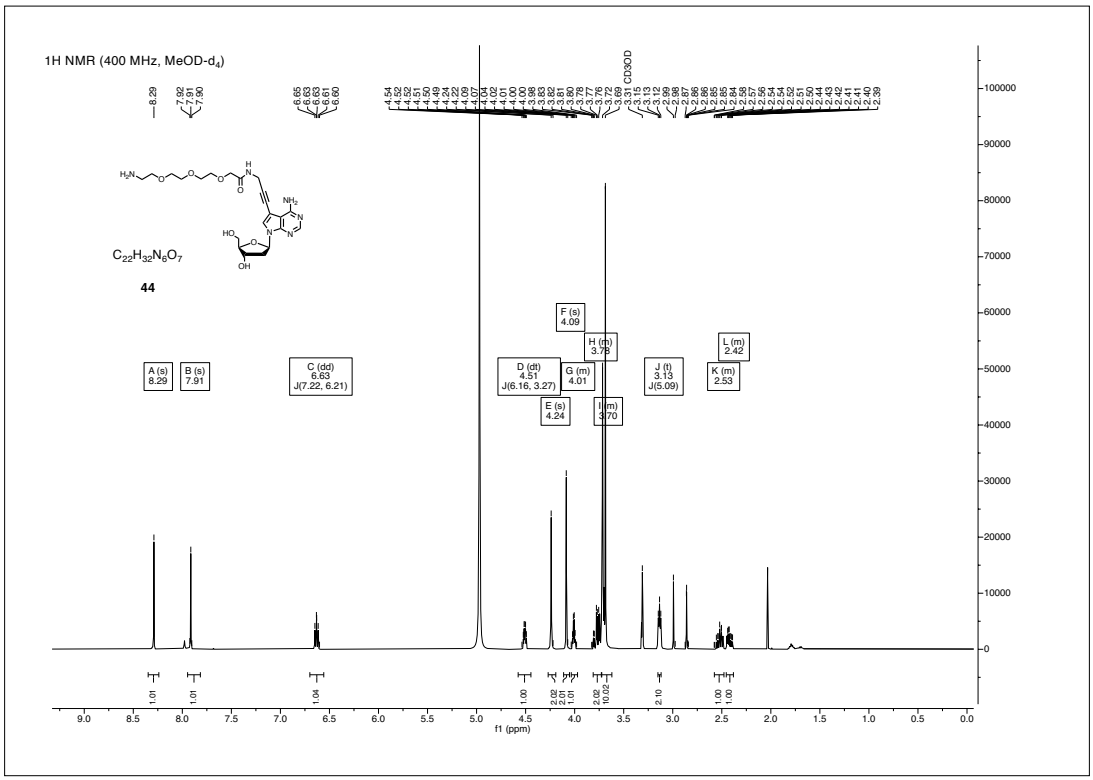
1H NMR (400 MHz, MeOD-d4)
C22H32N6O7
44
A (s) 8.29
B (s) 7.91
C (dd) 6.63 J(7.22, 6.21)
D (dt) 4.51 J(6.16, 3.27)
E (s) 4.24
F (s) 4.09
G (m) 4.01
H (m) 3.78
I (m) 3.70
J (t) 3.13 J(5.09)
K (m) 2.53
L (m) 2.42
f1 (ppm)

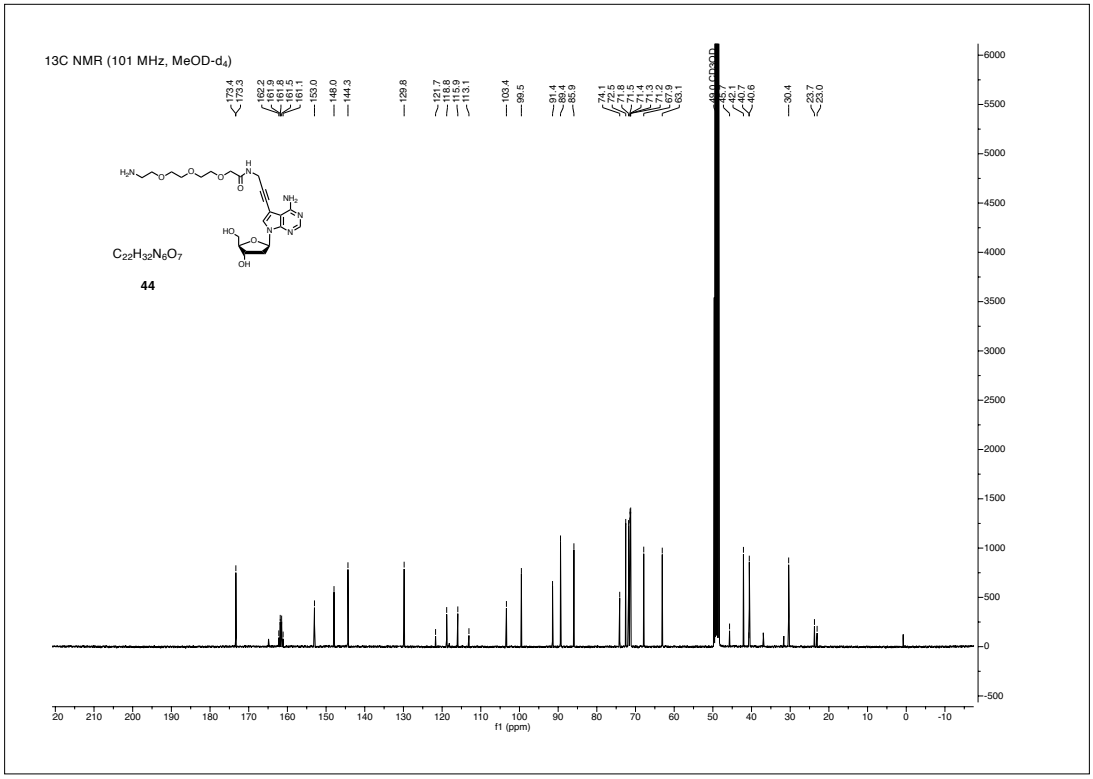
13C NMR (101 MHz, MeOD-d4)
C22H32N6O7
44
f1 (ppm)

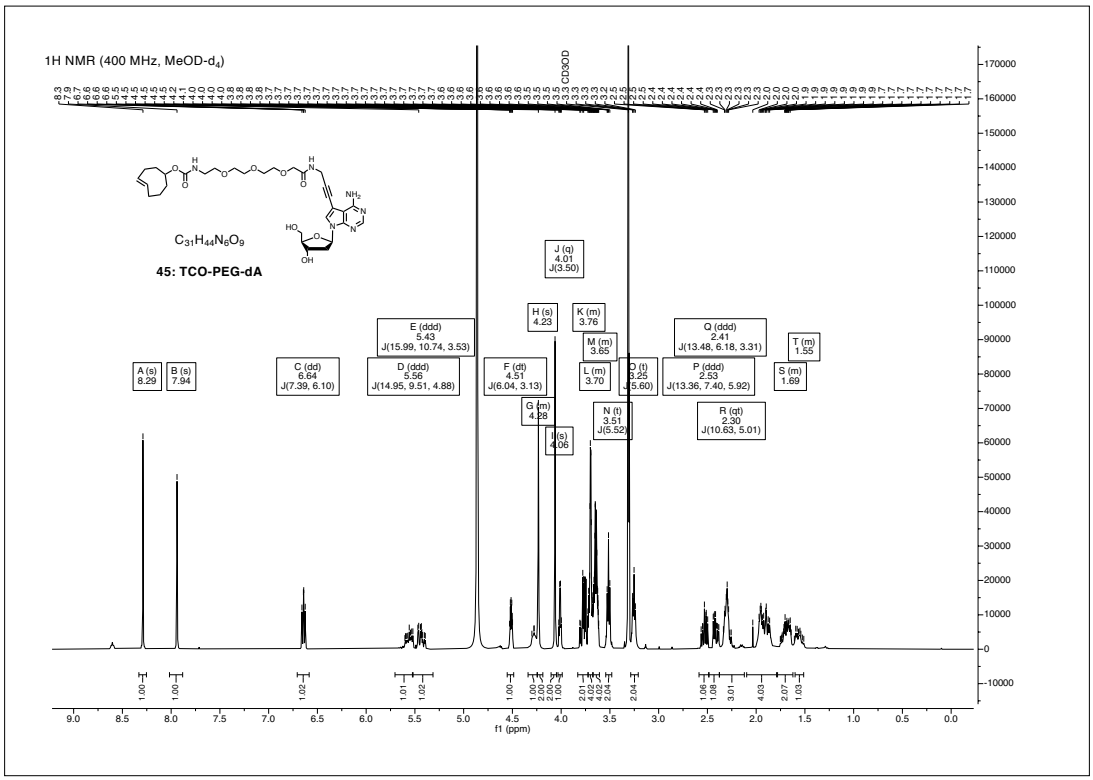
1H NMR (400 MHz, MeOD-d4)
C31H44N6O9
45: TCO-PEG-dA
A (s) 8.29
B (s) 7.94
C (dd) 6.64 J(7.39, 6.10)
D (ddd) 5.56 J(14.95, 9.51, 4.88)
E (ddd) 5.43 J(15.99, 10.74, 3.53)
F (dt) 4.51 J(6.04, 3.13)
G (m) 4.28
H (s) 4.23
I (s) 4.06
J (q) 4.01 J(3.50)
K (m) 3.76
L (m) 3.70
M (m) 3.65
N (t) 3.51 J(5.52)
O (t) 3.25 J(5.60)
P (ddd) 2.53 J(13.36, 7.40, 5.92)
Q (ddd) 2.41 J(13.48, 6.18, 3.31)
R (qt) 2.30 J(10.63, 5.01)
S (m) 1.69
T (m) 1.55
f1 (ppm)

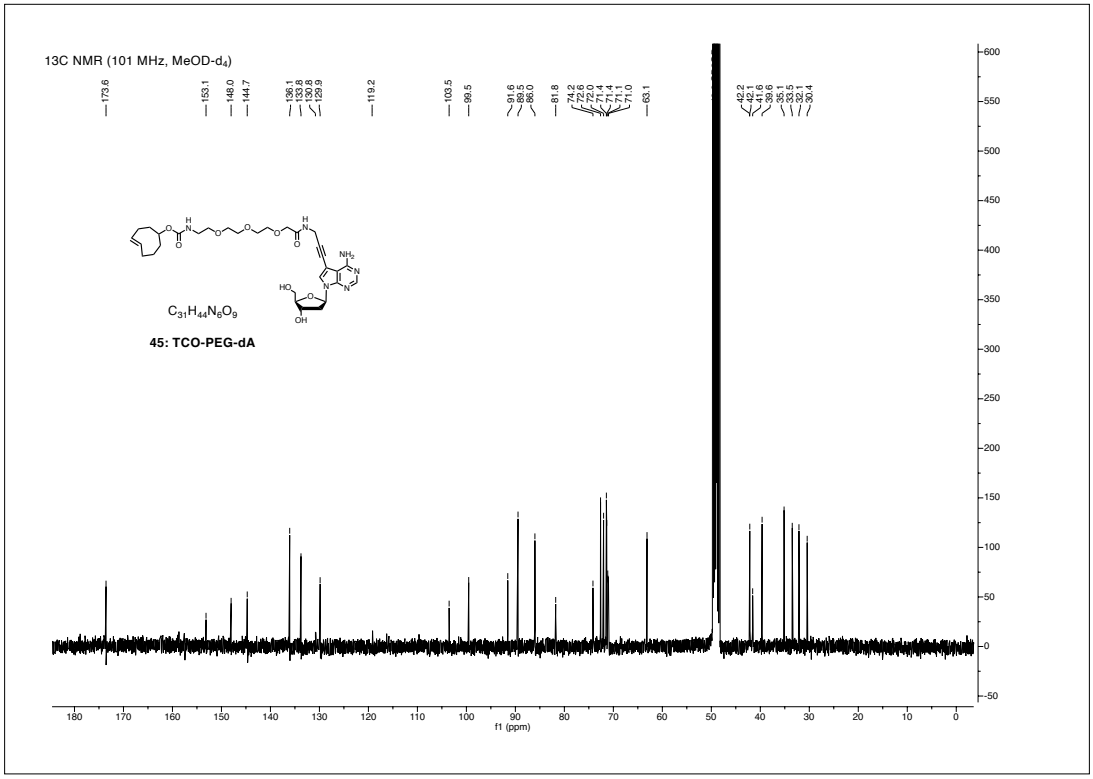
13C NMR (101 MHz, MeOD-d4)
173.6
153.1
148.0
144.7
136.1
135.8
130.8
129.9
119.2
103.5
99.5
91.6
89.5
86.0
81.8
74.2
73.6
72.0
71.4
71.1
71.0
63.1
42.2
42.1
41.6
39.6
35.1
33.5
32.1
30.4
C31H44N6O9
45: TCO-PEG-dA
f1 (ppm)

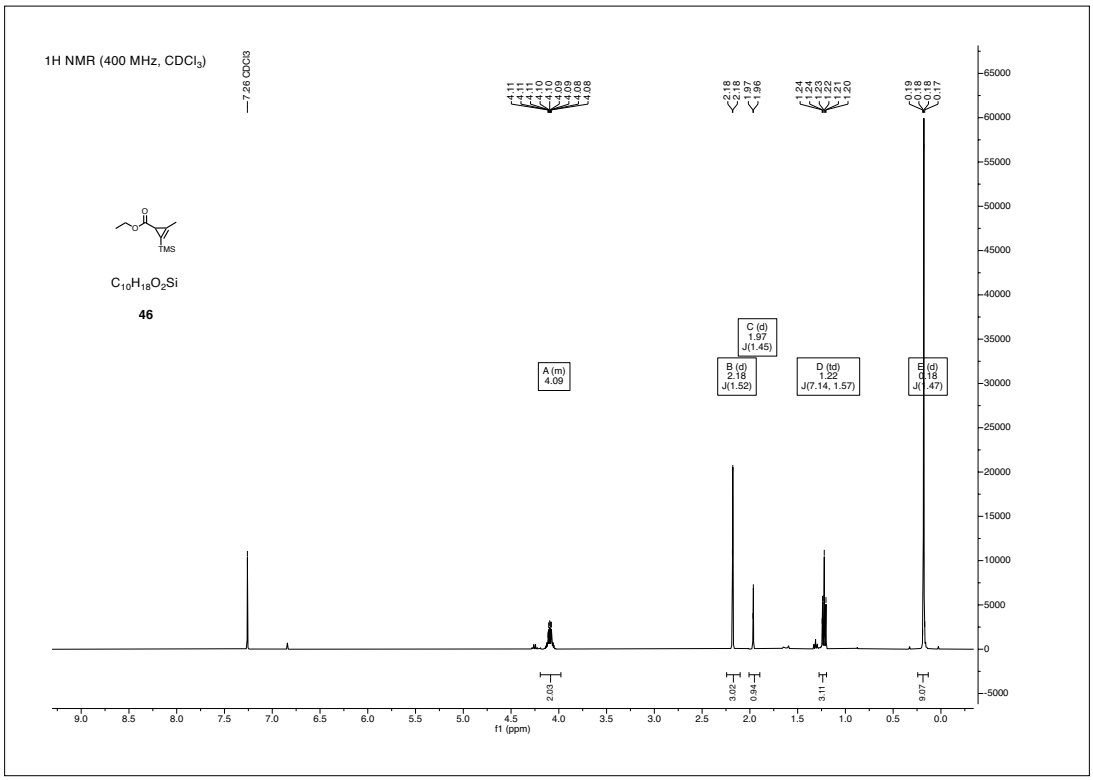
1H NMR (400 MHz, CDCl3)
7.26 CDCl3
4.11
4.11
4.11
4.10
4.10
4.09
4.09
4.08
4.08
2.18
2.18
2.17
1.96
1.24
1.24
1.23
1.22
1.21
1.20
0.19
0.18
0.18
0.18
0.17
TMS
C10H18O2Si
46
A (m)
4.09
B (d)
2.18
J(1.52)
C (d)
1.97
J(1.45)
D (td)
1.22
J(7.14, 1.57)
E (d)
0.18
J(1.47)
2.03
3.02
0.94
3.11
9.07
f1 (ppm)

13C NMR (101 MHz, $CDCl_3$)

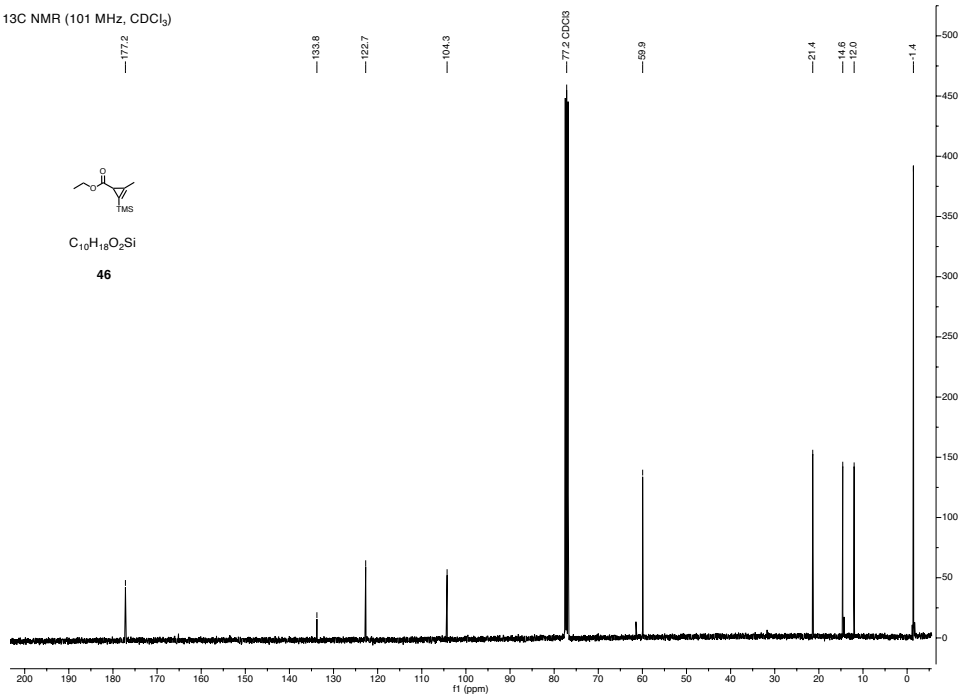

$C_{10}H_{18}O_2Si$

46

1H NMR (400 MHz, $CDCl_3$)

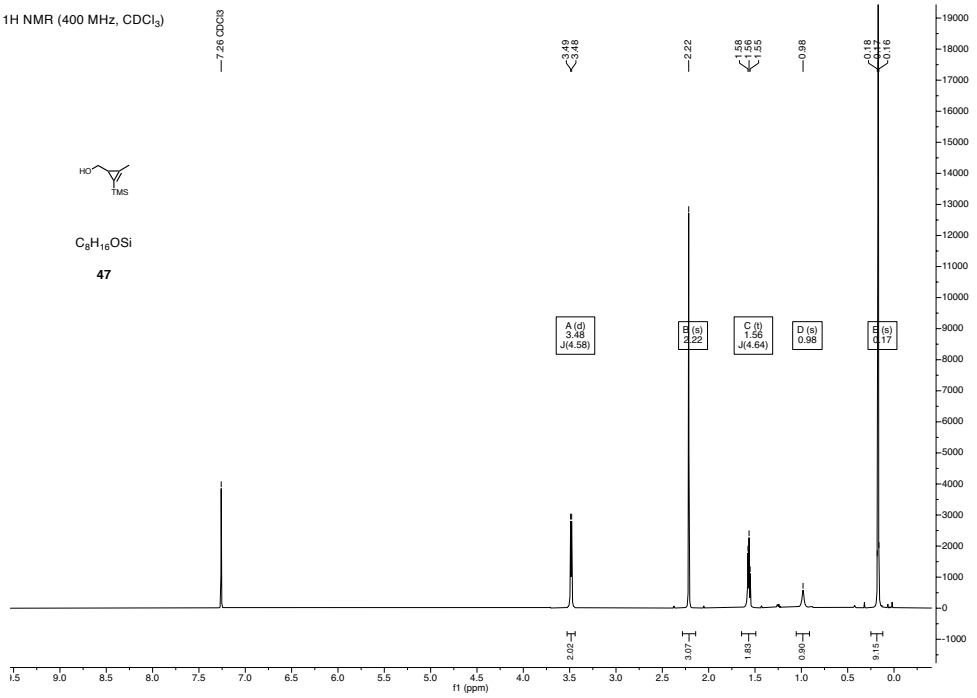

$C_8H_{16}OSi$

47

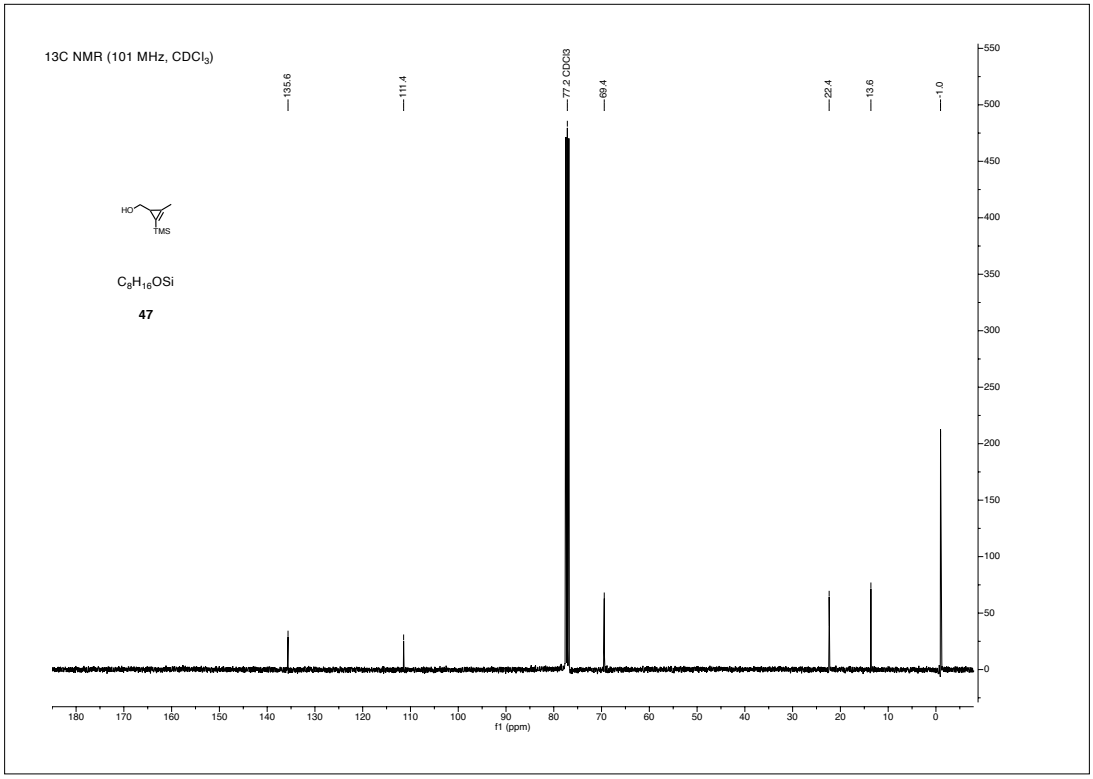
13C NMR (101 MHz, CDCl3)
135.6
111.4
77.2 CDCl3
69.4
22.4
13.6
1.0
HO
TMS
C8H16OSi
47
f1 (ppm)

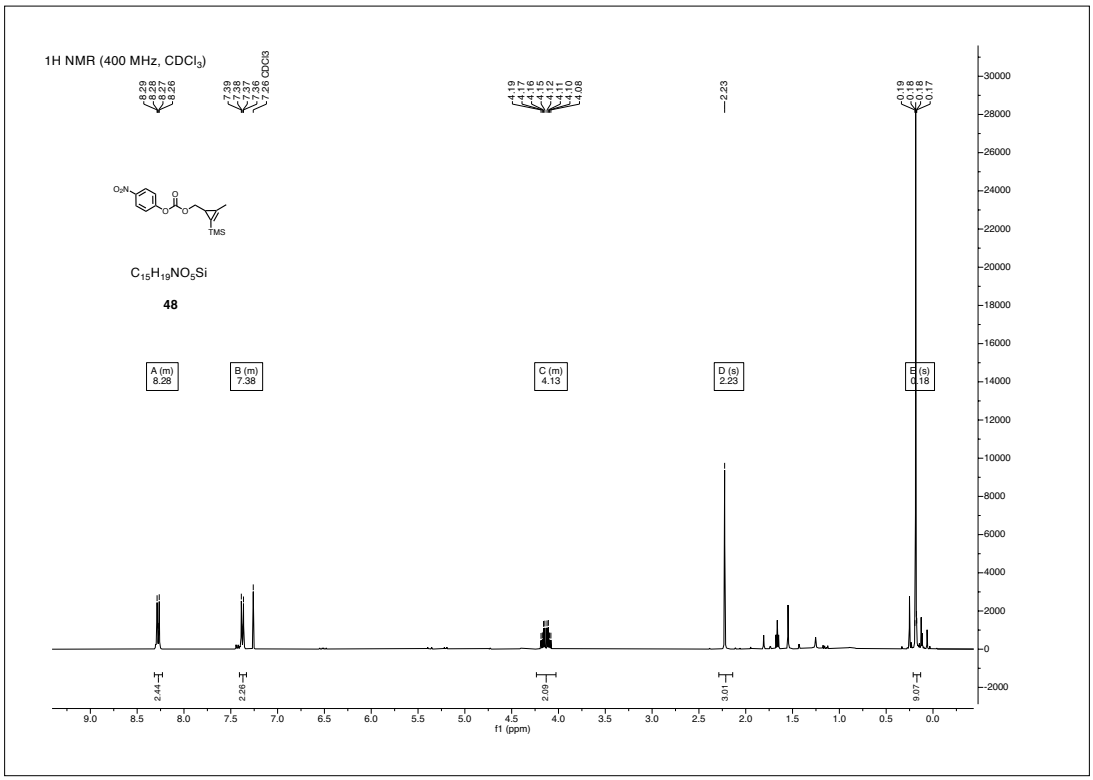
1H NMR (400 MHz, CDCl3)
8.29
8.28
8.27
8.26
7.39
7.38
7.37
7.36
7.26 CDCl3
4.19
4.17
4.16
4.15
4.12
4.11
4.10
4.08
2.23
0.19
0.18
0.18
0.17
O2N
O
O
O
TMS
C15H19NO5Si
48
A (m) 8.28
B (m) 7.38
C (m) 4.13
D (s) 2.23
E (s) 0.18
2.44
2.26
2.09
3.01
9.07
f1 (ppm)

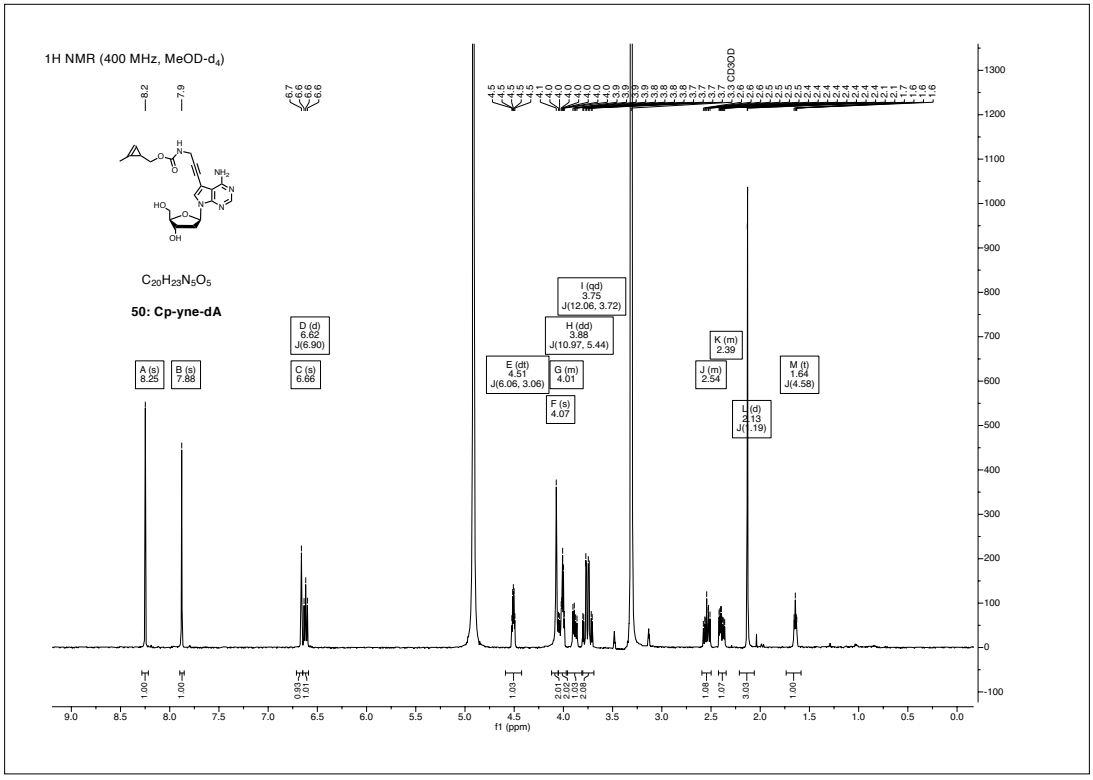
1H NMR (400 MHz, MeOD-d4)
C20H23N5O5
50: Cp-yne-dA
A (s) 8.25
B (s) 7.88
C (s) 6.66
D (d) 6.62 J(6.90)
E (dt) 4.51 J(6.06, 3.06)
F (s) 4.07
G (m) 4.01
H (dd) 3.88 J(10.97, 5.44)
I (qd) 3.75 J(12.06, 3.72)
J (m) 2.54
K (m) 2.39
L (d) 2.13 J(7.19)
M (t) 1.64 J(4.58)
CD3OD
f1 (ppm)

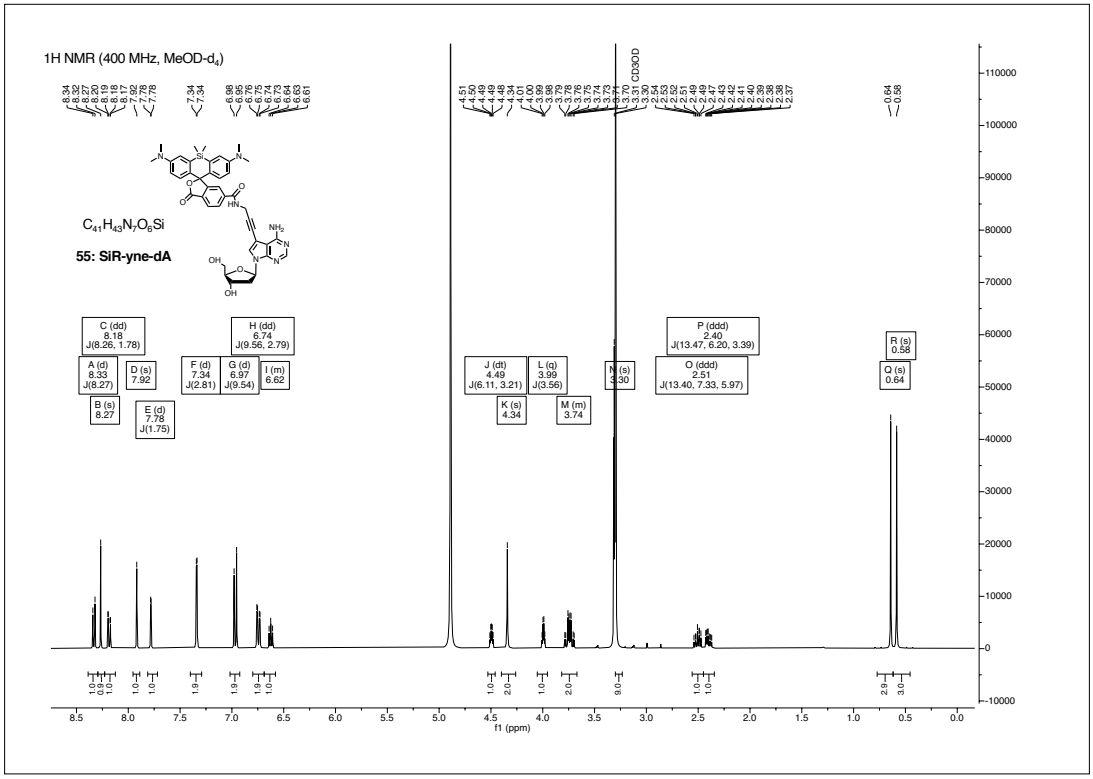
1H NMR (400 MHz, MeOD-d4)
C41H43N7O6Si
55: SiR-yne-dA
C (dd) 8.18 J(8.26, 1.78)
A (d) 8.33 J(8.27)
D (s) 7.92
B (s) 8.27
E (d) 7.78 J(1.75)
H (dd) 6.74 J(9.56, 2.79)
F (d) 7.34 J(2.81)
G (d) 6.97 J(9.54)
I (m) 6.62
J (dt) 4.49 J(6.11, 3.21)
L (q) 3.99 J(3.56)
K (s) 4.34
M (m) 3.74
N (s) 3.30
P (ddd) 2.40 J(13.47, 6.20, 3.39)
O (ddd) 2.51 J(13.40, 7.33, 5.97)
R (s) 0.58
Q (s) 0.64
CD3OD
f1 (ppm)

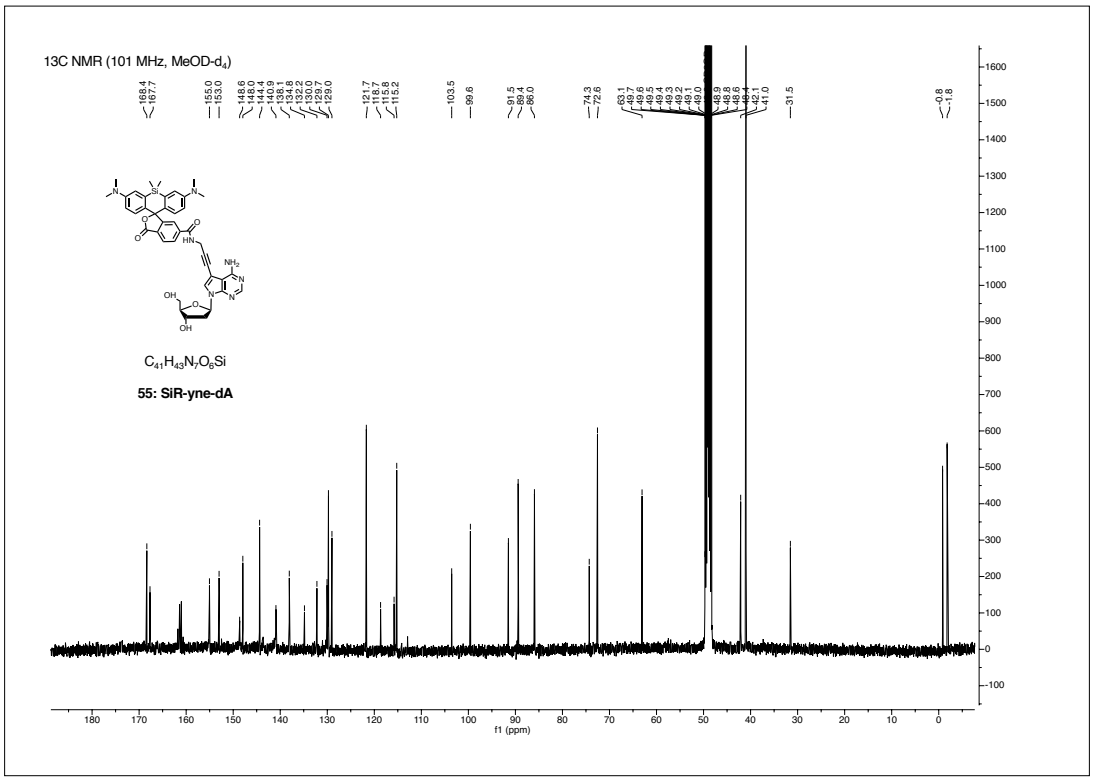
13C NMR (101 MHz, MeOD-d4)
C41H43N7O6Si
55: SiR-yne-dA
f1 (ppm)

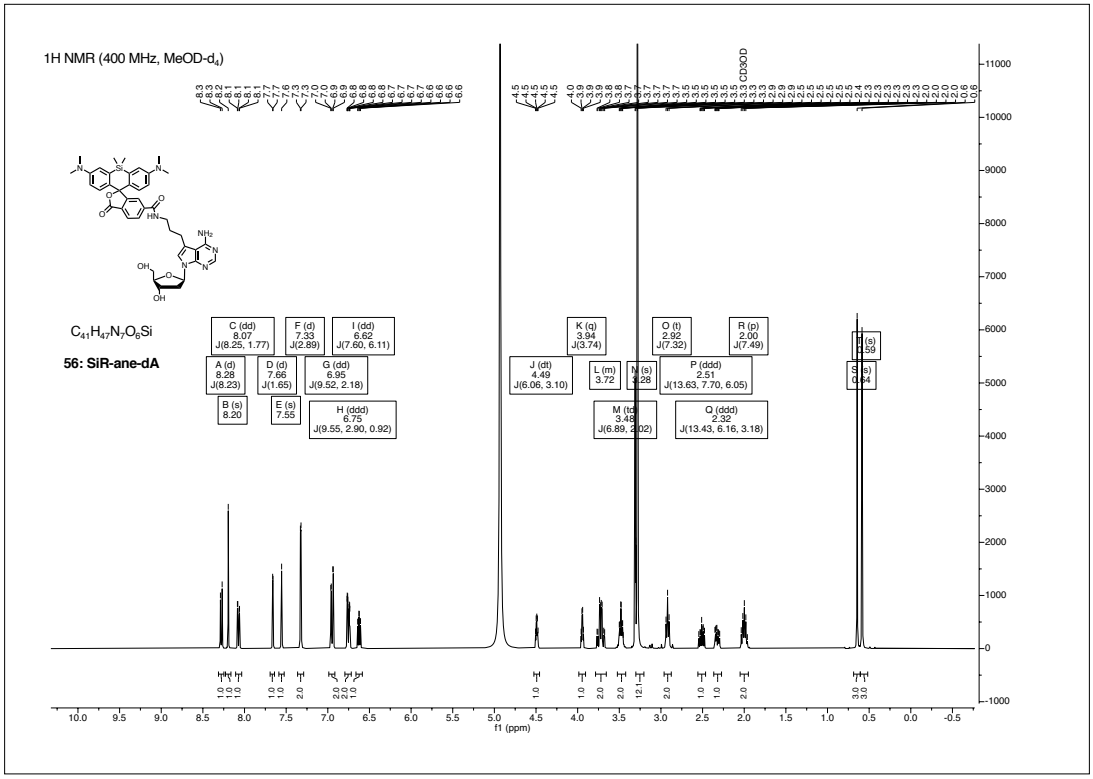
1H NMR (400 MHz, MeOD-d4)
C41H47N7O6Si
56: SiR-ane-dA
A (d) 8.28 J(8.23)
B (s) 8.20
C (dd) 8.07 J(8.25, 1.77)
D (d) 7.66 J(1.65)
E (s) 7.55
F (d) 7.33 J(2.89)
G (dd) 6.95 J(9.52, 2.18)
H (ddd) 6.75 J(9.55, 2.90, 0.92)
I (dd) 6.62 J(7.60, 6.11)
J (dt) 4.49 J(6.06, 3.10)
K (q) 3.94 J(3.74)
L (m) 3.72
M (td) 3.48 J(6.89, 2.02)
N (s) 3.28
O (t) 2.92 J(7.32)
P (ddd) 2.51 J(13.63, 7.70, 6.05)
Q (ddd) 2.32 J(13.43, 6.16, 3.18)
R (p) 2.00 J(7.49)
S (s) 0.64
T (s) 0.59
f1 (ppm)

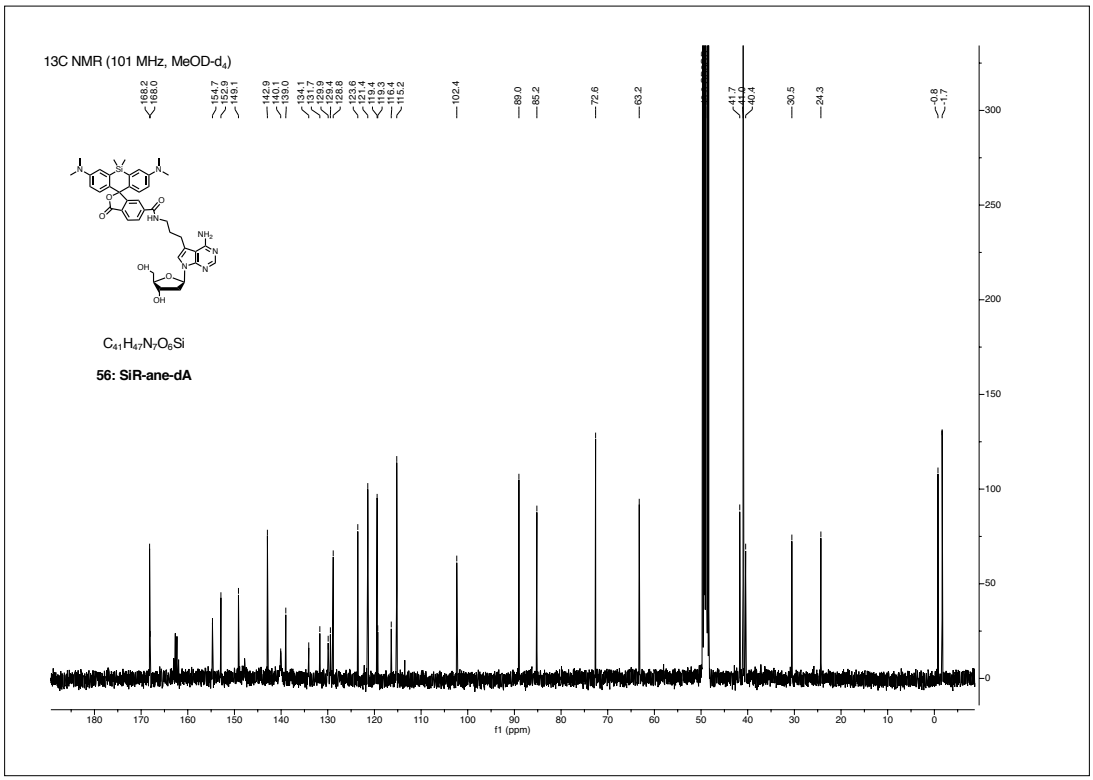
13C NMR (101 MHz, MeOD-d4)
C41H47N7O6Si
56: SiR-ane-dA
f1 (ppm)

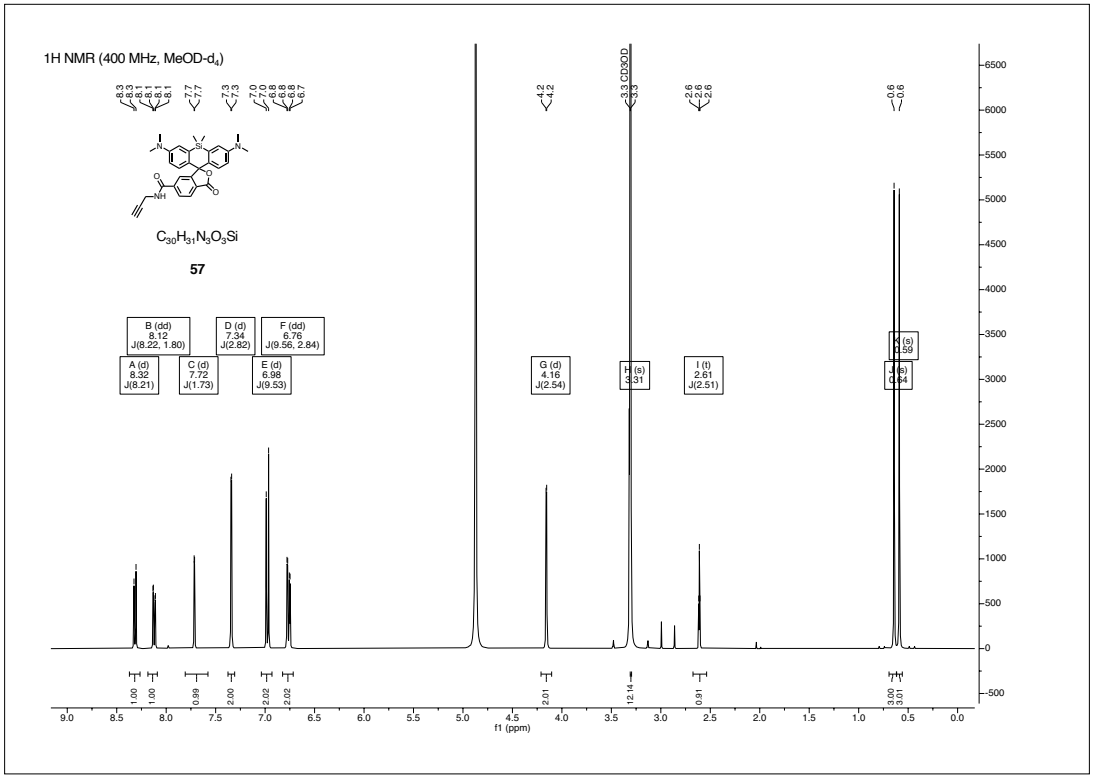
1H NMR (400 MHz, MeOD-d4)
C30H31N3O3Si
57
B (dd) 8.12 J(8.22, 1.80)
D (d) 7.34 J(2.82)
F (dd) 6.76 J(9.56, 2.84)
A (d) 8.32 J(8.21)
C (d) 7.72 J(1.73)
E (d) 6.98 J(9.53)
G (d) 4.16 J(2.54)
H (s) 3.31
I (t) 2.61 J(2.51)
J (s) 0.59
K (s) 0.54
f1 (ppm)

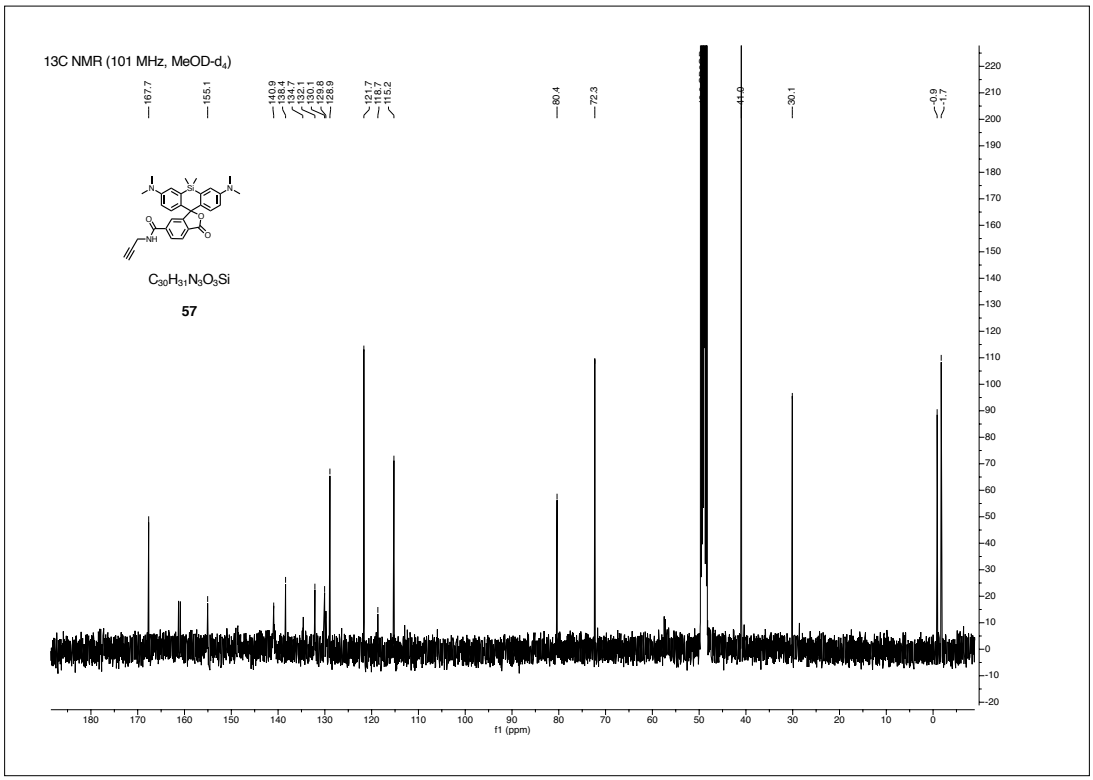
13C NMR (101 MHz, MeOD-d4)
C30H31N3O3Si
57
167.7
155.1
140.9
138.4
134.7
132.1
130.1
129.8
128.9
121.7
118.7
115.2
80.4
72.3
41.0
30.1
-0.9
-1.7
f1 (ppm)

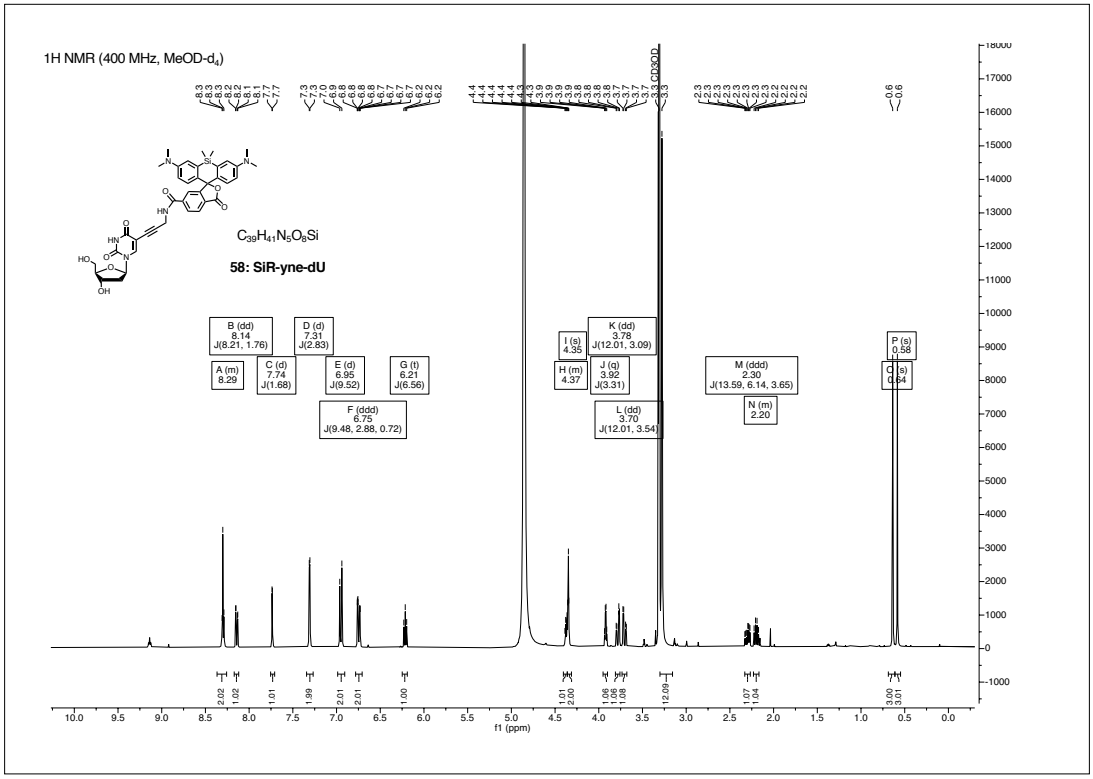
1H NMR (400 MHz, MeOD-d4)
C39H41N5O8Si
58: SiR-yne-dU
B (dd) 8.14 J(8.21, 1.76)
D (d) 7.31 J(2.83)
A (m) 8.29
C (d) 7.74 J(1.68)
E (d) 6.95 J(9.52)
G (t) 6.21 J(6.56)
F (ddd) 6.75 J(9.48, 2.88, 0.72)
I (s) 4.35
K (dd) 3.78 J(12.01, 3.09)
H (m) 4.37
J (q) 3.92 J(3.31)
L (dd) 3.70 J(12.01, 3.54)
M (ddd) 2.30 J(13.59, 6.14, 3.65)
N (m) 2.20
P (s) 0.58
O (s) 0.64
f1 (ppm)

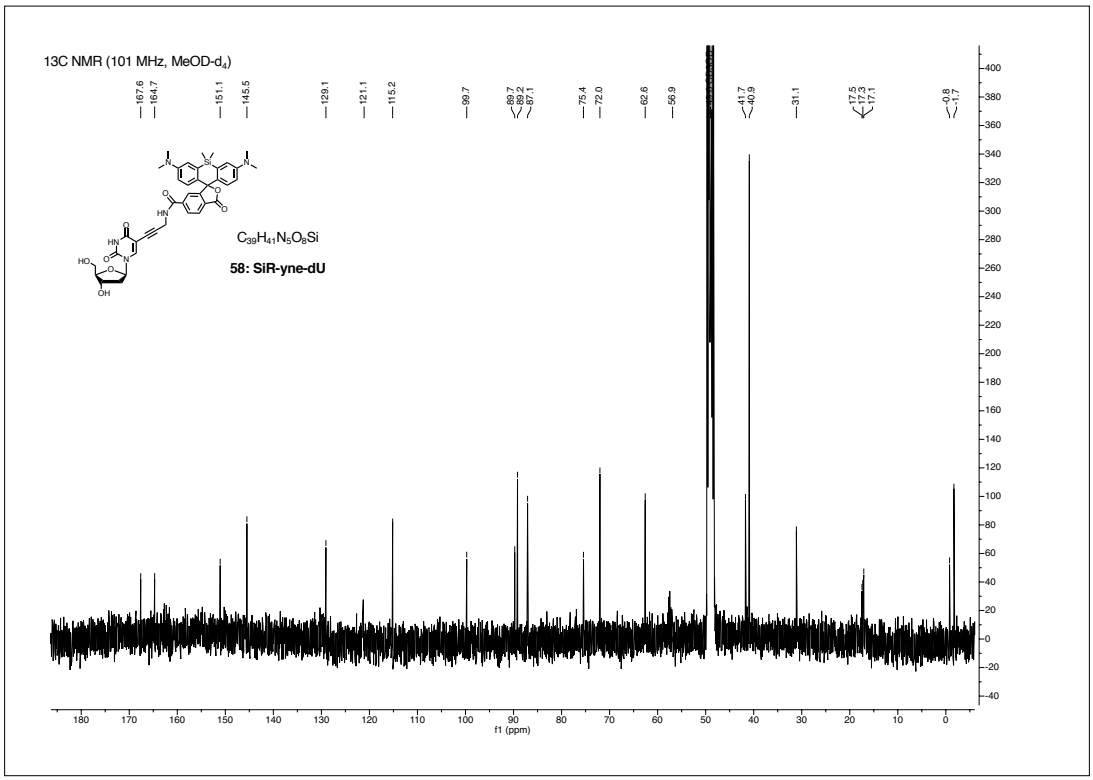
13C NMR (101 MHz, MeOD-d4)
C39H41N5O8Si
58: SiR-yne-dU
f1 (ppm)

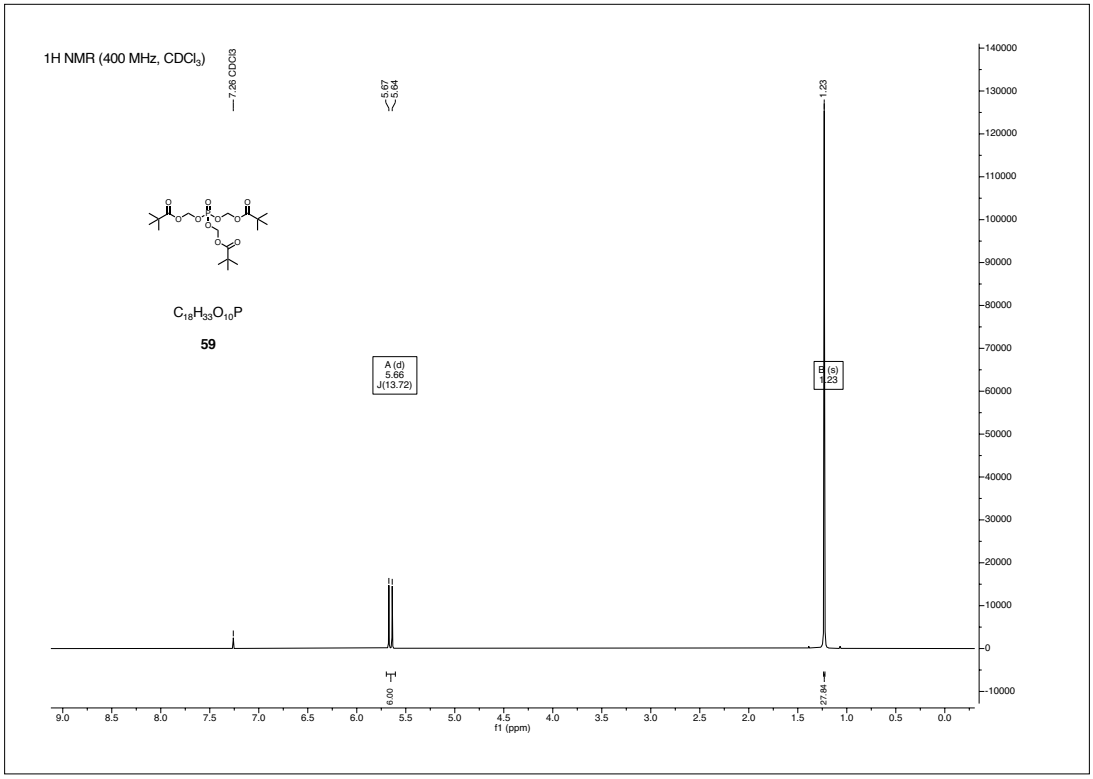
1H NMR (400 MHz, $CDCl_3$)
7.26 CDCl3
5.67
5.64
1.23
$C_{18}H_{33}O_{10}P$
59
A (d)
5.66
J(13.72)
B (s)
1.23
6.00
27.84
f1 (ppm)

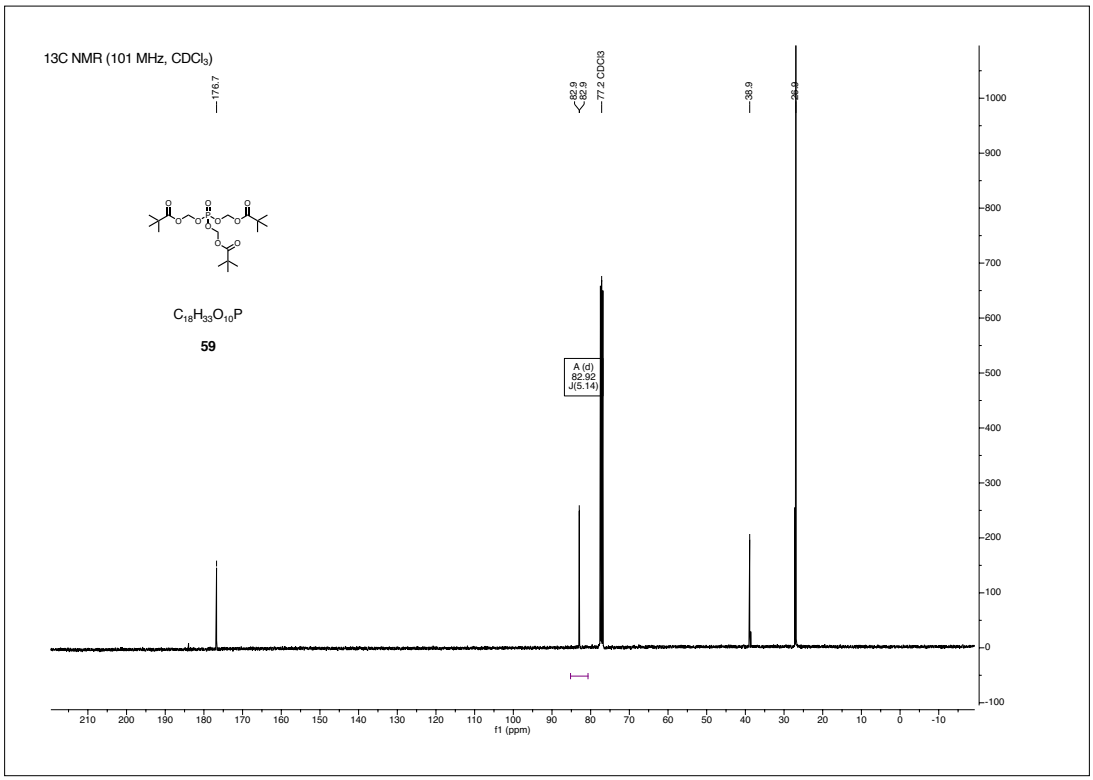
13C NMR (101 MHz, $CDCl_3$)
176.7
82.9
82.9
77.2 CDCl3
38.9
26.9
$C_{18}H_{33}O_{10}P$
59
A (d)
82.92
J(5.14)
f1 (ppm)

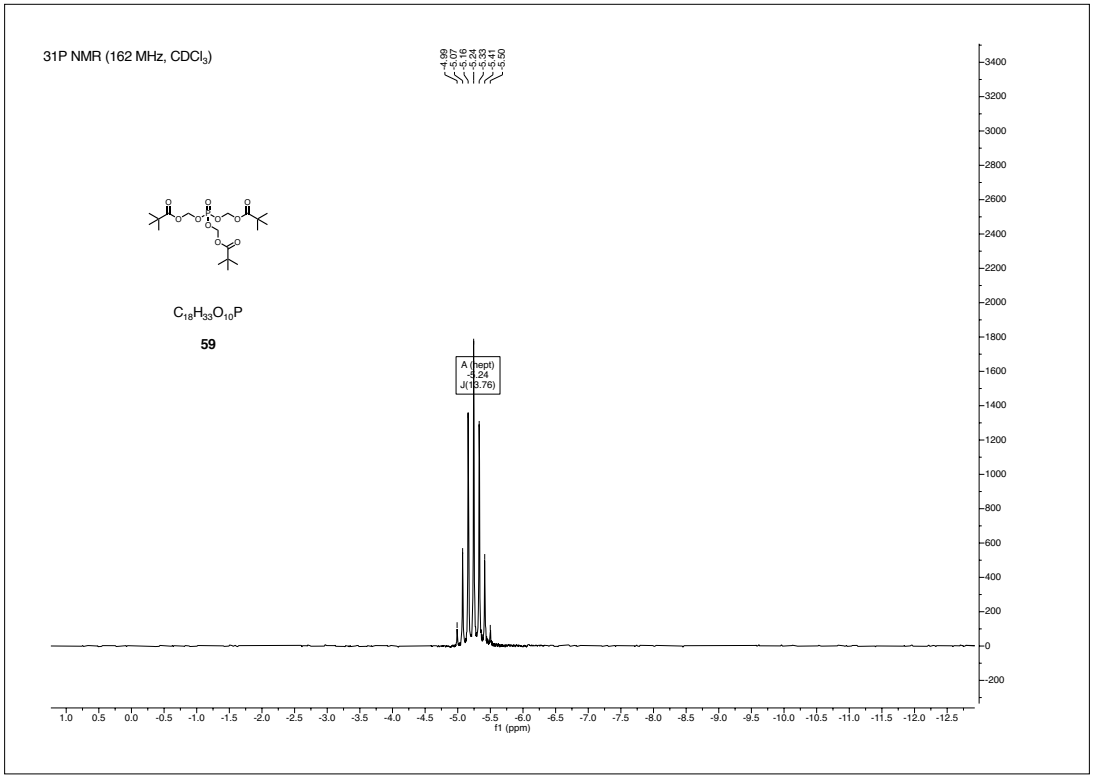

$C_{18}H_{33}O_{10}P$

59

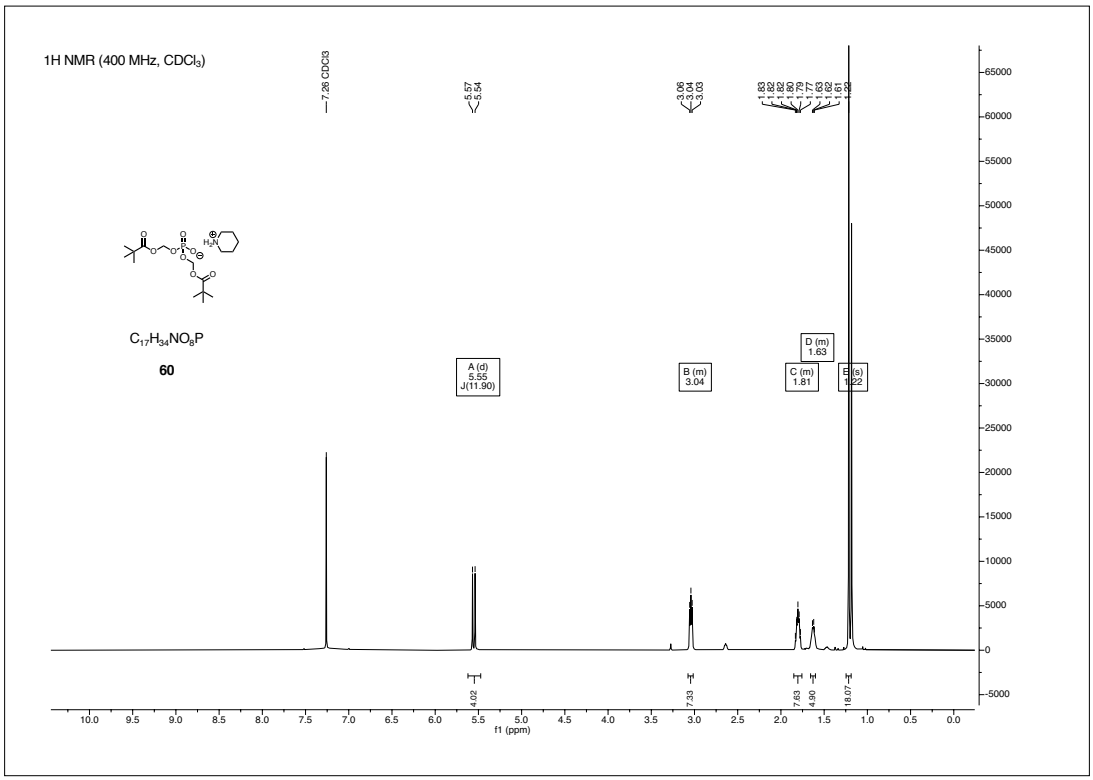

$C_{17}H_{34}NO_8P$

60

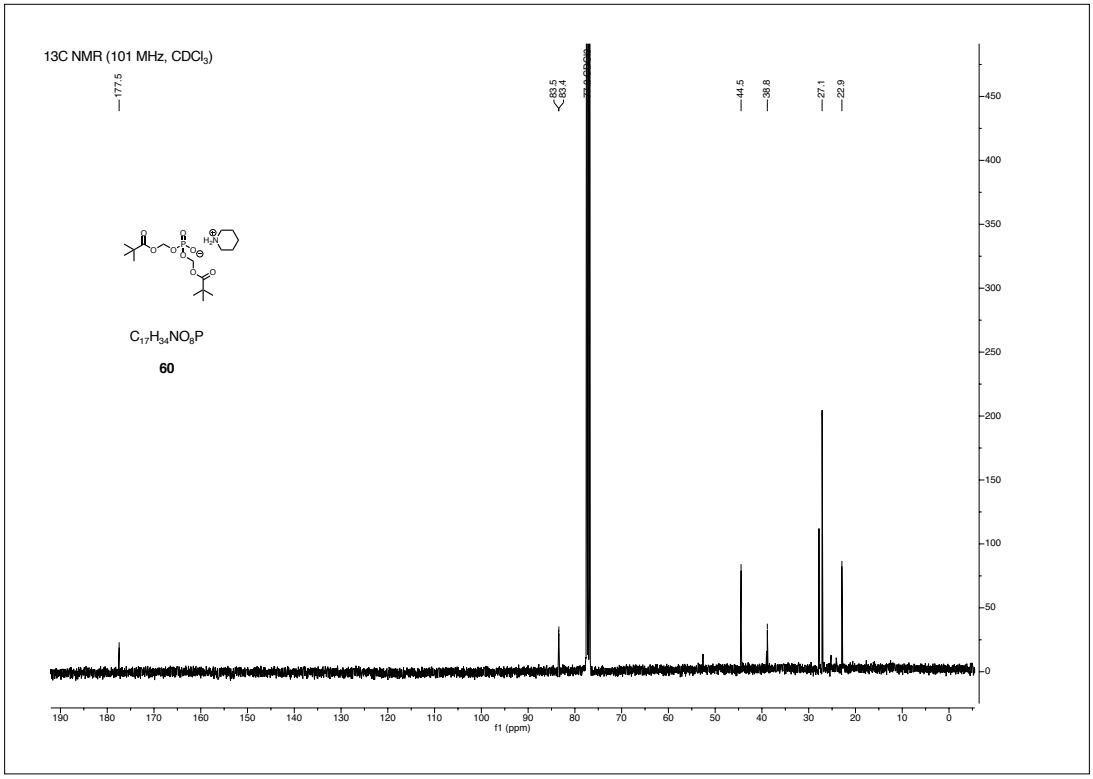
13C NMR (101 MHz, CDCl3)
177.5
83.5
83.4
77.0 CDCl3
44.5
38.8
27.1
22.9
C17H34NO8P
60
f1 (ppm)

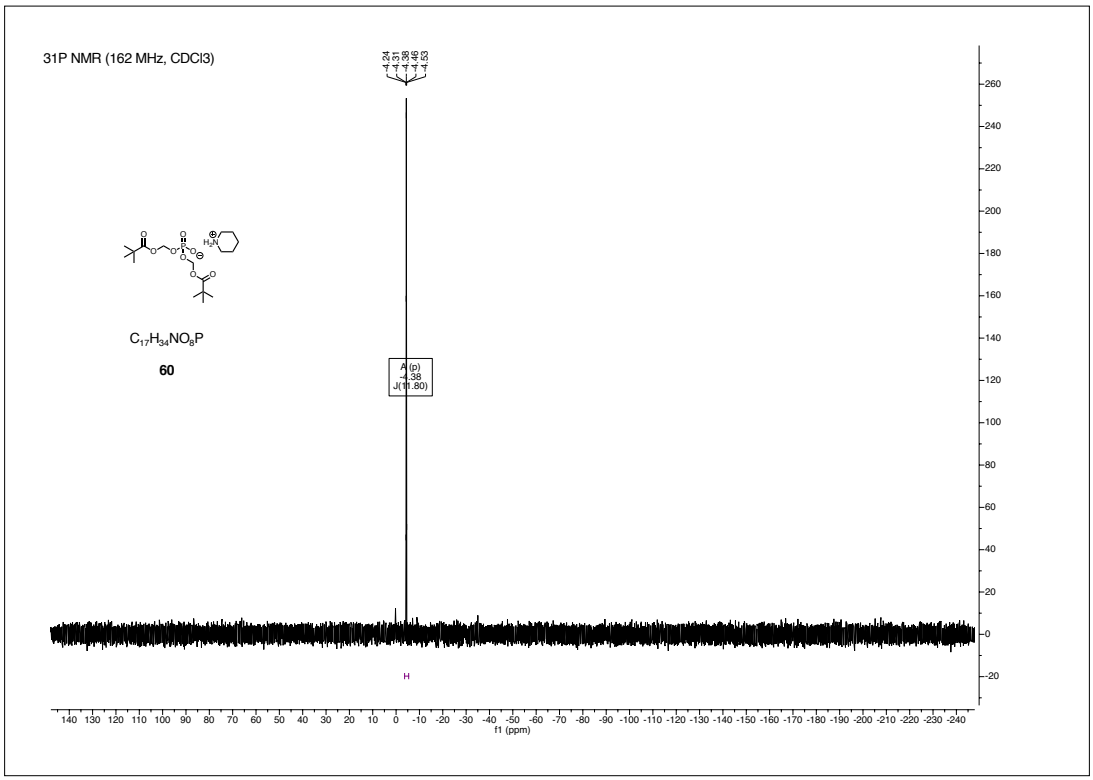
31P NMR (162 MHz, CDCl3)
-4.24
-4.33
-4.38
-4.46
-4.53
A (p)
-4.38
J(H,80)
C17H34NO8P
60
f1 (ppm)

1H NMR (400 MHz, $CDCl_3$)

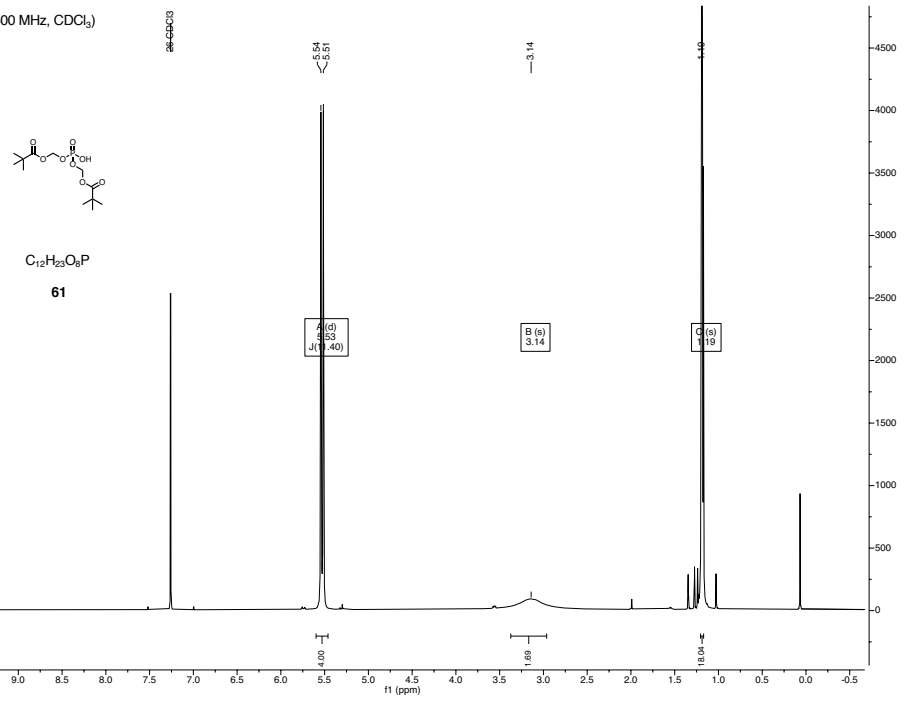

$C_{12}H_{23}O_8P$

61

13C NMR (101 MHz, $CDCl_3$)

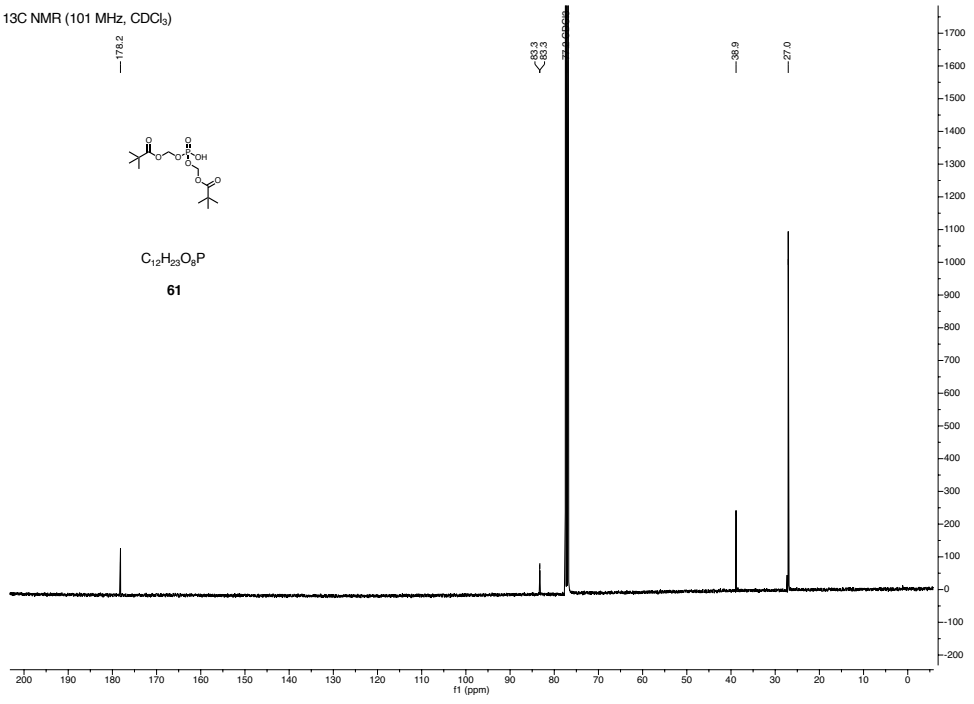

$C_{12}H_{23}O_8P$

61

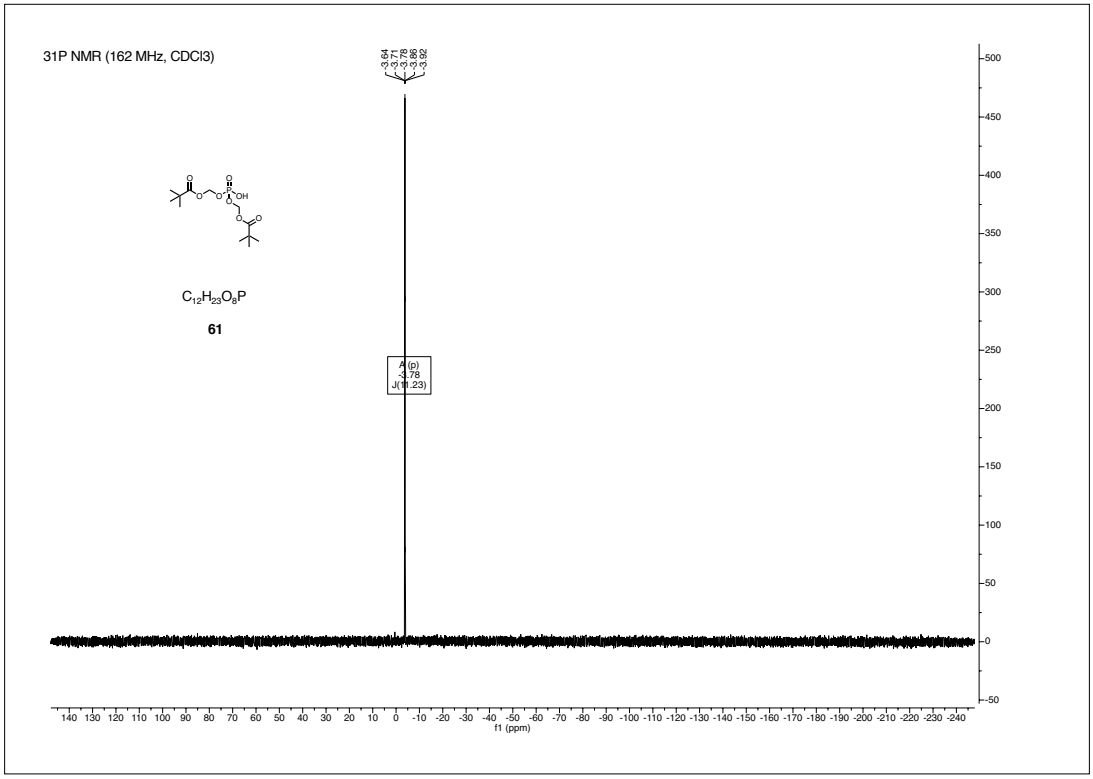

$C_{12}H_{23}O_8P$

61

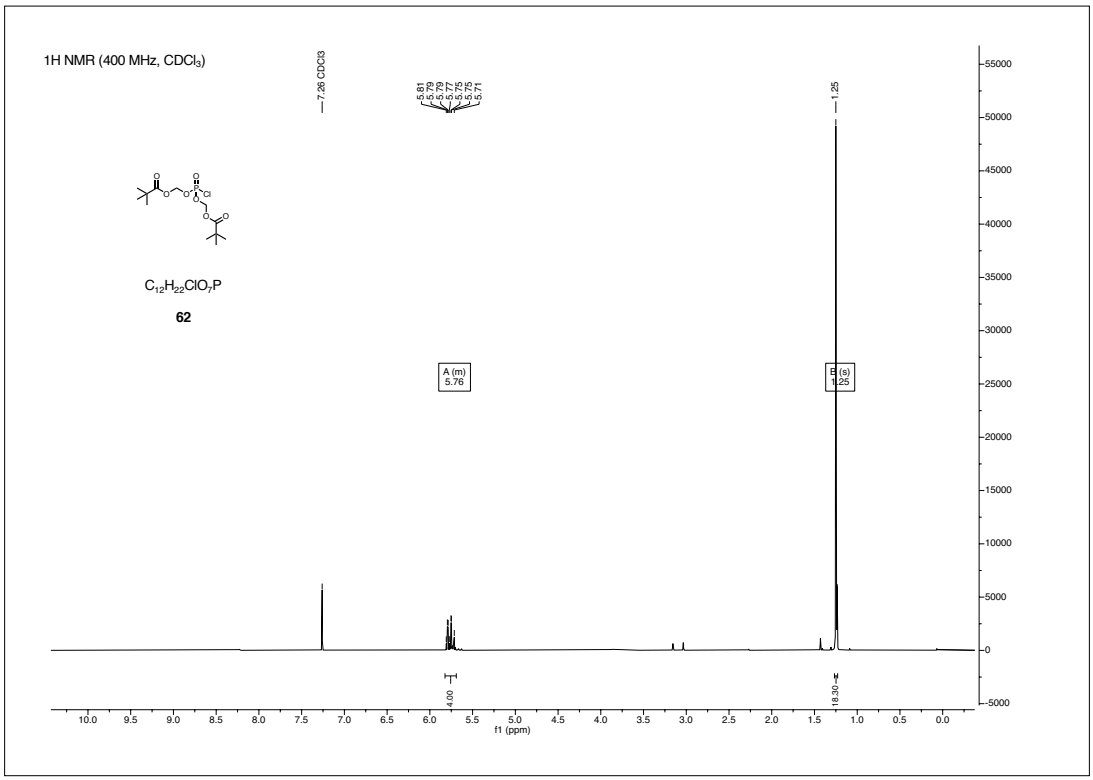

$C_{12}H_{22}ClO_7P$

62

13C NMR (101 MHz, $CDCl_3$)

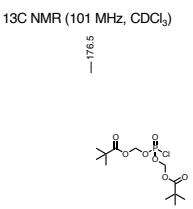

$C_{12}H_{22}ClO_7P$

62

31P NMR (162 MHz, $CDCl_3$)

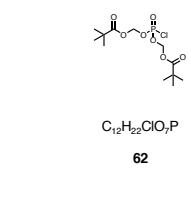

$C_{12}H_{22}ClO_7P$

62

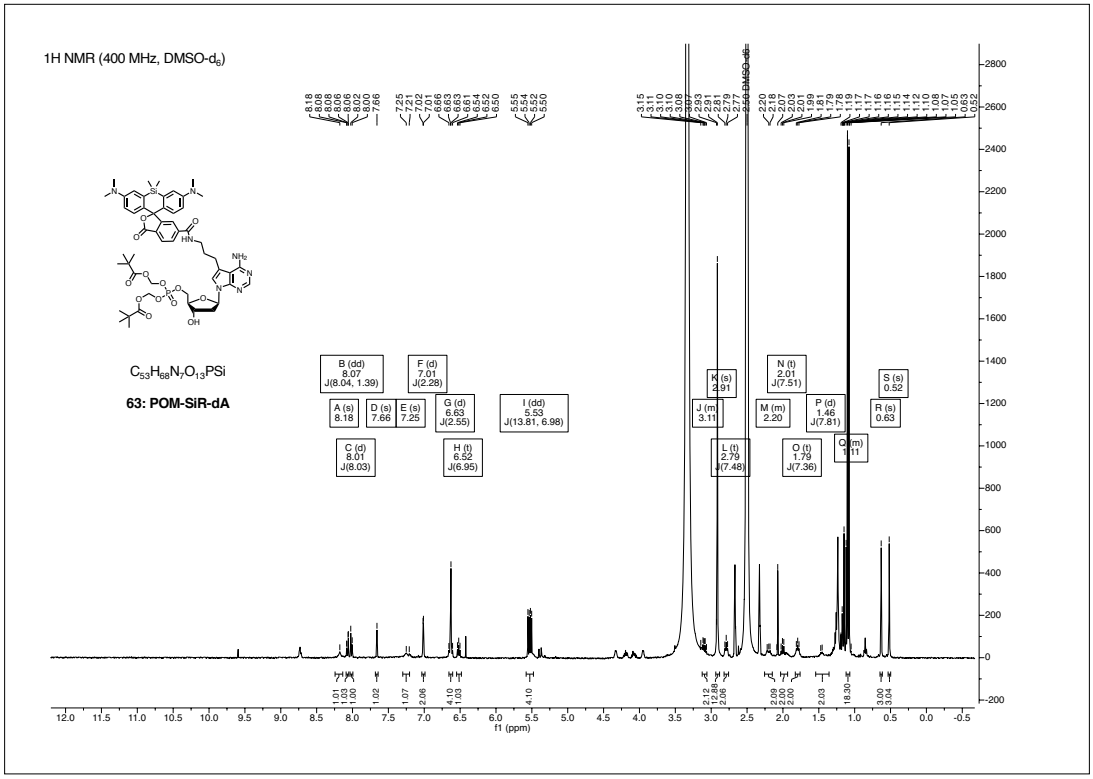
1H NMR (400 MHz, DMSO-d6)
C53H68N7O13PSi
63: POM-SiR-dA
A (s) 8.18
B (dd) 8.07 J(8.04, 1.39)
C (d) 8.01 J(8.03)
D (s) 7.66
E (s) 7.25
F (d) 7.01 J(2.28)
G (d) 6.63 J(2.55)
H (t) 6.52 J(6.95)
I (dd) 5.53 J(13.81, 6.98)
J (m) 3.11
K (s) 2.91
L (t) 2.79 J(7.48)
M (m) 2.20
N (t) 2.01 J(7.51)
O (t) 1.79 J(7.36)
P (d) 1.46 J(7.81)
Q (m) 1.11
R (s) 0.63
S (s) 0.52
f1 (ppm)

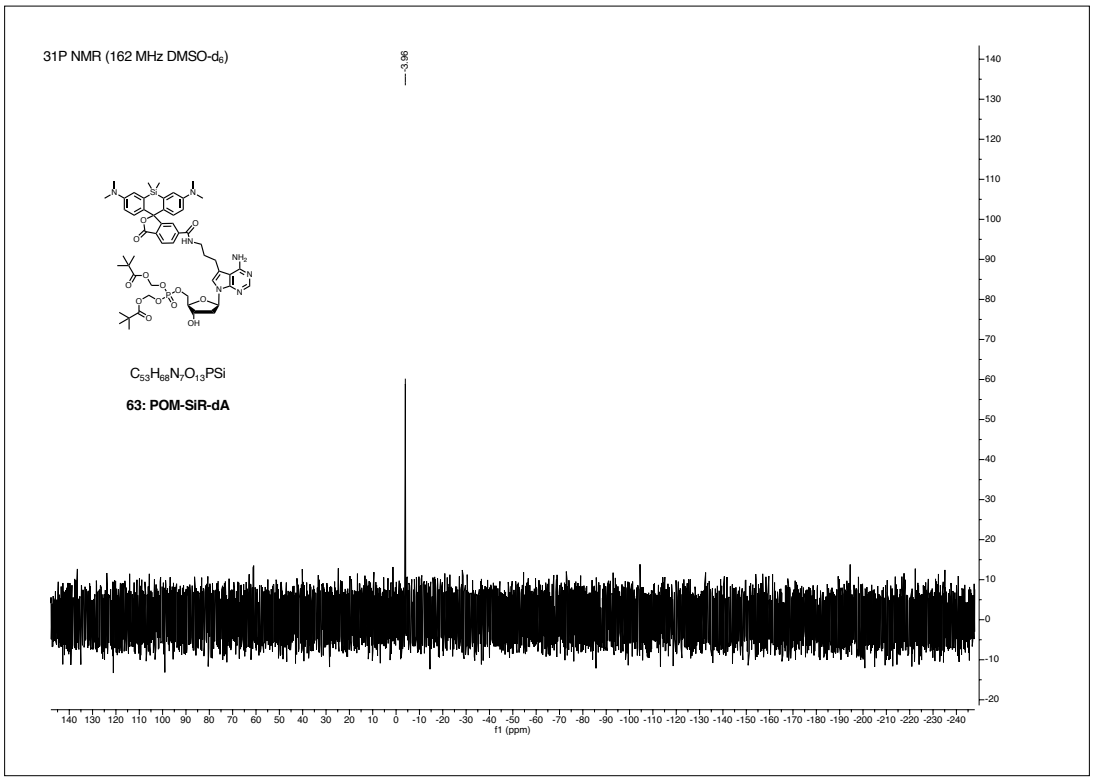
31P NMR (162 MHz DMSO-d6)
-3.96
C53H68N7O13PSi
63: POM-SiR-dA
f1 (ppm)

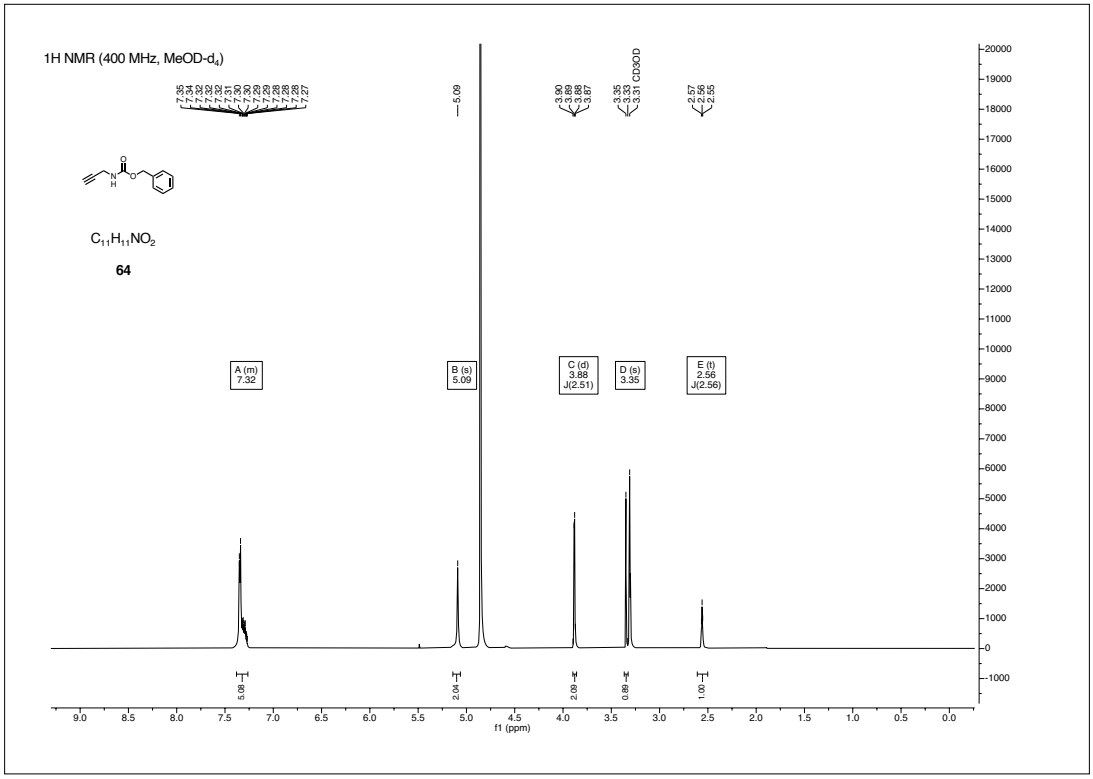
1H NMR (400 MHz, MeOD-d4)
7.35 7.34 7.34 7.32 7.32 7.31 7.30 7.30 7.29 7.29 7.28 7.28 7.28 7.27
5.09
3.90 3.89 3.88 3.87
3.35 3.33 3.31 CD3OD
2.57 2.56 2.55
C11H11NO2
64
A (m) 7.32
B (s) 5.09
C (d) 3.88 J(2.51)
D (s) 3.35
E (t) 2.56 J(2.56)
5.09
2.04
2.09
0.89
1.00
f1 (ppm)

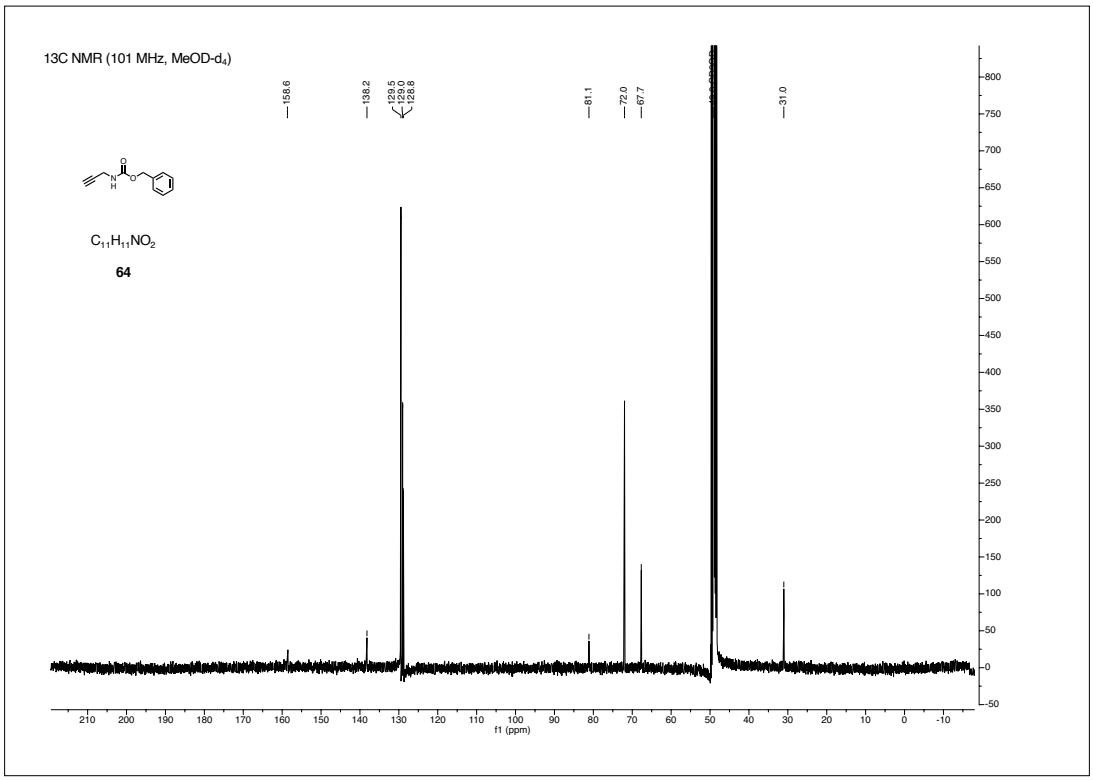
13C NMR (101 MHz, MeOD-d4)
158.6
138.2
129.5
129.0
128.8
81.1
72.0
67.7
49.2 49.0 48.8
31.0
C11H11NO2
64
f1 (ppm)

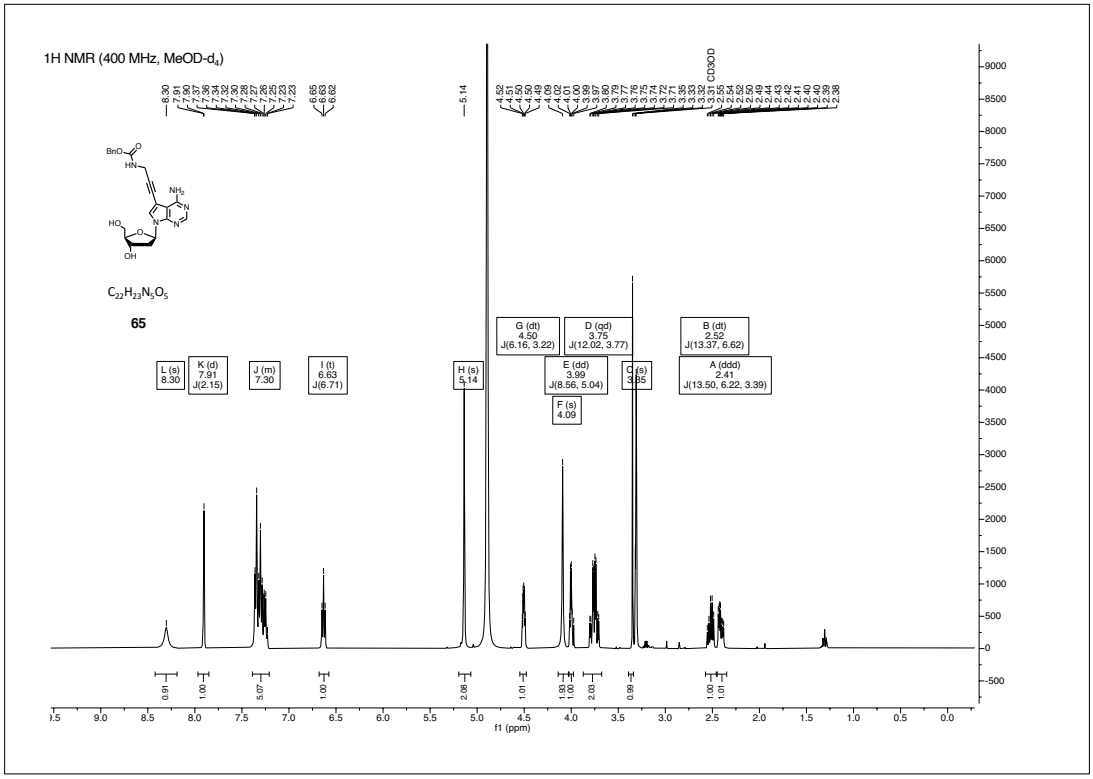
1H NMR (400 MHz, MeOD-d4)
C22H23N5O5
65
L (s) 8.30
K (d) 7.91 J(2.15)
J (m) 7.30
I (t) 6.63 J(6.71)
H (s) 5.14
G (dt) 4.50 J(6.16, 3.22)
D (qd) 3.75 J(12.02, 3.77)
E (dd) 3.99 J(8.56, 5.04)
F (s) 4.09
C (s) 3.85
B (dt) 2.52 J(13.37, 6.62)
A (ddd) 2.41 J(13.50, 6.22, 3.39)
f1 (ppm)

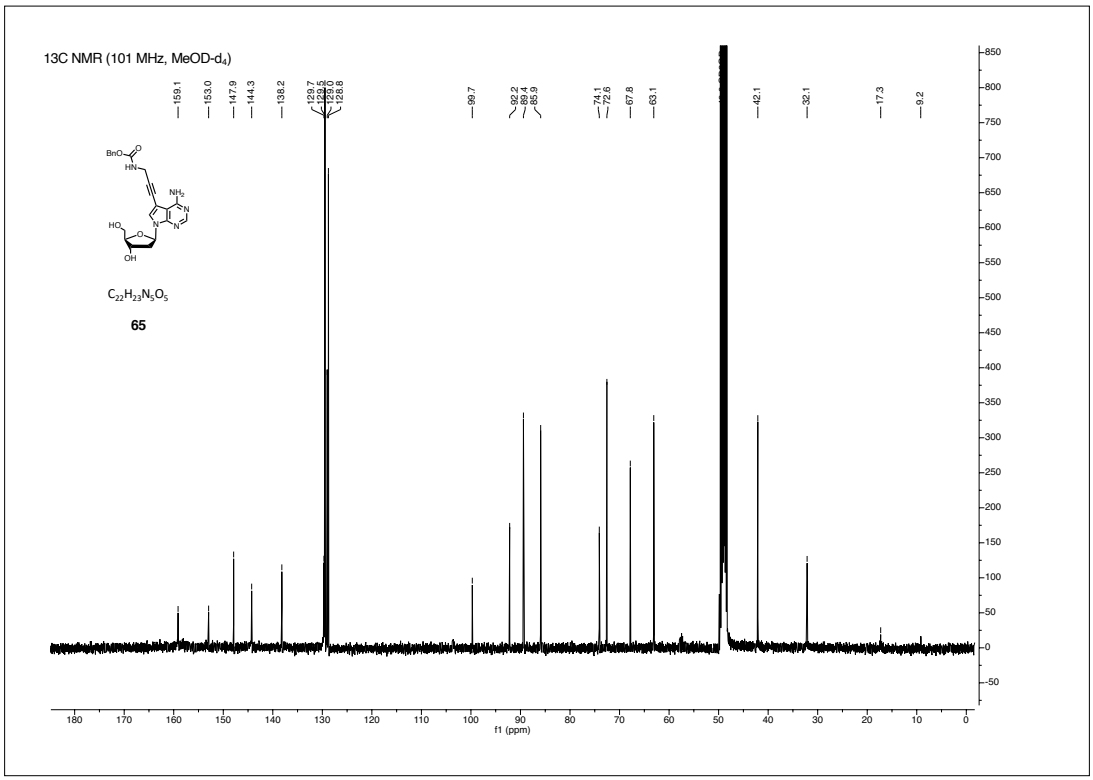
13C NMR (101 MHz, MeOD-d4)
C22H23N5O5
65
f1 (ppm)

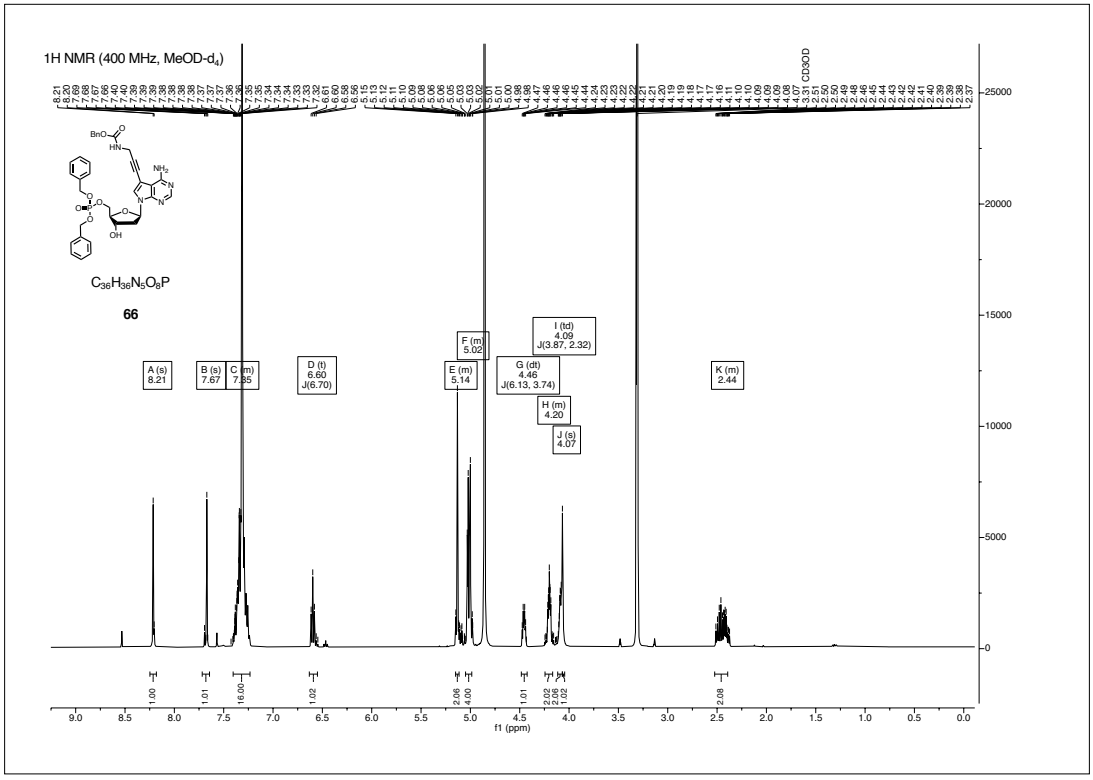

$C_{36}H_{36}N_5O_8P$

66

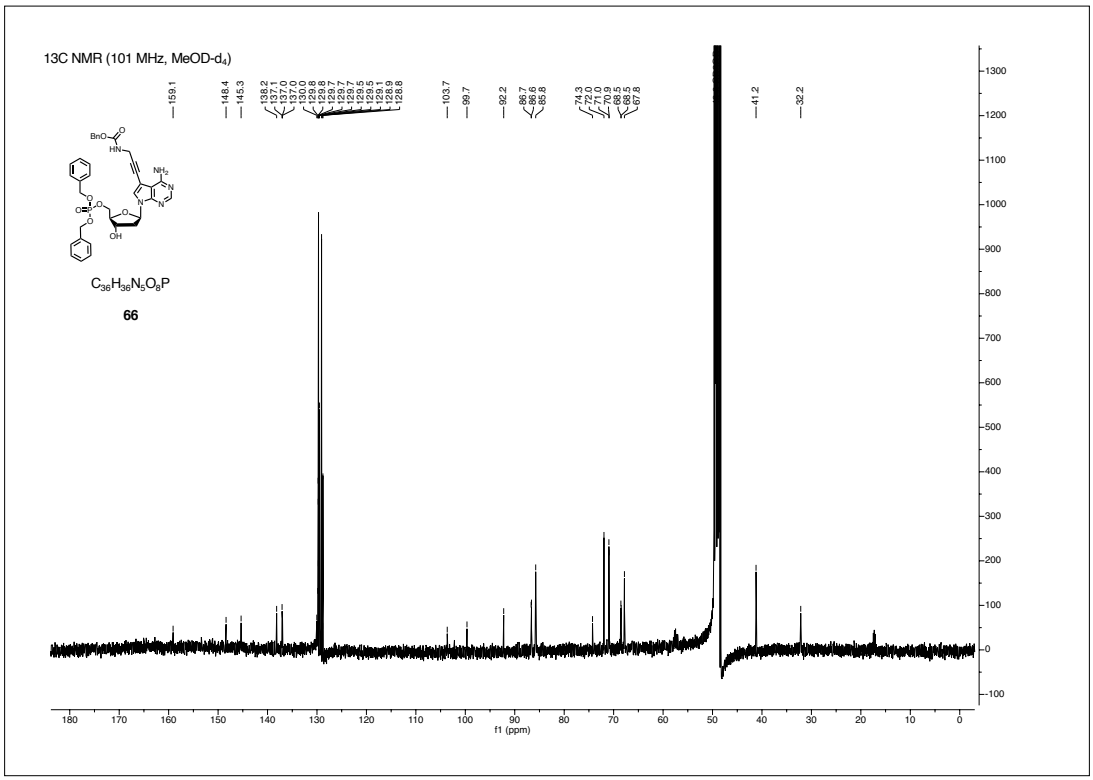

$C_{36}H_{36}N_5O_8P$

66

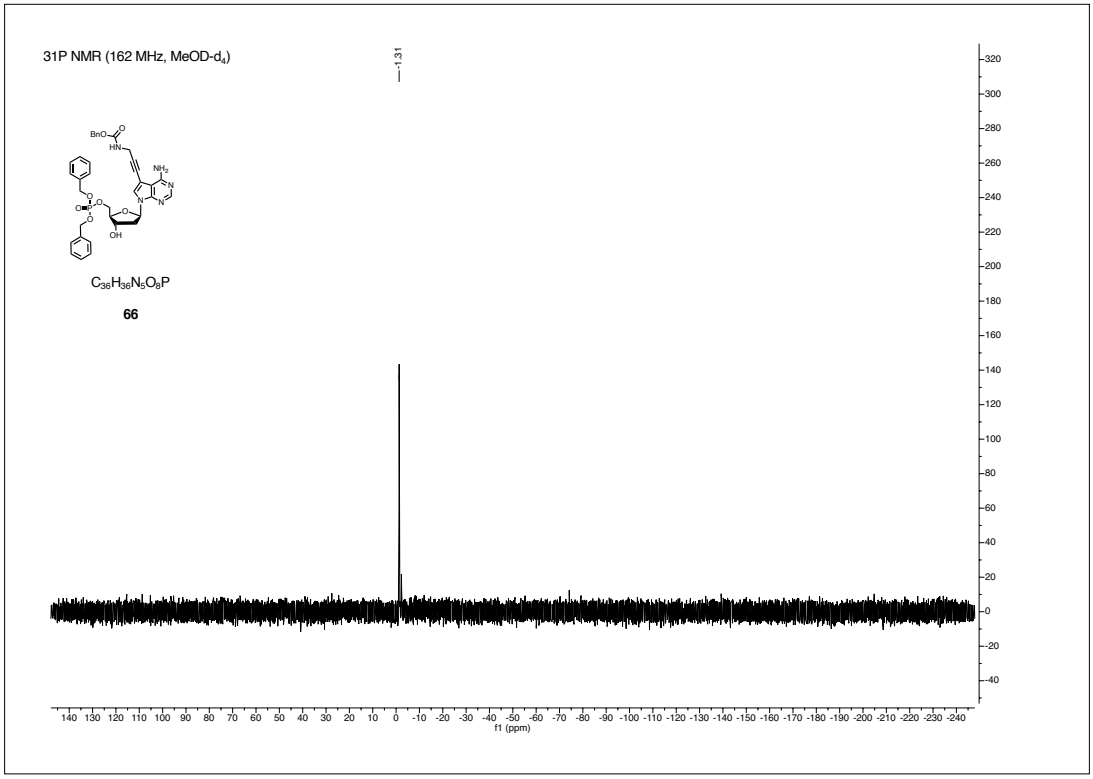

$C_{36}H_{36}N_5O_8P$

66

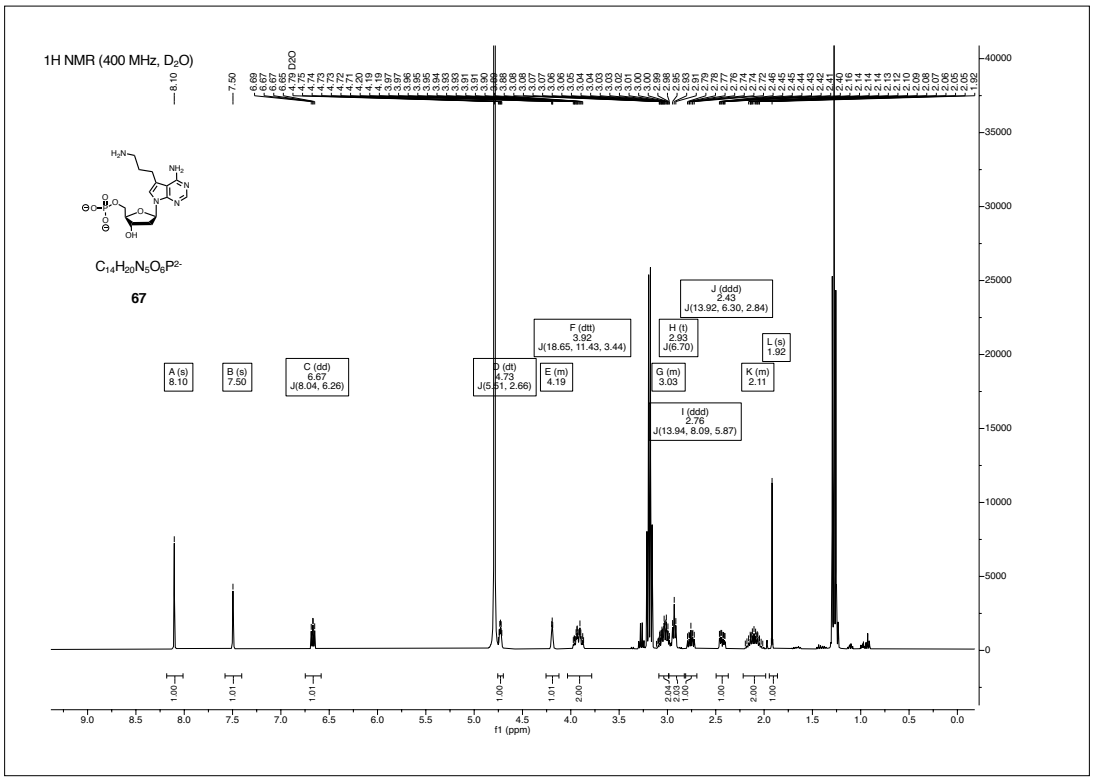

$C_{14}H_{20}N_5O_8P^{2-}$

67

13C NMR (101 MHz, D_2O)

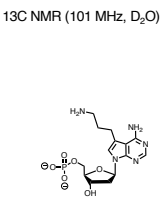

$C_{14}H_{20}N_5O_6P^{2-}$

67

31P NMR (162 MHz, D_2O)

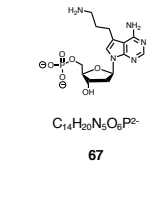

$C_{14}H_{20}N_5O_6P^{2-}$

67

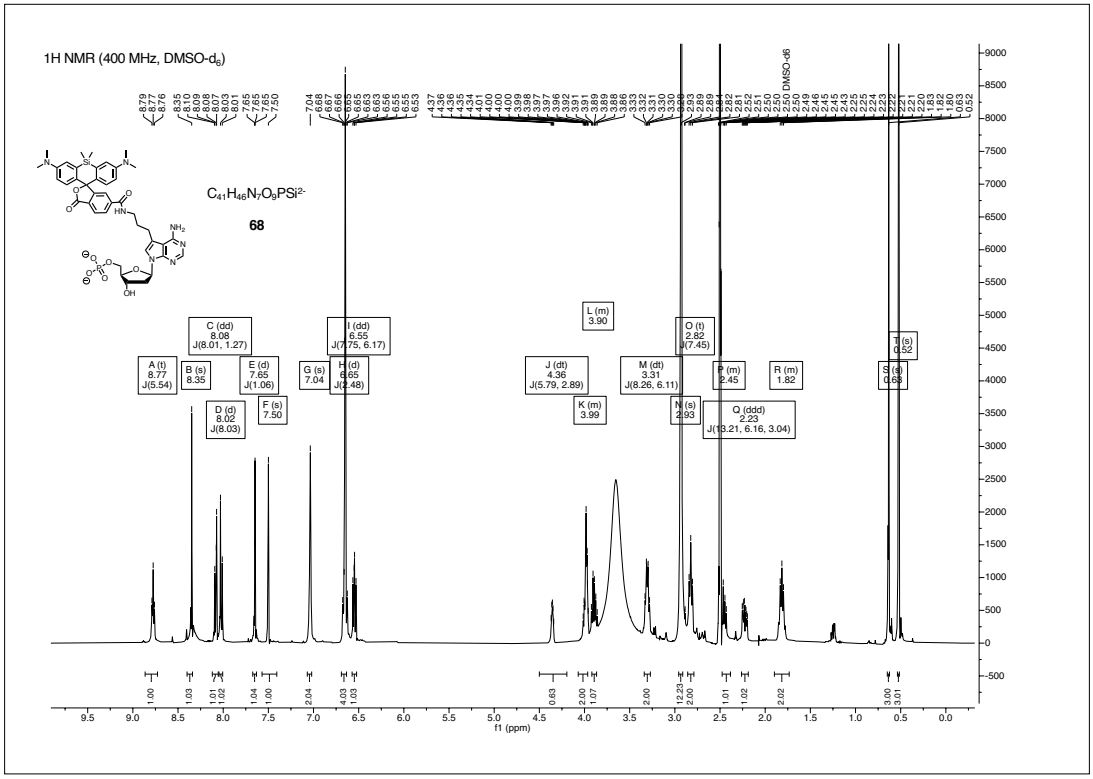
1H NMR (400 MHz, DMSO-d6)
C41H46N7O9PSi2-
68
A (t) 8.77 J(5.54)
B (s) 8.35
C (dd) 8.08 J(8.01, 1.27)
D (d) 8.02 J(8.03)
E (d) 7.65 J(1.06)
F (s) 7.50
G (s) 7.04
H (d) 6.65 J(2.48)
I (dd) 6.55 J(7.75, 6.17)
J (dt) 4.36 J(5.79, 2.89)
K (m) 3.99
L (m) 3.90
M (dt) 3.31 J(8.26, 6.11)
N (s) 2.93
O (t) 2.82 J(7.45)
P (m) 2.45
Q (ddd) 2.23 J(13.21, 6.16, 3.04)
R (m) 1.82
S (s) 0.63
T (s) 0.52
DMSO-d6
f1 (ppm)

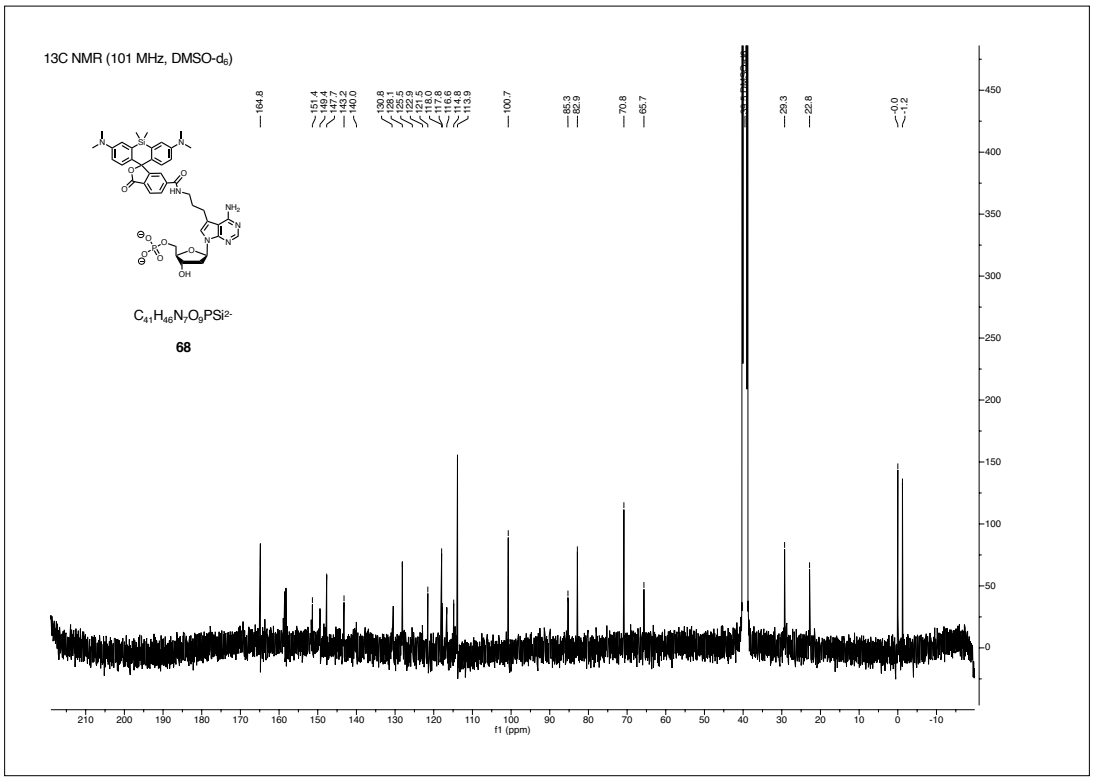
13C NMR (101 MHz, DMSO-d6)
C41H46N7O9PSi2-
68
164.8
151.4
149.4
147.7
143.2
140.0
130.8
128.1
125.5
122.9
121.5
118.0
117.7
116.6
114.8
113.9
100.7
85.3
82.9
70.8
65.7
29.3
22.8
0.0
-1.2
f1 (ppm)

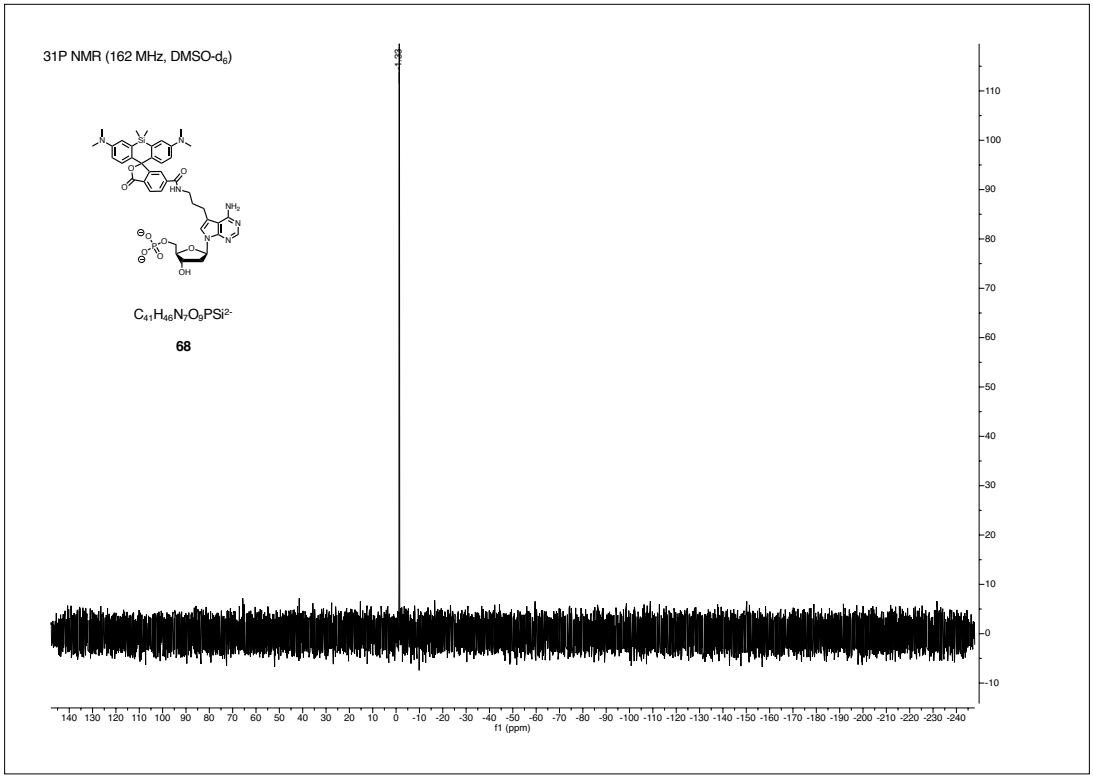

$C_{41}H_{46}N_7O_9PSi^{2-}$

68

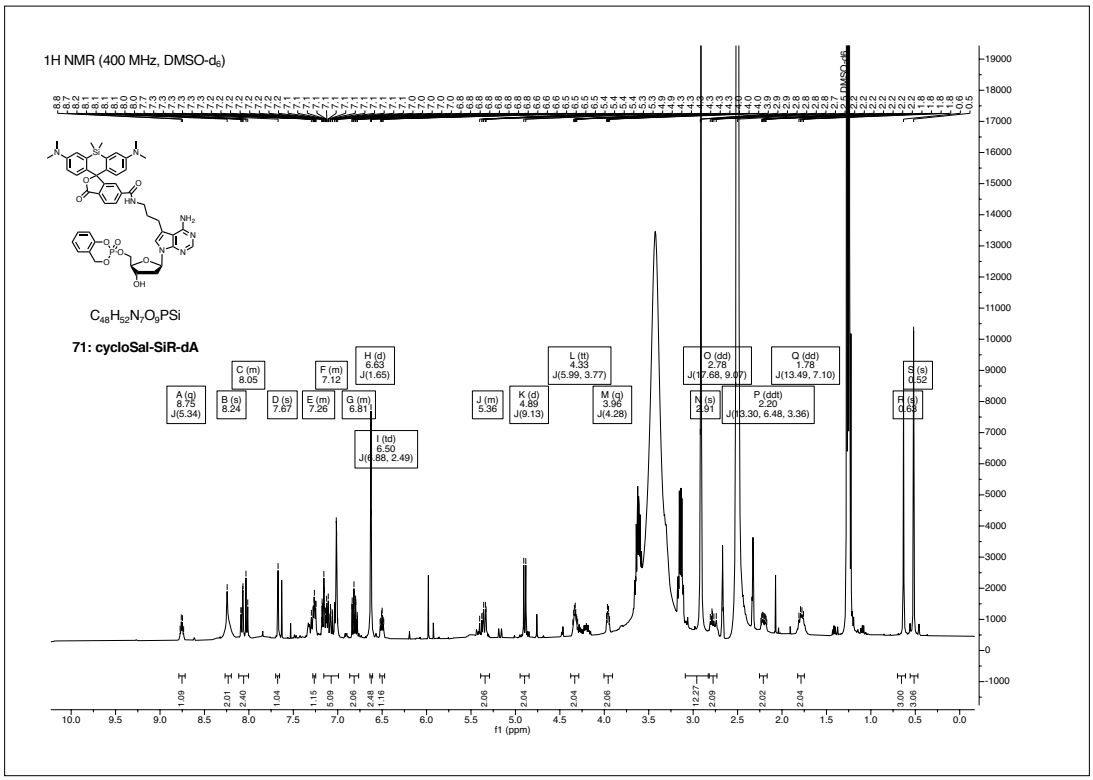

$C_{48}H_{52}N_7O_9PSi$

71: cycloSal-SiR-dA

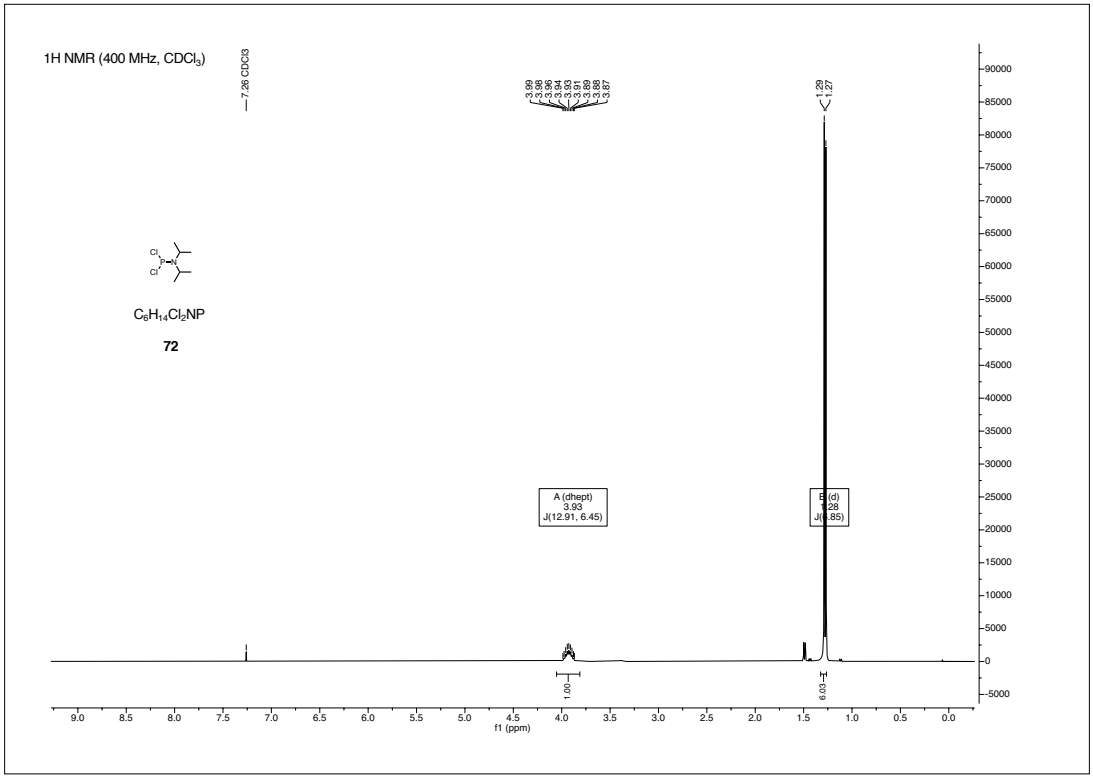
1H NMR (400 MHz, CDCl3)
7.26 CDCl3
3.99
3.98
3.96
3.94
3.93
3.91
3.89
3.88
3.87
1.29
1.27
C6H14Cl2NP
72
A (dhept)
3.93
J(12.91, 6.45)
B (d)
1.28
J(6.85)
1.00
6.03
f1 (ppm)

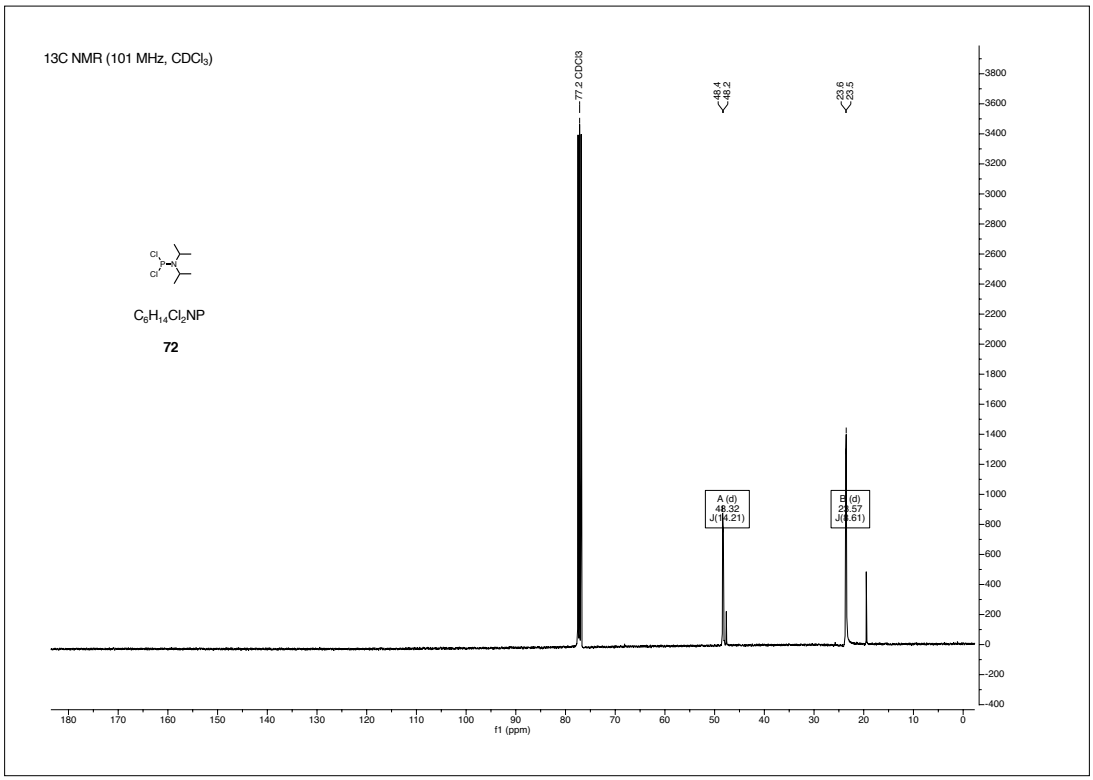
13C NMR (101 MHz, CDCl3)
77.2 CDCl3
48.4
48.2
23.6
23.5
C6H14Cl2NP
72
A (d)
48.32
J(14.21)
B (d)
23.57
J(6.61)
f1 (ppm)

31P NMR (162 MHz, CDCl3)

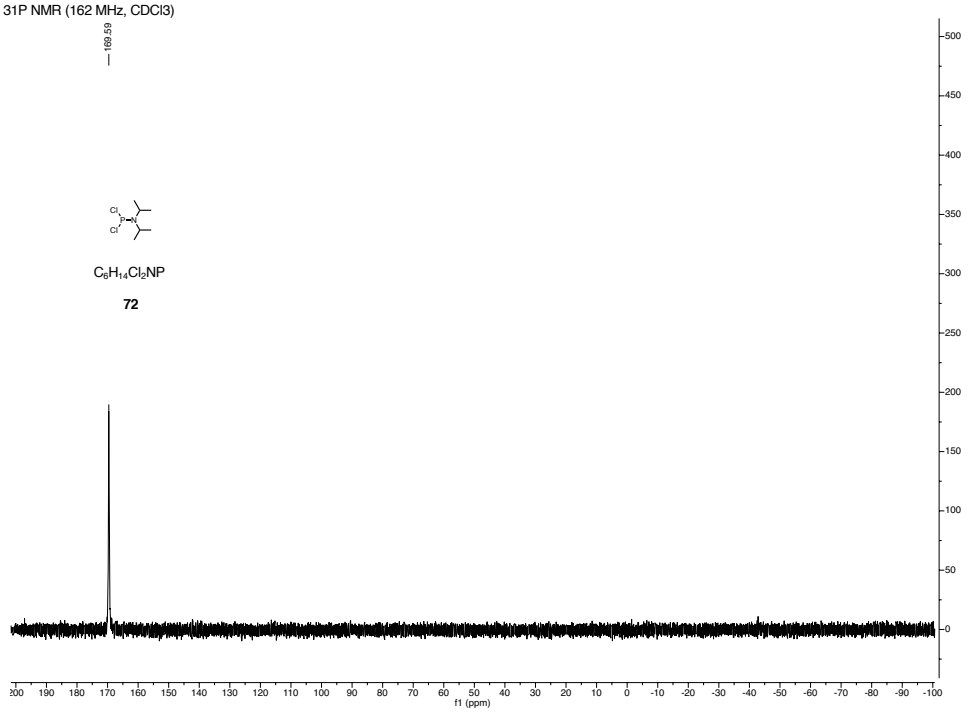

$C_6H_{14}Cl_2NP$

72

1H NMR (400 MHz, $CDCl_3$)

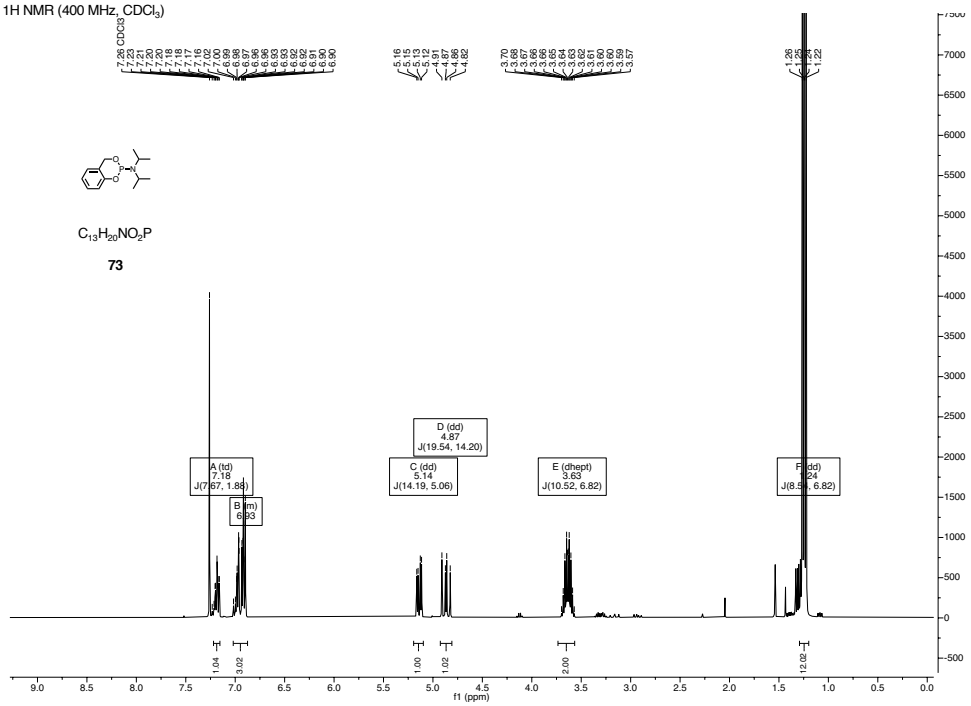

$C_{13}H_{20}NO_2P$

73

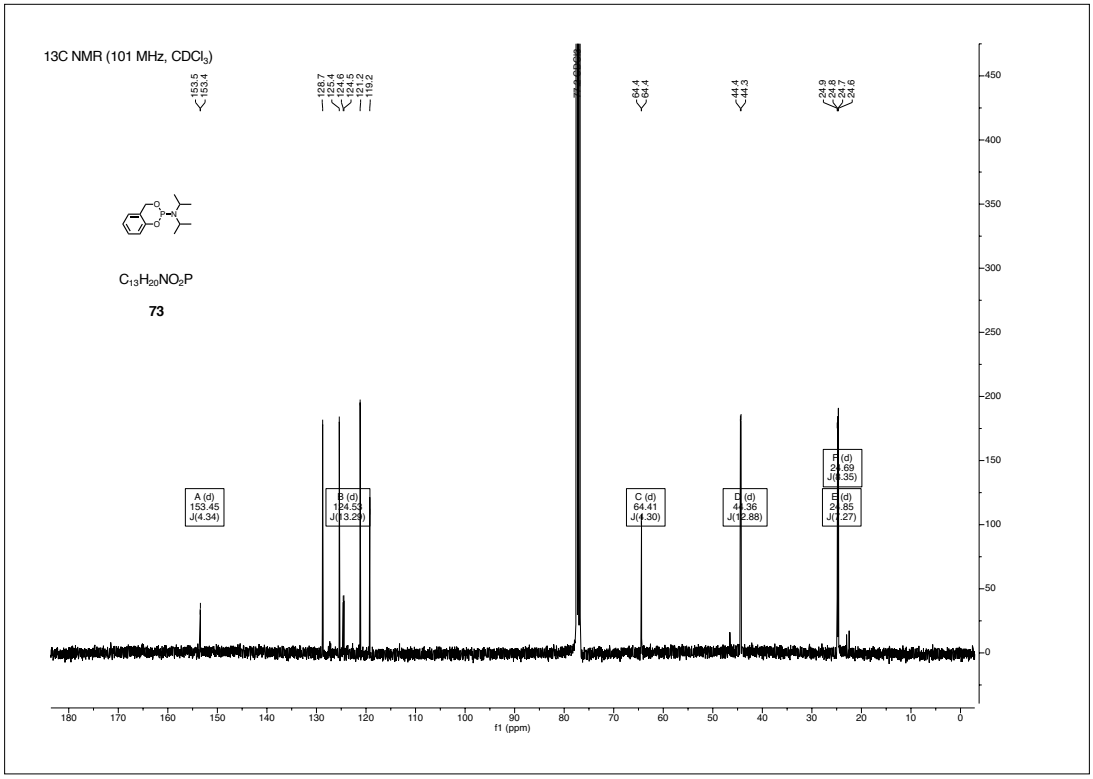
13C NMR (101 MHz, CDCl3)
153.5
153.4
128.7
125.4
124.6
124.5
121.2
119.2
64.4
64.4
44.4
44.3
24.9
24.8
24.7
24.6
C13H20NO2P
73
A (d)
153.45
J(4.34)
B (d)
124.53
J(13.29)
C (d)
64.41
J(4.30)
D (d)
44.36
J(12.88)
F (d)
24.69
J(8.35)
E (d)
24.85
J(7.27)
f1 (ppm)

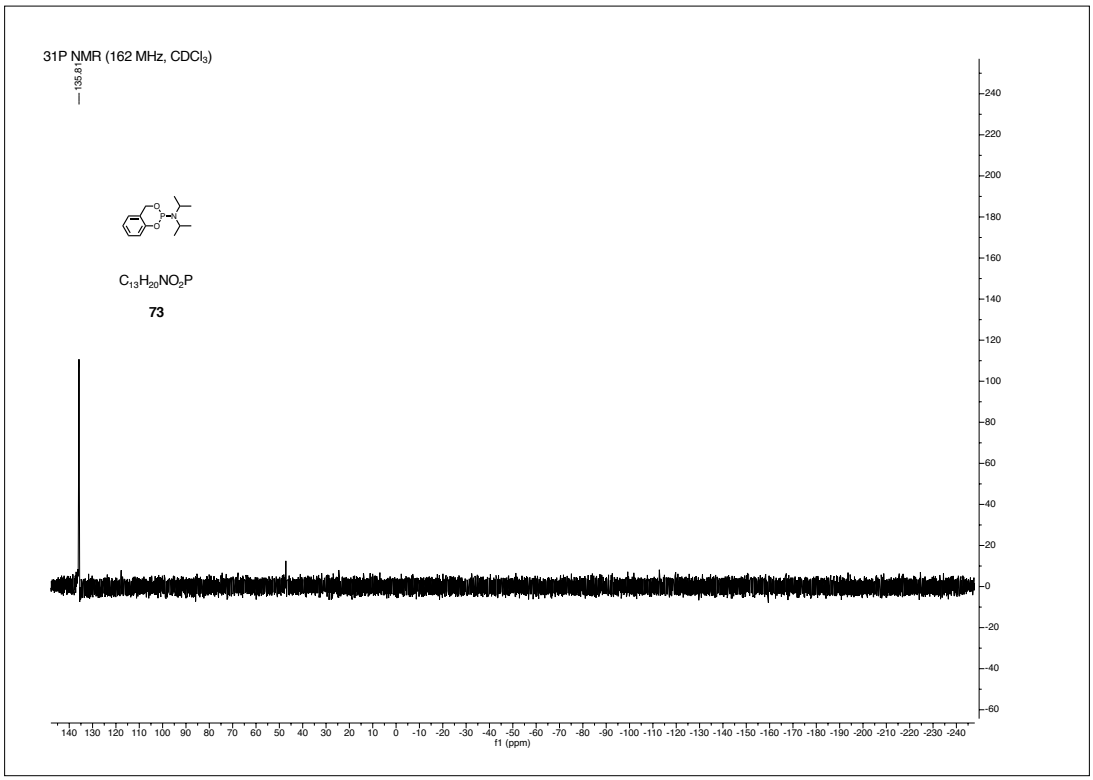
31P NMR (162 MHz, CDCl3)
135.81
C13H20NO2P
73
f1 (ppm)

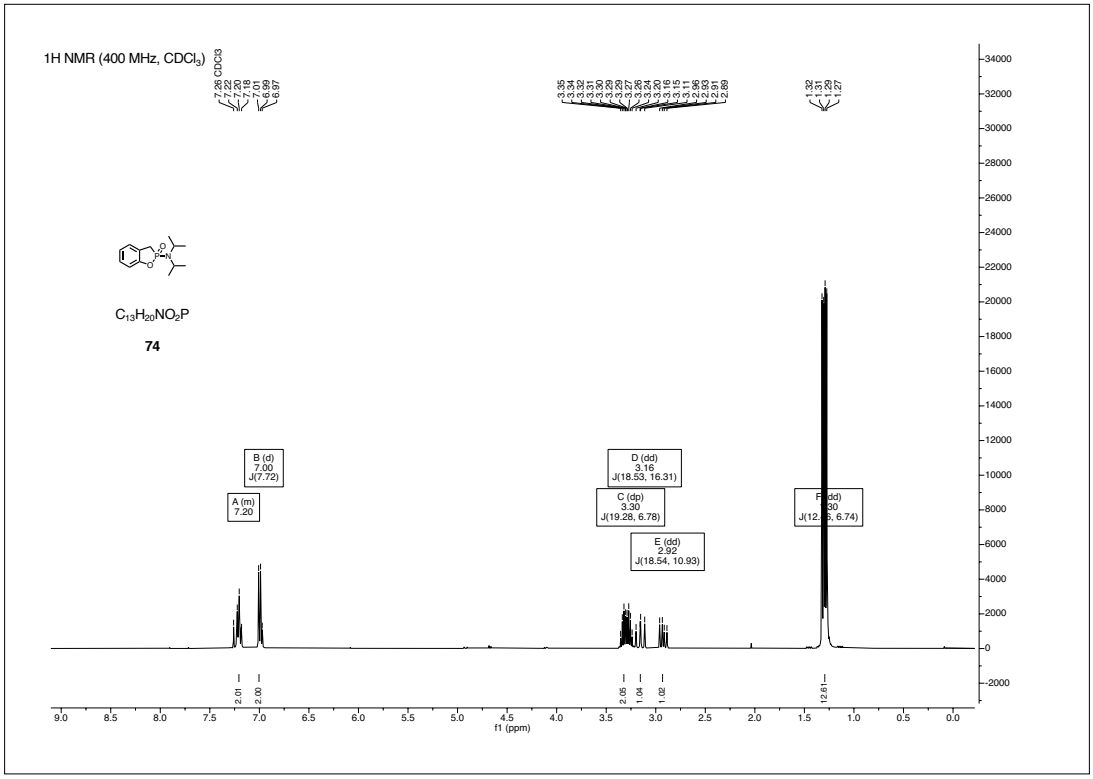
1H NMR (400 MHz, CDCl3)
C13H20NO2P
74
A (m)
7.20
B (d)
7.00
J(7.72)
C (dp)
3.30
J(19.28, 6.78)
D (dd)
3.16
J(18.53, 16.31)
E (dd)
2.92
J(18.54, 10.93)
f1 (ppm)

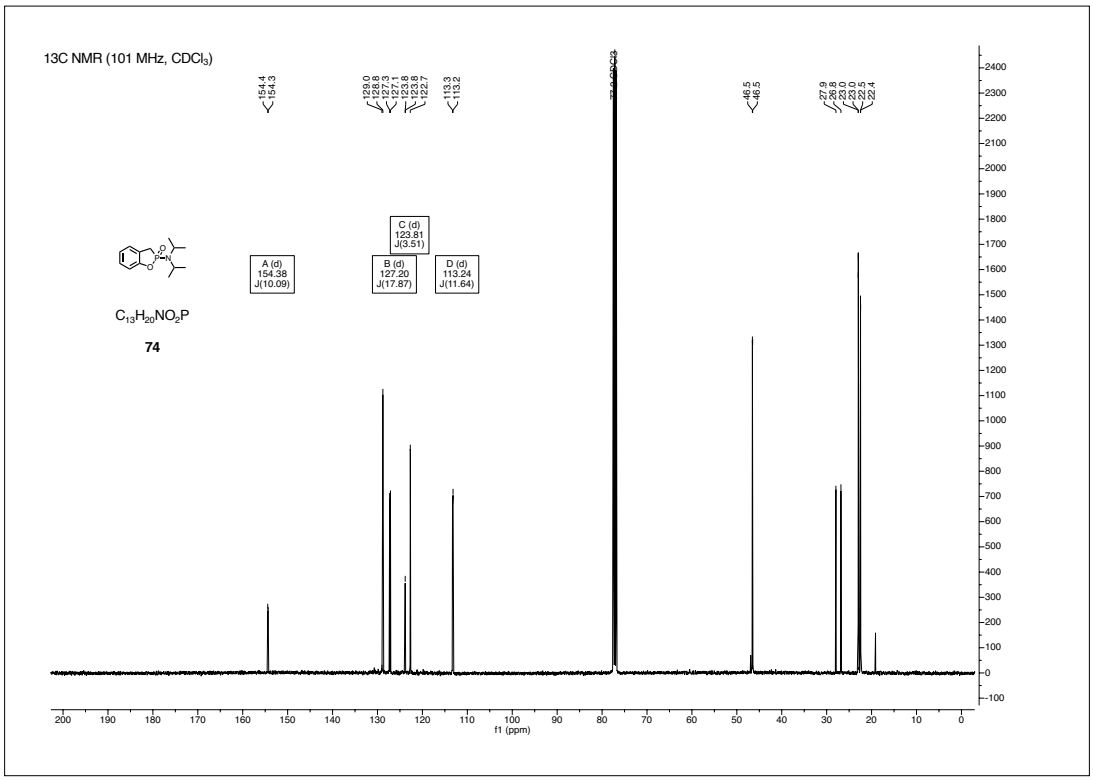
13C NMR (101 MHz, CDCl3)
C13H20NO2P
74
A (d)
154.38
J(10.09)
B (d)
127.20
J(17.87)
C (d)
123.81
J(3.51)
D (d)
113.24
J(11.64)
f1 (ppm)

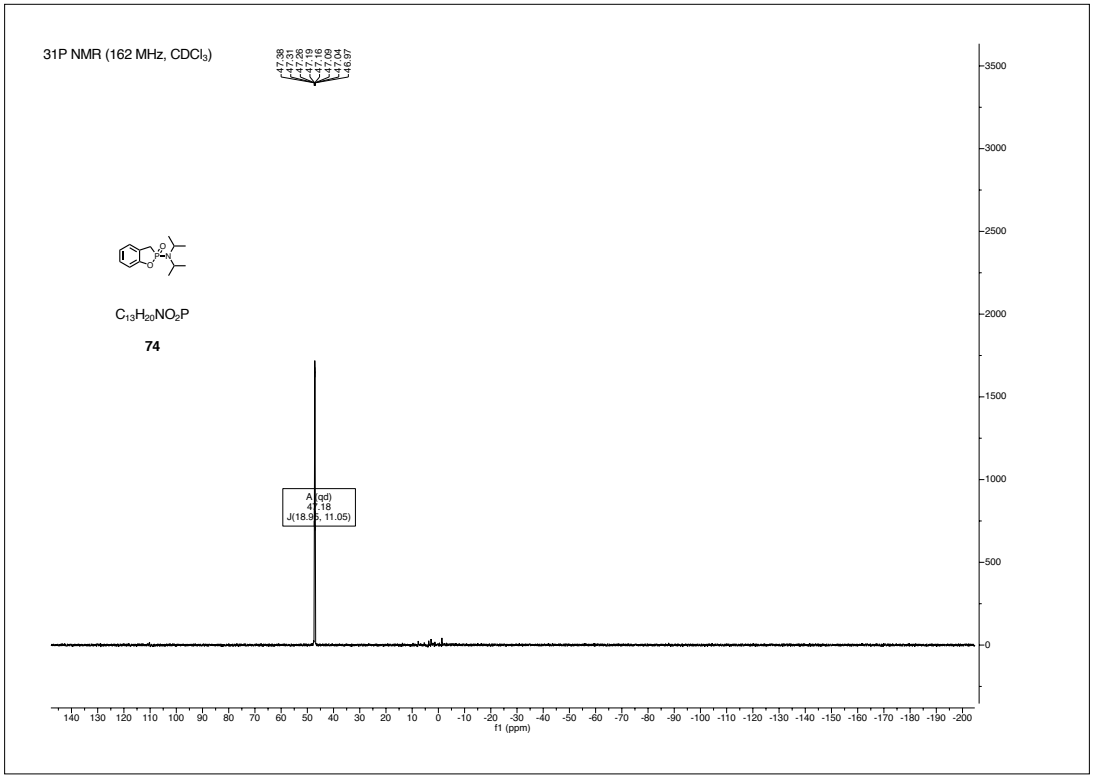
31P NMR (162 MHz, CDCl3)
47.38
47.31
47.26
47.19
47.18
47.16
47.09
47.04
46.97
C13H20NO2P
74
A (qd)
47.18
J(18.95, 11.05)
f1 (ppm)

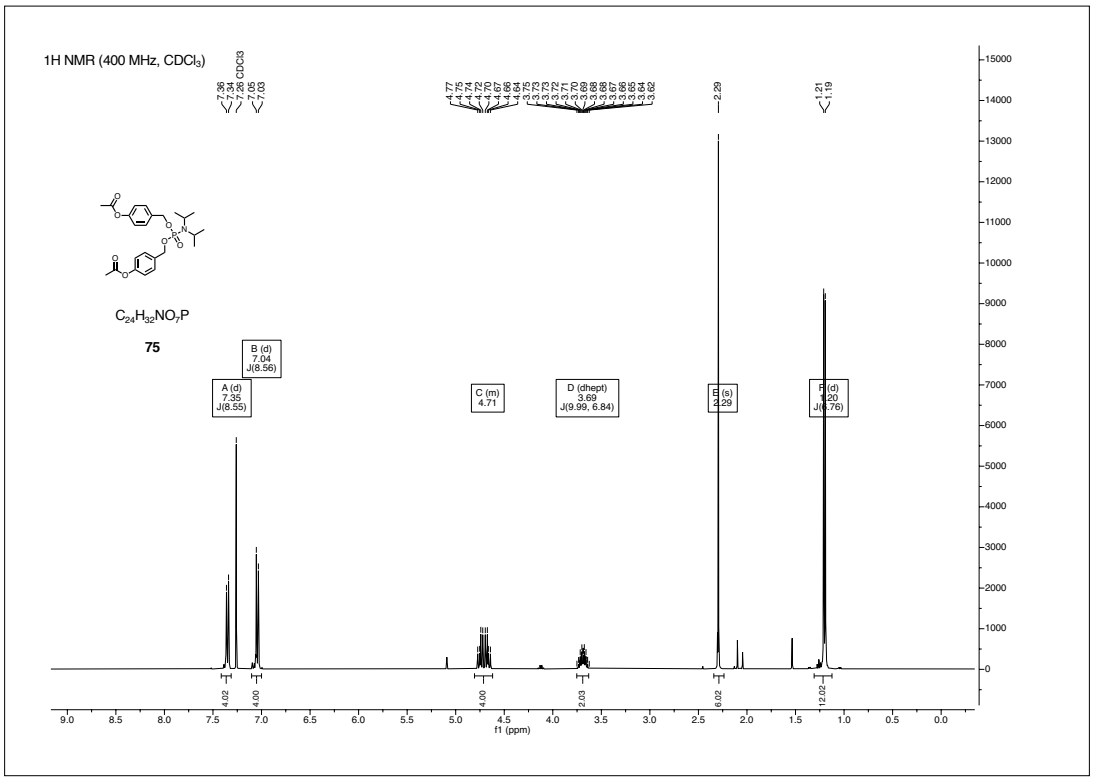
1H NMR (400 MHz, CDCl3)
7.36
7.34
CDCl3
7.05
7.03
4.77
4.75
4.74
4.72
4.70
4.67
4.66
4.64
3.75
3.73
3.72
3.71
3.70
3.69
3.68
3.67
3.66
3.65
3.64
3.62
2.29
1.21
1.19
C24H32NO7P
75
A (d)
7.35
J(8.55)
B (d)
7.04
J(8.56)
C (m)
4.71
D (dhept)
3.69
J(9.99, 6.84)
E (s)
2.29
F (d)
1.20
J(6.76)
4.02
4.00
4.00
2.03
6.02
12.02
f1 (ppm)

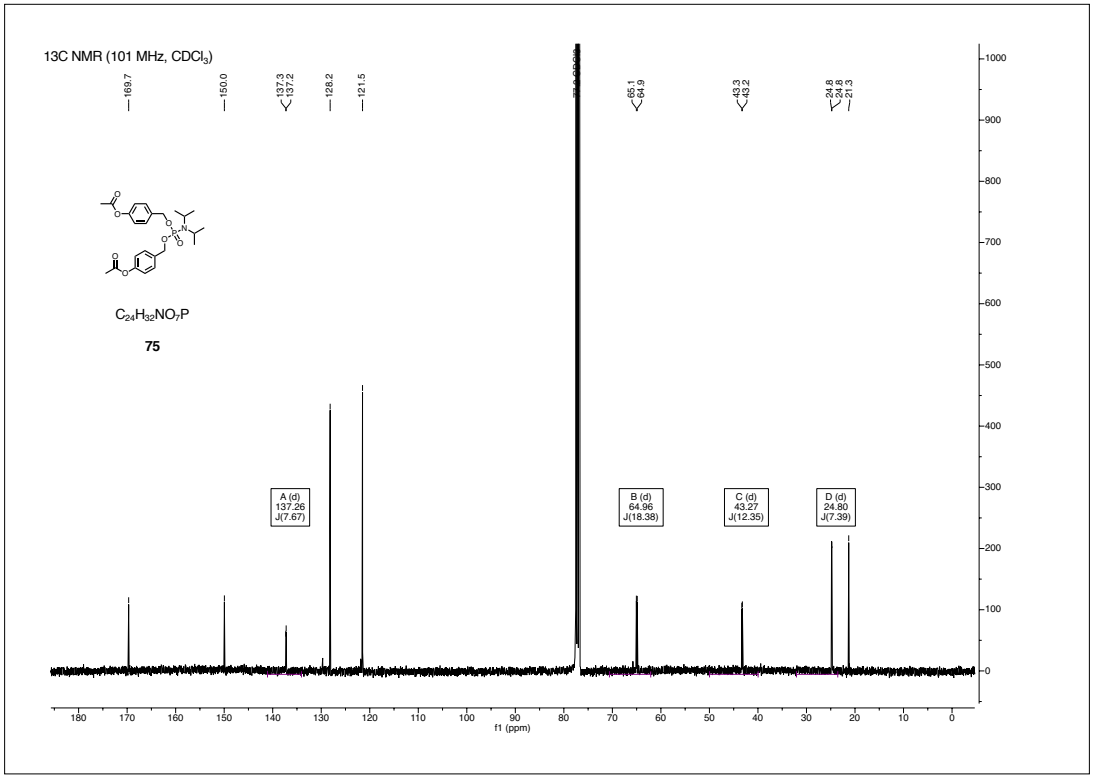
13C NMR (101 MHz, CDCl3)
169.7
150.0
137.3
137.2
128.2
121.5
65.1
64.9
43.3
43.2
24.8
24.8
21.3
A (d)
137.26
J(7.67)
B (d)
64.96
J(18.38)
C (d)
43.27
J(12.35)
D (d)
24.80
J(7.39)
C24H32NO7P
75
f1 (ppm)

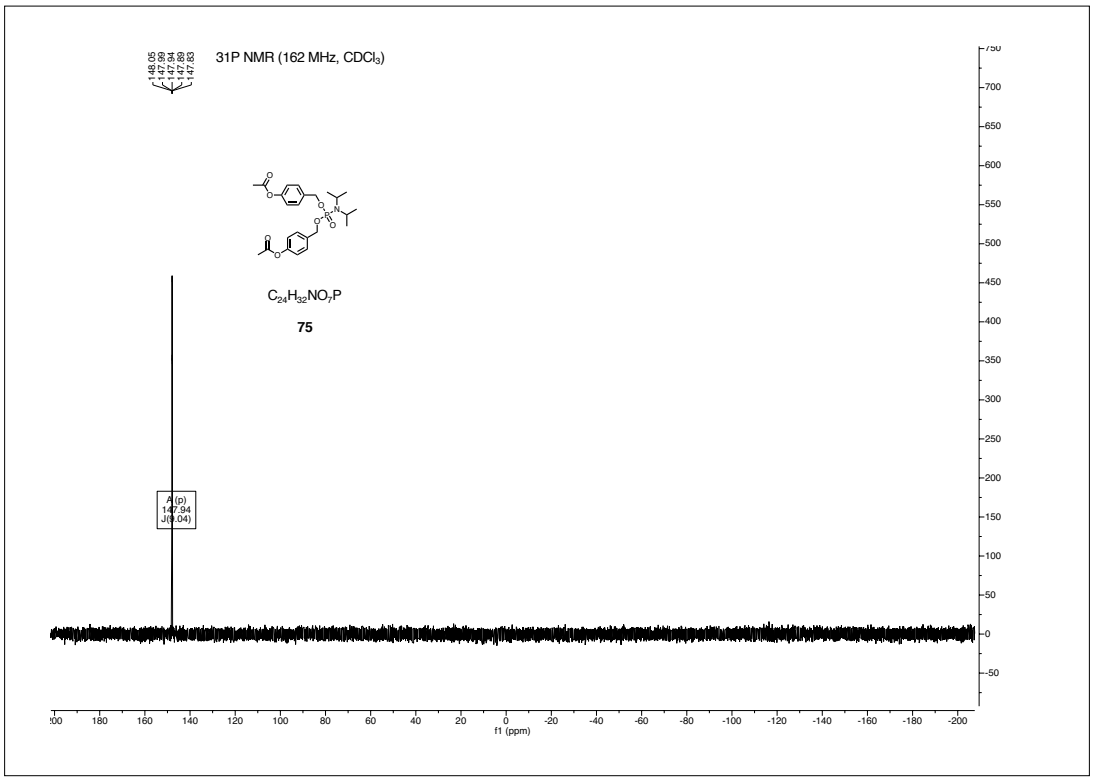
31P NMR (162 MHz, CDCl3)
148.05
147.99
147.94
147.89
147.83
A (p)
147.94
J(9.04)
C24H32NO7P
75
f1 (ppm)

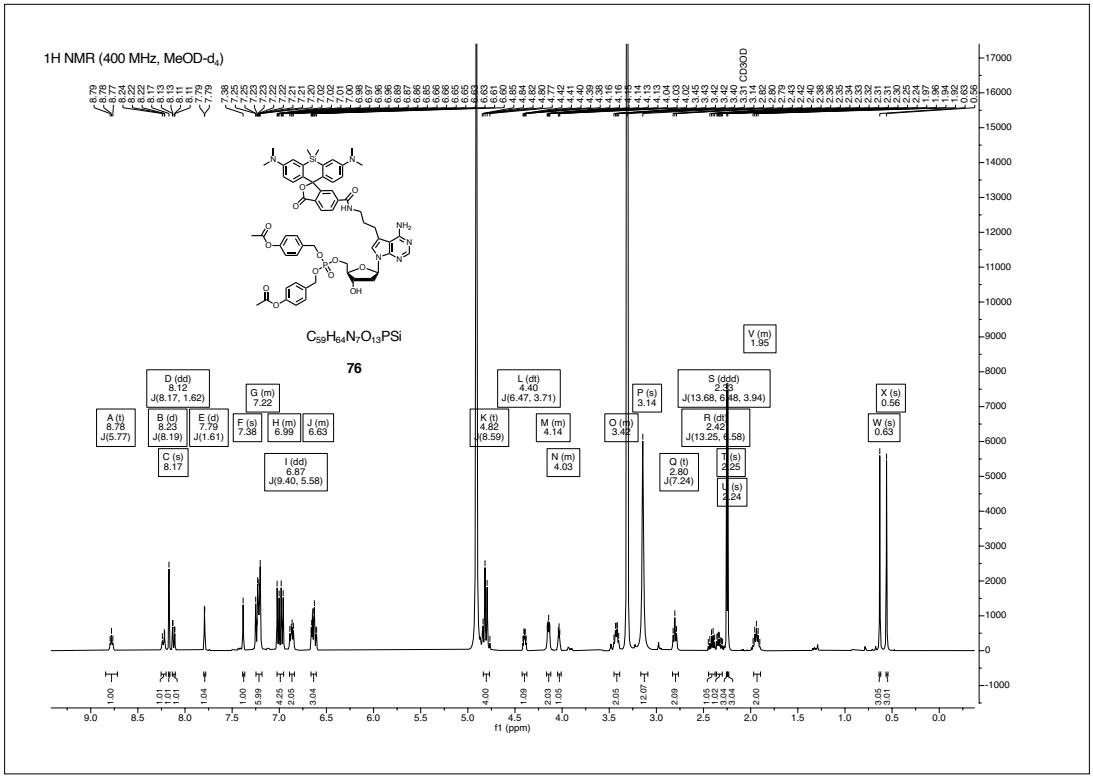
1H NMR (400 MHz, MeOD-d4)
CD3OD
C59H64N7O13PSi
76
A (t) 8.78 J(5.77)
B (d) 8.23 J(8.19)
C (s) 8.17
D (dd) 8.12 J(8.17, 1.62)
E (d) 7.79 J(1.61)
F (s) 7.38
G (m) 7.22
H (m) 6.99
I (dd) 6.87 J(9.40, 5.58)
J (m) 6.63
K (t) 4.82 J(8.59)
L (dt) 4.40 J(6.47, 3.71)
M (m) 4.14
N (m) 4.03
O (m) 3.42
P (s) 3.14
Q (t) 2.80 J(7.24)
R (dt) 2.42 J(13.25, 6.58)
S (ddd) 2.45 J(13.68, 6.48, 3.94)
T (s) 2.25
U (s) 2.24
V (m) 1.95
W (s) 0.63
X (s) 0.56
f1 (ppm)

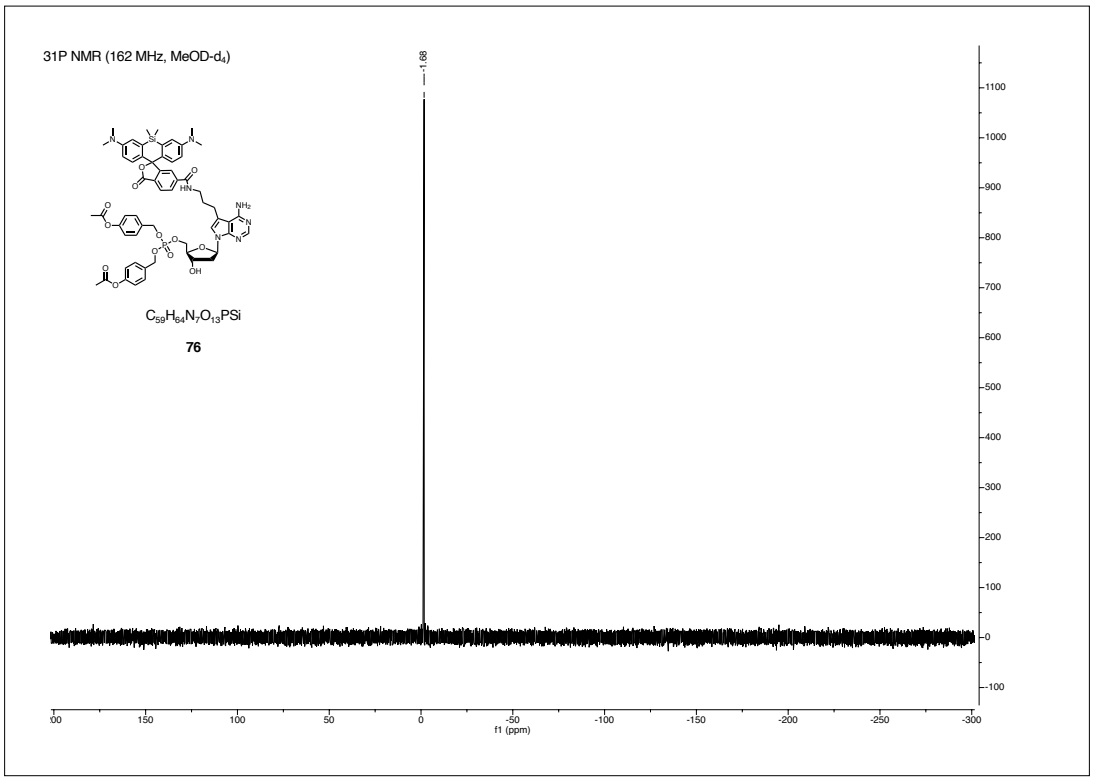
31P NMR (162 MHz, MeOD-d4)
-1.68
C59H64N7O13PSi
76
f1 (ppm)

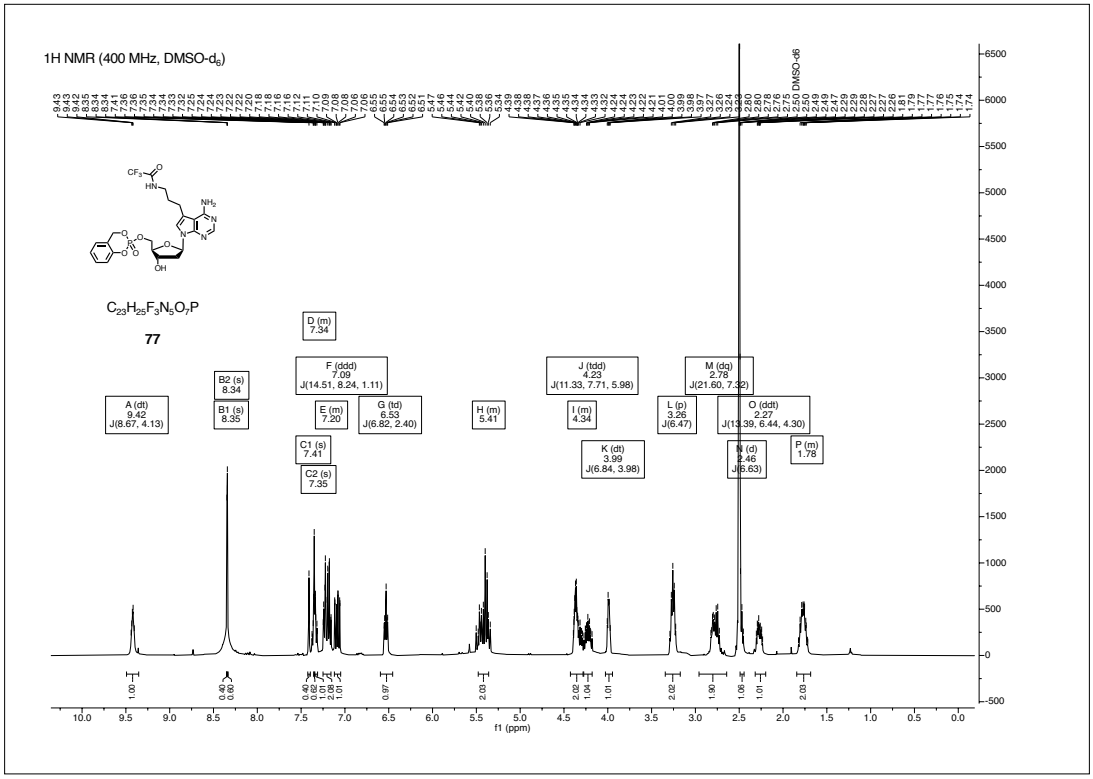
1H NMR (400 MHz, DMSO-d6)
C23H25F3N5O7P
77
A (dt) 9.42 J(8.67, 4.13)
B1 (s) 8.35
B2 (s) 8.34
C1 (s) 7.41
C2 (s) 7.35
D (m) 7.34
E (m) 7.20
F (ddd) 7.09 J(14.51, 8.24, 1.11)
G (td) 6.53 J(6.82, 2.40)
H (m) 5.41
I (m) 4.34
J (tdd) 4.23 J(11.33, 7.71, 5.98)
K (dt) 3.99 J(6.84, 3.98)
L (p) 3.26 J(6.47)
M (dq) 2.78 J(21.60, 7.32)
N (d) 2.46 J(5.63)
O (ddt) 2.27 J(13.39, 6.44, 4.30)
P (m) 1.78
DMSO-d6
f1 (ppm)

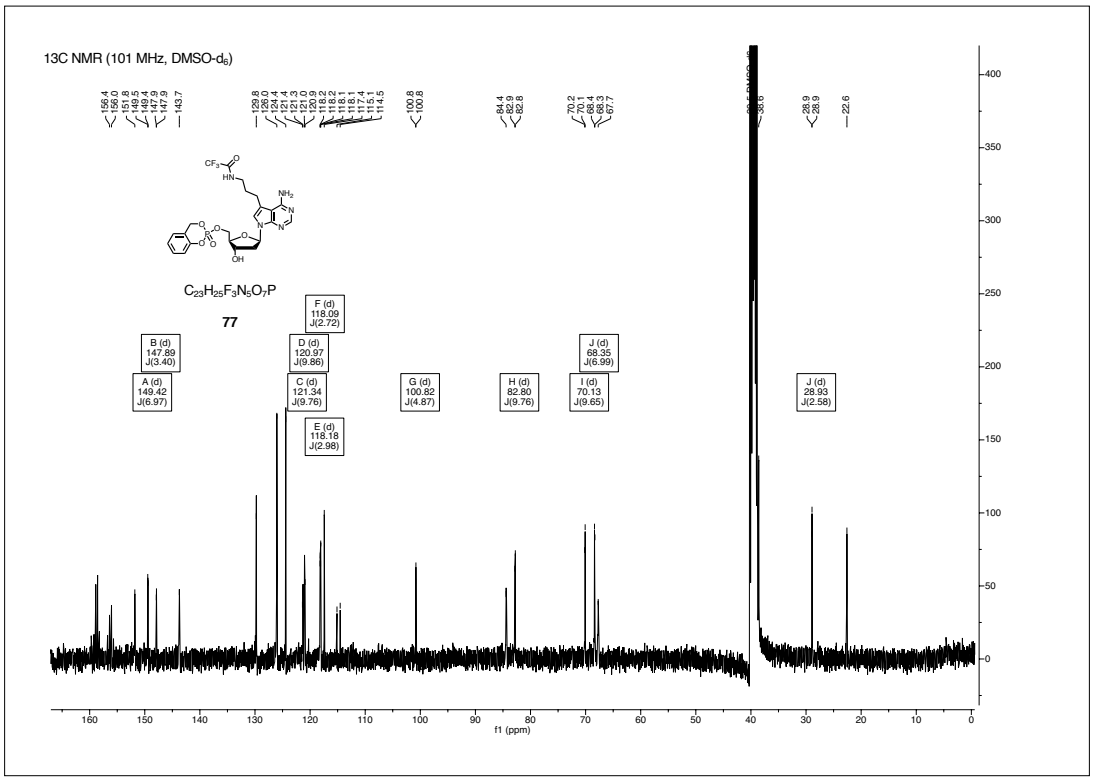
13C NMR (101 MHz, DMSO-d6)
C23H25F3N5O7P
77
A (d) 149.42 J(6.97)
B (d) 147.89 J(3.40)
C (d) 121.34 J(9.76)
D (d) 120.97 J(9.86)
E (d) 118.18 J(2.98)
F (d) 118.09 J(2.72)
G (d) 100.82 J(4.87)
H (d) 82.80 J(9.76)
I (d) 70.13 J(9.65)
J (d) 68.35 J(6.99)
J (d) 28.93 J(2.58)
DMSO-d6
f1 (ppm)

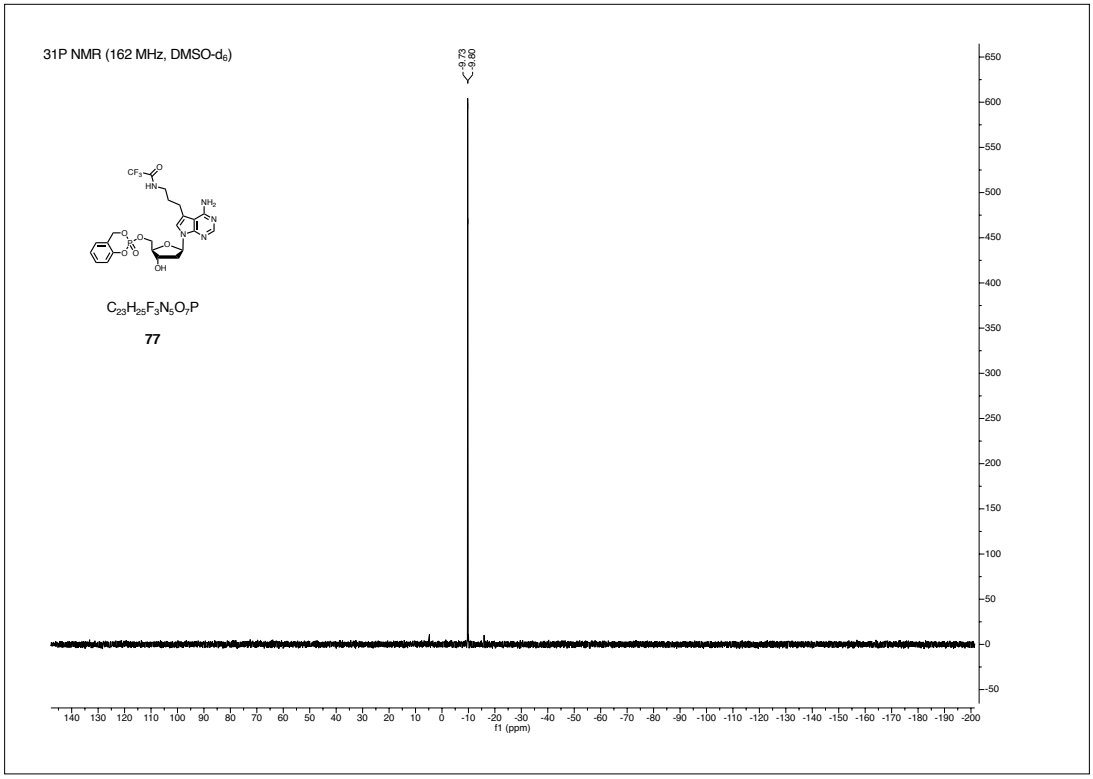

$C_{23}H_{25}F_3N_5O_7P$

77

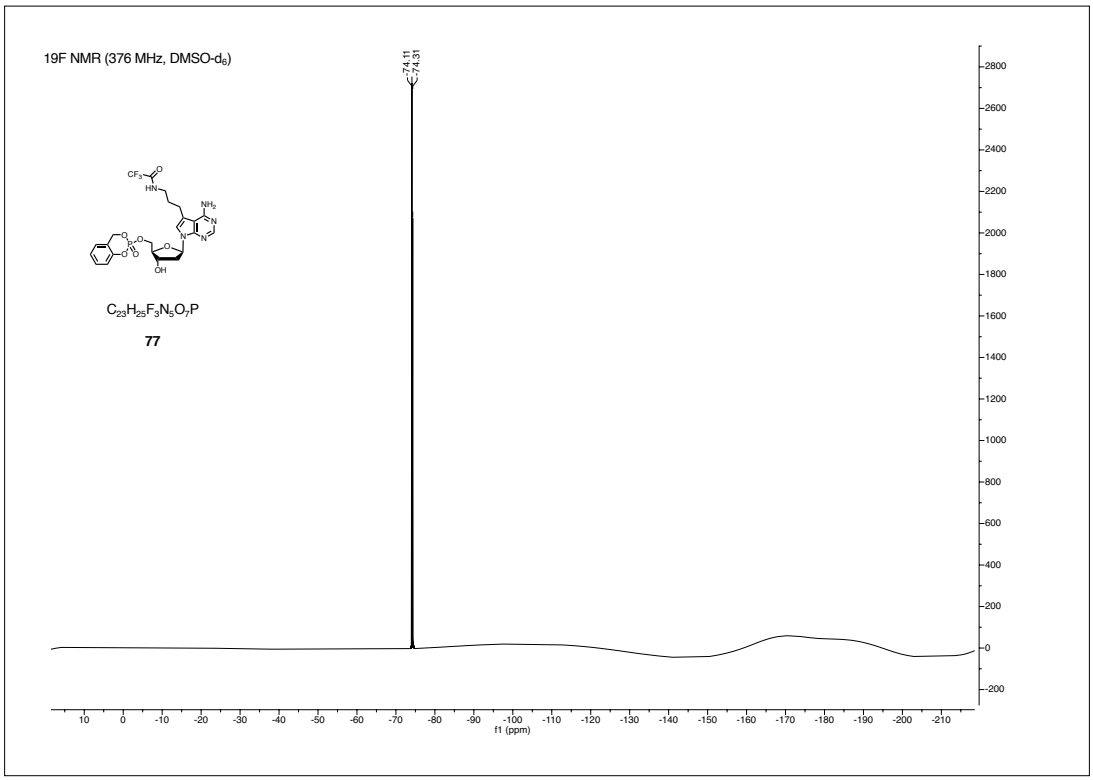

$C_{23}H_{25}F_3N_5O_7P$

77

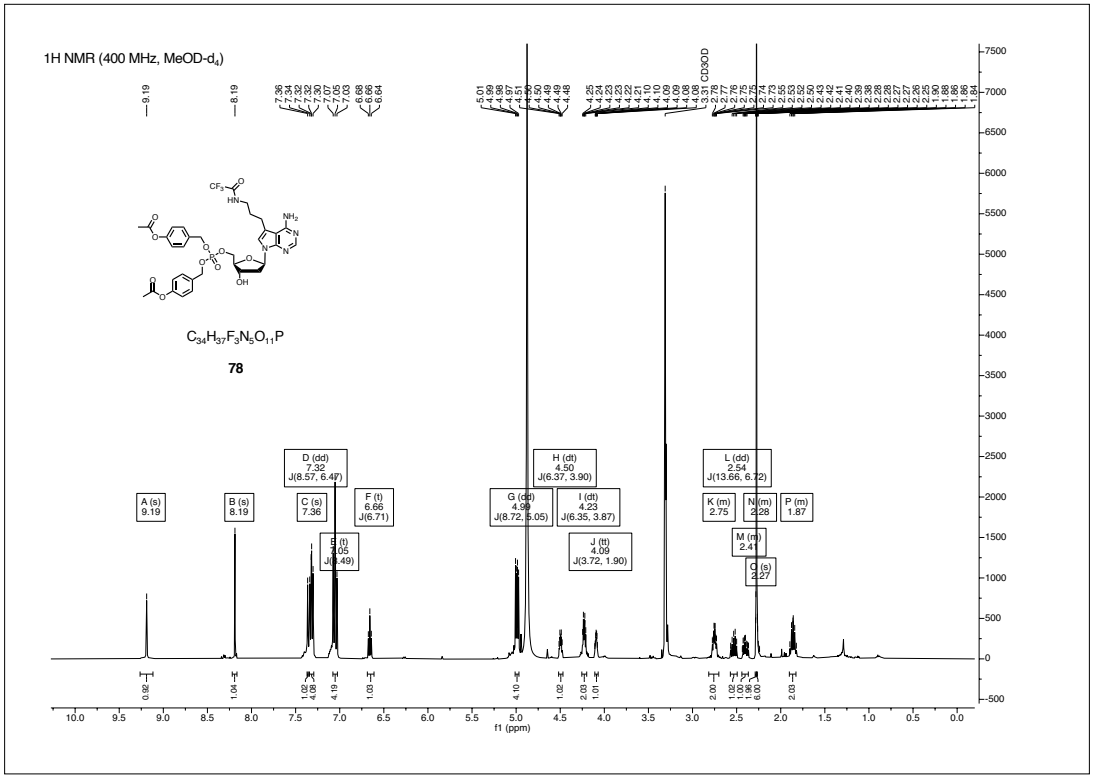
1H NMR (400 MHz, MeOD-d4)
C34H37F3N5O11P
78
A (s) 9.19
B (s) 8.19
C (s) 7.36
D (dd) 7.32 J(8.57, 6.47)
E (t) 7.05 J(0.49)
F (t) 6.66 J(6.71)
G (dd) 4.99 J(8.72, 5.05)
H (dt) 4.50 J(6.37, 3.90)
I (dt) 4.23 J(6.35, 3.87)
J (tt) 4.09 J(3.72, 1.90)
K (m) 2.75
N (m) 2.28
P (m) 1.87
M (m) 2.41
O (s) 2.27
L (dd) 2.54 J(13.66, 6.72)
f1 (ppm)

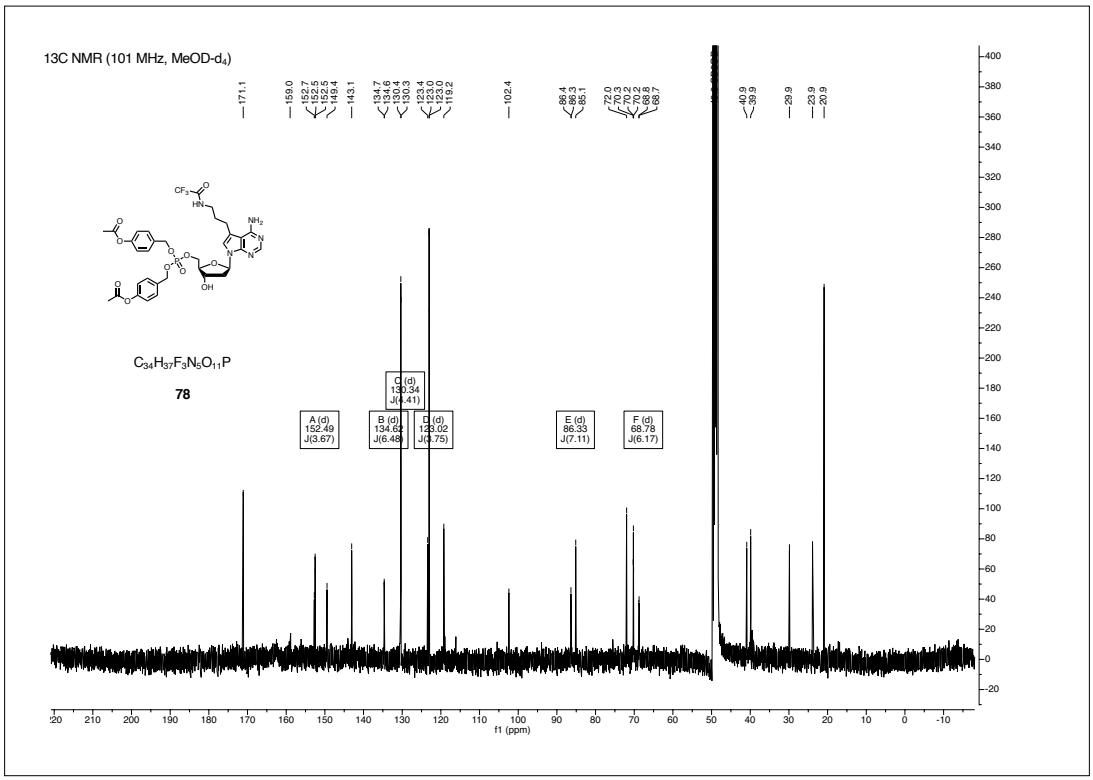
13C NMR (101 MHz, MeOD-d4)
C34H37F3N5O11P
78
A (d) 152.49 J(3.67)
B (d) 134.62 J(6.48)
C (d) 130.34 J(4.41)
D (d) 123.02 J(2.75)
E (d) 86.33 J(7.11)
F (d) 68.78 J(6.17)
f1 (ppm)

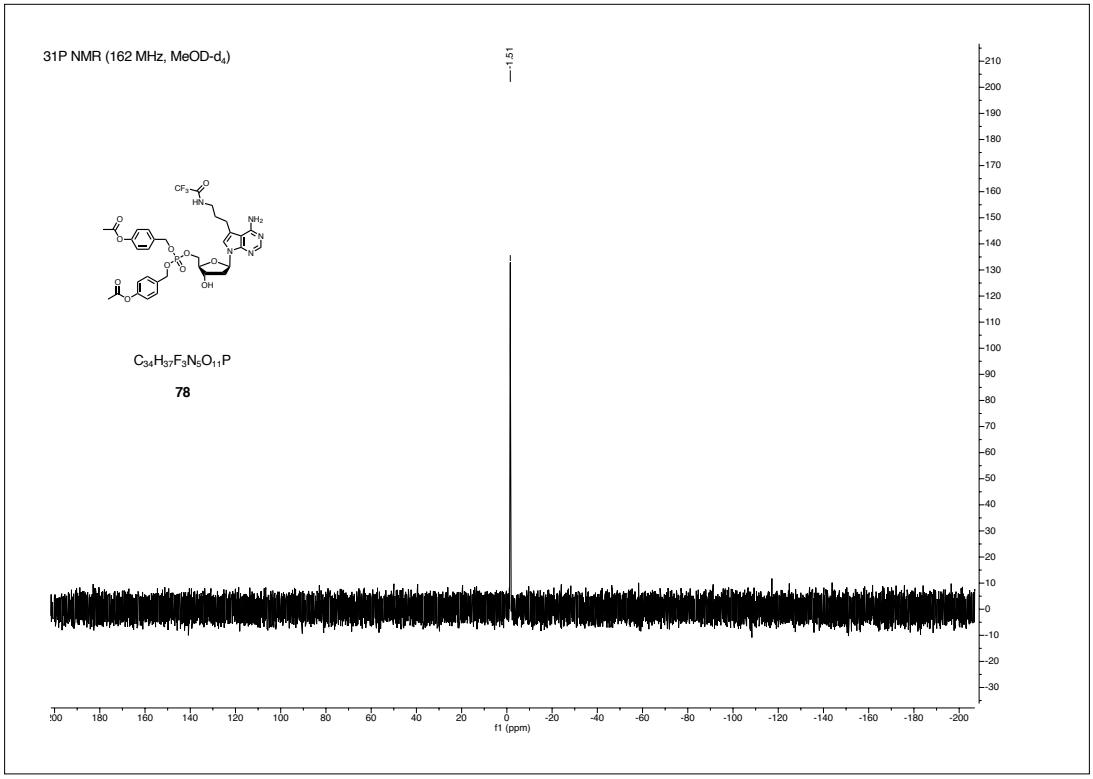

$C_{34}H_{37}F_3N_5O_{11}P$

78

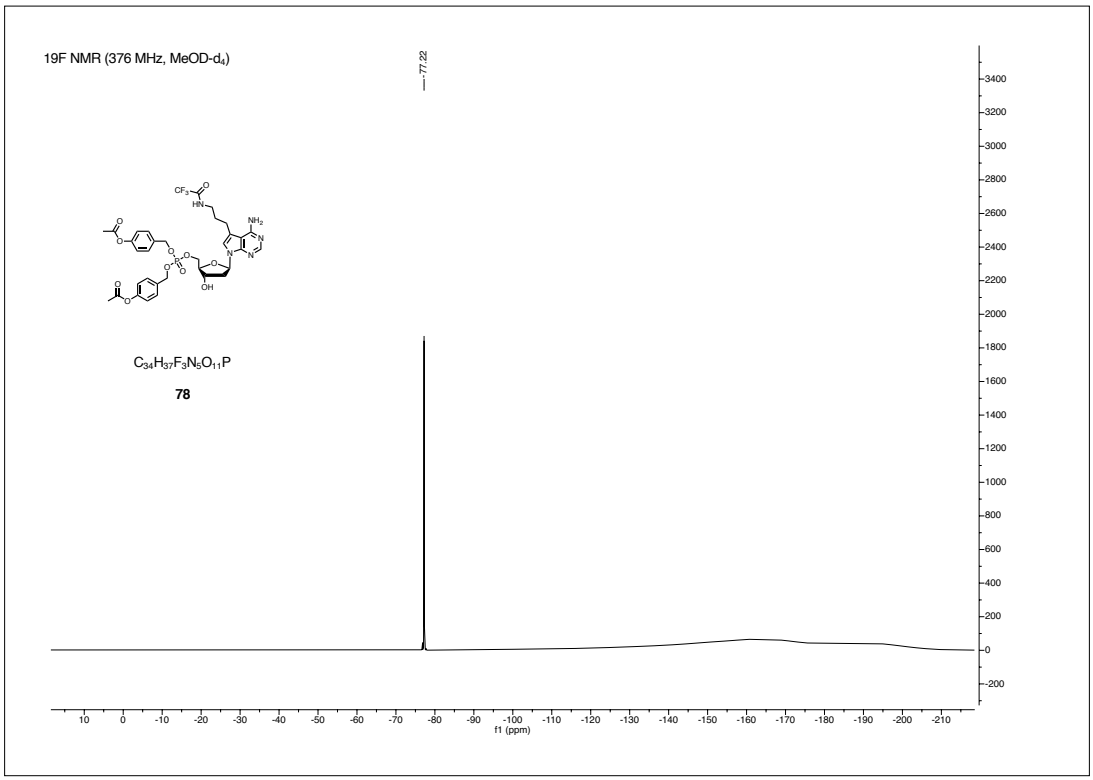

$C_{34}H_{37}F_3N_5O_{11}P$

78

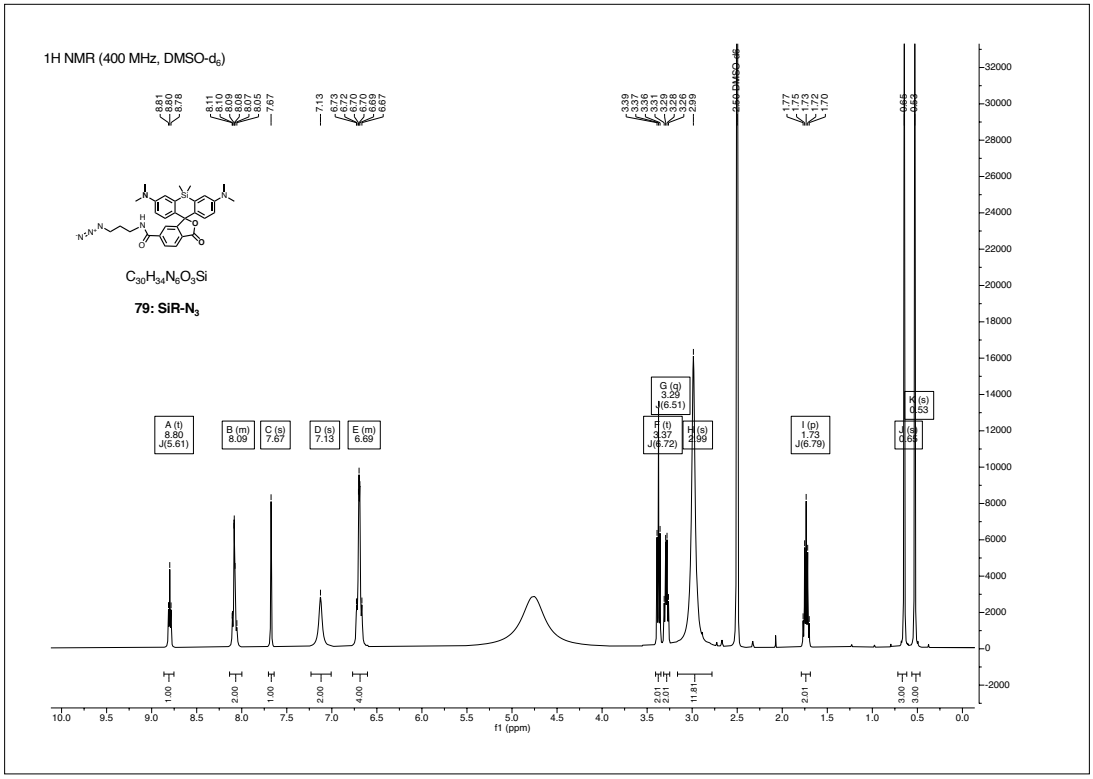
1H NMR (400 MHz, DMSO-d6)
C30H34N6O3Si
79: SiR-N3
A (t) 8.80 J(5.61)
B (m) 8.09
C (s) 7.87
D (s) 7.12
E (m) 6.89
F (t) 3.37 J(6.72)
G (q) 3.29 J(6.51)
H (s) 2.99
I (p) 1.73 J(6.79)
J (s) 0.65
K (s) 0.53
f1 (ppm)

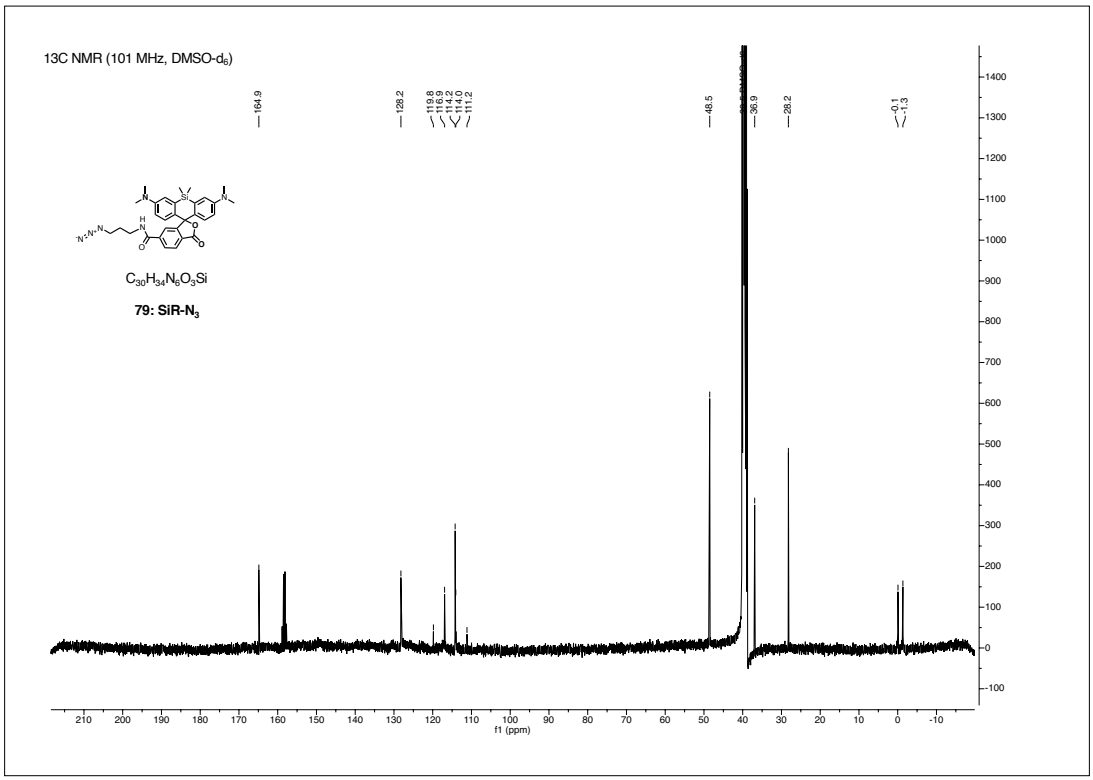
13C NMR (101 MHz, DMSO-d6)
C30H34N6O3Si
79: SiR-N3
164.9
139.2
119.8
118.0
114.2
114.0
111.2
48.5
36.9
29.2
-0.1
-1.3
f1 (ppm)

2 Analytical HPLC traces

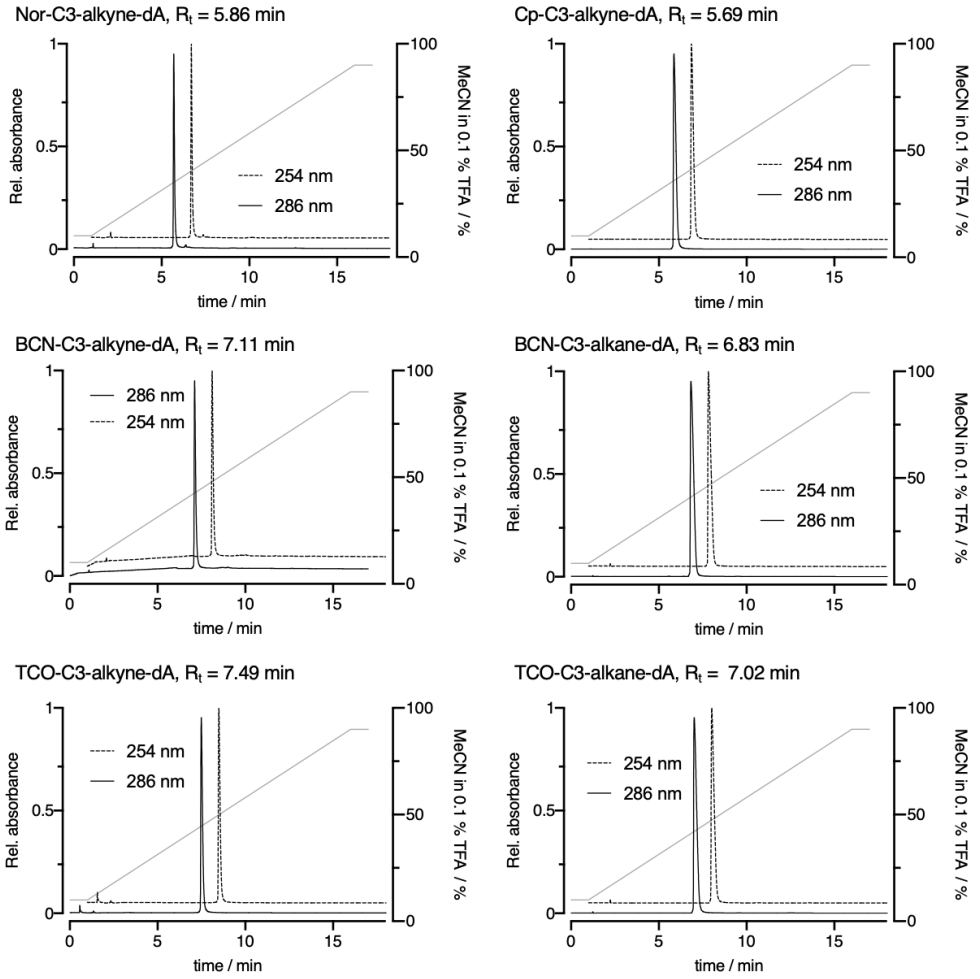

Figure 2.1: HPLC traces nucleoside analogs.

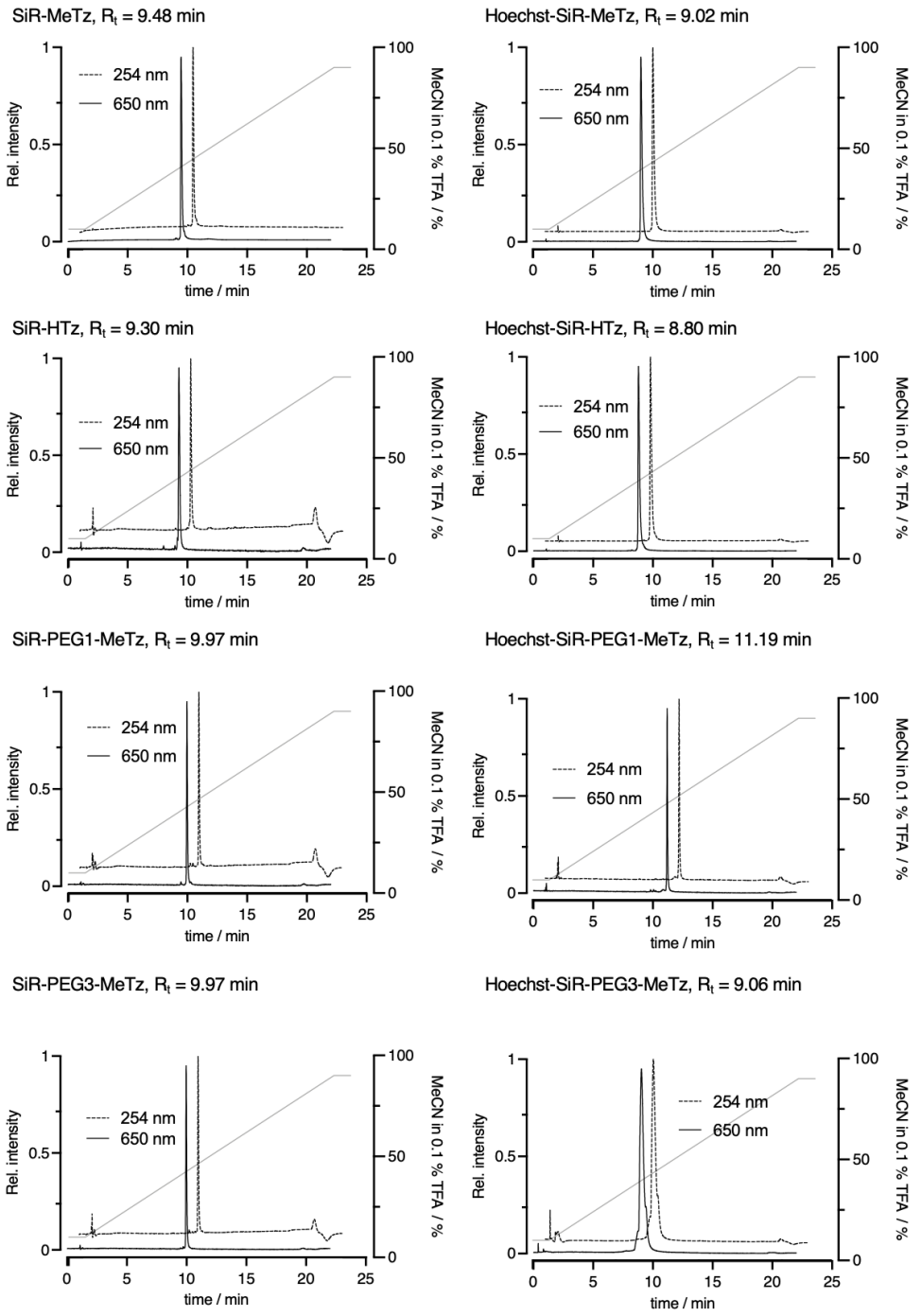

Figure 2.2: HPLC traces bifunctional probe.

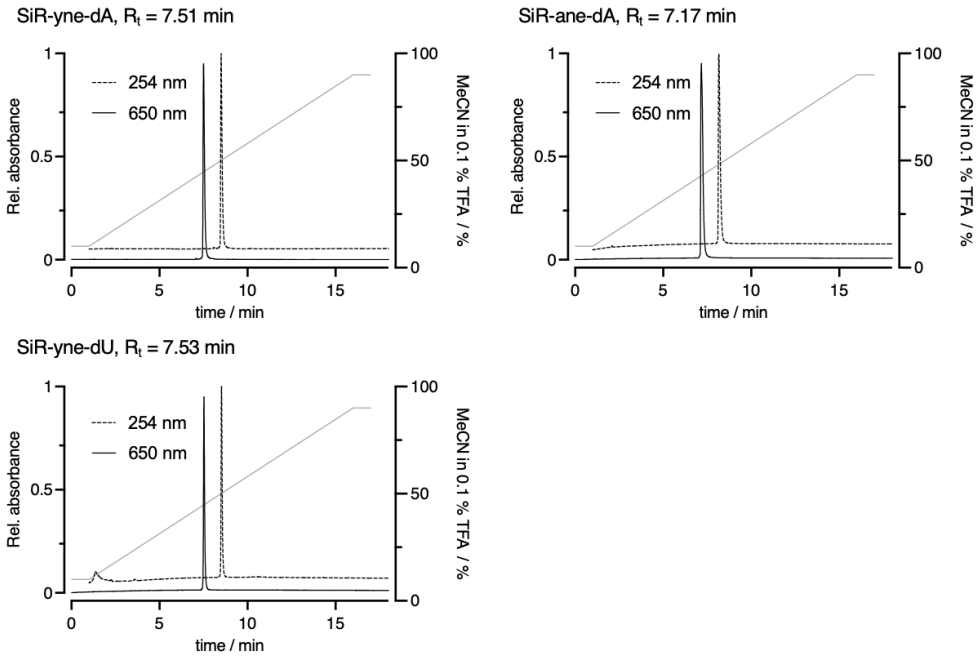

Figure 2.3: HPLC traces fluroescent nucleosides.

3 Additional *in vitro* experiments

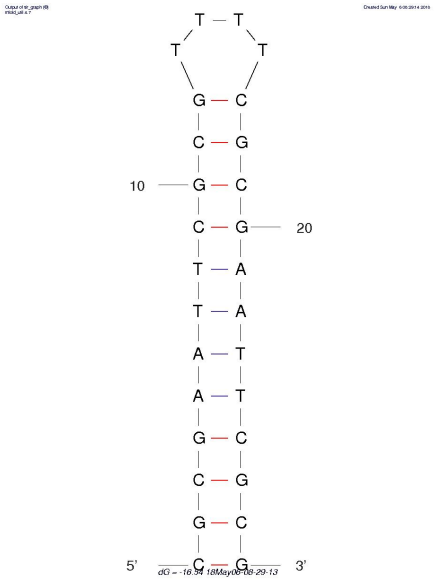

Figure 3.1: Hairpin structure predicted with mfold.

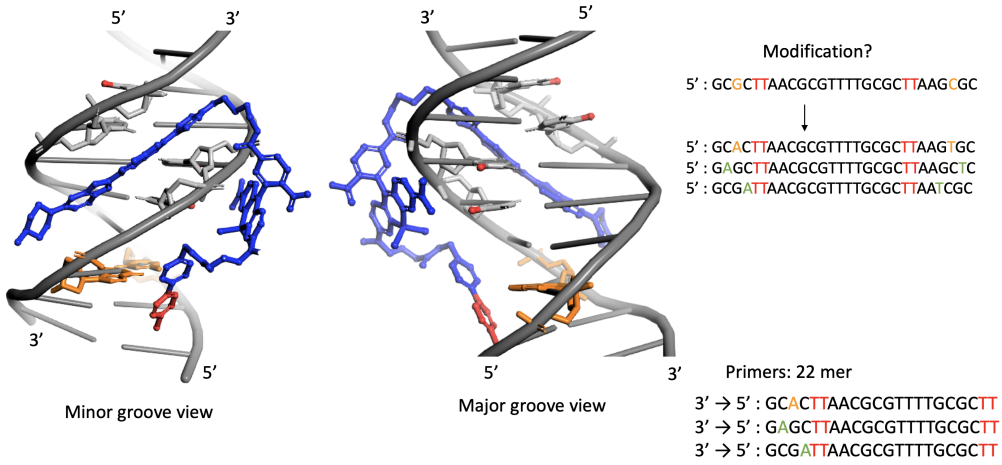

Figure 3.2: Structures from docking experiments with bifunctional probe and 8BNA oligonucleotide. Derived alternative sequences for oligos.

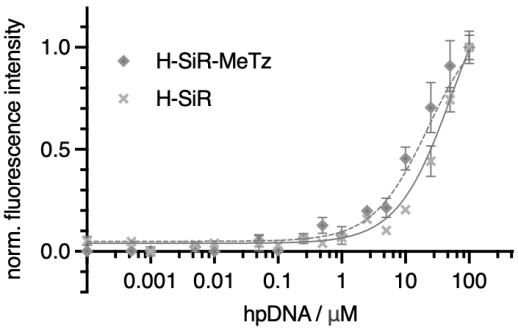

Figure 3.3: Titration 20 nM H-SiR-MeTz and H-SiR against hairpin DNA (1 nM to 100 µM) after 1 h incubation at room temperature.

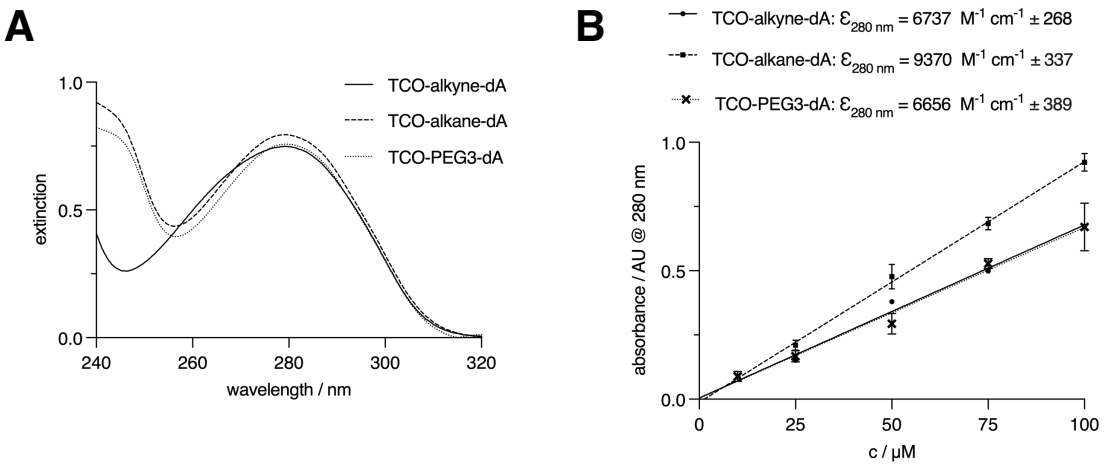

Figure 3.4: (A) UV/Vis spectra of TCO modified nucleosides with different linkers. (B) Linear regression of absorbance against concentration for determining the extinction coefficient at 280 nm.

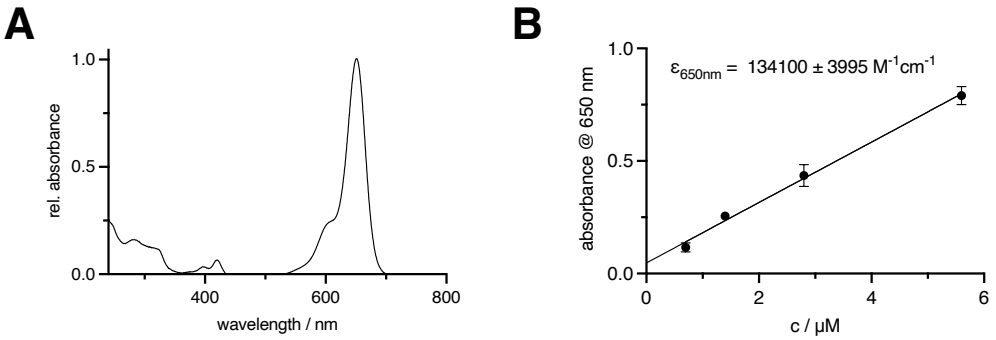

Figure 3.5: (A) UV/Vis spectrum of SiR-yne-dA. (B) Linear regression of absorbance against concentration for determining the extinction coefficient at 650 nm.

4 Additional *in cellulo* experiments

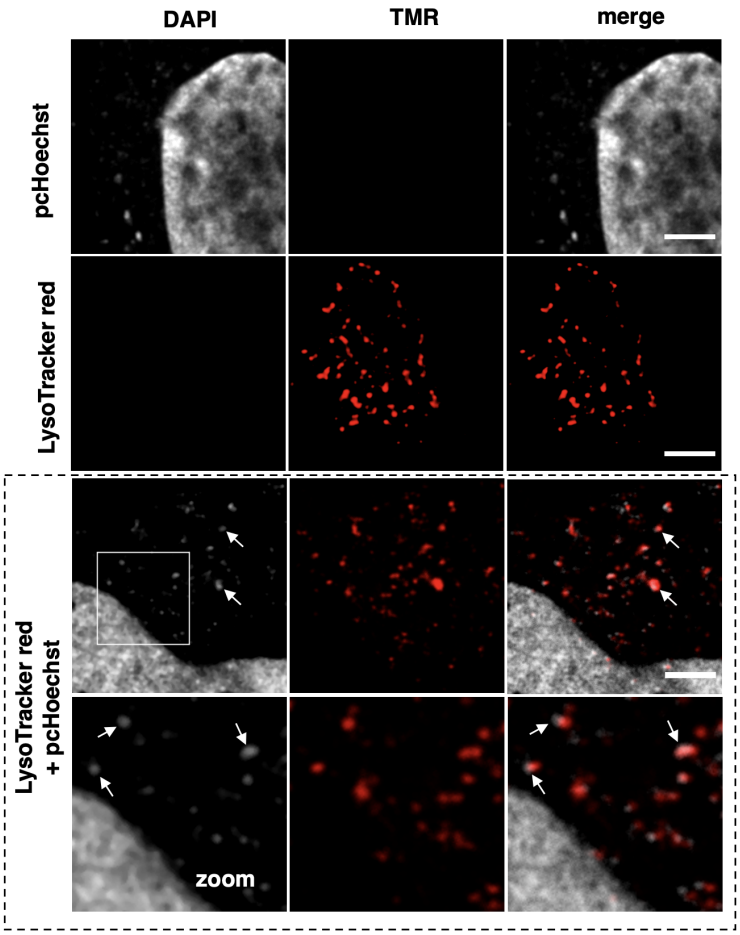

Figure 4.1: Confocal images of live Hela cells that were in the first row incubated with pcHoechst and globally uncaged or in the second row LysoTracker red only. The third and fourth rows are showing colocalizations with uncaged pcHoechst (gray) and LysoTracker red (red) that were incubated with the cells simultaneously. The more detailed views in row four clearly show colocalizing spots that were marked with white arrows.

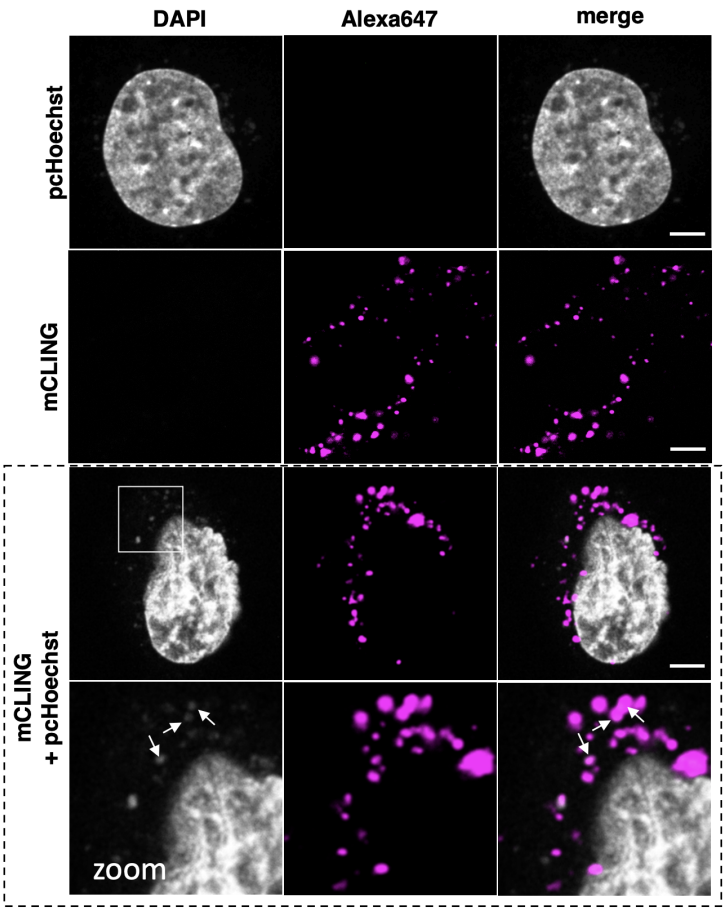

Figure 4.2: Confocal images of live Hela cells that were in the first row incubated with pcHoechst and globally uncaged or in the second row mCLING-Alexa647 only. The third and fourth rows are showing colocalizations with uncaged pcHoechst (gray) and mCLING-Alexa647 (magenta) that were incubated with the cells simultaneously. The more detailed views in row four clearly show colocalizing spots that were marked with white arrows.

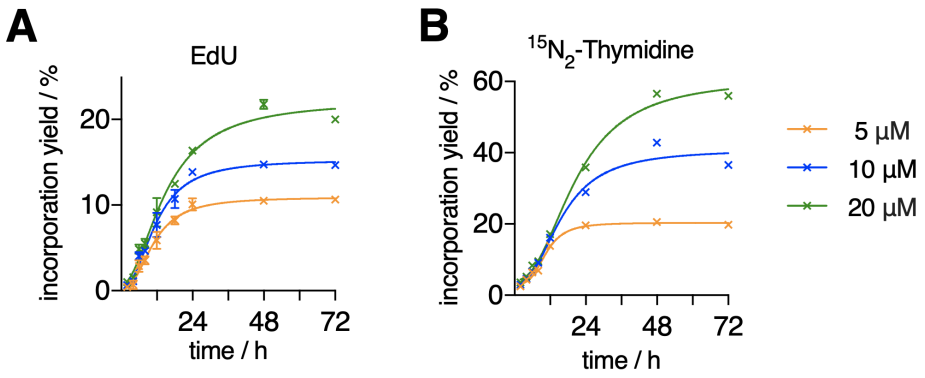

Figure 4.3: Incorporation yields of modified nucleoside analogs A) EdU and B) $^{15}N_2$-thymidine throughout 72 h determined by MRM quantification.

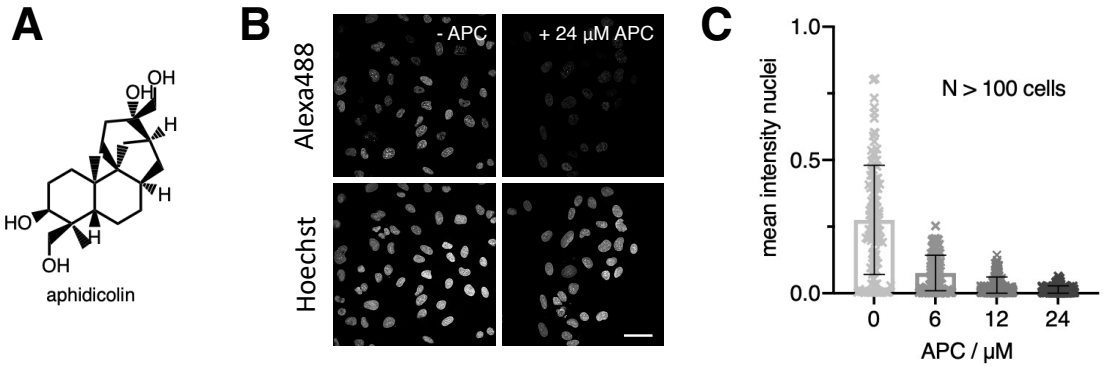

Figure 4.4: A) Structure of aphidicholin (APC). B) Confocal images of U2OS cells treated with 10 µM EdU for 8 h and optionally with 24 µM APC. The cells were fixed, labeled with Alexa488-azide in the presence of Cu(I), and counterstained with Hoechst33342. Scale bar = 50 µm. C) U2OS cells were treated with 10 µM EdU for 8 h and optionally with 6–24 µM APC. Quantification of mean fluorescence intensity in nuclei with N $>$100 cells.

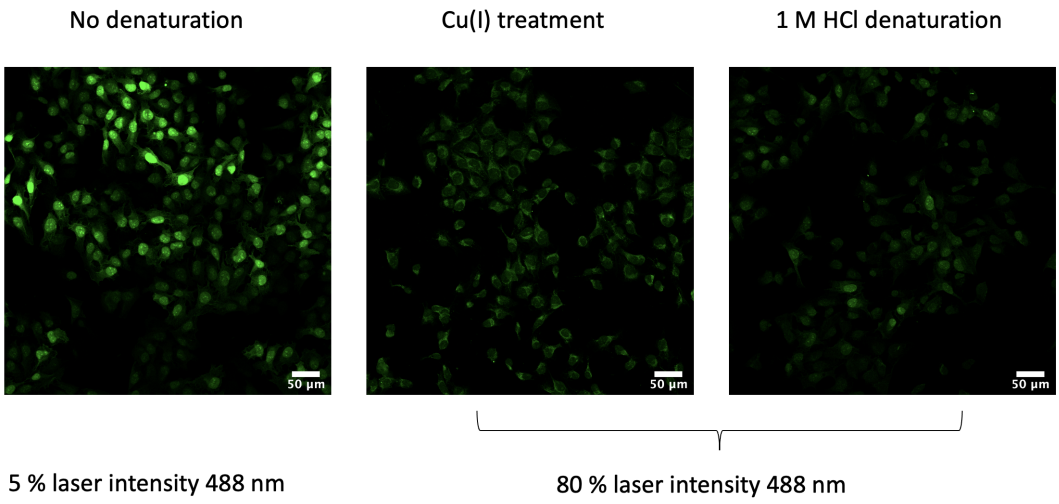

Figure 4.5: GFP signal in U2OS HSV-TK1-eGFP(+) cells. After PFA fixation and optional treatment with Cu(I) or 1 M HCl. Scale bar = 50 µm.

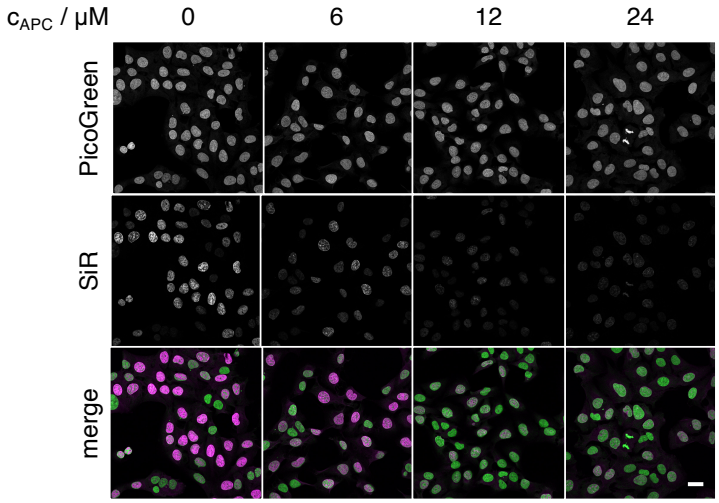

Figure 4.6: A) Confocal images of U2OS cells treated with 50 µM VdU for 8 h and optionally with 6–24 µM APC. The cells were fixed, labeled with 5 µM H-SiR-MeTz, and counterstained with PicoGreen. Scale bar = 50 µm.

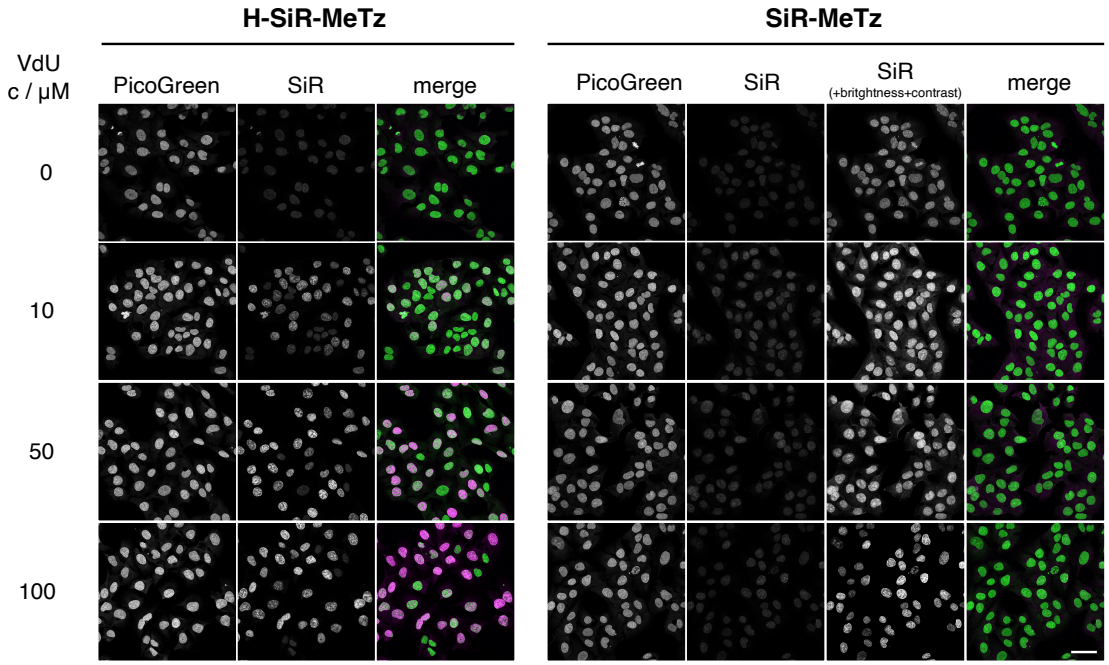

Figure 4.7: Representative confocal images of U2OS cells treated with various doses of VdU from 0–100 µM for 8 h and labeled with 5 µM of H-SiR-MeTz or SiR-MeTz. Cells were fixed with 4% PFA for 15 min, permeabilized with 0.2% Triton X-100 for 10 min, denatured with 1 M HCl for 30 min and labeled for 16 h at room temperature. Merge images show SiR signal in magenta and PicoGreen signal in green. Scale bar = 50 µm.

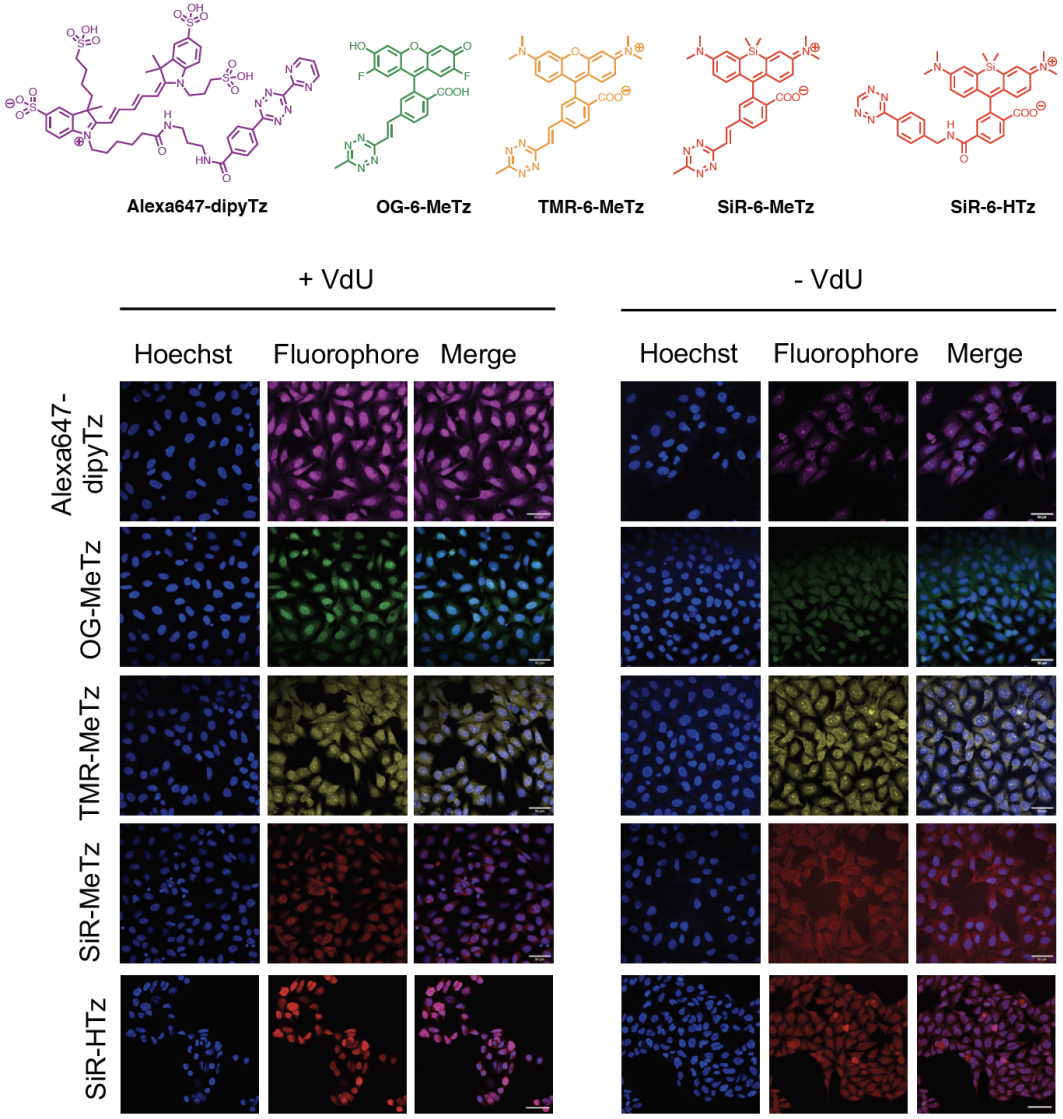

Figure 4.8: Confocal images of U2OS cells treated with 100 µM VdU, fixed with 4% PFA, permeabilized with 0.1% Triton X-100, denatured with 1 M HCl and labeled with 5 µM of the corresponding tetrazine dyes for 16 h at room temperature.

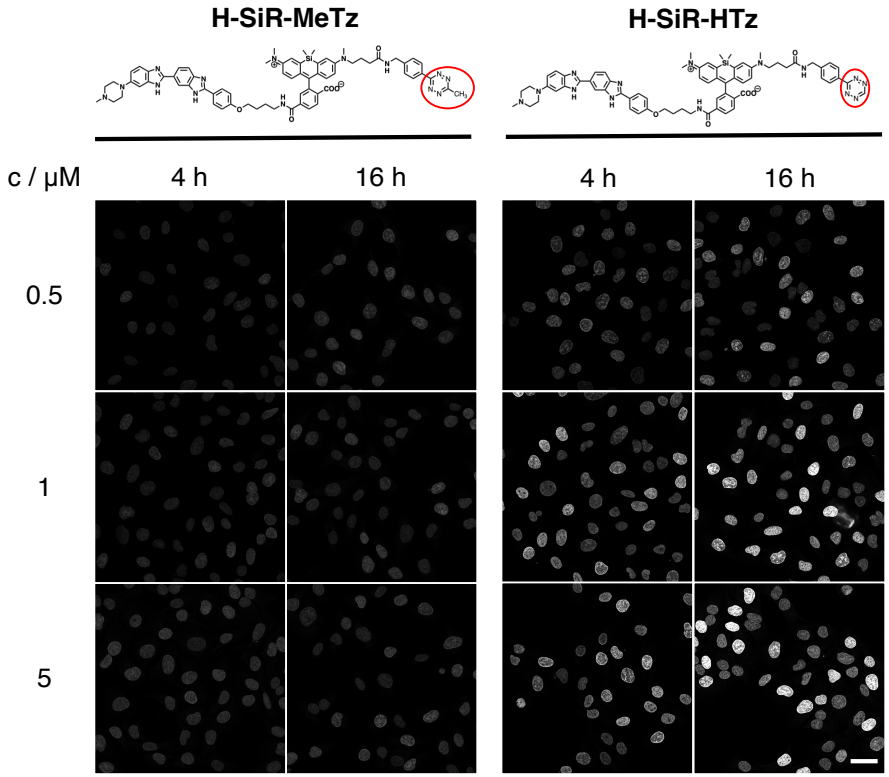

Figure 4.9: Representative confocal images of U2OS cells treated with VdU for 8 h and labeled with 0.5–5 µM of H-SiR-MeTz or H-SiR-HTz. Cells were fixed with 4% PFA for 15 min, permeabilized with 0.2% Triton X-100 for 10 min, denatured with 1 M HCl for 30 min and labeled for 4 or 16 h at room temperature. Scale bar = 50 µm.

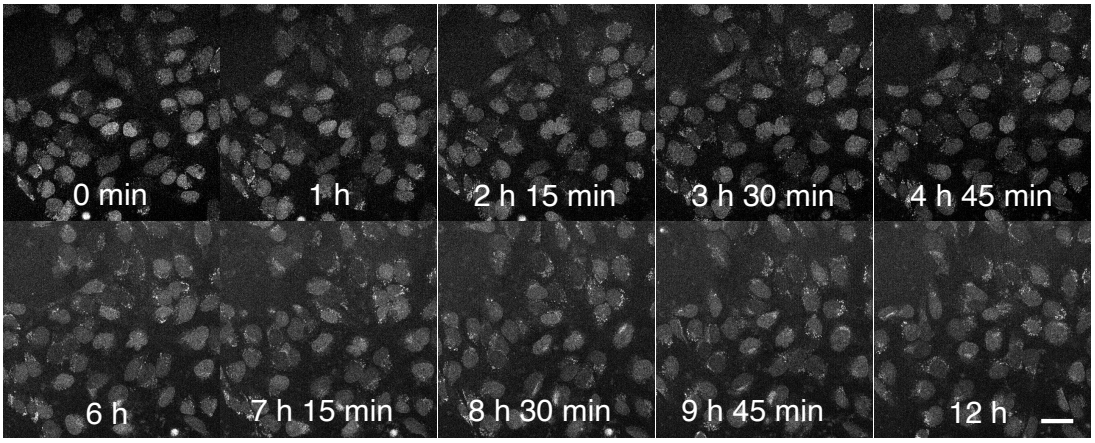

Figure 4.10: Representative confocal images of U2OS cells treated with VdU for 8 h and labeled with 5 µM H-SiR-HTz live for 16 h. Time course image acquisition started after labeling. Scale bar = 20 µm.

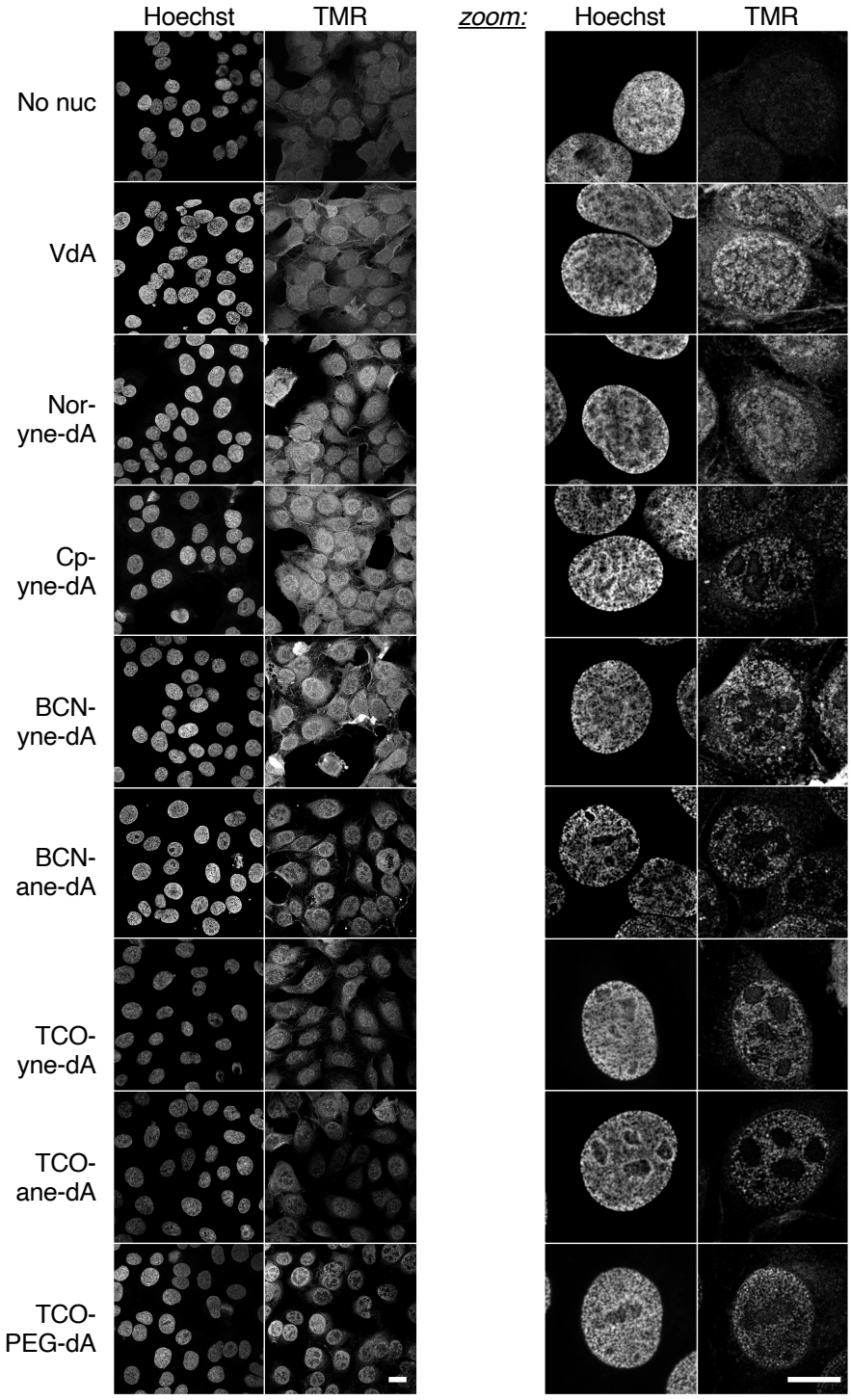

Figure 4.11: Representative confocal images of U2OS TREx cells after 8 h feeding with 100 µM nucleosides, PFA fixation, HCl denaturation, and labeling with 5 µM MAP-C1-MeTz **51** at room temperature for 16 h. Images were acquired using different laser intensities. One of two independent experiments is shown. Scale bar = 50 µm and 20 µm (details).

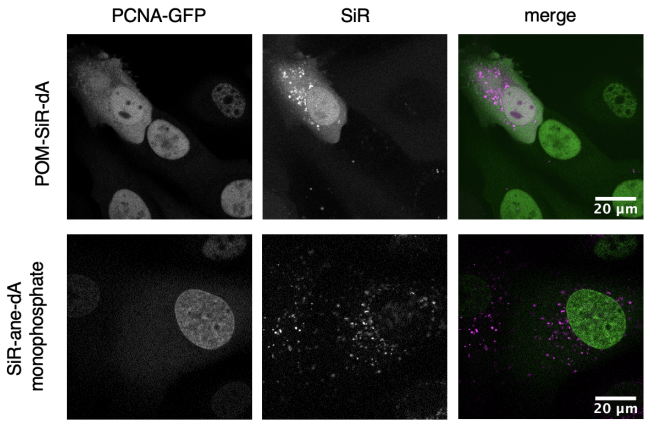

Figure 4.12: Confocal images of live U2OS PCNA-GFP cells treated with 5 µM POM-SiR-dA **63** for 8 h or 5 µM SiR-ane-dA monophosphate **68** for 6 h.

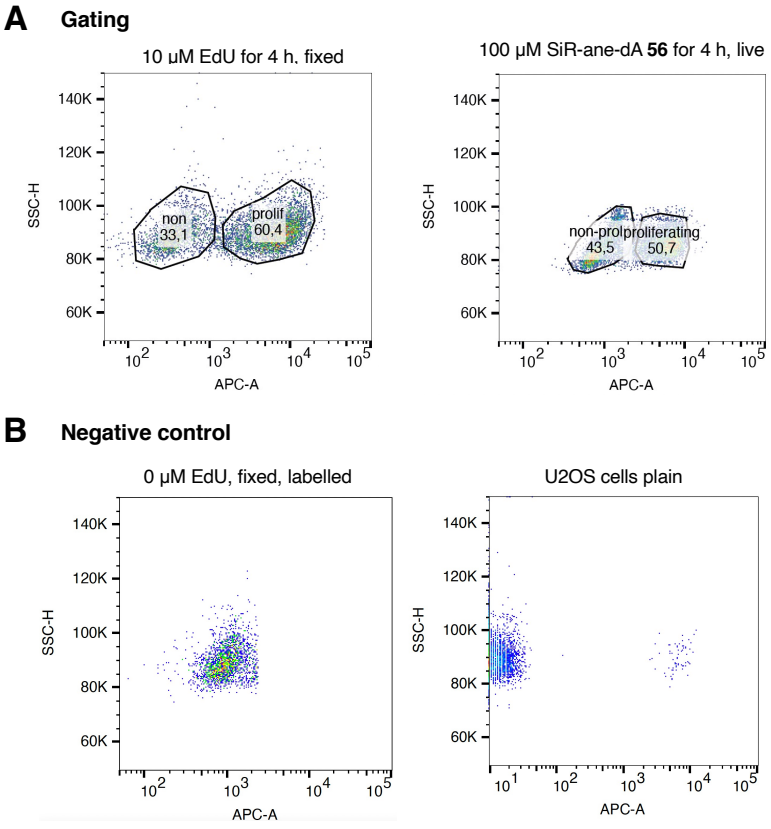

Figure 4.13: A) Flow cyteometry gating strategy to determine proliferating and non-proliferating U2OS cells feeding EdU or SiR-ane-dA **56** for 4 h. EdU treated cells were fixed and labeled with Alexa647-azide, SiR-ane-dA **56** treated cells labeled live. B) Negative control experiments for gating.

5 Additional tables

Table 5.1: Determination of UV laser power of SuperK white light CW laser (Coherent) at 355 nm and resulting laser intensity per surface area.

% UV laser	measured power / µW	calculated intensity / W cm^{-2}
100%	1260 ± 26.4	1451546
80%	1100 ± 25.1	1267223
60%	777 ± 15.8	895120
20%	110 ± 10.7	126722
5%	7.16 ± 0.247	8248

Table 5.2: Parameters predicted with Schrödinger Software for docking experiments with H-SiR-MeTz to hpDNA based on the PDB: 8BNA structure.

Binding mode	Glide score	ΔG_{bind} / kcal mol^{-1}
minor	-8.726	-119.08
minor	-6.744	-118.76
minor	-14.818	-109.76
minor	-10.202	-107.64
minor to major	-4.920	-98.66
minor	-7.474	-87.03
minor	-3.811	-81.14
minor	-0.713	-79.56
minor	-3.094	-78.22

Part V

Additional Information

Scientific meetings and conferences

2021	Boehringer Ingelheim Fonds Summer Retreat, talk
2019	Boehringer Ingelheim Fonds Summer Retreat, talk
2019	SFB1129 Retreat, poster contribution
2019	Seeing is believing, EMBL Heidelberg
2018	Chemical Biology, EMBL Heidelberg
2018	MPImR Intitute Retreat, talk
2012	Swiss Pharma Science Day, talk

Publications

- Laemmle C. A. et al: Photocaged Hoechst Enables Subnuclear Visualization and Cell Selective Staining of DNA in vivo, ChemBioChem 2020, 21, 1 – 10.
- Binder R., Laemmle C.: Reversed Phase High Performance Thin Layer Chromatography of Aqueous Samples in Student Laboratories Using the Example of Anthocyanin Patterns from Flower Petals, J. Chem. Educ. 2019, 96, 9, 1922–19.
- Laemmle C., Belladonna puzzle – Application of mass spectrometry, SWISS PHARMA 34 (2012) Nr. 10, conference proceedings.

Contributions to this project

Ideas for the project were proposed in the context of the SFB1129 proposal. Prior work on thymidine derivatives for metabolic DNA labeling was performed in the group of Prof. Dr. Carsten Schultz (back then: EMBL, Heidelberg) and Prof. Dr. Dr. h.c. Hans-Georg Kräusslich (University Hospital Heidelberg). Dr. Thorsten Müller (AK Kräusslich) introduced me to the topic and we collaborated on the project. Dr. Johannes Broichhagen supervised the project from April 2018 until September 2019 at MPImR. Franziska Walterspiel worked on tetrazine dyes in her Master's thesis from September 2019 until March 2020. Luis Hauptmann joined the project about proximity labeling as a research intern from mid-November 2020 until January 2021. The project on pcHoechst (Chapter 1) was published (see above) and collaborations were indicated separately.